THESIS
5
2003
V.1
54047655

LIBRARY
Michigan State
University

This is to certify that the
dissertation entitled

ANALYSES OF TOP-DOWN CRACKING IN RUBBLIZED AND FELXIBLE PAVEMENTS

presented by

Tunwin Svasdisant

has been accepted towards fulfillment
of the requirements for the

Ph.D. degree in Civil Engineering

Major Professor's Signature

8/21/03

Date

*MSU is an Affirmative Action/Equal Opportunity Institution*

**PLACE IN RETURN BOX** to remove this checkout from your record.
**TO AVOID FINES** return on or before date due.
**MAY BE RECALLED** with earlier due date if requested.

| DATE DUE | DATE DUE | DATE DUE |
|---|---|---|
| | | |
| | | |
| | | |
| | | |
| | | |
| | | |
| | | |
| | | |
| | | |
| | | |

6/01 c:/CIRC/DateDue.p65-p.15

ANAL

# ANALYSES OF TOP-DOWN CRACKING IN RUBBLIZED AND FLEXIBLE PAVEMENTS

Volume I

By

Tunwin Svasdisant

**A DISSERTATION**

Submitted to
Michigan State University
in partial fulfillment of the requirements
for the degree of

DOCTOR OF PHILOSOPHY

Department of Civil and Environmental Engineering

2003

ANALY

R

pavements

concrete s

reflective

top-down

pavement

R

the underp

activities

backcalcu

induced i

T

and after

investigat

after the c

concrete s

uneven in

## ABSTRACT

# ANALYSES OF TOP-DOWN CRACKING IN RUBBLIZED AND FLEXIBLE PAVEMENTS

By

Tunwin Svasdisant

Rubblization is one of the rehabilitation options for deteriorated concrete pavements. The main objectives of rubblization are to destroy the integrity of the concrete slabs and joints and to debond the temperature steel as to eliminate future reflective cracking potential. However, field investigation revealed that reflective cracks, top-down cracks (TDC) and segregation are the dominant distresses on rubblized pavements. TDC were also reported on conventional flexible pavements.

Recognizing the problems, this study was conducted to determine the causes of the underperformance of rubblized pavements and the causes of TDC. The research activities include field and laboratory investigations of rubblized and flexible pavements, backcalculation of pavement layer moduli and 2- and 3-dimensional analyses of stresses induced in the AC layer of rubblized and flexible pavements.

The field investigation consisted of two phases; during the rubblization operation and after construction. In the first phase 15 rubblized pavement projects were investigated whereas 87 rubblized and 10 flexible pavement projects were investigated after the completion of construction. Results of the former indicated that the rubblized concrete slabs consisted of two layers; a rubblized material and fractured concrete with uneven interface between them. Further, in the majority of cases, the temperature steel

was not deb

and cores w

were used t

verification

layers and

rubblized p

to stiff laye

Me

the load-in

the relaxat

the analys

edges of th

are caused

AC surfac

winter inc

TDC.

Ba

analyses.

Further, i

premature

selection

equipmen

was not debonded. In the latter, nondestructive deflection tests (NDT) were conducted and cores were extracted from rubblized and flexible pavements. The deflection data were used to backcalculate the layer moduli while the cores were used for TDC verification and for laboratory investigation. To overcome the problems (more than 5-layers and uneven interface between the layers) in the backcalculation of layer moduli of rubblized pavements, a backcalculation procedure and a procedure to estimate the depth to stiff layer were developed and implemented in this study.

Mechanistic analyses were conducted using finite element programs to determine the load-induced stresses in the AC layer. Whereas thermal stresses were calculated using the relaxation constitutive equation and the measured pavement temperatures. Results of the analyses indicated that, in certain scenarios, the potential of longitudinal TDC at the edges of the wheel paths is higher than that for bottom-up cracking and longitudinal TDC are caused by high stress ratio (the ratio of the tensile stress to the tensile strength) at the AC surface and are likely to initiate during summer. The high thermal tensile stresses in winter increase transverse TDC initiation potential and accelerate the propagation of TDC.

Based on the results of field and laboratory investigations and of mechanistic analyses, a guideline to determine TDC based on field observation was developed. Further, it was shown that when the rubblization objectives are not fully satisfied, premature distresses would occur. Consequently, two procedures were developed for the selection of candidate projects for rubblization and for the calibration of the rubblizing equipment as to improve the quality of the rubblization operation.

*To My Family*
*&*
*My Advisor*

The

Gilbert Bala

course of th

appreciated

Spec

people and

The

undergradu

appreciated

A th

understand

Uni

Uranwan, by

encouragem

Baladi's), I

from home

## ACKNOWLEDGEMENTS

The author likes to express my utmost appreciation to my major advisor, Dr. Gilbert Baladi, for his constant support, guidance and encouragement throughout the course of this study. The guidance from my doctoral committee members is also greatly appreciated.

Special thanks are due to the Michigan Department of Transportation and to the people and Government of Thailand for their financial and technical supports.

The contributions, suggestions and discussion of many graduate and undergraduate students especially Michael Schorsch and Michael Niederquell are greatly appreciated.

A thousand thanks to Nattaporn Tansawat for her support, encouragement and understanding throughout my tenure at Michigan State University.

Untold thanks to my family in Thailand especially my father Santi, mother, Uraiwan, brother, Taymee and sister Pattrapetra for their great spiritual supports and encouragement especially during the writing of this dissertation. To my other family (the Baladi's), I would like to express my true love and appreciation for giving me home away from home.

LIST OF T

LIST OF FI

CHAPTER

1.0 INTR
2.0 OBJ
3.0 HYP
4.0 RES
4.1
4.2
4.3
4.4
4.5
4.6
5.0 THE

CHAPTER

1.0 INT
2.0 TIR
2.1
2.2
3.0 TOP
4.0 CAL
5.0 FAC
5.1
5.2
5.3
5.4
5.5
6.0 FAC
6.1
6.2
6.3
7.0 TOP
8.0 SUM

## TABLE OF CONTENTS

**LIST OF TABLES** ..... xi

**LIST OF FIGURES** ..... xvii

**CHAPTER 1 - INTRODUCTION & OBJECTIVES** ..... 1

1.0 INTRODUCTION ..... 1
2.0 OBJECTIVES ..... 3
3.0 HYPOTHESES ..... 4
4.0 RESEARCH PLAN ..... 4
4.1 Literature Review ..... 5
4.2 Field Investigation ..... 5
4.3 Laboratory Investigation ..... 6
4.4 Analyses ..... 6
4.4.1 Analyses of the Measured FWD Deflection Data ..... 6
4.4.2 Mechanistic Analyses of Rubblized and Flexible Pavements ..... 7
4.5 Validation of the Results of the Analyses ..... 7
4.6 Conclusions and Recommendations ..... 8
5.0 THESIS STRUCTURE ..... 8

**CHAPTER 2 - LITERATURE REVIEW** ..... 10

1.0 INTRODUCTION ..... 10
2.0 TIRE-PAVEMENT INTERACTION ..... 12
2.1 Tire-Pavement Contact Area ..... 12
2.2 Tire-Pavement Contact Stresses ..... 13
2.2.1 Tire Type and Structure ..... 27
2.2.2 Wheel Load and Tire Inflation pressure ..... 31
2.2.3 Tire Motion ..... 35
3.0 TOP-DOWN CRACKS IN FLEXIBLE AND RUBBLIZED PAVEMENTS ..... 37
4.0 CAUSES OF TOP-DOWN CRACKS ..... 40
5.0 FACTORS AFFECTING TENSILE STRENGTH OF AC MIXTURES ..... 47
5.1 The AC Mix Design ..... 48
5.2 Temperature ..... 50
5.3 Particle Segregation ..... 51
5.4 Compaction ..... 52
5.5 Stress State ..... 53
6.0 FACTORS AFFECTING THE TENSILE STRESSES IN THE AC LAYER ..... 55
6.1 Magnitude and Configuration of Load ..... 55
6.2 Thickness and Modulus of Each Pavement Layer ..... 56
6.3 Temperature (Thermal stress) ..... 57
7.0 TOP-DOWN CRACK PROPAGATION MODELS ..... 62
8.0 SUMMARY ..... 64

CHAPTER

1.0 RUB
1.1

1.2
1.3
2.0 FIEI
2.1
2.2

3.0 LAB
3.1
3.2
3.3
3.4

4.0 SUM

CHAPTER 4

1.0 INTR
2.0 QUAL
2.1
2.2
2.3
2.4
3.0 CONS
4.0 THE
5.0 PROJ
6.0 SUM

CHAPTER 5

1.0 INTR
2.0 TDC
2.1
2.2
2.3
3.0 TDC

**CHAPTER 3 – FIELD AND LABORATORY INVESTIGATIONS** ..... 65

1.0 RUBBLIZATION ..... 65
1.1 Rubblizing Equipment ..... 67
1.1.1 Resonant Frequency Breaker ..... 67
1.1.2 Multi-Head Breaker ..... 71
1.2 Rubblization Objectives ..... 75
1.3 Rubblized and Conventional Flexible Pavement Cross-Sections ..... 77
2.0 FIELD INVESTIGATION ..... 79
2.1 Field Investigation during the Rubblization Operation ..... 79
2.2 Field Investigation after Completion of Construction ..... 87
2.2.1 FWD Testing and Coring ..... 89
2.2.2 Manual Distress Survey of Rubblized Pavements ..... 95
3.0 LABORATORY INVESTIGATION ..... 116
3.1 Sample Preparation ..... 118
3.2 Specific Gravity Test (SG test) ..... 123
3.3 Indirect Tensile Cyclic Load Tests (ITCLT) ..... 123
3.4 Indirect Tensile Strength Tests (ITST) ..... 131
3.4.1 Effect of Test Temperature ..... 134
3.4.2 Segregation and Moisture Conditioning ..... 136
4.0 SUMMARY ..... 140

**CHAPTER 4 - THE UNDERPERFORMANCE OF RUBBLIZED PAVEMENTS** ..... 141

1.0 INTRODUCTION ..... 141
2.0 QUALITY OF THE RUBBLIZATION OPERATION ..... 142
2.1 Rubblization Objectives ..... 142
2.2 Rubblization Procedure ..... 146
2.3 Measures of the Quality of the Rubblization Operation ..... 149
2.4 Equipment Calibration ..... 155
3.0 CONSTRUCTION PROCEDURES ..... 162
4.0 THE ASPHALT MIX DESIGN ..... 162
5.0 PROJECT SELECTION FOR RUBBLIZATION ..... 165
6.0 SUMMARY ..... 168

**CHAPTER 5 - CLASSIFICATION AND IDENTIFICATION OF TOP-DOWN CRACKS** ..... 169

1.0 INTRODUCTION ..... 169
2.0 TDC DESCRIPTIONS AND CLASSIFICATION ..... 169
2.1 Longitudinal Top-Down Cracks (LTDC) Category ..... 170
2.2 Transverse Top-Down Cracks (TTDC) Category ..... 176
2.3 Cracks in Segregated Areas Category ..... 176
3.0 TDC IDENTIFICATION ..... 180

3.1
3.2
3.3
4.0 SUM

CHAPTER

1.0 GEN
2.0 REPI
3.0 THE
4.0 BAC
5.0 BAC
5.1
5.2
5.3
5.4
5.5
6.0 VAR
6.1
6.2
6.3
7.0 TEM
MOD
8.0 DET
PAVI
8.1
8.2
8.3
9.0 BAC
10.0 SUM

CHAPTER

1.0 INTR
2.0 THE
3.0 PAVI
4.0 THE
4.1
4.2
4.3
4.4

3.1 Longitudinal Cracks ..... 180
3.2 Transverse Cracks ..... 182
3.3 Network of Longitudinal and Transverse Cracks ..... 183
4.0 SUMMARY ..... 184

**CHAPTER 6 - BACKCALCULATION OF LAYER MODULI** ..... 185

1.0 GENERAL ..... 185
2.0 REPEATABILITY AND LINEARITY OF THE DEFLECTION DATA ..... 188
3.0 THE DEFLECTION DATA ..... 192
4.0 BACKCALCULATION COMPUTER PROGRAMS ..... 200
5.0 BACKCALCULATION PROCEDURE ..... 205
5.1 Depth to Stiff Layer ..... 206
5.1.1 Equivalent Pavement Modulus ..... 208
5.1.2 Three- and four-layer systems ..... 210
5.2 Convergence Criteria ..... 215
5.3 Special Provisions for the Backcalculation of Rubblized Pavement Moduli ..... 218
5.4 Acceptance Criteria ..... 220
5.5 Determination of the Most Plausible RM Thickness ..... 221
6.0 VARIABLES AFFECTING THE BACKCALCULATION RESULTS ..... 227
6.1 The AC Thickness ..... 228
6.2 The RM and FC Thicknesses ..... 230
6.2.1 The Effect of Combining the RM and FC layers ..... 232
6.2.2 The Effect of the Thickness of the RM Layer ..... 232
6.3 The BS Thickness ..... 236
7.0 TEMPERATURE CORRECTION OF THE BACKCALCULATED AC MODULUS ..... 237
8.0 DETAILED EXAMPLE OF BACKCALCULATION OF RUBBLIZED PAVEMENT LAYER MODULI ..... 238
8.1 Examination of the Measured Deflection Data ..... 239
8.2 Determination of the Depth to Stiff Layer ..... 239
8.3 Final Selection of Layered Systems ..... 248
9.0 BACKCALCUALTION RESULTS ..... 259
10.0 SUMMARY ..... 273

**CHAPTER 7 - THERMAL STRESSES IN THE AC LAYER** ..... 274

1.0 INTRODUCTION AND OBJECTIVES ..... 274
2.0 THERMAL STRESSES ..... 274
3.0 PAVEMENT TEMPERATURE DATA ..... 279
4.0 THERMAL STRESSES IN AC SURFACED PAVEMENTS ..... 284
4.1 The Effect of the Duration Period on Thermal Stresses ..... 285
4.2 Daily Thermal Stress Variation ..... 286
4.3 Yearly Thermal Stress Variation ..... 288
4.4 Thermal Stress Variation between Test Sites ..... 290

5.0 SUM

CHAPTER

1.0 INT
2.0 CON
3.0 MEC
4.0 TWO
4.1
4.2

5.0 THRE
5.1
5.2
5.3

5.4

5.5

6.0 STRES
7.0 SUMM

CHAPTER 9

1.0 SUMM
2.0 CONC
2.1
2.2
2.3
2.4
2.5
3.0 RECO

5.0 SUMMARY ..... 294

**CHAPTER 8 - MECHANISTIC ANALYSES OF LAOD-INDUCED STRESSES AT THE AC SURFACE AND AT THE AC BOTTOM** ..... 296

1.0 INTRODUCTION ..... 296
2.0 COMPUTER PROGRAMS USED IN THE MECHANISTIC ANALYSES ..... 297
3.0 MECHNAISTIC ANALYSES ..... 302
4.0 TWO-DIMENSIONAL FINITE ELEMENT ANALYSES ..... 303
4.1 Partial Factorial ..... 303
4.2 Results of the 2-D Analyses ..... 306
4.2.1 Flexural Rigidity of the AC Layer ..... 320
4.2.2 Stress-Strain Relationship (Hooke's Law) ..... 320
4.2.3 Stress Decay ..... 321
4.2.4 Stiffness of the Support of the AC Layer ..... 323
4.2.5 Location of the Neutral Axis ..... 325
5.0 THREE-DIMENSIONAL FINITE ELEMENT ANALYES ..... 325
5.1 Tire-Pavement Contact Area and Contact Stresses ..... 326
5.2 Finite Element Models ..... 334
5.3 Lateral Stresses Induced in the AC Layer by Tire-Pavement Contact Stresses ..... 339
5.3.1 Superposition ..... 339
5.3.2 Lateral Contact Stresses ..... 342
5.3.3 Longitudinal Contact Stresses ..... 345
5.3.4 Vertical Contact Stresses and by Combination of Lateral and Vertical Contact Stresses ..... 347
5.4 The Effects of the Interface Geometry between the RM and the FC Layers ..... 357
5.5 The Lateral Stresses Induced in the AC Layer Due to Dual Wheel Load ..... 373
5.5.1 3-D Models, Contact Stresses and Contact Areas ..... 374
5.5.2 Results of the 3-D analyses of Single and Dual Wheel Loads ..... 377
6.0 STRESS RATIOS ..... 384
7.0 SUMMARY ..... 394

**CHAPTER 9 - SUMMARY, CONCLUSIONS AND RECOMMENDATIONS** ..... 395

1.0 SUMMARY ..... 395
2.0 CONCLUSIONS ..... 398
2.1 Hypotheses ..... 399
2.2 Rubblized Pavements and Top-Down Cracks ..... 399
2.3 NDT and Backcalculation of Layer Moduli ..... 400
2.4 Thermal Stresses ..... 400
2.5 Mechanistic Analyses ..... 401
3.0 RECOMMENDATIONS ..... 402

APPENDIX

REFERENCES

**APPENDIX A - Rubblized Pavement Projects in Michigan**.....403

**REFERENCES**.....413

Table 2.1

Table 2.2

Table 3.1

Table 3.2

Table 3.3

Table 3.4

Table 3.5

Table 3.6

Table 3.7

Table 3.8

Table 3.9

Table 3.10

Table 3.11

Table 3.12

Table 3.13

## LIST OF TABLES


Table 2.1 A summary of the tire-pavement contact stresses....36

Table 2.2 A summary of conclusions made by various investigators....46

Table 3.1 A summary of field and laboratory investigation activities on rubblized and flexible pavements of the two specified studies....66

Table 3.2 A summary of the rubblized equipment and trench locations....79

Table 3.3 A summary of rubblization variables and observations made during the investigation of various projects....8

Table 3.4 Comparison between the products of the resonant frequency and the multi-head breakers....81

Table 3.5 A summary of the repeatability and linearity tests....92

Table 3.6 A summary of rubblized pavement projects that were FWD tested and/or cored....93

Table 3.7 A summary of flexible pavement projects that were FWD tested and/or cored....94

Table 3.8 A summary of the number of rubblized and flexible pavement test sites that were FWD tested and cored....94

Table 3.9 A summary of the distresses survey of 86 rubblized pavement projects in 2001....98

Table 3.10 A summary of the distresses survey of 87 rubblized pavement projects in 2002....99

Table 3.11 A summary of the distresses survey of 87 rubblized pavement projects in 2003....100

Table 3.12 Number of projects having transverse TDC in and outside segregated areas....115

Table 3.13 Number of projects having longitudinal TDC in and outside segregated areas at different locations on the pavements....115

Table 3.14

Table 3.15

Table 3.16

Table 3.17

Table 3.18

Table 3.19

Table 3.20

Table 3.21

Table 3.22

Table 4.1

Table 6.1

Table 6.2

Table 6.3

Table 6.4

Table 3.14 A summary of the number of the no-rehabilitated rubblized pavement projects having TDC in 2003 sorted by the AC surface course mix types ..... 117

Table 3.15 A summary of the rehabilitated rubblized pavement projects and their average service life (years in service until the first rehabilitation) sorted by the original AC surface course mix types ..... 117

Table 3.16 Crack depth measurement of cores extracted from rubblized pavement projects to verify whether or not the cracks are TDC ..... 119

Table 3.17 A summary of the average total thickness of the cores and the average thickness of each AC course for 19 rubblized and 13 flexible pavement test sites ..... 124

Table 3.18 A summary of the average physical and engineering properties of the AC cores obtained from 19 rubblized and 13 flexible pavement test sites ..... 125

Table 3.19 Comparison of the average measured and predicted indirect tensile strengths (using equation 2.1) of the 4B mix ..... 135

Table 3.20 Sources of the aggregate gradations and the asphalt contents used in investigating the effect of segregation and moisture conditioning on the indirect tensile strengths of three asphalt mixes (Schorsch, 2003) ..... 135

Table 3.21 The average tensile strengths of three segregated and not segregated asphalt mixes (Schorsch, 2003) ..... 135

Table 3.22 Indirect tensile strengths of the 4B, 4C and 4E10 mixes at 39.2, 65.3 and 140.0° F for various mix conditions ..... 138

Table 4.1 Definition, objectives and score of the quality of the rubblization operation ..... 161

Table 6.1 Pavement projects where repeatability and linearity tests were conducted ..... 189

Table 6.2 The averages and standard deviations of deflections D1 through D7 at different load levels, I-69 EB, test site 1 of test section 1 ..... 189

Table 6.3 Typical averages of D1 through D7 deflections at different load levels, I-69 EB, test site 1 of test section 1 ..... 191

Table 6.4 D1 through D7 deflections, rubblized pavement, US-10 EB test section 1, test site 1 ..... 193

Table 6.5

Table 6.6

Table 6.7

Table 6.8

Table 6.9

Table 6.10

Table 6.11

Table 6.12

Table 6.13

Table 6.14

Table 6.15

Table 6.16

Table 6.17

Table 6.5 D1 through D7 deflections, rubblized pavement, US-10 EB, test section 1, test site 2 ..... 194

Table 6.6 D1 through D7 deflections, flexible pavement, US-27 SB, test section 1, test site 1 ..... 195

Table 6.7 Coefficients of variation in the measured D1 through D7 deflections for 26 test sites on rubblized pavements and 12 test sites on flexible pavements ..... 198

Table 6.8 Summaries of the MICHBACK, MODCOMP5, EVERCALC and MODULUS (version 4.0) backcalculation programs ..... 201

Table 6.9 The thicknesses and engineering properties of two pavement sections used in the forward analyses (MICHPAVE) ..... 201

Table 6.10 The deflection basins of the two pavement sections in Table 6.8 due to 9000-lb load calculated using MICHPAVE finite element program ..... 201

Table 6.11 Comparison of the results of MICHBACK, MODCOMP5, EVERCALC and MODULUS backcalculation programs of a pavement section with no stiff layer ..... 202

Table 6.12 Comparison of the results of MICHBACK, MODCOMP5, EVERCALC and MODULUS backcalculation programs of a pavement section with a depth to stiff layer of 200 in. ..... 203

Table 6.13 Thickness and moduli of AC, rubblized concrete slab (RCS), combination of base and subbase (BS) and roadbed soil (RB) of a pavement section having stiff layer at 300 in. ..... 216

Table 6.14 Thickness and moduli of AC, rubblized concrete slab (RCS), combination of base and subbase (BS) and roadbed soil (RB) of a pavement section having no stiff layer ..... 216

Table 6.15 Backcalculated moduli at 12 core locations on US-10 EB section 1 test site 1 using the average AC thickness of 6.5-in. and the measured core thicknesses ..... 229

Table 6.16 Layer thicknesses, moduli and Poisson ratios used in the forward calculation of the deflection basins of 223 pavement sections ..... 231

Table 6.17 Backcalculated layer moduli and errors due to incorrect RM thicknesses used in the backcalculation ..... 231

Table 6.18
Table 6.19
Table 6.20
Table 6.21
Table 6.22
Table 6.23
Table 6.24
Table 6.25
Table 6.26
Table 6.27
Table 6.28
Table 6.29
Table 6.30

Table 6.18 Backcalculated layer moduli using 4-layer system with various depths to stiff layer, US-10 EB test section 1 test site 1 ..... 245

Table 6.19 Backcalculated layer moduli using 3-layer system with various depths to stiff layer, US-10 EB test section 1 test site 1 ..... 245

Table 6.20 Backcalculated layer moduli using 4-layer system with various depths to stiff layer, US-10 EB test section 1 test site 2 ..... 246

Table 6.21 Backcalculated layer moduli using 3-layer system with various depths to stiff layer, US-10 EB test section 1 test site 2 ..... 246

Table 6.22 Results of backcalculation using 3- and 4-layer systems and depth to stiff layer of 500 in, US-10 EB test section1, test site 1 ..... 249

Table 6.23 Results of backcalculation using 3- and 4-layer systems and depth to stiff layer of 500 in, US-10 EB test section1, test site 2 ..... 252

Table 6.24 Final results of the backcalculation of US-10 EB test section 1, test site 1 ..... 255

Table 6.25 Final results of the backcalculation of US-10 EB test section 1, test site 2 ..... 256

Table 6.26 A summary of pavement cross sections, roadbed soil, depths to stiff layer and the observed pavement surface distresses at 18 rubblized pavement test sites where, in the backcalculation of layer moduli, the base and subbase layers and the roadbed were combined as one layer ..... 261

Table 6.27 A summary of pavement cross sections, roadbed soil, depths to stiff layer and the observed pavement surface distresses at six rubblized pavement test sites where the combined base and subbase layers and the roadbed soil were backcalculated as two layers. ..... 262

Table 6.28 A summary of the results of the backcalculation of layer moduli of 18 rubblized pavement test sites where the base, subbase layers and the roadbed soil were treated as one layer.. ..... 264

Table 6.29 A summary of the results of the backcalculation of 6 rubblized pavement test sites where the combined base and subbase layers and the roadbed soil were counted as two layers. ..... 265

Table 6.30 A summary of pavement cross sections, roadbed soil, depths to stiff layer and the observed distresses in 12 flexible pavement test sites (Schorsch, 2003) ..... 270

Table 6

Table 7

Table 7

Table 7.3

Table 7.4

Table 8.1

Table 8.2

Table 8.3

Table 8.4

Table 8.5

Table 8.6

Table 8.7

Table 8.8

Table 8.9

Table 6.31 A summary of the backcalculation of 12 flexible pavement test sites (Schorsch, 2003) ....271

Table 7.1 List of the pavement sections, thermocouples locations and the time period during which for temperature data were recorded ....280

Table 7.2 The lowest and the highest recorded pavement surface temperatures and the corresponding air temperatures and the temperatures at various depths in the pavements ....281

Table 7.3 Calculated thermals stresses at the surface and at the bottom of the AC layer for February 2 and June 19, 1996 using three time periods ....287

Table 7.4 The thermal stresses at the AC surface and at the AC bottom of five pavement sections in MI on February 2nd, 1996 ....293

Table 8.1 Assumptions used in the analyses and limitations of the CHEVRONX, MICHPAVE and ABAQUS programs ....299

Table 8.2 The range of pavement cross-sections and material properties used in the 2-D partial factorial sensitivity analyses ....305

Table 8.3 Results of the sensitivity analyses of the effects of the indicated properties on the radial stresses induced in the AC layer ....307

Table 8.4 A summary of the sensitivity of the radial stress at the surface at the tire edge and at the AC bottom under the tire center due to various variables (as the value of the variable increases) ....312

Table 8.5 Thicknesses, element sizes, moduli and Poison ratios assigned to pavement layers and the roadbed soil in the 3-D analyses ....336

Table 8.6 Pavement sections used in the 3-D analyses of the induced stresses in pavements due to the indicated contact stresses ....340

Table 8.7 Thicknesses and moduli of pavement layers and roadbed soil used in the analyses of the tire-induced lateral stresses in the AC layer by vertical contact stresses and by the combination of vertical and lateral contact stresses ....348

Table 8.8 Results of the 3-D analyses of the lateral stresses induced in the AC layer of the 12 pavement sections listed in Table 8.7 ....349

Table 8.9 Results of the 3-D analyses of the lateral stresses induced in the AC layer in rubblized pavement sections having the various interface geometries between the RM and the FC layers illustrated in Figures 8.37 to 8.39....358

Table 8.10
Table 8.11
Table 8.12
Table 8.13
Table 8.14
Table 8.15
Table 8.16
Table 8.17
Table 8.18
Table 8.19
Table A1

Table 8.10 Results of 3-D analyses of the lateral stresses induced in the AC layer in pavement sections with 4-in. thick AC and a channel of rubblized material under the tire (Geometry 4 of Figure 8.32) ..... 368

Table 8.11 Pavement layer thicknesses and moduli and the lateral stresses induced in the AC layer of the pavement sections with 6-in. AC and a channel of rubblized material under the tire (Geometry 4 of Figure 8.32) ..... 369

Table 8.12 Results of 3-D analyses of the lateral stresses induced in the AC layer in pavement sections with 9-in. thick AC and a channel of rubblized material under the tire (Geometry 4 of Figure 8.32) ..... 370

Table 8.13 A summary of the sensitivity of the lateral stress induced in the AC layer to various pavement layer and roadbed soil properties obtained from the 2-D and 3-D analyses ..... 372

Table 8.14 Pavement cross-sections, pavement layers and roadbed soil moduli used in the analyses of rubblized pavements subjected to the indicated wheel loads ..... 378

Table 8.15 Lateral stresses induced at the AC surface and AC bottom of the 19 rubblized pavement sections listed in Table 8.14 ..... 379

Table 8.16 The highest AC surface temperatures and the corresponding temperatures at the AC bottom measured by MDOT during 1994 through 1999, and the mid-depth temperatures of various asphalt pavements ..... 386

Table 8.17 Properties of the rubblized and flexible pavements, the interfaces between the RM and FC layers and the wheel loads used in the analyses of the load-induced stresses at the AC surface at the tire edge and at the AC bottom under the tire center ..... 387

Table 8.18 Stress ratios at the AC surface and AC bottom of three pavement sections in Table 8.17 subjected to single wheel load ..... 388

Table 8.19 Stress ratios at the AC surface and AC bottom of three pavement sections in Table 8.17 subjected to dual wheel load ..... 389

Table A1 List of 87 rubblized pavement projects in Michigan ..... 404

Figure 2.1
Figure 2.2
Figure 2.3
Figure 2.4
Figure 2.5
Figure 2.6
Figure 2.7
Figure 2.8
Figure 2.9
Figure 2.10
Figure 2.11
Figure 2.12
Figure 2.13

## LIST OF FIGURES


Figure 2.1 The SAE vehicle coordinates system (Gillespie, 1992) ..... 11

Figure 2.2 Tire prints of a radial and a bias ply tire having 9.2 kip wheel load and 104 psi inflation pressure (De Beer and Fisher, 1997); (the scale is in mm). ..... 14

Figure 2.3 Plots of the maximum vertical, lateral and longitudinal contact stresses of a bias-ply tire with various wheel loads and inflation pressures (after De Beer et al, 1997) ..... 16

Figure 2.4 Plots of the maximum vertical, lateral and longitudinal contact stresses of a radial tire with various wheel loads and inflation pressures (after De Beer et al, 1997) ..... 17

Figure 2.5 Relationship between the maximum vertical and the maximum lateral contact stresses (after De Beer et al, 1997) ..... 18

Figure 2.6 Tire print of the radial truck tire tested by Pottinger and McIntyre (1999) ..... 19

Figure 2.7 Variation in the vertical contact stresses of a radial truck tire (Pottinger and McIntyre, 1999) ..... 21

Figure 2.8 Variation in the lateral contact stresses of a radial truck tire (Pottinger and McIntyre, 1999) ..... 22

Figure 2.9 Variations in the measured vertical and lateral contact stresses across the tire along the lateral center line of a radial truck tire (after Pottinger and McIntyre, 1999) ..... 23

Figure 2.10 Variations in the measured vertical and lateral contact stresses in the longitudinal direction along the edge of a radial truck tire (after Pottinger and McIntyre, 1999) ..... 24

Figure 2.11 Lateral shear stresses under each tire rib of a radial truck tire (after Pottinger and McIntyre, 1999) ..... 25

Figure 2.12 Variation in the longitudinal direction of the longitudinal contact stress along the left edge of rib 5 (after Pottinger and McIntyre, 1999). ..... 26

Figure 2.13 Variation in the longitudinal contact stresses of a radial truck tire subjected to the rated load (De Beer et al, 1997) ..... 26

Figure 2.1
Figure 2.1
Figure 2.1
Figure 2.17
Figure 2.18
Figure 2.19
Figure 2.2
Figure 2.21
Figure 3.1
Figure 3.2
Figure 3.3
Figure 3.4
Figure 3.5
Figure 3.6
Figure 3.7
Figure 3.8
Figure 3.9
Figure 3.10
Figure 3.11

Figure 2.14 Load transfer mechanisms of a tire ..... 29

Figure 2.15 Lateral contact stresses due to the Pneumatic (a) and Poisson effects (b) and lateral contact stresses of a bias-ply (c) and of a radial tire (d) ..... 30

Figure 2.16 Comparisons between the maximum vertical and lateral contact stresses of radial and bias ply tires at various wheel loads and inflation pressures ..... 32

Figure 2.17 Variations in the vertical contact stresses of overloaded and under loaded radial tires (De Beer and Fisher, 1997) ..... 34

Figure 2.18 Top-down cracks in a rubblized pavement (US-131) ..... 38

Figure 2.19 Photographs showing the development of Top-Down Cracking (A = Stage 1, B = Stage 2, C = Stage 3) and the pictures of cores with Top-Down Cracks, Core 1- I-96, 2- M-20, 3- Marsh Road, 4- M-37, and 5- I-194 ..... 39

Figure 2.20 Different stress states at the top and bottom of the AC layer ..... 54

Figure 2.21 Master relaxation modulus and shift factor of the asphalt mixtures reported by Park (2000) ..... 60

Figure 3.1 A resonant frequency breaker and a smooth drum vibratory roller ..... 69

Figure 3.2 Schematic of the sonic shoe of the resonant frequency breaker ..... 70

Figure 3.3 Multi-head concrete pavement breaker ..... 72

Figure 3.4 Vibratory grid roller ..... 72

Figure 3.5 Schematic of the hammer configuration of the multi-head breaker ..... 74

Figure 3.6 Concrete and rubblized pavement cross-sections ..... 76

Figure 3.7 Rubblized and flexible pavement cross-sections ..... 78

Figure 3.8 Schematic of a rubblized concrete slab showing rubblized and fractured layers ..... 83

Figure 3.9 Close-up of the fractured concrete in a trench (M-50) ..... 83

Figure 3.10 Partial debonding of the temperature steel (M-21) ..... 84

Figure 3.11 Partial destruction of the joint integrity (US-131) ..... 84

Figure 3.1
Figure 3.1
Figure 3.1
Figure 3.15
Figure 3.16
Figure 3.17
Figure 3.18
Figure 3.19
Figure 3.20
Figure 3.21
Figure 3.22
Figure 3.23
Figure 3.24
Figure 3.25
Figure 3.26

Figure 3.12 Trapped water above the fractured concrete in a trench (M-18) .....85

Figure 3.13 A standard layout of the FWD tests used in this study .....90

Figure 3.14 The relative pavement conditions in segregated area (passing lane) and in a non-segregated area (traffic lane) 2 years after construction on US-23 SB, control section 47013, job number 29768, BMP 5.5 and EMP 7.0, May 2002. .....102

Figure 3.15 The pavement condition in segregated area on US-12 EB, control section 81063, job number 26796, BMP 3.6 and EMP 4.1, May 2002 ...103

Figure 3.16 Longitudinal and transverse TDC (LTDC and TTDC) on I-96 EB, control section 33084, job number 28213, BMP 9.0 and EMP 17.5, May 2002 .....104

Figure 3.17 Reflective joint crack on M-50, control section 46082, job number 30388, BMP 3.9 and EMP 4.4, May 2002 .....105

Figure 3.18 Crack reflective cracks on US-131, control section 41131, job number 21089, BMP 6.5 and EMP 10.1, May 2002 .....106

Figure 3.19 Alligator cracks in the wheel path, US-27, control section 37013, job number 28116, BMP 9.0, and EMP 11.7, June 2001 .....107

Figure 3.20 Pothole along US-131, control section 41133, job number 33914, BMP 3.2 and EMP 8.7, May 2002 .....109

Figure 3.21 Patches on M-53, control section 74012, job number 29729, BMP 9.0 and EMP 13.0, May 2002 .....110

Figure 3.22 A shear failure on I-196 NB, control section 70024, job number 35987, BMP 12.6 and EMP 15.6, May 2002 .....111

Figure 3.23 Deteriorated paving joint between lanes and longitudinal TDC at edge of the wheel path in the segregated area on US 131, control section 83032, job number 34060, BMP 13.0 and EMP 18.6, May 2002 .....112

Figure 3.24 The initiation of a temperature crack, US-27, control section 37014, job number 38206, BMP 7.2 and EMP 14.4, May 2003 .....113

Figure 3.25 TTDC associated with LTDC, M-27, control section 16302, job number 26672, BMP 9.3 and EMP 11.4, May 2003 .....114

Figure 3.26 Untrimmed (left) and trimmed (right) AC cores .....122

Figure 3.2
Figure 3.2
Figure 3.2
Figure 3.3
Figure 3.3
Figure 3.32
Figure 3.33
Figure 3.34
Figure 4.1
Figure 4.2
Figure 4.3
Figure 4.4
Figure 4.5
Figure 4.6
Figure 4.7
Figure 4.8
Figure 4.9
Figure 4.10

Figure 3.27 An AC test specimen (left) and a trimmed AC core (right) ..... 122

Figure 3.28 The ITCLT and ITST specimen holder for a 6-in. diameter and 3-in. thick test specimen ..... 126

Figure 3.29 Test specimen in the specimen holder during an ITCLT test ..... 127

Figure 3.30 One load cycle consisting of 0.1-second load-unload period and 0.4-second relaxation period ..... 127

Figure 3.31 Plots of the average bulk specific gravity and the average ITCLT modulus of the test specimens of 19 rubblized pavement test sites ..... 132

Figure 3.32 ITST loading frame and the specimen holder ..... 133

Figure 3.33 Comparison of the indirect tensile strengths at different temperatures obtained from ITST (Schorsch, 2003) and predicted using equation 2.5 ..... 133

Figure 3.34 The effect of temperature, segregation and moisture conditioning on the indirect tensile strengths of three asphalt mixes ..... 139

Figure 4.1 Schematic of concrete and rubblized pavement cross-sections ..... 144

Figure 4.2 Joint reflective cracking in rubblized pavements ..... 145

Figure 4.3 Reflective cracks in rubblized pavements ..... 147

Figure 4.4 Debonding between the AC layer and the original concrete pavement where the fractured concrete extends to the original pavement surface and the integrity of the slab including the transverse crack is not destroyed – Portage Road ..... 148

Figure 4.5 A shoe of the resonant frequency breaker ..... 150

Figure 4.6 Partial debonding of the temperature steel (M-21) ..... 150

Figure 4.7 Partial destruction of the joint integrity (US-131) ..... 152

Figure 4.8 Differential settlements between the two lanes along NB I-196, May 2002 ..... 152

Figure 4.9 The fractured concrete layer ..... 153

Figure 4.10 Excavated showing the sand subbase and the fractured concrete layer ..... 154

Figure 4.1
Figure 4.2
Figure 4.3
Figure 4.4
Figure 4.5
Figure 4.6
Figure 5.1
Figure 5.2
Figure 5.3
Figure 5.4
Figure 5.5
Figure 5.6
Figure 5.7
Figure 5.8
Figure 5.9

Figure 4.11 Two shear failures in the rubblized pavement on NB I-196 ..... 156

Figure 4.12 Initiation of a shear failure on rubblized pavement project on NB I-196 ..... 157

Figure 4.13 Calibration layouts for the multi hammer rubblizer ..... 159

Figure 4.14 Calibration layouts for the resonant frequency breaker ..... 160

Figure 4.15 Pavement condition in segregated and non-segregated areas along US-23 in May 2002, 2 years after construction ..... 163

Figure 4.16 Pavement condition in segregated and not segregated areas along US-131 in May 2002, 5 years after construction ..... 164

Figure 5.1 Longitudinal TDC at the edge of the wheel path on US-23, control section 04031, job number 32335, BMP 0.0 and EMP 7.9, May 2002 ... 171

Figure 5.2 Longitudinal TDC at the edge of the wheel path on US-131, control section 83032, job number 34060, BMP 13.0 and EMP 18.7, May 2002 ..... 172

Figure 5.3 Parallel longitudinal TDC at the edge of the inner and outer wheel paths on US-131 (same location as Figure 5.2), control section 83032, job number 34060, BMP 13.0 and EMP 18.7, May 2003 ..... 173

Figure 5.4 Transverse TDC associated with longitudinal TDC on M-27, control section 16302, job number 26672, BMP 9.3 and EMP 11.4, May 2003 ..... 174

Figure 5.5 The third stage of TDC development, LTDC and TTDC forming a networks on East Michigan Avenue, control section 39555, job number 39212, BMP 13.9 and EMP 15.2, May 2002 ..... 175

Figure 5.6 The three stages (A, B and C) of TDC development and pavement cores showing the extent of TDC propagation with depth ..... 177

Figure 5.7 Transverse TDC located at the center of the lane (compare the size to half of a 4-in core) ..... 178

Figure 5.8 Transverse TDC located at the middle of the lane ..... 179

Figure 5.9 Longitudinal TDC and raveling in segregated area ..... 181

Figure 6.1

Figure 6.2

Figure 6.3

Figure 6.4

Figure 6.5

Figure 6.6

Figure 6.7

Figure 6.8

Figure 6.9

Figure 6.10

Figure 6.11

Figure 6.12

Figure 6.13

Figure 6.14

Figure 6.15

Figure 6.1 Schematic of FWD load plate and the spacing of the deflection sensors ..... 186

Figure 6.2 Typical FWD tests and cores layout ..... 187

Figure 6.3 Average deflections of D1 to D7 versus load, I-69, test site 1 of section 1 ..... 191

Figure 6.4 Variations of D1 through D7 deflections, US-10 EB, test section 1, test site 1 ..... 196

Figure 6.4 Variations of D1 through D7 deflections, US-10 EB, test section 1, test site 2 ..... 196

Figure 6.6 Variations of D1 through D7 deflections, US-27 SB, test section 1, test site 1 ..... 197

Figure 6.7 A typical trench excavated in rubblized pavement showing RM and fractured concrete, US-10 SB ..... 197

Figure 6.8 A flowchart of the backcalculation procedure for rubblized pavements. 207

Figure 6.9 Plots of equivalent pavement modulus versus the distance from the center of load for 6 pavement sections having different depths to stiff layer ..... 211

Figure 6.10 Three and four layer systems for flexible and rubblized pavements used to determine the approximate stiff layer depth ..... 213

Figure 6.11 Backcalculated roadbed soil (RB) moduli and the moduli of the combination of base, subbase and roadbed soil (BSRB) of the pavement with a 300-in depth to stiff layer ..... 217

Figure 6.12 Backcalculated roadbed soil (RB) moduli and the moduli of the combination of base, subbase and roadbed soil (BSRB) of the pavement with no stiff layer (In the plot, 800 in. represents no stiff layer) ..... 217

Figure 6.13 Three multi-layer systems used in the backcalculation of rubblized pavement moduli ..... 219

Figure 6.14 Schematic of three possible outcomes of rubblizing pavements illustrating their impacts on the moduli of the RM and FC layers ..... 223

Figure 6.15 Comparison between the true moduli and the backcalculated moduli using 4-layer backcalculation (AC, RCS, BS and RB) ..... 233

Figure 6.1
Figure 6.1
Figure 6.1
Figure 6.1
Figure 6.2
Figure 6.2
Figure 6.22
Figure 6.23
Figure 7.1
Figure 7.2
Figure 7.3
Figure 7.3
Figure 7.4
Figure 7.5
Figure 7.6

Figure 6.16 The effects of the RM thickness on the backcalculated layer moduli .....235

Figure 6.17 Three deflection basins from test locations at the beginning, the middle and at the end of the US-10 EB test section 1, test sites 1 and 2 .....240

Figure 6.18 Variation in the pavement deflections (D1 and D7) along and across test site 1 .....241

Figure 6.19 Variation in the pavement deflections D1 and D7 along and across test site 2 .....242

Figure 6.20 Equivalent modulus versus lateral distance from the center of the load for 3 test locations, US-10 EB, test section 1, test sites 1 and 2 .....243

Figure 6.21 The average backcalculated moduli of the combination of base, subbase and roadbed soil (BSRB) and of the roadbed soil (RB) of test sites 1and 2 at various depths to stiff layer .....247

Figure 6.22 Extensive transverse and longitudinal cracks on the FWD test sites on I-75, and on M-37, test section 1, test site 1 .....260

Figure 6.23 Rubblized material (RM) layer thickness versus the backcalculated modulus of the rubblized concrete slab (RCS) .....268

Figure 7.1 Master relaxation modulus curve and shift factor of the asphalt mixtures reported by Park (2000) .....276

Figure 7.2 The shift factor ($a_T$) versus temperature .....276

Figure 7.3 Comparison between the estimated relaxation moduli using the Prony series developed by Park (2000) and using equation 7.4 and the master relaxation modulus curve .....278

Figure 7.3 Yearly temperature variations at the surface and the bottom of the AC layer, US-23, Alpena, MI .....283

Figure 7.4 Daily temperature variations at the surface and the bottom of the AC layer on the days at which the pavement surface experienced very low and very high temperatures (US-23, Alpena, MI) .....284

Figure 7.5 Variations of thermal stresses throughout one day (February 2$^{nd}$, 1996 and June 19$^{th}$ , 1996), (US-23, Alpena, MI) .....289

Figure 7.6 Variation in the thermal stresses throughout one year calculated around 8:30 AM and 2:20 PM (US-23, Alpena, MI) .....291

Figure 7.
Figure 7.
Figure 8.1
Figure 8.2
Figure 8.3
Figure 8.4
Figure 8.5
Figure 8.6
Figure 8.7
Figure 8.8
Figure 8.9
Figure 8.10
Figure 8.11
Figure 8.12

Figure 7.7 Variation of the pavement temperatures around 8:30 AM and 2:20 PM throughout one year (US-23, Alpena, MI).....292

Figure 7.8 Thermal stress ratios between the top and the bottom of the AC layer versus the thickness of the AC layer.....295

Figure 8.1 Comparison of the radial stresses at the top and at the bottom of the pavement obtained from the CHEVRONX, MICHPAVE and ABAQUS computer programs .....301

Figure 8.2 The pavement model used in the 2-D MICHPAVE analyses.....304

Figure 8.3 Radial tensile stresses at the AC bottom under the tire center versus the AC thicknesses for various AC surface course (ACS) moduli.....313

Figure 8.4 Radial tensile stresses at the AC bottom under the tire center versus the AC surface course moduli for various AC base course (ACB) moduli...313

Figure 8.5 Radial tensile stresses at the AC bottom under the tire center versus the AC base course moduli for various AC thicknesses.....314

Figure 8.6 Radial tensile stresses at the AC bottom under the tire center versus the rubblized material thicknesses for various fractured concrete (FC) moduli .....314

Figure 8.7 Radial tensile stresses at the AC bottom under the tire center versus the rubblized material (RM) moduli for various rubblized material Thicknesses .....315

Figure 8.8 Radial tensile stresses at the AC bottom under the tire center versus the fractured concrete moduli for various rubblized material (RM) moduli .....315

Figure 8.9 Radial tensile stresses at the AC bottom under the tire center versus the combination base and subbase moduli for various roadbed soil (RB) moduli .....316

Figure 8.10 Radial tensile stresses at the AC surface at the tire edge versus the AC thicknesses for various AC surface course (ACS) moduli.....316

Figure 8.11 Radial tensile stresses at the AC surface at the tire edge versus the AC surface course moduli for various AC base course (ACB) moduli .....317

Figure 8.12 Radial tensile stresses at the AC surface at the tire edge versus the AC base course moduli for various AC thicknesses .....317

Figure 8.
Figure 8.
Figure 8.
Figure 8.
Figure 8.
Figure 8.
Figure 8.
Figure 8.2
Figure 8.2
Figure 2.22
Figure 2.23
Figure 2.24
Figure 8.25
Figure 8.26

Figure 8.13 Radial tensile stresses at the AC surface at the tire edge versus the rubblized material (RM) moduli for various rubblized material thicknesses ..... 318

Figure 8.14 Radial tensile stresses at the AC surface at the tire edge versus the rubblized material thicknesses for various fractured concrete (FC) moduli ..... 318

Figure 8.15 Radial tensile stresses at the AC surface at the tire edge versus the fractured concrete moduli for various rubblized material (RM) moduli .319

Figure 8.16 Radial tensile stresses at the AC surface at the tire edge versus the combination of base and subbase moduli for various roadbed soil (RB) moduli ..... 319

Figure 8.17 Lower stress decay rates due to higher AC thicknesses (500-ksi AC surface and AC base course moduli) ..... 322

Figure 8.18 Lower stress decay rates due to higher AC base course (ACB) moduli (500-ksi AC surface course modulus and 4-in. total AC thickness)..... 322

Figure 8.19 Variations in the peak deflections due to different rubblized material (RM) thicknesses and different base and subbase (BS) moduli ..... 324

Figure 8.20 Lines of symmetry of the vertical and the lateral contact stresses of a radial truck tire having 8 ribs and 7 grooves (after Pottinger and McIntyre, 1999) ..... 327

Figure 8.21 Variation in the vertical contact stresses of a radial truck tire (Pottinger and McIntyre, 1999)..... 328

Figure 2.22 Variation in the lateral contact stresses of a radial truck tire (Pottinger and McIntyre, 1999)..... 329

Figure 2.23 Variations in the measured vertical and lateral contact stresses across the tire along the lateral center line of a radial truck tire (after Pottinger and McIntyre, 1999) ..... 330

Figure 2.24 Variations in the measured vertical and lateral contact stresses in the longitudinal direction along the edge of a radial truck tire (after Pottinger and McIntyre, 1999)..... 331

Figure 8.25 Variation in the longitudinal direction of the longitudinal contact stress along the left edge of rib 5 (after Pottinger and McIntyre, 1999)..... 333

Figure 8.26 Variation in the longitudinal contact stresses of a radial truck tire subjected to the rated load (De Beer et al, 1997)..... 333

Figure 8.2
Figure 8.2
Figure 8.2
Figure 8.3
Figure 8.3
Figure 8.3
Figure 8.3
Figure 8.3
Figure 8.35
Figure 8.36
Figure 8.37
Figure 8.38

Figure 8.27 The quarter model used in the 3-D FEM analyses of the vertical and lateral contact stresses ..... 335

Figure 8.28 The model used in the 3-D FEM analysis of the lateral stresses induced in the AC layer due to the longitudinal contact stresses ..... 338

Figure 8.29 Comparison of the lateral stresses induced at the AC surface by the vertical and lateral contact stresses obtained by superposition and by direct analyses of both contact stresses ..... 341

Figure 8.30 Comparison of the lateral stresses obtained from pavement sections 1 through 7 of Table 8.6 ..... 343

Figure 8.31 Lateral stresses induced at the pavement surface due to the longitudinal contact stresses ..... 346

Figure 8.32 The effects of the AC surface course modulus on the lateral stresses induced at the AC surface by vertical contact stresses and by the combination of vertical and lateral contact stresses ..... 350

Figure 8.33 The effects of the AC base course modulus on the lateral stresses induced at the AC surface by vertical contact stresses and by the combination of vertical and lateral contact stresses ..... 351

Figure 8.34 The effects of the AC thickness on the lateral stresses induced at the AC surface by vertical contact stresses and by the combination of vertical and lateral contact stresses ..... 352

Figure 8.35 The effects of properties of the rubblized concrete slab on the lateral stresses induced at the AC surface by vertical contact stresses and by the combination of vertical and lateral contact stresses ..... 353

Figure 8.36 The lateral stresses induced at the AC surface and the AC bottom by vertical contact stresses obtained from 2-D and 3-D analyses, pavement section 1 of Table 8.7 ..... 354

Figure 8.37 Geometries 1 through 3 of the interface between the RM and the FC layers used in the 3-D analyses of the effects of the uneven interface on the load-induced lateral stresses in the AC layer. ..... 359

Figure 8.38 Geometries 4 through 6 of the interface between the RM and the FC layers used in the 3-D analyses of the effects of the uneven interface on the load-induced lateral stresses in the AC layer ..... 360

Figure 8.
Figure 8.
Figure 8.
Figure 8.
Figure 8.
Figure 8.
Figure 8.

Figure 8.38 Geometries 7, 8 and 9 of the interface between the RM and the FC layers used in the 3-D analyses of the effects of the uneven interface on the load-induced lateral stresses in the AC layer .....361

Figure 8.40 Three-dimensional view of the quarter model with the interface geometry 4 of Figure 8.38 (uneven interface with RM channel under the tire) .....362

Figure 8.41 Lateral tensile stresses induced at the AC surface at the tire edge of pavement sections having the various geometries of the interface shown in Figure 8.37 through 8.40.....364

Figure 8.42 The upper portion of the models used in the analyses of lateral stresses induced by dual and single wheels.....375

Figure 8.43 Lateral stresses at the AC surface induced by the vertical contact stresses of each wheel of the dual wheels .....382

Figure 8.44 Lateral stresses at the AC bottom induced by the vertical contact stresses of each wheel of the dual wheels .....383

Figure 8.45 Confinement due to the interface frictional forces at the AC bottom.....392

1.0 IN

S

systems, v

have been

including

1. Pa

2. As

3. Cr

4. Ru

Par

and limited

10 years. T

severity an

The resultir

concrete pa

- The

- The

The crack a

and to exten

data indicate

# CHAPTER 1

# INTRODUCTION & OBJECTIVES

## 1.0 INTRODUCTION

Substantial resources are required to preserve and rehabilitate the aging highway systems, which is subjected to increasing traffic demand. Over time, various alternatives have been developed and used for the rehabilitation of deteriorated concrete pavements, including:

1. Partial and full depth repairs
2. Asphalt concrete (AC) overlay (composite pavement)
3. Crack and seat with AC overlay
4. Rubblization with AC overlay

Partial and full depth repairs are suitable for concrete pavements with low severity and limited extent of distresses; the expected service life of the repairs ranges from 6 to 10 years. The AC overlay option is typically applied to concrete pavements with higher severity and extent of distresses and it is expected service life ranges from 6 to 12 years. The resulting composite pavements will experience reflective cracks from the underlying concrete pavement within 3 to 5 years after construction depending on:

- The thickness of the AC overlay
- The pre-overlay repairs of the deteriorated concrete pavement.

The crack and seat with asphalt overlay option was thought to eliminate reflective cracks and to extend the service life of the pavement to 20 years. However, historical distress data indicate that reflective cracks were not eliminated and the service life of the

pavemen

develope

objective

reflective

data indic

is much s

underperf

Field inve

cracks (T

found in f

lives. Fin

reference

methods d

Currently,

over existi

applied at

Rec

of the facto

TDC, in pa

University

sponsored s

1. Det

This

pavement was much shorter than 20 years. Finally, rubblization with AC overlay was developed as a pavement rehabilitation method and it has been used since 1986 with the objective of breaking the concrete to aggregate size material thereby eliminating reflective cracking potential (see Chapter 3). Once again, historical pavement distress data indicate that the average service life of rubblized pavements is about 12 years, which is much shorter than the 20-year design life. The distress data indicate that the underperformance of rubblized pavements is manifested by various types of distress. Field investigation revealed that the two overwhelming types of distress are top-down cracks (TDC) and reflective cracks. In the USA and other countries, TDC have been found in flexible pavements and have been reported to cause reduction in their service lives. Finally, most, if not all, pavement management distress databanks do not include reference to TDC. The reason is that, for all pavement types, existing distress survey methods do not include any procedure to differentiate between TDC and regular cracks. Currently, the only available procedure to identify TDC is to core the pavement section over existing cracks. Such procedure is expensive and laborious and therefore cannot be applied at the network level.

Recognizing the dimensions of the problem and the need of a full understanding of the factors affecting the underperformance of rubblized pavements, in general, and TDC, in particular, research activities were initiated and developed at Michigan State University to solve the problem. These research activities include the following two sponsored studies, which were conducted under the direction of Dr. Gilbert Baladi:

1. **Determining the Causes of Top-Down Cracks in Bituminous Pavements -** This study was co-sponsored by the Michigan Asphalt Paving Association

2. I

P

T

of the da

dissertati

2.0 O

T

flexible a

For Flexi

1. Id

ve

2. De

do

3. Co

4. De

the

For Rubbl

5. Ana

crac

(MAPA) and the Michigan Department of Transportation (MDOT).

2. **Identify Causes for Underperforming Rubblized Concrete Pavement Projects** – A two-phase study that was sponsored by MDOT.

The research activities for this dissertation include the examination and analyses of the data obtained from the above two studies. The objectives and hypotheses of this dissertation are stated in the next two sections.

## 2.0 OBJECTIVES

The objectives of this dissertation are divided into two categories; one addressing flexible and rubblized pavements and the other addressing rubblized pavements only.

**For Flexible and Rubblized Pavements:**

1. Identify the causes of TDC and the materials, pavement, environmental and vehicle factors affecting top-down cracking potential.
2. Determine the effect of each of the above factors and their interactions on top-down cracking potential.
3. Compare top-down and bottom-up cracking potentials.
4. Develop methods and guidelines for the proper identification of TDC based on their appearance and characteristics.

**For Rubblized Pavements:**

5. Analyze the effects of the quality of the rubblization operation on top-down cracking potential.

6. I

s

r

**3.0 H**

In

follow ng

1. T

T

th

2. T

ch

3. Fo

ra

To

was drawn

**4.0 RE**

In c

research pl

6. Identify the causes of the underperformance of rubblized pavements and suggest solutions regarding the appropriate design(s) and construction method(s) of rubblized pavements.

## 3.0 HYPOTHESES

In this study, filed and laboratory investigations and the analyses are based on the following hypotheses:

1. TDC are fatigue cracks caused by high stress ratios at the AC surface course. Therefore, top-down cracking potential is affected by all the factors influencing the magnitude of the induced tensile stress and the tensile strength of the AC mix.
2. TDC can be distinguished from the other types of cracks based on their characteristics (appearance, location, and propagation)
3. For rubblized pavements, there exist a relationship between the quality of the rubblization operation and top-down cracking potential.

To accomplish the study objectives and to verify the hypotheses, a research plan was drawn and is presented in the next section.

## 4.0 RESEARCH PLAN

In order to accomplish the study objectives and to verify the hypotheses, a research plan was drawn. The plan consists of six categories as stated below.

## 4.1 Li

A

of TDC

review p

undertak

## 4.2 Fi

T

rubblizat

conventio

consists o

- Ev
- Ev

co

an

Th

convention

- Co
- Co

pa

- Co

## 4.1 Literature Review

Available literature regarding the performance of rubblized pavements, the causes of TDC and the factors affecting top-down cracking potential were reviewed. Such a review provided information regarding the various research activities that have been undertaken by various researchers and their conclusions.

## 4.2 Field Investigation

The field investigation consists of two parts; one was conducted during the rubblization operation and the other after completion of construction of rubblized and conventional flexible pavements. The field investigation during the rubblization operation consists of:

- Examining the rubblizing equipments and their operating parameters.
- Excavating trenches in rubblized concrete slabs at mid-slabs and at original concrete pavement joints to examine the condition of the rubblized concrete slab and whether or not the rubblization operation has met its objectives.

The field investigation after the completion of construction of rubblized and conventional flexible pavements includes:

- Conducting nondestructive deflection tests.
- Coring the AC layer and drilling through the base and/or subbase in some flexible pavements.
- Conducting distress surveys.

**4.3** I

T

- E

th

- C

A

- C

m

- Co

str

ma

seg

**4.4** An

Ba

the follow

**4.4.**

1.

2.

## 4.3 Laboratory Investigation

The laboratory investigation consists of the following activities:

- Examining the pavement cores and measuring of the core dimensions, the thicknesses of the various AC courses, and the depth and width of cracks, if any.
- Conducting specific gravity tests to determine the bulk specific gravity of each AC mix in each core when possible.
- Conducting indirect tensile cyclic load tests (ITCLT) to determine the resilient moduli of the various AC courses when possible.
- Conducting indirect tensile strength tests (ITST) to determine the indirect tensile strengths of the various AC courses when possible. Further, ITST of lab manufactured specimens were conducted to estimate the effects of temperature, segregation and moisture damage on the indirect tensile strength of AC mixes.

## 4.4 Analyses

Based on data obtained from the literatures, and the field and lab investigations, the following two types of analyses were conducted:

### 4.4.1 Analyses of the Measured FWD Deflection Data

The measured deflection data will be analyzed in two ways as follows:

1. Determine the variations in the deflection data along and across the pavement at each test site. Results of the analyses would indicate the degree of uniformity in the structural capacity of the pavements.
2. Backcalculate the pavement layer and roadbed soil moduli using the measured pavement deflections and cross-section data. The backcalculated

4.

1.

2.

3.

4.5 Val

Res

1.

moduli were used in the mechanistic analyses of rubblized and flexible pavements. Note that, for rubblized pavements, a new procedure for the backcalculation of rubblized pavement layer moduli was developed to address the high variability in the thicknesses and stiffnesses of the rubblized material and the fractured concrete layers. No such procedure has been developed by researchers.

### 4.4.2 Mechanistic Analyses of Rubblized and Flexible Pavements

The mechanistic analyses of rubblized and flexible pavements consist of:

1. Analyses of temperature-induced tensile stresses in the AC layer using existing models and equations.
2. Analyses of the sensitivity of the load-induced tensile stresses in the AC layer to the various factors affecting top-down and bottom-up cracking potentials.
3. Comparison of crack initiation potentials at the AC surface and AC bottom using the stress ratio concept.

## 4.5 Validation of the Results of the Analyses

Results of the analyses were validated as follow:

1. The accuracy of the results of the backcalculation of layer moduli using the MICHBACK computer program was checked using forward and backward analyses.

2

3.

4.

4.6 C

B

flexible p

conclusio

effects of

potential.

- Ru
- Ca

5.0 TH

Thi

Chapter 1

Chapter 2

Chapter 3

2. For rubblized and flexible pavements, the backcalculation routines and procedures were checked and validated using forward and backward mechanistic analyses.
3. For the same pavement sections and load conditions, results of the analyses using finite element programs (ABAQUS and MICHPAVE) were compared to those obtained from the CHEVRONX computer program.
4. The potential and locations of TDC obtained from the analyses will be compared to field observations.

### 4.6 Conclusions and Recommendations

Based on the results of the field and lab investigations, analyses of rubblized and flexible pavements, and the understanding obtained from the literature, the proper conclusions and recommendations will be made regarding: the causes of TDC and the effects of the various factors and the quality of the rubblization operation on TDC potential.

- Rubblization operation and performance of rubblized pavements; and
- Cause(s) of TDC in rubblized and flexible pavements

## 5.0 THESIS STRUCTURE

This thesis is organized in eight chapters and eight appendices as follows:

**Chapter 1 - Introduction and Objectives**

**Chapter 2 - Literature Review**

**Chapter 3 - Field and Laboratory Investigations**

Chapter
Chapter
Chapter
Chapter
Chapter
Chapter
Appendi

**Chapter 4 – The Underperformance of Rubblized Pavements**

**Chapter 5 – Classification and Identification of Top-Down Cracks**

**Chapter 6 - Backcalculation of Layer Moduli**

**Chapter 7 – Analyses of Thermal Stresses in the AC Layer**

**Chapter 8 - Mechanistic Analyses of Load-Induced Lateral Stresses in the AC Layer**

**Chapter 9 – Summary, Conclusions and Recommendations**

**Appendix A – Rubblized Pavement Projects in Michigan**

1.0 I

C

pavemer

pavemer

conven

pavemer

numerou

included

the envir

interactio

1. Ti

2. Ti

ve

(pa

sp

all

the

sho

(Gi

To

# CHAPTER 2

# LITERATURE REVIEW

## 1.0 INRODUCTION

Considerable literature regarding the design and performance of asphalt pavements are available. Most of which has been directed toward determining the pavement cross-section (design) and predicting pavement roughness, rutting and the conventional bottom-up fatigue cracking. Recently, top-down cracks (TDC) in flexible pavements have been widely reported by various researchers and highway authorities and numerous studies were conducted to determine the causes of TDC. The researched topics included the effects of tire-pavement interaction, pavement cross-section, axle load, and the environment on top-down cracking potential. Note that, the term "tire-pavement interaction" refers to the following:

1. The shape and size of the tire-pavement contact area.
2. The magnitude and distribution of the tire-pavement contact stresses including the vertical, lateral (perpendicular to the tire traveling direction), and longitudinal (parallel to the tire traveling direction) contact stresses. Unless otherwise specified, in the rest of this thesis, the term "contact stresses" is used to reference all three contact stresses between the tire and the pavement. Note that, in this thesis, the Society of Automotive Engineers (SAE) vehicle coordinate system shown in Figure 2.1 is used to label the positive and negative contact stresses (Gillespie, 1992).

   To this end, this literature review addresses the following topics:

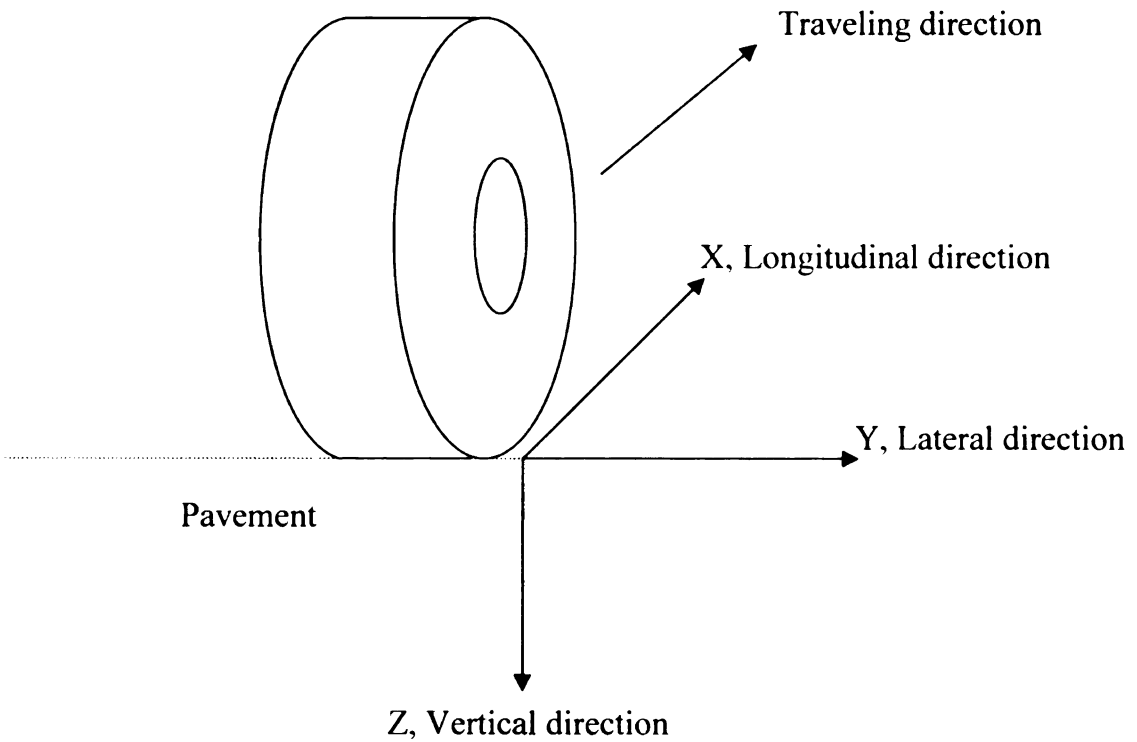


Figure 2.1 The SAE vehicle coordinates system (Gillespie, 1992)

- Tire-pavement interaction
- The causes and propagation of TDC in rubblized and flexible pavements.
- The factors affecting the tensile strength of AC mixtures.
- The factors affecting tensile stresses induced in the AC layer.
- Top-down crack propagation models

## 2.0 TIRE-PAVEMENT INTERACTION

Almost all vehicles use rubber-based pneumatic tires. The principal functions of a rubber tire include (Clark, 1981):

- Transferring the load from the vehicle to the pavement and providing wear resistance by being tough and minimizing cuts, tears and cracks by being resilient.
- Providing good friction and resisting the bruising impacts due to roadway defects.

Although the truck fleet in the USA and other countries uses a wide variety of pneumatic tires (which is referred to as "tire" in this thesis, unless otherwise specified), two tire types are heavily used; radial and bias ply with a high percentage of the truck fleet uses radial tires. Variations between tires include size, inflation pressure, tire structure, (ribs, grooves, and tire stiffness). The next sections present a literature review of the tire-pavement contact area and contact stresses and the factors affecting the magnitudes and distribution of the tire-pavement contact stresses.

### 2.1 Tire-Pavement Contact Area

The shape and size of the tire-pavement contact area are affected by various factors including tire type (e.g., radial versus bias ply), tire inflation pressure, axle load,

carcass

steering

(1997) c

and infl

- F
  - a
  - s
  - i
  - t
  - P
- F
  - T
  - in
  - k
  - A

into two

grooves.

also mad

## 2.2 T

D

smooth t

(VRSPT

carcass stiffness, the number and dimensions of the ribs and grooves, vehicle speed, steering, and the pavement micro and macro textures (Clark, 1981). De Beer and Fisher (1997) obtained tire-prints of bias-ply, radial and wide-base radial tires at different loads and inflation pressures. Examination of their tire prints indicates that:

- For radial tires, the shape of the contact area can be simulated by a rectangle with almost a constant width but a variable length. The constant width is equal to the sum of the widths of the ribs and grooves whereas the length increases with increasing wheel load and decreasing inflation pressure. Figure 2.2a illustrates the tire print of a radial truck tire having 9.2 kips wheel load and 104 psi inflation pressure (De Beer and Fisher, 1997).
- For bias ply tires, the shape of the contact area is rectangle with rounded ends. The width and the length are variables and function of the wheel load and inflation pressure. Figure 2.2b illustrates the tire print of a bias-ply tire having 9.2 kips wheel load and 104 psi inflation pressure (De Beer and Fisher, 1997).

As can be seen in Figure 2.2, the tire print area of both tire types can be divided into two zones; the actual contact area under the ribs and the non-contact area under the grooves. Similar observations regarding the shape of the contact area of radial tires were also made by Groenendijk (1998).

## 2.2 Tire-Pavement Contact Stresses

De Beer et al (1997) measured tire-pavement contact stresses of a slow rolling smooth tire (no grooves) using Vehicle-Road Surface Pressure Transducer Array (VRSPTA), which were spaced at 0.69 in. Their results indicated that:

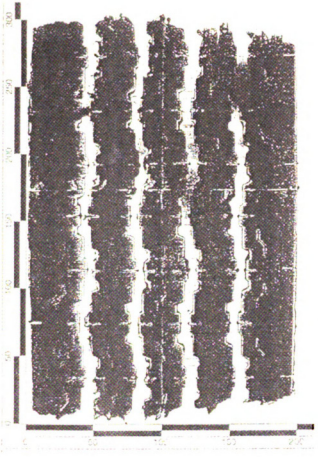

a) Tire print of a radial tire

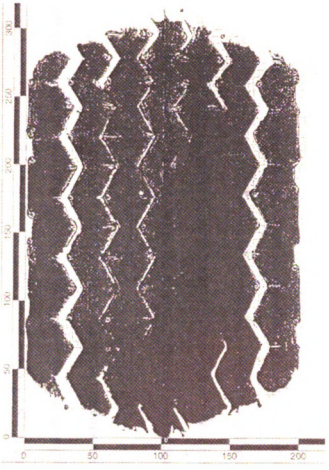


b) Tire print of a bias-ply tire

Figure 2.2 Tire prints of a radial and a bias ply tire having 9.2 kip wheel load and 104 psi inflation pressure (De Beer and Fisher, 1997); (the scale is in mm).

1.

2.

ro..ir

trans

respe

were

ure p

figur

abou

stress

induc

1.

2.

1. The vertical contact stresses were neither equal to the tire inflation pressure nor uniformly distributed throughout the contact area.
2. Among the three contact stress components, the maximum vertical contact stress is the highest and the longitudinal is the lowest as shown in Figures 2.3 and 2.4. This finding is similar to that reported by De Beer and Fisher (1997). Further, there is a relationship between the maximum vertical and the maximum lateral contact stresses shown in Figure 2.5.

Pottinger and McIntyre (1999) measured the contact stresses under straight free-rolling condition of a performance car tire and a radial truck tire using stress measuring transducers spaced at 0.15 and 0.10 in. in the lateral and longitudinal directions, respectively. The wheel load and the inflation pressure of the radial tire used in the test were 6,182 lb and 125 psi, respectively. Figure 2.6 shows the rounded-end rectangular tire print (contact area) and the eight ribs and seven grooves of the radial truck tire. The figure also shows that the ribs and grooves (the contact area) are almost symmetrical about the longitudinal and lateral centerlines of the tire. Note that, the measured contact stresses data obtained from Dr. Pottinger were used in the 3-D analyses of the load-induced stresses in the AC layer and results are presented in Chapter 8. The data include:

1. Complete vertical and lateral contact stresses over the contact area except those along two arrays of transducers on the right side of rib 8 which were excluded from the data because of their irregularities.
2. Longitudinal contact stresses that were measured using only one array of transducers located at the left edge of rib 5.

Contact stress (psi)
a) Con
Contact stress (psi)
16
12
8
4
b) Contact
lb

Figure 2.3

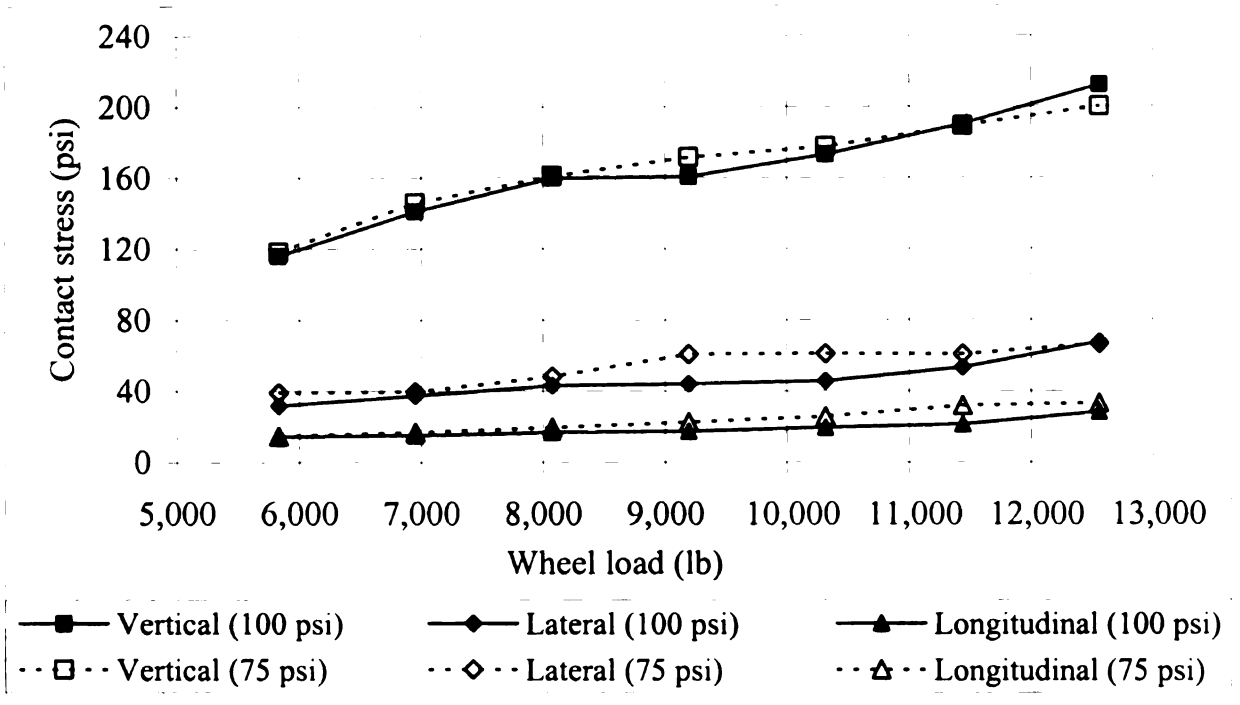


a) Contact stresses due to various wheel loads and inflation pressure of 75 and 100 psi

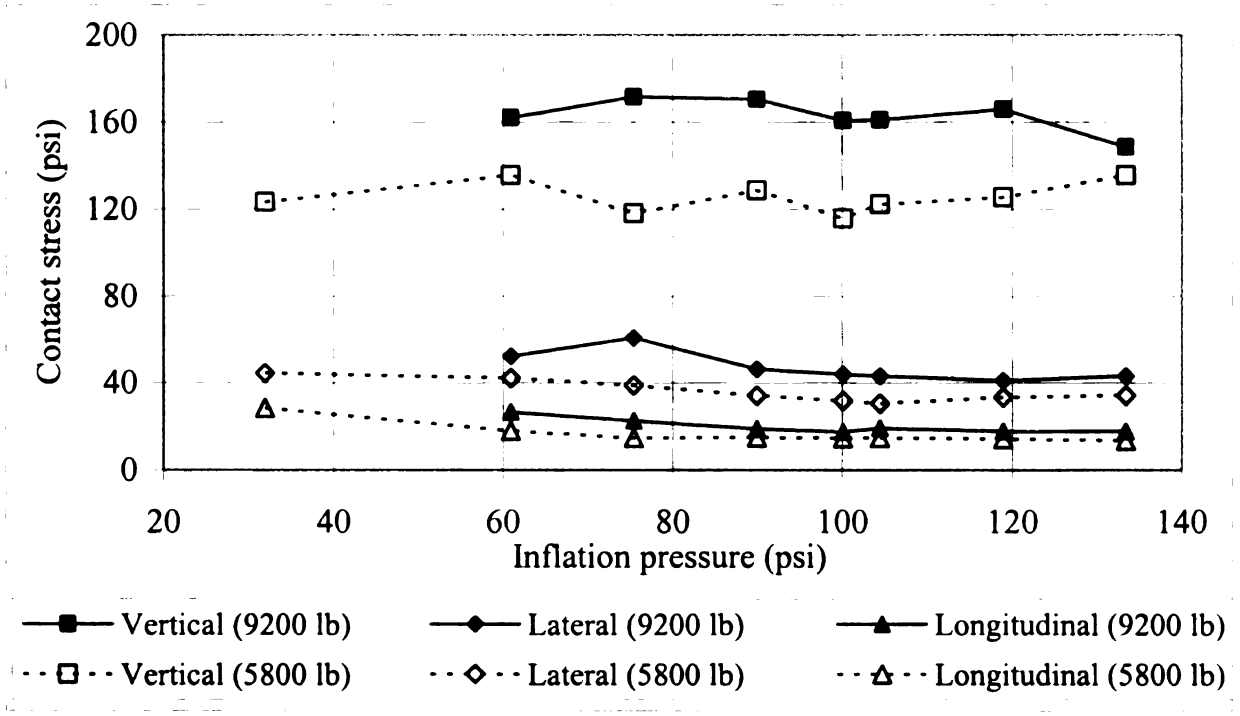


b) Contact stresses due to various inflation pressures and wheel loads of 5,800 and 9,200 lb

Figure 2.3 Plots of the maximum vertical, lateral and longitudinal contact stresses of a bias-ply tire with various wheel loads and inflation pressures (after De Beer et al, 1997).

Contact stress (psi)

a) C

Contact stress (psi)

b) Cor

9.2

Figure

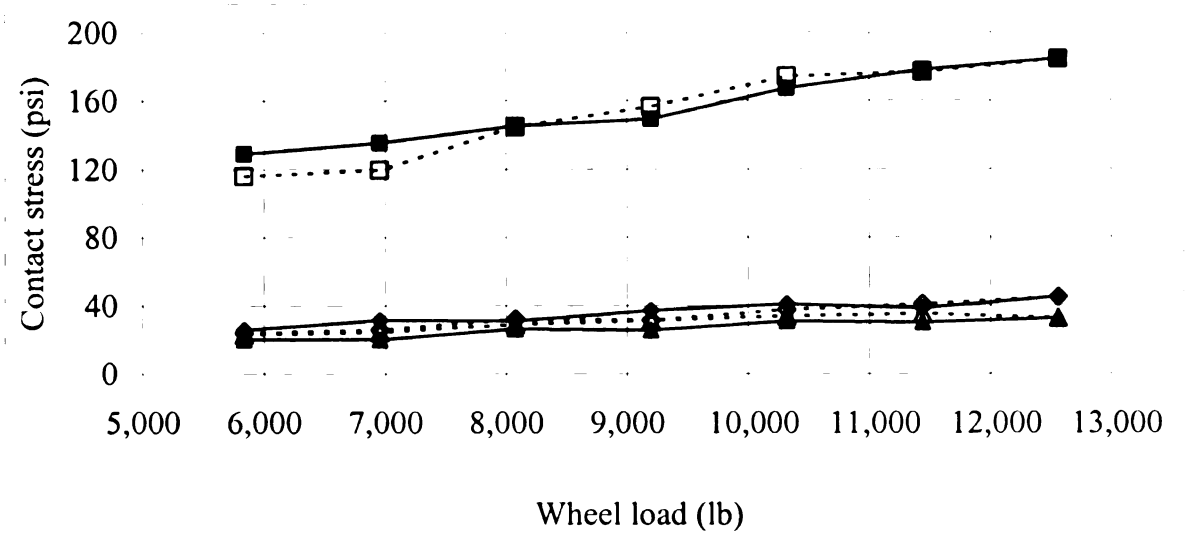


a) Contact stresses due to various wheel loads and inflation pressure of 75 and 100 psi

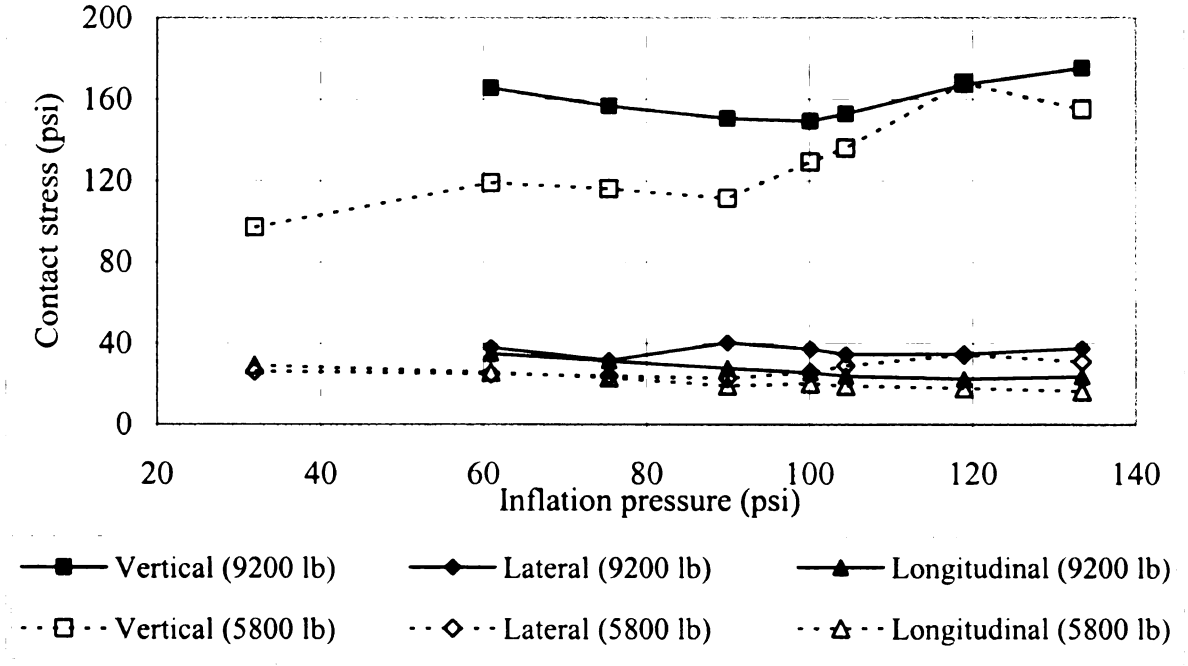


b) Contact stresses due to various inflation pressures and the wheel loads of 5,800 and 9,200 lb

Figure 2.4 Plots of the maximum vertical, lateral and longitudinal contact stresses of a radial tire with various wheel loads and inflation pressures (after De Beer et al, 1997).

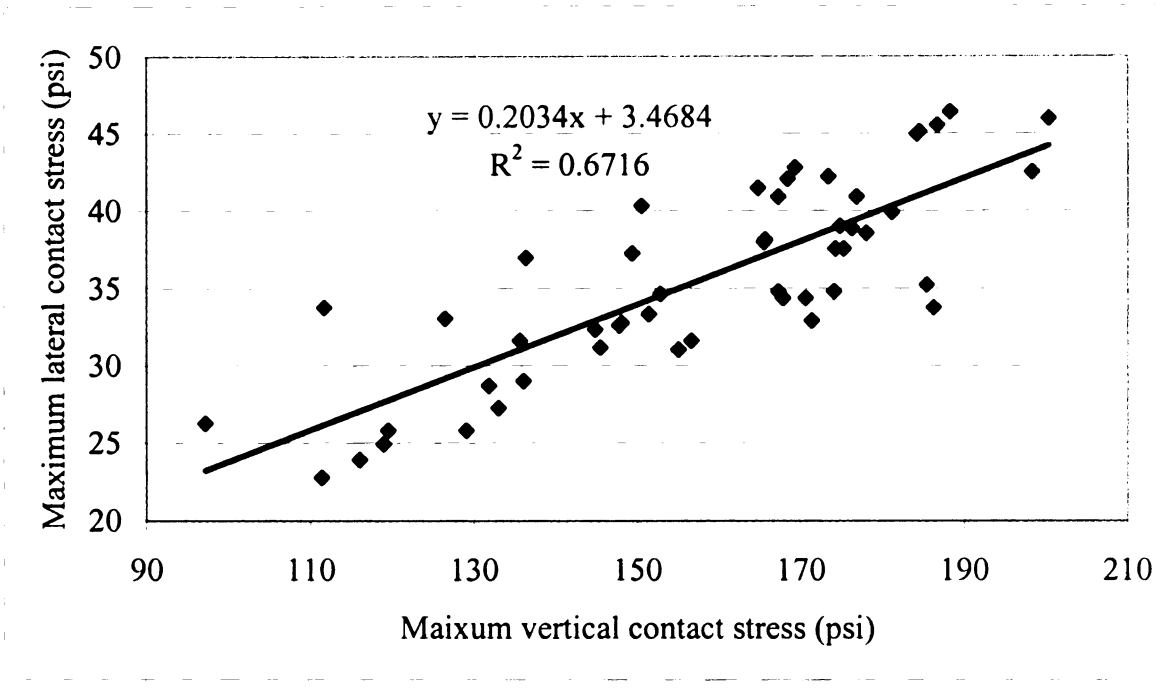


Figure 2.5 Relationship between the maximum vertical and the maximum lateral contact stresses (after De Beer et al, 1997).

Figure 2.

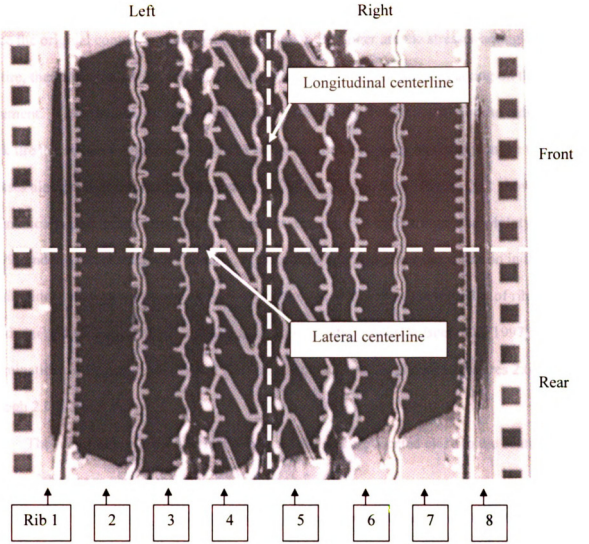


Figure 2.6 Tire print of the radial truck tire tested by Pottinger and McIntyre (1999)

Since t

the tire

pavem

track t

stresses

schema

(1999)

longitud

(Potting

Examin

through

1.

2.

3.

4.

Since the original contact stresses obtained from Dr. Pottinger are the stresses acting on the tire, their directions were reversed in this thesis to express the stresses acting on the pavement. Nevertheless, the measured vertical and lateral contact stresses for the radial truck tire are shown in Figures 2.7 and 2.8 in the form of 3-D plots. Variations in the two stresses along and across the tire are shown in Figures 2.9 and 2.10. Figure 2.11 shows a schematic diagram of the lateral contact stresses as measured by Pottinger and McIntyre (1999) under a radial truck tire. Finally, Figures 2.12 and 2.13 show the variation in the longitudinal contact shear stress along the longitudinal direction of the left edge of rib 5 (Pottinger and McIntyre, 1999) and along the entire contact area (De Beer et al, 1997). Examination of the measured vertical and lateral contact stresses shown in Figures 2.6 through 2.9 indicate that:

1. The maximum vertical and lateral contact stresses are located close to the center of the tire as shown in Figures 2.7 through 2.10.
2. As shown in the Figures 2.7 through 2.10, the vertical and lateral contact stresses are almost symmetrical about the lateral and longitudinal centerlines of the tire.
3. The lateral contact stresses under the inner ribs are outward shear stresses having direction away from the center of the ribs, while those under the two outer ribs (ribs 1 and 8) are inward shear stresses (toward the center of the tire) as shown in Figure 2.11. The latter finding from the measured data contradicts the conclusion made by Myers et al (1999) that radial truck tires produce only lateral outward shear stresses.
4. The distributions of the longitudinal contact shear stress along the front and rear portions of the contact area are different. Hence, the stress is not symmetrical

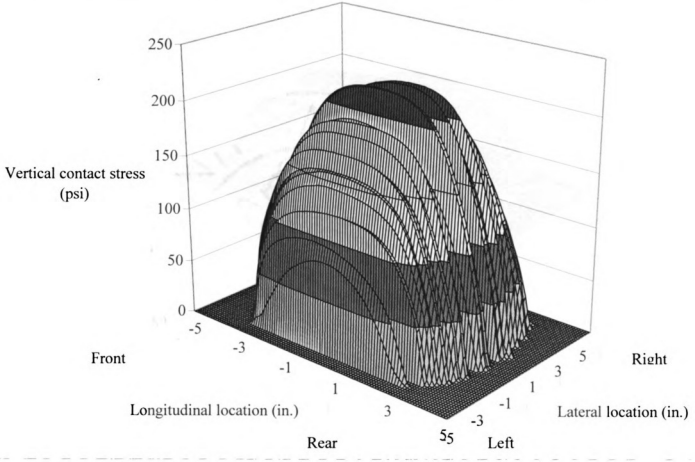


Figure 2.7 Variation in the vertical contact stresses of a radial truck tire (Pottinger and McIntyre, 1999)

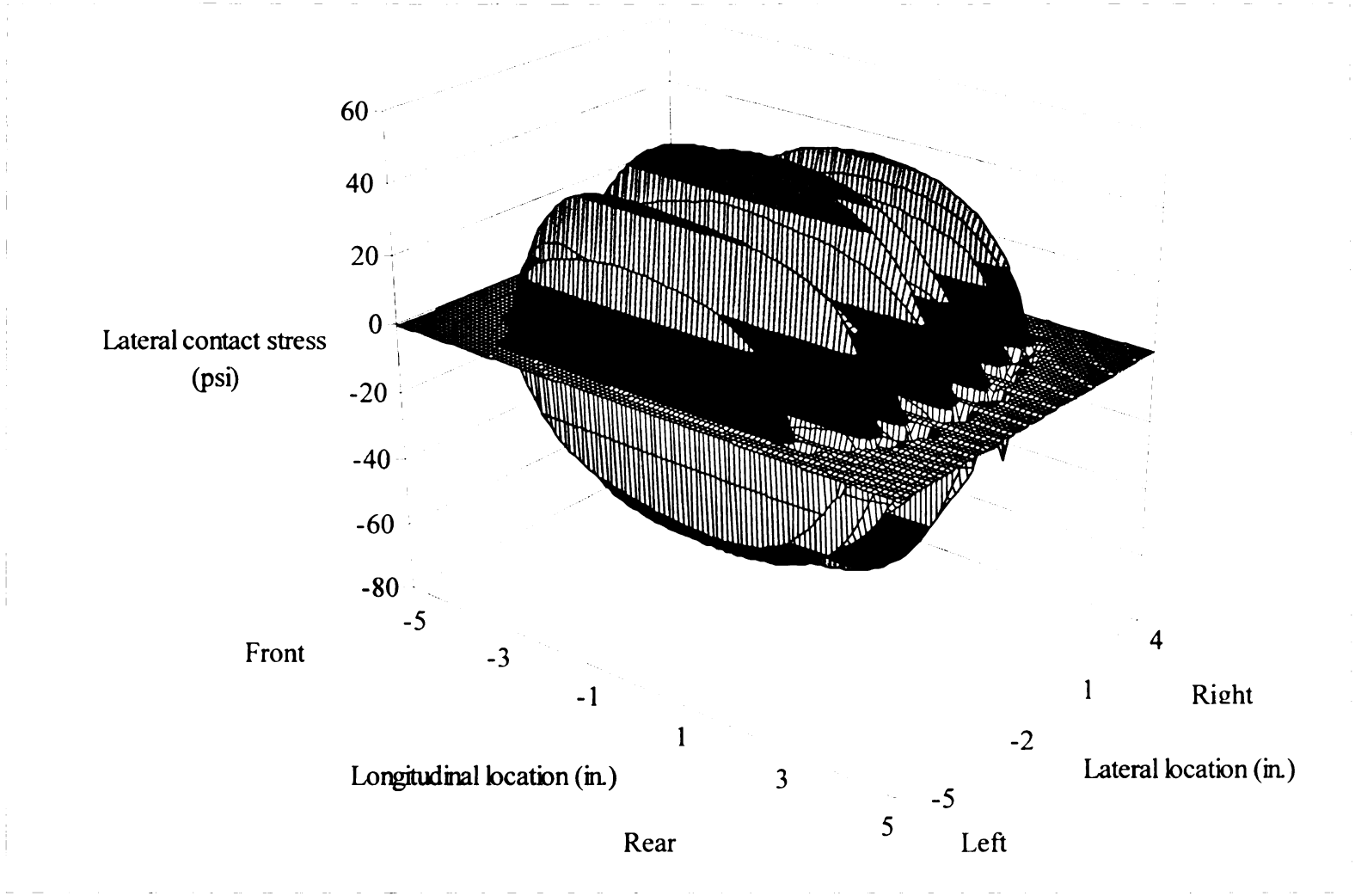


Figure 2.8 Variation in the lateral contact stresses of a radial truck tire (Pottinger and McIntyre, 1999)

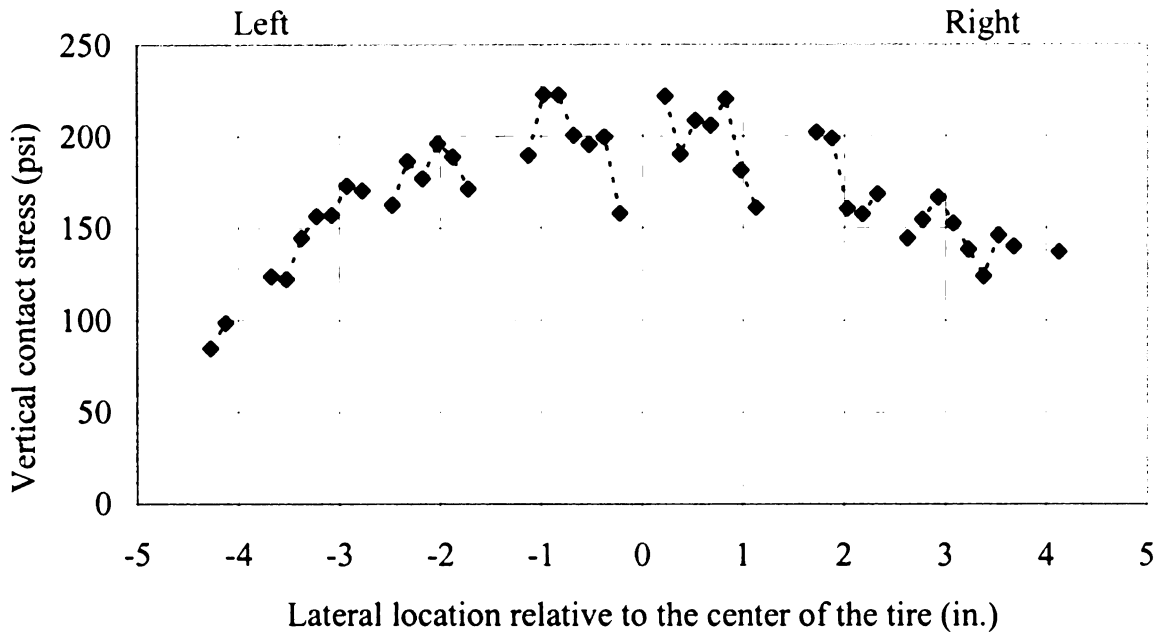


a) Vertical contact stresses

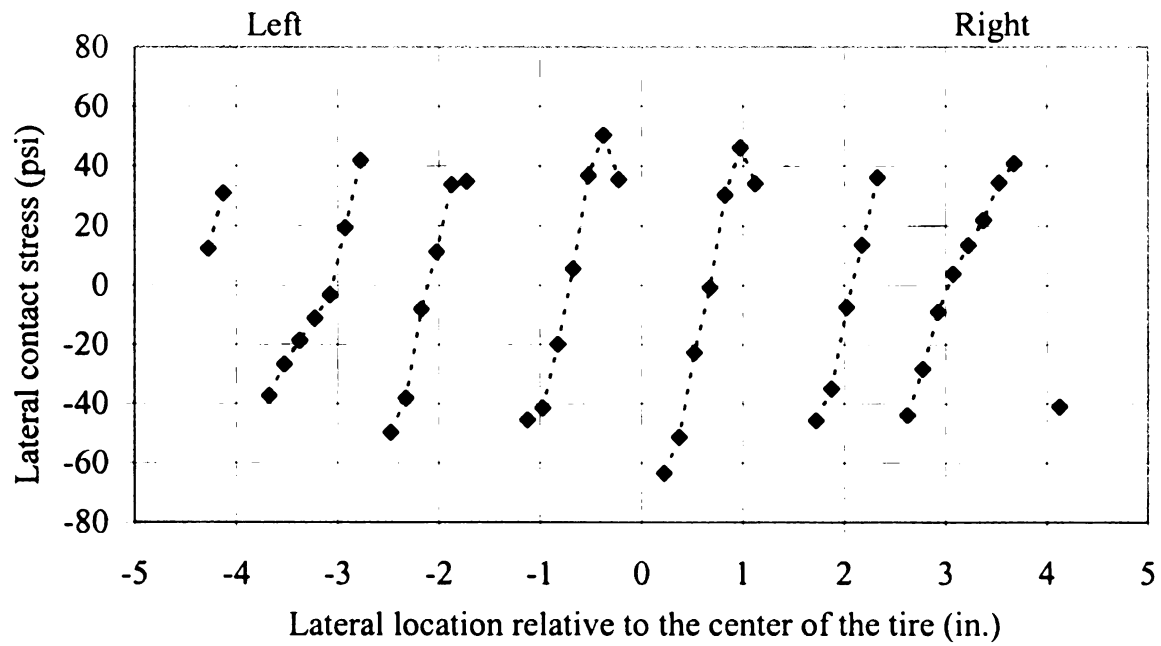


b) Lateral contact stresses

Figure 2.9 Variations in the measured vertical and lateral contact stresses across the tire along the lateral center line of a radial truck tire (after Pottinger and McIntyre, 1999)

Vertical contact stress (psi)

Lateral contact stress (psi)

Figure 2.2

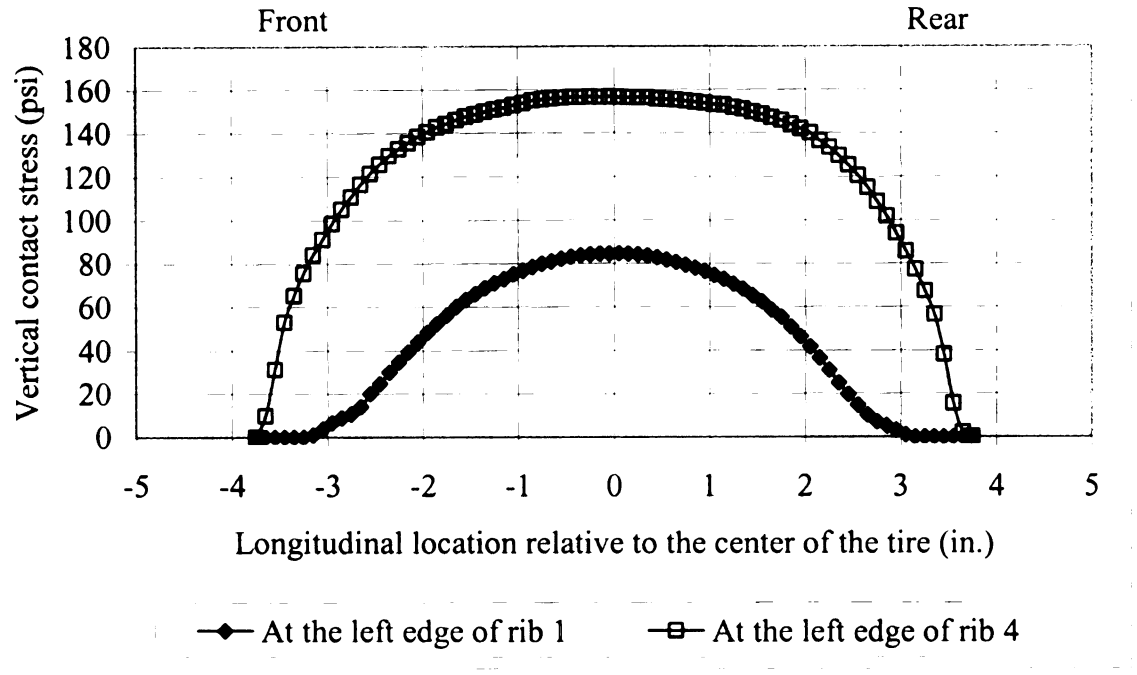


a) Vertical contact stress

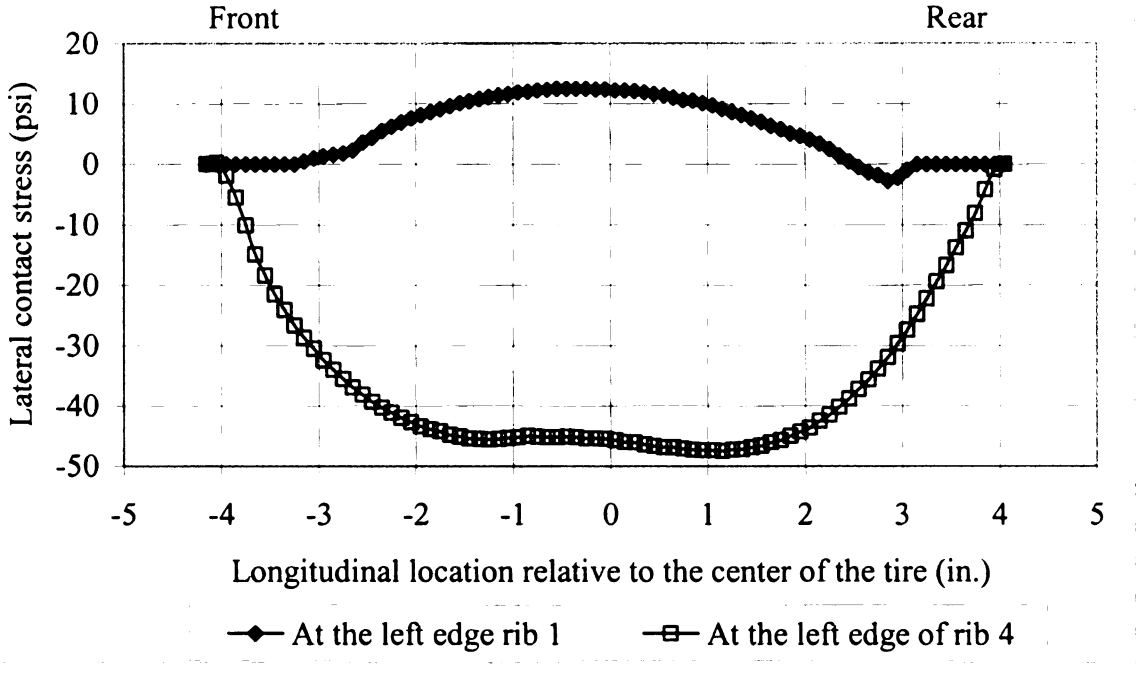


b) Lateral contact stress

Figure 2.10 Variations in the measured vertical and lateral contact stresses in the longitudinal direction along the edge of a radial truck tire (after Pottinger and McIntyre, 1999)

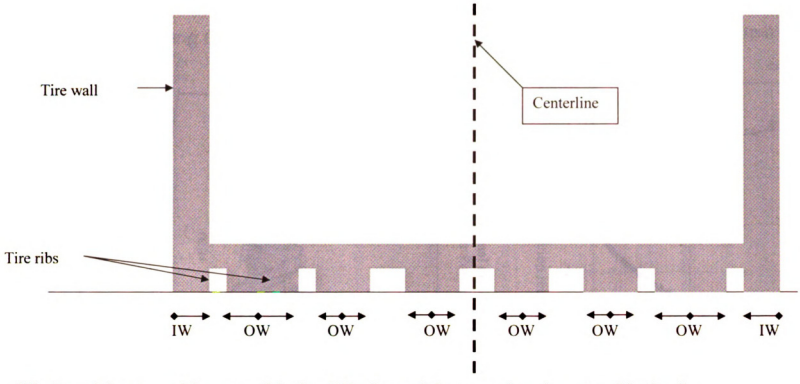


IW = Inward shear toward the center of the tire, OW = Outward shear away from the center of the tire rib

Figure 2.11 Lateral shear stresses under each tire rib of a radial truck tire (after Pottinger and McIntyre, 1999)

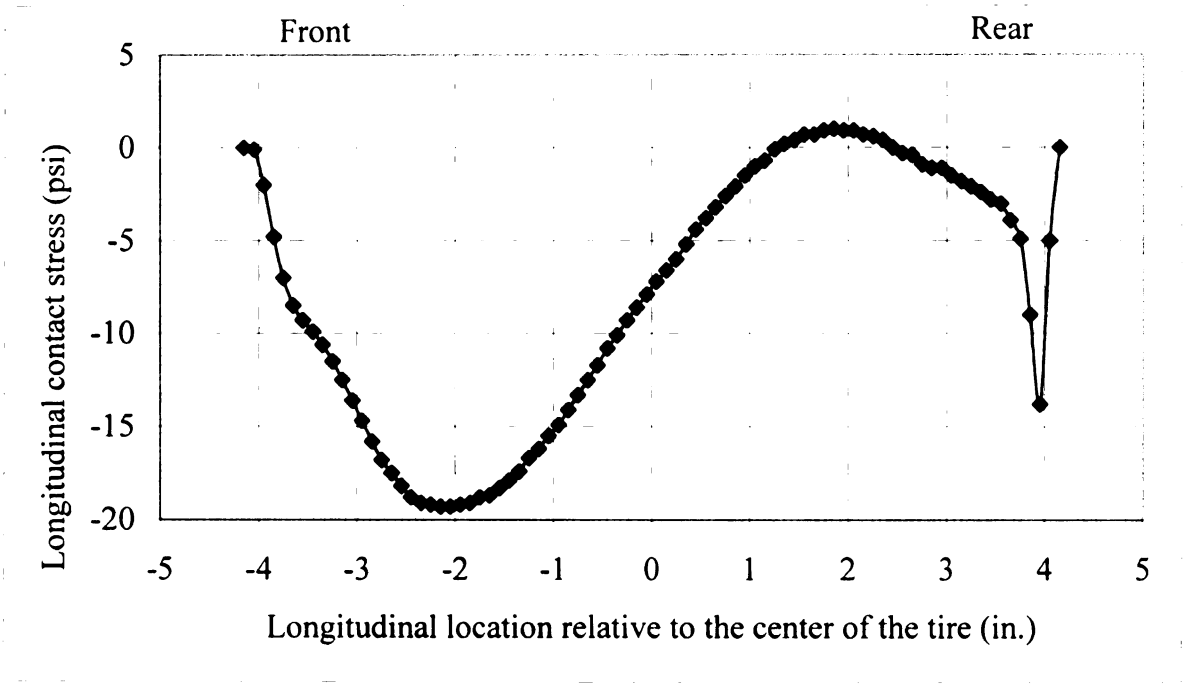


Figure 2.12 Variation in the longitudinal direction of the longitudinal contact stress along the left edge of rib 5 (after Pottinger and McIntyre, 1999)

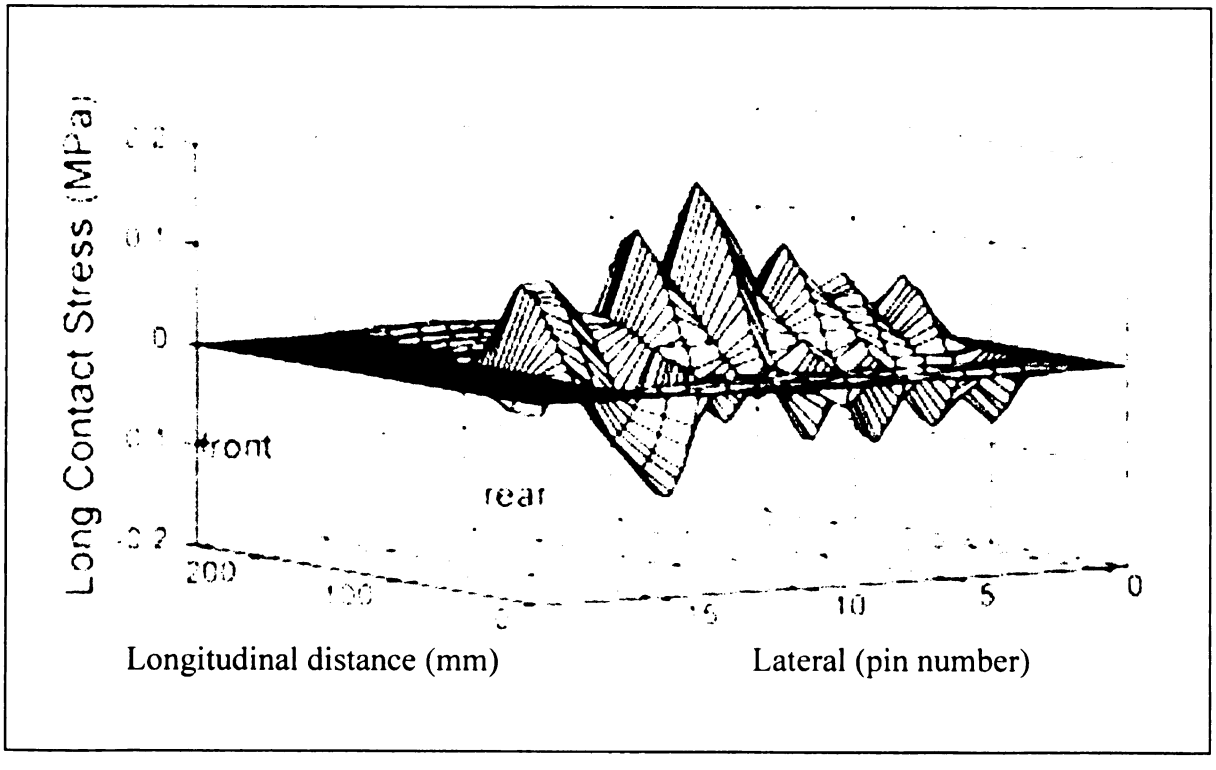


Figure 2.13 Variation in the longitudinal contact stresses of a radial truck tire subjected to the rated load (De Beer et al, 1997)

about the lateral centerline of the tire as shown in Figures 2.12 and 2.13. The first figure shows the distribution of the longitudinal contact stress along the left edge of rib 5 whereas the second figure shows the 3-D variation of said stresses. Note that the term "rated load" used in Figure 2.13 implies that the tire was loaded and pressurized as per manufacturer specifications.

Roque et al (2000) used the ABAQUS finite element computer program to analyze the tire-pavement contact stresses. They reported that the lateral contact shear stress is not affected by the thickness of the AC layer, and the moduli of the AC and aggregate base layers. However, the magnitude and the variation of the tire-pavement contact stresses are functions of various parameters including:

- Tire type and structure
- Wheel load and inflation pressure
- Tire motion (stationary or rolling)

The effects of these parameters on the tire-pavement contact stresses are addressed below.

### 2.2.1 Tire Type and Structure

As stated earlier, one of the functions of the pneumatic tire is to transfer the load from the vehicle to the pavement. The load can transfer to the tire-pavement interface through the tire walls at the edges of the tire and through the pressurized air over the tire tread as shown in Figure 2.14. According to Myers et al (1999), the "pneumatic effect" causes the tire tread to pull in toward the center of the tire inducing inward shear stress at the pavement surface as shown in

Figure 2.15a. On the other hand, the "Poisson's effect" causes each rib to deform outward relative to its center inducing outward shear on the pavement surface as shown in Figure 2.15b. All tires are subjected to certain degrees to both pneumatic and Poisson's effect. However, the pneumatic action controls bias ply tires behavior (see Figure 2.15c) because of their relatively rigid wall and flexible tread structure. Whereas, Poisson's effect controls radial tires behavior as shown in Figure 2.15d because of their rigid tread structure and relatively flexible wall structure. Hence, the two mechanisms affect the distribution of the tire-pavement contact stresses. It is important to note that the lateral contact shear stress under the outer ribs of radial tires can be either inward or outward shear depending on the load magnitude and the tire inflation pressure (more details can be found in section 1.2.2 below). In addition, the outward shear stresses due to Poison's effect decrease as the groove depth decreases due to tire wear and tear. Such wear and tear may reverse the lateral contact stresses from outward to inward under the edges of radial tires. In the Netherlands, Groenendijk (1998) reported that the maximum induced shear stress under a trimmed radial tire, which simulated wear-tear of the used tire, is an inward shear located at the edge of the tire. Pottinger (1992) measured the contact stresses of a stationary and rolling smooth-treaded (bald) radial tire. His results indicated that the shear stresses under the entire contact area are inward directed toward the center of the tire. De Beer and Fisher (1997) measured the contact stresses of bias ply and radial tires subjected to a wide range of tire inflation pressure and load. Their measurements indicated that, in general, the maximum lateral contact stresses and the maximum vertical

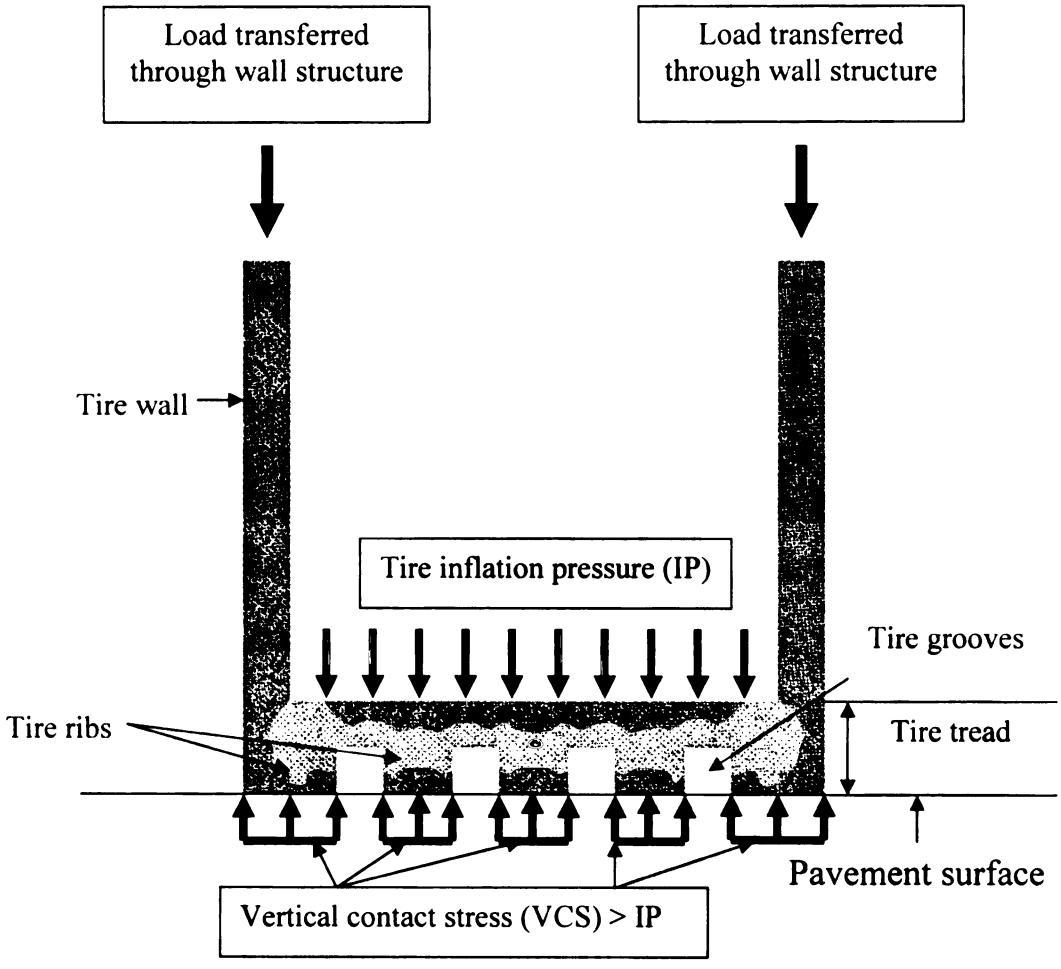


Figure 2.14 Load transfer mechanisms of a tire

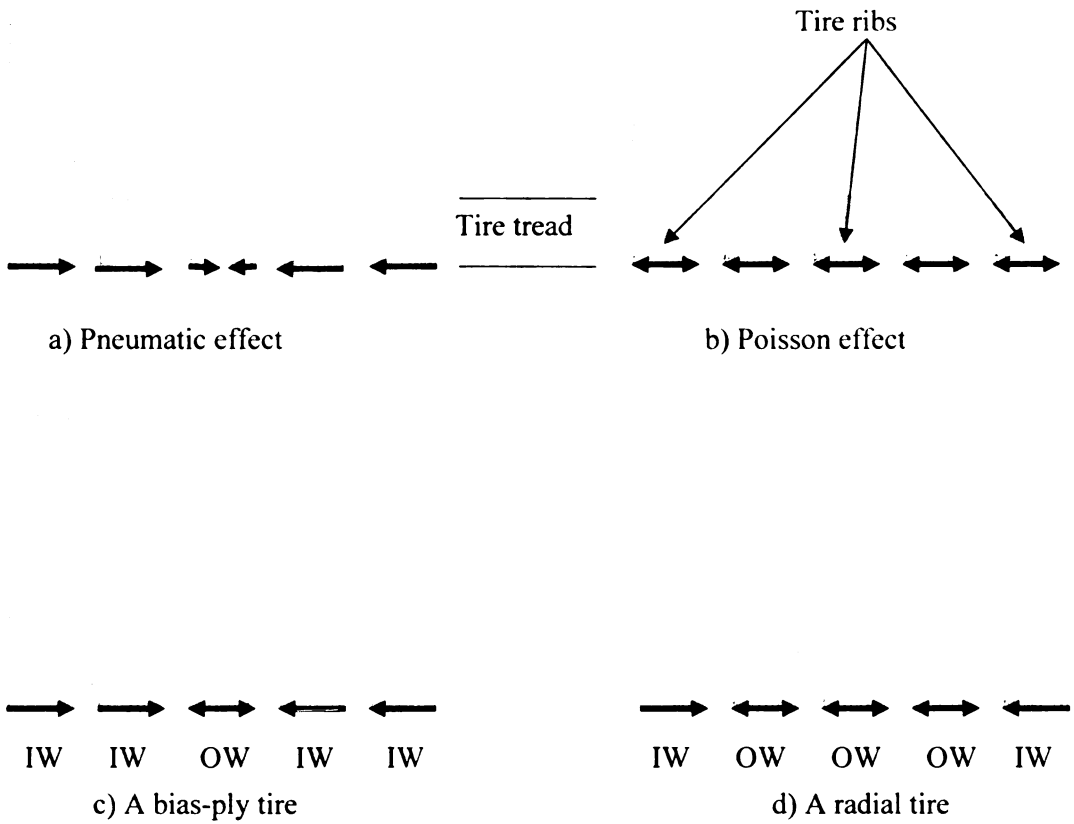


Note 1. IW = Inward shear toward the center of the tire, OW = Outward shear away from the center of the tire rib
2. The contact shears under the outer ribs of the radial tire can be either inward or outward shears

Figure 2.15 Lateral contact stresses due to the Pneumatic (a) and Poisson effects (b) and lateral contact stresses of a bias-ply (c) and of a radial tire (d)

contact stresses of a bias-ply tire are slightly higher than those of a similar size radial tire having the same inflation pressure and carrying the same load as shown in Figure 2.16. This finding contradicts that of Myer et al (1999) who concluded that radial tires induce greater lateral contact stresses relative to bias ply tires.

Finally, Markwick and Starks (1940) reported that the rib-hardness has significant impact on the frictional properties between the tire and the pavement and hence on the inward and outward shear stresses.

### 2.2.2 Wheel Load and Tire Inflation pressure

Many researchers have investigated the effects of wheel load and tire inflation pressure on the contact stresses. Their findings and conclusions are summarized below.

1. Both the average and the maximum vertical contact stresses are higher than the tire inflation pressure. Markwick and Starks (1940) concluded that the maximum vertical contact stresses are about 1.5 times higher than the inflation pressure. The average tire-pavement vertical contact stress $(VCS)_{avg}$ can be estimated by multiplying the tire inflation pressure (IP) by the ratio of the total contact area (TCA) to the area of the tire ribs (ATR) as follows:

$$VCS_{avg} \simeq IP*(TCA/ATR) \qquad (2.1)$$

Or by dividing the total load by ATR. Note that, the above estimates were developed in this study based on various data reported in the literature. Nevertheless, the maximum vertical contact stresses were found to be a

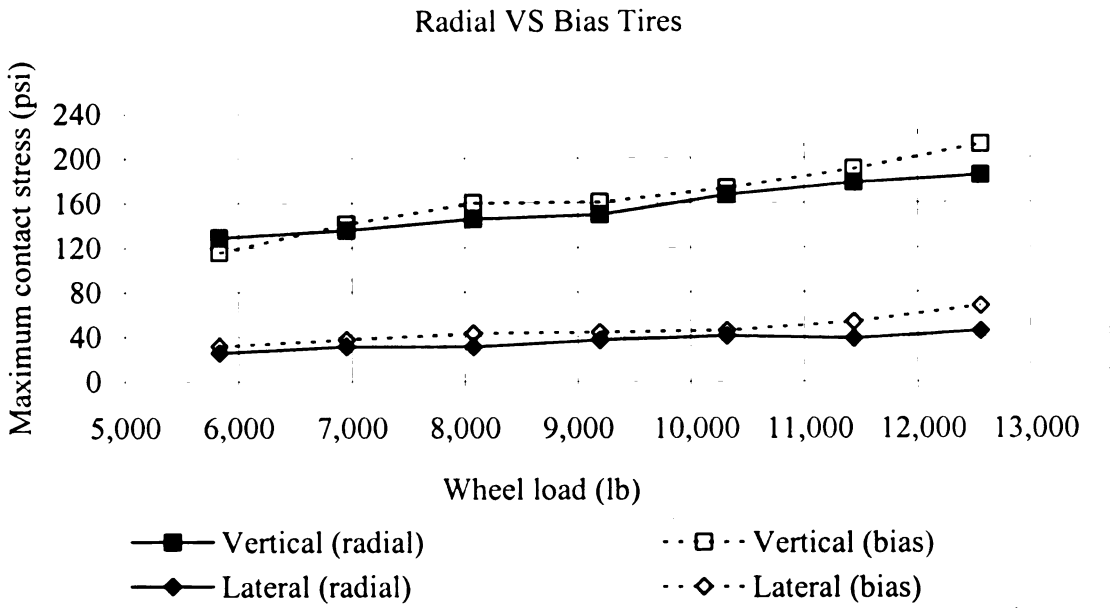


a) Maximum vertical and lateral contact stresses due to various wheel loads and 100 psi inflation pressure

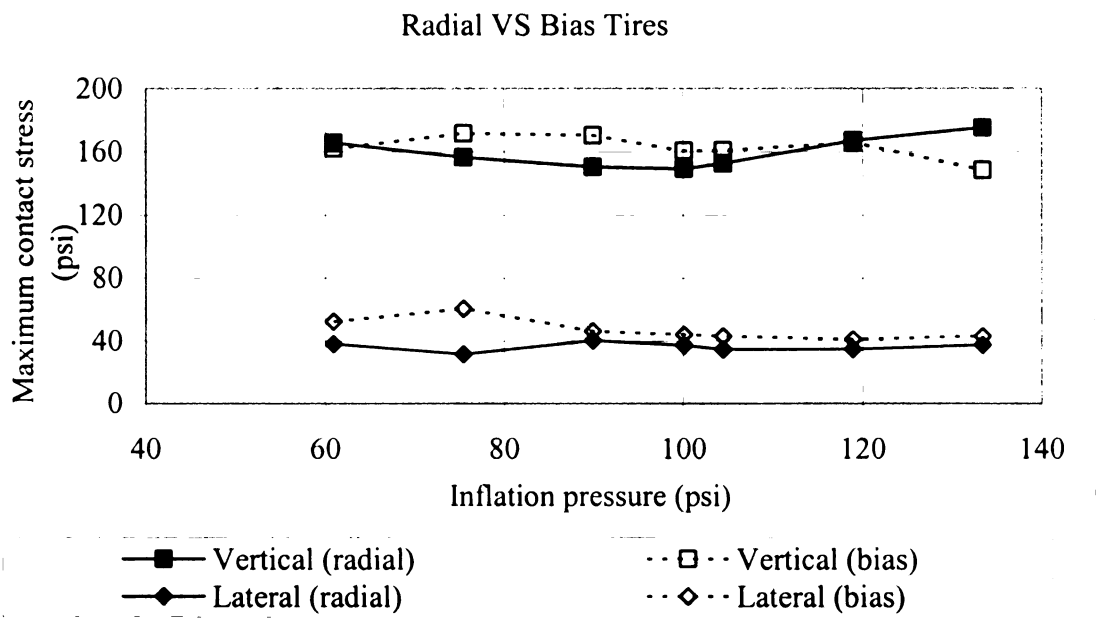


b) Maximum vertical and lateral contact stresses due to various inflation pressures and 9,200 lb wheel load

Figure 2.16 Comparisons between the maximum vertical and lateral contact stresses of radial and bias ply tires at various wheel loads and inflation pressures (After De Beer and Fisher, 1997)

function of both the tire inflation pressure and the wheel load (Markwick and Starks, 1940, Tielking and Abraham, 1994, Himeno et al, 1997, and De Beer et al, 1997). The tire inflation pressure controls the vertical contact stress at the tire center while the wheel load controls the contact stress at the tire edges.

2. All measurements indicated that the maximum shear stresses of bias ply tires are inward shear located at the edges of the tire (De Beer et al, 1997 and De Beer and Fisher (1997). Measurements made by De Beer and Fisher (1997) of the lateral contact stress of overloaded radial tires indicate inward shear stresses at the outer ribs. Groenendijk (1998) reported that the lateral contact stresses at the edges of a trimmed and overloaded radial tire are also inward shear toward the center of the tire.

Figure 2.17 depicts De Beer and Fisher (1997) measurements of the vertical contact stresses of overloaded and under-loaded radial tires. As can be seen from the figure, for overloaded (under-inflated) radial tires, the maximum contact stresses are located at the edges of the tire and their magnitudes are highly related to the wheel load. Increasing wheel load results in increases in the maximum contact stresses while increasing the tire inflation pressure has very small impacts on the maximum contact stresses (De Beer et al, 1997 and Groenendijk, 1998). On the other hand, the maximum contact stresses of under loaded (over inflated) tires are located at the center of the tires and their magnitudes are functions of the tire inflation pressure.

Table 2.1 provides a summary of the lateral contact stresses of bias-ply and radial tires tested under different loads, inflation pressures and tire tread conditions. The data indicate that the ranges of the measured inward shear stresses for radial and bias-ply tires are 7 to 45 psi and 32 to 73 psi, respectively.

### 2.2.3 Tire Motion

The differences in the tire-pavement contact stresses of stationary and rolling tires were addressed by Markwick and Starks (1940). They stated that under a stationary tire, the shear stresses are symmetrical around the center of the tire. The direction of said stresses is toward the center of the tire and their values decrease to zero at the center of the tire. Under a rolling tire, the shear stresses are no longer symmetrical. The resultant shear force on the pavement is in the opposite direction of the vehicle traveling direction. Pottinger (1992) measured the tire-pavement contact stresses of a smooth-tread radial tire under stationary and rolling conditions. He reported that the magnitude of the vertical contact stresses at the edges of the rolling tire are higher than those of the stationary tire, and vise versa for the lateral contact stresses. Another aspect of tire motion is the effect of vehicle speed on the induced strains. Siddharthan and Sebaaly (1999) investigated such effect using the 3D-MOVE computer program. Their results indicated that the load-induced strains in the AC layers decrease significantly due to moving-loads. These results agreed with field measurements reported by Chatti et al (1996) and (1997) and Dai et al (1997) that the measured strains at the mid-depth and at the bottom of the AC layer decrease as the truck speed increase.

Table 2.1 A summary of the tire-pavement contact stresses

| Sources | Tire types/conditions | Loads and inflation pressures | Reported lateral shear stress |
|---|---|---|---|
| Groenendijk, 1998 | Wide base radial/old and trimmed | 22.4 kips, 102 psi | Maximum inward shear of 29 psi at the outer rib. |
| | Wide base radial/new | 16.8 and 22.4 kips, 131 psi | Maximum inward shear of 29 psi at the outer rib for both load levels. |
| | | 11.2 kips, 131 psi | Maximum inward shear of 22 psi at the outer rib. |
| Myers et al, 1999 | Bias ply/unknown | 5.6 kips, 115 psi | Maximum inward shear of 36 psi at the outer rib. |
| | Radial/unknown | 5.6 kips, 115 psi | Maximum outward shear of 58 psi at the center rib. |
| | Wide base radial/unknown | 9.4 kips, 115 psi | Maximum outward shear of 73 psi at the center rib. |
| Pottinger, 1992 | Radial/bald | 0.8 kips, 29 psi | Maximum inward shear of 25 psi at the edge of a rolling tire and 15 psi for a static tire. |
| Pottinger and McIntyre, 1999 | Performance car tire/unknown | 1.1 kips, 38 psi | Maximum inward shear of 44 psi at the second rib from the edge. |
| | Radial/unknown | 6.2 kips, 125 psi | Maximum outward shear of 66 psi at the center rib and inward shear of 40 psi at the outer rib. |
| De Beer et al., 1997 | Bias-ply tire/smooth (buffed down or trimmed) | 9 and 18 kips, 90 psi | Maximum inward shear of 44 and 73 psi at the edge of the tire for 9 and 18 kip load, respectively. |
| | Bias ply/used | 4.5kips, 75 psi and 6.7 kips, 90 psi | Maximum inward shear of 29 psi at the edge of the tire for both cases. |
| | Radial/new | 9 kips, 116 psi | Maximum outward shear of 29 psi at the inner rib with inward shear of 15 psi at the outer rib. |
| | Wide base radial/new | 11.2 kips, 131 psi | Maximum outward shear of 29 psi at the second rib from the edge with inward shear of 7 psi at the outer rib. |
| De Beer and Fisher, 1997 | Bias-ply/used | 5.8 to 12.6 kips, 32 to 133 psi | The maximum values of the inward shear at the outer rib vary from 32 to 67 psi. In some cases, there are small outward shear at the outer rib with a maximum of 19 psi. |
| | Radial/new | 5.8 to 12.6 kips, 32 to 133 psi | The maximum values of the inward shear at the outer rib vary from 26 to 45 psi. In most cases, there are small outward shear at the outer rib with a maximum of 15 psi. |

## 3.0 TOP-DOWN CRACKS IN FLEXIBLE AND RUBBLIZED PAVEMENTS

Top-down cracks (TDC) are longitudinal and/or transverse cracks that initiate at the pavement surface and propagate downward and outward as shown in Figure 2.18. Based on the examination of pavement cores, various researchers have reported that TDC may propagate only within the AC surface course or throughout the entire depth of the AC layer (Myers et al, 1998, Gerristsen et al, 1987, Uhlmeyer et al, 2000, Niederquell et al, 2001, and Svasdisant et al, 2002). Field investigation has shown that most longitudinal TDC are located in the vicinity of the wheel paths (Myers et al, 1998, Gerristsen et al, 1987, Matsuno and Nishizawa, 1992, Niderquell et al, 2001, and Svasdisant et al, 2002). Also based on field observations, Svasdisant et al (2002) have divided the development of TDC into three stages as shown in Figure 2.19. The first stage consists of a single short longitudinal TDC appearing just outside the wheel path. Over time, the second stage develops where the short longitudinal TDC grow longer and new sister cracks develop parallel to the original crack. Finally, the TDC evolve into the third stage where the parallel longitudinal TDC are connected via short transverse TDC. TDC have been investigated and reported as a prominent distress in flexible pavements in various countries including Japan, Kenya, South Africa, France, and the Netherlands. In the United States, TDC are becoming a major distress in flexible pavements and are being or were investigated by several states including Florida, Michigan and Washington State. Most of the investigations are related to the causes of TDC in flexible pavements are few address TDC propagation models. These two topics are reviewed in the sections below.

Figure 2.18 Top-down cracks in a rubblized pavement (US-131)

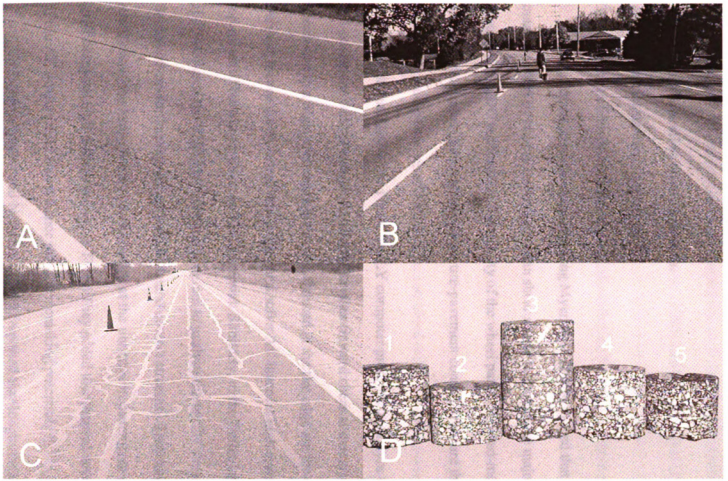


Figure 2.19 Photographs showing the development of Top-Down Cracking (A = Stage 1, B = Stage 2, C = Stage 3) and the pictures of cores with Top-Down Cracks, Core 1- I-96, 2- M-20, 3- Marsh Road, 4- M-37, and 5- I-194.

## 4.0 CAUSES OF TOP-DOWN CRACKS

Several factors have been studied and reported in the literature as the causes of TDC. These include:

1. Load-induced stresses and strains.
2. Thermal stresses.
3. Aging of the AC binder.

Since various researchers including Myers et al (1998) agreed that TDC are mainly caused by tensile stress rather than shear stress, and since the majority of longitudinal TDC are found in the vicinity of the wheel paths, the load-induced tensile stresses and strains in the vicinity of the tire-pavement contact areas are the most commonly studied causes of TDC.

Molenaar (1984) used the CIRCLY computer program to analyze the effects of tire-pavement vertical and lateral contact stresses (inward shear stresses) on TDC. He concluded that high surface tensile strains induced at the tire edge are the cause of TDC. Further, his results indicated that thicker and softer AC layer (at high temperatures) on top of a stiff base layer increase TDC potential. Similarly, in the Netherlands, Gerritsen et al (1987) used the CIRCLY computer program to analyze the tensile stresses induced at the pavement surface due to vertical and lateral contact stresses. They have found that, in some cases, the load-induced tensile strains at the tire edge in pavements with bound base (stiff base) are high enough to initiate TDC. They added that thermal stresses and aging of the AC binder could also enhance top-down cracking potential.

In Japan, Matsuno and Nishizawa (1992) reported that longitudinal TDC were found mostly along the wheel paths and they are absent in shadowy areas. They

conducted finite element analysis of flexible pavements in hot temperature and made the following two conclusions:

1. The load-induced tensile strains at the tire edge cause TDC initiation. This conclusion supports that of Molenaar (1984) and Gerritsen et al (1987). Park (2000) made similar conclusion.
2. The pavement cross section had little effect on the surface tensile strains.

Groenendijk (1998) used the 3-Dimensional (3-D) finite element computer program, CAPA, to analyze the load-induced surface tensile stresses at the pavement surface. He employed the three components of the tire-pavement contact stresses; vertical, lateral, and longitudinal contact stresses, to simulate different loads and different inflation pressures. He concluded that the combined influence of the non-uniform contact stresses and the aging of the AC at the surface could result in critical tensile stress at the AC surface instead of at the AC bottom. Finally, the values of the contact stresses used in Groenendijk's analyses were measured in South Africa using the Vehicle-Road Surface Pressure Transducer Array (VRSPTA). More details of the South Africa's measurements are presented in the tire-pavement interaction section.

Myers et al (1998), (1999) and (2001) studied the effects of the vertical and lateral contact stresses of radial and bias ply tires on the induced tensile stresses at the tire-pavement contact areas. They concluded that:

1. Lateral contact stresses (inward shear stresses) induce high surface tensile stresses in the pavement at the edges of bias ply tires and cause TDC (Myer et al, 1998). This conclusion was based on Jacobs (1996) data for bias ply tires.
2. Lateral contact stresses (outward shear stresses) under the outer ribs of radial tires

induce high surface tensile stresses at those locations, which cause TDC (Myers et al, 1998). This conclusion was based on the shear stresses data that were measured by Pottinger (1992) for radial tires. Further, based on another set of measured data, Myers et al (1999) concluded that the maximum surface radial tensile stress occurs under the center of the outer rib.

3. The tensile stresses under the tire ribs are localized phenomenon at the AC surface and they dissipate rapidly throughout the depth of the AC layer. The pavement structural characteristics such as moduli of the AC and base layers have insignificant effects on the magnitude of the induced surface tensile stresses (Myers et al, 1998 and 1999). This also support the conclusion made by Matsuno and Nishizawa (1992).

4. Radial and wide-base radial truck tires induce in the pavement higher surface lateral tensile stresses relative to bias ply tires. As a result, they are more detrimental to the pavements than the bias ply tires (Myers et al, 1999). Note that, to simulate the field condition, in their study higher wheel loads were assigned to the wide base radial truck tires than to the bias ply or to the radial tires.

5. Load-induced tensile stresses away from the edges of the tire are the driving mechanism for the propagation of TDC. The pavement layer stiffnesses and the location of the tire relative to TDC have significant impact on the magnitude of the load-induced tensile stresses away from the tire, Myers et al (2001).

Uhlmeyer et al (2000) studied of the causes of TDC in conjunction with the Washington State Department of Transportation. They observed that TDC occurred in and around the wheel paths in pavements 3 to 8 years old with AC thickness of more than

6.3-inch (16-cm). Hence, they concluded that pavement thickness has an effect on the initiation of TDC, which disagree with the conclusion made by Myers et al (1998), Myers et al (1999), and Matsuno and Nishizawa (1992).

A different mechanism of top-down cracking was reported by Bensalem et al (2000). They used finite element model to analyze the load induced stresses and strains in the pavement. They reported that:

- The load-induced shear strains at the tire edge on the vertical plane are higher than the load-induced lateral tensile strains at the same location on the pavement surface. Therefore, the shear strains on the vertical plane play an important role in TDC initiation and propagation.
- The magnitude of the shear strains on a vertical plane at the tire edge decreases rapidly with depth. This explains some of the field observations that TDC propagate through the upper AC courses.
- Decreasing the thickness of the AC layer results in increasing the load-induced shear strains. Hence, thinner AC layers are more vulnerable to TDC.
- Differential stiffness in the AC layer due to temperature gradient and the thermal stresses (tensile stresses) may have important roles in the initiation and propagation of TDC.

Note that, the first three conclusions represent a new view of the causes of TDC. However, field data collected during the field investigation of this dissertation and other studies (Myers et al, 1998) do not support the first two conclusions of Bensalem et al (2000). Cracks caused by shear failure along a vertical plane should be inclined at an angle from the vertical plane. The cracks found in numerous cores extracted from various

rubblized and flexible pavements, in this study, were aligned with the vertical plane.

The agreements and contradictions regarding the effect of the pavement cross-section on the induced tensile stress at the pavement surface were further scrutinized by examining the types of analyses conducted by the various researchers. Eventually, all sides have made the proper conclusions relative to their input data and results. To clarify, the tensile stress induced at the pavement surface due to the inward/outward shear is independent of the pavement cross-section. However, the tensile stress induced at the pavement surface due to the vertical contact stresses is a function of the pavement cross-section. The above implies that when only lateral stresses induced by vertical contact stress are analyzed, the results would show a significant role of the pavement cross-section. On the other hand, analyses of lateral stresses induced by inward and outward contact stresses (shears) would result in an opposite conclusion.

Thermal stresses and strains were also investigated as possible causes of TDC. Dauzats and Rampal (1987) reported that most of the TDC found in their test sections in southern France were located on the centerline side of the slow lane. They calculated thermal stresses, strains, and tensile strength of the AC using equations developed by Shahin (1977). Results of their study indicated that the surface tensile strains due to low temperatures could initiate TDC after a number of repeated temperature cycles. Similarly, Roque and Ruth (1990) used MEAPs/CRACK3 computer program to study TDC initiation potential in flexible pavements due to thermal and load-induced stresses. They concluded that the combination of thermal and load-induced stresses is the cause of TDC especially under critical condition such as fast cooling rate and spring thaw condition with more emphasis placed on the former condition than the latter one.

In South Africa, Hugo and Kennedy (1985) also investigated thermal stresses as a possible cause of TDCs. They calculated the thermal stresses in the AC layer using the CRACK computer program. They also studied the impact of several AC mix characteristics including aggregate gradation, air voids, and asphalt cement contents on the aging of the AC mix. They concluded that TDC could initiate due to load-associated or non-load associated causes (thermal stress and/or aging) or combination thereof.

In Kenya, Wambura et al (1999) tested cores obtained from pavements exhibiting TDC. They concluded that severe aging is the cause of TDC, said aging was the result of high air voids in the AC mixes used in Kenya. Similarly, Malan et al (1988) related aging of AC binder to TDC initiation. They studied premature surface cracking in South Africa and concluded that gap-graded AC mixes are more vulnerable to aging and TDC than dense graded mixes.

To this end, it becomes obvious that there is no consensus in the literature regarding the causes of TDC in flexible pavements. Several factors have been hypothesized as the causes of TDC as summarized in Table 2.2. As can be seen, the noted causes of TDC can be summarized into two categories as follows:

- High tensile stresses and strains induced by load and temperature.
- Low tensile strength or fatigue resistance of the AC materials due to the AC mix properties, and aging or hardening of the AC binder.

Some researchers only emphasized the effects of one category while the others emphasize the combined effects of some factors from both categories. In the study for this dissertation at Michigan State University (MSU), it was hypothesized that TDC are

Table 2.2 A summary of conclusions made by various investigators

| References | Conclusion |
|---|---|
| Svasdisant et al (2002) | TDC are located at the edge of the wheel path and differential stiffness in the A layer enhances TDC potential |
| Molenaar (1984) and Gerritsen et al (1987) | ➢ High tensile strains induced by the combination of vertical and lateral contact stresses at the tire edge cause TDC.<br>➢ Soft AC surface on top of stiff base causes TDC. |
| Matsuno and Nishizawa (1992) | Load-induced tensile strains are the cause of TDC and they are almost independent of the pavement structural properties. |
| Uhlmeyer et al (2000) | TDC occur in and around the wheel paths in pavements 3 to 8 years old with AC thickness of more than 6.3-inch (16-cm). |
| Myers et al (1998), (1999) and (2001) | ➢ Lateral contact stresses (inward shear stresses) induce high surface tensile stresses under the first tire rib at the edges of radial tires and cause TDC.<br>➢ The pavement structural characteristics such as moduli of the AC and base layers have insignificant effects on the magnitude of the induced surface tensile stresses.<br>➢ Radial and wide-base radial truck tires induce higher surface tensile stresses relative to bias ply tires.<br>➢ Load-induced tensile stresses away from the edges of the tire are the driving mechanism for the propagation of TDC. |
| Groenendijk (1998) | The combined influence of the non-uniform contact stress and the aging of the AC at the surface could result in critical tensile stress at the AC surface instead of at the AC bottom. |
| Dauzats and Rampal (1987) | Thermal tensile strains could initiate TDC after a number of repeated temperature cycles. |
| Roque and Ruth (1990) | The combination of thermal and load-induced stresses is the cause of TDC especially during fast cooling rate and the critical spring thaw condition. |
| Hugo and Kennedy (1985) | TDC initiate due to load- or non-load associated causes (aging) or combination. |
| Wambura et al (1999) and Malan et al (1988) | Severe aging of the AC binder causes the initiation of TDC at the AC surface. |
| Bensalem et al (2000) | Load-induced shear strains on vertical plane cause TDC. |

fatigue cracks caused by high stress ratios (high tensile stresses and/or low tensile strength) at the AC surface. Results of a study conducted at MSU by Baladi (1988) indicated that if AC mixes are subjected to stress ratios less than 0.35, their fatigue life would be unlimited. Whereas increasing stress ratios over 0.35 causes increases in fatigue cracking potential. Hence, to determine the causes of TDC, it is necessary to addresses the factors that affect the tensile stress and the tensile strength at the AC surface. In addition, this study addresses the potentials of TDC and bottom-up cracking. Hence the induced tensile stresses and the available tensile strengths at the bottom and at the top of the AC layer are considered. Therefore, in the next sections, available literature addressing the factors affecting tensile stresses and tensile strengths in the AC layer are reviewed.

## 5.0 FACTORS AFFECTING TENSILE STRENGTH OF AC MIXTURES

The tensile strength of the AC mixture is affected by several factors including:

- The AC mix design.
- Temperature
- Particle segregation.
- Compaction.
- Stress state

The effects of each of these factors on the tensile strength of the AC mix are presented in the subsections below.

## 5.1 The AC Mix Design

Because of several reasons including improving the ride quality, decreasing noise and decreasing bleeding/flushing potential, the AC surface course is typically designed to have smaller aggregate sizes (higher aggregate surface area) and slightly lower asphalt binder content relative to the AC base course. This double jeopardy (lower AC content and smaller aggregate sizes) results in thinner asphalt film coating the aggregates and hence, more stress concentration in the AC film (Harvey and Tsai, 1996), which leads to lower tensile strength of the AC mix. Further, the low AC contents tend to increase the percent air voids, which also cause low tensile strength (Button et al, 1990). Similarly, Jung and Vinson (1993) showed that the fracture strength of asphalt mix is most sensitive to the percent air void contents and aggregates type and Zubeck and Vinson (1996) showed that the tensile strength of an AC mix is a direct function of its fracture strength.

Brown and Bassett (1990) studied the effect of the maximum aggregate size on the properties of the AC mixes by conducting several tests including indirect tensile strength tests. They concluded that increasing the maximum aggregate size results in increasing tensile strengths of the AC specimens.

Baladi (1988) studied the effects of the asphalt mix parameters (kinematic viscosity of the AC binder, aggregate gradation, percent air void contents and test temperature) on the tensile strength and resilient modulus of asphalt mixtures. Based on their test results, they developed the following prediction equations:

$$\ln (ITS) = 8.016 - 0.0336*TT - 0.2605*AV + 0.051*ANG + 0.00077*KV \quad (2.2)$$

$$\ln (MR) = 16.092 - 0.03658*TT - 0.1401*AV - 0.0003409*CL + 0.04258*ANG + 0.0008364*KV \quad (2.3)$$

where

INTS = indirect tensile strength (psi);

MR = resilient modulus (psi);

TT = test temperature ($^{o}$F), 40 $^{o}$F $\leq$ TT $\geq$140 $^{o}$F

AV = percent air voids (%);

ANG = aggregate angularity;

KV = kinematic viscosity (centistokes); and

CL = cyclic load (lb).

Based on their test results, they concluded that the indirect tensile strength and modulus of an AC mix increases as the kinematic viscosity and the aggregate angularity increases and as the temperature and the per cent air voids decreases.

Equation 2.3 was rearranged and used in this study to correct the backcalculated layer moduli to the standard temperature of 68$^{o}$ F. Since, for a given AC mix, the percent air voids, the aggregate angularity and the kinematic viscosity are constants and since all FWD tests were conducted at constant load, equation 2.3 can be rewritten as follows:

$$\text{Ln (MR)} = A - 0.03658*TT, \text{ where A is constant}$$

Knowing the value of MR as MR1 and temperature TT1, then the modulus value "MR2" at temperature TT2 can be expressed as follows:

$$MR1 = e^{(A-0.03658*TT1)} \text{ and } MR2 = e^{(A-0.03658*TT2)}$$

$$(MR1/MR2) = e^{(0.03658*TT2-0.03658*TT1)} = e^{0.03658(TT2-TT1)} \text{ and}$$

$$MR2 = MR1[e^{0.03658(TT1-TT2)}] \qquad (2.4)$$

Similarly, equation 2.2 was rearranged and used in this study to predict the ITS at various temperatures as follows:

$$ITS2 = ITS1[e^{0.0336(TT1-TT2)}] \quad (2.5)$$

Where

ITS1 and ITS2 = indirect tensile strengths corresponding to the temperatures TT1 and TT2, respectively.

Khattak (1999) conducted indirect tensile strength and indirect tensile cyclic load tests to study the characteristics of PMA mixtures. He concluded that increases in the polymer content, up to an optimum value, result in improvement of the tensile and compressive strengths, fatigue life, rut potential and low temperature cracking resistances of PMA mixtures at low, moderate and high temperatures. Similarly, Chapuis and Gatien (1995) conducted four-point flexion tests to investigate the effect of temperature on the tensile strength of conventional and polymer modified AC mixtures. Their results indicated that the tensile strengths of the polymer modified AC mixtures are significantly higher than the conventional asphalt mixtures and the tensile strength of both conventional and polymer modified asphalt (PMA) mixtures increases with decreasing temperatures. Further discussion regarding the effect of temperature on the tensile strength of AC mixes is presented below.

## 5.2 Temperature

Zubeck and Vinson (1996) conducted low temperature cracking test of AC mix using Thermal Stress Restrained Specimen Test (TSRST). Their TSRST results indicated that the tensile strength of the AC increases as the temperature decreases to the glass transition point. As the temperature decreases below this point, the tensile strength of the AC decreases. Similarly, results of tests conducted by Heukelom (1966) indicated that the

tensile strength of the AC mixture increases as the stiffness of the asphalt cement increase (as a result of different temperatures and loading times) up to a certain value and then decreases as the stiffness of the asphalt cement increases.

## 5.3 Particle Segregation

Chang (2000) stated that particle segregation refers to the separation of coarse and fine aggregates in an asphalt mix. The mechanism of segregation is based on the motion of aggregates. Whenever aggregates are moved, there is a tendency for segregation to occur." He adopted the following Michigan Department of Transportation definition of particle segregation "areas of non-uniform distribution of coarse and fine aggregate particles in a bituminous pavement that are visually identifiable or can be determined by other methods." He defined three degrees of segregation as follows:

**Light** – The fine matrix in place, more stone than the surrounding mat.

**Medium** – Lack of surrounding fine matrix, significantly more stone than the surrounding mat.

**Heavy** – Stone against stone, little or no fine matrix.

Chang (2000) investigated 25 test sites located along various pavement projects that exhibiting segregation. His data indicated that raveling and cracking are segregation-related distresses, which results in reduction in the pavement service life. Chang et al (2001) reported that areas exhibiting medium to heavy degrees of segregation are expected to lose 56 to 73 percent of their design life due to raveling and cracking. The reduction in the pavement life is mainly due to the low asphalt contents and high percent air voids of the segregated mix, which cause lower tensile strength. Brown et al (1989),

and Khedaywi and White (1995) also draw similar conclusion that the tensile strength of the AC mix decrease with increasing degrees of segregation.

William et al (1996) used Khedaywi and White (1995) techniques to produce in the laboratory five levels of mixture segregation; very fine, fine, control, coarse, and very coarse. They tested all mixes using a wheel tracking device and made the following conclusions:

- The asphalt contents decrease and the percent air voids increase significantly from very fine to very coarse segregation.
- Segregated mixtures exhibit significant loss in performance when tested in the wheel tracking device.

## 5.4 Compaction

Rickards et al (1999) summarized the objectives of compaction of asphalt mixtures as follows:

4. Achieve optimum density.
5. Achieve aggregate particle contact to provide adequate deformation (shear) resistant.
6. Minimize air void contents.
7. Provide crack-free pavement surface to reduce permeability of the AC layer.

The second objective (increasing the AC mix resistance to shear deformation) can be achieved, if and only if, the tensile strength of the AC mix is increased. Marker (1967) explained that by moving aggregates particles closer together, the compaction helps the

asphalt films around the aggregates to develop the inter-particle cohesion force. The increase in particle cohesion force results in increasing tensile strength of the AC mix.

Mohammad and Paul (1993) conducted indirect tensile strength tests on specimens made using different compaction efforts and various AC mixtures (the asphalt binders were obtained from different sources). Their results indicated that higher densities due to higher compaction efforts result in higher indirect tensile strengths of the AC mixtures.

## 5.5 Stress State

As can be seen in Figure 2.20, the pavement surface at the tire edges is subjected to load-induced horizontal tensile stresses whereas the bottom of the AC layer under the tire is subjected to load-induced vertical compressive and horizontal tensile stresses. In addition, the bottom of the AC layer is also subjected to confining stresses due to the overburden pressure and the frictional force between the AC and the aggregate base layers (Zubeck and Vinson, 1986). The different states of stress between the top and the bottom of the AC layer impact the total tensile strengths at both locations. The total tensile strength herein is defined as "the true tensile strength of the AC mix, which could be the same at the top and the bottom of the AC layer, and the added apparent strength due to the different stress states and the frictional confinement." It should be noted that the total strength, not the true strength, controls cracking potential.

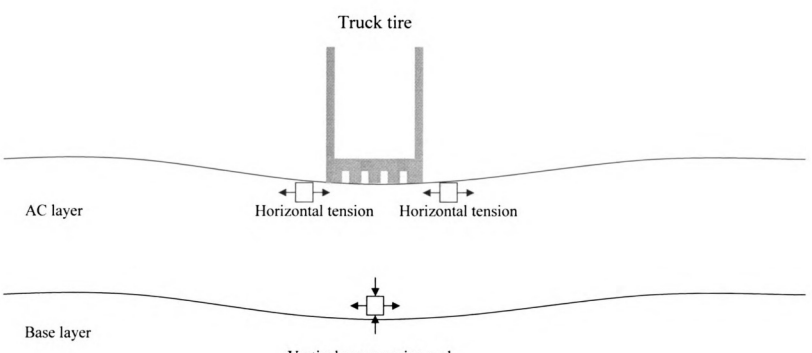


Figure 2.20 Different stress states at the top and bottom of the AC layer

## 6.0 FACTORS AFFECTING THE TENSILE STRESSES IN THE AC LAYER

In this section, the following factors affecting the load-induced tensile stress in the AC layer are reviewed:

- The magnitude and configuration of the load.
- Pavement structural properties (layer thickness and moduli).
- Temperature (thermal stress).

### 6.1 Magnitude and Configuration of Load

In conventional flexible pavement designs and analyses, the wheel load is assumed to be vertical and uniformly distributed over a circular area and the resulting tire-pavement contact stress is assumed to be equal to the tire inflation pressure (Yoderand Witczak, 1975 and Huang, 1993). Based on the two assumptions numerous articles were published addressing the sensitivity of the pavement responses to variations in the wheel load and the tire inflation pressure.

Later, researchers such as Bensalem et al (2000) and Huang (1993) addressed the effects of single and duel wheels on pavement responses. Their results indicate that a single wheel induced higher stresses and strains at the surface and the bottom of the AC layer relative to dual wheels for a given total load. Other researchers studied the effects of non-uniform tire-pavement contact stresses and the shape of the contact area on pavement response. Still others incorporated tire-pavement interaction (vertical, lateral and longitudinal stresses) into the analyses of flexible pavements (De Beer et al, 1997, Molenaar, 1984, Groenendijk, 1998, and Myers et al, 1998 and 1999). Their general conclusions are presented in section 1.0 of this chapter. One important conclusion that

was made by DeBeer et al (1997) is that, for conventional flexible pavement design and analyses, the uniformly distributed vertical contact stress assumption is adequate for the relatively thick AC layer (more than 4 in.). The reason for such conclusion is that the impact of the nonuniform vertical contact stress on the tensile stress at the bottom of a thick AC layer is insignificant.

## 6.2 Thickness and Modulus of Each Pavement Layer

Flexible pavement designs are accomplished by using either empirical or mechanistic-empirical approaches or both. Some empirical procedures (such as the AASHTO 1993) are based on the ride quality (serviceability index) whereas most mechanistic-empirical procedures are based on limited rut depth and pre-determined fatigue life. The common output of all pavement design methods is that thicker pavements are required for higher traffic levels or longer performance period. The implication of this is that the pavement layer thicknesses (especially the AC layer thickness) affect the ride quality, rutting and fatigue cracking. For example, higher AC layer thicknesses reduce the tensile stress/strains at the bottom of the AC layer and the compressive stress at the top of the subgrade thereby causing increases in the fatigue life and decreases in rut potential. The above scenario indicates that the modulus and thickness of the AC and the other pavement layers have significant impact on pavement performance relative to fatigue life, rut depth and ride quality.

The effects of the layer thickness on the load-induced stresses vary and depend on the type of the contact stresses. For example, the stresses induced by lateral and longitudinal contact stresses are independent of the thicknesses and moduli of the

pavement layers including the AC layer (Molenaar, 1984). On the other hand, the effects of the vertical contact stress on the induced stresses in the pavement layers are a function of the thicknesses and moduli of the pavement layers and the modulus ratios between the AC courses and between the pavement layers (Myers et al, 1999).

Svasdisant et al (2002) used 2-D analyses to study the induced tensile stress at the pavement surface due to vertical contact stress. He concluded that high modulus ratios between the AC surface and the AC base courses (high differential stiffness in the AC layer) result in higher induced tensile stress at the pavement surface. Such differential stiffness could be the product of the asphalt mix design practice, aging and temperature gradient. The idea of higher differential stiffness or high modulus ratio was also noted by other researchers. However, some such as (Roque et al, 2002) addressed differential stiffness within the AC layer, whereas (Molenaar, 1984) addressed the differential stiffness between the AC layer and the aggregate base. Myers and Roque (2002) concluded that the differential stiffness (higher modulus at the pavement surface) in the AC layer due to temperature gradient and aging results in higher tensile stresses at the crack tip. They concluded that temperature gradient accelerates the TDC propagation rate.

## 6.3 Temperature (Thermal stress)

Typically, thermal stresses in asphalt pavements are calculated based on the assumption of perfect restraint and using the following viscoelastic stress-strain relationship (Kim and Lee, 1995).

$$\sigma(t) = \int_0^t E(t-\tau)\frac{d\varepsilon}{d\tau}d\tau \tag{2.6}$$

where $\sigma(t)$ = thermal stress at the time in question t;

$\tau$ = time integration variable;

$\frac{d\varepsilon}{d\tau}$ = rate of change of strain at time $\tau$; and

E(t) = time-dependent relaxation modulus of the AC layer.

Since the AC can be considered as a thermo rheologically simple material, its responses under constant temperatures can be used to predict the responses under transient temperatures by imposing time-temperature superposition. The effect of the temperature on the modulus of the AC is incorporated in a parameter termed "the reduced time, $t_r$), which can be calculated as follow.

$$t_r = t/a_T \tag{2.7}$$

where $a_T$ = shift factor for temperature T, which can be calculated using the WLF (Williams, Landel and Frey) equation as follow (Park, 2000):

$$\log(a_T) = -\frac{c_1(T-T_o)}{c_2+T-T_o} \tag{2.8}$$

where $c_1$, $c_2$ = material constants and

$T_o$ = the reference temperature at which the master relaxation curve has been calculated.

Note that, equation 2.8 is applicable within a temperature range from the glass transition temperature (Tg) to Tg+100°C. The reason is that at temperatures below the glass transition temperature, the physical hardening of the AC binder becomes predominant and the material behaves like solid. While at high temperatures, the AC

binder behaves like a Newtonian material. Dividing the time, t and the incremental time $\tau$ in equation 2.6 by the shift factor $a_T$, the term $E(\frac{t-\tau}{a_T})$ becomes time-temperature dependent relaxation modulus as expressed in equation 2.9 (after Haddad, 1995).

$$\sigma(t) = \int_0^t E(\frac{t-\tau}{a_T})\frac{d\varepsilon}{d\tau}d\tau \qquad (2.9)$$

Figure 2.21 depicts plot of a master relaxation curve expressing the time-temperature dependent modulus of an AC mix as a function of the reduced time $t_r$ (Park, 2000). Note that, the master curve is based on base temperature of 25°C. Park (2000) developed the following regression equation that fits the master curve of Figure 2.8 well up to approximately 10 seconds with $R^2 = 0.99$.

$$E(t_r) = 14825 - 2209*(1-e^{-t_r/1.1447957}) - 4427.6*(1-e^{-t_r/.0006052}) - 4454.6*$$
$$(1-e^{-t_r/0.0173438}) - 2637.2*(1-e^{-t_r/0.0000131}) \qquad (2.10)$$

where $E(t_r)$ = time-temperature dependent relaxation modulus (MPa)

Based on equation 2.9, it can be seen that the thermal stress is a function of two parameters, the relaxation modulus and the rate of changes of strains of the AC material. The former parameter can be obtained using the master curves and the shift factor as explained above. The latter are functions of the rate of changes of the temperature and the coefficient of thermal contraction and expansion of the AC materials as shown in the following equations.

$$\Delta\varepsilon = \alpha\Delta T \qquad (2.11)$$

and hence

$$\varepsilon'(t) = \alpha T'(t) \qquad (2.12)$$

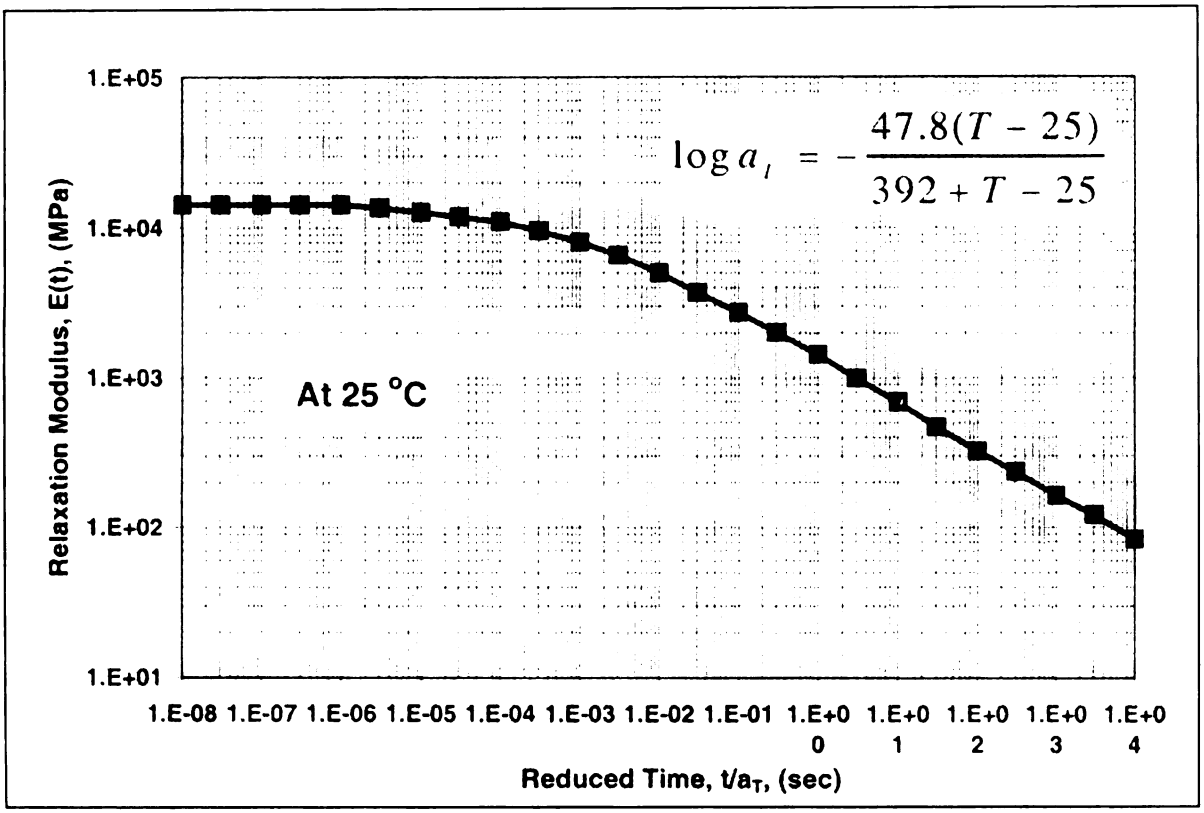


Figure 2.21 Master relaxation modulus and shift factor of the asphalt mixtures reported by Park (2000)

Where $\Delta T$ = the change in temperature, °C;

$\Delta\varepsilon$ = the corresponding change in strain;

$\alpha$ = the coefficient of thermal contraction and expansion, 1/°C;

$T''(t)$ = the rate of changes of the temperature, °C/unit time; and

$\varepsilon'(t)$ = the corresponding rate change of strain, 1/unit time.

Note that, the rate of change of temperature impacts both the rate of change of strain as shown in equation 2.12 and on the relaxation modulus, $E(t_r)$ (shorter or longer loading time, t). Rogue and Ruth (1990) concluded that low temperatures and fast cooling rates could result in high thermal stress. They added that the high thermal stresses combined with load-induced stresses can results in TDC initiation in flexible pavements.

The value of the coefficient of thermal contraction and expansion of an asphalt mixture is a function of the coefficient of thermal contraction and expansion of the AC binder and the aggregates and the volumetric relationship between the AC binder, aggregates and the air voids (Hiltunen and Rogue, 1994). Kim and Hussein (1996) reported ranges of the coefficient of thermal contraction of gravel, AC binder and AC mixture as $4\text{-}5*10^{-6}$/°C, $0.8\text{-}2.1*10^{-4}$/°C and $1.7\text{-}3.2*10^{-5}$/°C, respectively. Zeng and Shields (1999) conducted thermal expansion-contraction tests of asphalt concrete specimen in the temperature range from +40°C to -40°C. They concluded that the coefficient of thermal coefficient of the investigated AC mix can be assumed as "bi-constant"; $2.62*10^{-5}$/°C and $1.35*10^{-5}$/°C, for temperatures above and below the glass transition temperature of -17°C, respectively. They reported that the calculated thermal stresses in the asphalt concrete specimen using their predicted thermal coefficients agreed

very well with the measured stresses obtained from Thermal Stress Restrained Specimen Tests (TSRST).

Note that, thermal tensile stresses cannot exceed the fracture strength of the AC material. Once the thermal tensile stresses reach the fracture strength, micro-cracks will develop and the thermal stresses will be relaxed. In addition, in the field, the maximum contraction force due to thermal stresses at the bottom of the AC layer cannot exceed the restraining frictional force between the AC and the base layers. If the former is greater than the latter (without exceeding the fracture strength of the AC), the AC layer will slip on top of the base and the thermal stresses will be relaxed (Zubeck and Vinson, 1996).

## 7.0 TOP-DOWN CRACK PROPAGATION MODELS

While the state-of-the-art regarding the causes of TDC is relatively rich, it is poor relative to TDC propagation. Recently, Myers and Roque (2002) incorporated the effect of temperature gradient on differential stiffness in the AC layer in their analyses of tensile stresses at the TDC crack tip using a finite element program. They concluded that:

- Differential stiffness within the AC layer results in higher tensile stresses at the crack tip.
- Temperature gradient accelerates the TDC propagation rate.
- TDC propagate at relatively fast rate in the beginning and then at slower rate for a certain period of time. After this slow rate period, TDC propagate at fast rate again until they spread throughout the thickness of the AC layer.

Molenaar (1984) and Jacobs et al (1996) developed crack propagation model based on a simplified and modified form of Paris' law (equation 2.13).

$$\frac{dc}{dN} = AK^n \tag{2.13}$$

where dc/dN = crack length (mm) per loading cycle, N;

K = stress intensity factor ($N/mm^{1.5}$); and

A,n = crack propagation coefficients (material constant).

The modification allowed the determination of the crack propagation coefficients ("A" and "n") using simple static tests and master curves. However, they reported that their models contain some errors due to the simplifications of the models and the discrepancies between the linear-elastic and homogeneous material assumptions and the actual asphalt mix characteristics. Unfortunately, the accuracy of the TDC propagation models developed by the above researchers cannot be verified or calibrated since there is no currently available TDC historical data in any State Highway Agency database.

Schorsch (2003) developed a TDC propagation model based on historical TDC data that were collected by their research team and by Chang (2000). All their data were inside segregated areas along various pavement sections. Their crack propagation model is based on newly developed numerical values of the degrees of segregation and time as follows:

$$PC = 0.0602\,DS + 0.0093\,DS \ln(t) \tag{2.14}$$

where PC = Percent (TDC) cracking in segregated areas = crack length within an area showing certain degree of segregation/length of the area showing that degree of segregation * 100%;

DS = Numerical value of degree of segregation (Light = 2.5, Medium = 7.5, Heavy = 10); and

t = Pavement surface age (months).

Note that Schorsch (2003) re-arranged equation 2.14 to estimate the service life of areas showing various degrees of segregation based on any threshold value of the percent cracking.

## 8.0 SUMMARY

In this chapter, the following topics have been reviewed:

- Tire-pavement interaction
- Causes of the top-down cracks (TDC)
- Factors affecting tensile strength of the AC mixtures
- Factors affecting tensile stresses induced in the AC layer
- Top-down crack propagation models

# CHAPTER 3

# FIELD AND LABORATORY INVESTIGATIONS

During the course of this study, field and laboratory investigations were conducted on rubblized and conventional flexible pavement sections. The investigations of rubblized pavements were parts of a two-phase study titled "Identify causes for underperforming rubblized concrete pavement projects" (Baladi and Svasdisant, 2002). Those for flexible pavements were parts of a study titled "Determining the causes of top-down cracks in bituminous pavements" (Schorsch, 2003). Table 3.1 summarizes the field and laboratory investigation activities of the two studies. Detailed results of the field and laboratory investigations of rubblized pavements can be found in (Baladi and Svasdisant, 2002)

## 1.0 RUBBLIZATION

Substantial resources are required to preserve and rehabilitated the aging highway systems, which are subjected to increasing traffic demand. Over time, various alternatives have been developed and used for the rehabilitation of deteriorated concrete pavements. These include:

- Partial and full depth joint and crack repairs
- Asphalt concrete (AC) overlay (composite pavement)
- Crack and seat with AC overlay
- Rubblization with AC overlay

The first option is suitable for concrete pavements with low severity and limited extent of distresses. The AC overlay option is typically applied to concrete pavements

Table 3.1 A summary of field and laboratory investigation activities on rubblized and flexible pavements of the two specified studies

| Activities | Two studies | | |
|---|---|---|---|
| | Identify causes for underperforming rubblized concrete pavement projects | | Determining the causes of top-down cracks in bituminous pavements |
| | Phase I | Phase II | |
| Field investigation during the rubblization operation | | | |
| Investigation of the rubblizing equipment and their operating parameters | Yes | Yes | - |
| Excavating trenches in rubblized concrete slabs | Yes | Yes | - |
| Drainability tests | Yes | - | - |
| Field investigation after the completion of construction | | | |
| FWD testing | Yes | Yes | Yes |
| Coring | Yes | Yes | Yes |
| Distress surveys | - | Yes | Yes |
| Laboratory investigation | | | |
| Core and cracks measurements | - | Yes | Yes |
| Specific gravity tests | - | Yes | Yes |
| Indirect tensile cyclic load tests | - | Yes | Yes |
| Indirect tensile strength tests | - | Yes | Yes |

with higher degrees of severity and extent of distresses. The resulting composite pavements will experience within a relatively short time period (3 to 5 years after construction depending on the thickness of the AC overlay and the pre-overlay repairs of the deteriorated concrete pavement) reflective cracks from the underlying concrete pavement. Hence, crack and seat, and rubblization are two options that are applied with the intention to eliminate reflective cracks.

Since 1986 various highway agencies including the Michigan Department of Transportation (MDOT) have used rubblization as an option for a major rehabilitation of deteriorated concrete pavements. The rubblized pavement is typically designed for 20-years. The deteriorated concrete pavements that have been selected for rubblization have had a variety of distress conditions, traffic volumes, base/subbase and roadbed soil support. Finally, two types of equipment are currently available for the rubblization of deteriorated concrete pavements. They are presented in the next subsection.

## 1.1 Rubblizing Equipment

Two types of equipment are used in the rubblization of deteriorated concrete pavements; a resonant frequency breaker and a multi-head guillotine breaker, also known as the multi-head breaker. Some common characteristics and features of the equipment and their operational parameters are presented below.

### 1.1.1 Resonant Frequency Breaker

The resonant frequency breaker was developed and became operational in 1986. From 1986 to about 1995, no other rubblizing equipment was available and

therefore a large number of projects were rubblized using the resonant frequency breaker. As of 2001, more than thirty state highway agencies have used the equipment to rubblize more than 6,300 lane-miles of deteriorated concrete pavements.

The resonant frequency breaker (shown in Figure 3.1a) is a self-contained and propelled machine. The resonant rubblizer is composed of a shoe (hammer) located at the end of a pedestal, which is attached to 12.5-ft shaft (beam) whose thickness is 6.57 in. and loaded at the top by a 12,000-lb counter weight, which is adjustable. The principle on which the resonant breaker operates is that a sonic shoe delivers to the concrete slab low amplitude (0.5 in) energy at a frequency close to the natural frequency of the concrete (43 to 46 Hz). The applied energy causes high tension at the top of the slab, which causes the slab to fracture on a shear plane inclined at about 45-degrees from the pavement surface. Figure 3.2 shows a schematic of the sonic shoe of the resonant frequency breaker. After the rubblization operation is completed, the rubblized concrete slabs are compacted using a smooth drum roller as shown in Figure 3.1b.

Several variables affect the rubblized products including shoe size, beam width, operating frequency, loading pressure, velocity of the rubblizer and the degree of overlapping of the various shoe passes. Typical ranges of values for the first five variables are listed below. The rate of production of the resonant frequency breaker is approximately 1.0 to 1.5 lane-miles per day depending on the type of base/subbase material.

a) A resonant frequency breaker

b) A smooth drum vibratory roller

Figure 3.1 A resonant frequency breaker and a smooth drum vibratory roller

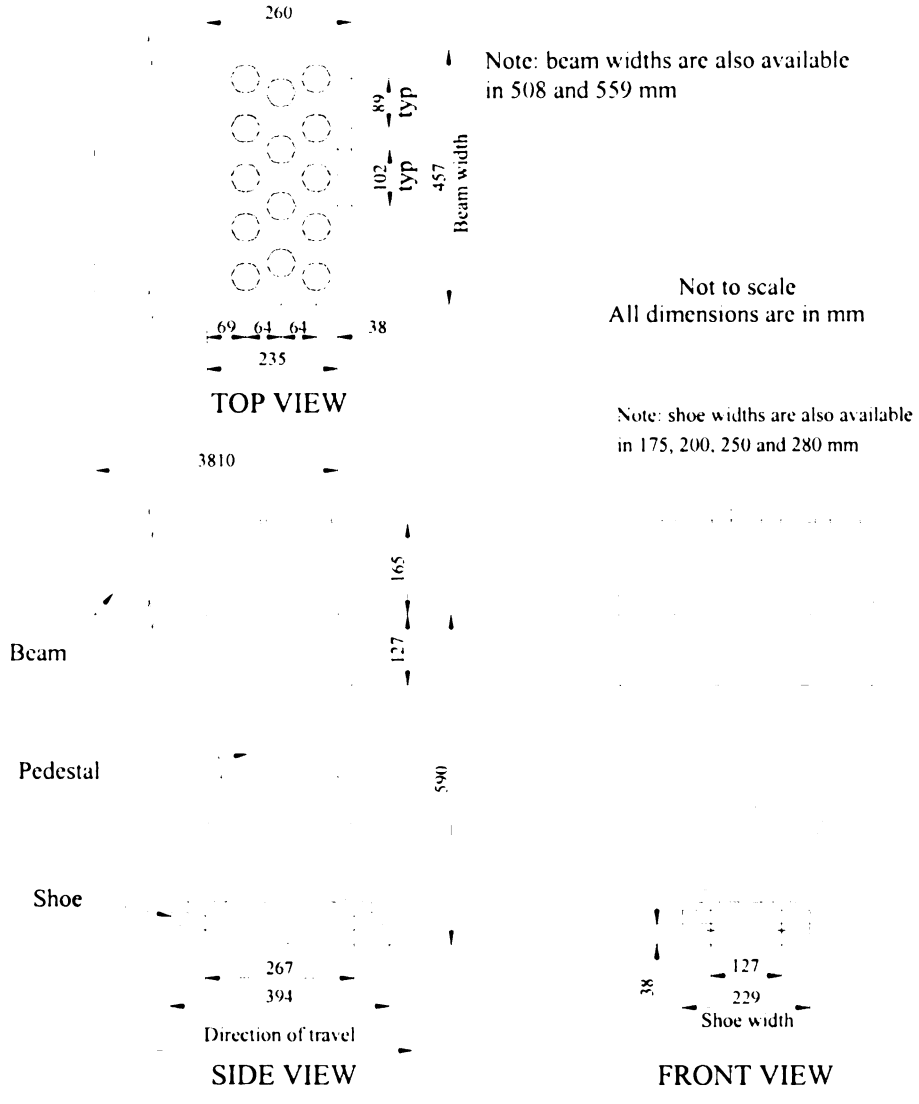


Figure 3.2 Schematic of the sonic shoe of the resonant frequency breaker

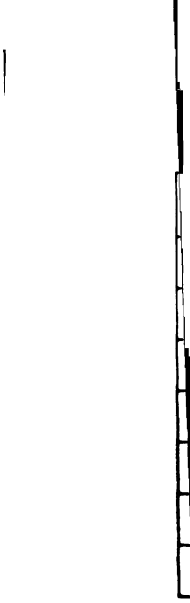

Duri

the vicinity

microproces

in the energ

asphalt over

loss in the e

bounces on

breakup the

and the tem

other hand,

1.1.2

mult

vibra

| Resonant rubblizer characteristics | Values |
|---|---|
| Resonant shoe width | 7 to 12 in. |
| Contact strip width | Approximately 2 in. |
| Beam width | 18, 20 and 22 in. |
| Loading force | 5,000 to 25,000 lbs |
| Loading pressure | 208 to 1,800 psi |
| Frequency | 43 to 46 Hz |
| Velocity | 2 to 4 mph |

During its operation, the resonant frequency rubblizer may encounter difficulty in the vicinity of pavement discontinuities, such as joints or cracks. At a discontinuity, the microprocessor controller automatically increases the rubblizer speed causing a decrease in the energy delivered to the concrete or a shut down. Bituminous patches or un-milled asphalt overlays present another problem. The shoe penetrates the asphalt causing a large loss in the energy delivered to the concrete. When the applied pressure is low, the shoe bounces on the concrete surface and the shoe does not transfer the needed energy to breakup the concrete. Hence, the effective depth of rubblization decreases substantially and the temperature steel may not debond from the concrete. High pressures, on the other hand, cause the shoe to penetrate into the concrete causing damage in the subbase.

### 1.1.2 Multi-Head Breaker

The multi-head breaker system (shown in Figures 3.3 and 3.4) includes multiple drop hammers arranged in two rows on a self-propelled unit and a vibratory grid roller. The bottom of the hammer is shaped as to strike the

Figure 3.3 Multi-head concrete pavement breaker

Figure 3.4 Vibratory grid roller

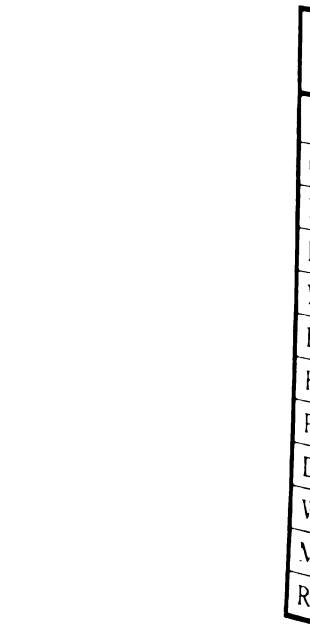

pavement on a 1.5-in. wide and 8-in. long loading strip. The hammers in the first row strike the pavement at an angle of 30 degrees from the transverse direction. The hammers in the second row strike the pavement parallel to the transverse direction. The hammers strike the pavement approximately every 4.5 in. along the direction of travel. Figure 3.5 shows a schematic diagram of a typical hammer configuration of the multi-head breaker. The sequence of hammer drops is irregular because each cylinder, which carries two hammers) is set on its own timer/frequency system. By disabling some cylinders, the width of the rubblized area can be varied from 2.5-ft to 12.67-ft. A 10-ton vibratory grid roller follows the multi-head breaker to reduce the size of the broken concrete.

The rate of production of the multi-head breaker is about 0.75 to 1 lane-mile per day depending on the type of base/subbase material. Some characteristics of the multi-head breaker are provided below.

| Multi-head breaker characteristics | Values |
|---|---|
| Rubblization width | 2.5 to 12.7 ft |
| Cylinders/row | 4 or less |
| Number of rows | 2 |
| Distance between rows | 20 in. |
| Number of hammers per cylinder | 2 |
| Hammer width | 8 in. |
| Hammer length | 12 in. |
| Pavement striking dimension | 1.5 by 8 in. |
| Distance between hammers in one row | 16 in. |
| Weight/hammer [wing hammer] | 1200 and [1500] lbs |
| Maximum drop height [wing hammer] | 48 and [60] in. |
| Rubblizer operating velocity | 500 to 950 ft/hr |

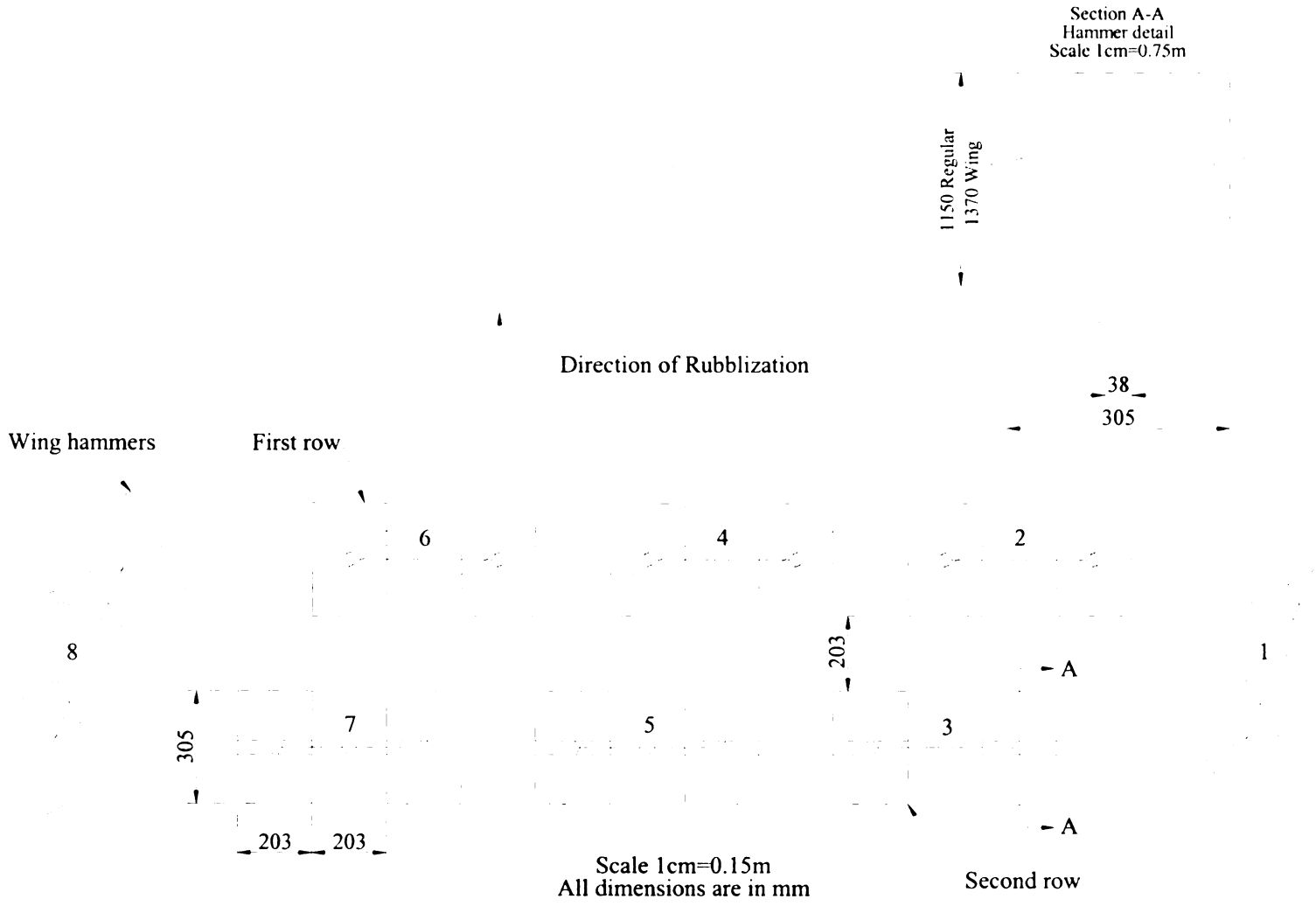


Figure 3.5 Schematic of the hammer configuration of the multi-head breaker

mu

and

dif

mo

pen

perf

## 1.2 Rub

As s

for the reha

of rubblizin

1. Des

crac

2. Des

avoi

3. Cha

than

If th

overlay alte

flexible pav

explained, n

Winkler's fo

Several variables affect the quality of the rubblization operation of the multi-head breaker. These include the speed of the rubblizer and height, weight and frequency of the drop hammers. The multi-head breaker encounters difficulties on saturated subbase and/or weak roadbed soil (less than 3000 psi modulus), which fail in shear causing large concrete pieces to rotate and/or penetrate the underlying material. Such failure would result in a poor pavement performance.

## 1.2 Rubblization Objectives

As stated in the previous section, rubblization and AC surfacing is an alternative for the rehabilitation of distressed concrete pavements. There are three main objectives of rubblizing concrete pavements. These are:

1. Destroying the integrity of the concrete pavement joints as to eliminate reflective cracks.
2. Destroying the integrity of the concrete slab by debonding the temperature steel to avoid reflective cracks and by producing full depth rubblized material.
3. Changing the concrete slab into a particulate media whose maximum size is less than 6 in. This allows the rubblized concrete slab to behave like a base layer.

If the above three objectives are successfully achieved, the rubblizing and AC overlay alternative changes the pavement cross-section and its behavior from rigid to flexible pavement as shown in Figure 3.6. Thus, rubblized pavement can be better explained, modeled and analyzed using the multi-layer elastic system rather than the Winkler's foundation, which is used in the analyses of rigid pavements.

a) (

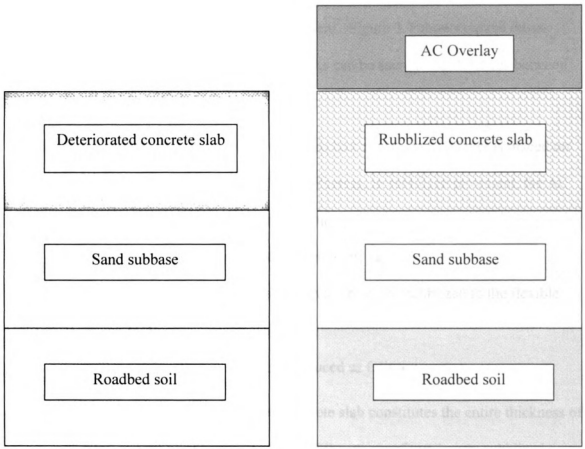


a) Original concrete pavement

b) Rubblized pavement

Figure 3.6 Concrete and rubblized pavement cross-sections

## 1.3 Ru

Th

rubblized

similar to t

sections of

the two cro

1. In c

   top

   laye

2. Rub

3. The

   pav

At this poi

**Rubblized**

the deterior

material an

**Rubblized**

concrete sl

size from d

**Fractured**

concrete sl

consists of

## 1.3 Rubblized and Conventional Flexible Pavement Cross-Sections

The above section indicates that when a deteriorated concrete pavement is rubblized and an asphalt layer is placed on top, the finished pavement cross-section is similar to that of a conventional flexible pavement. Figure 3.7 shows typical cross-sections of rubblized and flexible pavements. As can be seen, the differences between the two cross-sections include:

1. In conventional flexible pavement, the asphalt concrete (AC) layer is placed on top of a conventional aggregate base. Whereas, in rubblized pavement, the AC layer is placed on top of the rubblized material.
2. Rubblized pavements have a fractured concrete layer.
3. The thickness of the sand subbase may vary from the rubblized to the flexible pavement sections.

At this point, three definitions should be introduced as follows:

**Rubblized Concrete Slab** – A rubblized concrete slab constitutes the entire thickness of the deteriorated and rubblized concrete slab and it consists of two layers; rubblized material and fractured concrete.

**Rubblized Material** – The rubblized material layer is the upper portion of the rubblized concrete slab which was broken by the rubblizers into small concrete pieces ranging in size from dust to about 6-inch.

**Fractured concrete** – The fractured concrete layer is the lower portion of the rubblized concrete slab where the rubblizer did not break down the concrete. Fractured concrete consists of semi-solid concrete containing various hair lines to micro cracks.

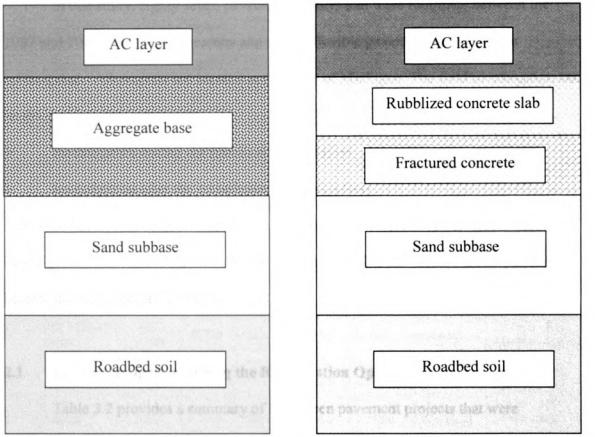


a) Rubblized pavement cross-section b) Flexible pavement cross-section

Figure 3.7 Rubblized and flexible pavement cross-sections

## 2.0 FIELD INVESTIGATION

In this study, eighty seven pavement projects that were rubblized between the 1987 and 2001 construction seasons and eleven flexible pavement projects were investigated. All projects are located in the State of Michigan. The field investigation can be divided into two categories:

- Investigation during the rubblization operation
- Investigation after the completion of construction

Note that the first investigation applies to rubblized pavements only whereas the second investigation was conducted on both rubblized and flexible pavements. Details of the investigations are presented below.

### 2.1 Field Investigation during the Rubblization Operation

Table 3.2 provides a summary of the fifteen pavement projects that were investigated during the rubblization operation. Six of these projects were rubblized using the resonant frequency breaker and nine using the multi-head breaker. Table 3.3 provides a summary of observations made during the investigation. The main objective of the investigation was to evaluate the quality of the rubblization operation, which can be determined from the degree that the objectives of the rubblization operation (stated in section 1.2 above) have been achieved.

During the rubblization operation of each of fifteen rubblized pavements, several trenches were excavated in the rubblized concrete slabs and the thickness of the rubblized material and fractured concrete layers were measured. Some of the trenches were located at mid-slab, others were located at joints and still others were located at a transverse

| No | |
|---|---|
| 1 | US |
| 2 | US |
| 3 | US |
| 4 | US |
| 5 | US |
| 6 | Old<br>EB |
| 7 | Old<br>NB |
| 8 | M-1 |
| 9 | M-2 |
| 10 | M-5 |
| 11 | M-5 |
| 12 | Port<br>Roa |
| 13 | Chi<br>Driv |
| 14 | US 2 |
| 15 | Beec<br>Roa |

IL =Inner la
crack, BMP

Table 3.2 A summary of the rubblized equipment and trench locations

| No | Project | Control section | Job number | Region | BMP | EMP | Rubblizing equipment | Trench locations |
|---|---|---|---|---|---|---|---|---|
| 1 | US-10 EB | 67022 | 44986 | North | 9.657 | 12.087 | Multi-head | 19+867 - MS<br>20+144 - MS<br>20+389 - MS |
| 2 | US-23 SB | 01052<br>04031<br>04031<br>04031<br>04031 | 32335<br>32335<br>32335<br>32335<br>44350 | North | 16.369<br>0.000<br>0.449<br>1.404<br>4.218 | 16.393<br>0.241<br>0.908<br>2.248<br>7.893 | Resonant | 465+21 -MS<br>465+85.5 - TJ |
| 3 | US-31 NB | 10032 | 44113 | North | 11.430<br>13.905 | 13.874<br>14.340 | Multi-head | 26+130 - MS<br>26+652 - MS<br>26+680 - MS<br>27+324 - TJ<br>27+385 - TJ |
| 4 | US-31 SB | 05011 | 44109 | North | 0.923 | 3.019 | Multi-head | 2+200 - MS<br>2+637 -MS |
| 5 | US-131 SB | 41133<br>59012 | 33914 | Grand | 3.200<br>0.000 | 8.691<br>4.214 | Resonant | 37+558.5 - MS<br>N/A - TJ<br>N/A - MS |
| 6 | Old US-10 EB | 56555<br>56041 | 48370 | Bay | 7.114 | 9.513 | Resonant | 25+064 - MS<br>25+594 - MS |
| 7 | Old US-131 NB | 41401<br>41013 | 49321<br>45797 | Grand | 2.669<br>0.000 | 2.820<br>2.232 | Resonant | 9+858 - MS<br>10+690 - MS<br>11+641 - MS |
| 8 | M-18 | 26011 | 45410 | North | 4.860 | 12.000 | Multi-head | 3+180 - MS<br>3+194 - MS<br>4+034 - TJ |
| 9 | M-21 | 25081 | 38028 | Bay | 4.981 | 7.285 | Multi-head | 1+200 IL - MS<br>1+200 OL - MS<br>1+309 IL - TC<br>1+684 IL -MS |
| 10 | M-50 | 58042 | 43523 | Univ. | 0.143 | 4.521 | Multi-head | 10+441 -MS<br>10+803 - MS<br>11+151 -MS<br>12+000 - TJ |
| 11 | M-53 | 50012<br>44031 | 36021 | Metro Bay | 4.438<br>0.000<br>2.820<br>6.466 | 4.458<br>1.588<br>6.130<br>6.940 | Multi-head | 53+621 - MS<br>53+886 - TJ<br>53+900 - MS<br>54+210 - MS |
| 12 | Portage Road | 39405 | 49551 | SW | 0.000 | 1.125 | Resonant | 3+609 - MS<br>3+901.5 - MS |
| 13 | Chicago Drive | 41401 | 50230 | Grand | N.A. | N.A. | Resonant | 149+22 - MS<br>146+26 - MS |
| 14 | US 27 | 37014 | 38205 | Bay | 0.00 | 1.53 | Multi-head | N/A - MS<br>N/A - TJ |
| 15 | Beecher Road | 25402 | 50078 | Bay | N.A. | N.A. | Multi-head | 1+480 - MS<br>1+485 - TJ<br>1+322 - MS<br>1+140 - MS |

IL =Inner lane, OL =Outer lane, TJ =Transverse joint, MS =Mid-slab, TC =Transverse crack, BMP and EMP = beginning and ending mile posts.

Table 3.3 A summary of rubblization variables and observations made during the investigation of various projects

| No. | Project | Rubblization process | Results of drainability test |
|---|---|---|---|
| 1 | US-10 EB | • The quality of rubblization of the original concrete slab and widening strip varies from one location to another. | • Good drainage. |
| 2 | US-23 SB | • The quality of rubblization was poor along the concrete widening strip.<br>• The original concrete slab was well rubblized to depths below the temperature steel.<br>• Poor rubblization at a transverse joint. | • No test was conducted. |
| 3 | US-31 NB | • Most aggregates were broken, which indicates that the strength of the aggregate is less than that of the cement paste.<br>• The quality of rubblization was good in all five trenches. | • Good drainage. |
| 4 | US-31 SB | • Shallow rubblization.<br>• No steel was debonded in two trenches. | • W ater drained laterally because of super-elevation. |
| 5 | US-131 SB | • Good rubblization in all three trenches.<br>• Dowel bars were exposed. | • No test was conducted. |
| 6 | Old US-10 EB | • Excellent rubblization through the entire concrete thickness in both trenches. | • Excellent drainage. |
| 7 | Old US-131 NB | • Good rubblization in two trenches.<br>• Fair rubblization at the third trench. | • Poor drainage in 2 trenches |
| 8 | M-18 NB | • High amount of dust.<br>• Poor quality of rubblization especially along the shoulder.<br>• Few fractures were observed in the fractured concrete.<br>• Dowel bars were exposed. | • Poor drainage in 2 trenches |
| 9 | M-21 WB | • Poor rubblization of the inner lane.<br>• Fair rubblization of the outer lane. | • Poor drainage in 2 trenches<br>• Excellent drainage along the 4-ft concrete widening strip. |
| 10 | M-50 EB | • The quality of rubblization was excellent.<br>• Dowel bars were exposed. | • No test was conducted. |
| 11 | M-53 NB | • Poor rubblization at speed of 275-m/hr.<br>• Good rubblization at speed of 245-m/hr.<br>• The steel was poorly debonded. | • Poor drainage. |
| 12 | Portage Road | • Excellent rubblization through the entire concrete thickness in both trenches. | • No test was conducted. |
| 13 | Chicago Drive | • Maximum of 4.5-in. rubblized material<br>• Large pieces (1.5 to 2 ft) of fractured concrete | • No test was conducted |
| 14 | US 27 | • Hammer bounces<br>• Frequent large pieces (more than 6 in.)<br>• No temperature steel debonding | • No test was conducted |
| 15 | Beecher Road | • Poor rubblization at MS, TJ and cracks<br>• Large pieces (more than 6 in.) throughout the project<br>• Asphalt patches at cracks were not removed | • No test was conducted |

cracks. For eight rubblized pavement projects, after excavating the trenches, the rubblized materials were piled to form the walls of a pool. The floor of the pool consisted of the fractured concrete layer. The pool was filled with water to test the drainability of the fractured concrete. Results of the investigation of the trenches indicated that:

1. The rubblization operation produced two distinctive layers in the rubblized concrete slab, a rubblized material layer at the top and a fractured concrete layer at the bottom as shown in Figures 3.8 through 3.12. The thickness of each layer varied from one location to another. In some areas, the fractured concrete extended to the original pavement surface while in other locations the rubblized material extended to the bottom of the original concrete slab. It was observed that the rigidity or stiffness of the rubblized material varies from one point to another depending on the size of the rubblized material. It was also observed that the stiffness of the fractured concrete is an order of magnitude higher than that of the rubblized material layer. Such differential stiffness causes high load-induced tensile stress at the top of the AC surface, which increases the top-down cracking potential.
2. In general, the interface between the rubblized material and the fractured concrete layer is uneven as shown in Figures 3.8 and 3.9. This creates differential stiffness in the horizontal direction. The implication of this is that, in the mechanistic analyses, the rubblized concrete slab must be modeled as non-homogeneous.
3. At most locations, the temperature steel was not debonded as shown in figure 3.10. This increases the reflective cracking potential.

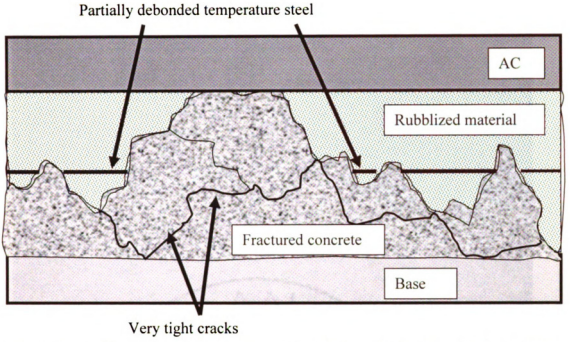


Figure 3.8 Schematic of a rubblized concrete slab showing rubblized and fractured layers

Figure 3.9 Close-up of the fractured concrete in a trench (M-50)

Figure 3.10 Partial debonding of the temperature steel (M-21)

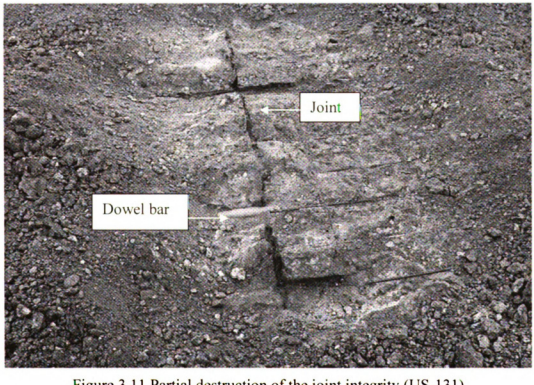


Figure 3.11 Partial destruction of the joint integrity (US-131)

Figure 3.12 Trapped water above the fractured concrete in a trench (M-18)

4. As shown in Figure 3.11, at some longitudinal and transverse joints, the integrity of the joints in the original slabs was not completely destroyed and some dowel bars were found embedded in the concrete on both sides of the joint. These cause the development of reflective cracks.

5. On some projects, the drainability of the fractured concrete layer was poor as shown in Figure 3.12. The water level in the pool did not drop (infiltrate the fractured concrete layer) in 4 hours. On four projects, after the water was placed on the fractured concrete surface, air bubbles were observed coming out of the cracks. When the cracks were saturated, the air bubbles stopped and the water did not drain. Another observation is that the water did not drain or permeate horizontally through the loose rubblized material, which made the pool walls. The implication of this observation is that if water infiltrates the AC layer through cracks, it is likely to be trapped. The trapped water may cause softening of the rubblized material and stripping in the asphalt layer, which lead to a lower pavement performance.

6. At some locations, the resonant frequency breaker caused some large concrete pieces (larger than 6 in.) to rotate and penetrate the underlying base and/or subbase material. This implies that the base and/or the subbase have failed in shear action (bearing capacity). This failure is mainly caused by soft and/or wet base, subbase and/or roadbed soil.

7. For some projects, the frequency of the hammer drops and the speed of the equipment were set such that some large concrete pieces (larger than 1-ft) that were broken due to the impact of the first row of hammers were often struck again

by the second row of hammers. At some locations, the second strike drove the broken concrete into the base/subbase layer causing shear failure. Such localized shear failure may cause pothole or depression in the AC layer. Calibration of the rubblizer speed and the drop frequency can overcome this problem.

8. In general, the resonant frequency breaker delivers better quality rubblization than the multi-head breaker. For examples, the resonant frequency breaker, relative to the multi-head breaker, delivers:

   - Thicker rubblized material layer.
   - Much higher areas of debonded steel.
   - More destruction of the joint integrity as measured by the number of loose dowel bars.

   Table 3.4 provides a summary of the observations made during the investigation of pavement projects that were rubblized using the resonant frequency and the multi-head breakers.

## 2.2 Field Investigation after Completion of Construction

After the completion of construction, rubblized and flexible pavement projects were also investigated. The investigation consisted of two activities as follows:

1. Nondestructive deflection tests were conducted on eighteen rubblized and eleven conventional flexible pavement projects using the MDOT falling weight deflectometer (FWD). On most test sites, after the completion of the FWD tests, pavement cores were extracted and transported to the laboratory for further investigation.

Table 3.4 Comparison between the products of the resonant frequency and the multi-head breakers

| Item | Resonant frequency breaker | Multi-head breaker |
|---|---|---|
| Rubblized concrete slab | The surface of the rubblized concrete slab is less than 1 in. higher than the original concrete surface. This was expected because the rubblized material has a higher air void contents than the original concrete slab. | In most cases, the surface of the rubblized concrete slab is about 1 in. lower than the original concrete surface. The rubblized slab penetrated the sand subbase. |
| Temperature steel | Most temperature steel throughout the trench is debonded. | The temperature steel is debonded in very limited area of the trenches. |
| Dowel bars | Most dowel bars are loose and removable by hand. | Most dowel bars are embedded in the concrete. |
| Rubblized material size | The size of most rubblized material ranged from dust to less than 4 in., few pieces larger than 6-in. | The size of the rubblized material ranged from dust to more than 12 in. with a high frequency of more than 6-in size material. |
| The fractured concrete layer | The surface of the fractured concrete is uneven and varies in thickness from 0.0 to less than 4.5 in. | The surface of the fractured concrete is uneven and varies in thickness from 0 to 9 in. |
| Shear failure in the base | None was observed. | Three were observed on three pavement projects. |

2. Three manual distress surveys were conducted on eighty seven rubblized and eleven conventional flexible pavement projects.

### 2.2.1 FWD Testing and Coring

Nondestructive deflection tests were conducted on 18 rubblized pavement projects each of which consists of one or more test sites. All tests were conducted using approximately 9,000-lb load. Each test consisted of four drops. The first drop was for instrument seating, which was not recorded while the last three drops were recorded and later analyzed. The standard layout of the FWD tests and core locations is shown in Figure 3.13. The letter "X" in the figure indicates an FWD test location while the circle indicates a core location. The measured FWD deflection data were used to accomplish the following objectives:

1. Analyze the variation in the measured deflection data and hence in the structural capacity along and across the pavements.
2. Compare the rubblized pavement responses (deflections) to load to those of conventional flexible pavements.
3. Backcalculate the pavement layer and roadbed soil moduli.
4. Relate, if possible, variations in the measured deflection data to variation in the quality of the rubblized pavements.

During the FWD testing, the general pavement condition (distresses, if any) was documented and digital image(s) were obtained from each test site. At most test sites, after the completion the FWD tests, 6-in. diameter asphalt cores were extracted from the pavement. Some cores were located over cracks to verify

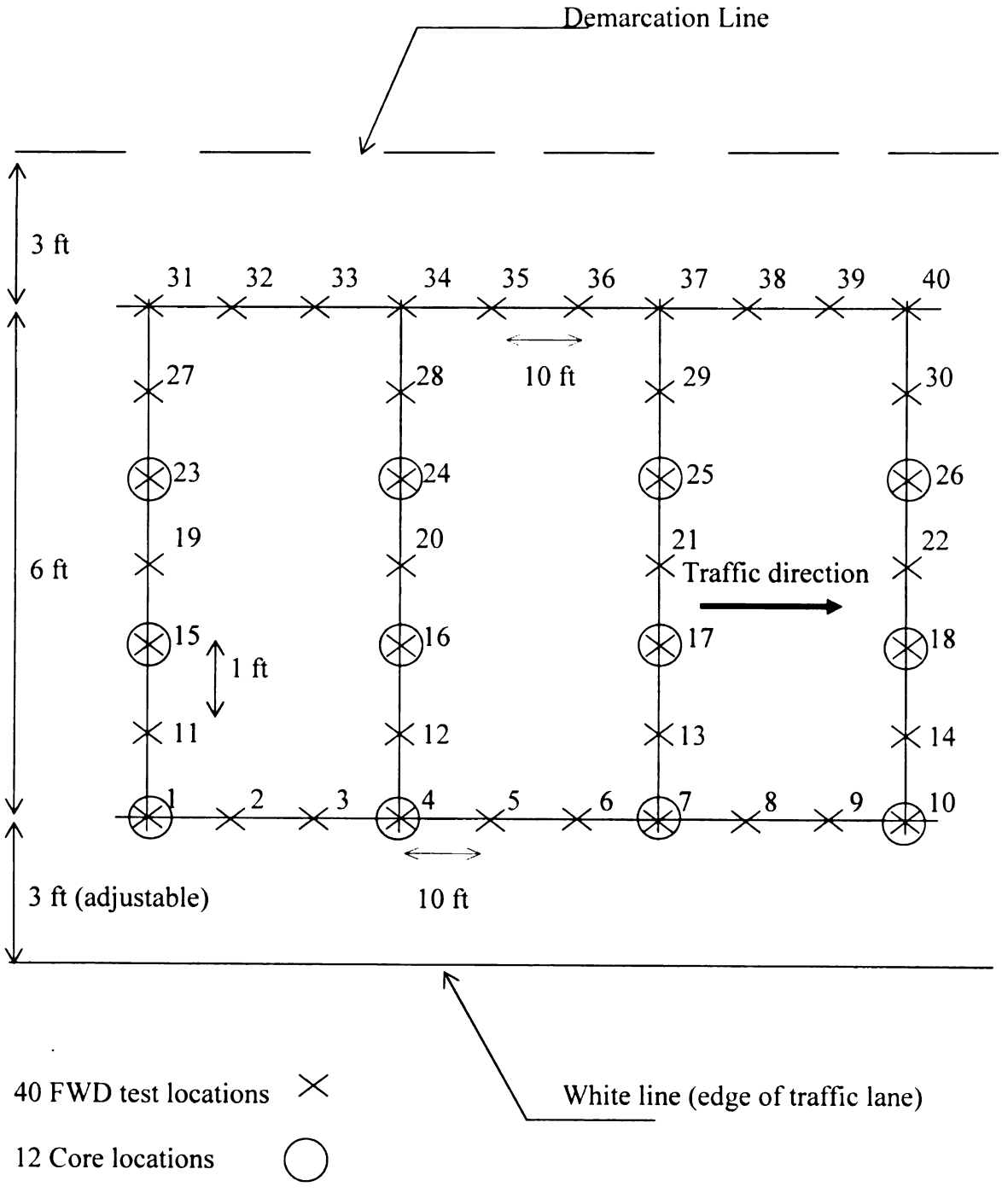


Figure 3.13 A standard layout of the FWD tests used in this study

whether or not the cracks are TDC. For these cores, the extent of the crack into each AC course was measured and recorded. The other cores were mostly located under the center of the load plate of the FWD. The cores were examined and their thickness and the thickness of each asphalt course were measured and recorded. The average core thickness was then calculated and used in the backcalculation of layer moduli. Most of the intact pavement cores were then tested to determine the physical and engineering properties (specific gravity, resilient modulus and indirect tensile strength) of the asphalt concrete. Note that, no FWD tests were conducted at test site 1 of test section 2 on M-53. However, pavement cores were extracted for verification of TDC and laboratory tests.

Note that, at some test sites, the standard FWD tests and cores layout shown in Figure 3.13 was modified for the following reasons:

1. Few FWD tests and/or core locations were added over existing cracks and/or in segregated areas.
2. The number of FWD tests and core locations were reduced on some projects due to logistic, safety and traffic control issues.
3. Additional FWD tests were conducted at four test sites to determine the repeatability of the measured deflection data and the linearity of the pavement responses to load. For each test site, the number of FWD tests (drops) and the corresponding load level are listed in Table 3.5.

Tables 3.6 and 3.7 provide lists of the rubblized and flexible pavement projects that were FWD tested and cored. The numbers of FWD tests and pavement cores are included in the tables. Finally, Table 3.8 provides a list of the

Table 3.5 A summary of the repeatability and linearity tests

| Test sites | Load (lb) | Number of drops | Load (lb) | Number of drops | Load (lb) | Number of drops | Load (lb) | Number of drops |
|---|---|---|---|---|---|---|---|---|
| 20273-21 | - | - | 9000 | 20 | 16000 | 10 | 21000 | 10 |
| 10692-12 | 5500 | 10 | 9000 | 20 | 16000 | 10 | 21000 | 10 |
| 30373-52 | 5500 | 10 | 9000 | 20 | 16000 | 10 | 21000 | 10 |
| 20102-11 | 5500 | 10 | 9000 | 20 | 16000 | 10 | 21000 | 10 |

Table 3.6 A summary of rubblized pavement projects that were FWD tested and/or cored

| Project number | Route | Control section | Job number | Test site designation number | Investigation date | Number of Cores | | | FWD test stations |
|---|---|---|---|---|---|---|---|---|---|
| | | | | | | Total | Intact | With cracks /defects | |
| 1 | I-69 | 25042 | 36020 | 10692-11 | 6/12/2001 | 12 | 10 | 0/2 | 40 |
| | I-69 | 25042 | 36020 | 10692-12 | 6/12/2001 | 12 | 9 | 0/3 | 40 |
| 2 | I-75 | 16092 | 25559 | 10753-11 | 10/24/2001 | 14 | 11 | 3/0 | 42 |
| | I-75 | 16092 | 25559 | 10753-12 | 10/24/2001 | 15 | 12 | 3/0 | 43 |
| 3 | I-96 | 23152 | 29581 | 10962-11 | 8/24/1999 | - | - | - | 28 |
| 4 | I-96 | 33084 | 28213 | 10962-21 | 8/24/1999 | 5 | - | 5/0 | 29 |
| | I-96 | 33084 | 28213 | 10962-31 | 8/24/1999 | 7 | 2 | 5/0 | 37 |
| | I-96 | 33084 | 28213 | 10964-51 | 10/21/1999 | 2 | - | 2/0 | 36 |
| 5 | I-194 | 13033 | 29670 | 11941-11 | 1999 | 10 | 0 | 10/0 | - |
| | I-194 | 13033 | 29670 | 11941-21 | 11/7/2001 | 15 | 10 | 5/0 | 43 |
| | I-194 | 13033 | 29670 | 11941-22 | 11/7/2001 | 15 | 8 | 5/2 | 43 |
| 6 | US-10 | 53022 | 37974 | 20102-11 | 6/28/2001 | 12 | 12 | - | 40 |
| | US-10 | 53022 | 37974 | 20102-12 | 6/28/2001 | 12 | 12 | - | 40 |
| 7 | US-23 | 4031 | 44350 | 20233-11 | 6/23/2001 | 11 | 10 | 0/1 | 52 |
| | US-23 | 4031 | 44350 | 20233-12 | 6/23/2001 | 10 | 7 | 0/3 | 30 |
| 8 | US-27 | 37013 | 28116 | 20273-21 | 6/4/2001 | 15 | 11 | 4/0 | 45 |
| 9 | US-27 | 37013 | 38205 | 20273-31 | 6/6/2001 | 12 | 12 | - | 40 |
| | US-27 | 37014 | 38205 | 20273-41 | 7/12/2001 | 12 | 12 | - | 40 |
| 10 | US-31 | 70013 | 38179 | 20311-11 | 6/26/2001 | 12 | 12 | - | 40 |
| 11 | US-131 | 41133 | 33914 | 21313-11 | 10/26/1999 | - | - | - | 30 |
| 12 | US-131 | 3112 | 28143 | 21311-21 | 11/3/1999 | - | - | - | 34 |
| 13 | US-131 | 3112 | 32373 | 21311-31 | 9/1/1999 | - | - | - | 51 |
| 14 | M-15 | 25092 | 45534 | 30153-11 | 11/21/2001 | 16 | 12 | 4/0 | 43 |
| 15 | M-37 | 41033 | 26691 | 30371-11 | 11/4/1999 | 5 | 0 | 5/0 | - |
| | M-37 | 41033 | 26691 | 30373-11 | 11/4/1999 | 4 | 0 | 4/0 | 83 |
| 16 | M-37 | 41033 | 38190 | 30373-51 | 6/19/2001 | 12 | 12 | - | 40 |
| | M-37 | 41033 | 38190 | 30373-52 | 6/19/2001 | 12 | 12 | - | 40 |
| 17 | M-37 | 41033 | 26691 | 30373-61 | 11/6/2001 | 18 | 15 | 2/1 | 42 |
| 18 | M-53 | 44031 | 36021 | 30531-11 | 11/02/1999 | - | - | - | 45 |
| 19 | M-53 | 74012 | 19729 | 30531-21 | 1999 | 20 | 14 | 6/0 | - |

The designation number of each test site consists of a seven-digit number. The first digit designates road type (1 = Interstate, 2 = U.S., 3 = Michigan). The second through the fourth digits express the highway/route number. The fifth digit designates the traffic direction (1 = North, 2 = East, 3 = South, 4 = West). The sixth digit designates the test section number. Finally, the seventh digit expresses the test site number. For example, a designation number of 11941-12 implies I-194, northbound section 1 test site 2

Table 3.7 A summary of flexible pavement projects that were FWD tested and/or cored

| Project number | Route | Control section | Job number | Test site designation number | Investigation date | Number of Cores | | | FWD test stations |
|---|---|---|---|---|---|---|---|---|---|
| | | | | | | Total | Intact | With cracks /defects | |
| 1 | I-96 | 23151 | 29581 | 10962-41 | 10/11/1999 | - | - | - | 34 |
| 2 | US-27 | 37014 | 38205 | 20273-11 | 6/04/2001 | 12 | 12 | 0/0 | 40 |
| 3 | US-41 | 07013 | 34037 | 20411-11 | 8/21/2001 | 14 | 12 | 2/0 | 42 |
| | US-41 | 07013 | 34037 | 20411-12 | 8/21/2001 | 14 | 12 | 2/0 | 42 |
| 4 | M-20 | 37022 | 38196 | 30202-11 | 6/06/2001 | 11 | 9 | 2/0 | 30 |
| | M-20 | 37022 | 38196 | 30202-12 | 6/06/2001 | 12 | 9 | 3/0 | 29 |
| 5 | M-42 | 83041 | 44396 | 30422-11 | 11/7/2002 | 27 | 24 | 3/0 | 52 |
| 6 | M-50 | 23052 | 41007 | 30502-11 | 11/21/2001 | 13 | 12 | 1/0 | 41 |
| 7 | M-50 | 23052 | 45984 | 30502-21 | 5/29/2002 | 38 | 22 | 16/0 | 48 |
| 8 | M-52 | 33051 | 34530 | 30521-11 | 11/13/2002 | 24 | 20 | 4/0 | 44 |
| 9 | M-52 | 76011 | 36580 | 30521-21 | 11/25/2002 | 10 | 6 | 4/0 | 40 |
| 10 | M-55 | 72022 | 31009 | 30552-11 | 8/20/2001 | 15 | 12 | 3/0 | 41 |
| | M-55 | 72022 | 31009 | 30552-12 | 8/20/2001 | 13 | 12 | 2/0 | 37 |
| 11 | Marsh Rd. | NA | NA | Marsh | 10/11/2000 | 8 | 2 | 6/0 | 58 |

The test site designation number is the same as that stated in Table 3.6

Table 3.8 A summary of the number of rubblized and flexible pavement test sites that were FWD tested and cored.

| Study | Number of test sites that were FWD tested | | Number of test sites that were cored | |
|---|---|---|---|---|
| | Rubblized pavements | Flexible pavements | Rubblized pavements | Flexible pavements |
| The underperformance of rubblized pavements and the causes of TDC | 27 | 2 | 25 | 1 |
| The study of TDC in flexible pavements | - | 12 | - | 12 |
| Total | 27 | 14 | 25 | 13 |

total number of rubblized and flexible test sites that were FWD tested and cored in this study.

### 2.2.2 Manual Distress Survey of Rubblized Pavements

MDOT surveys each pavement section every other year. Since rubblized pavements are relatively new, only limited historical distress data for rubblized pavements were available in the MDOT Pavement Management System (PMS) databank. Further, the distress data does not differentiate between TDC and other types of cracks. Consequently, three manual distress surveys of rubblized pavements were undertaken by the research team to accomplish the following objectives:

1. Determine the number of underperforming rubblized pavement projects exhibiting premature distresses including TDC.
2. Determine the causes, if possible, of the underperformance of rubblized pavements.
3. Document the characteristics of TDC for the purposes of developing a TDC identification procedure and understanding TDC initiation and propagation.

Seventy eight rubblized pavement projects were surveyed during each of the three distresses surveys in August and September 2001, May 2002 and May and June 2003 as listed in Appendix A. Only 67 projects were surveyed in all three distress surveys. The reason is that few projects are located in remote areas of the state. For the rubblized pavement projects that were surveyed only once or twice, the

data were simply transferred from one year to the other. By doing so, distress data for 87 rubblized pavement projects were obtained. Appendix A provides a list of the 87 rubblized pavement projects and the year during which each project was surveyed. Nevertheless, in all three surveys, the survey team consisted of two persons and used the following procedure:

1. For each rubblized project, the inventory data (project location and boundaries, pavement surface age, asphalt mix types and rubblizing equipment) and the pavement historical distress data, when available, were obtained from MDOT.
2. At each project location, the distress along the entire project was observed by driving on the right pavement shoulder at creep speed. During the drive, notes were taken as to the consistency and uniformity of the pavement condition along the project.
3. After observing the general pavement condition, the survey crew walked along one to three 300-ft long segments located along the project. When the overall pavement condition was inconsistent, the research team walked or drove at creep speed along three 300-ft segments located at the beginning, middle and the end of the project. On the other hand, when the pavement condition was uniform, the research team surveyed only one representative 300-ft long segment.
4. For each 300-ft segment, detailed distress data were observed and recorded and digital images were obtained when needed for later verification. The distress data included the location, type, extent and

severity of longitudinal and transverse cracks, raveling, segregation, patching, depression and other conditions that adversely affect pavement performance. For transverse cracks, notes were made whether the cracks were reflective or likely TDC. For longitudinal cracks, notes were made whether the cracks were reflective, alligator (bottom-up crack) or likely TDC. Notes were also taken when longitudinal and/or transverse cracks were located in segregated areas.

5. For each project where rut was evident, rut depth measurements were made at several locations using a 6-ft long beam.
6. For some projects, the research team drove along the project at the posted speed limit and observed and recorded the ride quality in terms of driving comfort.

Summaries of the three distress surveys are provided in Tables 3.9 through 3.11 in terms of the number of projects exhibiting certain types of distress. As can be seen from Table 3.11, the distress data collected in 2003 indicate that:

1. Eight rubblized pavement projects showed no signs of distress.
2. All projects that were constructed in 1996 and earlier exhibited certain type of distress.
3. Since 1987 when concrete pavement rubblization started, capital preventive maintenance and rehabilitation actions were taken on 19 rubblized projects. These actions included mill and fill, AC overlay, chip seal and micro surfacing. Hence, for those projects, the distress data listed were those observed on the new maintained and/or rehabilitated surface.

Table 3.9 A summary of the distresses survey of 86 rubblized pavement projects in 2001

| Year of Completion | Number of projects | Number of rubblized pavement projects with certain distress type in 2001 | | | | | | | | | | | | | | Number of projects with no distress | Rehabilitated projects | |
|---|---|---|---|---|---|---|---|---|---|---|---|---|---|---|---|---|---|---|
| | | Transverse | | | Longitudinal | | | Other types of distress | | | | | | | | | Number of projects | Age when rehabilitated (years) |
| | | TDC | RC | RJ | TDC | RC | ALC | S | RV | P | PH | R | BC | B | D | | | |
| 1987 | 1 | 1 | 1 | | | | | | | | | | | | | | 1 | 15 |
| 1988 | 2 | 1 | 1 | | 1 | | | 1 | | | | | | | | 1 | 1 | 11 |
| 1989 | 2 | 2 | 1 | | 1 | | | 1 | 1 | 1 | 1 | 1 | | | | | 1 | 11 |
| 1990 | 6 | 2 | 4 | | 5 | | | 4 | 1 | 1 | | 3 | | | | 1 | 3 | 6, 9 and 9 |
| 1991 | | | | | | | | | | | | | | | | | | |
| 1992 | 4 | 3 | 4 | 1 | 3 | | | 3 | 1 | | | | | | | | 1 | 8 |
| 1993 | 5 | 3 | 5 | | 3 | | 1 | 5 | 1 | 1 | 1 | 3 | | | | | 2 | 6 and 7 |
| 1994 | 4 | 2 | 1 | 1 | 2 | | | 2 | 1 | | | 1 | | 1 | | | 1 | 7 |
| 1995 | 4 | 4 | 1 | | 4 | | | 3 | 1 | 1 | | 2 | | | | | 1 | 6 |
| 1996 | 8 | 4 | 2 | | 6 | | 1 | 5 | 1 | 1 | | 2 | | 1 | | | | |
| 1997 | 11 | 4 | 1 | 3 | 7 | | | 7 | 3 | | | 5 | | | | 1 | 2 | 3 and 4 |
| 1998 | 17 | 6 | 4 | 2 | 13 | | 1 | 14 | 2 | 2 | 1 | 2 | | 1 | 1 | 1 | | |
| 1999 | 14 | 2 | 1 | 1 | 7 | | 1 | 10 | | 1 | | 2 | | 1 | | 2 | | |
| 2000 | 5 | | | | | | | 3 | | | 1 | | | | | 2 | | |
| 2001 | 3[1] | | | | | | | | | | | | | | | 3 | | |
| Total | 86 | 34 | 26 | 8 | 52 | | 4 | 58 | 12 | 8 | 4 | 21 | 0 | 4 | 1 | 11 | 13 | |

TDC = Top-down crack, RC = Reflective crack, RJ = Rough joint, ALC = Alligator crack, S = Segregation, RV = Raveling, P = Patches, PH = Pot hole, R = Rut, BC = Block crack, B = Bleeding, D = Depression

1 There was one rubblized pavement project under construction during the 2001 distress survey thus; only 3 projects were reported as completed in 2001 in Table 3.9 and 4 projects in Tables 3.10 and 3.11.

Table 3.10 A summary of the distresses survey of 87 rubblized pavement projects in 2002

| Year of Completion | Number of projects | Number of rubblized pavement projects with certain distress type in 2002 | | | | | | | | | | | | | | Number of projects with no distress | Rehabilitated projects | |
|---|---|---|---|---|---|---|---|---|---|---|---|---|---|---|---|---|---|---|
| | | Transverse | | | Longitudinal | | | Other types of distress | | | | | | | | | Number of projects | Age when rehabilitated (years) |
| | | TDC | RC | RJ | TDC | RC | ALC | S | RV | P | PH | R | BC | B | D | | | |
| 1987 | 1 | 1 | 1 | | | | | 1 | | | | | | | | | 1 | 15 |
| 1988 | 2 | 1 | 1 | | 1 | | | 1 | | | | | | | | 1 | 1 | 11 |
| 1989 | 2 | 2 | 1 | | 1 | | | 1 | 1 | 1 | 1 | 1 | | | | | 1 | 11 |
| 1990 | 6 | 3 | 5 | 1 | 5 | | | 4 | 1 | 1 | | 3 | | | | | 3 | 6, 9 and 9 |
| 1991 | | | | | | | | | | | | | | | | | | |
| 1992 | 4 | 2 | 4 | 1 | 3 | | | 3 | 1 | | | | | | | | 2 | 8 and 10 |
| 1993 | 5 | 3 | 5 | 1 | 3 | | 1 | 5 | 2 | 1 | 1 | 3 | | | | | 2 | 6 and 7 |
| 1994 | 4 | 4 | 2 | 1 | 3 | | | 2 | 1 | | | 1 | | 1 | | | 1 | 7 |
| 1995 | 4 | 3 | | | 3 | | | 3 | 1 | 1 | | 2 | | | | | 1 | 6 |
| 1996 | 8 | 4 | 2 | | 6 | | 1 | 5 | 2 | 2 | | 2 | 1 | 1 | | | 1 | 6 |
| 1997 | 11 | 4 | 2 | 3 | 8 | | | 7 | 3 | | | 5 | | | | 1 | 2 | 3 and 4 |
| 1998 | 17 | 7 | 4 | 2 | 13 | | 1 | 14 | 4 | 2 | 1 | 3 | | 1 | 1 | 1 | | |
| 1999 | 14 | 2 | 1 | 2 | 7 | | 1 | 10 | 2 | 2 | 1 | 2 | | 1 | | 2 | | |
| 2000 | 5 | | | | | | | 3 | | | 1 | | | | | 2 | | |
| 2001 | 4 | | | 1 | | | | 1 | | | | | | | | 3 | | |
| Total | 87 | 36 | 28 | 12 | 53 | | 4 | 60 | 18 | 10 | 5 | 22 | 1 | 4 | 1 | 10 | 15 | |

TDC = Top-down crack, RC = Reflective crack, RJ = Rough joint, ALC = Alligator crack, S = Segregation, RV = Raveling, P = Patches, PH = Pot hole, R = Rut, BC = Block crack, B = Bleeding, D = Depression

*Table 3.11 A summary of the distresses survey of 87 rubblized pavement projects in 2003*

| Number of rubblized pavement projects with certain distress type in 2003 | | |

Table 3.11 A summary of the distresses survey of 87 rubblized pavement projects in 2003

| Year of Completion | Number of projects | Number of rubblized pavement projects with certain distress type in 2003 | | | | | | | | | | | | | | Number of projects with no distress | Rehabilitated projects | |
|---|---|---|---|---|---|---|---|---|---|---|---|---|---|---|---|---|---|---|
| | | Transverse | | | Longitudinal | | | Other types of distress | | | | | | | | | Number of projects | Age when rehabilitated (years) |
| | | TDC | RC | RJ | TDC | RC | ALC | S | RV | P | PH | R | BC | B | D | | | |
| 1987 | 1 | 1 | 1 | | 1 | | | 1 | 1 | | | | | | | | 1 | 15 |
| 1988 | 2 | 1 | 2 | | 1 | | | 1 | | | | | | | | | 1 | 11 |
| 1989 | 2 | 2 | 1 | | 1 | | | 1 | 1 | 1 | 1 | 1 | | | | | 1 | 11 |
| 1990 | 6 | 3 | 6 | 1 | 6 | 1 | | 4 | 1 | 1 | | 3 | | | | | 4 | 6, 9, 9 and 13 |
| 1991 | | | | | | | | | | | | | | | | | | |
| 1992 | 4 | 3 | 4 | 1 | 3 | | | 3 | 1 | | | | | | | | 2 | 8 and 10 |
| 1993 | 5 | 5 | 5 | 2 | 5 | | 1 | 5 | 2 | 1 | 1 | 3 | | | | | 3 | 6, 7 and 10 |
| 1994 | 4 | 3 | 3 | 1 | 3 | | | 2 | 1 | | | 1 | | 1 | | | 1 | 7 |
| 1995 | 4 | 4 | 2 | | 4 | | | 3 | 1 | 1 | | 2 | | | | | 1 | 6 |
| 1996 | 8 | 2 | 3 | | 5 | | 1 | 4 | 2 | 3 | | 2 | 1 | 1 | | | 2 | 6 and 7 |
| 1997 | 11 | 4 | 5 | 3 | 8 | | | 8 | 3 | 1 | | 5 | | | | 1 | 2 | 3 and 4 |
| 1998 | 17 | 10 | 6 | 4 | 14 | | 1 | 14 | 3 | 2 | 1 | 2 | | 1 | 1 | 1 | 1 | 5 |
| 1999 | 14 | 7 | 1 | 2 | 9 | | 1 | 10 | 2 | 3 | 1 | 2 | | 1 | | 2 | | |
| 2000 | 5 | 2 | 1 | | 3 | | | 3 | | | 1 | | | | | 2 | | |
| 2001 | 4 | 1 | 0 | 1 | 2 | | | 1 | | | | | | | | 2 | | |
| Total | 87 | 48 | 40 | 15 | 65 | 1 | 4 | 60 | 18 | 13 | 5 | 21 | 1 | 4 | 1 | 8 | 19 | |

TDC = Top-down crack, RC = Reflective crack, RJ = Rough joint, ALC = Alligator crack, S = Segregation, RV = Raveling, P = Patches, PH = Pot hole, R = Rut, BC = Block crack, B = Bleeding, D = Depression

4. Sixty rubblized pavement projects exhibited various degrees of segregation. On most of these projects, longitudinal and transverse TDC can be found in the segregated areas. Further, eighteen of these projects have developed various degrees of raveling in the segregated areas (see Figures 3.14 and 3.15).

5. Longitudinal and transverse cracks are the dominant types of distress. Several types of longitudinal and transverse cracks were found as follows:

   a) Sixty five projects exhibited longitudinal TDC as shown in Figure 3.16.

   b) Forty eight projects exhibited transverse TDC as shown in Figure 3.16.

   c) Forty projects exhibited reflective cracks as shown in Figures 3.17 and 3.18.

   d) Four projects exhibited alligator cracks in the wheel paths as shown in Figure 3.19.

6. Fifteen projects exhibited roughness over transverse joints of the original concrete pavements. A rough joint is a forerunner of reflective transverse cracks and is defined as a slight but measurable hump in the AC surface along the joint. On five of these projects, transverse reflective cracks have already developed at some locations while other locations showed rough joints only. Ten of the fifteen projects exhibited rough joints only and the reflective transverse cracks were not developed as of May 2003, which represents an increase of 2 projects since the 2001 distress survey.

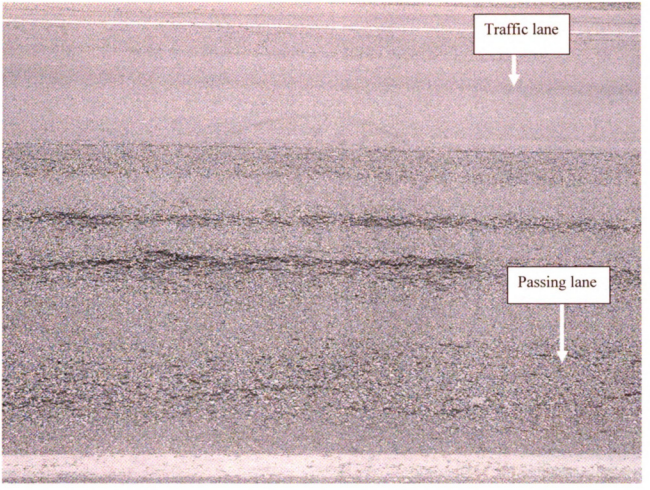


Figure 3.14 The relative pavement conditions in segregated area (passing lane) and in a non-segregated area (traffic lane) 2 years after construction on US-23 SB, control section 47013, job number 29768, BMP 5.5 and EMP 7.0, May 2002.

Figure 3.15 The pavement condition in segregated area on US-12 EB, control section 81063, job number 26796, BMP 3.6 and EMP 4.1, May 2002

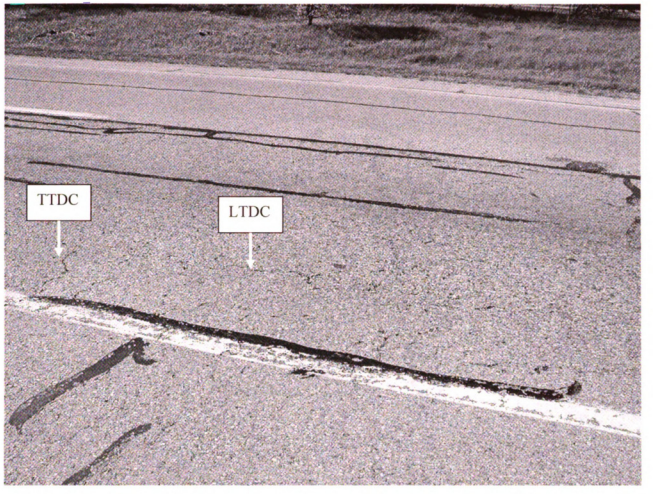


Figure 3.16 Longitudinal and transverse TDC (LTDC and TTDC) on I-96 EB, control section 33084, job number 28213, BMP 9.0 and EMP 17.5, May 2002

Figure 3.17 Reflective joint crack on M-50, control section 46082, job number 30388, BMP 3.9 and EMP 4.4, May 2002

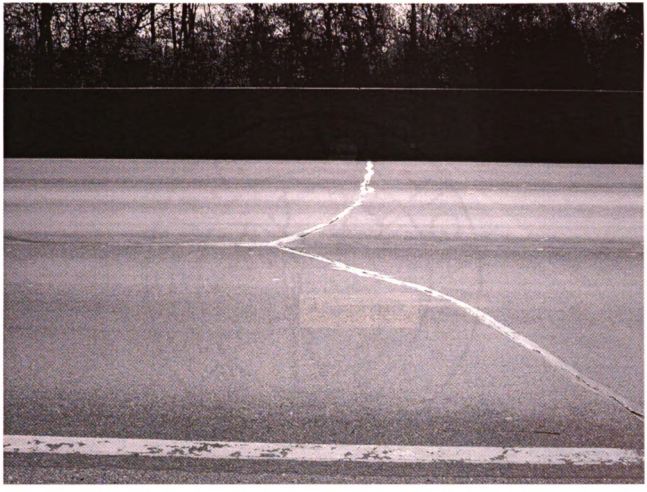

Figure 3.18 Crack reflective cracks on US-131, control section 41131, job number 21089, BMP 6.5 and EMP 10.1, May 2002

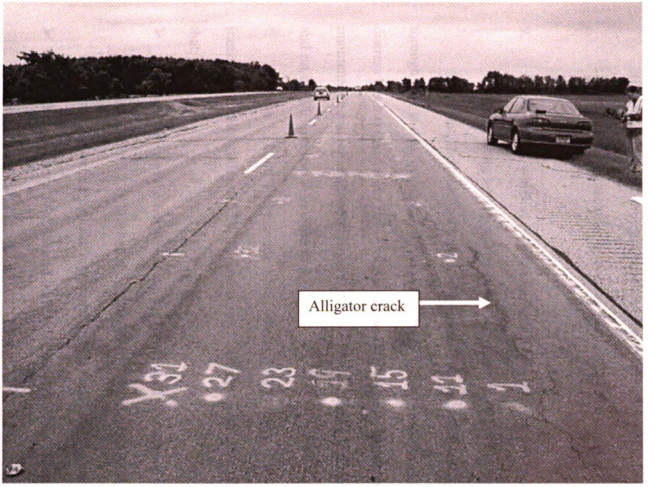


Figure 3.19 Alligator cracks in the wheel path, US-27, control section 37013, job number 28116, BMP 9.0, and EMP 11.7, June 2001

7. Twenty one projects exhibited measurable rut. The rut depth varied from about 0.125 to 1.0 in.

8. Potholes were found on five projects (see Figure 3.20), patches on 13 projects (Figure 3.21); four projects exhibited low severity bleeding; one project exhibited block cracking, and one project exhibited depression along a limited area.

9. Shear failure, which is reported in Table 3.8 as patches, was found at three locations along I-196 south of Grand Rapids as shown in Figure 3.22.

Note that, the basic difference between the distress data listed in Tables 3.9 through 3.11 is that, in general, the total number of projects exhibiting certain type of distress has increased from 2001 to 2002 and to 2003 surveys. However, Due to maintenance and rehabilitation activities, the numbers of projects exhibiting raveling and rut in 2003 are less than those in 2002.

Tables 3.12 and 3.13 provide more information regarding the locations of the transverse and longitudinal TDC. Examination of the data in the two tables indicates that:

- The majority of the transverse and longitudinal TDC occurred in segregated areas (Figure 3.23). Further, the longitudinal TDC are frequently found at the edges of the wheel path for both segregated and non segregated areas.
- For the transverse TDC located outside segregated areas, they are either temperature cracks (Figure 3.24) or transverse TDC associated with longitudinal TDC (Figure 3.25).

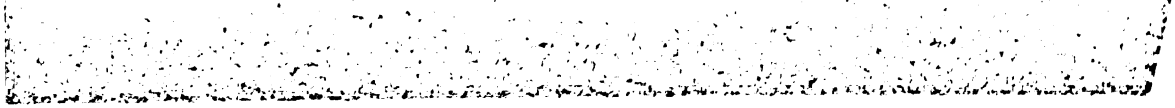

Figure 3.20 Pothole along US-131, control section 41133, job number 33914, BMP 3.2 and EMP 8.7, May 2002

Figure 3.21 Patches on M-53, control section 74012, job number 29729, BMP 9.0 and EMP 13.0, May 2002

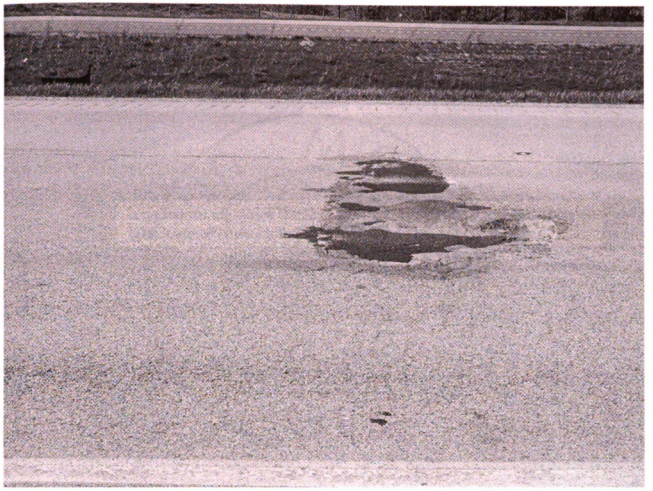

Figure 3.22 A shear failure on I-196 NB, control section 70024, job number 35987, BMP 12.6 and EMP 15.6, May 2002

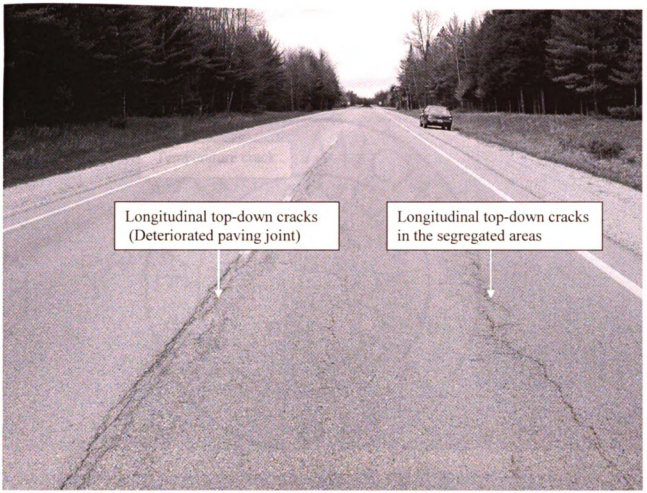


Figure 3.23 Deteriorated paving joint between lanes and longitudinal TDC at edge of the wheel path in the segregated area on US 131, control section 83032, job number 34060, BMP 13.0 and EMP 18.6, May 2002

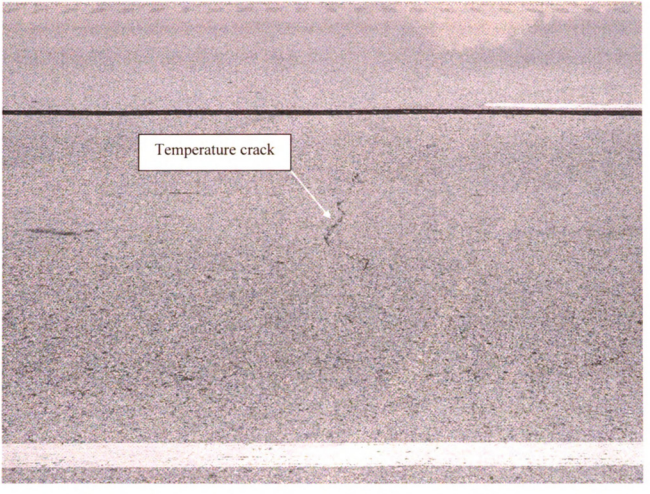


Figure 3.24 The initiation of a temperature crack, US-27, control section 37014, job number 38206, BMP 7.2 and EMP 14.4, May 2003

Figure 3.25 TTDC associated with LTDC, M-27, control section 16302, job number 26672, BMP 9.3 and EMP 11.4, May 2003

Table 3.12 Number of projects having transverse TDC in and outside segregated areas

| Inside SG areas | Outside SG areas | | |
|---|---|---|---|
| | Total | Temperature cracks | Associated with LTDC |
| 30 | 25 | 24 | 9 |

Table 3.13 Number of projects having longitudinal TDC in and outside segregated areas at different locations on the pavements

| Locations of LTDC | Number of projects exhibiting LTDC and their locations | | | Percent of projects exhibiting LTDC in the specified location | |
|---|---|---|---|---|---|
| | Total | In segregated areas | Outside segregated areas | In segregated areas | Outside segregated areas |
| Edges of wheel path | 49 | 33 | 21 | 67 | 43 |
| In wheel path | 29 | 20 | 12 | 69 | 41 |
| Center of lane | 38 | 31 | 9 | 82 | 24 |
| Between lanes | 43 | 32 | 15[1] | 74 | 35 |
| Edge of lane | 16 | 11 | 6 | 69 | 38 |
| Total | 65 | 49 | 31 | 75 | 48 |

1 – The LTDC are deterioration of the paving joints (see Figure 3.23).

Table 3.14 provides a summary of the rubblized pavement projects having TDC sorted by their AC surface course mix type. Further, the original AC mix type of rehabilitated rubblized pavement projects are summarized in Table 3.15. Examination of the data in the two tables indicates that:

- The average service life (time between rubblization and rehabilitation) of nineteen of the 87 rubblized projects (see Table 3.15) is about 7 years compared to the 20 years design period.
- Most asphalt mixes of the AC surface course show underperformance in terms of LTDC and TTDC including the superpave mixes. The exemptions are the 3 projects that were surfaced with 13A-MOD and SMA-C mixes. The pavements are more than 5 year old and showing no sign of distress.
- The 4B and 4C mixes show one of the worst performances. This was expected because all three mixes are well known to be brittle and relatively dry (low asphalt contents). The two mixes were originally designed to overcome the problem of rutting in Michigan.

## 3.0 LABORATORY INVESTIGATION

After the AC cores were extracted from the pavements during the field investigation, they were transported to the Pavement Research Center of Excellence (PRCE) laboratory for testing. Since one of the purposes of coring was to verify whether or not the cracks found on the pavements are TDC, a good number of cores were obtained over cracks. In the laboratory, the thickness of each core and the thickness of

Table 3.14 A summary of the number of the no-rehabilitated rubblized pavement projects having TDC in 2003 sorted by the AC surface course mix types

| AC surface course mix type | Average pavement surface age (years) | Number of Projects | | | | Percent of the projects with the specified mix type | | | |
|---|---|---|---|---|---|---|---|---|---|
| | | Total | With TDC | With LTDC | With TTDC | Total | With TDC | With LTDC | With TTDC |
| 1100-20AA | 13 | 3 | 3 | 3 | 3 | 100 | 100 | 100 | 100 |
| 1100-20AAA | 13 | 1 | 1 | 1 | 1 | 100 | 100 | 100 | 100 |
| 1300-20AAA | 11 | 2 | 1 | 1 | 1 | 100 | 50 | 50 | 50 |
| 1300T-20AAA | 7 | 1 | 1 | 1 | 0 | 100 | 100 | 100 | 0 |
| 13A | 5 | 8 | 5 | 4 | 5 | 100 | 63 | 50 | 63 |
| 13A-MOD | 5 | 1 | 0 | 0 | 0 | 100 | 0 | 0 | 0 |
| 1500 T | 5 | 1 | 1 | 1 | 1 | 100 | 100 | 100 | 100 |
| 3B | 10 | 1 | 1 | 1 | 1 | 100 | 100 | 100 | 100 |
| 4B | 7 | 13 | 13 | 13 | 11 | 100 | 100 | 100 | 85 |
| 4C | 6 | 15 | 14 | 13 | 9 | 100 | 93 | 87 | 60 |
| 4C-MOD | 5 | 1 | 1 | 1 | 0 | 100 | 100 | 100 | 0 |
| 4C-SHRP | 7 | 1 | 1 | 1 | 0 | 100 | 100 | 100 | 0 |
| SMA-C | 6 | 2 | 0 | 0 | 0 | 100 | 0 | 0 | 0 |
| Superpave | 4 | 18 | 12 | 12 | 6 | 100 | 67 | 67 | 33 |
| All mix types | 6 | 68 | 54 | 52 | 38 | 100 | 79 | 76 | 56 |

Table 3.15 A summary of the rehabilitated rubblized pavement projects and their average service life (years in service until the first rehabilitation) sorted by the original AC surface course mix types

| The original AC surface course mix type | Number of rehabilitated projects | Average time between rubblization and rehabilitation (years) |
|---|---|---|
| 4C | 3 | 5 |
| 4B | 6 | 6 |
| 3B | 1 | 6 |
| SMA-C, SMA-P, 4C | 1 | 7 |
| 1500-20AAA-MOD | 1 | 8 |
| 1500-20AAA | 4 | 10 |
| 1100-20AA | 3 | 11 |
| 1300T-20AAA | 1 | Unknown |
| All mix types | 19 | 7 |

each AC course were measured at the four ends of two orthogonal diameters. The average thickness of the core and the average thickness of each AC course were calculated and are listed in Table 3.16. In addition, for each core, the width of the crack was examined and its extent through each AC course was measured. The extent of the crack through each AC course was then normalized relative to the course thickness. The results (the percent of crack propagation through each AC course) are also provided in Table 3.16. The data in the table indicate that, for some cores, the cracks have propagated through the AC surface layer only while for others; the cracks have propagated through the AC leveling and/or base courses. For six of the eight cores that the cracks have propagated throughout the AC layer, the width of the cracks was wider at the top than at the bottom of the cores. For the other two cores (shaded rows in Table 3.16), the cracks are wider at the bottom of the core. This was expected because the two cores were taken over two joint reflective cracks. Later, during the course of the study, pavement cores were obtained from cracked and non-cracked areas. The former cores were used to verify the existence of TDC and the latter for laboratory testing. The steps that were taken during the sample preparation and details of each test are presented in the next sections.

## 3.1 Sample Preparation

In general, the AC cores that were extracted from the pavements could be divided into two categories; intact cores and cores with cracks and/or defects. Each core was carefully examined and cataloged. After cataloging all cores of one test site, the following steps were taken to prepare them for testing:

Table 3.16 Crack depth measurement of cores extracted from rubblized pavement projects to verify whether or not the cracks are TDC

| Test site | Crack type | Thickness (in.) | | | | | Crack depth per AC course (%) | | | | TDC |
|---|---|---|---|---|---|---|---|---|---|---|---|
| | | Total | O | S | L | B | O | S | L | B | |
| 11942-11 | TJ | 4.9 | - | 1.3 | 1.6 | 2.0 | - | 100 | 100 | 100 | No |
| | LC | 5.0 | - | 1.5 | 1.6 | 1.9 | - | 100 | 100 | 100 | Yes |
| | LC | 5.0 | - | 1.2 | 1.8 | 2.0 | - | 100 | 100 | 100 | Yes |
| | DC | 6.3 | - | 1.5 | 2.2 | 2.6 | - | 100 | 100 | 0 | Yes |
| | LC | 6.0 | - | 1.6 | 1.6 | 2.8 | - | 100 | 100 | 25 | Yes |
| | TJ | 4.8 | - | 1.4 | 1.4 | 2.0 | - | 100 | 100 | 100 | No |
| | LC/TC | 5.9 | - | 1.7 | 2.4 | 1.8 | - | 100 | 100 | 100 | Yes |
| | TC | 6.1 | - | 1.7 | 2.2 | 2.2 | - | 100 | 100 | 100 | Yes |
| | LC | 6.0 | - | 1.3 | 2.6 | 2.1 | - | 100 | 100 | 0 | Yes |
| | LC | 6.4 | - | 1.3 | 2.4 | 2.7 | - | 100 | 100 | 0 | Yes |
| 30371-11 | TC/LC | 6.2 | - | 1.8 | 2.2 | 2.2 | - | 100 | 20 | 0 | Yes |
| | LC | 6.4 | - | 1.7 | 2.2 | 2.5 | - | 100 | 0 | 0 | Yes |
| | LC | 4.9 | - | 1.3 | 1.6 | 2.0 | - | 100 | 100 | 0 | Yes |
| | LC | 5.1 | - | 1.6 | 1.5 | 2.0 | - | 100 | 100 | 0 | Yes |
| | LC | 5.1 | - | 1.6 | 1.5 | 2.0 | - | 100 | 10 | 0 | Yes |
| 30373-11 | LC | 5.6 | - | 1.1 | 1.8 | 2.7 | - | 100 | 90 | 0 | Yes |
| | LC | 6.1 | - | 1.3 | 1.9 | 2.9 | - | 100 | 10 | 0 | Yes |
| | LC | 6.2 | - | 1.4 | 1.8 | 3.0 | - | 100 | 50 | 0 | Yes |
| | TC | 4.4 | - | 1.2 | 1.6 | 1.6 | - | 100 | 100 | 100 | Yes |
| 10962-21 | LC | 6.8 | - | 1.3 | 1.6 | 3.9 | - | 100 | 45 | 0 | Yes |
| | LC | 7.2 | - | 1.2 | 1.6 | 4.4 | - | 100 | 50 | 0 | Yes |
| | LC | 6.9 | - | 1.1 | 1.7 | 4.1 | - | 100 | 75 | 0 | Yes |
| | LC | 6.5 | - | 1.1 | 1.7 | 3.7 | - | 100 | 30 | 0 | Yes |
| | LC | 6.4 | - | 1.1 | 1.5 | 3.8 | - | 100 | 0 | 0 | Yes |
| | None | 6.8 | - | 1.1 | 1.8 | 3.9 | - | 0 | 0 | 0 | No |
| | None | 7.0 | - | 1.2 | 1.7 | 4.1 | - | 0 | 0 | 0 | No |
| 10962-31 | LC | 6.3 | - | 1.2 | 1.8 | 3.3 | - | 100 | 60 | 0 | Yes |
| | LC | 6.5 | - | 1.2 | 1.6 | 3.7 | - | 100 | 75 | 0 | Yes |
| | TC | 6.4 | - | 1.2 | 2.0 | 3.2 | - | 100 | 40 | 0 | Yes |
| | TC | 5.7 | - | 1.2 | 1.7 | 2.8 | - | 100 | 100 | 30 | Yes |
| | TC | 6.1 | - | 1.3 | 1.9 | 2.9 | - | 100 | 100 | 100 | Yes |
| 109642 | LC | 7.5 | - | 1.5 | 1.8 | 4.2 | - | 100 | 0 | 0 | Yes |
| | TC | 7.9 | - | 1.3 | 2.0 | 4.6 | - | 100 | 0 | 0 | Yes |

O=Overlay, S=Surface, L=Leveling, B=Base, DC=Diagonal cracks, LC=Longitudinal cracks, TC=Transverse cracks, TJ=Transverse joint and N/A=Not available or undetermined

Table 3.16 Crack depth measurement of cores extracted from rubblized pavement projects to verify whether or not the cracks are TDC (continued)

| Test site | Crack type | Thickness (in.) | | | | | Crack depth per AC course (%) | | | | TDC |
|---|---|---|---|---|---|---|---|---|---|---|---|
| | | Total | O | S | L | B | O | S | L | B | |
| 10753-11 | LC | 4.7 | - | 1.8 | 1.0 | 1.8 | - | 60 | 0 | 0 | Yes |
| | LC | 4.7 | - | 1.8 | 1.4 | 1.5 | - | 100 | 100 | 100 | Yes |
| | TC | 4.5 | - | 1.8 | 1.0 | 1.9 | - | 100 | 100 | 100 | Yes |
| 10753-12 | DC | 3.5 | - | 1.0 | 1.5 | 1.0 | - | 100 | 100 | 100 | N/A |
| | TC | 3.9 | - | 1.5 | 1.0 | 1.4 | - | 100 | 100 | 100 | Yes |
| | DC | 3.5 | - | 1.0 | 1.4 | 1.1 | - | 100 | 100 | 100 | Yes |
| 11941-21 | N/A | 8.0 | 1.5 | 1.6 | 2.1 | 2.7 | 0 | 100 | 100 | 0 | Yes |
| | N/A | 7.7 | 1.3 | 1.6 | 2.3 | 2.6 | 0 | 100 | 100 | 100 | N/A |
| | LC | 7.8 | 1.4 | 1.6 | 2.5 | 2.3 | 100 | 100 | 100 | 100 | Yes |
| | TC | 7.3 | 1.4 | 1.5 | 2.3 | 2.1 | 100 | 100 | 100 | 100 | N/A |
| | LC | 7.9 | 1.4 | 1.6 | 2.3 | 2.7 | 100 | 100 | 100 | 100 | N/A |
| 11941-22 | TC | 7.1 | 1.4 | 1.5 | 2.0 | 2.2 | 30 | 0 | 0 | 0 | Yes |
| | TC | 7.8 | 1.5 | 1.4 | 2.2 | 2.7 | 65 | 0 | 0 | 0 | Yes |
| | LC | Broken to pieces | | | | | 100 | 100 | 100 | 100 | N/A |
| | TJ | 7.4 | 1.5 | 1.5 | 1.8 | 2.7 | 100 | 100 | 100 | 100 | No |
| 20273-21 | LC | 4.6 | - | 1.3 | 1.3 | 2.1 | - | 0 | 100 | 100 | No |
| | LC | 4.7 | - | 1.1 | 1.6 | 2.0 | - | 100 | 100 | 100 | No |
| | LC | 4.8 | - | 1.4 | 1.6 | 1.8 | - | 100 | 100 | 100 | No |
| | LC | 4.6 | - | 1.3 | 1.4 | 2.0 | - | 100 | 100 | 100 | No |
| 30153-11 | TC | 4.6 | - | 1.1 | 1.9 | 1.6 | - | 100 | 100 | 70 | Yes |
| | LC | 4.9 | - | 1.5 | 1.8 | 1.6 | - | 100 | 0 | 0 | Yes |
| | LC | 5.5 | - | 1.6 | 1.9 | 2.0 | - | 40 | 0 | 0 | Yes |
| | N/A | 5.2 | - | 1.5 | 1.8 | 1.9 | - | 40 | 0 | 0 | Yes |
| 30373-31 | N/A | 5.1 | - | 1.4 | 1.5 | 2.3 | - | 60 | 0 | 0 | Yes |
| | N/A | 5.0 | - | 1.3 | 1.5 | 2.2 | - | 100 | 20 | 0 | Yes |
| | N/A | 5.3 | - | 1.0 | 1.9 | 2.5 | - | 100 | 10 | 0 | Yes |
| | N/A | 5.1 | - | 1.3 | 1.5 | 2.3 | - | 100 | 20 | 0 | Yes |
| 30373-61 | LC | 5.5 | - | 1.6 | 2.2 | 1.7 | - | 50 | 0 | 0 | Yes |
| | LC | 5.5 | - | 1.5 | 2.4 | 1.6 | - | 100 | 0 | 0 | Yes |
| 30531-11 | N/A | 6.0 | - | 1.3 | 2.5 | 2.6 | - | 100 | 10 | 0 | Yes |
| | N/A | 6.0 | - | 1.0 | 2.4 | 2.6 | - | 100 | 100 | 100 | Yes |
| | N/A | 5.9 | - | 1.1 | 3.4 | 2.8 | - | 100 | 75 | 0 | Yes |
| | N/A | 4.5 | - | 1.4 | 1.1 | 2.0 | - | 100 | 100 | 100 | Yes |
| | N/A | 4.9 | - | 1.4 | 3.3 | 1.4 | - | 100 | 60 | 0 | Yes |
| | N/A | 4.8 | - | 1.4 | 2.0 | 1.5 | - | 100 | 100 | 100 | Yes |

O=Overlay, S=Surface, L=Leveling, B=Base, DC=Diagonal cracks, LC=Longitudinal cracks, TC=Transverse cracks, TJ=Transverse joint and N/A=Not available or undetermined

1. For each intact core, the diameter and thickness of the core and the thickness of each AC course were measured. All thicknesses were measured at the four ends of two orthogonal diameters and the average core thickness was calculated, recorded, and used in the backcalculation of the pavement layer moduli.
2. The bottom of each core, which had some aggregates or rubblized material attached to it, was trimmed off by sawing (see Figure 3.26).
3. The specific gravity of the entire core was then determined according to the ASTM standard test procedure D-2726 (ASTM, 1994).
4. The AC cores were then sawn to separate the various AC courses and to produce test specimens for the indirect tensile cyclic load test (ITCLT) and the indirect tensile strength test (ITST). Note that, for both tests, the ideal theoretical test specimen thickness is 3.0 in. (see Figure 3.27) and, because of edge effects, the absolute minimum thickness is 2.2 in. Due of this constraint, some test specimens contained more than one AC course. For example, the test specimen representing the AC surface course contained about 1.5-in. thick AC surface course and a minimum of 0.7 in. leveling course. Likewise, when an AC course was less than 2.2-in. thick, a part of the adjacent course was included in the test specimen.
5. The specific gravity of each test specimen was then determined according to the ASTM standard test procedure D-2726 (ASTM, 1994).
6. Each test specimen was subjected to ITCLT (details of the test are presented in a later section).
7. After the completion of the ITCLT, the test specimen was then subjected to ITST (details of the test are presented in a later section).

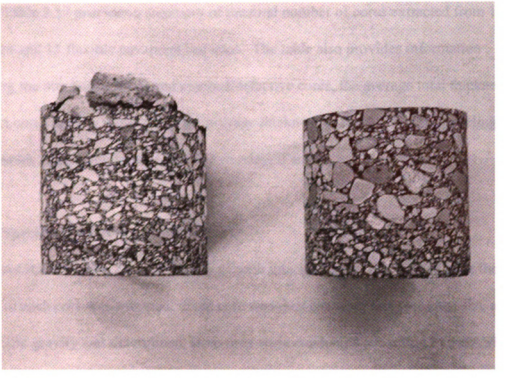

Figure 3.26 Untrimmed (left) and trimmed (right) AC cores

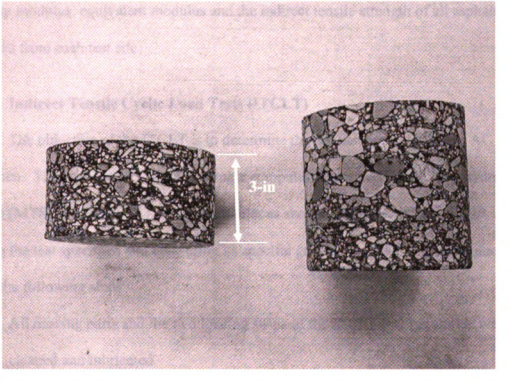


Figure 3.27 An AC test specimen (left) and a trimmed AC core (right)

Table 3.17 provides a summary of the total number of cores extracted from 19 rubblized and 13 flexible pavement test sites. The table also provides information regarding the number of intact and cracked/defective cores, the average total thickness of all intact cores of each test site and the average thickness of the AC surface, leveling and base courses and the thickness of the AC overlay, if any.

## 3.2 Specific Gravity Test (SG test)

As stated earlier, specific gravity of each intact core was determined after the bottom of each core was trimmed. Each core was then sawed to test specimen size and the specific gravity was determined. Both tests were conducted according to the ASTM standard test procedure D 2726.

Table 3.18 provides a summary of the averages of the bulk specific gravity, resilient modulus, equivalent modulus and the indirect tensile strength of all asphalt cores obtained from each test site.

## 3.3 Indirect Tensile Cyclic Load Tests (ITCLT)

The objective of the ITCLT is to determine the resilient modulus of the AC specimen. The tests were conducted using a computer-controlled closed-loop hydraulic system (MTS) and the ITCLT specimen holder as shown in Figures 3.28 and 3.29. After sawing the test specimen and measuring its specific gravity, the ITCLT was conducted using the following steps:

1. All moving parts and the two loading strips of the ITCLT loading device were cleaned and lubricated.

Table 3.17 A summary of the average total thickness of the cores and the average thickness of each AC course for 19 rubblized and 13 flexible pavement test sites

| Test sites | Number of Cores | | | Average thickness (in) | | | | |
|---|---|---|---|---|---|---|---|---|
| | Total | Intact | With cracks /defects | Total core | Overlay | AC surface course | AC leveling course | AC base course |
| Rubblized Pavements | | | | | | | | |
| 10692-11 | 12 | 10 | 0/2 | 8.2 | - | 1.5 | 2.2 | 4.5 |
| 10692-12 | 12 | 9 | 0/3 | 8.0 | - | 1.6 | 2.3 | 4.1 |
| 10753-11 | 14 | 11 | 3/0 | 4.5 | - | 1.6 | 1.0 | 1.8 |
| 10753-12 | 15 | 12 | 3/0 | 4.1 | - | 1.6 | 1.0 | 1.5 |
| 11941-21 | 15 | 10 | 5/0 | 7.8 | 1.5 | 1.6 | 2.3 | 2.6 |
| 11941-22 | 15 | 8 | 5/2 | 7.4 | 1.5 | 1.4 | 2.1 | 2.4 |
| 20102-11 | 12 | 12 | - | 6.5 | - | 1.4 | 2.1 | 2.9 |
| 20102-12 | 12 | 12 | - | 6.4 | - | 1.5 | 2.1 | 2.8 |
| 20233-11 | 11 | 10 | 0/1 | 5.5 | - | 1.5 | 1.8 | 2.2 |
| 20233-12 | 10 | 7 | 0/3 | 5.5 | - | 1.3 | 2.4 | 1.7 |
| 20273-21 | 15 | 11 | 4/0 | 4.6 | - | 1.3 | 1.5 | 2.0 |
| 20273-31 | 12 | 12 | - | 7.0 | - | 1.8 | 2.5 | 2.6 |
| 20273-41 | 12 | 12 | - | 6.5 | - | 1.7 | 2.0 | 2.8 |
| 20311-11 | 12 | 12 | - | 6.9 | - | 1.2 | 1.8 | 3.9 |
| 30153-11 | 16 | 12 | 4/0 | 5.3 | - | 1.4 | 1.8 | 1.8 |
| 30373-51 | 12 | 12 | - | 6.6 | - | 1.5 | 1.8 | 3.4 |
| 30373-52 | 12 | 12 | - | 6.4 | - | 1.4 | 1.8 | 3.3 |
| 30373-61 | 18 | 15 | 2/1 | 5.7 | - | 1.6 | 2.1 | 2.0 |
| 30531-21 | 20 | 14 | 6/0 | 5.5 | - | 1.2 | 2.2 | 2.1 |
| Flexible Pavements | | | | | | | | |
| 20273-11 | 12 | 12 | 0/0 | 9.0 | - | 1.7 | 2.3 | 4.9 |
| 20411-11 | 14 | 12 | 2/0 | 3.3 | - | 1.4 | 1.9 | - |
| 20411-12 | 14 | 12 | 2/0 | 2.8 | - | 1.2 | 1.6 | - |
| 30202-11 | 11 | 9 | 2/0 | 4.7 | - | 1.1 | 1.5 | 2.1 |
| 30202-12 | 12 | 9 | 3/0 | 4.5 | - | 1.0 | 1.4 | 2.1 |
| 30422-11 | 27 | 24 | 3/0 | 3.7 | - | 1.1 | 1.9 | 0.6 |
| 30502-11 | 13 | 12 | 1/0 | 6.1 | 1.1 | 0.8 | 1.2 | 3.0 |
| 30502-21 | 38 | 22 | 16/0 | 7.1 | 2.7 | 1.0 | 1.1 | 2.3 |
| 30521-11 | 24 | 20 | 4/0 | 5.9 | 1.2 | 0.8 | 1.4 | 2.4 |
| 30521-21 | 10 | 6 | 4/0 | 9.1 | 3.7 | 1.4 | 1.5 | 2.4 |
| 30552-11 | 15 | 12 | 3/0 | 3.0 | - | 1.6 | 1.4 | - |
| 30552-12 | 13 | 12 | 2/0 | 3.1 | - | 1.4 | 1.6 | - |
| Marsh | 8 | 2 | 6/0 | 10.6 | 1.7 | 1.9 | 4.1 | 3.0 |

Table 3.18 A summary of the average physical and engineering properties of the AC cores obtained from 19 rubblized and 13 flexible pavement test sites

| Test sites | Bulk specific gravity | Resilient modulus (ksi) | | Equivalent elastic modulus (ksi) | Indirect tensile strength (psi) |
|---|---|---|---|---|---|
| | | One-dimension | Three-dimensions | | |
| Rubblized pavements | | | | | |
| 10692-11 | 2.32 | 177 | 171 | 52 | 97 |
| 10692-12 | 2.31 | 179 | 173 | 65 | 107 |
| 10753-11 | 2.38 | 209 | 202 | 62 | 146 |
| 10753-12 | 2.39 | 196 | 189 | 73 | 171 |
| 11941-21 | 2.40 | 203 | 196 | 85 | 211 |
| 11941-22 | 2.40 | 214 | 206 | 85 | 241 |
| 20102-11 | 2.33 | 188 | 181 | 61 | 126 |
| 20102-12 | 2.31 | 207 | 200 | 62 | 118 |
| 20233-11 | 2.39 | 202 | 195 | 73 | 138 |
| 20233-12 | 2.38 | 213 | 205 | 50 | 120 |
| 20273-21 | 2.45 | 291 | 281 | 108 | 213 |
| 20273-31 | 2.44 | 217 | 209 | 44 | 101 |
| 20273-41 | 2.45 | 258 | 249 | 41 | 100 |
| 20311-11 | 2.46 | 234 | 226 | 61 | 123 |
| 30153-11 | 2.35 | 220 | 212 | 84 | 172 |
| 30373-51 | 2.36 | 186 | 179 | 66 | 167 |
| 30373-52 | 2.35 | 196 | 189 | 70 | 154 |
| 30373-61 | 2.45 | 273 | 263 | 71 | 143 |
| 30531-21 | 2.33 | 170 | 164 | 84 | 172 |
| Flexible pavements | | | | | |
| 20273-11 | 2.44 | 214 | 206 | 36 | 82 |
| 20411-11 | 2.50 | 181 | 175 | 42 | 93 |
| 20411-12 | 2.48 | 212 | 205 | 28 | 82 |
| 30202-11 | 2.46 | 185 | 178 | 88 | 165 |
| 30202-12 | 2.46 | 178 | 172 | 95 | 183 |
| 30422-11 | 2.38 | N/A | N/A | N/A | N/A |
| 30502-11 | 2.36 | 195 | 188 | 88 | 122 |
| 30502-21 | 2.38 | 172 | 166 | 79 | 137 |
| 30521-11 | 2.32 | N/A | N/A | N/A | N/A |
| 30521-21 | 2.39 | N/A | N/A | N/A | N/A |
| 30552-11 | 2.40 | 189 | 182 | 60 | 114 |
| 30552-12 | 2.41 | 189 | 182 | 59 | 116 |
| Marsh | 2.33 | 198 | 191 | 75 | 115 |

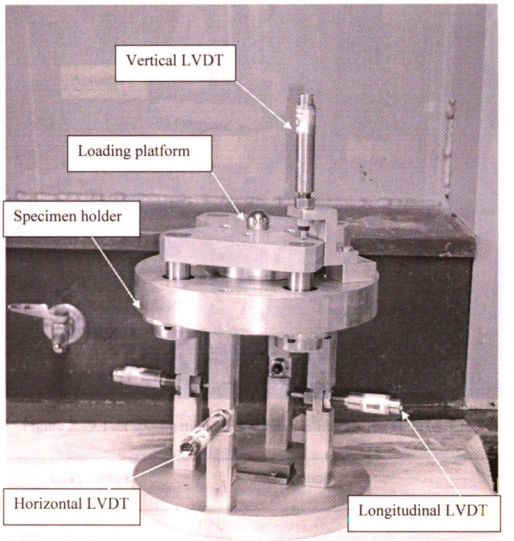


Figure 3.28 The ITCLT and ITST specimen holder for a 6-in. diameter and 3-in. thick test specimen

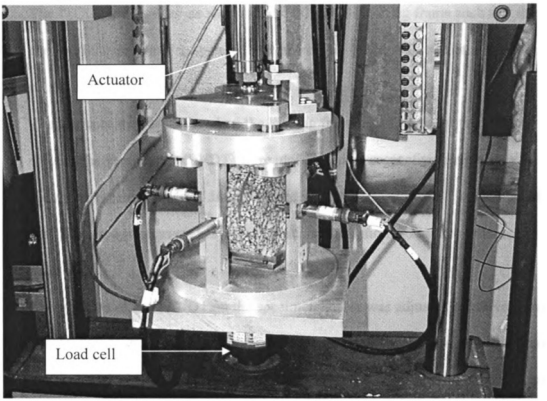


Figure 3.29 Test specimen in the specimen holder during an ITCLT test

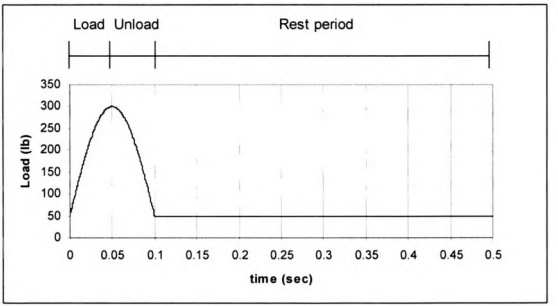


Figure 3.30 One load cycle consisting of 0.1-second load-unload period and 0.4-second relaxation period

2. The ITCLT loading device was placed on the MTS loading frame such that the center of the device corresponded with the center of the MTS actuator and the center of the load cell.
3. The test specimen was placed on the loading frame and five linear variable differential transducers (LVDT) were placed in their respective positions as shown in Figure 3.29. In addition, the sixth LVDT placed inside the MTS actuator was also used to measure the test specimen deformation along the vertical diameter.
4. The position of each LVDT on the specimen holder was adjusted by moving the LVDT core toward or away from the test specimen using two position adjustment knots until the LVDT signal indicates that the LVDT position relative to the core would allow the use of a high percentage of the LVDT range.
5. A 50-lb sustained load was placed on the test specimen by lowering the actuator of the MTS. The resulting test specimen deformations were recorded.
6. When the rate of deformation due to the sustained load was small enough (not measurable), a 250-lb cyclic load was applied to the test specimen at a frequency of 2 Hz. Each cycle consisted of 0.1-second of load-unload and 0.4-second relaxation periods. Figure 3.30 illustrates a plot of one load cycle as a function of time.
7. Each test specimen was subjected to a minimum of 700 load cycles. At certain specified cycles (e.g., the 200 and 500 cycles), the load magnitude and the deformations of the test specimen in three directions were recorded for three consecutive cycles. The rate of data collection was set at one set of deformation

readings every 0.0004-second. Hence, 250 deformation readings were collected by each LVDT during the load-unload cycle and 1,000 readings during the rest period. Note that the load data were collected using a 1000-lb capacity load cell located under the ITCLT loading frame.

8. The test was terminated and the data was downloaded for analysis.

9. The load and deformation data corresponding to load cycles 499, 500 and 501 were used to calculate the resilient modulus of the test specimen using one- and three-dimensional analyses as follows: .

**a) One-Dimensional Analysis** – The resilient modulus of the test specimen was calculated using the deformation measured along the vertical diameter of the test specimen, equation 3.1 (after Baladi, 1988). In this calculation, since the impact of Poisson's ratio on the value of the resilient modulus is insignificant, a Poisson's ratio of 0.3 was assumed for all test specimens.

$$MR_v = \frac{P * (4.085950 - 0.0417333 * \upsilon)}{L * D_v} \qquad (3.1)$$

Where $MR_v$ = Resilient modulus based on vertical deformation (psi);

$P$ = peak cyclic load (lb);

$\upsilon$ = Poisson's ratio;

$L$ = thickness of the test specimen (in.); and

$D_v$ = the deformation of the specimen along the vertical diameter (in.).

b) **Three-Dimensional Analyses** - The resilient moduli of the test specimens were calculated using the deformations measured along the vertical and

horizontal diameters and along the thickness of each test specimen using the equations below (after Baladi, 1988). .

$$MR_{3D} = \frac{(0.1832585H + 4.2817159V - 0.0215089A)}{D} \qquad (3.2)$$

$$D = 1.0468779(H^2 + V^2 + A^2) - (H - 0.0417333V + 0.212453A)^2;$$

$$H = \frac{D_h * L}{P};\ V = \frac{D_v * L}{P};\ \text{and}\ A = \frac{D_l}{P}$$

Where $MR_{3D}$ = Resilient modulus based on 3-D deformations (psi);

L = thickness of the test specimen (in.);

P = peak cyclic load (lb);

$D_h$ = the horizontal deformation = the sum of the displacements measured by the two LVDT along the horizontal diameter of the test specimen (in.);

$D_v$ = the deformation of the test specimen along the vertical diameter (in.); and

$D_l$ = the longitudinal deformation = the sum of the displacements measured by the two LVDT along the thickness of the test specimen (in.).

Note that, the vertical deformation used in equations 3.1 through 3.2 was that obtained from the LVDT placed inside the MTS actuator. The reason is that the actuator and the LVDT were positioned at the center of the test specimen. The outside mounted LVDT was positioned at the corner of the top plate of the ITCLT device which may be affected by the rocking motion of the test specimen during the cyclic load test. Nevertheless, the resilient moduli obtained from equations 3.1 and 3.2 were compared. It was found that

the differences between the two values are insignificant. Table 3.18 provides a summary of the average resilient moduli of the AC specimen calculated using equations 3.1 and 3.2. Figure 3.31 depicts a plot of the average resilient modulus of the test specimens obtained from the ITCLT using equation 3.1 versus the average bulk specific gravity of the test specimens of each test site. The data in the figure indicate that, higher the bulk specific gravities yield higher resilient moduli. This finding agrees with the lab test results conducted by Baladi (1988) that increases in the air voids of the AC mixes results in decreases in the resilient modulus of the AC mixes.

## 3.4 Indirect Tensile Strength Tests (ITST)

After all ITCLT were concluded, the ITST were commenced. The objectives of the latter tests are to determine the indirect tensile strengths (ITS) and the equivalent moduli (EM) of the test specimens. The tests were conducted at 70°F using the ITCLT specimen holder and Marshall loading frame (see Figure 3.32). The load was increased to failure by means of the constant rate of movement of the loading frame of 2 in. per minute. The vertical deformation and the applied load were recorded and used in the calculation of the ITS and the EM of the test specimen using equations 3.3 and 3.4.

$$\text{ITS} = \frac{2P}{\pi DL} \tag{3.3}$$

$$\text{EM} = \frac{\frac{P}{2} * (4.085950 - 0.0417333 * \nu)}{1000 * L * D_{HL}} \tag{3.4}$$

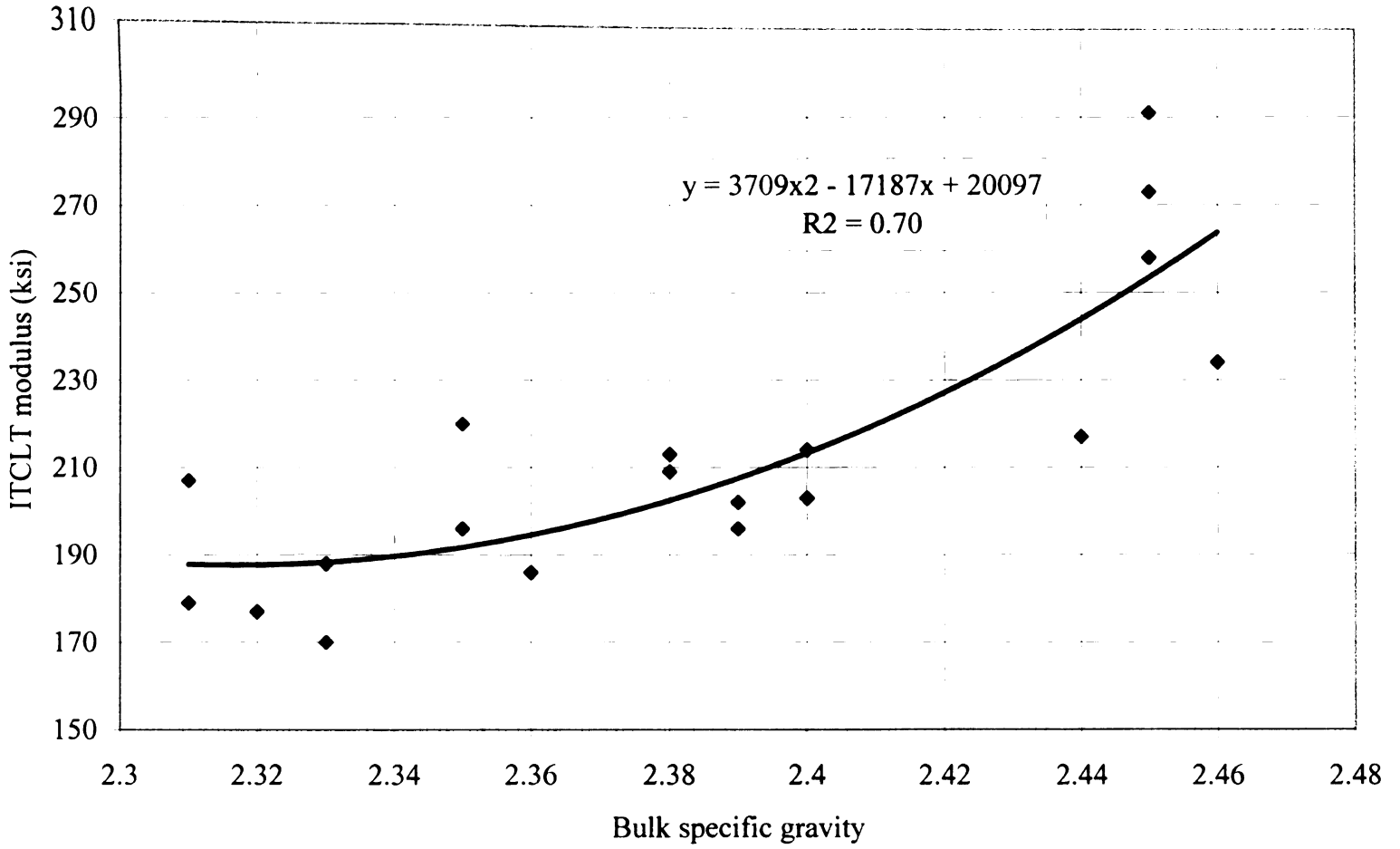


Figure 3.31 Plots of the average bulk specific gravity and the average ITCLT modulus of the test specimens of 19 rubblized pavement test sites

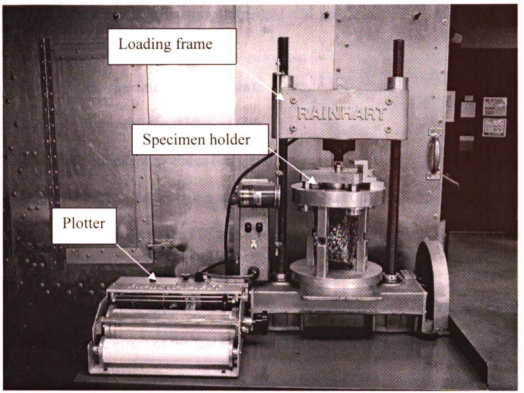


Figure 3.32 ITST loading frame and the specimen holder

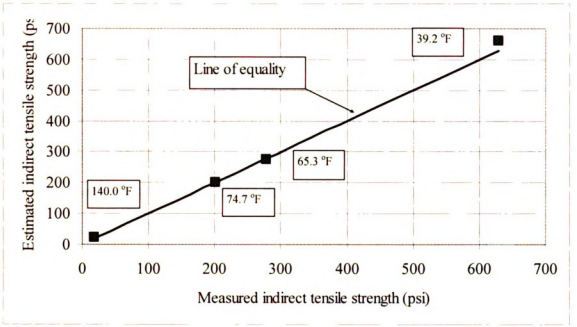


Figure 3.33 Comparison of the indirect tensile strengths at different temperatures obtained from ITST (Schorsch, 2003) and predicted using equation 2.5

where ITS = indirect tensile strength (psi);

P = peak load at failure (lb);

D = test specimen diameter (in);

L = test specimen thickness (in);

EM = equivalent modulus (ksi); and

$D_{HL}$ = vertical deformation at half the peak load (in).

The average values of the ITS and the EM of the test specimens of each test site are listed in Table 3.18.

In addition, special indirect tensile strength tests were conducted to determine the effect of the test temperature, segregation and moisture on the tensile strength of asphalt mixtures. These tests and the test results are addressed in the next two subsections.

### 3.4.1 Effect of Test Temperature

In order to validate equation 2.5, Schorsch (2003) conducted indirect tensile strength tests (ITST) on four triplicates. One triplicate was tested at 39°F, another at 74.7°F (room temperature), the third at 65.3°F, and the fourth at 140°F. The average indirect tensile strength of each triplicate was then calculated and is listed in Table 3.19. Figure 3.33 depicts the average tensile strengths of the four triplicates and the strengths predicted using equation 2.5 based on the lab test tensile strength at 74.7°F. The solid line in the figure depicts the locus of the points of equality. As can be seen, equation 2.5 is reliable and predicts the

Table 3.19 Comparison of the average measured and predicted indirect tensile strengths (using equation 2.1) of the 4B mix

| Temperature | | Indirect tensile strength (psi) | |
|---|---|---|---|
| Fahrenheit | Centigrade | Tested | Estimated |
| 39.2 | 4.0 | 629 | 662 |
| 65.3 | 18.5 | 278 | 275 |
| 74.7 | 23.7 | 201 | 201 |
| 140.0 | 60.0 | 18 | 22 |

Table 3.20 Sources of the aggregate gradations and the asphalt contents used in investigating the effect of segregation and moisture conditioning on the indirect tensile strengths of three asphalt mixes (Schorsch, 2003)

| Mix type | Segregation | Gradation | Asphalt content |
|---|---|---|---|
| 4B | Non-segregated | Cores | Cores |
| | Segregated | Cores | Cores |
| 4C | Non-segregated | JMF | JMF |
| | Segregated | Cores | Film thickness |
| 4E10 | Non-segregated | Cores | Film thickness |
| | Segregated | Cores | Film thickness |

Table 3.21 The average tensile strengths of three segregated and not segregated asphalt mixes (Schorsch, 2003)

| Mix type | Non-segregated | | Segregated | |
|---|---|---|---|---|
| | Unconditioned | Conditioned | Unconditioned | Conditioned |
| 4B | 278 | 190 | 274 | 158 |
| 4C | 240 | 246 | 203 | 161 |
| 4E10 | 190 | 172 | 203 | 143 |
| Normalized to Non-segregated unconditioned tensile strength of each mix | | | | |
| 4B | 1 | 0.68 | 0.98 | 0.57 |
| 4C | 1 | 1.03 | 0.85 | 0.67 |
| 4E10 | 1 | 0.90 | 1.07 | 0.75 |

measured data well. That is if the indirect tensile strength at any temperature is known, equation 2.5 can be used to calculate the strength at other temperatures.

### 3.4.2 Segregation and Moisture Conditioning

In a concurrent study of top-down cracks in flexible pavements, Schorsch (2003) conducted indirect tensile strength tests to determine the effect of moisture damage on segregated and non-segregated AC mixes. The tests were conducted in accordance with the ASTM D 4867M standard test procedure (ASTM, 1994). Three asphalt mixes, 4B, 4C and 4E10, which are commonly used as the AC surface course in Michigan, were tested. For each mix, 12 test samples were compacted. Six samples were mixed and compacted as to duplicate the aggregate gradation and asphalt content obtained from cores that were extracted from segregated areas along the test section. Three of these samples (a triplicate) were subjected to moisture conditioning and then tested while the other three samples (another triplicate) were tested dry. The aggregate gradation and asphalt content of the other six samples (control, non-segregated, samples) were in accordance with either the gradation and asphalt contents of cores that were extracted from non-segregated areas or with the job-mix-formula (JMF), which was obtained from MDOT. Once again, three samples were subjected to moisture conditioning and then tested while the other three were tested dry. Table 3.20 summarizes the source of aggregate gradations and the asphalt contents used. The test results (the average indirect tensile strengths of all twelve triplicates are listed in Table 3.21.

The table also provides a list of the same data normalized to the average strength of non-segregated and unconditioned triplicate of each mix. Note that, all tests were conducted at a room temperature of 65.3°F. The data in Table 3.21 indicate that, for all three mixes:

- The differences between the indirect tensile strengths of unconditioned (dry), segregated and non-segregated mixes are statistically insignificant. The strengths of the segregated mixes vary from about 85 to about 107 percent of the non-segregated mixes. The 4B mix is highly moisture susceptible while the superpave mix 4E10 is moderately susceptible. The former (non-segregated conditioned 4B mix) shows reduction in the indirect tensile strength of 32 percent relative to the unconditioned mix. The 4E10 mix shows a reduction of only 10 percent. According to ASTM 4867M, the mix is considered moisture susceptible if the reduction in the tensile strength is greater than 10 percent.
- All three mixes show substantial reduction in the indirect tensile strengths for the segregated and conditioned samples. The strengths of said samples vary from 57 to 75 percent depending on the mix type and degree of segregation.

Finally, it should be noted that the ITS of each of the three mixes listed in Table 3.21 would experience higher reduction at higher temperatures. Said strengths were calculated using the data in Table 3.21 and equation 2.2 and the results are listed in Table 3.22 and shown in Figure 3.34.

Table 3.22 Indirect tensile strengths of the 4B, 4C and 4E10 mixes at 39.2, 65.3 and 140.0° F for various mix conditions

| Mix type | Non-segregated | | | | | | Segregated | | | | | |
|---|---|---|---|---|---|---|---|---|---|---|---|---|
| | Unconditioned | | | Conditioned | | | Unconditioned | | | Conditioned | | |
| | Temperature (°F) | | | | | | | | | | | |
| | 39.2 | 65.3 | 140.0 | 39.2 | 65.3 | 140.0 | 39.2 | 65.3 | 140.0 | 39.2 | 65.3 | 140.0 |
| | Indirect tensile strength (psi) | | | | | | | | | | | |
| 4C | 577 | 240 | 19 | 592 | 246 | 20 | 488 | 203 | 16 | 387 | 161 | 13 |
| 4B | 669 | 278 | 23 | 457 | 190 | 15 | 659 | 274 | 22 | 380 | 158 | 13 |
| 4E10 | 457 | 190 | 15 | 414 | 172 | 14 | 488 | 203 | 16 | 344 | 143 | 12 |

Note that, the ITST were conducted at 65.3 °F. The indirect tensile strengths at 39.2 and 140.0°F were calculated using equation 2.1

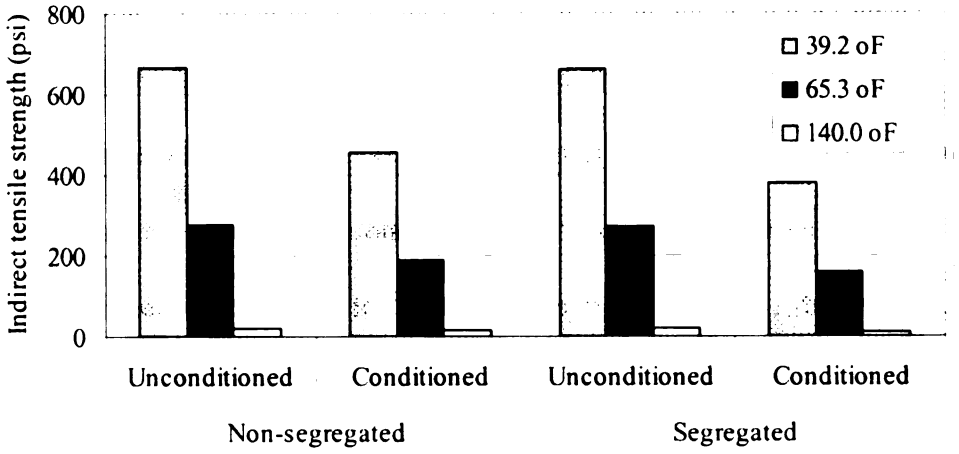


a) 4B mix

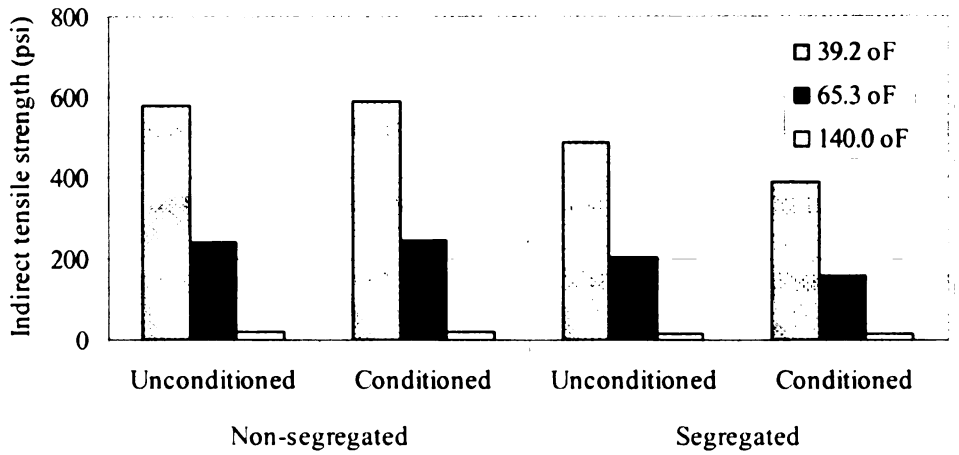


b) 4C mix

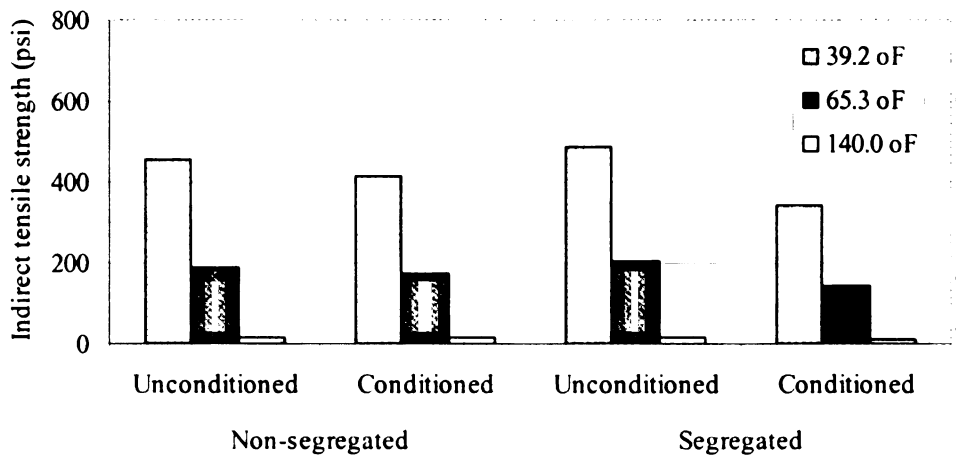


c) 4E10 mix

Figure 3.34 The effect of temperature, segregation and moisture conditioning on the indirect tensile strengths of three asphalt mixes

## 4.0 SUMMARY

In this chapter, the objectives, equipment and procedures for rubblizing deteriorated concrete pavements are presented. The terms "rubblized concrete slab", "rubblized material" and "fractured concrete" are introduced and defined. The last two terms were established in this study to describe the condition of the rubblized concrete slab. The chapter also addresses the field and laboratory investigations of rubblized and conventional flexible pavements that were conducted in this study. The filed investigation consisted of examination of the rubblization operation and its products, distresses surveys, and FWD testing and coring. The laboratory investigation included core and cracks measurements, specific gravity tests, indirect tensile cyclic load tests and indirect tensile strength tests of the asphalt cores. The latter test was also used to assess the impact of temperature, segregation and moisture conditioning on the indirect tensile strength of some asphalt mixes.

# CHAPTER 4

# THE UNDERPERFORMANCE OF RUBBLIZED PAVEMENTS

## 1.0 INTRODUCTION

During the course of this study, three manual distress surveys of 87 rubblized pavement projects in the State of Michigan were conducted. In addition, the available 1991 through 1999 historical distress data of rubblized pavement projects were obtained from the MDOT pavement management system (PMS) databank. The two sets of distress data (from the two manual distress surveys and from the PMS databank) were compared and their accuracy was checked. The 2001, 2002 and 2003 manual distress survey data were summarized and are provided in Tables 3.9 through 3.10. Examination of the data listed in the three tables indicates that the most predominant distress type is cracking, although few projects showed signs of raveling and rutting. The cracks can be divided into five categories:

1. Longitudinal cracks that initiate at the pavement surface and propagate downward and outward, they are referred to as "longitudinal top-down cracks (LTDC)."
2. Longitudinal bottom-up fatigue cracks (alligator cracks).
3. Longitudinal reflective cracks.
4. Transverse cracks that also initiate at the pavement surface and propagate downward and outward. These types of cracks are referred to as "transverse top-down cracks (TTDC)."
5. Transverse joint or transverse cracks reflective cracks.

The distress data and the observations made during the rubblization operation and after the completion of construction (see Chapter 3) indicate that the underperformance of

rubblized concrete pavements could be attributed to several variables. These variables can be classified into four categories as follows:

1. The quality of the rubblization operation
2. Construction procedure
3. The asphalt mix design
4. The project scoping/selection process

The four categories of variables are addressed below.

## 2.0 QUALITY OF THE RUBBLIZATION OPERATION

The quality of the rubblization operation is defined herein as "the degree of which the rubblized products satisfy the rubblization objectives." These objectives are stated in Chapter 3 and, for convenience, are repeated in the next section. The quality of the rubblization operation is affected by the rubblization equipment and procedure. The former is included in Chapter 3 and the latter is addressed in section 2.2 below. Finally, section 2.3 presents and discusses quantified measures for the purpose of assigning numerical values to the quality of the rubblization operation.

### 2.1 Rubblization Objectives

As stated in Chapter 3, there are three main objectives of rubblizing concrete pavements. These are:

1. Destroying the integrity of the concrete pavement joints as to eliminate reflective cracks.

2. Destroying the integrity of the concrete slab by debonding the temperature steel to avoid reflective cracks and by producing full depth rubblized material.

3. Changing the concrete slab into a particulate media whose maximum size is less than 6 in., this would allow the rubblized concrete slab to behave like a base layer.

If the above three objectives are successfully achieved, the rubblizing alternative changes the pavement cross-section from rigid to flexible pavement as shown schematically in Figure 4.1. Thus, rubblized pavement will have flexible-like behavior and can be better explained, modeled and analyzed using the multi-layer elastic system. On the other hand, if one or more of the above objectives are only partially achieved, then the rubblized pavement may have flexible-, flexible-composite-, or composite-like behavior.

The purposes of the above stated objectives are to assure that the pavement will perform well during its assumed design life of 20-years. Violations of one or more objectives would result in unintended and premature pavement distresses as illustrated in the following case studies:

**Case Study 1** - If the integrity of the joints in the original concrete pavements is not completely destroyed, joint reflective cracks will develop as shown in Figure 4.2.

**Case Study 2** - If the temperature steel is only occasionally debonded, then the integrity of that portion of the concrete slab where the steel is not debonded remains intact. The slab will expand and contract due to temperature changes causing movements and perhaps reflective cracking in the AC layer as shown in Figure 4.3.

.

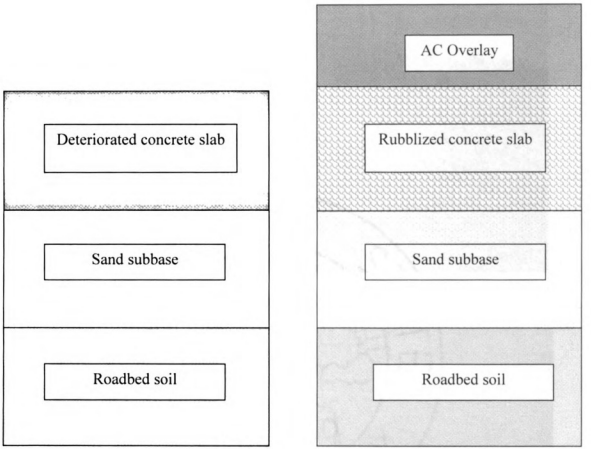


a) Original concrete pavement b) Rubblized pavement

Figure 4.1 Schematic of concrete and rubblized pavement cross-sections

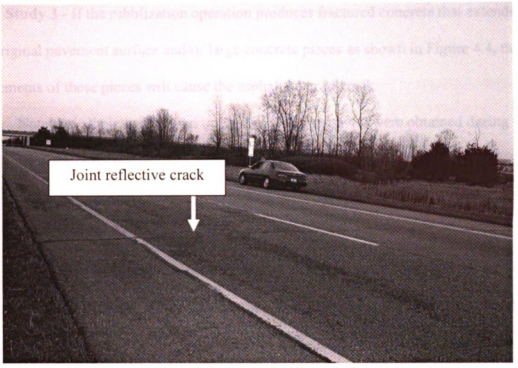


a) US 10

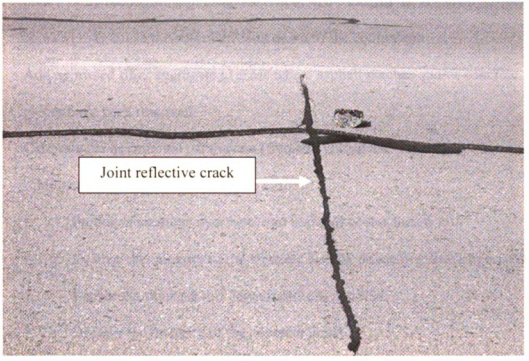


b) M-50

Figure 4.2 Joint reflective cracking in rubblized pavements

**Case Study 3** - If the rubblization operation produces fractured concrete that extends to the original pavement surface and/or large concrete pieces as shown in Figure 4.4, the movements of these pieces will cause the asphalt layer to crack

Note that all pictures shown in Figures 4.2 through 4.4 were obtained during the May 2002 distress survey.

## 2.2 Rubblization Procedure

A typical rubblization procedure consists of several steps that affect the quality of the rubblization operation. Some steps are applicable to the resonant frequency breaker, others to the multi-head breaker and still others apply to both. These steps are:

1. Remove all asphalt overlays and/or asphalt patches. Failure to do so would cause poor quality rubblization in these areas and, in the case of the resonant frequency breaker, may cause the automatic shut down of the equipment.
2. Add approved filler aggregate to areas where asphalt patches and/or concrete pieces have been removed.
3. Calibrate the operational parameters (frequency, load and velocity) of the rubblizer at the start of every project as to:
   - Produce maximum size rubblized material of less than 6 in.
   - Destroy the integrity of the concrete slab by debonding the temperature steel and producing full depth rubblized material.
   - Destroy the integrity of the concrete joints.

   Two calibration schemes developed for the resonant frequency breaker and the multi-head breaker are presented in the next section.

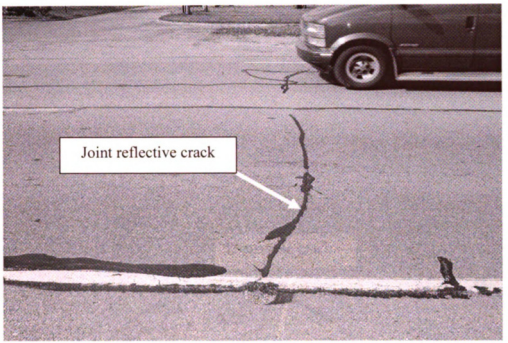


a) M-50

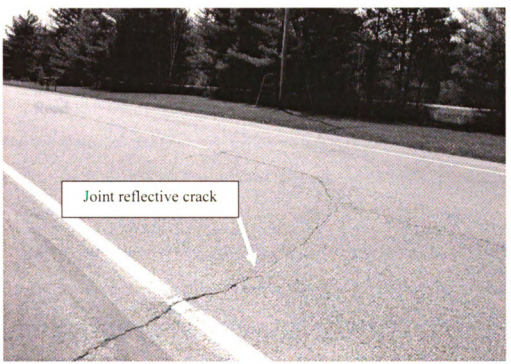


b) Saginaw Road

Figure 4.3 Reflective cracks in rubblized pavements

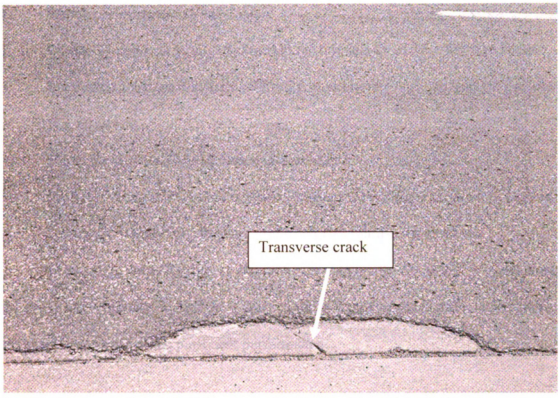


Figure 4.4 Debonding between the AC layer and the original concrete pavement where the fractured concrete extends to the original pavement surface and the integrity of the slab including the transverse crack is not destroyed – Portage Road

4. Rubblize the same area only once.

5. For the sonic breaker, slightly overlap the boundaries of the rubblized strips.

6. Spray the rubblized materials with water to minimize dust and prevent the loss of fine materials.

7. Cut and remove all exposed temperature steel.

8. Compact the rubblized materials uniformly using vibratory roller (for resonant frequency breaker) or vibratory grid roller (for multi-head breaker).

In practice, the calibration of the rubblizer is typically neglected. Nevertheless, the above steps literally control the quality of the rubblized material (see next section) and significantly affect the pavement performance.

## 2.3 Measures of the Quality of the Rubblization Operation

Once again, the quality of the rubblization operation is defined herein in terms of achieving the three main objectives of rubblization and in terms of pavement performance. Hence the quality of rubblization can be thought of as a measure of the degree of success of the rubblization operation. In this study, the quality of rubblization is defined in the following five terms:

1. **Breaking the Concrete Slab** - Breaking the concrete slabs into small pieces (less than 6 in. maximum dimension) as shown in Figure 4.5. This would eliminate independent movement of large pieces, which leads to reflective cracks.

2. **Steel Debonding** - Debonding the temperature steel (Figure 4.6) to decrease the magnitude of temperature expansion and contraction of the rubblized concrete slab and hence, to reduce the potential of reflective cracking

Figure 4.5 A shoe of the resonant frequency breaker

Figure 4.6 Partial debonding of the temperature steel (M-21)

3. **Joint Integrity** - Destroying the integrity of the concrete joints to prevent reflective joint cracking. Figure 4.7 shows a rubblized concrete slab where the integrity of a transverse joint is preserved. The partial destruction of the integrity of a longitudinal joint (the rubblizer produces rubblized material on one side of the joint and fractured concrete on the other side), will be manifested in differential settlement between the two lanes as shown in Figure 4.8.

4. **Rubblized material and fractured concrete Layers** - Eliminating or decreasing the potential of rubblizing the concrete slab into two distinctive layers; rubblized material and fractured concrete. The uneven interface between the two layers and the high modulus fractured concrete layer result in higher potential for TDC initiation. Figures 4.9 shows a rubblized concrete slab where the rubblized material layer has been removed and the fractured concrete layer has been exposed. Figure 4.10 shows rubblized material next to fractured concrete, which produces horizontal differential stiffness.

5. **Shear Failure** – Eradicating shear failure in the subbase and/or roadbed soil. When the subbase and/or roadbed soil are weak or saturated, the rubblization operation may cause large pieces (e.g., 3-ft by 3-ft) of the concrete slab to break off, rotate and penetrate the subbase. This is called shear failure of the subbase. Such shear failure, if not treated properly, would reflect through the AC layer within a relatively short time period (2 to 5 years) as a depression and finally would develop to a shear failure in the pavement structure. Figures 4.11 shows a shear failure along I-196 where the rubblizer caused large concrete pieces to break off, rotate and penetrate the subbase. Likewise, Figure 4.12 shows the initiation of

Figure 4.7 Partial destruction of the joint integrity (US-131)

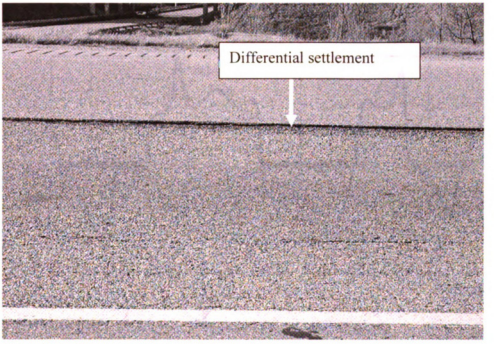


Figure 4.8 Differential settlements between the two lanes along NB I-196, May 2002

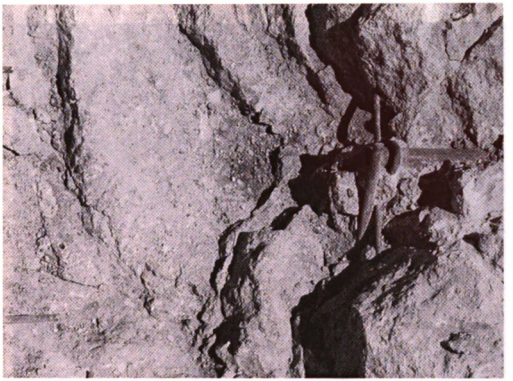

a) A close-up of the fractured concrete in a trench (M-50)

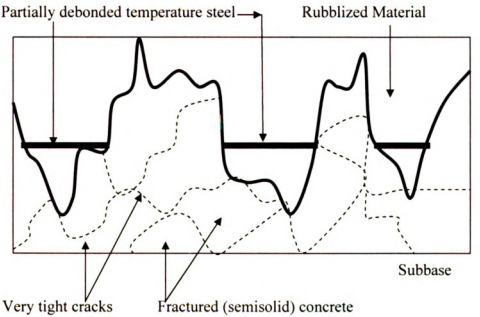


b) Schematic of the fractured layer and partial steel debonding

Figure 4.9 The fractured concrete layer

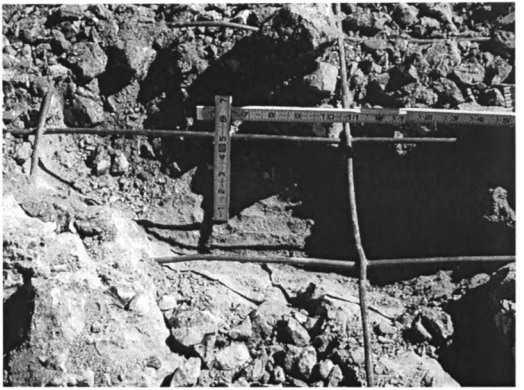

a) A trench showing the fractured concrete and the rubblized material

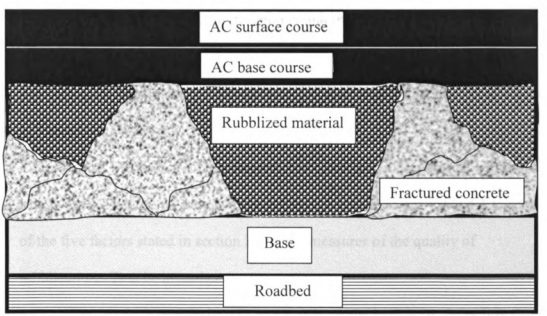


b) Schematic representation of the trench area

Figure 4.10 Excavated showing the sand subbase and the fractured concrete layer

shear failure along I-196. Note that, I-196 was rubblized immediately after two days of sustained rain. During the rubblization operation, the subbase and the roadbed soil were wet and soft.

To assure better measures of the quality of rubblization, equipment calibration must be performed prior to the commencement of the rubblization operation. This is presented in the next section.

## 2.4 Equipment Calibration

The quality of the rubblization procedure could be improved by calibrating the rubblizing equipment prior to the commencement of full-scale rubblization. Such calibration should be conducted at one end of the project using the following steps:

1. Divide the slabs along one lane into twelve adjacent sections such that each section is 6-ft wide (across the slab) and 12-ft long (along the slab) as shown in Figures 4.13 and 4.14 for the multi-hammer and the resonant frequency breakers, respectively.
2. Rubblize each section using different setting of the rubblizer parameters as shown in Figures 4.13 and 4.14.
3. Excavate two 3-ft wide trenches along the rubblized portion of the slab as shown in Figures 4.13 and 4.14 and examine and assign a score as per Table 4.1 to each of the five factors stated in section 2.3 under measures of the quality of rubblization. That is, investigate:
   a) The degree at which the concrete slab has been broken to pieces less than 6-inch in size. This can be estimated by the number of larger than 6-inch concrete pieces found in the trench.

a) Shear failure in a rubblized pavement

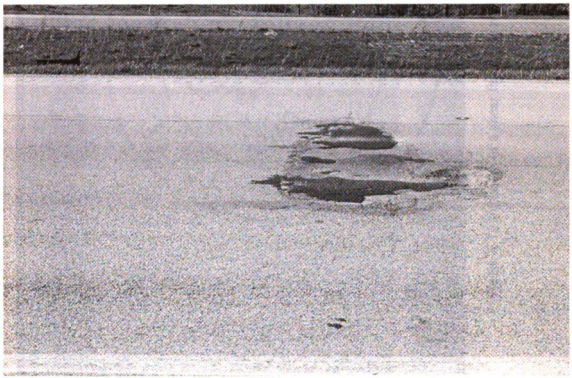

b) Another shear failure in a rubblized pavement

Figure 4.11 Two shear failures in the rubblized pavement on NB I-196

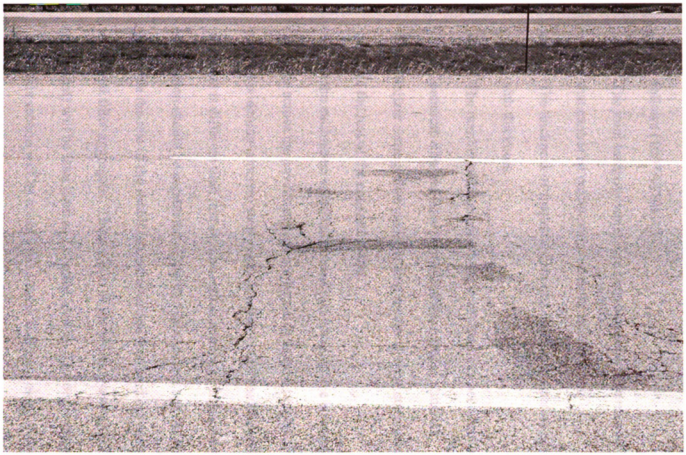

Figure 4.12 Initiation of a shear failure on rubblized pavement project on NB I-196

b) The degree of debonding of the temperature steel. This can be estimated as the trench area where the temperature steel has been debonded (ATSB) divided by to the total area of the trench (AT) and expressed in percent as follows [100*ATSB/AT].

c) The joint integrity which can be estimated by the number of dowel bars that cannot be easily removed from the concrete.

d) The thickness of fractured concrete layer expressed in percent of the total slab thickness.

e) The number of large concrete pieces that have been broken-off the concrete slab and have penetrated the subbase material.

4. The rubblizer settings that yield the best results (lowest score) should be used to rubblize the rest of the concrete slabs.

5. Repeat the calibration when the unconfined compressive strength of the concrete along or across the pavement changes by more than 50 percent. For example when a widening concrete strip exists, it is likely that the strength of the newer concrete is different than that of the original concrete. In such a scenario, the calibration should be conducted along the old concrete and the widening strip.

6. Excavate the rest of the rubblized material and fractured concrete and replace with approved filler aggregate. This section of the project (conventional flexible pavement) will be later used as a control section. Historical distress data collected along this section will be compared to those collected along the rubblized section, which would help the highway agency to compare the performance of rubblized pavement to that of flexible pavement.

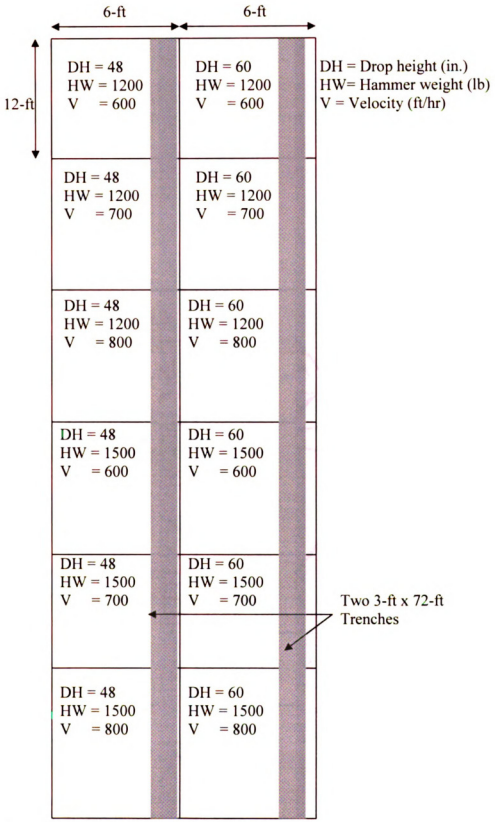


Figure 4.13 Calibration layouts for the multi hammer rubblizer

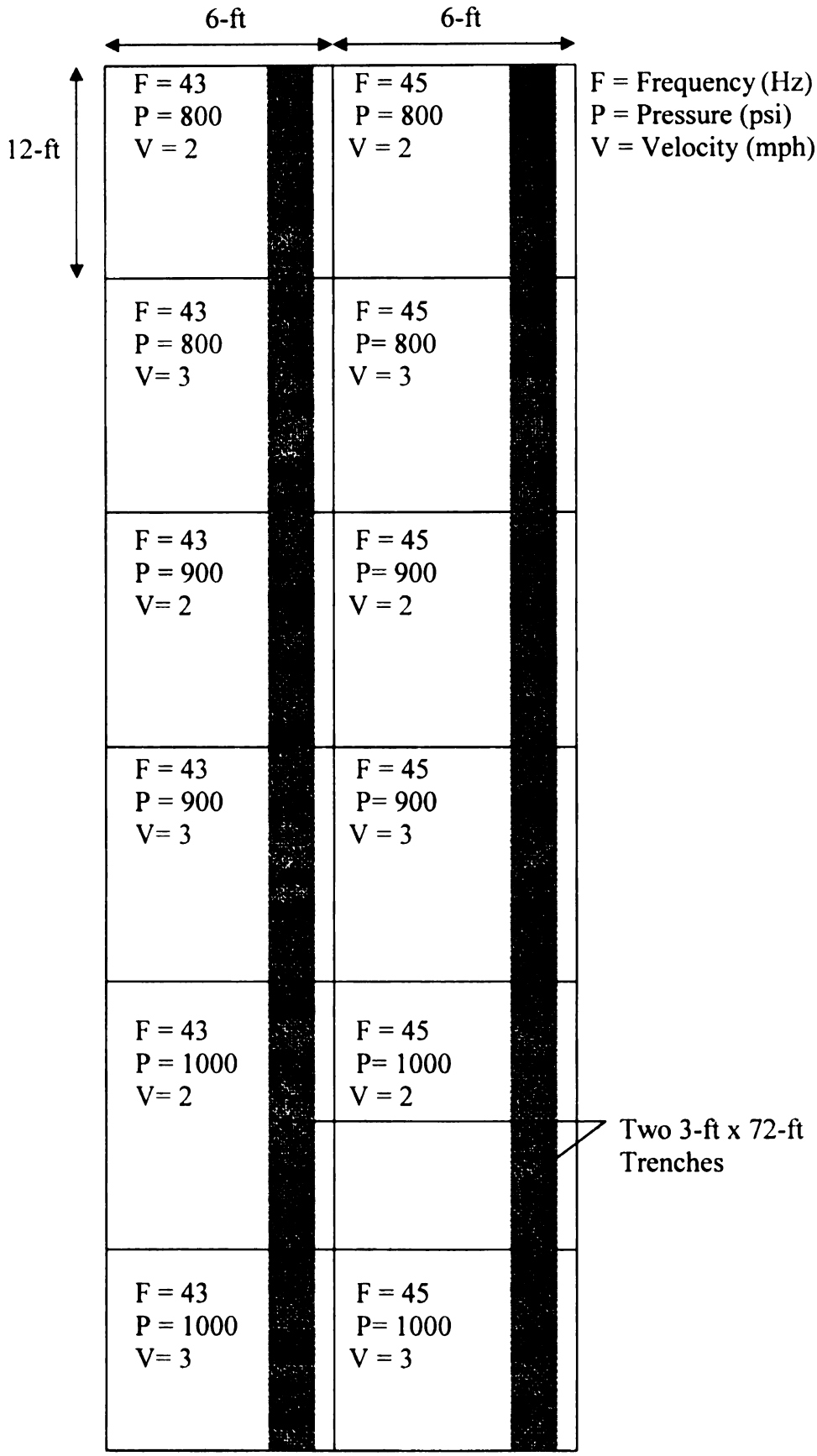


Figure 4.14 Calibration layouts for the resonant frequency breaker

Table 4.1 Definition, objectives and score of the quality of the rubblization operation

Rating of the rubblization operation

**Rubblization Definition and Objectives**

The quality of rubblization is a measure of the degree of success to which the rubblization procedure satisfies the following objectives.

1. Breaking the concrete slabs to pieces smaller than 6 in. (152 mm)
2. Completely debonding the temperature Steel
3. Destroying joint integrity
4. Producing full-depth rubblization
5. No large concrete pieces have penetrated the subbase

The rating of the quality of rubblization can be calculated using the following equation:

$$\mathbf{QR = Max\ (S_i)}$$

Where QR = quality of rubblization and $S_i$ is a score relative to the $i^{th}$ objective.

Lower QR values imply better rubblization quality. A QR value of 50 is the threshold value above which the quality of rubblization is not acceptable. The proposed values of $S_i$ are listed below.

Score of each objective of the rubblization operation

| Objective | Measurements within a 3-ft wide and 6-ft long trench | Best score | Maximum acceptable score |
|---|---|---|---|
| 1 | 30*the number of loose pieces larger than 6 in. | 0 | 50 |
| 2 | 100* the area of the trench where steel is not debonded/the total area of the trench (%) | 0 | 50 |
| 3 | 25* the number of dowel bars that cannot be easily extracted from the trench. | 0 | 50 |
| 4 | 100* the thickness of the fractured concrete in the trench/the total slab thickness (%) | 0 | 50 |
| 5 | 51* the number of large concrete pieces that were broken-off and penetrated the subbase | 0 | 50 |

## 3.0 CONSTRUCTION PROCEDURES

The performance of both flexible and rubblized pavements is also a function of the construction procedures. In this study, the most predominant and construction-related distress found in rubblized and flexible pavements is particle segregation in the AC layer. Particle or physical segregation causes high percent air void contents in the AC layer and raveling, and substantially decreases the tensile strength of the AC (Chang et al, 2001 and 2002). The high percent air void contents accelerate the aging process and moisture damage of the AC binder, whereas the low tensile strengths increase the TDC potential. Figure 4.15 shows a general and a close-up view of a segregated area along the passing lane of US-23 where raveling has taken place within two years after the completion of construction. Note that the traffic lane is in perfect condition. Figure 4.16 shows an end-of-load segregated area and strip segregation where TDC can be found. The main cause of these TDC is the low tensile strength of the AC due to segregation.

## 4.0 THE ASPHALT MIX DESIGN

Based on the result of three manual distress surveys of 87 rubblized pavement projects and the information regarding the type of asphalt mixes used on those projects (see Tables 3.14 and 3.15), it appears that the 4B and 4C mixes show one of the worst performance. This was expected because the two mixes are known to be brittle and relatively dry. The two mixes were originally designed to overcome the problem of rutting in Michigan. It is recommended that AC mixes with higher tensile strength and less brittleness be used to reduce TDC potential. In addition, past and current research activities indicate that:

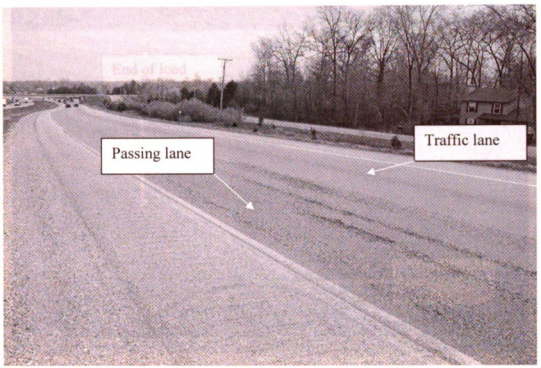


b) General view of a segregated area

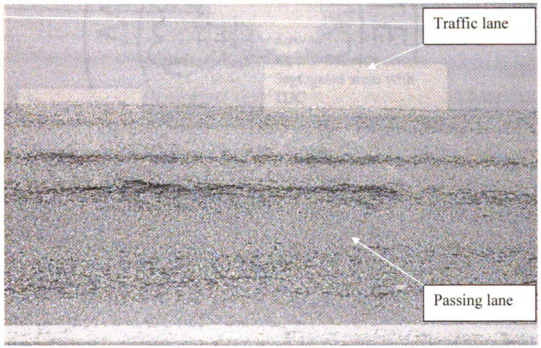


b) A close-up view of a segregated area

Figure 4.15 Pavement condition in segregated and non-segregated areas along US 23 in May 2002, 2 years after construction

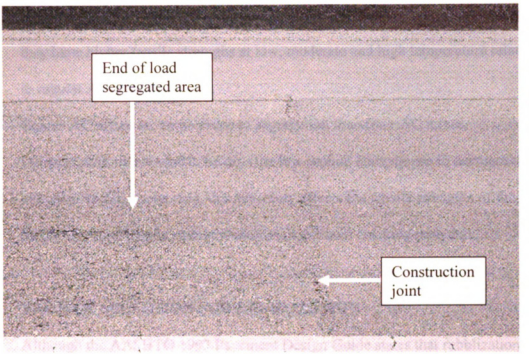


a) End of load segregated area

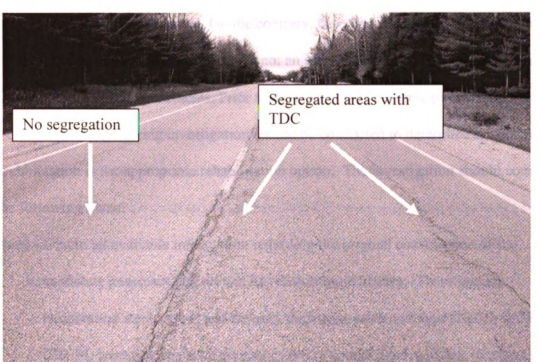


b) General pavement condition of segregated and not segregated areas

Figure 4.16 Pavement condition in segregated and not segregated areas along US-131 in May 2002, 5 years after construction

1. Polymer modified asphalt mixes could be used as the AC surface course since they have higher tensile strengths at low, moderate and high temperature relative to regular AC mixes.
2. Coarse AC mixes are more prone to segregation than finer AC mixes.
3. Dense asphalt mixes tend to be dry (the low asphalt contents are to decrease the bleeding/flushing potential); this adversely affects the tensile strengths of the mixes. The low tensile strengths increase top-down cracking potential.

## 5.0 PROJECT SELECTION FOR RUBBLIZATION

Although the AASHTO 1993 Pavement Design Guide states that rubblization can be used as a rehabilitation option for any distressed concrete pavement condition; field data do not support such statement. On the contrary, based on field observations that were conducted during this study, rubblization is not an appropriate rehabilitation option for some distressed concrete pavements. Prior to the selection of concrete pavement projects for rubblization, engineering investigation should be conducted to determine whether or not rubblization is the appropriate rehabilitation option. The investigation should consist of the following items:

**History** - Obtain all available information regarding the original construction of the candidate pavement project and its rehabilitation history. These include: temperature steel, dowel and tie bars, thickness, pavement type (JRCP, JPCP or CRCP), joint spacing, widening strip, full or partial depth patches, overlays and so forth.

**Distress** - Obtain all available historical distress data and conduct distress survey to determine the extent of longitudinal and transverse cracks and other defects and discontinuities such as asphalt patches in the concrete pavement.

**Nondestructive Deflection Test (NDT)** – Conduct FWD tests at 500-ft interval along the project. Use the deflection data to backcalculate the stiffness or modulus of the roadbed soil.

**Coring** – Obtain one concrete core for each 500-ft interval along the project. Examine the cores for delamination type cracks and record the width of the cracks. Determine the compressive strength of each core. If asphalt overlay is present, determine the thickness of the overlay (for milling purposes and for backcalculation). If widening strips exist, obtain cores from the widening strip as well to determine the compressive strength of the concrete along the strip.

**Soil boring** - At two to three core locations, drill through the base, subbase and at least 2 ft through the roadbed soil. The objectives of the drilling are to document the type of base, subbase and roadbed materials and to determine whether or not the roadbed soil is saturated.

Based on the analysis of the above data, the following pavements should not be selected for rubblization:

1. Composite or concrete pavements that have extensive discontinuities. The rubblization energy will dissipate in the gaps at discontinuities instead of breaking the concrete slab. Such discontinuities include:
   a) Extensive longitudinal and transverse cracks. The term "extensive cracks" is defined herein as follows "a pavement section would have extensive

cracks when the crack ratio (CR) is equal to or exceed 1.0." The crack ratio is defined as follows:

$$CR = \frac{CCL}{PL}$$

where CR = crack ratio;

CCL = cumulative crack length (mile); and

PL = pavement length (lane-mile).

b) Concrete pavements that were previously rehabilitated using crack and seat method. A good part of the rubblization energy would be consumed in closing the cracks.

c) Concrete pavements with frequent delamination type cracks.

2. Concrete pavements that are supported on soft or saturated subbase and/or roadbed soil. The term "soft subbase" refers to any subbase material having resilient modulus of less than 7000 psi. The term "soft roadbed soil" refers to any roadbed soil having a resilient modulus of less than 3000 psi.

3. Concrete pavements supported on a considerable soft subbase relative to the stiffness of the roadbed soil. The rubblization energy causes shear failure and lateral displacement of the subbase. For example, if a concrete pavement is supported on a base material with 10,000-psi modulus and a roadbed soil with 20,000-psi modulus, the rubblization energy may cause the softer subbase to fail in shear or be displaced laterally.

In addition, the timing of the rubblization operation is very crucial to its success. For example, the operation should not commence immediately after a period of sustained rain (few days). The deteriorated and cracked concrete pavements would allow

considerable water infiltration into the subbase causing softening of the subbase material and the roadbed soil. Likewise, commencing the rubblization operation shortly after the end of a thaw period is not desirable; it is highly likely that the subbase and the roadbed soils are saturated.

## 6.0 SUMMARY

In this chapter, the quality and objectives of rubblization are defined. It is shown, using several pavement examples, that when the rubblization objectives are not fully satisfied, premature distress would occur. Based on examination of the rubblization operation on various projects, equipment calibrations schemes are presented. Finally, the factors that need to be examined during the selection of rubblization projects are presented and discussed.

# CHAPTER 5

# CLASSIFICATION AND IDENTIFICATION OF TOP-DOWN CRACKS

## 1.0 INTRODUCTION

This chapter was developed in cooperation with Michael Schorsch who is studying the causes of TDC in flexible pavements. Part of the problem associated with TDC is that PMS databases make no distinction between TDC and other cracks. Since most databases do not include data regarding crack locations, it is not possible to decipher the distress data and to separate regular cracks from TDC.

The main reason for the lack of TDC data is that no identification procedure has been developed whereby the TDC can be correctly documented either by manual or videotape survey. The lack of such data creates various problems including:

1. Inappropriate selection of rehabilitation alternatives; the rehabilitation options for TDC are different than those for regular cracks.
2. It is not possible to assess the impact of TDC on pavement conditions or on its remaining service life.
3. TDC propagation models cannot be verified.

Recognizing the dimension of the problem, one of the objectives of this study is to develop TDC identification procedure based on crack appearance, location and the mechanics of crack propagation. Such procedure was developed and is presented below.

## 2.0 TDC DESCRIPTIONS AND CLASSIFICATION

TDC were typically observed in the field as:

- Individual longitudinal or transverse cracks.
- Groups of parallel longitudinal cracks.
- Networks of longitudinal cracks.

Based on field observations and depending on the type and causes of the first observed crack, TDC can be classified into three categories as presented in the next sections.

## 2.1 Longitudinal Top-Down Cracks (LTDC) Category

The main cause of LTDC in this category is the induced tensile stress at the pavement surface. Such tensile stress could be a combination of the tensile stress due to tire-pavement interaction and thermal stress. The magnitude of the tensile stress could be increased due to differential stiffness between the AC courses and the pavement layers and, for rubblized pavement only, the geometry of the interface between the fractured concrete and the rubblized material layers. The LTDC develop in three stages (Svasdisant et al, 2002) as follows:

- In the first stage, a single short longitudinal crack develops in the vicinity of the edge of the wheel path. Over time, the crack propagates parallel to the wheel path as shown in Figures 5.1 and 5.2.
- In the second stage, sister cracks develop and propagate parallel to the wheel path as shown in Figure 5.3 or in some pavements, transverse TDC may develop connecting to the existing LTDC as shown in Figure 5.4.
- In the third stage, two or more LTDC connect via transverse TDC as shown in Figure 5.5.

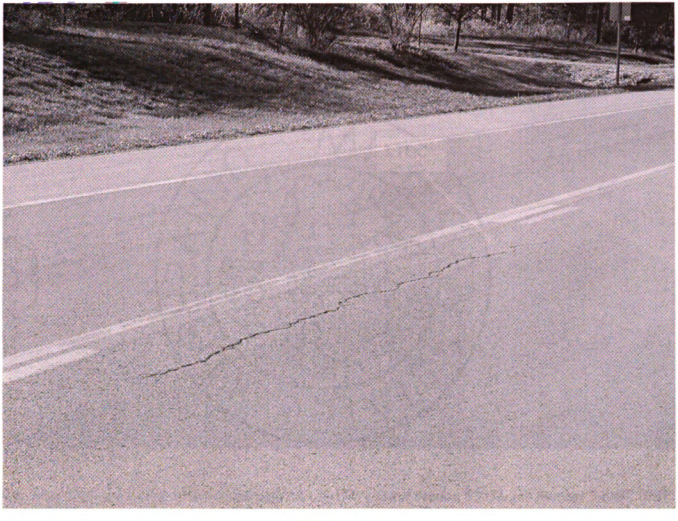

Figure 5.1 Longitudinal TDC at the edge of the wheel path on US-23, control section 04031, job number 32335, BMP 0.0 and EMP 7.9, May 2002

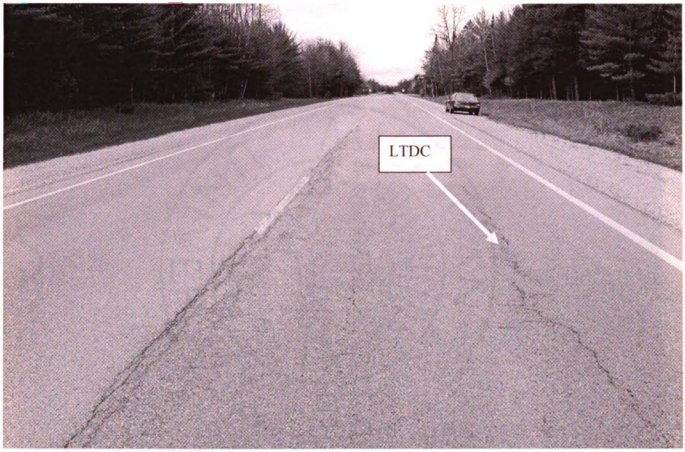


Figure 5.2 Longitudinal TDC at the edge of the wheel path on US-131, control section 83032, job number 34060, BMP 13.0 and EMP 18.7, May 2002

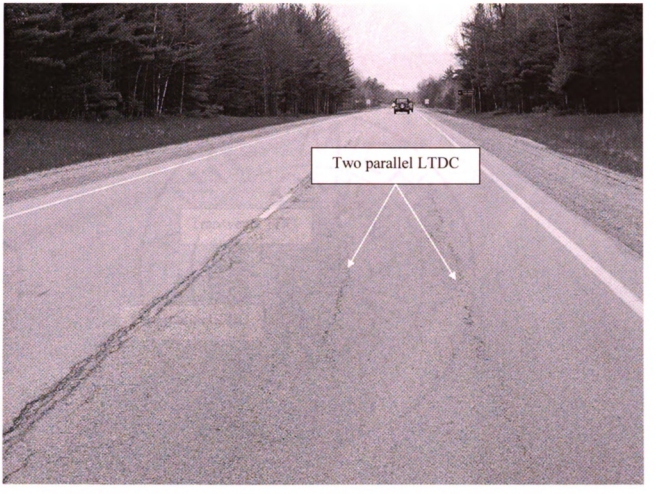


Figure 5.3 Parallel longitudinal TDC at the edge of the inner and outer wheel paths on US-131 (same location as Figure 5.2), control section 83032, job number 34060, BMP 13.0 and EMP 18.7, May 2003

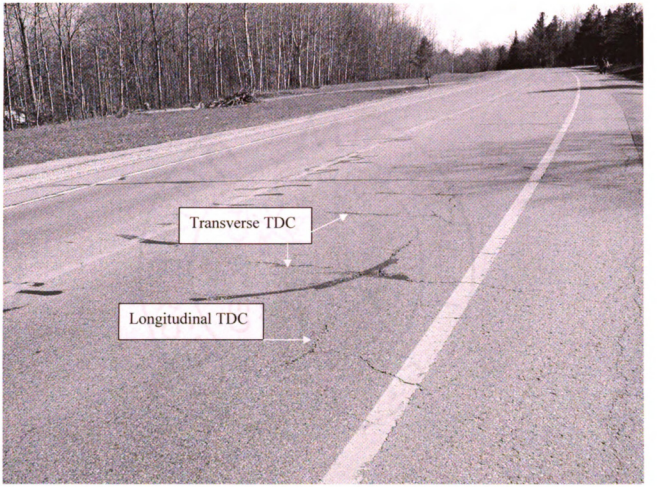


Figure 5.4 Transverse TDC associated with longitudinal TDC on M-27, control section 16302, job number 26672, BMP 9.3 and EMP 11.4, May 2003

Figure 5.5 The third stage of TDC development, LTDC and TTDC forming a networks on East Michigan Avenue, control section 39555, job number 39212, BMP 13.9 and EMP 15.2, May 2002

Figure 5.6 depicts the three stages of TDC and some pavement cores showing partial propagation of TDC. Since the 5 cores were extracted from pavements with various AC thicknesses, it can be concluded that the initiation and propagation of TDC is independent of the pavement thickness

## 2.2 Transverse Top-Down Cracks (TTDC) Category

The likely cause of TTDC is thermal stresses due to cold temperatures and low tensile strength AC mixes. Most of the TTDC appear as short transverse cracks located at the center of the lane as shown in Figures 5.7 and 5.8. Over time, the cracks propagate across the lane and other transverse cracks develop. The TTDC may or may not be connected with LTDC depending on the state of the tensile stress at the pavement surface in the vicinity of the wheel path. Finally, the main reason that most TTDC initiate in the middle of the lane is because the crack in the wheel path is delayed due to the tires kneading action.

## 2.3 Cracks in Segregated Areas Category

The cause of TDC in this category is particle segregation in the AC mat. Further, because of the high air voids in segregated areas, the AC mix is more susceptible to oxidation and moisture damage resulting in substantial decreases in the tensile strength of the mix. Particle segregation may cause up to 60 percent reduction in the tensile strength of the AC mix in the segregated areas (Brown et al, 1989 and Khedaywi and White, 1995). Depending on the shape of the segregated area, the crack could be longitudinal or

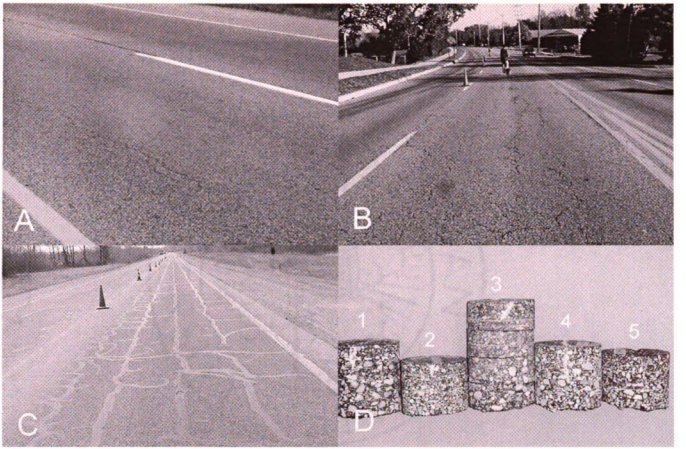


Figure 5.6 The three stages (A, B and C) of TDC development and pavement cores showing the extent of TDC propagation with depth

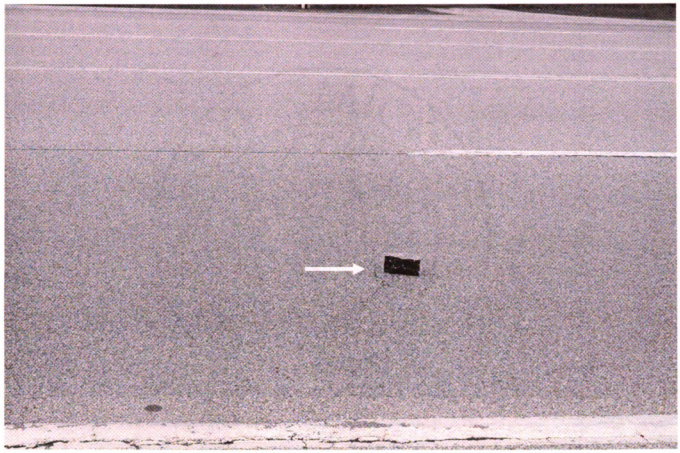

Figure 5.7 Transverse TDC located at the center of the lane (compare the size to half of a 4-in core)

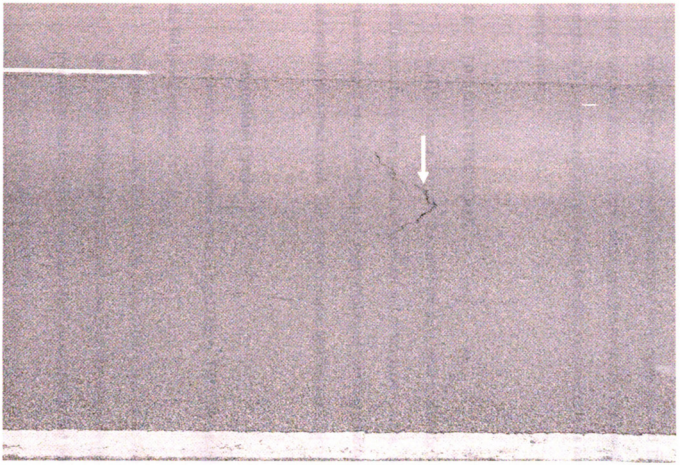

Figure 5.8 Transverse TDC located at the middle of the lane

transverse, although most observed TDC in this category are longitudinal. The TDC propagate within the segregated area at a relatively fast rate, which decreases as the cracks begin to penetrate non- segregated areas.

Another type of distress that associated with segregation and TDC in segregated areas is raveling. Figure 5.9 shows raveling of the outer lane of a two-lane highway. The pavement is two years old and the traffic lane (the inner lane) shows no sign of distress and/or raveling.

## 3.0 TDC IDENTIFICATION

As stated earlier, no procedure has been developed to identify TDC and to differentiate them from regular longitudinal and/or transverse cracks. Such a procedure was developed and is based on field observations and the understanding of TDC initiation and propagation mechanism. This section presents and discusses the procedure.

### 3.1 Longitudinal Cracks

An observed longitudinal crack is highly likely TDC if it satisfies one or more of the following criteria:

1. Longitudinal cracks located at the edges of the wheel paths. These LTDC are most likely initiated by the induced tensile stresses due to tire-pavement interaction and temperature and are likely accelerated by the low tensile strength of the AC mix at the pavement surface.
2. A group of parallel longitudinal cracks separated by 1 to 3 ft. and located at the edges of, or within, the wheel paths.

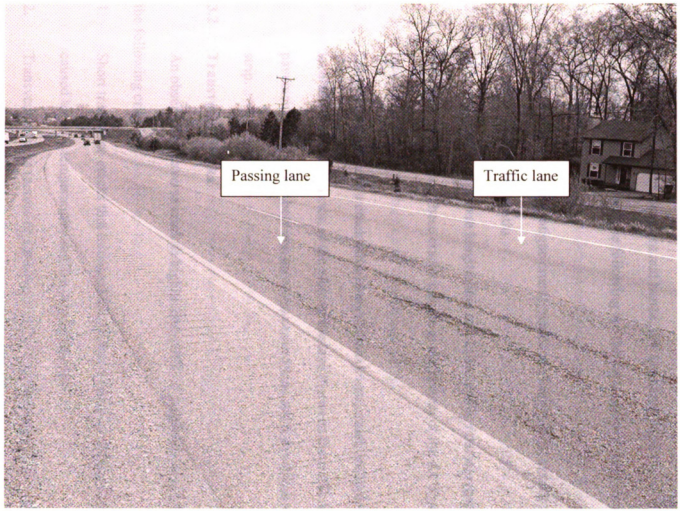


Figure 5.9 Longitudinal TDC and raveling in segregated area

3. Longitudinal cracks located between two lanes. These longitudinal TDC are caused by the opening of the paving joint.

4. Longitudinal cracks that are located in segregated areas or in areas where the AC mix is dry (low asphalt content and hence, low tensile strength).

For comparison purposes, the following are the locations of other types of longitudinal cracks.

1. Low to medium severity fatigue cracks, which are longitudinal cracks located at the center of the wheel paths.

2. Stripping cracks, which are longitudinal cracks located in non-segregated areas at the center of the lane. These cracks initiate at the bottom of the AC layer and propagate upward.

3. Longitudinal reflective cracks from longitudinal joints, which are typically located between two lanes, at the edge of the lane (between the traffic lane and the pavement shoulder) or between an old pavement lane and a pavement widening strip.

### 3.2 Transverse Cracks

An observed transverse crack is highly likely TDC if it satisfies one or more of the following criteria.

1. Short transverse cracks that initiate at the center of the lane. These TTDC are caused by cold temperatures and low tensile strength.

2. Transverse cracks (across or almost across the lane) that appear at a constant interval throughout the pavement section. These cracks can be identified by their low profile at the crack edges, which causes roughness. The cracks initiate at the

pavement surface and propagate downward because the thermal stress at the pavement surface is much higher than that at the bottom of the AC layer.

3. All short transverse cracks connecting LTDC. These short cracks could be located anywhere along the pavement.

4. Transverse cracks in segregated areas.

For rubblized and composite pavements only, straight transverse cracks that appear at a constant interval equal to the joint spacing of the original concrete slab are joint reflective cracks. The cracks start at the bottom of the AC and propagate upward. Reflective cracks typically have higher profiles at the center of the cracks.

### 3.3 Network of Longitudinal and Transverse Cracks

An observed network of longitudinal and transverse cracks is TDC if the cracks in the network satisfy one or more of the following criteria:

1. The network of cracks is located in and around the wheel paths and the distance between two longitudinal cracks is less than 3 ft.

2. A network of meandering cracks that extends throughout the pavement surface. This type of network is indicative of block cracking. The cracks are TDC caused by hardening of the AC binder.

Finally, a localized network of cracks is not TDC if it is located around the center of the wheel paths. These cracks are fatigue cracks.

## 4.0 SUMMARY

In this chapter, TDC were classified into three categories; LTDC, TTDC and TDC in segregated areas, based on field observations and the type and causes of the first observed crack. Further, a procedure to identify TDC and to differentiate them from regular longitudinal and/or transverse cracks was developed and presented in this chapter. The procedure is based on field observations and the understanding of TDC initiation and propagation mechanism.

S
2003
v.2
54847655

LIBRARY
Michigan State
University

**PLACE IN RETURN BOX** to remove this checkout from your record.
**TO AVOID FINES** return on or before date due.
**MAY BE RECALLED** with earlier due date if requested.

| DATE DUE | DATE DUE | DATE DUE |
|---|---|---|
| | | |
| | | |
| | | |
| | | |
| | | |
| | | |
| | | |
| | | |
| | | |
| | | |

6/01 c:/CIRC/DateDue.p65-p.15

ANALYSI

# ANALYSES OF TOP-DOWN CRACKING IN RUBBLIZED AND FLEXIBLE PAVEMENTS

Volume II

By

Tunwin Svasdisant

**A DISSERTATION**

Submitted to
Michigan State University
in partial fulfillment of the requirements
for the degree of

DOCTOR OF PHILOSOPHY

Department of Civil and Environmental Engineering

2003

1.0 GENE

Durin

conducted on s

falling weight

sensors of the

on-board comp

measure and re

objectives of th

- Analyz
  pavem
- Backcal
- Assess

At each

test section was

separated by 1

marked on the

the figure indic

All FW

recorded while

were conducte

sites, about 10

# CHAPTER 6

# BACKCALCULATION OF LAYER MODULI

## 1.0 GENERAL

During the course of this study, nondestructive deflection tests (NDT) were conducted on several rubblized and flexible pavement projects using the MDOT KUAB falling weight deflectometer (FWD). The configuration and spacing of the 9 deflection sensors of the FWD are shown in Figure 6. 1. The capabilities of the FWD include an on-board computer to record the deflection data to within 0.01 mils (0.00001 in.) and to measure and record the pavement and air temperatures at each test location. The objectives of the NDT include:

- Analyzing the variations in the pavement deflections along and across the pavements.
- Backcalculating the moduli of the rubblized and flexible pavement layers.
- Assessing the linearity of the pavement response to load.

At each rubblized and flexible pavement project included in the FWD testing, a test section was selected and the section was divided into one or two 100-ft long test sites separated by 100-ft of pavement. At each test site, about forty FWD test locations were marked on the pavement surface as shown in Figure 6. 2. The circles and the letter "X" in the figure indicate core and FWD test locations, respectively.

All FWD tests consisted of 4 drops, the deflection data from the first drop was not recorded while the data from the other three drops were recorded. Further, most tests were conducted using a target load of 9000-lb. At one FWD test location along some test sites, about 10 FWD tests were conducted at each of four load levels to assess the

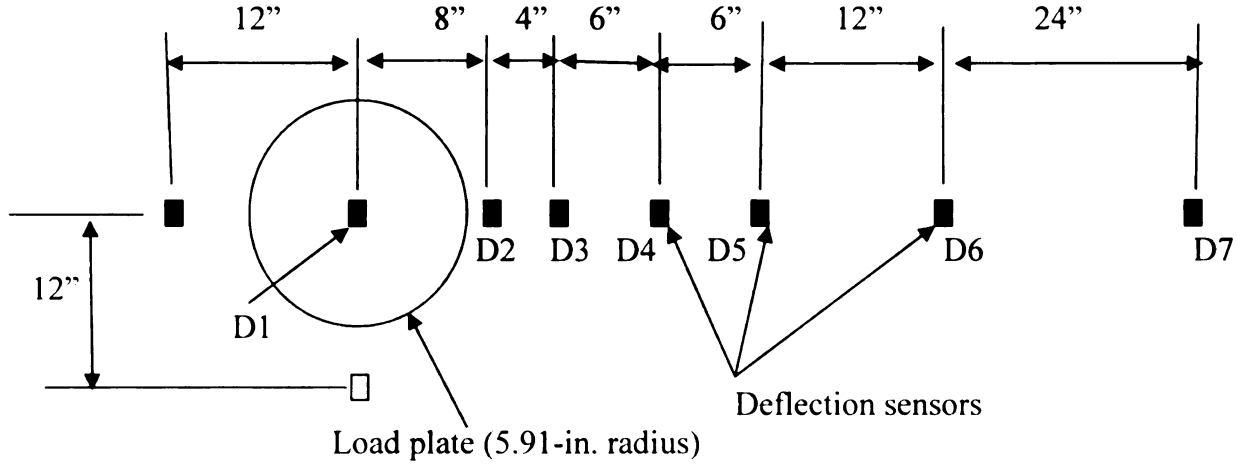


Figure 6.1 Schematic of FWD load plate and the spacing of the deflection sensors

40 FWD test lo

12 Core locatio

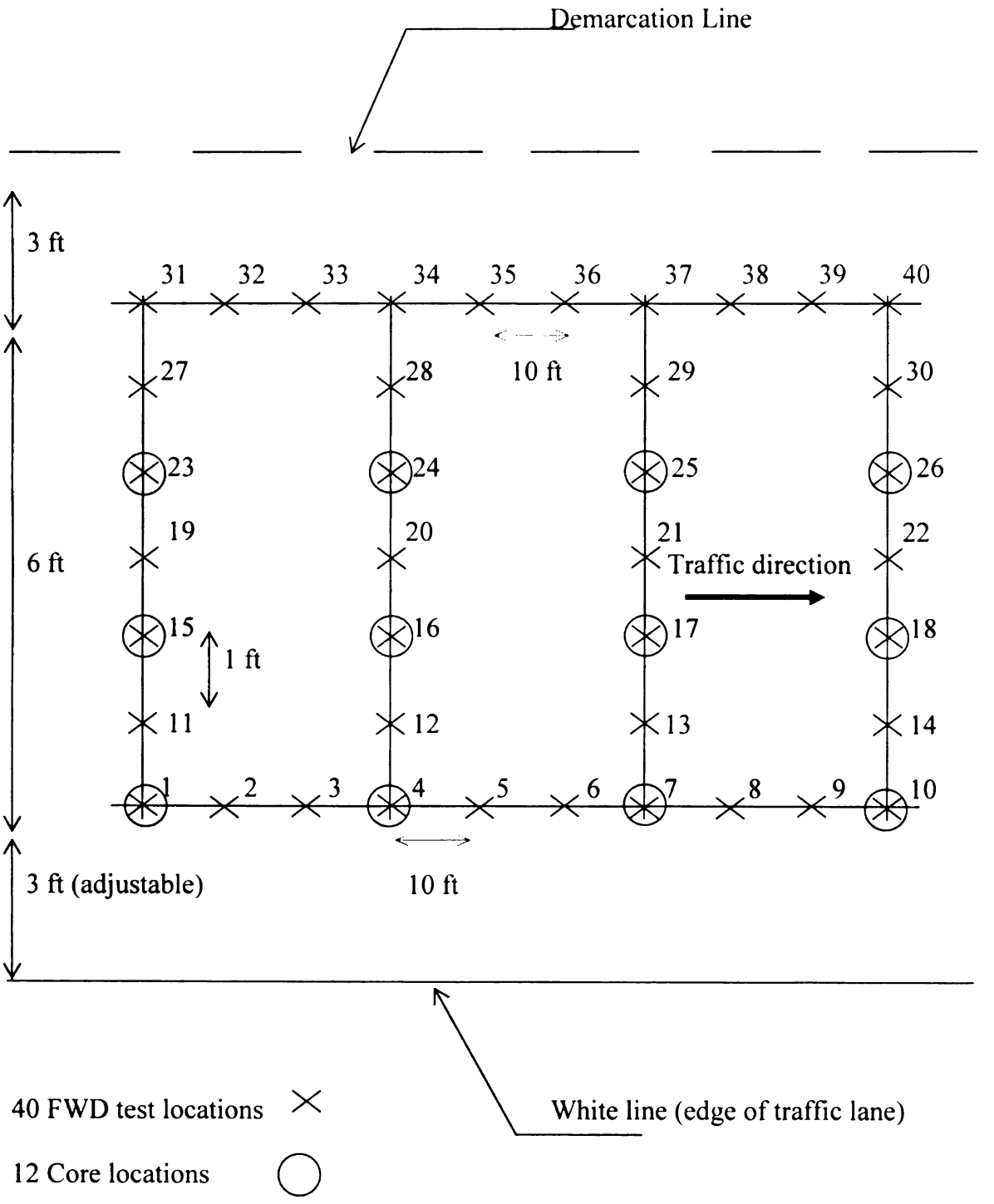


Figure 6.2 Typical FWD tests and cores layout

repeatability o

Both the linear

After a

extracted. The

was measured

were used as in

used to backca

Finally,

chapters 6, 7 an

1. Asphalt

2. Base =

3. Subbase

4. Roadbe

5. Rubbli

6. Rubbli

7. Fractur

8. Combi

9. Combi

## 2.0 REPE

On fou

location for ea

of the tests is

repeatability of the deflection data and the linearity of the pavement response to load. Both the linearity and repeatability are discussed in the next section.

After all FWD tests were completed, between 5 and 12 pavement cores were extracted. The thickness of each core at each of the 4 ends of two orthogonal diameters was measured and the average core thickness was then calculated. The thickness data were used as input to the backcalculation program. The D1 through D7deflections were used to backcalculate the layer moduli using the MICHBACK computer software.

Finally, for convenience, the following abbreviations are used throughout chapters 6, 7 and 8:

1. Asphalt concrete = AC
2. Base = B
3. Subbase = S
4. Roadbed soil = RB
5. Rubblized concrete slab = RCS
6. Rubblized material = RM
7. Fractured concrete = FC
8. Combined base and subbase = BS
9. Combination of base, subbase and roadbed soil = BSRB

## 2.0 REPEATABILITY AND LINEARITY OF THE DEFLECTION DATA

On four pavement projects, several FWD tests were conducted at the same location for each of the following loads: 5,500, 9,000, 16,000 and 21,000 lb. The purpose of the tests is to examine the repeatability of the deflection data at all seven deflection

Table 6.1 Pav

| Test sites |
| --- |
| 3973-21 |
| 1992-12 |
| 3973-52 |
| 2702-11 |

*refer to the te

Table 6.2 The a
load

| Load (pound) | Num of dr |
| --- | --- |
| 5500 | 1 |
| 9900 | 2 |
| 16000 | 1 |
| 21000 | 1 |

STDEV = Stan
CV = Coefficie

Table 6.1 Pavement projects where repeatability and linearity tests were conducted

| Test sites | Load (lb) | Number of drops | Load (lb) | Number of drops | Load (lb) | Number of drops | Load (lb) | Number of drops |
|---|---|---|---|---|---|---|---|---|
| 20273-21 | | | 9000 | 20 | 16000 | 10 | 21000 | 10 |
| 10692-12 | 5500 | 10 | 9000 | 20 | 16000 | 10 | 21000 | 10 |
| 30373-52 | 5500 | 10 | 9000 | 20 | 16000 | 10 | 21000 | 10 |
| 20102-11 | 5500 | 10 | 9000 | 20 | 16000 | 10 | 21000 | 10 |

* refer to the test sites reported in Chapter 3.

Table 6.2 The averages and standard deviations of deflections D1 through D7 at different load levels, I-69 EB, test site 1 of test section 1

| Load (pound) | Number of drops | Statistics | Deflection (mils) | | | | | | |
|---|---|---|---|---|---|---|---|---|---|
| | | | D1 | D2 | D3 | D4 | D5 | D6 | D7 |
| 5500 | 10 | Average | 4.93 | 3.40 | 2.85 | 2.42 | 2.09 | 1.56 | 0.84 |
| | | STDEV (mils) | 0.07 | 0.04 | 0.04 | 0.04 | 0.03 | 0.03 | 0.04 |
| | | CV (%) | 1.4 | 1.1 | 1.3 | 1.5 | 1.5 | 1.9 | 4.4 |
| 9000 | 20 | Average | 8.00 | 5.63 | 4.87 | 4.17 | 3.58 | 2.62 | 1.37 |
| | | STDEV (mils) | 0.06 | 0.05 | 0.04 | 0.04 | 0.03 | 0.02 | 0.02 |
| | | CV (%) | 0.8 | 0.9 | 0.9 | 0.9 | 0.8 | 0.9 | 1.6 |
| 16000 | 10 | Average | 14.35 | 10.24 | 8.93 | 7.59 | 6.58 | 4.77 | 2.55 |
| | | STDEV (mils) | 0.04 | 0.04 | 0.10 | 0.04 | 0.03 | 0.03 | 0.03 |
| | | CV (%) | 0.3 | 0.4 | 1.2 | 0.5 | 0.4 | 0.7 | 1.3 |
| 21000 | 10 | Average | 18.60 | 13.37 | 11.58 | 9.83 | 8.55 | 6.22 | 3.36 |
| | | STDEV (mils) | 0.05 | 0.04 | 0.10 | 0.03 | 0.02 | 0.02 | 0.03 |
| | | CV (%) | 0.3 | 0.3 | 0.9 | 0.3 | 0.3 | 0.3 | 0.8 |

STDEV = Standard deviation

CV = Coefficient of variation = standard deviation as a percent of the average

sensor location

list of the proje

with the numb

tests for I-69 E

list of the aver

(STDEV) and

As can be seen

load levels on

FWD (Irwin, I

sensors and fo

standard devia

Linear

four load level

The average o

Typical results

Figure 6.3 dep

Table 6.3 and

to load is linea

data were used

system.

sensor locations and the linearity of the pavement response to load. Table 6.1 provides a list of the projects along which the repeatability and linearity tests were conducted along with the number of weight drops for each load level. Typical results of the repeatability tests for I-69 EB, test site 1 of test section 1, are listed in Table 6.2. The table provides a list of the average measured deflection at each sensor location, the standard deviation (STDEV) and the coefficient of variation (CV) of the deflection data at each load level. As can be seen, the standard deviation for sensor 3 (D3), at the 16,000 and 21,000 pound load levels only, is ten percent, which satisfies the performance specifications for the FWD (Irwin, L.H., W.S., Yang, and R.N. Stubstad, 1989). For all other deflection sensors and for the D3 sensor at the 5,500 and 9,000 pound load levels, the maximum standard deviation is 0.07 mils, well below the FWD performance specifications.

Linearity tests were also conducted on seven pavement sections. At each of the four load levels used in the repeatability tests, ten or twenty FWD drops were conducted. The average of the measured deflection data for each load level was then calculated. Typical results from I-69 EB, test site 1 of test section 1, are provided in Table 6.3. Figure 6.3 depicts the average measured deflections versus the applied load. The data in Table 6.3 and Figure 6.3 indicate that, for all practical purposes, the pavement response to load is linear. Based on the linearity of the pavement response to load, the deflection data were used in the backcalculation of layer moduli using a linear elastic layered system.

Table 6.3 Typ
EB

| Load (pound) | |
|---|---|
| 55(0) | |
| 9(0) | |
| 16(0) | |
| 2(000) | |

Figure 6.3 A

Table 6.3 Typical averages of D1 through D7 deflections at different load levels, I-69 EB, test site 1 of test section 1

| Load (pound) | Deflection (mils) | | | | | | |
|---|---|---|---|---|---|---|---|
| | D1 | D2 | D3 | D4 | D5 | D6 | D7 |
| 5500 | 4.93 | 3.40 | 2.85 | 2.42 | 2.09 | 1.56 | 0.84 |
| 9000 | 8.00 | 5.63 | 4.87 | 4.17 | 3.58 | 2.62 | 1.37 |
| 16000 | 14.35 | 10.24 | 8.93 | 7.59 | 6.58 | 4.77 | 2.55 |
| 21000 | 18.60 | 13.37 | 11.58 | 9.83 | 8.55 | 6.22 | 3.36 |

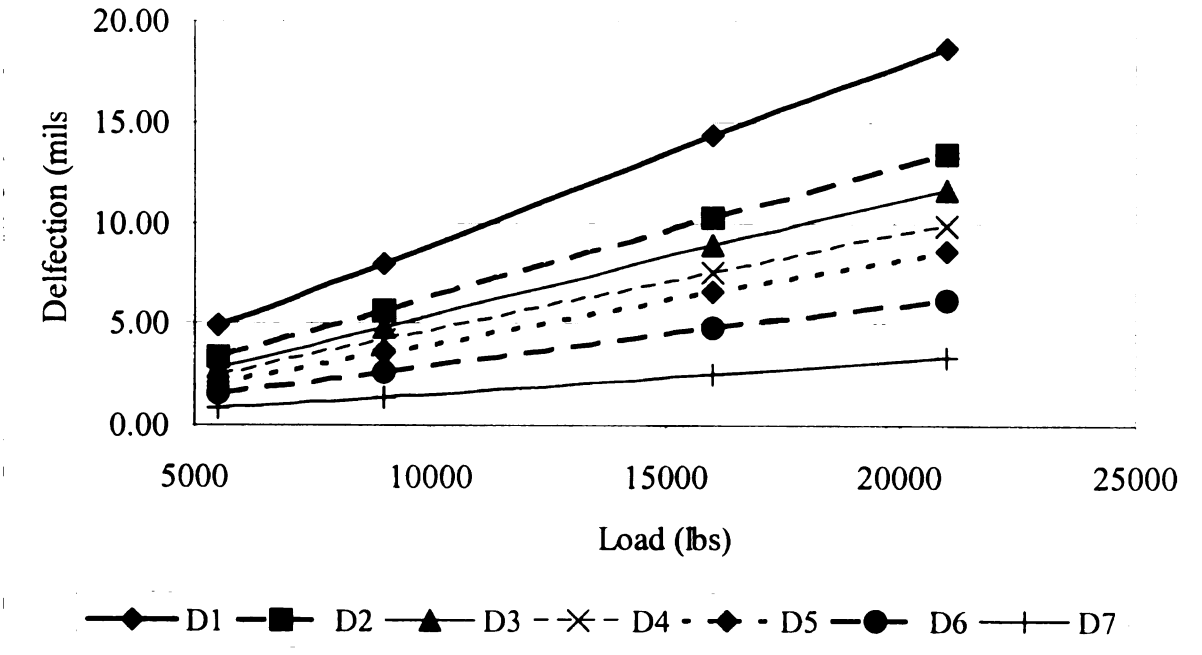


Figure 6.3 Average deflections of D1 to D7 versus load, I-69, test site 1 of section 1

3.0 THE I

Pavem

as an index ev

measured defl

Tables

pavement of U

similar inform

site 1 of sectio

deflections are

deflections alo

data in the tabl

rubblized conc

deflections of t

Table 6.7 prov

for 26 rubblize

variation for th

pavement sites

illustrate, the m

sections is the

directly related

more details, s

The th

and the

## 3.0 THE DEFLECTION DATA

Pavement deflections are its direct response to load. Deflection can be thought of as an index expressing the structural capacity of the pavement. Hence, variation in the measured deflection reflects parallel variation in the structural capacity of the pavement.

Tables 6.4 and 6.5 list the measured pavement deflections along and across the pavement of US-10 EB, test section 1, test sites 1 and 2, respectively. Table 6.6 provides similar information for a typical conventional flexible pavement along US-27 SB, test site 1 of section 1. The average and the coefficient of variation for D1 through D7 deflections are also listed in the three tables. Plots of the variation in D1 through D7 deflections along and across the three test sites are shown in Figures 6.4 through 6.6. The data in the tables and in the figures indicate that the variations in the deflections of the rubblized concrete pavements on US-10 EB are much higher than the variation in the deflections of the conventional flexible pavement on US-27 SB.

Table 6.7 provides a list of the values of the coefficient of variations of D1 through D 7 for 26 rubblized and 12 flexible pavement test sites. As can be seen, the coefficients of variation for the rubblized pavement sites are generally higher than those of the flexible pavement sites. Said variations reflect similar variability in the pavement structure. To illustrate, the main difference between conventional flexible and rubblized pavement sections is the rubblized concrete slab (RCS). Hence, the variations in the deflections are directly related to variations and/or non-uniformity of the RCS. Such non-uniformity (for more details, see Chapter 4) includes:

- The thickness of the rubblized material (RM) and fractured concrete (FC) layers and the geometry of their interface as shown in Figure 6.7.

Table 6.4 D
s

| FWD Station |
|---|
| 1 |
| 2 |
| 3 |
| 4 |
| 5 |
| 6 |
| 7 |
| 8 |
| 9 |
| 10 |
| 11 |
| 12 |
| 13 |
| 14 |
| 15 |
| 16 |
| 17 |
| 18 |
| 19 |
| 20 |
| 21 |
| 22 |
| 23 |
| 24 |
| 25 |
| 26 |
| 27 |
| 28 |
| 29 |
| 30 |
| 31 |
| 32 |
| 33 |
| 34 |
| 35 |
| 36 |
| 37 |
| 38 |
| 39 |
| 40 |
| Average |
| CV (%) |

CV = C

Table 6.4 D1 through D7 deflections, rubblized pavement, US-10 EB test section 1 test site 1

| FWD Station | Deflection (mils) | | | | | | |
|---|---|---|---|---|---|---|---|
| | D1 | D2 | D3 | D4 | D5 | D6 | D7 |
| 1 | 9.93 | 8.52 | 7.51 | 6.23 | 5.28 | 3.84 | 2.21 |
| 2 | 10.24 | 8.70 | 7.62 | 6.32 | 5.35 | 3.85 | 2.16 |
| 3 | 9.89 | 8.40 | 7.40 | 6.18 | 5.26 | 3.84 | 2.17 |
| 4 | 9.47 | 8.09 | 7.07 | 5.87 | 5.00 | 3.65 | 2.13 |
| 5 | 10.66 | 9.14 | 8.17 | 6.88 | 5.81 | 4.21 | 2.28 |
| 6 | 10.51 | 9.03 | 8.02 | 6.71 | 5.62 | 3.95 | 2.25 |
| 7 | 9.73 | 8.23 | 7.34 | 6.24 | 5.37 | 3.98 | 2.29 |
| 8 | 10.90 | 9.16 | 8.01 | 6.61 | 5.52 | 3.96 | 2.23 |
| 9 | 10.48 | 8.92 | 7.91 | 6.67 | 5.74 | 4.31 | 2.43 |
| 10 | 11.66 | 9.66 | 8.43 | 6.92 | 5.86 | 4.21 | 2.34 |
| 11 | 9.54 | 8.10 | 7.08 | 5.85 | 4.94 | 3.62 | 2.12 |
| 12 | 9.53 | 8.11 | 7.09 | 5.77 | 4.78 | 3.50 | 2.03 |
| 13 | 9.62 | 8.08 | 7.09 | 5.90 | 5.05 | 3.75 | 2.20 |
| 14 | 11.29 | 9.43 | 8.21 | 6.76 | 5.75 | 4.15 | 2.29 |
| 15 | 9.36 | 7.98 | 6.99 | 5.83 | 4.87 | 3.55 | 2.07 |
| 16 | 9.26 | 7.82 | 6.88 | 5.72 | 4.81 | 3.52 | 2.00 |
| 17 | 9.39 | 7.81 | 6.85 | 5.74 | 4.89 | 3.65 | 2.15 |
| 18 | 10.87 | 9.09 | 7.95 | 6.54 | 5.48 | 3.98 | 2.24 |
| 19 | 9.39 | 7.99 | 7.06 | 5.87 | 4.92 | 3.51 | 2.03 |
| 20 | 9.21 | 7.76 | 6.80 | 5.72 | 4.84 | 3.56 | 2.02 |
| 21 | 9.15 | 7.60 | 6.57 | 5.57 | 4.86 | 3.69 | 2.17 |
| 22 | 10.44 | 8.80 | 7.65 | 6.35 | 5.34 | 3.91 | 2.20 |
| 23 | 9.58 | 8.04 | 6.98 | 5.79 | 4.85 | 3.45 | 1.96 |
| 24 | 9.06 | 7.69 | 6.76 | 5.65 | 4.78 | 3.51 | 1.95 |
| 25 | 9.00 | 7.45 | 6.56 | 5.54 | 4.78 | 3.55 | 2.13 |
| 26 | 10.30 | 8.69 | 7.59 | 6.30 | 5.33 | 3.86 | 2.21 |
| 27 | 9.76 | 8.26 | 7.22 | 5.91 | 4.87 | 3.44 | 1.91 |
| 28 | 9.42 | 7.94 | 6.92 | 5.72 | 4.80 | 3.48 | 1.93 |
| 29 | 9.13 | 7.62 | 6.65 | 5.55 | 4.76 | 3.53 | 2.09 |
| 30 | 10.52 | 8.84 | 7.79 | 6.42 | 5.43 | 3.91 | 2.24 |
| 31 | 10.20 | 8.55 | 7.37 | 6.01 | 4.94 | 3.41 | 1.91 |
| 32 | 10.34 | 8.65 | 7.54 | 6.13 | 5.07 | 3.60 | 1.97 |
| 33 | 10.04 | 8.43 | 7.29 | 5.95 | 4.90 | 3.44 | 1.97 |
| 34 | 9.90 | 8.16 | 7.04 | 5.77 | 4.78 | 3.40 | 1.88 |
| 35 | 10.90 | 8.87 | 7.65 | 6.21 | 5.09 | 3.58 | 2.02 |
| 36 | 10.64 | 8.88 | 7.72 | 6.24 | 5.13 | 3.52 | 1.96 |
| 37 | 9.63 | 7.95 | 6.90 | 5.67 | 4.71 | 3.42 | 2.05 |
| 38 | 10.95 | 8.89 | 7.68 | 6.21 | 5.16 | 3.66 | 2.07 |
| 39 | 10.97 | 9.11 | 7.92 | 6.60 | 5.57 | 4.06 | 2.29 |
| 40 | 11.05 | 9.23 | 8.04 | 6.64 | 5.53 | 3.96 | 2.24 |
| Average | 10.05 | 8.44 | 7.38 | 6.11 | 5.15 | 3.72 | 2.12 |
| CV (%) | 7 | 7 | 7 | 7 | 7 | 7 | 6 |

CV = Coefficient of variation = standard deviation as a percent of the average

Table 6.5 D
site

| FWD Station | |
|---|---|
| 1 | |
| 2 | |
| 3 | |
| 4 | |
| 5 | |
| 6 | |
| 7 | |
| 8 | |
| 9 | |
| 10 | |
| 11 | |
| 12 | |
| 13 | |
| 14 | |
| 15 | |
| 16 | |
| 17 | |
| 18 | |
| 19 | |
| 20 | |
| 21 | |
| 22 | |
| 23 | |
| 24 | |
| 25 | |
| 26 | |
| 27 | |
| 28 | |
| 29 | |
| 30 | |
| 31 | |
| 32 | |
| 33 | |
| 34 | |
| 35 | |
| 36 | |
| 37 | |
| 38 | |
| 39 | |
| 40 | |
| Average | |
| CV | |
| CV | |

Table 6.5 D1 through D7 deflections, rubblized pavement, US-10 EB, test section 1, test site 2

| FWD Station | Deflection (mils) | | | | | | |
|---|---|---|---|---|---|---|---|
| | D1 | D2 | D3 | D4 | D5 | D6 | D7 |
| 1 | 13.49 | 11.22 | 9.85 | 8.03 | 6.64 | 4.50 | 2.27 |
| 2 | 11.91 | 10.22 | 8.93 | 7.33 | 6.07 | 4.18 | 2.21 |
| 3 | 10.57 | 8.72 | 7.66 | 6.37 | 5.35 | 3.83 | 2.06 |
| 4 | 11.39 | 9.37 | 8.19 | 6.65 | 5.55 | 3.97 | 2.17 |
| 5 | 10.94 | 9.16 | 8.06 | 6.70 | 5.63 | 4.07 | 2.15 |
| 6 | 11.39 | 9.56 | 8.38 | 6.85 | 5.73 | 4.03 | 2.17 |
| 7 | 13.04 | 10.71 | 9.30 | 7.66 | 6.41 | 4.52 | 2.32 |
| 8 | 12.25 | 10.23 | 8.87 | 7.20 | 5.95 | 4.23 | 2.31 |
| 9 | 11.08 | 9.02 | 7.80 | 6.40 | 5.34 | 3.87 | 2.18 |
| 10 | 13.26 | 11.06 | 9.49 | 7.36 | 5.88 | 3.94 | 2.16 |
| 11 | 13.32 | 11.06 | 9.54 | 7.79 | 6.40 | 4.34 | 2.24 |
| 12 | 11.29 | 9.36 | 8.13 | 6.59 | 5.47 | 3.94 | 2.16 |
| 13 | 12.78 | 10.58 | 9.12 | 7.43 | 6.16 | 4.33 | 2.28 |
| 14 | 12.72 | 10.57 | 8.99 | 7.00 | 5.65 | 3.91 | 2.19 |
| 15 | 13.29 | 11.05 | 9.50 | 7.67 | 6.24 | 4.28 | 2.23 |
| 16 | 10.83 | 8.81 | 7.61 | 6.17 | 5.12 | 3.76 | 2.14 |
| 17 | 12.80 | 10.40 | 8.88 | 7.22 | 5.98 | 4.19 | 2.26 |
| 18 | 11.61 | 9.53 | 8.09 | 6.40 | 5.31 | 3.81 | 2.18 |
| 19 | 13.53 | 11.07 | 9.44 | 7.54 | 6.13 | 4.17 | 2.16 |
| 20 | 10.68 | 8.84 | 7.48 | 6.06 | 5.08 | 3.70 | 2.08 |
| 21 | 12.35 | 10.16 | 8.74 | 7.03 | 5.77 | 4.03 | 2.21 |
| 22 | 11.36 | 9.21 | 7.84 | 6.22 | 5.17 | 3.79 | 2.12 |
| 23 | 13.72 | 11.17 | 9.47 | 7.54 | 6.15 | 4.16 | 2.17 |
| 24 | 11.01 | 8.93 | 7.63 | 6.17 | 5.10 | 3.73 | 2.10 |
| 25 | 12.37 | 9.90 | 8.57 | 6.97 | 5.68 | 3.98 | 2.20 |
| 26 | 11.41 | 9.40 | 8.03 | 6.36 | 5.28 | 3.78 | 2.12 |
| 27 | 13.66 | 11.37 | 9.79 | 7.77 | 6.21 | 4.11 | 2.12 |
| 28 | 11.07 | 8.93 | 7.67 | 6.27 | 5.23 | 3.80 | 2.08 |
| 29 | 12.28 | 9.85 | 8.49 | 6.84 | 5.63 | 3.88 | 2.14 |
| 30 | 11.41 | 9.38 | 8.10 | 6.56 | 5.40 | 3.80 | 2.14 |
| 31 | 13.80 | 11.52 | 9.86 | 7.72 | 6.21 | 4.08 | 2.16 |
| 32 | 12.66 | 10.35 | 8.93 | 7.22 | 5.89 | 4.03 | 2.14 |
| 33 | 11.59 | 9.24 | 7.90 | 6.32 | 5.23 | 3.64 | 2.02 |
| 34 | 12.34 | 9.86 | 8.47 | 6.75 | 5.52 | 3.80 | 2.12 |
| 35 | 11.68 | 9.43 | 8.12 | 6.56 | 5.32 | 3.64 | 2.06 |
| 36 | 13.21 | 10.59 | 9.06 | 7.26 | 5.83 | 3.88 | 2.04 |
| 37 | 12.44 | 10.01 | 8.60 | 6.92 | 5.65 | 3.90 | 2.19 |
| 38 | 12.21 | 10.00 | 8.63 | 6.97 | 5.84 | 4.11 | 2.28 |
| 39 | 11.20 | 9.02 | 7.80 | 6.33 | 5.25 | 3.69 | 2.15 |
| 40 | 11.62 | 9.45 | 8.12 | 6.56 | 5.41 | 3.81 | 2.13 |
| Average | 12.14 | 9.96 | 8.58 | 6.92 | 5.70 | 3.98 | 2.17 |
| CV (%) | 8 | 8 | 8 | 8 | 7 | 6 | 3 |

CV = Coefficient of variation = standard deviation as a percent of the average

Table 6.6 D

| FWD Station | 1 |
|---|---|
| 1 | |
| 2 | |
| 3 | |
| 4 | |
| 5 | |
| 6 | |
| 7 | |
| 8 | |
| 9 | |
| 10 | |
| 11 | |
| 12 | |
| 13 | |
| 14 | |
| 15 | |
| 16 | |
| 17 | |
| 18 | |
| 19 | |
| 20 | |
| 21 | |
| 22 | |
| 23 | |
| 24 | |
| 25 | |
| 26 | |
| 27 | |
| 28 | |
| 29 | |
| 30 | |
| 31 | |
| 32 | |
| 33 | |
| 34 | |
| 35 | |
| 36 | |
| 37 | |
| 38 | |
| 39 | |
| 40 | |
| Average | |
| CV | |
| CV | |

Table 6.6 D1 through D7 deflections, flexible pavement, US-27 SB, test section 1, test site 1

| FWD Station | Deflection (mils) | | | | | | |
|---|---|---|---|---|---|---|---|
| | D1 | D2 | D3 | D4 | D5 | D6 | D7 |
| 1 | 7.50 | 6.48 | 5.81 | 4.91 | 4.18 | 2.93 | 1.43 |
| 2 | 7.39 | 6.36 | 5.68 | 4.79 | 4.07 | 2.86 | 1.44 |
| 3 | 7.33 | 6.34 | 5.69 | 4.80 | 4.07 | 2.85 | 1.37 |
| 4 | 7.58 | 6.48 | 5.80 | 4.85 | 4.11 | 2.86 | 1.36 |
| 5 | 7.32 | 6.27 | 5.64 | 4.75 | 4.03 | 2.84 | 1.40 |
| 6 | 7.52 | 6.40 | 5.74 | 4.85 | 4.12 | 2.91 | 1.40 |
| 7 | 7.68 | 6.60 | 5.90 | 4.97 | 4.24 | 2.99 | 1.47 |
| 8 | 7.51 | 6.45 | 5.78 | 4.91 | 4.15 | 2.95 | 1.44 |
| 9 | 7.58 | 6.41 | 5.80 | 4.93 | 4.18 | 2.94 | 1.46 |
| 10 | 7.43 | 6.34 | 5.71 | 4.84 | 4.12 | 2.90 | 1.46 |
| 11 | 7.44 | 6.36 | 5.75 | 4.89 | 4.14 | 2.90 | 1.43 |
| 12 | 7.44 | 6.34 | 5.66 | 4.75 | 3.99 | 2.80 | 1.36 |
| 13 | 7.49 | 6.37 | 5.73 | 4.87 | 4.15 | 2.90 | 1.44 |
| 14 | 7.24 | 6.22 | 5.59 | 4.75 | 4.03 | 2.87 | 1.44 |
| 15 | 7.23 | 6.23 | 5.60 | 4.71 | 4.03 | 2.82 | 1.43 |
| 16 | 7.32 | 6.20 | 5.55 | 4.64 | 3.93 | 2.75 | 1.35 |
| 17 | 7.28 | 6.30 | 5.65 | 4.79 | 4.10 | 2.91 | 1.42 |
| 18 | 7.12 | 6.12 | 5.51 | 4.69 | 3.98 | 2.78 | 1.44 |
| 19 | 7.05 | 6.14 | 5.53 | 4.68 | 3.97 | 2.85 | 1.41 |
| 20 | 7.16 | 6.13 | 5.48 | 4.60 | 3.93 | 2.74 | 1.34 |
| 21 | 7.09 | 6.11 | 5.50 | 4.71 | 3.98 | 2.86 | 1.45 |
| 22 | 7.13 | 6.09 | 5.50 | 4.66 | 3.97 | 2.81 | 1.44 |
| 23 | 7.03 | 6.08 | 5.46 | 4.64 | 3.96 | 2.86 | 1.45 |
| 24 | 7.17 | 6.12 | 5.47 | 4.62 | 3.93 | 2.79 | 1.39 |
| 25 | 7.06 | 6.07 | 5.48 | 4.67 | 4.01 | 2.86 | 1.46 |
| 26 | 7.22 | 6.20 | 5.60 | 4.72 | 4.04 | 2.86 | 1.48 |
| 27 | 7.14 | 6.20 | 5.57 | 4.69 | 4.01 | 2.80 | 1.38 |
| 28 | 7.15 | 6.19 | 5.58 | 4.75 | 4.05 | 2.93 | 1.45 |
| 29 | 7.27 | 6.25 | 5.65 | 4.80 | 4.07 | 2.94 | 1.49 |
| 30 | 7.17 | 6.22 | 5.60 | 4.75 | 4.06 | 2.89 | 1.45 |
| 31 | 7.32 | 6.31 | 5.71 | 4.80 | 4.08 | 2.88 | 1.45 |
| 32 | 7.43 | 6.41 | 5.80 | 4.93 | 4.15 | 2.93 | 1.45 |
| 33 | 7.23 | 6.26 | 5.66 | 4.81 | 4.10 | 2.88 | 1.43 |
| 34 | 7.06 | 6.10 | 5.47 | 4.67 | 3.97 | 2.79 | 1.39 |
| 35 | 7.10 | 6.13 | 5.53 | 4.73 | 4.04 | 2.88 | 1.42 |
| 36 | 7.31 | 6.29 | 5.69 | 4.83 | 4.13 | 2.91 | 1.44 |
| 37 | 7.22 | 6.21 | 5.58 | 4.72 | 4.02 | 2.85 | 1.45 |
| 38 | 7.15 | 6.18 | 5.56 | 4.75 | 4.02 | 2.88 | 1.49 |
| 39 | 7.51 | 6.43 | 5.76 | 4.89 | 4.15 | 2.92 | 1.45 |
| 40 | 7.27 | 6.19 | 5.55 | 4.62 | 3.92 | 2.74 | 1.39 |
| Average | 7.29 | 6.26 | 5.63 | 4.77 | 4.05 | 2.87 | 1.43 |
| CV (%) | 3 | 2 | 2 | 2 | 2 | 2 | 2 |

CV = Coefficient of variation = standard deviation as a percent of the average

Figure 6.4 Va




Figure 6.4 Va

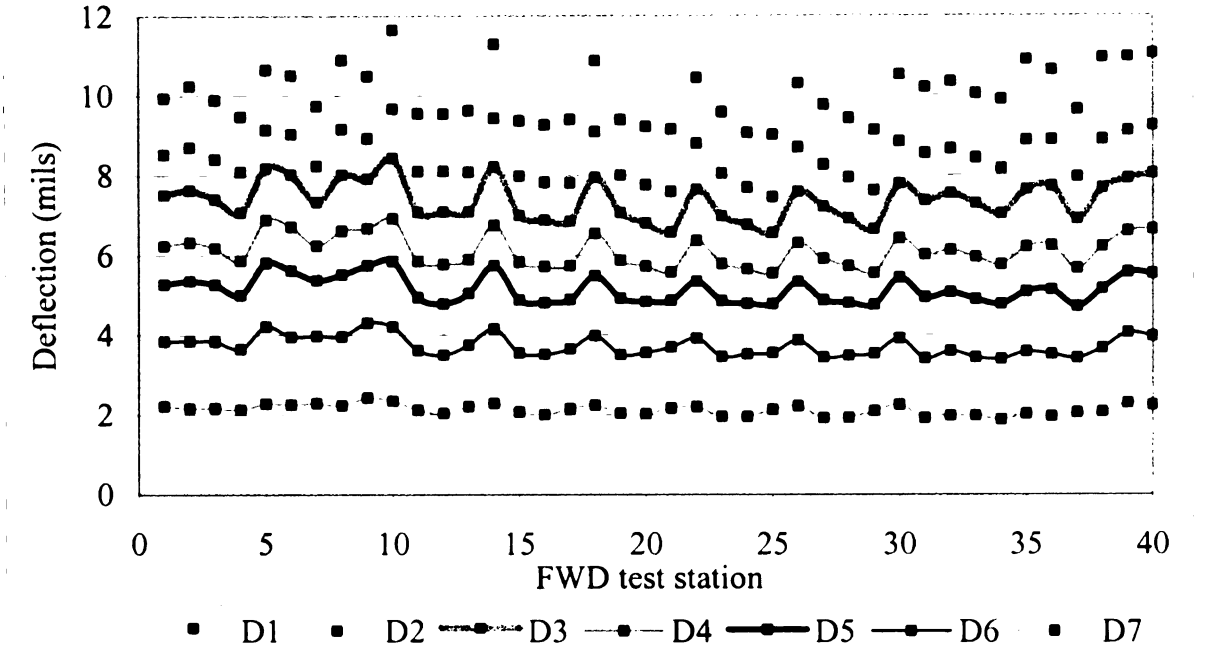


Figure 6.4 Variations of D1 through D7 deflections, US-10 EB, test section 1, test site 1

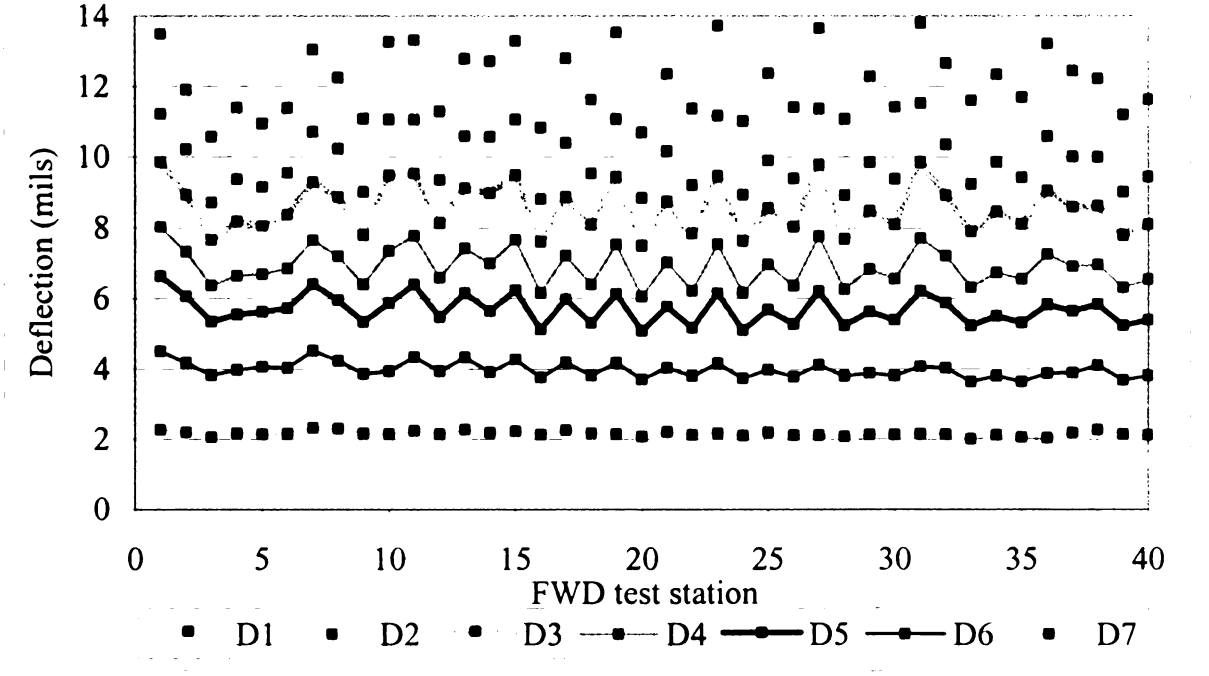


Figure 6.4 Variations of D1 through D7 deflections, US-10 EB, test section 1, test site 2

Figure 6.6 V



Figure 6.7

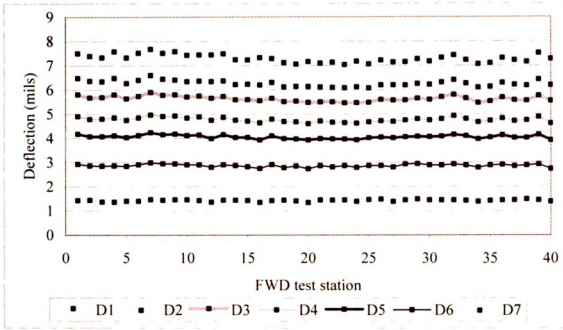


Figure 6.6 Variations of D1 through D7 deflections, US-27 SB, test section 1, test site 1

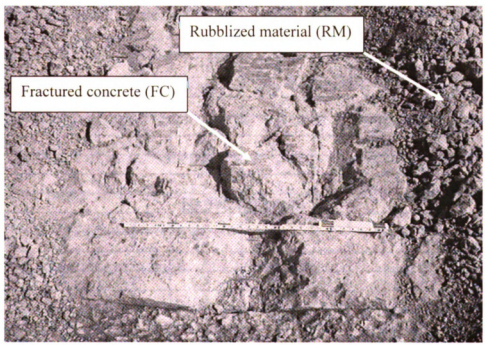


Figure 6.7 A typical trench excavated in rubblized pavement showing RM and fractured concrete, US-10 SB,

Table 6.7 Co-

| Test site | — |
|---|---|
| [illegible]2-11 | |
| [illegible]2-12 | |
| [illegible]53-11 | |
| [illegible]53-12 | |
| [illegible]62-11 | |
| [illegible]62-21 | |
| [illegible]62-31 | |
| [illegible]62-51 | |
| [illegible]63-21 | |
| [illegible]63-22 | |
| 2032-11 | |
| 2032-12 | |
| 2033-11 | |
| 2033-12 | |
| 2073-21 | |
| 2073-31 | |
| 2073-41 | |
| 2311-11 | |
| 2311-31 | |
| 2311-21 | |
| 2311-31 | |
| 3073-21 | |
| 3073-51 | |
| 3073-52 | |
| 3073-61 | |
| 3631-11 | |
| 2273-11 | |
| 2411-11 | |
| 2411-12 | |
| 3022-11 | |
| 3022-12 | |
| 3422-11 | |
| 3562-11 | |
| 3562-21 | |
| 3621-11 | |
| 3621-21 | |
| 3652-11 | |
| 3652-12 | |

Table 6.7 Coefficients of variation in the measured D1 through D7 deflections for 26 test sites on rubblized pavements and 12 test sites on flexible pavements

| Test site | Coefficient of variation of the measured D1 through D7 deflections (%) | | | | | | |
|---|---|---|---|---|---|---|---|
| | D1 | D2 | D3 | D4 | D5 | D6 | D7 |
| Rubblized pavements | | | | | | | |
| 10692-11 | 9 | 10 | 10 | 9 | 7 | 6 | 11 |
| 10692-12 | 9 | 10 | 11 | 10 | 10 | 10 | 15 |
| 10753-11 | 14 | 13 | 12 | 10 | 8 | 5 | 6 |
| 10753-12 | 16 | 14 | 12 | 11 | 10 | 10 | 13 |
| 10962-11 | 10 | 10 | 10 | 8 | 7 | 6 | 2 |
| 10962-21 | 11 | 10 | 9 | 8 | 8 | 6 | 3 |
| 10962-31 | 5 | 6 | 5 | 5 | 5 | 5 | 5 |
| 10964-51 | 4 | 3 | 3 | 3 | 3 | 5 | 7 |
| 11941-21 | 8 | 7 | 7 | 7 | 7 | 7 | 4 |
| 11941-22 | 11 | 8 | 7 | 7 | 6 | 6 | 5 |
| 20102-11 | 7 | 7 | 7 | 7 | 7 | 7 | 6 |
| 20102-12 | 8 | 8 | 8 | 8 | 7 | 6 | 3 |
| 20233-11 | 12 | 12 | 11 | 10 | 8 | 7 | 15 |
| 20233-12 | 8 | 9 | 9 | 9 | 9 | 10 | 10 |
| 20273-21 | 15 | 13 | 11 | 8 | 6 | 4 | 4 |
| 20273-31 | 6 | 6 | 5 | 5 | 5 | 5 | 6 |
| 20273-41 | 8 | 12 | 11 | 9 | 7 | 6 | 4 |
| 20311-11 | 10 | 10 | 9 | 7 | 7 | 8 | 10 |
| 21313-11 | 4 | 4 | 4 | 3 | 3 | 4 | 2 |
| 21311-21 | 11 | 10 | 10 | 9 | 8 | 6 | 5 |
| 21311-31 | 4 | 4 | 4 | 4 | 4 | 3 | 4 |
| 30373-21 | 19 | 14 | 10 | 17 | 14 | 12 | 10 |
| 30373-51 | 7 | 8 | 7 | 6 | 6 | 5 | 5 |
| 30373-52 | 15 | 16 | 15 | 14 | 14 | 13 | 11 |
| 30373-61 | 10 | 9 | 9 | 8 | 6 | 6 | 8 |
| 30531-11 | 7 | 7 | 6 | 5 | 4 | 3 | 3 |
| Flexible pavements | | | | | | | |
| 20273-11 | 3 | 2 | 2 | 2 | 2 | 2 | 2 |
| 20411-11 | 3 | 3 | 4 | 6 | 6 | 7 | 7 |
| 20411-12 | 2 | 3 | 4 | 4 | 5 | 6 | 11 |
| 30202-11 | 6 | 5 | 5 | 5 | 6 | 8 | 10 |
| 30202-12 | 4 | 3 | 3 | 3 | 4 | 3 | 3 |
| 30422-11 | 13 | 8 | 7 | 10 | 8 | 6 | 4 |
| 30502-11 | 8 | 7 | 6 | 6 | 8 | 13 | 21 |
| 30502-21 | 7 | 7 | 7 | 8 | 8 | 10 | 12 |
| 30521-11 | 4 | 4 | 3 | 4 | 5 | 5 | 3 |
| 30521-21 | 7 | 7 | 7 | 8 | 8 | 10 | 12 |
| 30552-11 | 6 | 6 | 6 | 7 | 6 | 5 | 4 |
| 30552-12 | 9 | 9 | 9 | 9 | 9 | 6 | 4 |

- The occasional debonding of the temperature steel.

This non-uniformity is directly related to the quality of the rubblization process and it impacts the variations in the measured deflection data. The implication is that the FWD data along and across rubblized pavements could be used as quality control measures to assess the quality and uniformity of the RCS.

Finally, variation in the deflection of the outer sensor (D7) is mainly related to the roadbed response to load. Such variation is related to:

1. Roadbed soil variability in terms of moisture content, density, and material type.
2. Variability in the load distribution mechanism through the pavement layers. For example, variation in the RM and FC thicknesses (see Figure 6.7) alter the stress distribution mechanism. In areas where the FC layer (stiff layer) is thick, lower stress is delivered to the roadbed soil. Whereas, thicker RM layer (soft layer) causes increases in the stress delivered to the roadbed soil. These cause substantial variation in the deflection of the roadbed soil, which is reflected in D7 deflections. The above scenarios imply that, for some pavements or for some test locations, where the pavement layers are not homogeneous and their thicknesses are not exactly known, the D7 deflections may not correlate on one to one basis to the backcalculated roadbed soil modulus.

In this study, the measured deflection data obtained from 24 rubblized and 12 flexible pavement test sites were used to backcalculate the pavement layer moduli. First, the capability and the accuracy of the backcalculation program used in the analyses are presented in the next section.

4.0 BAC

Nam

methods inclu

Prior to the i

using 4 comp

MODULUS

Typically, the

analyses of as

backcalculate

backcalculate

sections were

computer pro

no stiff layer.

200-in from th

6.9 and the MI

Table 6.10. Fo

was conducted

1. 4-layer

2. 4-layer

3. 5-layer

Tables 6

the error of eac

tables indicates

## 4.0 BACKCALCULATION COMPUTER PROGRAMS

Numerous computer programs are available for the backcalculation of layer moduli including Modulus, MICHBACK, MOD-COMP and Evercalc. In this study, Prior to the initiation of the backcalculation, the accuracy of the backcalculated moduli using 4 computer programs was checked; MICHBACK, MODCOMP5, EVERCALC and MODULUS version 4.0. Table 6.8 provides some information of the four programs. Typically, the accuracy of any backcalculation program is tested by conducting forward analyses of assumed pavement sections using a multilayer elastic computer program, backcalculating the layer moduli using the generated deflection basins and comparing the backcalculated moduli with the true moduli used in the forward analysis. Two pavement sections were analyzed using the linear analyses option of the MICHPAVE finite element computer program. Both sections consist of 4 layers, AC, RM, FC and roadbed soil with no stiff layer. One section has no stiff layer whereas the other a stiff layer was located at 200-in from the pavement surface. The properties of the two sections are listed in Table 6.9 and the MICHPAVE calculated deflections due to 9000 lb wheel load are listed in Table 6.10. For all four programs and for each pavement section, the backcalculation was conducted using the following systems:

1. 4-layer system (AC, RCS, BS and R)
2. 4-layer system (AC, RM, FC, and BSRB)
3. 5-layer system (AC, RM, FC, BS and RB)

Tables 6.11 and 6.12 provide a summary of the backcalculated results along with the error of each backcalculated modulus value. Examination of the data listed in the tables indicates that:

*Table 6.8 Summaries of the MICHBACK, MODCOMP5, EVERCALC and MODULUS (version 4.0) backcalculation programs*

| *Program* | *Forward engine* | Maximum number of layers in the backcalculation | Specified depth to stiff layer |
|---|---|---|---|
| *MICHBACK* | | | |

Table 6.8 Summaries of the MICHBACK, MODCOMP5, EVERCALC and MODULUS (version 4.0) backcalculation programs

| Program | Forward engine | Maximum number of layers in the backcalculation | Specified depth to stiff layer |
|---|---|---|---|
| MICHBACK | CHEVRONX | 5 | Yes |
| MODCOMP5 | CHEVLAY2 | 12 | Yes |
| EVERCALC | WESLEA | 5 | Yes |
| MODULUS | None (Built-in deflection database in the program) | 4 | No |

Table 6.9 The thicknesses and engineering properties of two pavement sections used in the forward analyses (MICHPAVE)

| Layer | Thickness (in.) | Modulus (ksi) | Poisson ratio | Thickness (in.) | Modulus (ksi) | Poisson ratio |
|---|---|---|---|---|---|---|
| | Section 1 | | | Section 2 | | |
| AC | 6 | 1,000 | 0.3 | 6 | 1,000 | 0.3 |
| Rubblized material | 4 | 40 | 0.4 | 4 | 40 | 0.4 |
| Fractured concrete | 5 | 1,800 | 0.2 | 5 | 1,800 | 0.2 |
| Base and subbase | 18 | 25 | 0.4 | 18 | 25 | 0.4 |
| Roadbed soil | infinite | 15 | 0.45 | 167 | 15 | 0.45 |
| Stiff layer | None | | | infinite | 2,000 | 0.2 |

Table 6.10 The deflection basins of the two pavement sections in Table 6.8 due to 9000-lb load calculated using MICHPAVE finite element program

| Section | Deflection (mils) | | | | | | |
|---|---|---|---|---|---|---|---|
| | D1 | D2 | D3 | D4 | D5 | D6 | D7 |
| 1 | 8.290 | 7.016 | 6.287 | 5.423 | 4.758 | 3.784 | 2.563 |
| 2 | 7.119 | 5.845 | 5.116 | 4.253 | 3.590 | 2.622 | 1.417 |

*Table 6.11 Comparison of the results of MICHBACK, MODCOMP5, EVERCALC and MODULUS backcalculation programs of a pavement section with no stiff layer*

| | AC | | RCS | | RM | | EC | | BSRB | | BS | | RB | |
|---|---|---|---|---|---|---|---|---|---|---|---|---|---|---|
| | Modulus | Error (%) | Modulus | Error | Modulus | Error | Modulus | Error | Modulus | Error | Modulus | Error | Modulus | Error |

Table 6.11 Comparison of the results of MICHBACK, MODCOMP5, EVERCALC and MODULUS backcalculation programs of a pavement section with no stiff layer

| Program | AC | | RCS | | RM | | FC | | BSRB | | BS | | RB | |
|---|---|---|---|---|---|---|---|---|---|---|---|---|---|---|
| | Modulus | Error (%) | Modulus | Error (%) | Modulus | Error (%) | Modulus | Error (%) | Modulus | Error (%) | Modulus | Error (%) | Modulus | Error (%) |
| | True moduli (ksi) | | | | | | | | | | | | | |
| | 1,000 | | | | 40 | | 1,800 | | | | 25 | | 15 | |
| | 4-layer system (AC, RCS, BS and RB) | | | | | | | | | | | | | |
| MICHBACK | 872 | -12.8 | 119 | N/A | | | | | | | 41 | 64.9 | 16 | 6.9 |
| MODCOMP5 | 856 | -14.4 | 123 | N/A | | | | | | | 41 | 62.4 | 16 | 7.3 |
| EVERCALC | 995 | -0.5 | 106 | N/A | | | | | | | 43 | 70.1 | 16 | 6.4 |
| MODULUS | 808 | -19.2 | 665 | N/A | | | | | | | 24 | -3.3 | 6 | -58.1 |
| | 4-layer system (AC, RM, FC and BSRB) | | | | | | | | | | | | | |
| MICHBACK | 997 | -0.3 | | | 41 | 3.0 | 2,767 | 53.7 | 16 | N/A | | | | |
| MODCOMP5 | 869 | -13.1 | | | 92 | 130.0 | 409 | -77.3 | 18 | N/A | | | | |
| EVERCALC | 620 | -38.0 | | | 20 | -49.0 | 4,000 | 122.2 | 16 | N/A | | | | |
| MODULUS | N/A | | | | | | | | | | | | | |
| | 5-layer system (AC, RM, FC, BS and RB) | | | | | | | | | | | | | |
| MICHBACK | No convergence | | | | | | | | | | | | | |
| MODCOMP5 | 899 | -10.1 | | | 88 | 119.5 | 243 | -86.5 | | | 33 | 32.8 | 16 | 8.7 |
| EVERCALC | No convergence | | | | | | | | | | | | | |
| MODULUS | N/A | | | | | | | | | | | | | |

AC=asphalt concrete, RCS=rubblized concrete slab, RM=rubblized material, FC=fractured concrete, BS=the combination of base and subbase layers, RB=Roadbed soil, BSRB=the combination of base, subbase and roadbed soil.

*Table 6.12 Comparison of the results of MICHBACK, MODCOMP5, EVERCALC and MODULUS backcalculation programs of a pavement section with a depth to stiff layer of 200 in.*

Table 6.12 Comparison of the results of MICHBACK, MODCOMP5, EVERCALC and MODULUS backcalculation programs of a pavement section with a depth to stiff layer of 200 in.

| Program | AC | | RCS | | RM | | FC | | BSRB | | BS | | RB | |
|---|---|---|---|---|---|---|---|---|---|---|---|---|---|---|
| | Modulus | Error (%) | Modulus | Error (%) | Modulus | Error (%) | Modulus | Error (%) | Modulus | Error (%) | Modulus | Error (%) | Modulus | Error (%) |
| | True moduli (ksi) | | | | | | | | | | | | | |
| | 1,000 | | | | 40 | | 1,800 | | | | 25 | | 15 | |
| | 4-layer system (AC, RCS, BS and RB) | | | | | | | | | | | | | |
| MICHBACK | 847 | -15.3 | 127 | N/A | | | | | | | 38 | 51.3 | 17 | 11.2 |
| MODCOMP5 | 856 | -14.4 | 126 | N/A | | | | | | | 38 | 52.0 | 17 | 11.3 |
| EVERCALC | 1791 | 79.1 | 44 | N/A | | | | | | | 57 | 127.6 | 16 | 6.7 |
| MODULUS | 808 | -19.2 | 787 | N/A | | | | | | | 13 | -49.2 | 6 | -60.7 |
| | 4-layer system (AC, RM, FC and BSRB) | | | | | | | | | | | | | |
| MICHBACK | 959 | -4.1 | | | 54 | 34.2 | 1,297 | -27.9 | 17 | N/A | | | | |
| MODCOMP5 | 874 | -12.6 | | | 92 | 128.8 | 379 | -78.9 | 19 | N/A | | | | |
| EVERCALC | 1286 | 28.6 | | | 49 | 21.4 | 866 | -51.9 | 17 | N/A | | | | |
| MODULUS | N/A | | | | | | | | | | | | | |
| | 5-layer system (AC, RM, FC, BS and RB) | | | | | | | | | | | | | |
| MICHBACK | No convergence | | | | | | | | | | | | | |
| MODCOMP5 | 899 | -10.1 | | | 87 | 117.0 | 285 | -84.2 | | | 29 | 14.0 | 17 | 15.3 |
| EVERCALC | No convergence | | | | | | | | | | | | | |
| MODULUS | N/A | | | | | | | | | | | | | |

AC=asphalt concrete, RCS=rubblized concrete slab, RM=rubblized material, FC=fractured concrete, BS=the combination of base and subbase layers, RB=Roadbed soil, BSRB=the combination of base, subbase layers and roadbed soil.

1. Nom
accu
2. Base
syste
elimi
yield
(EVE
3. For th
MOD
the ba
in the
4. The va
system
RCS. B
BSRB
high th
relative

Based on the ab

backcalculation

read the format

Once aga

system. Since so

backcalculation

1. None of the programs is capable of backcalculating the moduli of 5-layer system accurately.
2. Based on the errors in the backcalculated modulus values of the two 4-layer systems, the MODULUS program produced the worst results and therefore it was eliminated from any further consideration. Further, the MICHBACK program yields either similar to, or better results than, the other two programs (EVERCALC and MODCOMP5).
3. For the 4-layer system (AC, RCS, BS, and RB), all programs (except MODULUS) produce relatively accurate results for the roadbed soil. However, the backcalculated modulus of the BS layer is over estimated, which caused error in the backcalculated RCS modulus.
4. The value of the backcalculated BSRB modulus from the AC, RM, FC and BSRB system is very close to that the roadbed modulus (RB) obtained from the AC, RCS, BS and RB system. Hence, the influence of the RB over the backcalculated BSRB modulus is much higher than that of the BS layer. This is mainly due to the high thickness (the RB extends to the depth of the stiff layer) of the roadbed soil relative to the BS layer.

Based on the above observations, the MICHBACK computer program was used for the backcalculation of layer moduli. Another advantage of MICHBACK is that it directly read the format of the deflection data from the MDOT FWD file output.

Once again, like the other programs, MICHBACK is not accurate for the 5-layer system. Since some pavement sections consist of 5-layers, a procedure for the backcalculation of layer moduli was developed and is presented below.

## 5.0 BAC

As st

developed an

following ste

1. Obtai
   - T
     da
   - T
   - T
     sc
   - Pa
2. For ea
   irregul
   includ
   results
   -
   -
   -
3. Use Bo
   deep an
   determi
4. Set the c
   section 5

## 5.0 BACKCALCULATION PROCEDURE

As stated above, a procedure for the backcalculation of layer moduli was developed and implemented throughout this study. The procedure consists of the following steps:

1. Obtain the following information/data:
   - The thicknesses of the pavement layers and material types from the inventory data and/or from coring and drilling;
   - The pavement condition at the FWD test site;
   - The measured deflection data and the distances between the deflection sensors; and
   - Pavement temperature and time of the day for each FWD test.
2. For each test site, examine the deflection basins for possible irregularities. Highly irregular deflection basins relative to other basins within the test site should not be included in the backcalculation. The irregular deflection basins could be the results of:
   - Cracks in the vicinity of the FWD test.
   - Edge effect of the RCS.
   - Underground utility pipes or drainage pipes/culverts.
3. Use Boussinesq equation to determine whether or not a stiff layer is shallow or deep and conduct trial backcalculation using 3- and 4-layer systems as to determine the approximate depth to stiff layer (for details see section 5.1).
4. Set the convergence criteria in the backcalculation software as recommended in section 5.2 below.

5. Con

back

5.3.

6. Bas

the b

7. For

accep

RM

8. Calcu

the ba

using

9. For ea

variat

only,

the av

The ab

illustrated in th

## 5.1 Depth

The loa

almost zero val

the soil. Hence

based computer

5. Conduct backcalculation of layer moduli. Special provisions for the backcalculation of layer moduli of rubblized pavements are provided in section 5.3.

6. Based on engineering judgment, establish acceptance criteria to accept or reject the backcalculated results at each FWD test station (see section 5.4).

7. For each FWD test station, examine the backcalculated results against the acceptance criteria. For rubblized pavement only, determine the most plausible RM thickness (see section 5.5)

8. Calculate the temperature corrected AC moduli (TCAC). Note that, in this study the backcalculated AC moduli were adjusted to the standard temperature of $68^{o}$ F using equation 2.4 (see section 7.0).

9. For each test site, calculate and report the average values and the coefficients of variation (CV) of each backcalculated layer moduli. For rubblized pavements only, calculate and report the average values and the CV of the RCS modulus and the average thickness of the RM layer.

The above backcalculation procedure for rubblized pavements is summarized and illustrated in the form of a flowchart shown in Figure 6.8.

## 5.1 Depth to Stiff Layer

The load induced-stresses and strains in most pavement sections dissipate to almost zero value within few feet from the pavement surface due to the arching effects in the soil. Hence, such stresses cause no measurable deflection. An elastic layered system based computer program calculates stresses and deflections to great depths from the

Figure 6.8 A fl

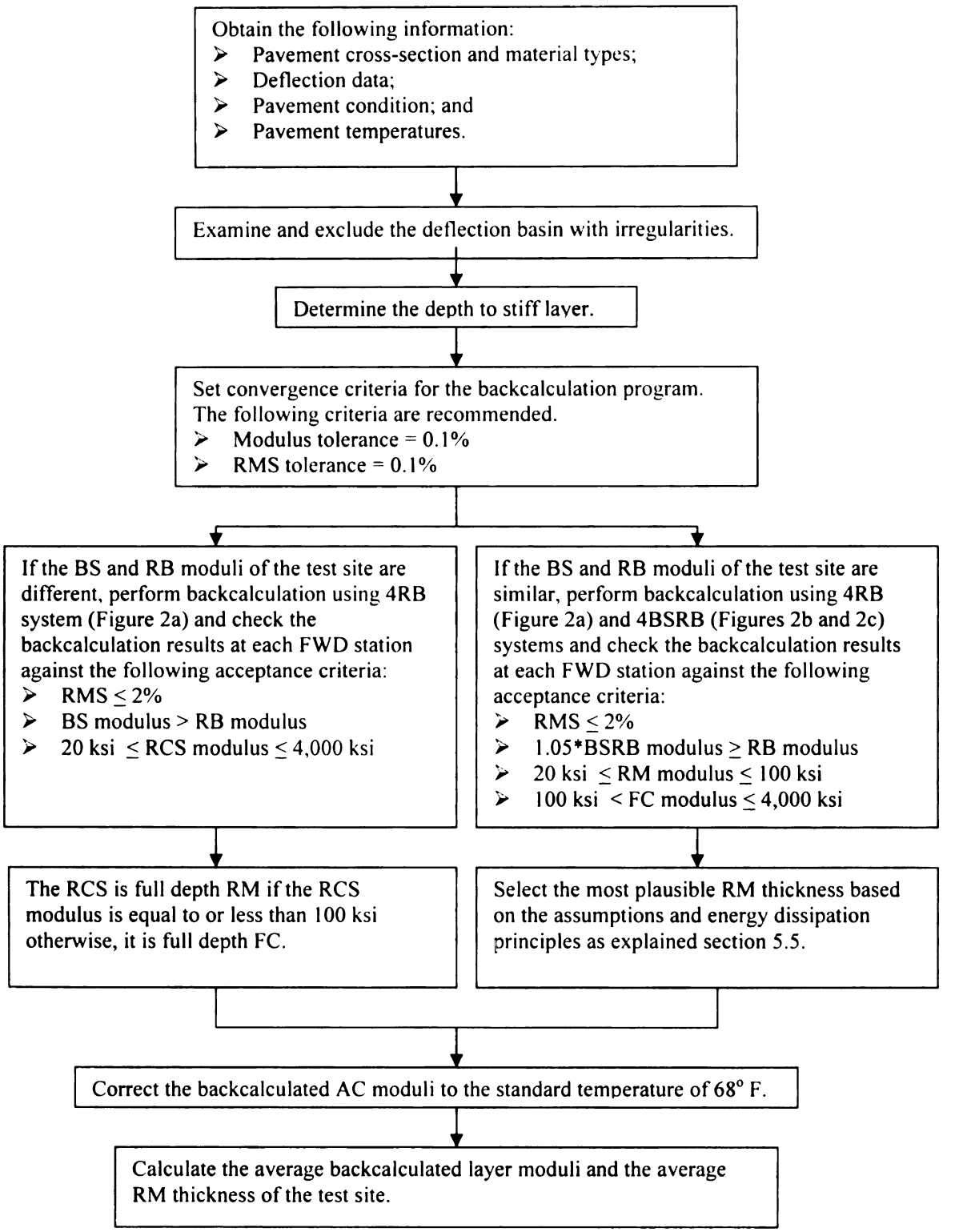


Figure 6.8 A flowchart of the backcalculation procedure for rubblized pavements

pavement s

backcalcula

layered elas

software (in

certain dept

estimated d

moduli. For

than the true

moduli could

innovative p

estimate the

### 5.1.1 Equiv

for co

follow

1.

pavement surface. In the backcalculation process, such calculations affect mainly the backcalculated modulus of the roadbed soil. To alleviate the problem and to force the layered elastic program to slow down the calculation of deflection, most backcalculation software (including the MICHBACK program) allow the users to place a stiff layer at a certain depth below the pavement surface. Such placement is problematic in that, if the estimated depth to stiff layer is incorrect, it produces errors in the backcalculated layer moduli. For example, if the depth to stiff layer is erroneously estimated at 400 in. rather than the true 200 in. then the errors in the backcalculated roadbed, subbase, base and AC moduli could be as high as70, 40, 20, and 10 percent, respectively. In this study, an innovative procedure based on two independent methods was developed to accurately estimate the depth to stiff layer. The procedure is detailed in the next two subsections.

### 5.1.1 Equivalent Pavement Modulus

The approximate depth to stiff layer can be estimated using the equivalent (or composite) modulus of the pavement and the roadbed soil as explained in the following steps:

1. Select a minimum of three deflection basins (one at the beginning, one in the middle and one at the end of the test site) and calculate the equivalent modulus of the pavement layers and the roadbed soil at deflection sensors D2 through D7 using the following Boussinesq's equation (Ullidtz, 1987):

$$E = \frac{P\left(1-\upsilon^2\right)}{\pi(r)\left(d_r\right)} \tag{6.1}$$

Where: E = equivalent modulus (psi);

P = applied load = 9000 lb in this study;

$\upsilon$ = Poisson's ratio (assume 0.4);

r = radial distance from the center of the load to the sensor in question (in.); and

$d_r$ = deflection at distance r from the center of the load (in.)

2. Plot the calculated E versus the distance "r" as shown in Figure 6.9. The resulting curve would have three possible shapes as follows:

   a) The E values at the tail of the curve increases with increasing distance $d_r$. This indicates possible shallow stiff layer. Higher rates of increasing E relative to $d_r$ imply shallower depth to stiff layer as shown in Figure 6.9.

   b) The E value at the tail of the curve is constant with increasing distance. This implies relatively deep (400 to 660-in) stiff layer.

   c) The E value continuously decreases with distance, which implies deep or no stiff layer is needed as shown in Figure 6.9.

   If the plots from the three deflection basins indicate different depths to stiff layer (e.g., one basin shows shallow stiff layer while the others show deep stiff layer), the following two scenarios are possible.

   a) There may be underground facilities such as drainage culvert or utilities pipe under the FWD test locations.

   b) There may be cracks in the vicinity of the FWD test location, especially under the load plate or between the load plate and the deflection sensors.

layer

by it

done

**5.1.2**

be est

as out

1.

2.

Regardless which scenario is true, it should be verified and deflection basins from those locations should be dropped or treated differently from the rest of the data.

Note that this method can only be used to determine whether or not a stiff layer should be incorporated in the backcalculation of layer moduli. The method by itself cannot be used to closely estimate the depth to stiff layer. This can be done using the next method.

### 5.1.2 Three- and four-layer systems

For a given set of deflection data, the approximate depth to stiff layer can be estimated by backcalculating the layer moduli for three and four layer systems as outlined in the following steps:

1. Based on Boussinesq's equation results, obtain a rough estimate of the range of the depth to stiff layer (e.g., between 100 and 400-in). Divide this range to three or four equal increments. For example, 100, 200, 300 and 400-in.
2. For each incremental depth to stiff layer and for each deflection basin of one test site, perform backcalculation of layer moduli for the 3- and 4-layer systems shown in Figure 6.10. The two systems for rubblized and flexible pavements are detailed below.
   - For rubblized pavements, the 3-layer system consists of AC, RCS and BSRB. Whereas the 4-layer system consists of AC, RCS, BS and RB.

Figure 6.9 P
lo

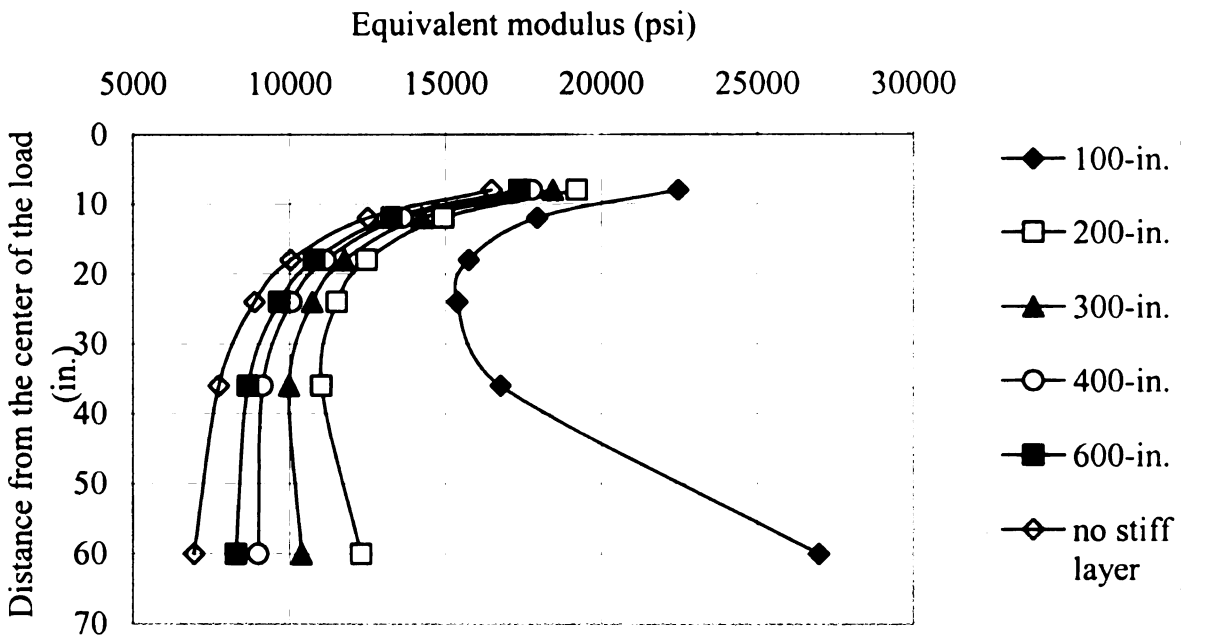


Figure 6.9 Plots of equivalent pavement modulus versus the distance from the center of load for 6 pavement sections having different depths to stiff layer

3.

4.

5.

6.

- For 4-layers (AC, B, S and RB) flexible pavements, the 3-layer system consists of AC, BS and RB. Whereas the 4-layer system consists of AC, BS, RB1 and RB2. That is split the roadbed soil into two zones; RB1 and RB2. Assume the thickness of the upper zone (RB1) 12-in. For 3-layers (AC, B and RB) flexible pavements, the 3-layer system consists of AC, B and RB. Whereas the 4-layer system consists of AC, B, RB1 and RB2 or AC, B1, B2 and RB. That is either split the RB or the base into two layers.

3. For rubblized pavements and for each test site, calculate the average backcalculated BSRB moduli from the results of the 3-layer system and the average RB modulus from the 4-layer system. Whereas for flexible pavements, calculate the average modulus of RB1 and RB2.
4. Plot the average backcalculated BSRB modulus and the average backcalculated RB modulus (the average RB1 and RB2 moduli for flexible pavements) against the depth to stiff layer.
5. If the two curves do not intersect, no stiff layer should be incorporated into the backcalculation of layer moduli.
6. Obtain the approximate depth to stiff layer as the depth of the intersection of the two curves where the average BSRB and RB moduli (RB1 and RB2 moduli for flexible pavements) are equal.
   - For flexible pavements, the true depth to stiff layer is the depth at which the two curves representing the moduli of RB1 and RB2 or B1 and B2 intersect.

Figure 6.10 Th
de

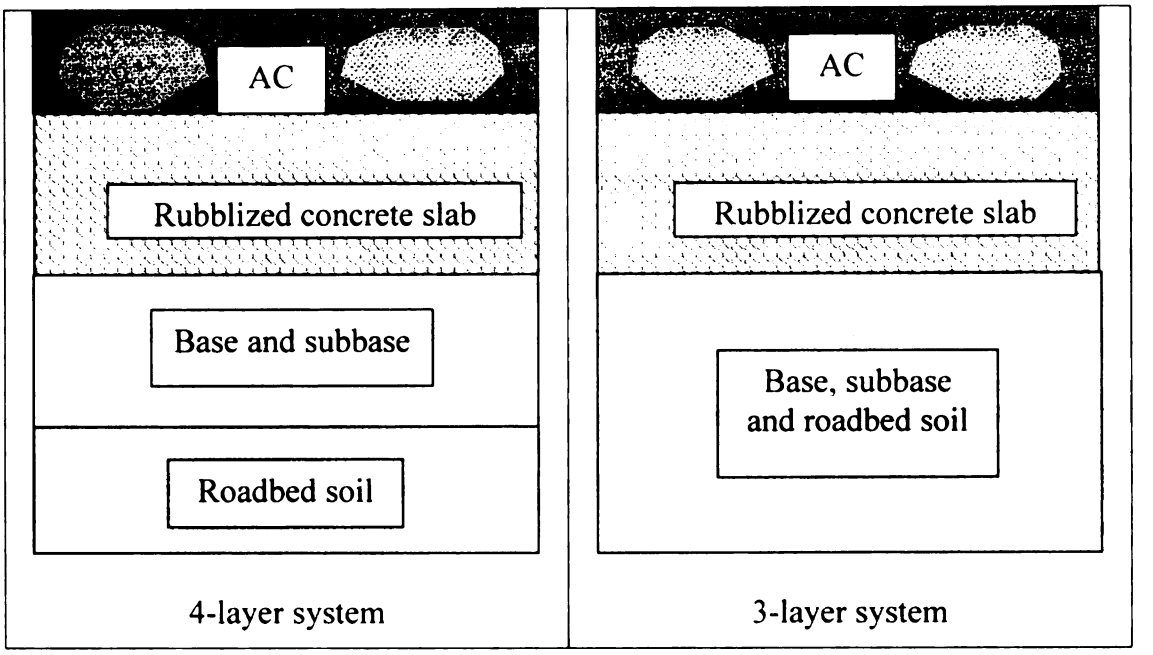


a) Three and four layer systems for rubblized pavements

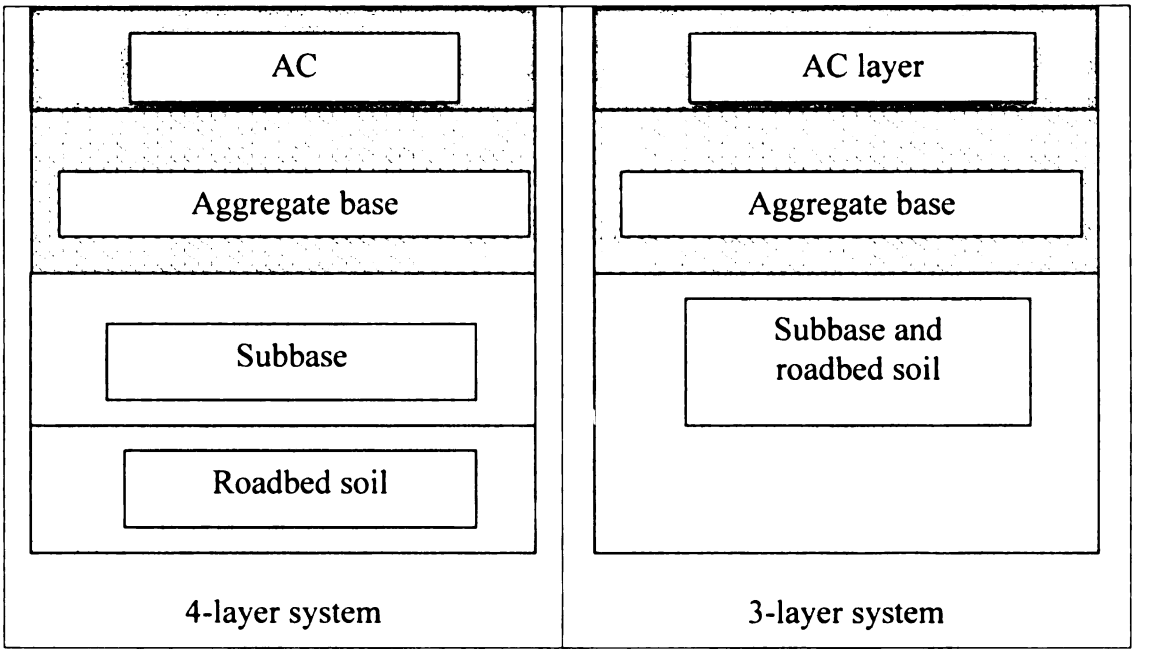


b) Three and four layer systems for flexible pavements

Figure 6.10 Three and four layer systems for flexible and rubblized pavements used to determine the approximate stiff layer depth

- For rubblized pavements, based on information obtained from soil maps and/or other sources, the true depth to stiff layer could be in accordance with one of the following three scenarios:

  a) The depth at which the BSRB and RB curves intersect (the two moduli are equal). This is the likely scenario for pavement having the same type base subbase and roadbed soil.

  b) Shallower than the depth at which the two curves intersect when the BSRB modulus is higher than the RB modulus, the likely scenario for most pavements. The higher is the BSRB modulus relative to the RB modulus, the shallower is the true depth to stiff layer relative to the depth of intersection.

  c) Deeper than the depth at which the two curves intersect when the BSRB modulus is lower than the RB modulus. This is the likely scenario when the RB is hard and desiccated clay or hard pan. The lower is the BSRB modulus relative to the RB modulus, the deeper is the true depth to stiff layer relative to the depth of intersection.

Finally, the selected depth to stiff layer should yield reasonable values for all the backcalculated moduli, and the backcalculation should satisfy the convergence criteria, which is explained in section 5.2.

To

using the C

300-in dep

basins. Th

are listed in

modulus.

must be hig

modulus fr

layer system

the two curv

shallower th

second set of

not intersect

## 5.2 Conv

In this

computer pro

calculated an

criteria are:

1. The m

2. The ro

deflect

subseq

To illustrate the above procedure, two sets of 15 deflection basins were generated using the CHEVRONX computer program. One set of 15 deflection basins is based on 300-in depth to stiff layer whereas no stiff layer was incorporated in the second set of 15 basins. The pavement cross-section and the layer moduli used in the forward analyses are listed in Tables 6.13 and 6.14. Note that the BS modulus is higher than the RB modulus. Hence, if the BS and RM are combined into a BSRB layer, the BSRB modulus must be higher than the RB. Figures 6.11 and 6.12 depict the average backcalculated RB modulus from the 4-layer system and the average backcalculated BS modulus from the 3-layer system. As can be seen, for the set of deflection basins with 300-in deep stiff layer, the two curves intersect at the depth to stiff layer of 350 in. implying that the stiff layer is shallower than 350-in (the BSRB modulus must be higher than the RB modulus). For the second set of deflection basins where no stiff layer was incorporated, the two curves do not intersect even at a stiff layer depth of 800-in. implying that no stiff layer is required.

## 5.2 Convergence Criteria

In this study, several convergence criteria are specified in the MICHBACK computer program, which are automatically checked to determine whether or not the calculated and the measured deflection basin in any given iteration converged. These criteria are:

1. The modulus tolerance between two subsequent iterations is 0.1 %
2. The root mean square (RMS) error between the calculated and the measured deflection basins does not change by more than 0.1 percent between two subsequent iterations.

Table 6.13

| AC Thickness (in.) |
|---|
| 5 |
| 5 |
| 5 |
| 5.5 |
| 5.5 |
| 5.5 |
| 6 |
| 6 |
| 6 |
| 6.5 |
| 6.5 |
| 6.5 |
| - |
| - |
| - |

Table 6.14 T
ba
st

| AC Thickness (in.) | M |
|---|---|
| 5 | |
| 5 | |
| 5 | |
| 5.5 | |
| 5.5 | |
| 5.5 | |
| 6 | |
| 6 | |
| 6 | |
| 6.5 | |
| 6.5 | |
| 6.5 | |
| 7 | |
| 7 | |
| 7 | |

Table 6.13 Thickness and moduli of AC, rubblized concrete slab (RCS), combination of base and subbase (BS) and roadbed soil (RB) of a pavement section having stiff layer at 300 in.

| AC | | RCS | | BS | | RB | | Stiff layer | |
|---|---|---|---|---|---|---|---|---|---|
| Thickness (in.) | Mod (ksi) | Thickness (in.) | Mod (ksi) | Thickness (in.) | Mod (ksi) | Thickness (in.) | Mod (ksi) | Depth (in.) | Mod (ksi) |
| 5 | 1000 | 9 | 50 | 15 | 20 | 271 | 15 | 300 | 2000 |
| 5 | 1000 | 9 | 100 | 15 | 20 | 271 | 15 | 300 | 2000 |
| 5 | 1000 | 9 | 300 | 15 | 20 | 271 | 15 | 300 | 2000 |
| 5.5 | 1000 | 9 | 50 | 15 | 20 | 270.5 | 15 | 300 | 2000 |
| 5.5 | 1000 | 9 | 100 | 15 | 20 | 270.5 | 15 | 300 | 2000 |
| 5.5 | 1000 | 9 | 300 | 15 | 20 | 270.5 | 15 | 300 | 2000 |
| 6 | 1000 | 9 | 50 | 15 | 20 | 270 | 15 | 300 | 2000 |
| 6 | 1000 | 9 | 100 | 15 | 20 | 270 | 15 | 300 | 2000 |
| 6 | 1000 | 9 | 300 | 15 | 20 | 270 | 15 | 300 | 2000 |
| 6.5 | 1000 | 9 | 50 | 15 | 20 | 269.5 | 15 | 300 | 2000 |
| 6.5 | 1000 | 9 | 100 | 15 | 20 | 269.5 | 15 | 300 | 2000 |
| 6.5 | 1000 | 9 | 300 | 15 | 20 | 269.5 | 15 | 300 | 2000 |
| 7 | 1000 | 9 | 50 | 15 | 20 | 269 | 15 | 300 | 2000 |
| 7 | 1000 | 9 | 100 | 15 | 20 | 269 | 15 | 300 | 2000 |
| 7 | 1000 | 9 | 300 | 15 | 20 | 269 | 15 | 300 | 2000 |

Table 6.14 Thickness and moduli of AC, rubblized concrete slab (RCS), combination of base and subbase (BS) and roadbed soil (RB) of a pavement section having no stiff layer

| AC | | RCS | | BS | | RB | | Stiff layer | |
|---|---|---|---|---|---|---|---|---|---|
| Thickness (in.) | Mod (ksi) | Thickness (in.) | Mod (ksi) | Thickness (in.) | Mod (ksi) | Thickness (in.) | Mod (ksi) | Depth (in.) | Mod (ksi) |
| 5 | 1000 | 9 | 50 | 15 | 20 | Infinite | 15 | No Stiff layer | |
| 5 | 1000 | 9 | 100 | 15 | 20 | Infinite | 15 | No Stiff layer | |
| 5 | 1000 | 9 | 300 | 15 | 20 | Infinite | 15 | No Stiff layer | |
| 5.5 | 1000 | 9 | 50 | 15 | 20 | Infinite | 15 | No Stiff layer | |
| 5.5 | 1000 | 9 | 100 | 15 | 20 | Infinite | 15 | No Stiff layer | |
| 5.5 | 1000 | 9 | 300 | 15 | 20 | Infinite | 15 | No Stiff layer | |
| 6 | 1000 | 9 | 50 | 15 | 20 | Infinite | 15 | No Stiff layer | |
| 6 | 1000 | 9 | 100 | 15 | 20 | Infinite | 15 | No Stiff layer | |
| 6 | 1000 | 9 | 300 | 15 | 20 | Infinite | 15 | No Stiff layer | |
| 6.5 | 1000 | 9 | 50 | 15 | 20 | Infinite | 15 | No Stiff layer | |
| 6.5 | 1000 | 9 | 100 | 15 | 20 | Infinite | 15 | No Stiff layer | |
| 6.5 | 1000 | 9 | 300 | 15 | 20 | Infinite | 15 | No Stiff layer | |
| 7 | 1000 | 9 | 50 | 15 | 20 | Infinite | 15 | No Stiff layer | |
| 7 | 1000 | 9 | 100 | 15 | 20 | Infinite | 15 | No Stiff layer | |
| 7 | 1000 | 9 | 300 | 15 | 20 | Infinite | 15 | No Stiff layer | |

Figure 6.11




Figure 6.12 B
o
(1

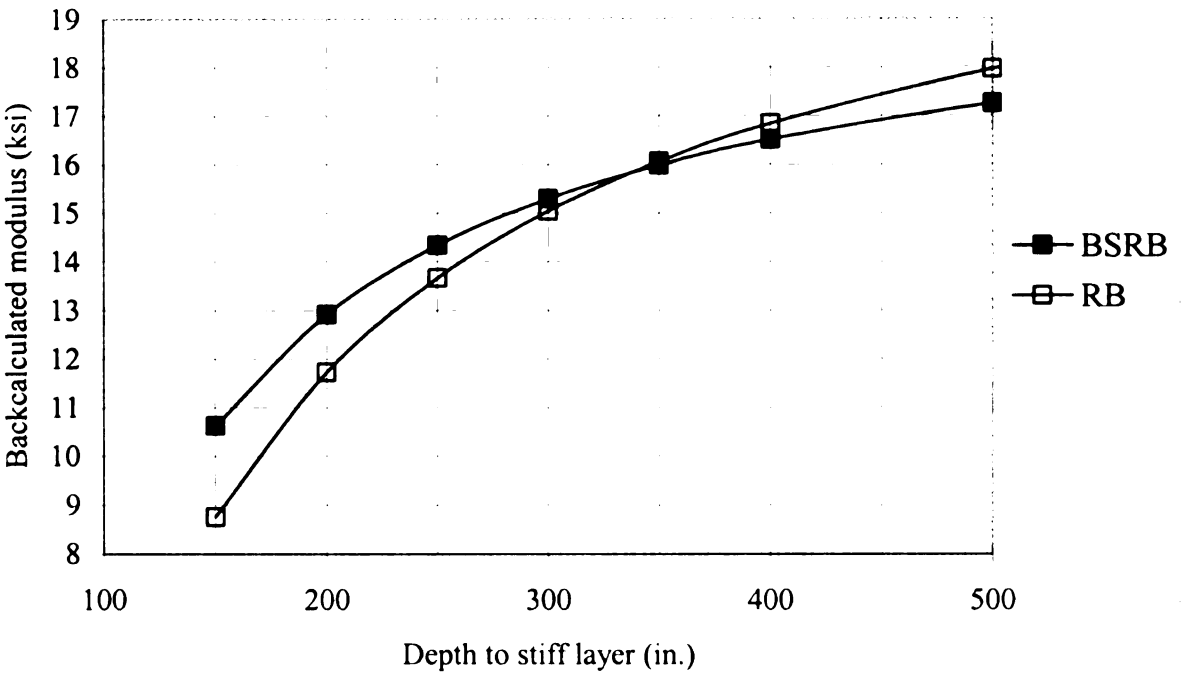


Figure 6.11 Backcalculated roadbed soil (RB) moduli and the moduli of the combination of base, subbase and roadbed soil (BSRB) of the pavement with a 300-in depth to stiff layer

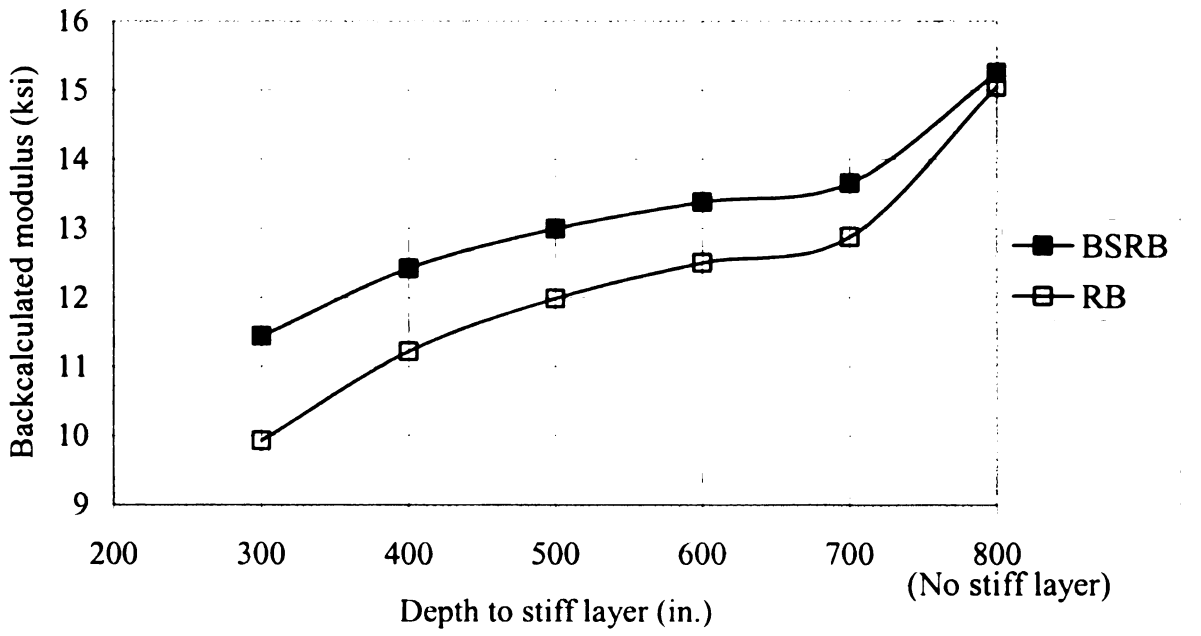


Figure 6.12 Backcalculated roadbed soil (RB) moduli and the moduli of the combination of base, subbase and roadbed soil (BSRB) of the pavement with no stiff layer (In the plot, 800 in. represents no stiff layer)

5.3 Sp

Th

pavement

- Th

to

- So

FC

stud

mod

To

backcalcula

provisions w

trenching) a

dissipation o

observations.

backcalculat

1. 4-laye

6.13a.

2. 4-layer

Figure

of laye

4. 5 an

layer a

## 5.3 Special Provisions for the Backcalculation of Rubblized Pavement Moduli

There are two special problems associated with the backcalculation of rubblized pavement moduli. These are:

- The thicknesses of the RM and the FC layers are unknown and they vary from 0.0 to 9.0-in along and across the pavement.
- Some rubblized pavement sections consist of more than 4 layers (e.g., AC, RM, FC, B, S and RB). Whereas none of the backcalculation software tested in this study (see section 4.0) is capable of performing accurate backcalculation of the moduli of more than 4-layers.

To overcome the two problems and to accomplish part of the objectives of the backcalculation (estimating the RM and the FC moduli), special backcalculation provisions were developed. The special provisions are based on field investigation (by trenching) and observations of rubblized pavement sections and on the principles of dissipation of the rubblizer energy through the depth of the concrete slabs. Based on field observations, rubblized pavement sections could be simulated and their moduli could be backcalculated using the following two 4-layer systems:

1. 4-layer system (4RB) consisting of AC, RCS, BS and RB as shown in Figure 6.13a.
2. 4-layer system (4BSRB) consisting of AC, RM, FC and BSRB as shown in Figures 6.13b and 6.13c. Since the RM thickness is unknown, the backcalculation of layer moduli should be repeated for each of the following RM thicknesses 0, 3, 4, 5 and 7 in. When the RM thickness is 0.0-in, the 4BSRB system becomes 3-layer and the RCS could be either a full depth RM or a full depth FC layer.

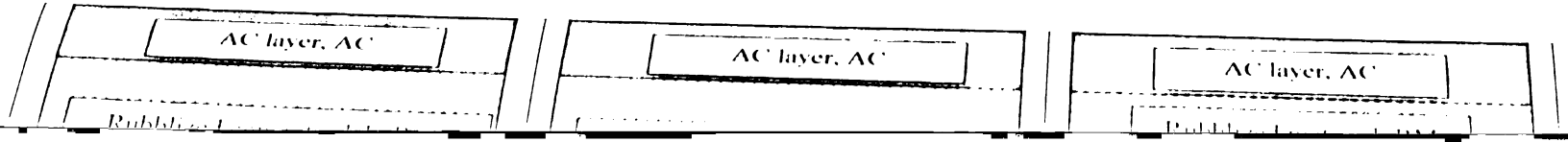
AC layer, AC
AC layer, AC
AC layer, AC

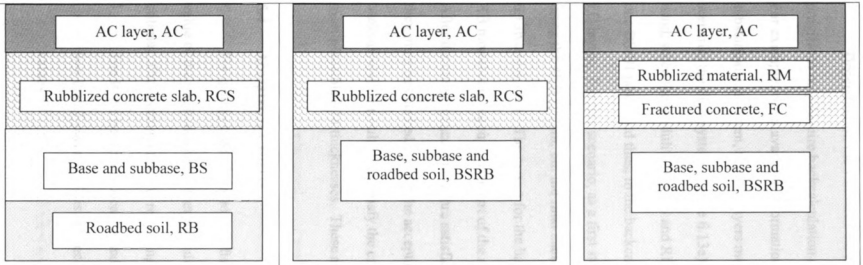


Figure 6.13 Three multi-layer systems used in the backcalculation of rubblized pavement moduli

D.

provisions

For exam

substantia

scenario, t

hand, whe

one BSRB

FC layers.

using the 4

6.13b and

RB modulu

After the co

they must b

backcalcula

most plausib

## 5.4 Accep

For q

value of the

criteria. The

1. The R

less th

values

Depending on the values of the BS and RB moduli of the test site, the special provisions may require backcalculation of the first or both 4-layer systems listed above. For example, when available information indicates that the moduli of the BS and RB are substantially different, the two layers must be backcalculated separately. For this scenario, the 4RB system (Figure 6.13a) is the only backcalculation option. On the other hand, when the moduli of the BS and RB are similar, the two layers can be combined into one BSRB layer, and thus, in the backcalculation, the RCS can be divided into RM and FC layers. For this scenario, as a first step, the layer moduli must be backcalculated using the 4RB system, but the final backcalculation option is the 4BSRB system (Figures 6.13b and 6.13c). The reason for the backcalculation using the 4RB system is that the RB modulus is required as a part of the acceptance criteria stated in the next section. After the convergence criteria are satisfied and the backcalculated moduli are obtained, they must be checked against the acceptance criteria listed in section 5.3. The backcalculation results that satisfy the criteria will then be examined to determine the most plausible RM thicknesses. These and other issues are presented in the next section.

## 5.4 Acceptance Criteria

For quality control purposes, after the convergence criteria are satisfied, each value of the backcalculated layer moduli were scrutinized based on several acceptance criteria. These criteria and the reasoning behind them are listed below.

1. The RMS between the calculated and the measured deflection basins is equal to or less than 2 percent. This enhances the accuracy of the backcalculated modulus values.

2. The BS modulus must be greater than the RB modulus. This criterion is based on the principles of pavement design, decreasing layer modulus with depth (Huang, 1993). This criterion could be waived, if and only if, available and reliable information indicate that the RB modulus is higher than the BS modulus.

3. When the 4BSRB system is used, the BSRB must satisfy the following equation

$$1.05*\text{BSRB modulus} \geq \text{RB modulus (obtained from the 4RB system)}$$

This criterion could be waved, if and only if, the RMS of the 4RB system is greater than 2 percent. Finally, the purpose of this criterion is to check whether or not the BS and the RB moduli are similar.

4. Based on the definitions of the RM and FC material; the RM modulus must be equal to or higher than 20 ksi but less than or equal to 100 ksi and the FC modulus must be higher than 100 ksi but less than or equal to 4,000 ksi. Whereas the RCS modulus must be equal to or greater than 20 ksi but equal to or less than 4,000 ksi.

For the backcalculation of rubblized pavement only, after the backcalculation results were checked against the acceptance criteria, the most plausible RM thickness are to be determined as presented in the next section.

## 5.5. Determination of the Most Plausible RM Thickness

From the outset, it should be recalled that the RM material is defined as the broken portion of the concrete with concrete chunks varying in size from dust to 6-in. Further, based on various field examinations of the RM and FC layers, it was assumed that the ranges of the two moduli are as follows:

$$20 \text{ ksi} \leq \text{RM modulus} \leq 100 \text{ ksi}$$

For the

2[-ksi w

frequen

occasion

observ a

rubbiliza

typically s

the thinne

the FC wh

modulus o

that the thic

pavements d

1. Soma

temp

lower

concr

were

2. The c

anoth

rubbli

the co

$$100 \text{ ksi} < \text{FC modulus} \leq 4000 \text{ ksi}$$

For the RM, the 100-ksi modulus is associated with larger concrete pieces whereas the 20-ksi with small ones. For the FC layer, the 100 ksi modulus is associated with frequently cracked concrete while the 4000-ksi designates solid concrete (no fracture or occasional fracture). Once again, the above assumptions were based on field observations and on the principles of energy dissipation with depth, which dictate that the rubblization energy decreases with increasing depth. Hence, the original concrete slab is typically subjected to better rubblization at the top than at the bottom. This implies that the thinner is the RM; the lower is its modulus and the higher is the average modulus of the FC whereas the thicker is the RM, the higher is its modulus and the lower is the modulus of the FC as shown in Figure 6.14. Further, field investigation also indicated that the thickness of the RM and FC layers could vary from 0 to 9 in. across and along the pavements depending on the quality of the rubblization. The reasons for that are:

1. Some of the rubblization energy is consumed by breaking the bond between the temperature steel and the concrete. Hence, lower energy level is delivered to the lower concrete causing it to fracture. This scenario could be different when plain concrete pavements are rubblized. Unfortunately, no plain concrete pavements were rubblized in Michigan and therefore they were not included in this study.
2. The condition of the concrete slab prior to rubblization varies from one point to another. A cracked area in the concrete slab will consume some of the rubblization energy, which tends to close the cracks. Hence, the thicknesses and the conditions of the RCS and the RM layers vary from one location to another.

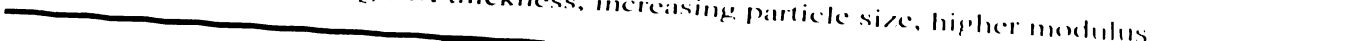
Increasing RM thickness, increasing particle size, higher modulus

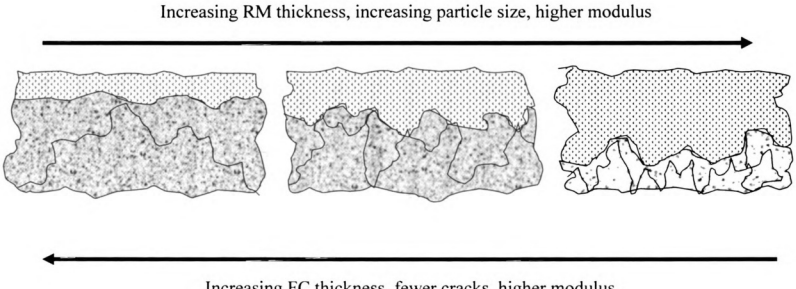




Figure 6.14 Schematic of three possible outcomes of rubblizing pavements illustrating their impacts on the moduli of the RM and FC layers

Based on the results of the filed investigation, the principles of energy dissipation with depth and the above discussions, the most plausible RM thickness can be determined as follows:

2a) If the 4RB system is used, the RCS must be counted as a full depth RM or a full depth FC depending on the modulus value of the RCS (less or greater than 100-ksi). The accuracy of the backcalculated moduli of the 4-RB system was studied using more than 200 forward and backward analyses. It was found that the accuracy of the backcalculated moduli varies from one layer to another as follows:

- The backcalculated AC modulus is relatively accurate and is not affected by combining the RM and FC layers. The accuracy of the AC modulus is a function of the accuracy of the AC thickness used in the backcalculation.
- The backcalculated RCS modulus is low and the backcalculated BS modulus is high, which indicate interaction between the two layers. On average, the backcalculated BS modulus should be divided by a factor of about 1.5 and the backcalculated RCS modulus should be increased by a factor of about 1.5. The value of the exact factor to be used depends on the relative thickness of the BS and RCS. Higher BS thickness would decrease the value of the base factor and increase the RCS factor.
- The error in the backcalculated RB modulus is insignificant.

The disadvantage of the 4RB system is that the moduli of the RM and FC layers cannot be determined. Alternatively, if these moduli are of interest, the B, S and

RB could be combined into one BSRB and the RM and FC moduli could be backcalculated as stated below.

2b) If the 4BSRB system is used, then the backcalculated moduli obtained from each RM thickness must be examined to determine the most plausible RM thickness and layer moduli. Such examination should be based on the principles of energy dissipation with depth and on the results of field investigation as follows:

- The BSRB modulus should satisfy the acceptance criteria stated in section 5.3 and repeated here for convenience.

  1.05*BSRB modulus $\geq$ RB modulus (obtained from the 4RB system)

- **Partial depth RM (3, 4, 5 and 7-in)** – The RM and FC moduli for the partial depth RM should be as follow:

  a) If the RM thickness is selected as 3 in., it is likely that the RM modulus is relatively low (e.g. less than 40 ksi). The FC modulus should be less than 1,000 ksi. The reasons for these include: a1) It is likely that the 3-in RM consists mainly of small pieces (.1 to 1-in) of broken concrete and the number of large pieces (1 to 6-in) is very limited. A2) The rubblization energy has fractured the lower portion of the concrete slab, the space between the cracks increases with depth. Hence, the modulus of the FC is likely between 250 and 100-ksi. If the FC modulus is higher than 1000-ksi, results of the backcalculation at that FWD station should be rejected.

  b) If the RM thickness is selected as 4 or 5 in., the RM modulus have any value between 20 and 100-ksi depending on the dominant size

of the broken concrete. Higher RM modulus indicates lower quality rubblization and higher number of large pieces of broken concrete. The FC modulus should be higher than 100 but lower than 1000-ksi. Further, higher RM modulus should correspond to higher FC modulus. That is the closer is the RM modulus to 100 ksi, the closer is the FC modulus to 1000-ksi. For example, if the modulus of a 4-in. thick RM layer is 70 ksi, the modulus of the FC layer should be at least 250 ksi. However, if the RM modulus is 30 ksi, the FC modulus could be higher than 100 but lower than 500 ksi depending on the degree to which the temperature steel has been debonded.

c) If the RM thickness is selected as 7 in., the RM modulus could also be higher than 20 but lower than 100-ksi depending on the number of large broken concrete pieces. The FC modulus should be higher than 100 but lower than 500-ksi.

- **Full depth RM or full depth FC** - If none of the backcalculation results (using 3, 4, 5 and 7-in. RM thickness) satisfy the above scenarios, the RCS is either a full depth RM or a full depth FC depending on the value of the backcalculated modulus of the RCS from the 3-layer system.

Finally, if none of the backcalculation results can be selected in accordance with the above, no backcalculation results should be reported at that test station.

One important point should be made regarding the backcalculation of the 4BSRB moduli. The backcalculated moduli of the AC layer for the 0, 3, 4, 5, and 7-in thick RM options should be similar. Large differences indicate interaction between the RM and the AC layers and the results for that thickness should be rejected.

Examples for the determination of the most plausible RM thickness are provided in section 8.0 of this chapter together with the example of backcalculation of layer moduli of two rubblized pavement test sites on US-10 eastbound.

## 6.0 VARIABLES AFFECTING THE BACKCALCULATION RESULTS

During the course of field investigation, it was found that the thickness of each pavement layer varies along and across a given test site. Core measurements and drilling of more than twenty test sites indicate that:

- The AC thickness varies along and across the project by about $\pm$ 1-in.
- The interfaces between the RM and the FC layers are uneven and their thicknesses vary along and across the pavement from zero to the original thickness of the concrete slab.
- The thicknesses of the aggregate base and the sand subbase vary along and across the project by about $\pm$ 2 in.

Such variations have impact on the accuracy of the backcalculated moduli. This impact and other issues related to the thickness of the pavement layers are presented and discussed in the next sections.

## 6.1. T

After the
projects.
cores we
of TDC.
since the
Chapter 3
was calcu
was calcu
no cores w
The effect
assessed (u
site 1) as fo

1. The
core

2. The
aver

Tabl
scenarios ste
backcalculat
the AC modu
the average h

## 6.1. The AC Thickness

In this study, 26 rubblized and 12 flexible pavement test sites were FWD tested. After the test, 10 to 18 cores were extracted from each of 19 rubblized and 12 flexible projects. In a preliminary study, at three rubblized tests sites along I-96 only 2, 5 and 7 cores were extracted The reason is that the purpose of the core was to verify the existence of TDC. In addition, no cores were extracted from four rubblized pavement test sites since there were no cracks. Nevertheless, the thickness of each core was measured (see Chapter 3) at the four ends of two orthogonal diameters and the average core thickness was calculated. After word, for each test site, the average of the average core thicknesses was calculated and used in the backcalculation of layer moduli. For those projects where no cores were extracted, the thickness of the AC was obtained from the MDOT records. The effect of using the average core thickness on the backcalculated layer moduli was assessed (using the deflection data that were measured on US-10 EB, test section 1, test site 1) as follows:

1. The layer moduli at each core location were backcalculated using the measured core thickness.
2. The layer moduli for the twelve core locations were backcalculated using the average measured AC thickness of 6.5-in.

Table 6.15 provides a list of the backcalculated moduli of the two backcalculation scenarios stated above. For each pavement layer, the percent error between the two backcalculation schemes is stated in the table. It can be seen that the maximum error in the AC modulus is about 7 percent due to error in the AC thickness of 0.4-inch. Further, the average backcalculated AC modulus from the two schemes is almost the same.

*Table 6.15 Backcalculated moduli at 12 core locations on US-10 EB section 1 test site 1 using the average AC thickness of 6.5-in. and the measured core thicknesses*

Table 6.15 Backcalculated moduli at 12 core locations on US-10 EB section 1 test site 1 using the average AC thickness of 6.5-in. and the measured core thicknesses

| Core no. | Measured core thickness (in.) | Backcalculated modulus (psi) | | | | | | | | |
|---|---|---|---|---|---|---|---|---|---|---|
| | | Using the average AC thickness of 6.5-in. | | | Using the measured AC thickness at each core location | | | Error (%) | | |
| | | AC | Rubblized | Roadbed | AC | Rubblized | Roadbed | AC | Rubblized | Roadbed |
| 4 | 6.1 | 593,308 | 117,592 | 16,842 | 638,486 | 127,150 | 16,857 | -7 | -8 | 0 |
| 16 | 6.2 | 624,477 | 110,572 | 17,683 | 654,573 | 118,199 | 17,689 | -5 | -6 | 0 |
| 1 | 6.3 | 633,726 | 99,602 | 16,084 | 657,589 | 103,990 | 16,087 | -4 | -4 | 0 |
| 24 | 6.3 | 700,981 | 105,098 | 17,936 | 727,063 | 109,878 | 17,938 | -4 | -4 | 0 |
| 7 | 6.4 | 624,280 | 123,957 | 15,525 | 633,640 | 126,743 | 15,527 | -1 | -2 | 0 |
| 10 | 6.5 | 449,885 | 84,145 | 14,912 | 449,882 | 84,143 | 14,912 | 0 | 0 | 0 |
| 25 | 6.5 | 479,011 | 177,691 | 17,127 | 476,651 | 178,319 | 17,127 | 0 | 0 | 0 |
| 17 | 6.5 | 481,336 | 152,459 | 16,838 | 477,940 | 153,219 | 16,837 | 1 | 0 | 0 |
| 18 | 6.6 | 499,286 | 90,203 | 15,722 | 489,909 | 88,508 | 15,720 | 2 | 2 | 0 |
| 26 | 6.6 | 538,983 | 100,909 | 16,051 | 520,122 | 97,031 | 16,045 | 4 | 4 | 0 |
| 15 | 6.7 | 619,067 | 110,782 | 17,315 | 595,696 | 106,642 | 17,309 | 4 | 4 | 0 |
| 23 | 6.7 | 583,352 | 97,567 | 17,968 | 566,073 | 93,208 | 17,967 | 3 | 5 | 0 |
| Average | 6.5 | 568,974 | 114,215 | 16,667 | 573,969 | 115,586 | 16,668 | -1 | -1 | 0 |
| CV | 0.03 | 0.14 | 0.23 | 0.06 | 0.16 | 0.24 | 0.06 | | | |

CV = Coefficient of variation = standard deviation divided by average value

The abo

are the r

extracte

backcalc

across th

F

regardin

backcalc

MDOT re

is 6.5-in.

errors in

AC cores

thickness.

**6.2. The**

As

on the B. S

thicknesses

the RM and

the backcalc

and backwa

Table 6.16.

Various assu

The above observations imply that the higher is the number of cores, the more accurate are the results of the backcalculation. However, if for some reason only 2 or 3 cores were extracted, and their average thickness is used in the backcalculation, the error in the backcalculated modulus could be minimized if the cores are randomly located along and across the pavement.

For the 4 test sites were no pavement cores were extracted and the MDOT record regarding the thickness of the AC layer was used in the backcalculation, the errors in the backcalculated layer moduli depend on the accuracy of the record. For example, the MDOT record of the AC thickness on US-10 is 6.0-in whereas the average core thickness is 6.5-in. So if thickness from the MDOT record is used, it would contribute to some errors in the backcalculation results. Therefore, it is highly recommended that enough AC cores be extracted from the FWD test sites to capture the variation of the AC thickness.

## 6.2. The RM and FC Thicknesses

As stated in section 5.4, the RCS is backcalculated as one or two layers depending on the B, S and RB moduli. This was accomplished by assigning the following thicknesses to the RM layer: 0, 3, 4, 5, and 7 in. An RM thickness of 0 in. implies that the RM and the FC layers are combines into one RCS layer. Nevertheless, the errors in the backcalculation results due to variable RM thickness are examined by the forward and backward analyses of 223 rubblized pavement sections having the properties listed in Table 6.16. Table 6.17 provides the backcalculated layer moduli and the errors due to various assumed RM thicknesses used in the backcalculation.

Table 6.16 Layer thicknesses, moduli and Poisson ratios used in the forward calculation of the deflection basins of 223 pavement sections.

| Layer | Thickness (in) | Modulus (ksi) | Poisson ratio |
|---|---|---|---|
| AC | 4 and 6 | 500, 1000 and 2000 | 0.3 |
| Rubblized material | 0, 3, 4.5, 5, 6, 7 and 9 | 15, 30, 50 and 100 | 0.4<br>0.2 |
| Fractured concrete | 0, 2, 3, 4, 4.5, 6 and 9 | 100, 200, 300, 500, 1000, 2000 and 2500 | 0.2 |
| Combination of base and subbase | 9, 12, 15 and 18 | 15, 20, 30 and 40 | 0.4 |
| Roadbed soil | infinite | 5, 10 and 20 | 0.45 |

Table 6.17 Backcalculated layer moduli and errors due to incorrect RM thicknesses used in the backcalculation

| RM thickness assumed in the backcalculation (in.) | Backcalculated moduli (ksi) | | | | Error (%) | | | |
|---|---|---|---|---|---|---|---|---|
| | AC | RM | FC | BSRB | AC | RM | FC | BSRB |
| 0 | 727 | - | 102 | 21 | -27 | - | -80 | 3 |
| 3 | 1,025 | 18 | 607 | 20 | 3 | -39 | 21 | 1 |
| 4 | 1,011 | 28 | 426 | 20 | 1 | -6 | -15 | 1 |
| 4.5 | 1,008 | 32 | 412 | 20 | 1 | 6 | -18 | 1 |
| 5 | 1,004 | 35 | 420 | 20 | 0 | 17 | -16 | 1 |
| 7 | 992 | 45 | 596 | 20 | -1 | 49 | 19 | 1 |
| True RM thickness and layer moduli | | | | | | | | |
| 4.5 | 1,000 | 30 | 500 | 20 | | | | |

layers (F

backcalc

### 6.2.1 T

F

versus th

that comp

on the ba

1. N

ba

2. Si

0.8

Th

the RM th

### 6.2.2 The

In

variable RM

the backcalc

Tabl

the backcalc

backcalculat

The data in Table 6.17 address two issues, the effect of combining the RM and FC layers (RM thickness = 0.0-in) and the effect of the RM thickness on the accuracy of the backcalculated moduli. These two issues are discussed in the next two subsections.

### 6.2.1 The Effect of Combining the RM and FC layers

Figure 6.15 provides plots of the backcalculated moduli of the AC, BS and RB versus the true moduli used in the forward analyses. Examination of the figure indicates that combining the RM and the FC layers into one layer results in the following impact on the backcalculated moduli:

1. Negligible impact on the backcalculated RB modulus and small impact on the backcalculated AC modulus as shown in Figures 6.15a and 6.15c.
2. Significant impact (the ratio of the backcalculated to the true moduli varies from 0.8 to 4.3) on the backcalculated BS modulus as shown in Figure 6.15b.

The reasons for the above observations are explained together with the effect of the RM thickness assumed in the backcalculation of layer moduli and presented below.

### 6.2.2 The Effect of the Thickness of the RM Layer

In the backcalculation of layer moduli of some pavement sections, the highly variable RM thickness was assigned various values. The effects of such assignment on the backcalculated layer moduli are addressed in this section.

Table 6.17 provides a list of the true layer moduli and the thickness of the RM, the backcalculated layer moduli and the percent errors between the true and the backcalculated layer moduli due to the RM thicknesses assumed in the backcalculation.

Backcalculated roadbed soil modulus (ksi)
25
20
15
10
5
0
Backcalculated base and subbase modulus (ksi)
Backcalculated AC

Figure 6.15 (

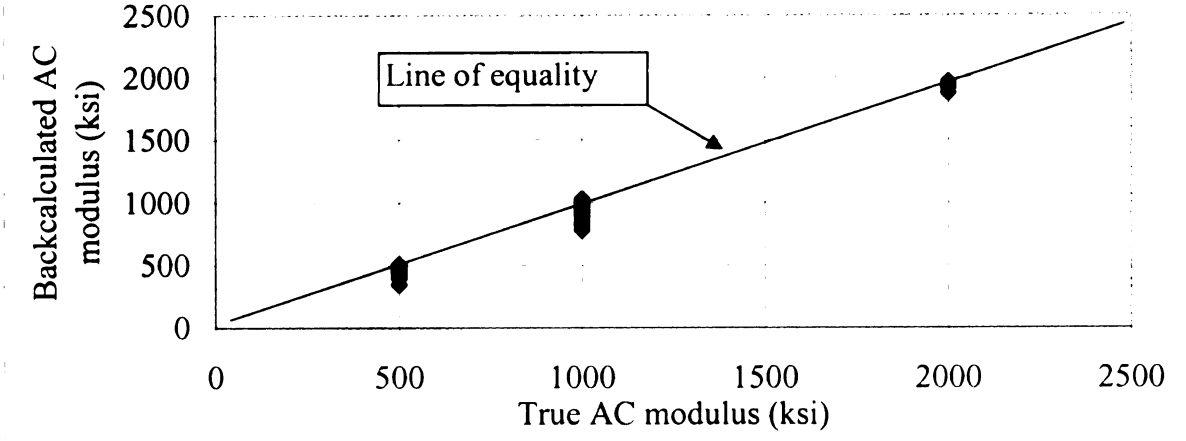


a) AC

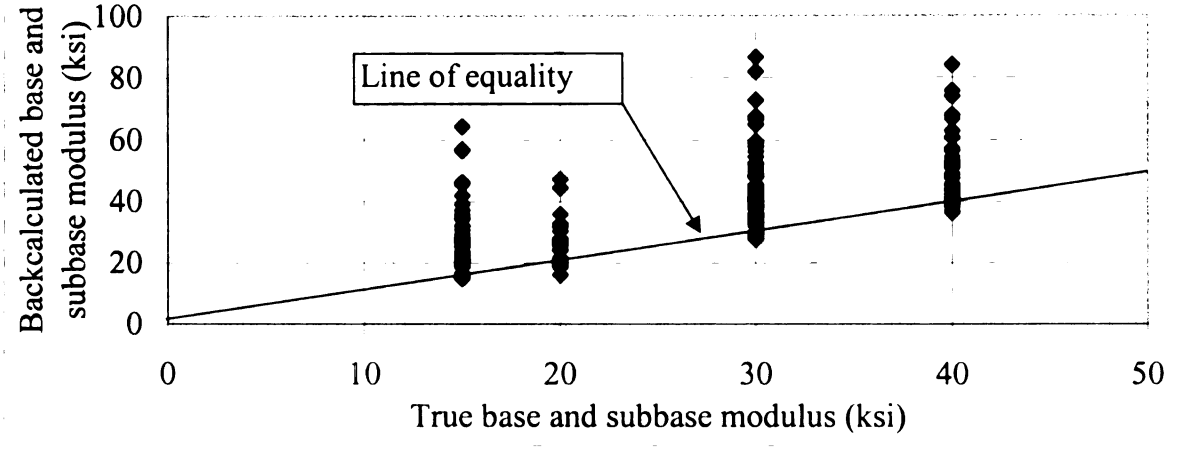


b) Base and subbase (BS)

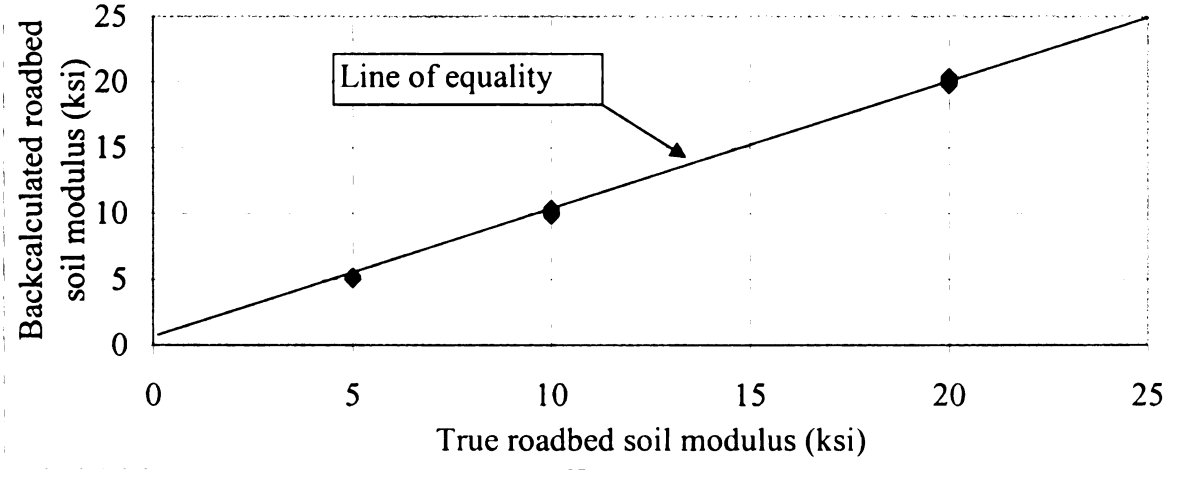


c) Roadbed soil (RB)

Figure 6.15 Comparison between the true moduli and the backcalculated moduli using 4-layer backcalculation (AC, RCS, BS and RB)

Figure 6.16 depicts the backcalculated layer moduli as a function of the assumed RM thickness. Examination of the data listed in Table 6.17 and depicted in Figure 6.16 indicates that:

1. The assumed RM thickness has no impact on the backcalculated BSRB modulus as shown in Figure 6.16c. The BSRB modulus remains almost constant and equal to the true modulus regardless of the RM thickness.
2. The assumed RM thickness has little to no effect on the backcalculated AC modulus except for zero thickness of the RM.
3. The backcalculated RM and FC moduli are very sensitive to the assumed RM thicknesses. The errors in the backcalculated RM and FC moduli can be as high as 49 and 80 percent, respectively.
4. When the true RM thickness of 4.5 is used in the backcalculation, the percent errors in the backcalculated moduli relative to the true ones for the AC, RM, FC and BSRB are 1, 6, -18, and 1, respectively.

The above four observations and the two stated in section 6.2.1 were expected because an error in the assumed RM thickness produces similar but opposite error in the FC thickness (the sum of the two thicknesses is constant and equal to the original thickness of the concrete slab). Said interaction between the two thicknesses produce similar interaction in their backcalculated moduli. Hence, an error in the backcalculated RM modulus is generally compensated by an opposite error in the FC modulus. This causes, more or less, stability in the backcalculated moduli of the other layers. When the RM thickness is assumed zero, the error in the FC thickness and hence in its modulus must be compensated for by errors in the backcalculated moduli of the other layers.

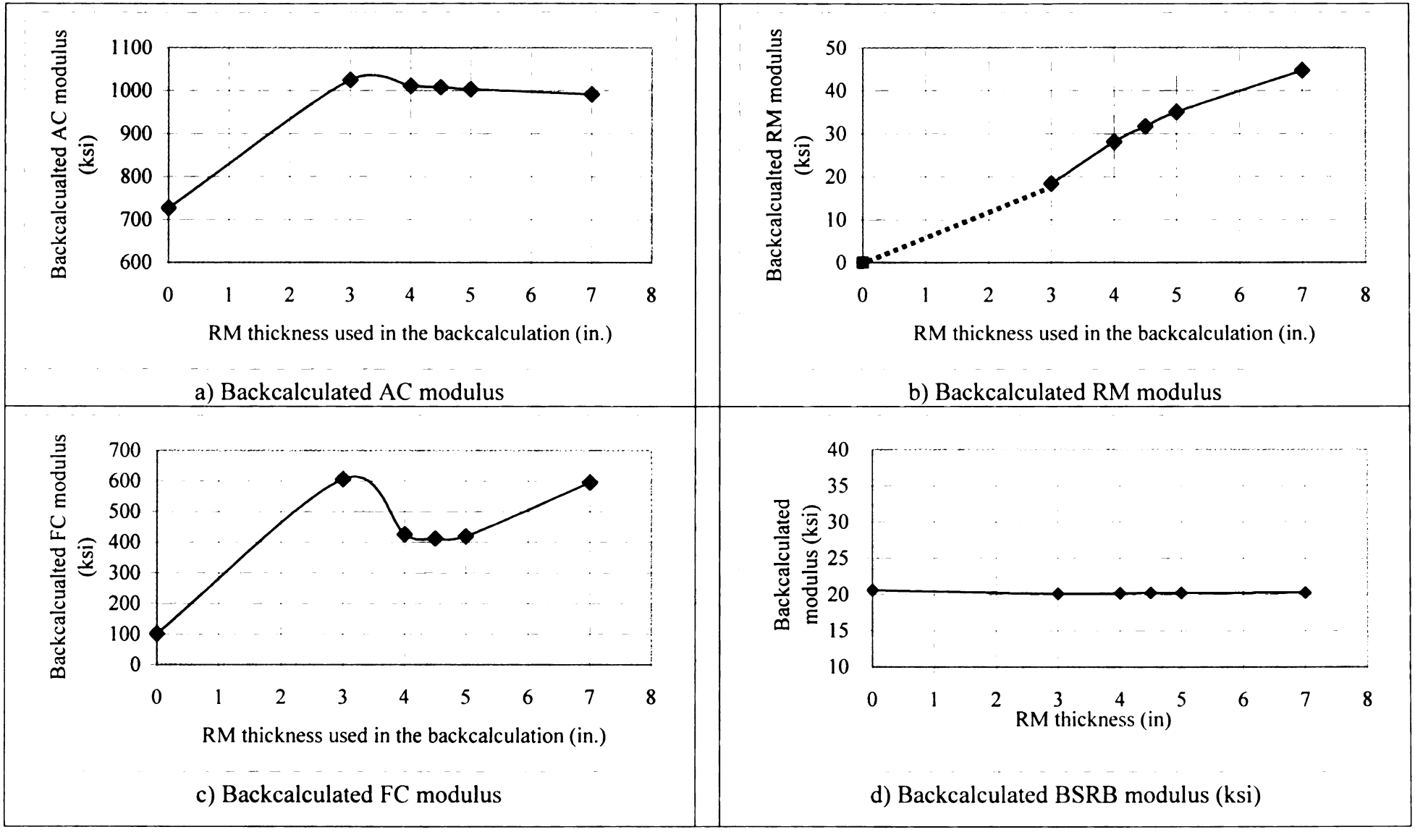


Figure 6.16 The effects of the RM thickness on the backcalculated layer moduli

For example, in a 4-layer system (see Figure 6.13a) consisting of AC, RCS, BS and RB, (the RM layer do exist but it is not counted), the error in the RCS is compensated for by error in the modulus of the BS as shown in Figure 6.15b. While for 3-layer system consisting of AC, RCS and BSRB (Figure 6.13b); an error in the RCS input produces error in its backcalculated modulus, which is compensated for by errors in both the backcalculated AC and RB moduli as shown in Table 6.17. Stated differently, an error in the thickness of one layer only causes errors in the backcalculated moduli of at least one and perhaps two other layers. But, when the thicknesses of two adjacent layers are oppositely erroneous such as in the RM and FC layers, their backcalculated moduli, however erroneous, are balanced as to yield a calculated deflection basin similar to the measured one.

## 6.3. The BS Thickness

The impact of errors in the thicknesses of the BS layer on the backcalculated layer moduli was studied using forward and backward analyses. Since, for rubblized pavements, the BS is separated from the applied load by the AC and the RCS layer, the load induced stresses in the BS layer are relatively small. Hence, the impact of errors in its thickness was found to be insignificant. For example, variations in the BS thicknesses of $\pm$ 2 in. yield less than ten percent error in the backcalculated layer moduli. Based on the results of the analyses, it was concluded that the BS thickness can be obtained from available cross-section records (drilling is not required). Note that, in some rubblized pavement test sites where the thicknesses of the B and S layers are not available, the thickness of the BS layer was assumed 15 in. Said assumption is based on MDOT general

practice for concrete pavements. One exception was found, US-23 near Alpena, Michigan was constructed on 30-in. thick wood logs and sand.

## 7.0 TEMPERATURE CORRECTION OF THE BACKCALCULATED AC MODULUS

The backcalculated AC moduli were corrected to the standard temperature of 68° F using the following temperature correction equation (after Baladi, 1988).

$$TCAC = E_{AC} * e^{0.03658(68-To)} \quad (6.2)$$

$$T_o = T_S + \sin(-6.3252t + 5.0967)*(-0.8767*\frac{h}{2} + 0.2788*(\frac{h}{2})^2 + 0.0321*(\frac{h}{2})^3) \quad (6.3)$$

Where TCAC = AC modulus corrected to standard temperature of 68° F (psi);

$E_{AC}$ = Backcalculated AC modulus at the measured pavement surface temperature ($T_S$), (psi);

$T_o$ = Mid-depth temperature of the AC layer (° F);

h = AC thickness (in.); and

t = time of the day. For example 1:30 PM = 13.5/24 = 0.5625

It should be noted that during sunny days, the pavement surface temperature may vary from one FWD test station to another depending on the wind speed, clouds and tree shadow. Therefore, abrupt changes in the measured pavement surface temperature (such as 3°F or more) between two FWD test stations were smoothened by replacing the odd temperature by the measured temperature at the two adjacent FWD test stations. After this, the moving 5-test location average temperature was employed to minimize the differences between the temperatures of two adjacent FWD stations. The reason for such temperature adjustment is that the time between two FWD tests is about 2 minutes, it is

physically not possible for the pavement surface temperature to rise by more than 3°F and then drop. After calculating the 5-station moving average of, the mid-depth pavement temperature was then calculated using equation 6.3 (Park, 2000).

## 8.0 DETAILED EXAMPLE OF BACKCALCULATION OF RUBBLIZED PAVEMENT LAYER MODULI

To illustrate the backcalculation procedure, a detailed example is presented in this section. A test section consisting of two test sites located on EB US-10 east of Custer City was FWD tested and cored on June 28, 2001. The original concrete pavement was rubblized in 2000, and it was capped with a 6-in thick asphalt layer. The cross-section of the original concrete pavement consisted of:

1. Nine inch thick concrete at the edges of the lane tapered to 7 in. at the center of the lane.
2. Aggregate base and sand subbase layers situated on a relatively deep deposit of sand roadbed soil.

During the investigation on June 28, pavement distress survey was conducted, no surface distress was observed. At each test site, forty FWD tests were conducted using the MDOT KUAB FWD and twelve 6-in. diameter cores were extracted. The core thickness for test site 1 varied from 6.1 to 6.7 in. with an average of 6.5 in whereas for test site 2, they varied from 6.0 to 6.8 with an average of 6.4. During the FWD testing, the pavement surface temperatures and the time of testing were recorded along with the measured deflection data. The deflection data were then examines and the layer moduli were backcalculated, the results are presented in the next subsections.

## 8.1. Examination of the Measured Deflection Data

First, the measured deflection data were examined for possible irregularities in the deflection basins. Figure 6.17 illustrates three measured deflection basins located at the beginning, the middle and at the end of each test site. As can be seen from the figure, the deflections at both tests sites vary from one test location to another. To study said variation for each test site, the measured D1 and D7 at various test locations along and across the pavement were normalized relative to D1 and D7 of the first test location of that site. Figures 6.18 and 6.19 depict the normalized D1 and D7 deflections along and across the pavements of test sites 1 and 2, respectively. The data in the figures indicate that the measured deflections show relatively high variations. Nevertheless, all deflection basins were smooth and no irregularities were found. Therefore, the FWD data from all test locations were included in the backcalculation.

## 8.2 Determination of the Depth to Stiff Layer

First, the equivalent pavement modulus was calculated using equation 6.1and the deflection data from three test stations (1, 16 and 26) positioned at the beginning, the middle and at the end of test sites 1 and 2. Figure 6.20 depicts plots of the equivalent modulus from the two test sites versus the radial distance from the center of the load plate. Two observations can be made as follows:

1. All curves for test sites 1 and 2 have similar shape. This implies the depth to stiff layer for both test sites is almost the same.
2. The tails of the curves show slight increases in the modulus at increasing radial distance. This indicates intermediate depth to stiff layer (300 to 500 in).

Deflection (mils)

Deflection (mils)

Figure

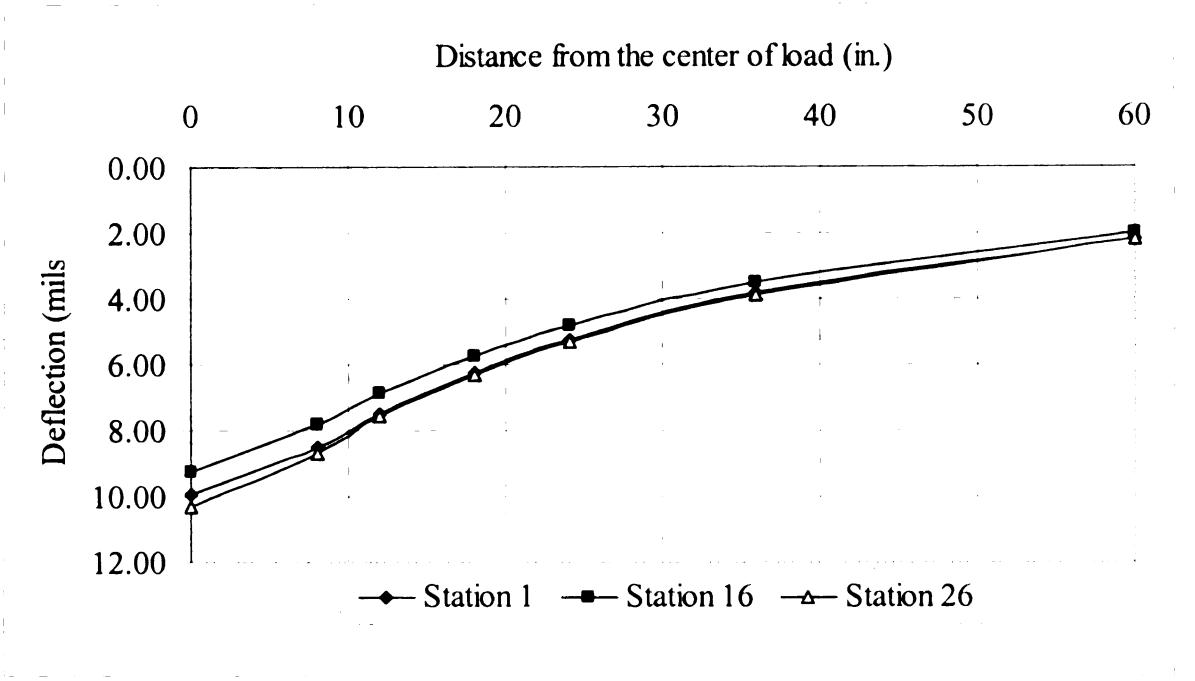


a) Test site 1

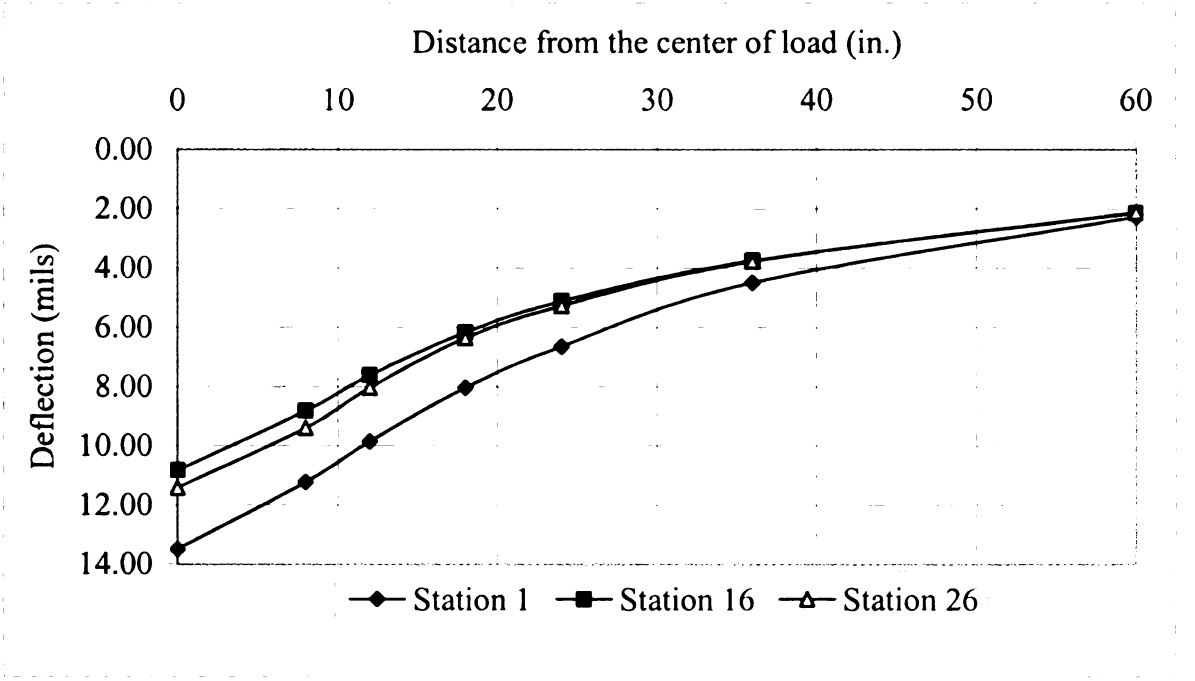


b) Test site 2

Figure 6.17 Three deflection basins from test locations at the beginning, the middle and at the end of the US-10 EB test section 1, test sites 1 and 2

Normalized deflection

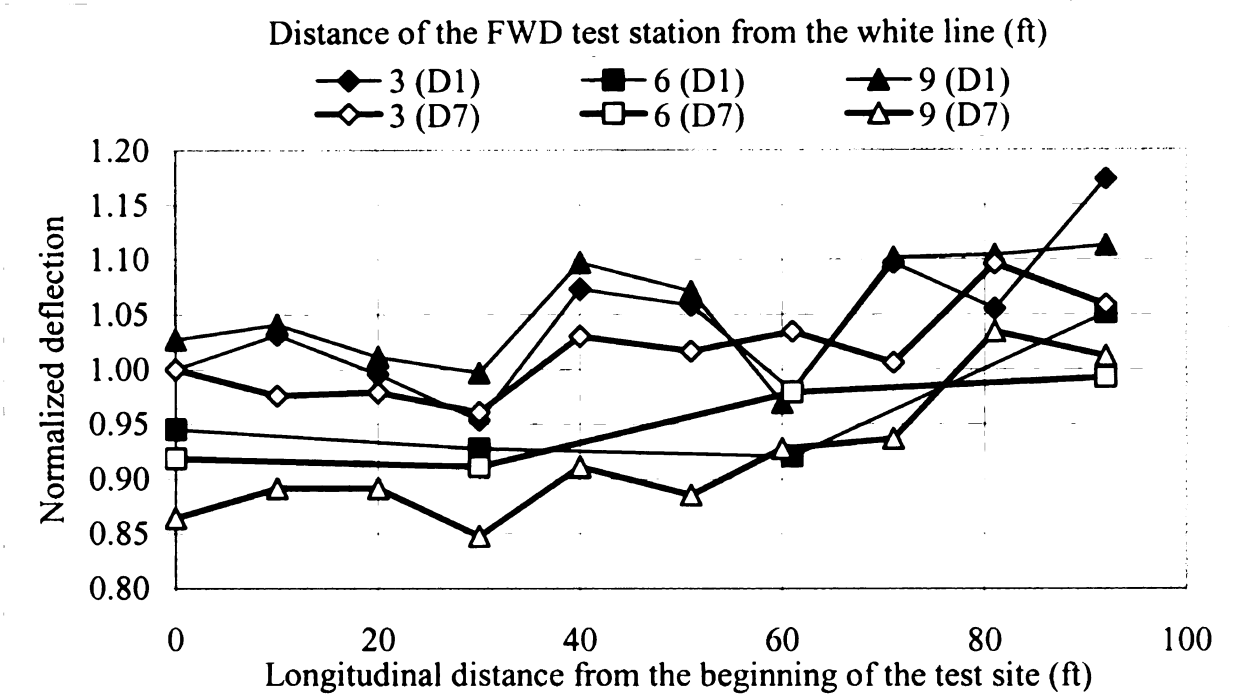


a) Variation along the pavement

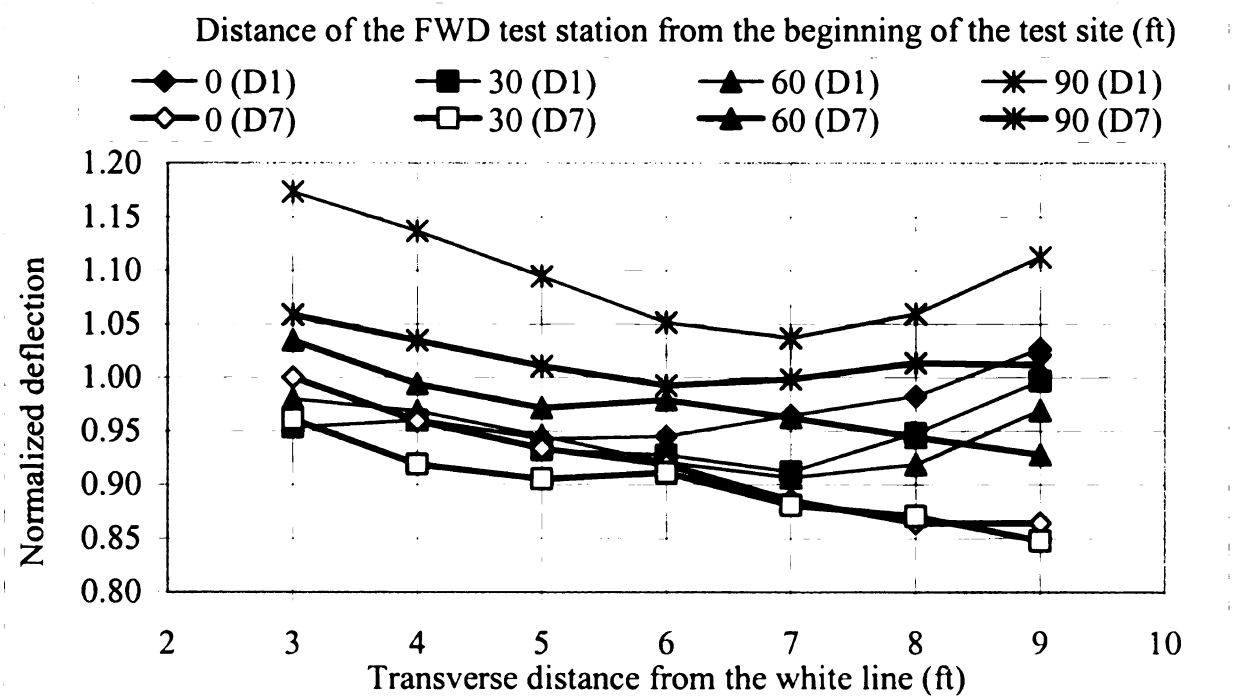


b) Variation across the pavement

Figure 6.18 Variation in the pavement deflections (D1 and D7) along and across test site 1

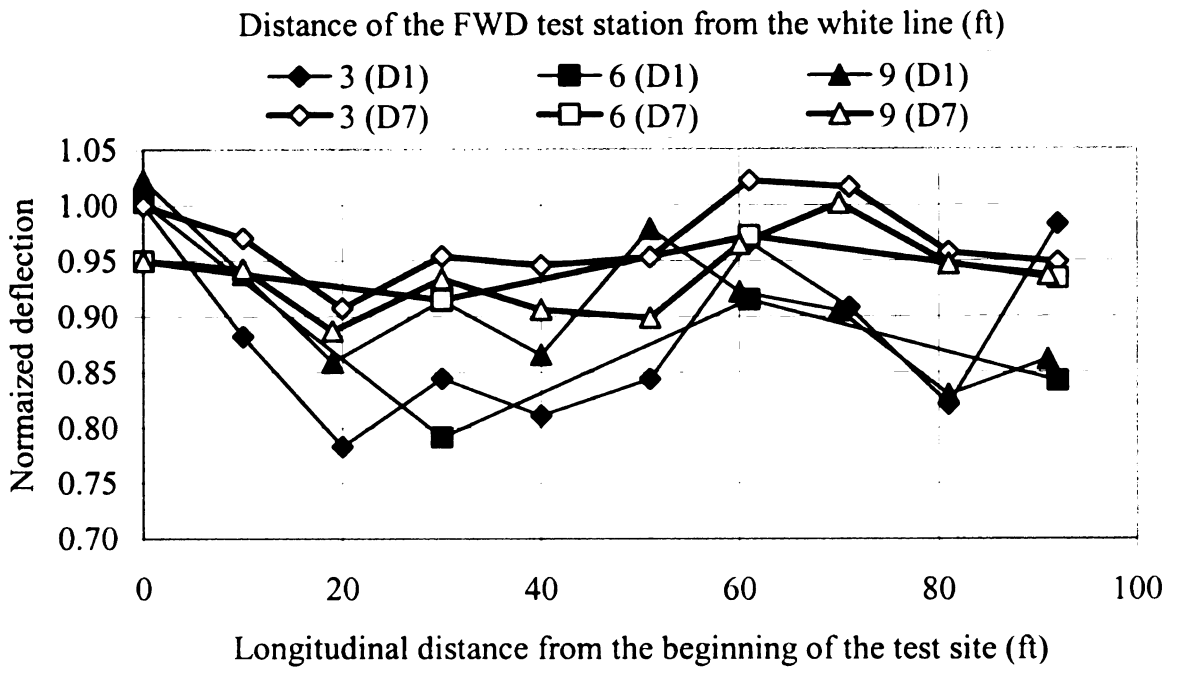


a) Variation along the pavement

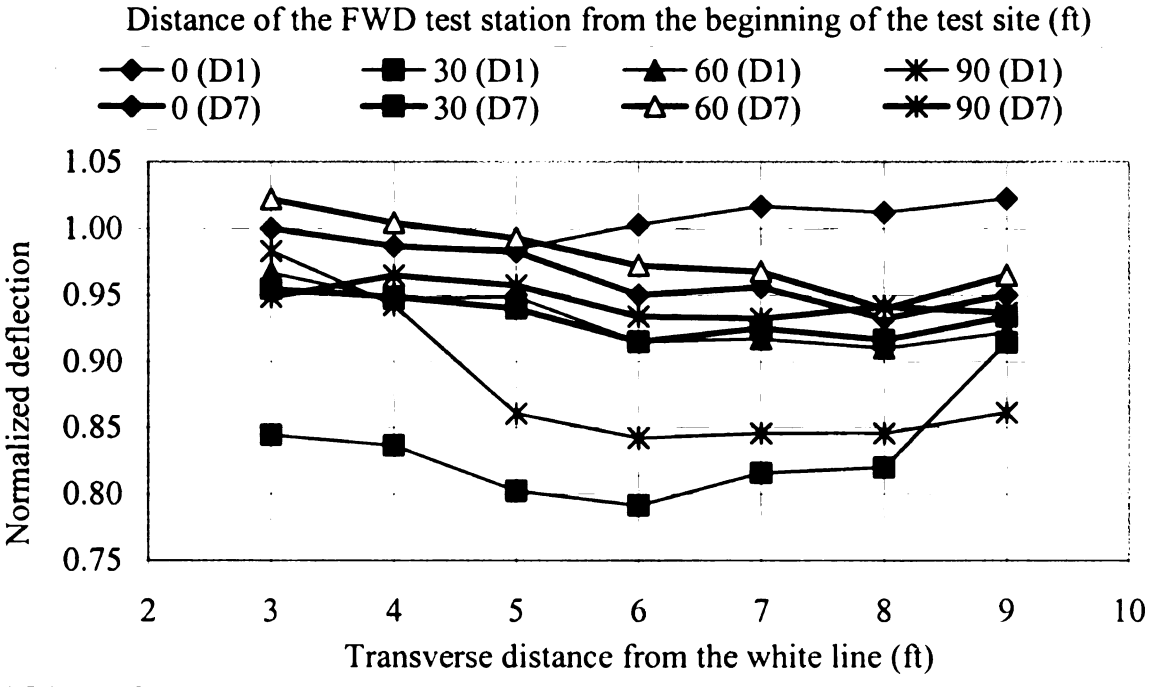


b) Variation across the pavement

Figure 6.19 Variation in the pavement deflections D1 and D7 along and across test site 2

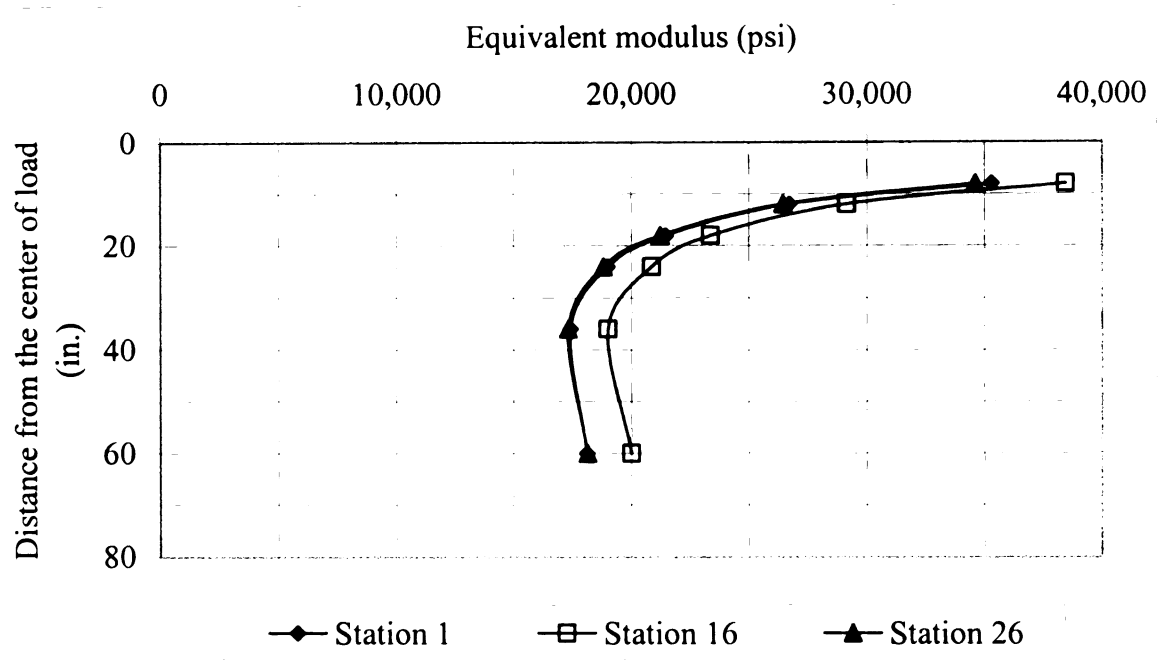


a) Test site 1

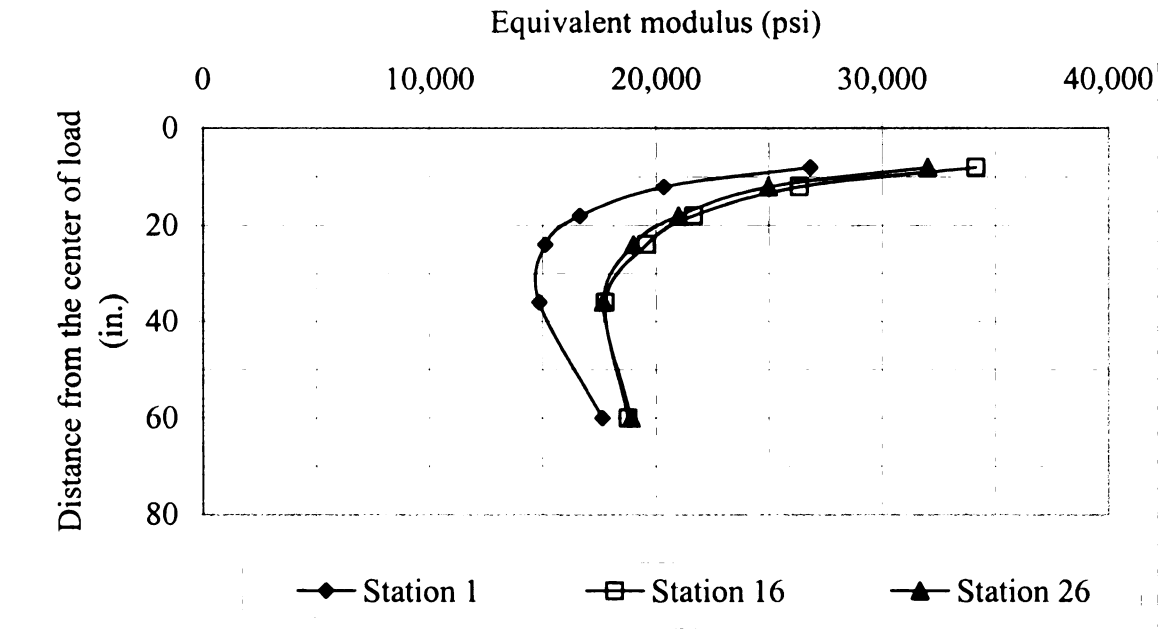


b) Test site 2

Figure 6.20Equivalent modulus versus lateral distance from the center of the load for 3 test locations, US-10 EB, test section 1, test sites 1 and 2

Second, the moduli of 3- and 4-layer systems (see Figure 6.10a) were backcalculated using various depths to stiff layer. Results of the backcalculation are listed in Tables 6.18 through 6.21. Figure 6.21 depicts plots of the average backcalculated BSRB (from the 3-layer system) and RB (from the 4-layer system) versus the depth to stiff layer. As can be seen from the figure, the curves intersect at the depths to stiff layer of about 700 and 600 in. for test sites 1 and 2, respectively. In reality, the true depth to stiff layer for both test sites is shallower than 600-in. The reason is that the modulus of the BSRB (base, subbase and roadbed soil) must be higher than the modulus of the RB. For the two test sites, a depth to stiff layer between 400 and 500-in is acceptable because of the following reasons:

1. The values of the backcalculated layer moduli of the 4-layer system (see Tables 6.18 and 6.20) are reasonable and consistent with the material types.
2. The values of the BS material at 300-in deep stiff layer is relatively high (38 kips) implying that the untreated aggregate base must be above 40 ksi.
3. At depths to stiff layer of 500 and 400-in for test sites 1 and 2, respectively, the moduli of the BS and RB are almost the same for both sites.

For the two test sites, a depth to stiff layer of 500-in was selected. Eventually, any depth to stiff layer between 400 and 500-in could be selected. Such depths have minimum impact on the values of the backcalculated layer moduli (see Tables 6.18 through 6.21). One important observation could be made by examining the values of the AC modulus of the 4- and 3-layer systems. As it was expected, for the 3-layer systems, the error in the modulus of the RCS (due to combining the RM and the FC layers) are compensated for by errors in the AC modulus. This can clearly be seen from examining the AC modulus

*Table 6.18 Backcalculated layer moduli using 4-layer system with various Asphalt*

Table 6.18 Backcalculated layer moduli using 4-layer system with various depths to stiff layer, US-10 EB test section 1 test site 1

| Depth to stiff layer (in.) | Number of stations converged | Average value (ksi) and coefficient of variation (CV) of the backcalculated layer moduli | | | | | | | | Average RMS (%) |
|---|---|---|---|---|---|---|---|---|---|---|
| | | AC | CV | RCS | CV | BS | CV | RB | CV | |
| 100 | 22 | 805 | 0.12 | 30 | 0.32 | 137 | 0.26 | 4 | 0.07 | 0.36 |
| 200 | 39 | 777 | 0.15 | 39 | 0.42 | 69 | 0.53 | 11 | 0.06 | 0.34 |
| 300 | 40 | 737 | 0.16 | 51 | 0.4 | 38 | 0.34 | 14 | 0.06 | 0.37 |
| 400 | 40 | 718 | 0.17 | 58 | 0.38 | 30 | 0.28 | 15 | 0.06 | 0.41 |
| 500 | 40 | 712 | 0.17 | 62 | 0.37 | 26 | 0.26 | 16 | 0.06 | 0.45 |
| 600 | 40 | 707 | 0.17 | 64 | 0.36 | 24 | 0.25 | 17 | 0.06 | 0.46 |
| 700 | 40 | 699 | 0.17 | 67 | 0.35 | 23 | 0.25 | 17 | 0.06 | 0.46 |
| 800 | 40 | 665 | 0.17 | 78 | 0.32 | 17 | 0.23 | 20 | 0.06 | 0.55 |

Table 6.19 Backcalculated layer moduli using 3-layer system with various depths to stiff layer, US-10 EB test section 1 test site 1

| Depth to stiff layer (in.) | Number of stations converged | Average value (ksi) and coefficient of variation (CV) of the backcalculated layer moduli | | | | | | | | Average RMS (%) |
|---|---|---|---|---|---|---|---|---|---|---|
| | | AC | CV | RCS | CV | | | BSRB | CV | |
| 100 | 40 | 336 | 0.22 | 462 | 0.44 | | | 7 | 0.07 | 7.32 |
| 200 | 40 | 423 | 0.13 | 187 | 0.24 | | | 13 | 0.07 | 3.84 |
| 300 | 40 | 478 | 0.14 | 137 | 0.25 | | | 15 | 0.06 | 2.32 |
| 400 | 40 | 525 | 0.15 | 115 | 0.27 | | | 16 | 0.06 | 1.62 |
| 500 | 40 | 562 | 0.16 | 103 | 0.28 | | | 17 | 0.06 | 1.25 |
| 600 | 40 | 588 | 0.17 | 96 | 0.29 | | | 17 | 0.06 | 1.04 |
| 700 | 40 | 605 | 0.17 | 91 | 0.3 | | | 18 | 0.06 | 0.90 |
| 800 | 40 | 733 | 0.18 | 65 | 0.35 | | | 19 | 0.06 | 0.78 |

RCS = rubblized concrete slab, BS = he combination of base and subbase, RB=roadbed soil, BSRB = the combination of base, subbase and roadbed soil, RMS = root mean square.

Table 6.20 Backcalculated layer moduli using 4-layer system with various depths to stiff layer, US-10 EB test section 1 test site 2

| Depth to stiff layer (in.) | Number of stations converged | Average value (ksi) and coefficient of variation (CV) of the backcalculated layer moduli | | | | | | | | Average RMS (%) |
|---|---|---|---|---|---|---|---|---|---|---|
| | | AC | CV | RCS | CV | BS | CV | RB | CV | |
| 100 | 25 | 619 | 0.11 | 22 | 0.3 | 140 | 0.27 | 4 | 0.06 | 0.44 |
| 200 | 29 | 573 | 0.13 | 31 | 0.39 | 53 | 0.55 | 11 | 0.04 | 0.43 |
| 300 | 40 | 538 | 0.13 | 41 | 0.38 | 31 | 0.47 | 13 | 0.03 | 0.45 |
| 400 | 40 | 522 | 0.14 | 46 | 0.36 | 24 | 0.36 | 15 | 0.03 | 0.49 |
| 500 | 40 | 516 | 0.14 | 49 | 0.35 | 21 | 0.33 | 16 | 0.03 | 0.53 |
| 600 | 40 | 512 | 0.14 | 51 | 0.34 | 20 | 0.31 | 16 | 0.03 | 0.54 |
| 700 | 40 | 507 | 0.14 | 53 | 0.34 | 19 | 0.3 | 17 | 0.03 | 0.55 |
| 800 | 40 | 483 | 0.14 | 60 | 0.31 | 14 | 0.27 | 19 | 0.03 | 0.63 |



Table 6.21 Backcalculated layer moduli using 3-layer system with various depths to stiff layer, US-10 EB test section 1 test site 2

| Depth to stiff layer (in.) | Number of stations converged | Average value (ksi) and coefficient of variation (CV) of the backcalculated layer moduli | | | | | | | | Average RMS (%) |
|---|---|---|---|---|---|---|---|---|---|---|
| | | AC | CV | RCS | CV | | | BSRB | CV | |
| 100 | 36 | 227 | 0.27 | 419 | 0.45 | | | 7 | 0.04 | 8.53 |
| 200 | 40 | 326 | 0.14 | 127 | 0.26 | | | 12 | 0.05 | 4.06 |
| 300 | 40 | 380 | 0.17 | 91 | 0.29 | | | 14 | 0.05 | 2.23 |
| 400 | 40 | 422 | 0.19 | 75 | 0.32 | | | 15 | 0.05 | 1.48 |
| 500 | 40 | 454 | 0.21 | 67 | 0.33 | | | 16 | 0.04 | 1.16 |
| 600 | 40 | 478 | 0.21 | 62 | 0.35 | | | 16 | 0.04 | 1.02 |
| 700 | 40 | 494 | 0.22 | 58 | 0.36 | | | 17 | 0.04 | 0.95 |
| 800 | 40 | 602 | 0.23 | 41 | 0.42 | | | 19 | 0.04 | 1.16 |

RCS = rubblized concrete slab, BS = he combination of base and subbase, RB=roadbed soil, BSRB = the combination of base, subbase and roadbed soil, RMS = root mean square.

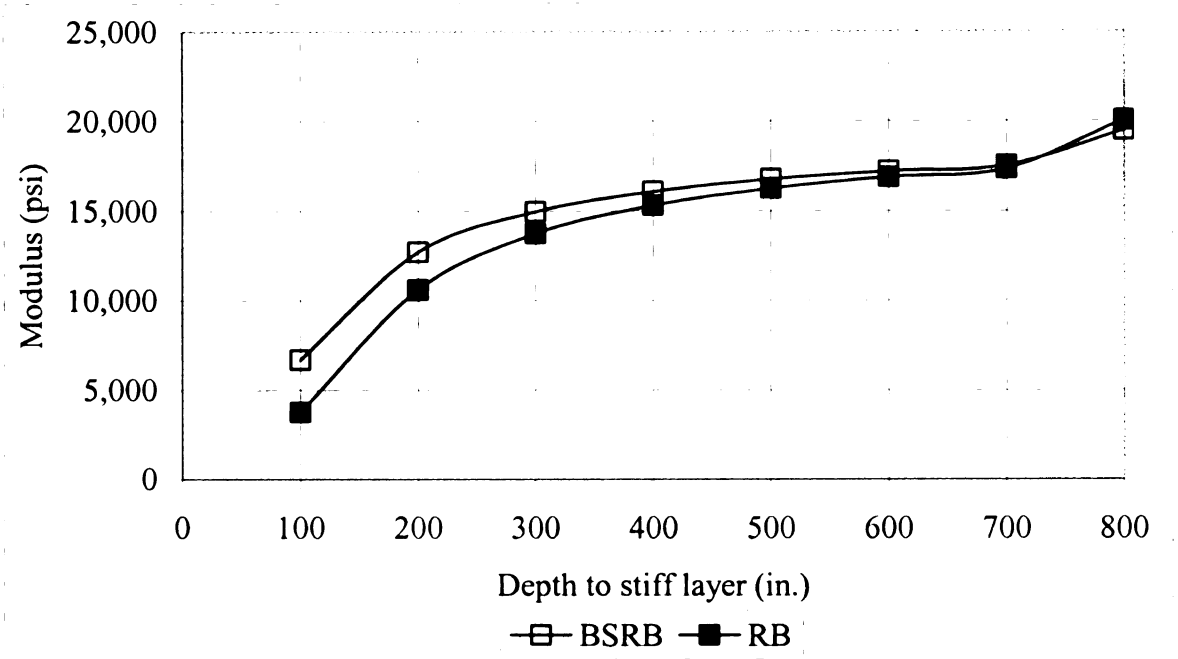


a) Test site 1

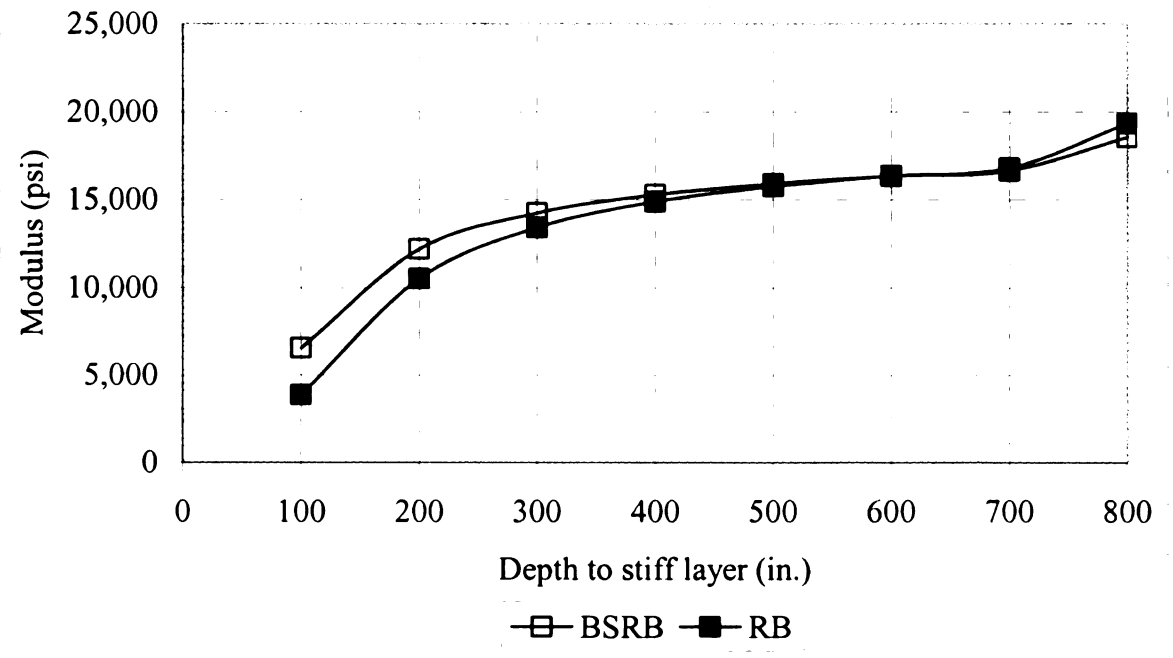


b) Test site 2

Figure 6.21 The average backcalculated moduli of the combination of base, subbase and roadbed soil (BSRB) and of the roadbed soil (RB) of test sites 1 and 2 at various depths to stiff layer

values of the 3- and the 4-layer systems. When a second 4-layer system is used in the backcalculation (AC RM, FC and BSRB), the moduli of the AC layer at the various test locations were more or less similar to those reported in Tables 6.18 and 6.20.

## 8.3 Final Selection of Layered Systems

Recall that field investigation revealed that the thickness of the RM layer varies from one point to another. Further, no backcalculation program was found that can produce accurate moduli of 5-layer system. Therefore, in this study, the moduli of the RM and FC layers were backcalculated using the 3- and 4-layer systems shown in Figures 6.13. The three layered systems consist of:

- 3-layer, AC, 9-in thick RCS, and BSRB.
- 4-layer, AC,9-in thick RCS, BS and RB
- 4-layer, AC, variable thickness RM and FC layers and BSRB.

In the backcalculation of the latter 4-layer system, the thickness of the RM layer was changed from 3 to 4 to 5 and to 7-in. Tables 6.22 and 6.23 summarize the backcalculated layer moduli of the three layered systems. Having obtained the results for the three layered systems, two questions arise:

1. For each FWD test location which layered system should be selected?
2. What is the most plausible RM layer thickness?

The answers to these questions can be obtained by a careful examination of the results listed in Tables 6.22 and 6.23. After such examination, the final results for each FWD test location were obtained and are listed in Tables 6.24 and 6.25. These are illustrated below using examples of four test stations on US-10 test site1.

Table 6.22 Results of backcalculation using 3- and 4-layer systems and depth to stiff layer of 500 in, US-10 EB test section1, test site 1

| FWD test number | 4-layer (AC, RCS, BS and RB) | | | | | | 3-layer (AC, RCS and BSRB) | | | | |
|---|---|---|---|---|---|---|---|---|---|---|---|
| | Modulus (ksi) | | | | RMS (%) | Conv | Modulus (ksi) | | | RMS (%) | Conv |
| | AC | RCS | BS | RB | | | AC | RCS | BSRB | | |
| 1 | 863 | 47 | 28 | 15 | 0.49 | Y | 634 | 100 | 16 | 1.38 | Y |
| 2 | 736 | 59 | 21 | 16 | 0.51 | Y | 621 | 87 | 16 | 0.88 | Y |
| 3 | 736 | 74 | 20 | 16 | 0.47 | Y | 628 | 101 | 16 | 0.76 | Y |
| 4 | 818 | 57 | 30 | 16 | 0.64 | Y | 593 | 118 | 17 | 1.58 | Y |
| 5 | 787 | 72 | 13 | 16 | 0.27 | Y | 842 | 62 | 15 | 0.35 | Y |
| 6 | 1,016 | 24 | 33 | 15 | 0.29 | Y | 732 | 70 | 16 | 1.17 | Y |
| 7 | 694 | 102 | 18 | 15 | 0.22 | Y | 624 | 124 | 16 | 0.46 | Y |
| 8 | 667 | 51 | 22 | 15 | 0.34 | Y | 534 | 83 | 16 | 1.02 | Y |
| 9 | 623 | 99 | 16 | 15 | 0.70 | Y | 590 | 110 | 15 | 0.74 | Y |
| 10 | 515 | 64 | 18 | 15 | 0.52 | Y | 450 | 84 | 15 | 0.83 | Y |
| 11 | 801 | 50 | 33 | 16 | 0.53 | Y | 558 | 119 | 17 | 1.87 | Y |
| 12 | 853 | 35 | 42 | 16 | 0.77 | Y | 570 | 105 | 18 | 2.25 | Y |
| 13 | 680 | 74 | 28 | 16 | 0.56 | Y | 501 | 139 | 16 | 1.63 | Y |
| 14 | 531 | 72 | 17 | 15 | 0.72 | Y | 486 | 85 | 15 | 0.83 | Y |
| 15 | 891 | 45 | 34 | 16 | 0.36 | Y | 619 | 111 | 17 | 1.64 | Y |
| 16 | 796 | 65 | 26 | 17 | 0.43 | Y | 624 | 111 | 18 | 1.14 | Y |
| 17 | 644 | 83 | 29 | 16 | 0.39 | Y | 481 | 152 | 17 | 1.61 | Y |
| 18 | 613 | 58 | 22 | 15 | 0.52 | Y | 499 | 90 | 16 | 1.10 | Y |
| 19 | 982 | 36 | 35 | 17 | 0.19 | Y | 682 | 97 | 17 | 1.46 | Y |
| 20 | 713 | 88 | 22 | 17 | 0.45 | Y | 614 | 118 | 18 | 0.80 | Y |
| 21 | 523 | 127 | 26 | 16 | 0.97 | Y | 432 | 193 | 17 | 1.58 | Y |
| 22 | 628 | 68 | 21 | 16 | 0.68 | Y | 526 | 98 | 16 | 1.09 | Y |
| 23 | 746 | 57 | 26 | 17 | 0.39 | Y | 583 | 98 | 18 | 1.16 | Y |
| 24 | 762 | 89 | 20 | 18 | 0.63 | Y | 701 | 105 | 18 | 0.71 | Y |
| 25 | 644 | 97 | 30 | 16 | 0.35 | Y | 479 | 178 | 17 | 1.61 | Y |
| 26 | 691 | 59 | 24 | 16 | 0.49 | Y | 539 | 101 | 16 | 1.24 | Y |
| 27 | 848 | 38 | 29 | 18 | 0.35 | Y | 654 | 76 | 18 | 1.18 | Y |
| 28 | 721 | 72 | 22 | 18 | 0.64 | Y | 630 | 96 | 18 | 0.88 | Y |
| 29 | 672 | 82 | 30 | 16 | 0.51 | Y | 496 | 156 | 17 | 1.73 | Y |
| 30 | 702 | 53 | 25 | 15 | 0.36 | Y | 535 | 96 | 16 | 1.26 | Y |
| 31 | 768 | 33 | 31 | 18 | 0.40 | Y | 573 | 72 | 18 | 1.40 | Y |
| 32 | 689 | 49 | 23 | 17 | 0.51 | Y | 576 | 74 | 18 | 0.96 | Y |
| 33 | 792 | 30 | 39 | 17 | 0.33 | Y | 540 | 85 | 18 | 1.88 | Y |
| 34 | 612 | 63 | 23 | 18 | 0.41 | Y | 520 | 89 | 19 | 0.90 | Y |
| 35 | 563 | 45 | 27 | 17 | 0.15 | Y | 431 | 82 | 17 | 1.45 | Y |
| 36 | 752 | 29 | 31 | 17 | 0.29 | Y | 564 | 64 | 18 | 1.34 | Y |
| 37 | 722 | 41 | 45 | 16 | 0.15 | Y | 449 | 128 | 18 | 2.67 | Y |
| 38 | 525 | 52 | 26 | 16 | 0.31 | Y | 405 | 91 | 17 | 1.51 | Y |
| 39 | 541 | 72 | 20 | 15 | 0.44 | Y | 458 | 100 | 15 | 0.92 | Y |
| 40 | 633 | 49 | 23 | 15 | 0.29 | Y | 492 | 85 | 16 | 1.17 | Y |

RCS = rubblized concrete slab, BS = combination of base and subbase, RB = roadbed soil, BSRB = combination of base, subbase and roadbed soil, RMS = root mean square error, Conv = Converged

Table 6.22 Results of backcalculation using 3- and 4-layer systems and depth to stiff layer of 500 in, US-10 EB test section1, test site 1 (continued)

| FWD test number | 4-layer (AC, 3-in. RM, 6-in. FC and BSRB) | | | | | | 4-layer (AC, 4-in. RM, 5-in. FC and BSRB) | | | | | |
|---|---|---|---|---|---|---|---|---|---|---|---|---|
| | Modulus (ksi) | | | | RMS (%) | Conv | Modulus (ksi) | | | | RMS (%) | Conv |
| | AC | RM | FC | BSRB | | | AC | RM | FC | BSRB | | |
| 1 | 974 | 8 | 2385 | 16 | 0.38 | Y | 958 | 12 | 3313 | 16 | 0.37 | N |
| 2 | 773 | 29 | 159 | 16 | 0.46 | Y | 770 | 36 | 168 | 16 | 0.47 | Y |
| 3 | 776 | 40 | 150 | 16 | 0.41 | Y | 773 | 47 | 158 | 16 | 0.41 | Y |
| 4 | 929 | 11 | 2121 | 16 | 0.52 | Y | 932 | 14 | 3280 | 16 | 0.52 | Y |
| 5 | 784 | 92 | 57 | 15 | 0.33 | Y | 785 | 85 | 54 | 15 | 0.32 | Y |
| 6 | 1122 | 4 | 4317 | 16 | 0.35 | N | 1129 | 5 | 7645 | 16 | 0.34 | N |
| 7 | 730 | 68 | 149 | 15 | 0.20 | Y | 726 | 76 | 155 | 15 | 0.20 | Y |
| 8 | 702 | 22 | 204 | 15 | 0.28 | Y | 698 | 28 | 207 | 16 | 0.28 | Y |
| 9 | 658 | 70 | 126 | 14 | 0.66 | Y | 649 | 79 | 128 | 14 | 0.66 | Y |
| 10 | 547 | 36 | 124 | 15 | 0.46 | Y | 544 | 42 | 131 | 15 | 0.46 | Y |
| 11 | 908 | 9 | 2850 | 16 | 0.37 | Y | 904 | 12 | 4459 | 16 | 0.37 | Y |
| 12 | 923 | 7 | 3788 | 17 | 0.56 | Y | 921 | 10 | 6176 | 17 | 0.56 | Y |
| 13 | 807 | 14 | 1853 | 16 | 0.41 | N | 717 | 40 | 389 | 16 | 0.48 | Y |
| 14 | 559 | 46 | 108 | 15 | 0.66 | Y | 557 | 52 | 113 | 15 | 0.67 | Y |
| 15 | 997 | 8 | 3059 | 17 | 0.23 | Y | 998 | 11 | 4984 | 17 | 0.24 | Y |
| 16 | 836 | 29 | 262 | 17 | 0.36 | Y | 831 | 37 | 267 | 17 | 0.36 | Y |
| 17 | 694 | 34 | 400 | 16 | 0.29 | Y | 686 | 45 | 390 | 16 | 0.29 | Y |
| 18 | 647 | 27 | 185 | 15 | 0.44 | Y | 643 | 34 | 192 | 15 | 0.44 | Y |
| 19 | 1086 | 6 | 3647 | 17 | 0.29 | Y | 1083 | 9 | 5911 | 17 | 0.26 | N |
| 20 | 852 | 23 | 597 | 16 | 0.96 | N | 754 | 57 | 182 | 17 | 0.38 | Y |
| 21 | 568 | 63 | 311 | 16 | 0.85 | Y | 563 | 77 | 323 | 16 | 0.85 | Y |
| 22 | 663 | 34 | 169 | 16 | 0.60 | Y | 660 | 41 | 178 | 16 | 0.60 | Y |
| 23 | 792 | 23 | 303 | 18 | 0.36 | Y | 785 | 30 | 287 | 18 | 0.37 | Y |
| 24 | 804 | 57 | 132 | 18 | 0.57 | Y | 795 | 65 | 136 | 18 | 0.58 | Y |
| 25 | 705 | 40 | 428 | 17 | 0.35 | Y | 698 | 52 | 425 | 17 | 0.35 | Y |
| 26 | 730 | 25 | 263 | 16 | 0.43 | Y | 725 | 32 | 261 | 16 | 0.44 | Y |
| 27 | 939 | 7 | 2452 | 18 | 0.18 | Y | 940 | 9 | 3992 | 18 | 0.18 | Y |
| 28 | 760 | 39 | 148 | 18 | 0.57 | Y | 756 | 46 | 156 | 18 | 0.57 | Y |
| 29 | 726 | 31 | 493 | 17 | 0.43 | Y | 713 | 44 | 446 | 17 | 0.44 | Y |
| 30 | 791 | 12 | 1174 | 15 | 0.32 | Y | 736 | 28 | 307 | 15 | 0.33 | Y |
| 31 | 854 | 6 | 2882 | 18 | 0.44 | Y | 860 | 8 | 4899 | 18 | 0.43 | N |
| 32 | 720 | 22 | 170 | 17 | 0.44 | Y | 716 | 28 | 177 | 17 | 0.44 | Y |
| 33 | 875 | 6 | 3841 | 18 | 0.33 | Y | 870 | 8 | 6198 | 18 | 0.32 | Y |
| 34 | 649 | 31 | 161 | 18 | 0.33 | Y | 646 | 38 | 170 | 18 | 0.33 | Y |
| 35 | 620 | 11 | 1077 | 17 | 0.14 | N | 597 | 22 | 458 | 17 | 0.10 | Y |
| 36 | 834 | 5 | 3027 | 18 | 0.35 | Y | 827 | 7 | 4769 | 18 | 0.35 | Y |
| 37 | 826 | 8 | 4384 | 17 | 0.26 | Y | 827 | 10 | 7264 | 17 | 0.25 | Y |
| 38 | 596 | 13 | 956 | 16 | 0.18 | Y | 609 | 16 | 1656 | 16 | 0.23 | Y |
| 39 | 577 | 38 | 157 | 15 | 0.35 | Y | 574 | 46 | 165 | 15 | 0.36 | Y |
| 40 | 672 | 19 | 277 | 15 | 0.24 | Y | 665 | 26 | 256 | 15 | 0.24 | Y |

RM = rubblized material, FC = fractured concrete, BSRB = combination of base, subbase and roadbed soil, RMS = root mean square error, Conv = Converged

Table 6.22 Results of backcalculation using 3- and 4-layer systems and depth to stiff layer of 500 in, US-10 EB test section1, test site 1 (continued)

| FWD test number | 4-layer (AC, 5-in. RM, 4-in. FC and BSRB) | | | | | | 4-layer (AC, 7-in. RM, 2-in. FC and BSRB) | | | | | |
|---|---|---|---|---|---|---|---|---|---|---|---|---|
| | Modulus (ksi) | | | | RMS (%) | Conv | Modulus (ksi) | | | | RMS (%) | Conv |
| | AC | RM | FC | BSRB | | | AC | RM | FC | BSRB | | |
| 1 | 1003 | 12 | 7408 | 16 | 0.38 | N | 872 | 39 | 651 | 16 | 0.47 | Y |
| 2 | 766 | 41 | 183 | 16 | 0.47 | Y | 760 | 47 | 273 | 16 | 0.47 | Y |
| 3 | 769 | 53 | 171 | 16 | 0.42 | Y | 763 | 60 | 246 | 16 | 0.42 | Y |
| 4 | 841 | 36 | 476 | 16 | 0.60 | Y | 832 | 46 | 678 | 16 | 0.61 | Y |
| 5 | 786 | 82 | 51 | 15 | 0.32 | Y | 784 | 80 | 33 | 15 | 0.31 | Y |
| 6 | 1124 | 7 | 13829 | 16 | 0.32 | N | 1031 | 13 | 40000 | 15 | 0.29 | N |
| 7 | 722 | 81 | 164 | 15 | 0.20 | Y | 718 | 88 | 213 | 15 | 0.20 | Y |
| 8 | 694 | 33 | 223 | 16 | 0.28 | Y | 688 | 40 | 338 | 16 | 0.29 | Y |
| 9 | 655 | 80 | 137 | 14 | 0.66 | Y | 650 | 85 | 169 | 14 | 0.67 | Y |
| 10 | 541 | 47 | 142 | 15 | 0.46 | Y | 536 | 53 | 201 | 15 | 0.47 | Y |
| 11 | 889 | 16 | 7112 | 16 | 0.37 | N | 805 | 43 | 1021 | 16 | 0.51 | Y |
| 12 | 921 | 12 | 11344 | 17 | 0.56 | Y | 756 | 34 | 13550 | 16 | 0.71 | N |
| 13 | 711 | 48 | 406 | 16 | 0.49 | Y | 703 | 59 | 597 | 16 | 0.49 | Y |
| 14 | 555 | 56 | 121 | 15 | 0.67 | Y | 551 | 61 | 161 | 15 | 0.68 | Y |
| 15 | 980 | 14 | 8022 | 17 | 0.23 | N | 894 | 39 | 1101 | 17 | 0.35 | Y |
| 16 | 827 | 43 | 288 | 17 | 0.36 | Y | 819 | 52 | 433 | 17 | 0.36 | Y |
| 17 | 680 | 54 | 412 | 16 | 0.29 | Y | 671 | 66 | 605 | 16 | 0.30 | Y |
| 18 | 639 | 39 | 209 | 15 | 0.44 | Y | 633 | 47 | 314 | 16 | 0.45 | Y |
| 19 | 1083 | 11 | 10940 | 17 | 0.24 | N | 988 | 31 | 2168 | 17 | 0.18 | Y |
| 20 | 749 | 63 | 197 | 17 | 0.38 | Y | 743 | 71 | 280 | 17 | 0.39 | Y |
| 21 | 558 | 88 | 348 | 16 | 0.86 | Y | 551 | 101 | 493 | 16 | 0.87 | Y |
| 22 | 657 | 47 | 194 | 16 | 0.61 | Y | 651 | 54 | 285 | 16 | 0.61 | Y |
| 23 | 780 | 36 | 302 | 18 | 0.37 | Y | 772 | 45 | 452 | 18 | 0.38 | Y |
| 24 | 794 | 70 | 146 | 18 | 0.58 | Y | 793 | 74 | 196 | 18 | 0.58 | Y |
| 25 | 691 | 62 | 449 | 17 | 0.36 | Y | 681 | 75 | 654 | 17 | 0.36 | Y |
| 26 | 721 | 38 | 279 | 16 | 0.44 | Y | 713 | 47 | 419 | 16 | 0.45 | Y |
| 27 | 923 | 12 | 6261 | 18 | 0.18 | N | 856 | 31 | 691 | 18 | 0.32 | Y |
| 28 | 753 | 51 | 170 | 18 | 0.57 | Y | 748 | 58 | 247 | 18 | 0.58 | Y |
| 29 | 707 | 53 | 462 | 17 | 0.45 | Y | 697 | 65 | 674 | 17 | 0.45 | Y |
| 30 | 731 | 34 | 317 | 15 | 0.33 | Y | 723 | 42 | 471 | 15 | 0.34 | Y |
| 31 | 849 | 10 | 8412 | 18 | 0.44 | Y | 775 | 27 | 1216 | 18 | 0.39 | Y |
| 32 | 713 | 33 | 192 | 17 | 0.45 | Y | 706 | 39 | 294 | 17 | 0.45 | Y |
| 33 | 872 | 10 | 11717 | 18 | 0.35 | Y | 667 | 142 | 229 | 22 | 0.45 | N |
| 34 | 642 | 44 | 185 | 18 | 0.33 | Y | 635 | 51 | 276 | 18 | 0.34 | Y |
| 35 | 589 | 28 | 394 | 17 | 0.10 | Y | 580 | 36 | 555 | 17 | 0.11 | Y |
| 36 | 822 | 9 | 8549 | 18 | 0.32 | N | 756 | 24 | 1634 | 17 | 0.28 | Y |
| 37 | 816 | 13 | 12935 | 17 | 0.24 | Y | 681 | 36 | 12534 | 16 | 0.45 | N |
| 38 | 699 | 9 | 26751 | 16 | 0.31 | N | 544 | 41 | 487 | 17 | 0.25 | Y |
| 39 | 570 | 51 | 179 | 15 | 0.36 | Y | 565 | 58 | 258 | 15 | 0.37 | Y |
| 40 | 661 | 32 | 269 | 15 | 0.24 | Y | 654 | 39 | 404 | 15 | 0.25 | Y |

RM = rubblized material, FC = fractured concrete, BSRB = combination of base, subbase and roadbed soil, RMS = root mean square error, Conv = Converged

Table 6.23 Results of backcalculation using 3- and 4-layer systems and depth to stiff layer of 500 in, US-10 EB test section1, test site 2

| FWD test number | 4-layer (AC, RCS, BS and RB) | | | | | | 3-layer (AC, RCS and BSRB) | | | | |
|---|---|---|---|---|---|---|---|---|---|---|---|
| | Modulus (ksi) | | | | RMS (%) | Conv | Modulus (ksi) | | | RMS (%) | Conv |
| | AC | RCS | BS | RB | | | AC | RCS | BSRB | | |
| 1 | 532 | 50 | 10 | 15 | 0.23 | Y | 667 | 29 | 15 | 0.80 | Y |
| 2 | 784 | 33 | 17 | 15 | 0.45 | Y | 736 | 40 | 15 | 0.50 | Y |
| 3 | 552 | 90 | 15 | 17 | 0.20 | Y | 591 | 80 | 17 | 0.36 | Y |
| 4 | 529 | 63 | 18 | 16 | 0.58 | Y | 475 | 78 | 16 | 0.78 | Y |
| 5 | 571 | 89 | 13 | 17 | 0.57 | Y | 660 | 69 | 16 | 0.81 | Y |
| 6 | 638 | 56 | 16 | 16 | 0.45 | Y | 617 | 61 | 16 | 0.47 | Y |
| 7 | 404 | 78 | 10 | 15 | 0.54 | Y | 519 | 51 | 14 | 1.18 | Y |
| 8 | 563 | 45 | 19 | 15 | 0.63 | Y | 479 | 65 | 15 | 0.97 | Y |
| 9 | 493 | 67 | 22 | 16 | 0.41 | Y | 399 | 101 | 16 | 1.23 | Y |
| 10 | 602 | 14 | 43 | 15 | 0.73 | Y | 433 | 41 | 16 | 1.97 | Y |
| 11 | 517 | 45 | 13 | 15 | 0.37 | Y | 567 | 37 | 15 | 0.52 | Y |
| 12 | 561 | 57 | 20 | 16 | 0.71 | Y | 479 | 78 | 16 | 1.05 | Y |
| 13 | 471 | 57 | 14 | 15 | 0.60 | Y | 483 | 54 | 15 | 0.62 | Y |
| 14 | 562 | 20 | 38 | 15 | 0.91 | Y | 387 | 57 | 16 | 2.45 | Y |
| 15 | 523 | 38 | 15 | 15 | 0.50 | Y | 510 | 41 | 15 | 0.51 | Y |
| 16 | 512 | 60 | 27 | 16 | 0.72 | Y | 388 | 108 | 17 | 1.91 | Y |
| 17 | 415 | 57 | 16 | 15 | 0.51 | Y | 389 | 65 | 15 | 0.60 | Y |
| 18 | 508 | 39 | 31 | 15 | 1.02 | Y | 361 | 88 | 16 | 2.55 | Y |
| 19 | 443 | 42 | 15 | 16 | 0.55 | Y | 451 | 41 | 15 | 0.56 | Y |
| 20 | 525 | 59 | 26 | 16 | 1.14 | Y | 409 | 102 | 17 | 1.98 | Y |
| 21 | 525 | 41 | 21 | 15 | 0.43 | Y | 432 | 63 | 16 | 1.07 | Y |
| 22 | 449 | 54 | 27 | 16 | 1.24 | Y | 345 | 97 | 17 | 2.31 | Y |
| 23 | 423 | 41 | 15 | 16 | 0.57 | Y | 416 | 43 | 15 | 0.58 | Y |
| 24 | 477 | 59 | 27 | 16 | 0.85 | Y | 368 | 103 | 17 | 1.96 | Y |
| 25 | 449 | 51 | 20 | 16 | 0.19 | Y | 376 | 72 | 16 | 0.92 | Y |
| 26 | 529 | 43 | 27 | 16 | 1.00 | Y | 398 | 83 | 17 | 2.07 | Y |
| 27 | 582 | 22 | 19 | 16 | 0.33 | Y | 530 | 30 | 16 | 0.51 | Y |
| 28 | 431 | 79 | 20 | 17 | 0.71 | Y | 384 | 98 | 17 | 0.99 | Y |
| 29 | 458 | 49 | 20 | 16 | 0.22 | Y | 389 | 68 | 16 | 0.85 | Y |
| 30 | 581 | 42 | 25 | 16 | 0.27 | Y | 439 | 78 | 16 | 1.46 | Y |
| 31 | 587 | 16 | 26 | 15 | 0.60 | Y | 477 | 33 | 16 | 1.16 | Y |
| 32 | 504 | 44 | 17 | 16 | 0.17 | Y | 477 | 50 | 16 | 0.29 | Y |
| 33 | 442 | 55 | 22 | 17 | 0.39 | Y | 365 | 79 | 17 | 1.17 | Y |
| 34 | 466 | 40 | 24 | 16 | 0.23 | Y | 361 | 69 | 16 | 1.43 | Y |
| 35 | 569 | 34 | 28 | 16 | 0.35 | Y | 414 | 70 | 17 | 1.63 | Y |
| 36 | 455 | 39 | 17 | 17 | 0.24 | Y | 439 | 42 | 16 | 0.27 | Y |
| 37 | 491 | 38 | 24 | 15 | 0.23 | Y | 370 | 69 | 16 | 1.50 | Y |
| 38 | 484 | 53 | 20 | 15 | 0.55 | Y | 407 | 74 | 15 | 1.04 | Y |
| 39 | 540 | 45 | 30 | 16 | 0.33 | Y | 373 | 98 | 17 | 2.09 | Y |
| 40 | 507 | 49 | 23 | 16 | 0.32 | Y | 400 | 79 | 16 | 1.33 | Y |

RCS = rubblized concrete slab, BS = combination of base and subbase, RB = roadbed soil, BSRB = combination of base, subbase and roadbed soil, RMS = root mean square error, Conv = Converged

Table 6.23 Results of backcalculation using 3- and 4-layer systems and depth to stiff layer of 500 in, US-10 EB test section1, test site 2 (continued)

| FWD test number | 4-layer (AC, 3-in. RM, 6-in. FC and BSRB) | | | | | | 4-layer (AC, 4-in. RM, 5-in. FC and BSRB) | | | | | |
|---|---|---|---|---|---|---|---|---|---|---|---|---|
| | Modulus (ksi) | | | | RMS (%) | Conv | Modulus (ksi) | | | | RMS (%) | Conv |
| | AC | RM | FC | BSRB | | | AC | RM | FC | BSRB | | |
| 1 | 444 | 185 | 18 | 15 | 0.40 | Y | 459 | 127 | 15 | 15 | 0.37 | Y |
| 2 | 810 | 18 | 64 | 15 | 0.43 | Y | 808 | 21 | 68 | 15 | 0.43 | Y |
| 3 | 538 | 117 | 73 | 17 | 0.28 | Y | 539 | 109 | 70 | 17 | 0.28 | Y |
| 4 | 561 | 37 | 110 | 16 | 0.51 | Y | 559 | 43 | 116 | 16 | 0.51 | Y |
| 5 | 556 | 141 | 57 | 16 | 0.72 | Y | 558 | 124 | 52 | 16 | 0.71 | Y |
| 6 | 661 | 42 | 70 | 16 | 0.43 | Y | 660 | 45 | 72 | 16 | 0.43 | Y |
| 7 | 356 | 216 | 35 | 15 | 0.87 | Y | 363 | 162 | 29 | 15 | 0.84 | Y |
| 8 | 591 | 22 | 124 | 15 | 0.55 | Y | 587 | 27 | 129 | 15 | 0.55 | Y |
| 9 | 530 | 32 | 198 | 16 | 0.29 | Y | 526 | 39 | 206 | 16 | 0.30 | Y |
| 10 | 634 | 3 | 3594 | 16 | 0.61 | Y | 636 | 5 | 6079 | 16 | 0.61 | Y |
| 11 | 490 | 81 | 30 | 15 | 0.42 | Y | 566 | 10 | 320 | 16 | 1.13 | N |
| 12 | 594 | 29 | 136 | 16 | 0.63 | Y | 592 | 35 | 144 | 16 | 0.63 | Y |
| 13 | 487 | 52 | 55 | 15 | 0.62 | Y | 486 | 53 | 55 | 15 | 0.62 | Y |
| 14 | 608 | 4 | 3289 | 16 | 0.73 | Y | 602 | 6 | 5239 | 16 | 0.70 | N |
| 15 | 544 | 27 | 49 | 15 | 0.47 | Y | 544 | 29 | 51 | 15 | 0.48 | Y |
| 16 | 637 | 11 | 1,860 | 16 | 0.42 | N | 543 | 31 | 378 | 16 | 0.62 | Y |
| 17 | 436 | 39 | 80 | 15 | 0.46 | Y | 434 | 44 | 83 | 15 | 0.46 | Y |
| 18 | 581 | 8 | 2364 | 16 | 0.71 | Y | 579 | 11 | 3732 | 16 | 0.72 | Y |
| 19 | 458 | 37 | 43 | 15 | 0.56 | Y | 456 | 39 | 42 | 15 | 0.56 | Y |
| 20 | 574 | 22 | 385 | 17 | 0.89 | N | 552 | 32 | 319 | 17 | 1.04 | Y |
| 21 | 749 | 3 | 7851 | 16 | 0.28 | N | 551 | 23 | 172 | 15 | 0.36 | Y |
| 22 | 563 | 10 | 1965 | 16 | 0.86 | N | 480 | 27 | 455 | 16 | 1.12 | Y |
| 23 | 438 | 32 | 48 | 15 | 0.55 | Y | 437 | 34 | 49 | 15 | 0.56 | Y |
| 24 | 607 | 10 | 1821 | 16 | 0.55 | N | 506 | 31 | 348 | 16 | 0.74 | Y |
| 25 | 483 | 25 | 137 | 16 | 0.26 | Y | 479 | 30 | 143 | 16 | 0.26 | Y |
| 26 | 613 | 8 | 1926 | 16 | 0.69 | Y | 614 | 11 | 3086 | 16 | 0.72 | Y |
| 27 | 635 | 5 | 1103 | 16 | 0.19 | Y | 635 | 6 | 1766 | 16 | 0.19 | N |
| 28 | 463 | 46 | 138 | 17 | 0.60 | Y | 460 | 53 | 145 | 17 | 0.60 | Y |
| 29 | 489 | 24 | 126 | 16 | 0.26 | Y | 486 | 30 | 132 | 16 | 0.26 | Y |
| 30 | 666 | 8 | 1633 | 16 | 0.17 | Y | 651 | 12 | 1997 | 16 | 0.16 | Y |
| 31 | 637 | 3 | 2558 | 16 | 0.55 | Y | 635 | 4 | 4195 | 16 | 0.54 | Y |
| 32 | 522 | 30 | 62 | 16 | 0.14 | Y | 520 | 34 | 65 | 16 | 0.14 | Y |
| 33 | 476 | 25 | 173 | 17 | 0.35 | Y | 472 | 32 | 178 | 17 | 0.35 | Y |
| 34 | 478 | 19 | 246 | 16 | 0.27 | N | 498 | 20 | 343 | 16 | 0.24 | Y |
| 35 | 665 | 6 | 2498 | 17 | 0.64 | Y | 662 | 8 | 3940 | 17 | 0.63 | Y |
| 36 | 456 | 34 | 46 | 16 | 0.26 | Y | 456 | 35 | 47 | 16 | 0.26 | Y |
| 37 | 555 | 6 | 293 | 16 | 0.45 | N | 446 | 100 | 24 | 16 | 0.29 | N |
| 38 | 516 | 26 | 139 | 15 | 0.49 | Y | 671 | 15 | 425 | 13 | 2.79 | N |
| 39 | 644 | 8 | 2407 | 16 | 0.65 | Y | 628 | 12 | 3347 | 16 | 0.64 | Y |
| 40 | 598 | 10 | 1113 | 16 | 0.22 | N | 557 | 19 | 793 | 16 | 0.29 | N |

RM = rubblized material, FC = fractured concrete, BSRB = combination of base, subbase and roadbed soil, RMS = root mean square error, Conv = Converged

Tab

RM = rub
and roadh

Table 6.23 Results of backcalculation using 3- and 4-layer systems and depth to stiff layer of 500 in, US-10 EB test section1, test site 2 (continued)

| FWD test number | 4-layer (AC, 5-in. RM, 4-in. FC and BSRB) | | | | | | 4-layer (AC, 7-in. RM, 2-in. FC and BSRB) | | | | | |
|---|---|---|---|---|---|---|---|---|---|---|---|---|
| | Modulus (ksi) | | | | RMS (%) | Conv | Modulus (ksi) | | | | RMS (%) | Conv |
| | AC | RM | FC | BSRB | | | AC | RM | FC | BSRB | | |
| 1 | 473 | 98 | 11 | 15 | 0.33 | Y | 499 | 69 | 5 | 15 | 0.28 | Y |
| 2 | 806 | 24 | 75 | 15 | 0.43 | Y | 801 | 27 | 111 | 15 | 0.44 | Y |
| 3 | 541 | 104 | 66 | 17 | 0.27 | Y | 542 | 100 | 46 | 17 | 0.26 | Y |
| 4 | 556 | 47 | 125 | 16 | 0.51 | Y | 551 | 52 | 175 | 16 | 0.52 | Y |
| 5 | 559 | 115 | 45 | 16 | 0.70 | Y | 553 | 110 | 17 | 16 | 0.67 | Y |
| 6 | 658 | 47 | 75 | 16 | 0.43 | Y | 655 | 50 | 93 | 16 | 0.43 | Y |
| 7 | 367 | 138 | 21 | 15 | 0.81 | Y | 378 | 106 | 6 | 15 | 0.70 | Y |
| 8 | 586 | 31 | 143 | 15 | 0.56 | Y | 580 | 37 | 215 | 15 | 0.56 | Y |
| 9 | 522 | 45 | 223 | 16 | 0.30 | Y | 515 | 53 | 330 | 16 | 0.31 | Y |
| 10 | 630 | 6 | 11,165 | 16 | 0.59 | N | 624 | 9 | 40,000 | 16 | 0.85 | N |
| 11 | 495 | 63 | 23 | 15 | 0.41 | Y | 500 | 55 | 12 | 15 | 0.39 | Y |
| 12 | 586 | 40 | 156 | 16 | 0.63 | Y | 582 | 46 | 233 | 16 | 0.64 | Y |
| 13 | 483 | 54 | 54 | 15 | 0.62 | Y | 482 | 55 | 53 | 15 | 0.62 | Y |
| 14 | 595 | 8 | 9,127 | 16 | 0.70 | N | 715 | 2 | 40,000 | 18 | 0.90 | N |
| 15 | 541 | 31 | 54 | 15 | 0.48 | Y | 538 | 33 | 69 | 15 | 0.48 | Y |
| 16 | 536 | 38 | 380 | 16 | 0.62 | Y | 528 | 48 | 553 | 16 | 0.63 | Y |
| 17 | 432 | 47 | 88 | 15 | 0.47 | Y | 429 | 50 | 114 | 15 | 0.47 | Y |
| 18 | 581 | 13 | 6,971 | 16 | 0.74 | Y | 506 | 34 | 1,096 | 16 | 0.99 | Y |
| 19 | 454 | 40 | 42 | 15 | 0.56 | Y | 452 | 41 | 42 | 15 | 0.56 | Y |
| 20 | 547 | 39 | 331 | 17 | 1.05 | Y | 540 | 48 | 493 | 17 | 1.06 | Y |
| 21 | 547 | 27 | 185 | 15 | 0.36 | Y | 541 | 33 | 283 | 15 | 0.37 | Y |
| 22 | 469 | 35 | 396 | 16 | 1.13 | Y | 459 | 45 | 558 | 16 | 1.13 | Y |
| 23 | 435 | 36 | 51 | 15 | 0.56 | Y | 433 | 38 | 60 | 15 | 0.56 | Y |
| 24 | 500 | 38 | 353 | 16 | 0.75 | Y | 492 | 47 | 516 | 16 | 0.75 | Y |
| 25 | 476 | 35 | 156 | 16 | 0.25 | Y | 470 | 41 | 234 | 16 | 0.24 | Y |
| 26 | 545 | 27 | 491 | 16 | 0.93 | Y | 533 | 36 | 618 | 16 | 0.94 | Y |
| 27 | 598 | 14 | 110 | 16 | 0.29 | Y | 592 | 18 | 180 | 16 | 0.30 | Y |
| 28 | 456 | 59 | 155 | 17 | 0.61 | Y | 451 | 65 | 215 | 17 | 0.61 | Y |
| 29 | 482 | 34 | 144 | 16 | 0.26 | Y | 477 | 40 | 216 | 16 | 0.26 | Y |
| 30 | 605 | 26 | 388 | 16 | 0.22 | Y | 597 | 34 | 539 | 16 | 0.23 | Y |
| 31 | 629 | 6 | 7,263 | 16 | 0.56 | Y | 609 | 8 | 40,000 | 16 | 0.56 | N |
| 32 | 518 | 36 | 69 | 16 | 0.14 | Y | 516 | 39 | 91 | 16 | 0.15 | Y |
| 33 | 468 | 37 | 193 | 17 | 0.35 | Y | 462 | 44 | 291 | 17 | 0.36 | Y |
| 34 | 492 | 25 | 318 | 16 | 0.25 | Y | 484 | 32 | 454 | 16 | 0.25 | Y |
| 35 | 547 | 45 | 69 | 16 | 0.49 | N | 589 | 27 | 1,162 | 16 | 0.37 | Y |
| 36 | 455 | 36 | 48 | 16 | 0.25 | Y | 454 | 37 | 57 | 16 | 0.25 | Y |
| 37 | 519 | 22 | 436 | 16 | 0.28 | Y | 510 | 30 | 559 | 16 | 0.28 | Y |
| 38 | 509 | 36 | 158 | 15 | 0.50 | Y | 503 | 42 | 236 | 15 | 0.50 | Y |
| 39 | 596 | 15 | 1,222 | 16 | 0.38 | N | 561 | 36 | 1,112 | 16 | 0.36 | Y |
| 40 | 644 | 12 | 5,918 | 16 | 0.52 | N | 526 | 39 | 385 | 16 | 0.26 | Y |

RM = rubblized material, FC = fractured concrete, BSRB = combination of base, subbase and roadbed soil, RMS = root mean square error, Conv = Converged

Table 6.24 Final results of the backcalculation of US-10 EB test section 1, test site 1

| FWD test number | Mid-depth temperature (°F) | Modulus (ksi) | | | | | | | RM thickness (in.) |
|---|---|---|---|---|---|---|---|---|---|
| | | AC | TCAC | RM | FC | BS | RB | RCS | |
| 1 | 92.0 | 634 | 1522 | 100 | - | 16 | 16 | 100 | 9 |
| 2 | 91.9 | 760 | 1822 | 47 | 273 | 16 | 16 | 87 | 7 |
| 3 | 91.9 | 763 | 1826 | 60 | 246 | 16 | 16 | 101 | 7 |
| 4 | 91.8 | 841 | 2009 | 36 | 476 | 16 | 16 | 118 | 5 |
| 5 | 91.8 | 842 | 2007 | 62 | - | 15 | 15 | 62 | 9 |
| 6 | 91.7 | 732 | 1742 | 70 | - | 16 | 16 | 70 | 9 |
| 7 | 91.7 | 718 | 1706 | 88 | 213 | 15 | 15 | 124 | 7 |
| 8 | 91.6 | 688 | 1629 | 40 | 338 | 16 | 16 | 83 | 7 |
| 9 | 91.5 | 650 | 1538 | 85 | 169 | 14 | 14 | 110 | 7 |
| 10 | 91.9 | 536 | 1284 | 53 | 201 | 15 | 15 | 84 | 7 |
| 11 | 92.4 | 558 | 1362 | | 119 | 17 | 17 | 119 | 0 |
| 12 | 92.7 | None of the backcalculation results was accepted | | | | | | | |
| 13 | 93.5 | 717 | 1823 | 40 | 389 | 16 | 16 | 139 | 4 |
| 14 | 94.6 | 551 | 1461 | 61 | 161 | 15 | 15 | 85 | 7 |
| 15 | 95.3 | 619 | 1681 | - | 111 | 17 | 17 | 111 | 0 |
| 16 | 95.7 | 831 | 2287 | 37 | 267 | 17 | 17 | 111 | 4 |
| 17 | 96.6 | 694 | 1976 | 34 | 400 | 16 | 16 | 152 | 3 |
| 18 | 97.4 | 633 | 1851 | 47 | 314 | 16 | 16 | 90 | 7 |
| 19 | 97.3 | 682 | 1989 | 97 | - | 17 | 17 | 97 | 9 |
| 20 | 97.4 | 743 | 2178 | 71 | 280 | 17 | 17 | 118 | 7 |
| 21 | 98.2 | 558 | 1684 | 88 | 348 | 16 | 16 | 193 | 5 |
| 22 | 98.7 | 651 | 2001 | 54 | 285 | 16 | 16 | 98 | 7 |
| 23 | 98.8 | 780 | 2409 | 36 | 302 | 18 | 18 | 98 | 5 |
| 24 | 99.6 | 793 | 2516 | 74 | 196 | 18 | 18 | 105 | 7 |
| 25 | 100.1 | 698 | 2259 | 52 | 425 | 17 | 17 | 178 | 4 |
| 26 | 100.5 | 713 | 2339 | 47 | 419 | 16 | 16 | 101 | 7 |
| 27 | 100.8 | 654 | 2171 | 76 | - | 18 | 18 | 76 | 9 |
| 28 | 101.1 | 748 | 2514 | 58 | 247 | 18 | 18 | 96 | 7 |
| 29 | 101.3 | 713 | 2411 | 44 | 446 | 17 | 17 | 156 | 4 |
| 30 | 101.5 | 731 | 2484 | 34 | 317 | 15 | 15 | 96 | 5 |
| 31 | 101.4 | 573 | 1942 | 72 | - | 18 | 18 | 72 | 9 |
| 32 | 101.2 | 706 | 2373 | 39 | 294 | 17 | 17 | 74 | 7 |
| 33 | 101.1 | 540 | 1812 | 85 | - | 18 | 18 | 85 | 9 |
| 34 | 101.1 | 635 | 2131 | 51 | 276 | 18 | 18 | 89 | 7 |
| 35 | 101.0 | 431 | 1441 | 82 | - | 17 | 17 | 82 | 9 |
| 36 | 101.0 | 564 | 1884 | 64 | - | 18 | 18 | 64 | 9 |
| 37 | 101.0 | None of the backcalculation results was accepted | | | | | | | |
| 38 | 100.9 | 544 | 1814 | 41 | 487 | 17 | 17 | 91 | 7 |
| 39 | 100.9 | 565 | 1883 | 58 | 258 | 15 | 15 | 100 | 7 |
| 40 | 100.8 | 661 | 2197 | 32 | 269 | 15 | 15 | 85 | 5 |
| Average | | 670 | 1946 | 59 | 294 | 17 | 16.5 | 103 | 6.4 |
| Coefficient of variation | | 0.14 | 0.17 | 0.33 | 0.34 | 0.07 | 0.07 | 0.28 | 0.36 |

TCAC = temperature corrected asphalt concrete, RM = rubblized material, FC=fractured concrete, BS = combination of base and subbase, RB = roadbed soil, RCS = rubblized concrete slab

Table 6.25 Final results of the backcalculation of US-10 EB test section 1, test site 2

| FWD test number | Mid-depth temperature (°F) | Modulus (ksi) | | | | | | | RM thickness (in.) |
|---|---|---|---|---|---|---|---|---|---|
| | | AC | TCAC | RM | FC | BS | RB | RCS | |
| 1 | 99.8 | None of the backcalculation results was accepted | | | | | | | |
| 2 | 99.7 | 736 | 2351 | 40 | - | 15 | 15 | 40 | 9 |
| 3 | 99.7 | 591 | 1883 | 80 | - | 17 | 17 | 80 | 9 |
| 4 | 99.7 | 551 | 1755 | 52 | 175 | 16 | 16 | 78 | 4 |
| 5 | 99.8 | 660 | 2113 | 69 | - | 16 | 16 | 69 | 9 |
| 6 | 100.0 | 617 | 1986 | 61 | - | 16 | 16 | 61 | 9 |
| 7 | 100.3 | None of the backcalculation results was accepted | | | | | | | |
| 8 | 100.7 | 580 | 1918 | 37 | 215 | 15 | 15 | 65 | 5 |
| 9 | 101.3 | 526 | 1777 | 39 | 206 | 16 | 16 | 101 | 4 |
| 10 | 101.8 | 433 | 1493 | 41 | - | 16 | 16 | 41 | 9 |
| 11 | 102.8 | 567 | 2023 | 37 | - | 15 | 15 | 37 | 9 |
| 12 | 103.7 | 582 | 2151 | 46 | 233 | 16 | 16 | 78 | 4 |
| 13 | 104.7 | 483 | 1848 | 54 | - | 15 | 15 | 54 | 9 |
| 14 | 105.5 | None of the backcalculation results was accepted | | | | | | | |
| 15 | 106.0 | 510 | 2047 | 41 | - | 15 | 15 | 41 | 9 |
| 16 | 106.2 | 543 | 2193 | 31 | 378 | 16 | 16 | 108 | 4 |
| 17 | 106.1 | 429 | 1731 | 50 | 114 | 15 | 15 | 65 | 7 |
| 18 | 106.1 | None of the backcalculation results was selected | | | | | | | |
| 19 | 106.1 | 451 | 1813 | 41 | - | 15 | 15 | 41 | 9 |
| 20 | 106.2 | 552 | 2235 | 32 | 319 | 17 | 17 | 102 | 4 |
| 21 | 106.4 | 541 | 2200 | 33 | 283 | 15 | 15 | 63 | 7 |
| 22 | 106.5 | 469 | 1919 | 35 | 396 | 16 | 16 | N/A | 5 |
| 23 | 106.7 | 416 | 1713 | 43 | - | 15 | 15 | 43 | 9 |
| 24 | 106.9 | 506 | 2098 | 31 | 348 | 16 | 16 | 103 | 4 |
| 25 | 106.8 | 470 | 1945 | 41 | 234 | 16 | 16 | 72 | 4 |
| 26 | 107.0 | 545 | 2270 | 27 | 491 | 16 | 16 | N/A | 5 |
| 27 | 107.4 | 530 | 2238 | 30 | - | 16 | 16 | 30 | 9 |
| 28 | 107.7 | 451 | 1931 | 65 | 215 | 17 | 17 | 98 | 4 |
| 29 | 108.1 | 477 | 2068 | 40 | 216 | 16 | 16 | 68 | 5 |
| 30 | 108.5 | 439 | 1932 | 78 | - | 16 | 16 | 78 | 9 |
| 31 | 108.6 | 477 | 2111 | 33 | - | 16 | 16 | 33 | 9 |
| 32 | 108.6 | 477 | 2108 | 50 | - | 16 | 16 | 50 | 9 |
| 33 | 108.6 | 462 | 2038 | 44 | 291 | 17 | 17 | 79 | 4 |
| 34 | 108.6 | 484 | 2136 | 32 | 454 | 16 | 16 | 69 | 7 |
| 35 | 108.6 | 414 | 1824 | 70 | - | 17 | 17 | 70 | 9 |
| 36 | 108.5 | 439 | 1934 | 42 | - | 16 | 16 | 42 | 9 |
| 37 | 108.5 | 370 | 1628 | 69 | - | 16 | 16 | 69 | 9 |
| 38 | 108.5 | 503 | 2211 | 42 | 236 | 15 | 15 | 74 | 5 |
| 39 | 108.4 | 561 | 2462 | 36 | 1112 | 16 | 16 | N/A | 7 |
| 40 | 108.4 | 526 | 2308 | 39 | 385 | 16 | 16 | 79 | 7 |
| Average | | 509 | 1998 | 46 | 288 | 16 | 16 | 66 | 7.5 |
| Coefficient of variation | | 0.15 | 0.10 | 0.31 | 0.35 | 0.04 | 0.04 | 0.33 | 0.23 |

TCAC = temperature corrected AC modulus, RM = rubblized material, FC = fractured concrete, BS = combination of base and subbase, RB = roadbed soil, RCS = rubblized concrete slab, N/A = Not available because the backcalculation results was rejected

Recall that the selection of the final layer moduli and RM thickness was based on few concepts and assumptions that were detailed in section 5.5 and summarized below for convenience.

1. It is assumed that the RM modulus is greater than or equal to 20 ksi but less than or equal to 100 ksi. It is further assumed that the modulus of the FC is greater than 100 ksi but equal to or less than 4,000 ksi.
2. Based on field observations and on the principle of the rubblizer energy dissipation with depth, the moduli and thicknesses of the RM and FC layers must be reasonable and compatible as illustrated schematically in Figure 6.14 and detailed in section 5.5.

The four FWD test stations on EB US 10, test section 1 and test site 1 used in the examples are stations 4, 5, 11 and 12.

**Station 4** – At this station, the RM thickness of 5 in. was selected as the most plausible value. The selection was accomplished using the following steps:

1. For all RM thicknesses, the modulus of the BSRB is similar to the modulus of the RB from the 4RB system and the backcalculated results pass the acceptance criteria.
2. Since the backcalculation results of 3 and 4-in. RM did not satisfy the acceptance criteria, only the backcalculation results from the 0, 5 and 7-in. thick RM were considered at this station.
3. The backcalculation results of the 7-in. thick RM were not selected because the FC modulus of 678 ksi was too high for the 2-in. thick FC layer. Whereas the RM

and FC moduli of 36 and 476 ksi were reasonable for 5-in. thick RM and 4-in. thick FC layers.

4. The full depth FC was not selected as the most plausible scenario because the backcalculated AC modulus of the 3-layer system was significantly different from the AC moduli of all other backcalculation results. This indicated high interaction between the AC and the RCS moduli. It should be noted that for most of the backcalculation results, full depth RM or FC was considered only when none of the backcalculation results of partial depth RM thickness (3, 4, 5 and 7 in) was reasonable. This agrees with the results of the field investigation that the RCS typically consists of RM and FC layers.

**Station 5**- At this station, full depth RM was elected as the most plausible RM thickness because none of the backcalculation results for partial depth RM was acceptable. Further, the RCS was determined as full depth RM since the RCS modulus was less than 100 ksi. Note that, the backcalculated AC modulus of the 3-layer system was similar to the AC moduli of the other backcalculation results. This indicated that, in the 3-layer system, there was no interaction between the AC and the RCS moduli.

**Station 11** - At this station, full depth FC (RM thickness = 0-in.) was selected. Said selection was made based on the following steps.

1. Since the backcalculation results for 3, 4 and 5-in. RM thickness did not satisfy the acceptance criteria. Only the backcalculation results of 0 and 7 in. thick RM were considered for this station.

2. The 7-in. RM thickness was not selected as the most plausible RM thickness because the FC modulus of 1,021 ksi modulus was too high for 2-in. FC layer.

3.

It sh

syst

Since

modu

Static

accept

were s

adjuste

provid

estima

modul

each te

are pres

9.0

one test

because

summary

3. Since the RCS modulus was greater than 100 ksi, the RCS was considered as full depth FC.

It should be noted that for this station, the backcalculated AC modulus of the 3-layer system is significantly different from the AC moduli of the other backcalculation results. Since said results were not acceptable (did not pass the acceptance criteria), the AC modulus from the 3-layer system should not be compared to that from the 4-layer system.

**Station 12 -** Since none of the backcalculation results of the 4BSRB system was accepted, no backcalculation results was selected for this test station.

Similarly, the backcalculation results at the other test stations of test site 1 and 2 were selected. After the selection was completed, the backcalculated AC moduli were adjusted to the standard temperature of 68°F using the temperature correction model provided in equation 6.2. The AC mid-depth temperature used in the equation was estimated using equation 6.3. Finally, the average and the coefficient of variation of the moduli of each layer and the average RM thickness of the accepted test station results of each test site were calculated and are listed in Table 6.24 and 6.25.

Results of the backcalculation of 24 rubblized and 12 flexible pavement test sites are presented in the next section.

## 9.0 BACKCALCUALTION RESULTS

The measured deflection data from 2 test sites on I-75 (10752-11, 10752-12) and one test site on M-37 and (30373-11) were excluded from the backcalculation analyses because of extensive cracks as sown in Figure 6.22. Table 6.26 and 6.27 provide a summary of the pavement cross section, type of roadbed soil, depth to stiff layer used in

Figure 6.

a) Transverse and longitudinal cracks on I-75, test section 1, test site 1

b) Transverse and longitudinal cracks on M-37, test section 1, test site 1

Figure 6.22 Extensive transverse and longitudinal cracks on the FWD test sites on I-75, and on M-37, test section 1, test site 1

*Table 6.26 A summary of pavement cross sections, roadbed soil, depths to stiff layer and the observed pavement surface distresses at 18 rubblized pavement test sites where, in the backcalculation of layer moduli, the base and subbase layers and the roadbed were combined*

Table 6.26 A summary of pavement cross sections, roadbed soil, depths to stiff layer and the observed pavement surface distresses at 18 rubblized pavement test sites where, in the backcalculation of layer moduli, the base and subbase layers and the roadbed were combined as one layer.

| No | Test site | Pavement cross section | | | | | | | Thicknesses used in the backcalculation (in.) | | | Roadbed soil | Depth to stiff layer (in.) | Pavement distresses at the test site |
|---|---|---|---|---|---|---|---|---|---|---|---|---|---|---|
| | | AC thickness (in.) | | JRCP slab thickness (in.) | Base | | Subbase | | | | | | | |
| | | Inventory data | Core | | Material type | Thickness (in.) | Material type | Thickness (in.) | AC | Slab | Base & subbase | | | |
| 1 | 10962-11 | 6 to 13 | NA | 9 | Agg. | 4 | Sand | 10 | 6.5 | 9 | 14 | Loamy sand | 500 | None |
| 2 | 10962-21 | 5.5 to 11 | 6.8 | 9 | Agg. | 4 | Sand | 10 | 6.8 | 9 | 14 | Loamy sand | 700 | Cracks |
| 3 | 10962-31 | 5.5 to 11 | 6.2 | 9 | Agg. | 4 | Sand | 10 | 6.2 | 9 | 14 | Loamy sand | 700 | Cracks |
| 4 | 10964-51 | 5.5 to 11 | 7.7 | 9 | Agg. | 4 | Sand | 10 | 7.7 | 9 | 14 | Loamy sand | 500 | Cracks |
| 5 | 11941-21 | 6.25 | 7.8 | 9 | Agg. | 4 | NA | 10 | 7.8 | 9 | 14 | Sand | None | Cracks |
| 6 | 11941-22 | 6.25 | 7.4 | 9 | Agg. | 4 | NA | 10 | 7.4 | 9 | 14 | Sand | None | Cracks |
| 7 | 20102-11 | 6 | 6.5 | 9-7-9 | NA | NA | NA | NA | 6.5 | 9 | 15 | Sand | 500 | None |
| 8 | 20102-12 | 6 | 6.4 | 9-7-9 | NA | NA | NA | NA | 6.4 | 9 | 15 | Sand | 500 | None |
| 9 | 20273-21 | 5.5 | 4.6 | 9 | Agg. | 3 | Sand | 11 | 4.6 | 9 | 14 | Loamy sand | 300 | Cracks |
| 10 | 20273-31 | 6.5 | 7.0 | 9 | NA | NA | NA | NA | 7.0 | 9 | 15 | Loamy sand | 225 | None |
| 11 | 20273-41 | 6.5 | 6.5 | 9 | NA | NA | NA | NA | 6.5 | 9 | 15 | Loamy and sandy soil | 300 | None |
| 12 | 20311-11 | 6.5 | 6.9 | 9 | NA | NA | NA | NA | 6.9 | 9 | 15 | Sandy soil | 500 | None |
| 13 | 21313-11 | 6.0 | NA | 9 | Agg. | 4 | Sand | 12 | 6.0 | 9 | 16 | Sandy soil | 165 | None |
| 14 | 21311-21 | 7.25 | NA | 9 | Agg. | 3 | NA | 10 | 7.3 | 9 | 13 | Sandy loam | 225 | None |
| 15 | 21311-31 | 6.0 | NA | 9 | Agg. | 3 | Sand | NA | 6.0 | 9 | 15 | Sandy loam | None | None |
| 16 | 30153-11 | 5.5 | 5.3 | 8 | None | 0 | Sand | 12 | 5.3 | 8 | 12 | Sandy loam | 500 | Cracks |
| 17 | 30373-51 | 6.5 | 6.6 | 9 | NA | NA | NA | NA | 6.6 | 9 | 15 | Loamy and sandy soil | 400 | None |
| 18 | 30373-52 | 6.5 | 6.4 | 9 | NA | NA | NA | NA | 6.4 | 9 | 15 | Loamy and sandy soil | 400 | None |

JRCP = Joint reinforced concrete pavement, X-Y-X = X-in. of concrete at the edges and Y-in. at the center of the lane, Agg. = Aggregate

*Table 6.22 A summary of pavement cross sections, roadbed soil, depths to stiff layer and the observed pavement surface distresses at*

Table 6.27 A summary of pavement cross sections, roadbed soil, depths to stiff layer and the observed pavement surface distresses at six rubblized pavement test sites where the combined base and subbase layers and the roadbed soil were backcalculated as two layers.

| No | Test site | Pavement cross section | | | | | | | Thicknesses used in the backcalculation (in.) | | | Roadbed soil | Depth to stiff layer (in.) | Pavement distresses at the test site |
|---|---|---|---|---|---|---|---|---|---|---|---|---|---|---|
| | | AC thickness (in.) | | Original JRCP slab thickness (in.) | Base | | Subbase | | | | | | | |
| | | Inventory data | Core | | Material type | Thickness (in.) | Material type | Thickness (in.) | AC | Slab | Base & subbase | | | |
| 1 | 10692-11 | 8.75 | 8.2 | 9 | Agg. | 4 | Sand | 12 | 8.2 | 9 | 16 | Loam | 150 | None |
| 2 | 10692-12 | 8.75 | 8.0 | 9 | Agg. | 4 | Sand | 12 | 8.0 | 9 | 16 | Loam | 150 | None |
| 3 | 20233-11 | 5 | 5.5 | 9 | None | 0 | Sand | 30 | 5.5 | 9 | 30 | Peat | 200 | None |
| 4 | 20233-12 | 5 | 5.5 | 9 | None | 0 | Sand | 30 | 5.5 | 9 | 30 | Peat | 200 | None |
| 5 | 30373-61 | 5.75 | 5.7 | 9 | Agg. | 12 | None | 0 | 5.7 | 9 | 12 | Loamy and sandy soil | 200 | Cracks |
| 6 | 30531-11<br>30531-11<br>30531-11 | 6.00 | N/A | 8<br>9-7-9<br>10-8-10 | None | 0 | Sand | NA | 6 | 9 | 15 | Loamy clay | 175 | Cracks |

JRCP = Jointed reinforced concrete pavement, X-Y-X = X-in. of concrete at the edges and Y-in. at the center of the lane, Agg. = Aggregate

the bac

Tables

24 test

include

1.

2.

the backcalculation of layer moduli of, and the observed distresses along, 24 test sites. Tables 6.28 and 6.29 provide the final results of the backcalculation layer moduli of the 24 test sites on rubblized pavements. For each test site, the results listed in the tables include:

- The number of FWD test stations where the RCS is full or partial depth RM or full depth FC.
- The average and the coefficient of variation of the backcalculated layer moduli, RCS moduli and the temperature correct AC moduli.
- The average thickness of the RM layer.

Examination of the data in Tables 6.26 through 6.29 indicates that:

1. The RB soil of the rubblized pavement test sites listed in Table 6.26 is sand, sandy soil, sandy loam or loamy sand. The base material is aggregate but only 3- or 4-in. thick, and the material of most subbase is sand with thicknesses from 9- to 14-in. Given such information and knowing that the above stated types of roadbed soil have moduli values close to that of compacted sand and aggregate, the backcalculation of layer moduli for the test sites listed in the table were performed by combining the BS and the RB into one BSRB layer.
2. Except for the test site 30373-61 (M-37 SB), the cross-sections of the rubblized pavement test sites listed in Table 6.27 show either thin aggregate base on top of thick sand subbase or just sand subbase. For test site 30373-61, the base is 12-in. thick with no sand subbase. For test site 30533-11 (M-53 SB), where the thickness of the subbase layer is not available, a 15-in. thick subbase was assumed. Said thickness is estimated based on MDOT practice and the 14.6-in.

*Table 6.28 A summary of the results of the backcalculation of layer moduli of 18 rubblized pavement test sites where the base,*

Table 6.28 A summary of the results of the backcalculation of layer moduli of 18 rubblized pavement test sites where the base, subbase layers and the roadbed soil were treated as one layer.

| No. | Test site | Number of FWD test stations determined as | | | Backcalculated moduli (ksi) | | | | | | | | | | | | | | RM thickness (in.) |
|---|---|---|---|---|---|---|---|---|---|---|---|---|---|---|---|---|---|---|---|
| | | Full depth RM | Partial depth RM | Full depth FC | AC | | TCAC | | RM | | FC | | BS | | RB | | RCS | | |
| | | | | | Avg | CV | Avg | CV | Avg | CV | Avg | CV | Avg | CV | Avg | CV | Avg | CV | |
| 1 | 10962-11 | 0 | 0 | 9 | 457 | 0.23 | 405 | 0.18 | - | - | 879 | 0.77 | 32 | 0.11 | 32 | 0.11 | 879 | 0.77 | 0.0 |
| 2 | 10962-21 | 0 | 0 | 21 | 651 | 0.17 | 662 | 0.17 | - | - | 487 | 0.26 | 29 | 0.02 | 29 | 0.02 | 487 | 0.26 | 0.0 |
| 3 | 10962-31 | 0 | 11 | 25 | 627 | 0.29 | 655 | 0.29 | 73 | 0.24 | 290 | 0.58 | 28 | 0.03 | 28 | 0.03 | 208 | 0.19 | 1.3 |
| 4 | 10964-51 | 1 | 6 | 24 | 1,630 | 0.19 | 692 | 0.17 | 66 | 0.32 | 222 | 0.49 | 27 | 0.05 | 27 | 0.05 | 171 | 0.22 | 1.1 |
| 5 | 11941-21 | 0 | 0 | 28 | 1,454 | 0.22 | 1,119 | 0.20 | - | - | 352 | 0.25 | 24 | 0.04 | 24 | 0.04 | 352 | 0.25 | 0.0 |
| 6 | 11941-22 | 1 | 5 | 18 | 1,482 | 0.24 | 1,546 | 0.20 | 77 | 0.19 | 358 | 0.55 | 21 | 0.05 | 21 | 0.05 | 271 | 0.32 | 1.2 |
| 7 | 20102-11 | 9 | 27 | 2 | 670 | 0.14 | 1,946 | 0.17 | 59 | 0.33 | 294 | 0.34 | 17 | 0.07 | 17 | 0.07 | 103 | 0.28 | 6.4 |
| 8 | 20102-12 | 17 | 18 | 0 | 509 | 0.15 | 1,998 | 0.10 | 46 | 0.31 | 288 | 0.35 | 16 | 0.04 | 16 | 0.04 | 66 | 0.33 | 7.5 |
| 9 | 20273-21 | 0 | 17 | 8 | 1,810 | 0.26 | 2,144 | 0.26 | 74 | 0.21 | 460 | 0.47 | 21 | 0.03 | 21 | 0.03 | 220 | 0.26 | 3.0 |
| 10 | 20273-31 | 16 | 20 | 0 | 460 | 0.16 | 951 | 0.15 | 56 | 0.29 | 208 | 0.43 | 13 | 0.05 | 13 | 0.05 | 73 | 0.30 | 7.8 |
| 11 | 20273-41 | 0 | 0 | 22 | 195 | 0.08 | 567 | 0.09 | - | - | 2,777 | 0.19 | 20 | 0.04 | 20 | 0.04 | 2,777 | 0.19 | 0.0 |
| 12 | 20311-11 | 0 | 1 | 25 | 517 | 0.23 | 1,428 | 0.25 | 35 | - | 826 | 0.91 | 21 | 0.10 | 21 | 0.10 | 707 | 0.64 | 0.1 |
| 13 | 21313-11 | 6 | 17 | 0 | 363 | 0.22 | 878 | 0.21 | 64 | 0.26 | 232 | 0.40 | 20 | 0.04 | 20 | 0.04 | 87 | 0.25 | 7.3 |
| 14 | 21311-21 | 0 | 3 | 18 | 1,169 | 0.23 | 612 | 0.25 | 78 | 0.15 | 264 | 0.47 | 16 | 0.03 | 16 | 0.03 | 231 | 0.28 | 0.6 |
| 15 | 21311-31 | 0 | 0 | 47 | 1,509 | 0.25 | 494 | 0.23 | - | - | 1,166 | 0.28 | 33 | 0.03 | 33 | 0.03 | 1,166 | 0.28 | 0.0 |
| 16 | 30153-11 | 7 | 7 | 16 | 1,971 | 0.22 | 1,564 | 0.24 | 68 | 0.30 | 206 | 0.65 | 20 | 0.07 | 20 | 0.07 | 142 | 0.59 | 3.5 |
| 17 | 30373-51 | 0 | 0 | 31 | 374 | 0.14 | 1,227 | 0.13 | - | - | 395 | 0.30 | 18 | 0.05 | 18 | 0.05 | 395 | 0.30 | 0.0 |
| 18 | 30373-52 | 2 | 19 | 16 | 394 | 0.27 | 1,681 | 0.26 | 76 | 0.24 | 268 | 0.51 | 16 | 0.11 | 16 | 0.11 | 180 | 0.57 | 3.4 |
| Average | | | | | 902 | | 1,143 | | 64 | | 554 | | 22 | | 22 | | 473 | | 2.4 |
| Maximum | | | | | 1,971 | | 2,144 | | 78 | | 2,777 | | 33 | | 33 | | 2,777 | | 7.8 |
| Minimum | | | | | 195 | | 405 | | 35 | | 206 | | 13 | | 13 | | 66 | | 0.0 |

TCAC=temperature corrected asphalt concrete, RM=rubblized material, FC=fractured concrete, BS=base and subbase, RB=roadbed soil, RCS=rubblized concrete slab, Avg=average value, CV=coefficient of variation

*Table 6.29 A summary of the results of the backcalculation of* [illegible]
*layers and the* [illegible]

Table 6.29 A summary of the results of the backcalculation of 6 rubblized pavement test sites where the combined base and subbase layers and the roadbed soil were counted as two layers.

| No. | Test site | Number of FWD test stations determined as | | | Backcalculated moduli (ksi) | | | | | | | | | | | | | | RM thickness (in.) |
|---|---|---|---|---|---|---|---|---|---|---|---|---|---|---|---|---|---|---|---|
| | | Full depth RM | Partial depth RM | Full depth FC | AC | | TCAC | | RM | | FC | | BS | | RB | | RCS | | |
| | | | | | Avg | CV | Avg | CV | Avg | CV | Avg | CV | Avg | CV | Avg | CV | Avg | CV | |
| 1 | 10692-11 | 19 | 0 | 20 | 317 | 0.14 | 534 | 0.14 | 79 | 0.24 | 163 | 0.31 | 25 | 0.24 | 14 | 0.11 | 122 | 0.47 | 4.4 |
| 2 | 10692-12 | 8 | 0 | 32 | 295 | 0.20 | 572 | 0.23 | 85 | 0.09 | 177 | 0.22 | 29 | 0.21 | 17 | 0.15 | 159 | 0.32 | 1.8 |
| 3 | 20233-11 | 33 | 0 | 0 | 396 | 0.20 | 2,079 | 0.20 | 45 | 0.25 | - | - | 22 | 0.10 | 7 | 0.04 | 45 | 0.25 | 9.0 |
| 4 | 20233-12 | 12 | 0 | 8 | 159 | 0.30 | 1,076 | 0.29 | 73 | 0.23 | 123 | 0.28 | 21 | 0.12 | 6 | 0.10 | 93 | 0.38 | 5.4 |
| 5 | 30373-61 | 2 | 0 | 15 | 2,126 | 0.29 | 2,005 | 0.32 | 67 | 0.71 | 256 | 0.46 | 38 | 0.39 | 16 | 0.05 | 234 | 0.55 | 1.1 |
| 6 | 30531-11 | 17 | 0 | 8 | 1,918 | 0.13 | 620 | 0.13 | 58 | 0.49 | 118 | 0.08 | 19 | 0.37 | 11 | 0.04 | 75 | 0.49 | 6.4 |
| Average | | | | | 869 | | 1,148 | | 68 | | 168 | | 26 | | 12 | | 121 | | 4.7 |
| Maximum | | | | | 2,126 | | 2,079 | | 85 | | 256 | | 38 | | 17 | | 234 | | 9.0 |
| Minimum | | | | | 159 | | 534 | | 45 | | 118 | | 19 | | 6 | | 45 | | 1.1 |

TCAC=temperature corrected asphalt concrete, RM=rubblized material, FC=fractured concrete, BS=base and subbase, RB=roadbed soil, RCS=rubblized concrete slab, Avg=average value, CV=coefficient of variation

average BS thickness of the test sites with known BS thickness excluding US-23. For the latter pavement, the sand subbase thickness is 30 in. and is occasionally supported on wood logs placed on top of the peat roadbed. Given these cross-sections of the six test sites and the type of the roadbed soil, it was decided to backcalculate the layer moduli using the 4RB system.

3. Only one test site showed full depth RM at each FWD test station where the backcalculated results were accepted. The weighted average RM modulus for that site is 45-ksi.
4. Six test sites showed full depth FC with a weighted average modulus of 988-ksi..
5. Five test sites showed both full depth RM and full depth FC. The weighted average modulus of the RM is 72-ksi and that of the FC is 177-ksi.
6. Twelve tests sites showed partial depth RM. The weighted average thickness and modulus of the RM are 3.8-in and 62-ksi, respectively. The weighted average thickness and modulus of the FC are 5.2-in and 329-ksi
7. The full depth FC layer stated in Table 6.28 for test site 20273-41 agrees with the field thickness of the FC layer measured during the rubblization operation. In addition, the average RM thickness obtained from the backcalculation of the layer moduli of the following test sites; 20102-11, 20102-12 and 21313-11 of Table 6.28 and 20232-11, 20232-12 and 30532-11 of Table 6.29 vary from 5.4 to 9.0 in. Filed investigation of these test sites during the rubblization operation indicated that the thickness of the rubblized material varied from 0.0 to 9.0 in. with about 50 percent of the trenched areas showing RM thickness of about 4-in. To a certain

extent, these field observations also agree with the range of the calculated RM thickness.

8. The TCAC moduli vary from 405 to 2,144 ksi for the 24 rubblized pavements. This range was expected because of the various AC mixtures used on those projects and the aging effects.

9. For some test sites listed in Table 6.29, the coefficients of variation of the BS moduli are relatively high. This may be due to combining the RM and FC into one layer. On the other hand, the high variations in the backcalculated RM and FC moduli do not necessarily mean interactions between the moduli of the two layers. Since the thicknesses and moduli of the two layers vary substantially within one test site.

Figure 6.23 depicts a plot of the average RM thickness of each test site and its average RCS modulus listed in Tables 6.28 and 6.29. The figure also shows the best fit line and the resulting regression equation. Examination of the figure indicates that:

- Lower RCS modulus values indicate thicker RM layer. This finding was expected because of the principle of energy dissipation. If the rubblizer energy penetrates and breaks the concrete slab to higher depths, the modulus of the RCS is low. The data in the figure indicates that results of the backcalculation are reasonable and relatively accurate.
- The average RM thicknesses of a test site can be predicted based on the average backcalculated RCS modulus and the following regression equation.

$$T_{RM} = 27.995 - 4.8887 * \mathrm{Ln}(E_{RCS}) \qquad \text{For } 49 \leq E_{RCS} \leq 307 \qquad (6.4)$$

Where $T_{RM}$ = average RM thickness of a test site (in.); and

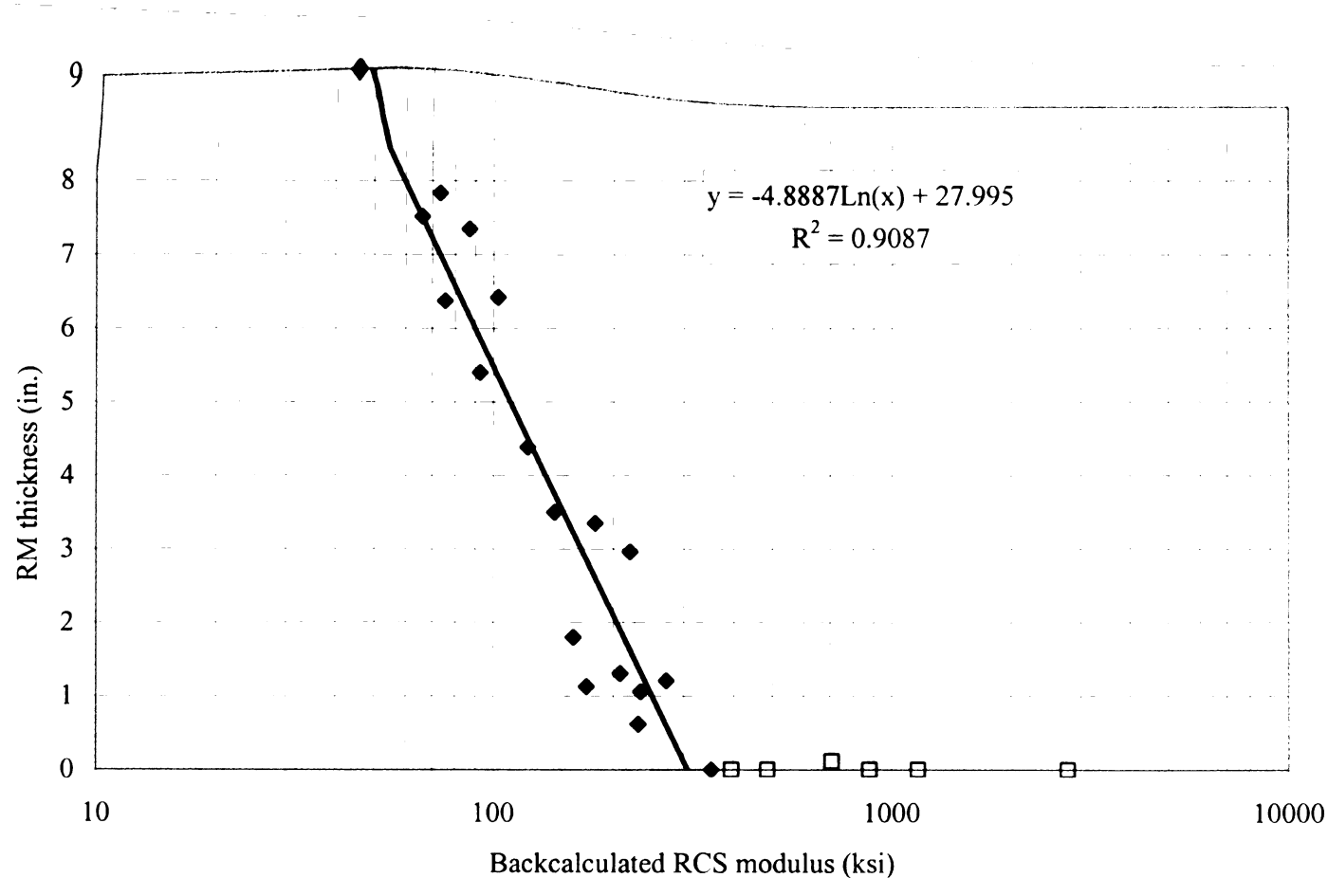


Figure 6.23 Rubblized material (RM) layer thickness versus the backcalculated modulus of the rubblized concrete slab (RCS)

$E_{RCS}$ = average backcalculated RCS modulus of that test site (ksi).

It should be noted that only the solid data points in Figure 6.23 were used to develop the regression equation. The open data points were excluded. The reason is that, on average, when the RCS modulus is greater than 307 ksi, it is likely that the RCS consists mainly of full depth FC. Whereas when the RCS modulus is less than 49 ksi, the RCS is a full depth RM. The significance of equation 6.4 is that State Highway Agencies can use the equation to estimate the average RM thickness of the test site based on its average RCS modulus without going through the steps for the determination of the most plausible RM thickness.

Table 3.30 provides the cross sections, depth to stiff layer and condition of the FWD test sites of 12 flexible pavements (Schorsch, 2003). Table 6.30 provides the results of the backcalculation of layer moduli of the 12 sites using the procedure listed in section 4.0. Because of lack of information concerning the thickness of the subbase layer for all test sites but one, Schorsch combined the two layers and performed three layers (AC, combined base and subbase and roadbed soil) backcalculation of layer moduli. After which, he evenly split the combined base and subbase layer into two individual layers and performed 4-layer backcalculation of layer moduli using various depths to stiff layer. He compared the backcalculated moduli of the two individual layers and selected the final depth to stiff layer where the two moduli were equal. Because the measured core thicknesses from M-42 test section 1 test site 1 showed significant variations; two AC thicknesses were used; 3.3-in was assigned to 38 FWD test stations and 4.7-in to 14 locations. Similar scenario existed on M-52 test section 1 site 1; three AC thicknesses were assigned as follows: 5.3-in for 4 test stations, 5.9-in for 37 test stations and 6.5-in

Table 6.30 A summary of pavement cross sections, roadbed soil, depths to stiff layer and the observed distresses in 12 flexible pavement test sites (Schorsch, 2003)

| No | Test Site | Pavement Cross Section | | | | | | Thickness used in the backcalculation (in) | | | | Type of Roadbed Soil | Depth to stiff layer (in.) | Pavement distresses at the test site |
|---|---|---|---|---|---|---|---|---|---|---|---|---|---|---|
| | | AC Thickness (in) | | Base (B) | | Subbase (S) | | AC | BS | B | S | | | |
| | | Inventory Data | Core | Material type | Thickness (in.) | Material type | Thickness (in.) | | | | | | | |
| 1 | 20273-11 | N/A | 9.0 | Agg. | N/A | N/A | N/A | 9.0 | 27 | - | - | Loamy sand | 200 | None |
| 2 | 20411-11[1] | 2.6 | 3.3 | Sand | 12 | Loamy Gravel | 39 | 3.3 | - | 12 | 39 | Sandy and mucky loam | None | Cracks |
| 3 | 20411-12 | 2.6 | 2.8 | Sand | 12 | Loamy Gravel | 39 | 2.8 | - | 12 | 39 | Sandy and mucky loam | None | Cracks |
| 4 | 30202-11 | 4.9 | 4.7 | Sand | N/A | Sand | N/A | 4.7 | 30 | - | - | Loamy sand | 150 | Cracks |
| 5 | 30202-12 | 4.9 | 4.5 | Sand | N/A | Sand | N/A | 4.5 | 30 | - | - | Sand | 150 | Cracks |
| 6 | 30422-11[2] | N/A | 3.3 | N/A | N/A | N/A | N/A | 3.3 | 30 | - | - | Sand | 250 | Cracks |
| | | | 4.7 | N/A | N/A | N/A | N/A | 4.7 | 30 | - | - | Sand | 250 | Cracks |
| 7 | 30502-12 | N/A | 6.1 | Agg. | N/A | N/A | N/A | 6.1 | 30 | - | - | Sandy loam | 120 | Cracks |
| 8 | 30502-21 | N/A | 6.9 | Agg. | N/A | N/A | N/A | 6.9 | 30 | - | - | Sandy loam | 150 | Cracks |
| 9 | 30521-11[1, 2] | N/A | 5.3 | N/A | N/A | N/A | N/A | 5.3 | 36 | - | - | Loam | None | Cracks |
| | | | 5.9 | N/A | N/A | N/A | N/A | 5.9 | 36 | - | - | Loam | None | Cracks |
| | | | 6.5 | N/A | N/A | N/A | N/A | 6.5 | 36 | - | - | Loam | None | Cracks |
| 10 | 30521-21 | N/A | 9.1 | N/A | N/A | N/A | N/A | 9.1 | 36 | - | - | Loam | 500 | Cracks |
| 11 | 30552-11[3] | 3.1 | 3.0 | Agg. | N/A | N/A | N/A | 3.0 | - | 15 | - | Sand | None | Cracks |
| 12 | 30552-12[3] | 3.1 | 3.0 | Agg. | N/A | N/A | N/A | 3.0 | - | 15 | - | Sand | None | Cracks |

BS=the combination of base and subbase; Agg. = Aggregate

[1] The old pavements underneath the existing pavements were treated as part of the roadbed soil in the backcalculation.

[2] The test sites were divided into sub-areas. Each sub-area was backcalculated using different average AC thicknesses; and

[3] The S and RB moduli at these test sites are similar, hence they were backcalculated as one layer.

Table 6.31 A summary of the backcalculation of 12 flexible pavement test sites (Schorsch, 2003)

| No | Test site | Number of the accepted backcalculation results | | Backcalculated moduli (ksi) | | | | | | | | | |
|---|---|---|---|---|---|---|---|---|---|---|---|---|---|
| | | | | AC | | TCAC | | B | | S | | RB | |
| | | | | Avg | CV | Avg | CV | Avg | CV | Avg | CV | Avg | CV |
| 1 | 20723-11 | 40 | | 851 | 0.05 | 905 | 0.10 | 29 | 0.07 | 29 | 0.07 | 17 | 0.03 |
| 2 | 20411-11 | 42 | | 2,268 | 0.11 | 1,084 | 0.15 | 38 | 0.07 | 17 | 0.08 | 41 | 0.07 |
| 3 | 20411-12 | 42 | | 3,098 | 0.16 | 1,151 | 0.17 | 44 | 0.06 | 16 | 0.05 | 56 | 0.11 |
| 4 | 30202-11 | 30 | | 1,017 | 0.12 | 1,248 | 0.11 | 38 | 0.08 | 38 | 0.08 | 22 | 0.10 |
| 5 | 30202-12 | 29 | | 952 | 0.09 | 1,559 | 0.08 | 37 | 0.05 | 37 | 0.05 | 26 | 0.03 |
| 6 | 30422-11 | 49 | | 1,083 | 0.28 | 2,376 | 0.27 | 17 | 0.09 | 17 | 0.09 | 12 | 0.03 |
| 7 | 30502-11 | 28 | | 670 | 0.24 | 457 | 0.21 | 22 | 0.09 | 22 | 0.09 | 16 | 0.16 |
| 8 | 30502-21 | 48 | | 312 | 0.15 | 584 | 0.15 | 28 | 0.09 | 28 | 0.09 | 17 | 0.12 |
| 9 | 30521-11 | 43 | | 865 | 0.15 | 579 | 0.15 | 21 | 0.08 | 21 | 0.08 | 36 | 0.03 |
| 10 | 30521-21 | 40 | | 1,063 | 0.22 | 456 | 0.24 | 18 | 0.13 | 18 | 0.13 | 34 | 0.11 |
| 11 | 30552-11 | 33 | | 1,728 | 0.18 | 2,546 | 0.20 | 42 | 0.14 | 42 | 0.14 | 27 | 0.04 |
| 12 | 30552-12 | 32 | | 1,256 | 0.27 | 2,794 | 0.30 | 48 | 0.17 | 48 | 0.17 | 21 | 0.04 |
| Total | | 456 | Average | 1,264 | | 1,312 | | 32 | | 28 | | 27 | |
| | | | Maximum | 3,098 | | 2,794 | | 48 | | 48 | | 56 | |
| | | | Minimum | 312 | | 456 | | 17 | | 16 | | 12 | |

for 3 test stations. Examination of the backcalculation results indicate that for test sites on US-41 and M-52 (20411-11, 20411-12, 30521-11 and 3052-12), the backcalculated roadbed soil moduli are greater than the base and/or subbase moduli. This occurs because these pavements are located over previously constructed pavements. On US-41, the original pavement is a PCC pavement located approximately 4.5 ft below the pavement surface. On M-52, the original pavement is a gravel road located approximately 3 ft below the pavement surface.

Comparing results of the backcalculation of layer moduli of rubblized and flexible pavements and their cross sections indicates that:

- The average TCAC of the all 12 flexible and all 24 rubblized pavement test sites are similar (1,144 vs. 1,312 ksi). Further, the ranges of the TCAC of rubblized and flexible pavements are also similar (405 to 2,144 ksi vs. 456 to 2,794 ksi.).
- The range of the backcalculated BS moduli of rubblized pavements of 19 to 38 ksi listed in Table 6.29 is similar to that of the base and subbase of the flexible pavements of 17 to 44 ksi. This reflects the fact that in general, the B and S materials for rubblized and flexible pavements are the same.
- Except for few unique test sites, the backcalculated RB moduli of rubblized and flexible pavements have similar range. This is compatible with the fact that the majority of the roadbed soils at the test sites vary from sand, to sandy loam to loamy sand.
- In general, for both rubblized and flexible pavements, the coefficient of variation of the backcalculated AC moduli is higher than those of the B, S, BS, and RB. This was expected and it indicates that the impact of variations in the AC layer

flexi

back

balar

10.0

pave

from

modi

discu

and

thickness on its modulus is higher than those of the other layers on their respective moduli.

Based on the results of the backcalculation of layer moduli of 24 rubblized and 12 flexible pavement test sites, it can be concluded that the newly developed procedures for backcalculation of layer moduli and for estimating the depth to stiff layer are relatively balanced and applicable to both rubblized and flexible pavements.

## 10.0 SUMMARY

In this chapter, variations in the deflection data of rubblized and flexible pavements are presented and discussed. The results of the repeatability and linearity tests from 4 rubblized pavements are presented. Two procedures for backcalculation of layer moduli and estimating the depth to stiff layer were developed, implemented and discussed with examples. Results of the backcalculation of layer moduli of 24 rubblized and 12 flexible pavement test sites using the new procedures are presented and discussed.

# CHAPTER 7

# THERMAL STRESSES IN THE AC LAYER

## 1.0 INTRODUCTION AND OBJECTIVES

One of the objectives of this research is to analyze the effects of tire-pavement interaction and the pavement and environmental factors on top-down and bottom up cracking potentials. The effects of the tire-pavement interaction and pavement factors are addressed in Chapter 8. This chapter presents and discusses the effects of temperature-induced thermal stresses.

As stated in the literature review, thermal stresses in the AC layer were studied by various researchers. Some, such as Zubeck and Vinson (1996) and Kim and Lee (1995) analyzed the impact of thermal stresses on transverse temperature cracks. While others, such as Rogue and Ruth (1990), Hugo and Kennedy (1985), and Dauzats and Rampal (1987), studied the impact of thermal stresses on top-down cracking potential.

In this study, the analyses of thermal stresses induced at the top and at the bottom of the AC layer were calculated using the relaxation constitutive equation. The results are presented and discussed below.

## 2.0 THERMAL STRESSES

The following relaxation constitutive equation for viscoelastic materials is used in the analyses of thermal stresses at the top and bottom of the AC layer (after Haddad, 1995).

$$\sigma(t) = \int_0^t E\left(\frac{t-\tau}{a_T}\right)\varepsilon'(\tau)d\tau \qquad (7.1)$$

where $\sigma(t)$ = Stress at time t;

$\varepsilon'(t)$ = Rate of change of the strain, $\varepsilon(t)$, at time t;

$E(t)$ = Time-dependent relaxation modulus;

$t$ = Time in question at which the stress is being calculated;

$\tau$ = Time integration variable; and

$a_T$ = Shift factor for temperature, T.

$$\log(a_T) = \frac{47.8*(T - 25)}{392 + (T - 25)} \qquad (7.2)$$

The master relaxation curve at the temperature of 25°C, $E(t_r)$ and its shift factor, $a_T$, of an asphalt mixture reported by Park (2000) was used in the analyses of thermal stresses. Plots of the master curve and the shift factor are presented in Figures 7.1 and 7.2, respectively. Park (2000) used the Prony series algorithm and regression analyses to develop equation 7.3, which expresses the master curve.

$$E(t_r) = 14825 - 2209*(1-e^{-t_r/1.1447957}) - 4427.6*(1-e^{-t_r/0.0006052}) - 4454.6*$$
$$(1-e^{-t_r/0.0173438}) - 2637.2*(1-e^{-t_r/0.0000131}) \qquad (7.3)$$

where $t_r$ = Reduced time = $t/a_T$

Figure 7.3 depicts a plot of the master curve and the Prony series (equation 7.3). Although Park stated that equation 7.3 accurately describes the master curve for reduced times of up to 10 seconds, the observations made in this study revealed that:

1. For a reduced time of 0.1 seconds or greater, the difference between the estimated and actual relaxation moduli becomes more prevalent as shown in Figure 7.3.
2. Because of the four exponential functions in the equation, when the value of the reduced time becomes greater than about 10, the values of the exponential

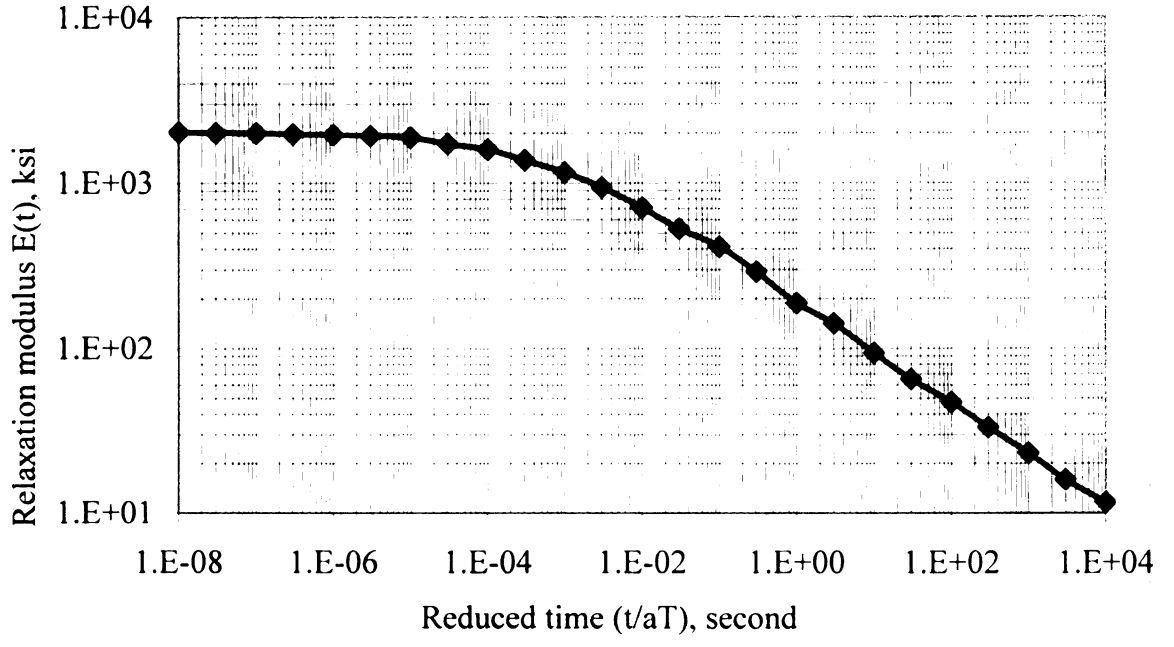


Figure 7.1 Master relaxation modulus curve and shift factor of the asphalt mixtures reported by Park (2000)

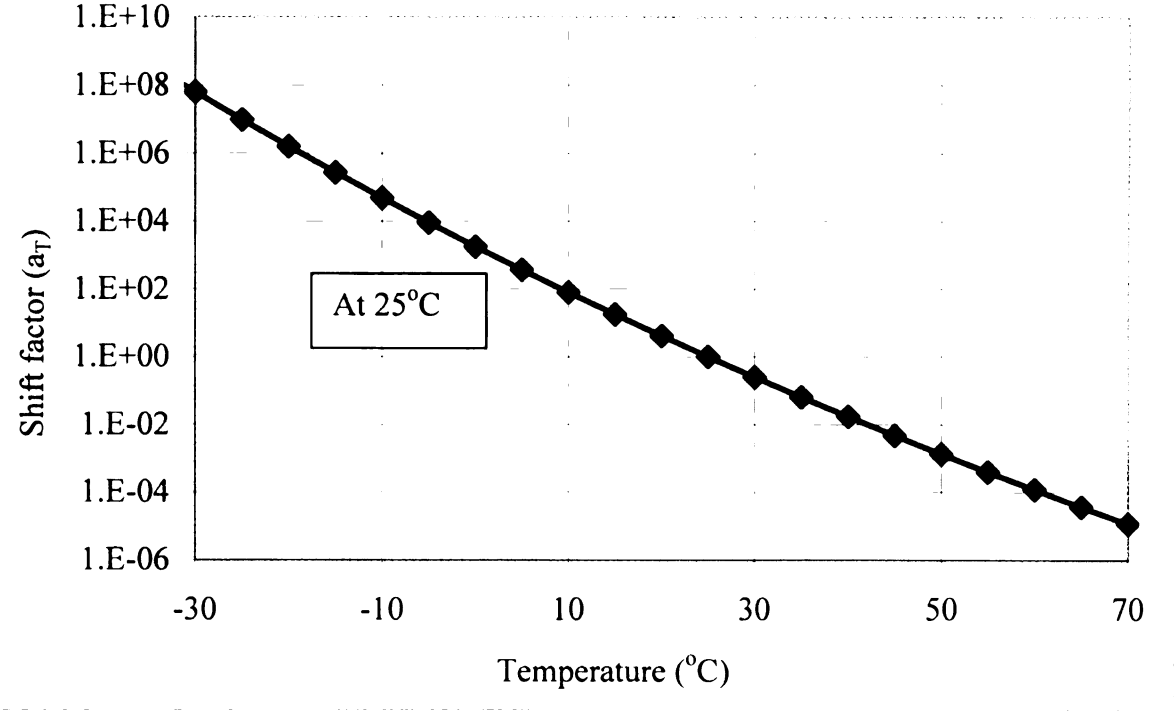


Figure 7.2 The shift factor ($a_T$) versus temperature

functions become negligible and hence, the value of $E(t_r)$ becomes constant. This represents significant departure from the relaxation curve as shown in Figure 7.3.

Based on the above observations, a two tears approach was used in this study to calculate the induced thermal stresses in the asphalt layer. In the first tear, equation 7.3 was used to calculate the relaxation modulus for all reduced times of less than 0.1 second. In the second tear, equation 7.4, which was developed in this study, was used to calculate the relaxation modulus for reduced times higher than 0.1 second. The values of the relaxation modulus calculated using equation 7.4 (for times higher than 0.1 second) are also shown in Figure 7.3. As can be seen, these values agree very well with the relaxation modulus values of the master curve. The figure also shows the values of the relaxation modulus for times greater than 10,000 seconds, which is the limiting value of the master curve. Such extrapolation of the relaxation modulus has insignificant impact (less than 0.1 psi) on the calculated thermal stress.

$$E(t_r) = 10^{3.13701-0.30525*LOG(t_r)} \tag{7.4}$$

The rates of change for strain, $\varepsilon'(t)$, were calculated using the following equation.

$$\varepsilon'(t) = \alpha T' \tag{7.5}$$

where: $\varepsilon'(t)$ = Corresponding rate of change for strain, 1/unit time;

$\alpha$ = Coefficient of thermal contraction and expansion per $^{o}C$; and

$T'$ = Rate of change of temperature, $^{o}C$/unit time.

The coefficient of thermal contraction and expansion of the AC mixture was assumed as $2.62*10^{-5}$ /$^{o}C$ for temperatures above the glass transition temperature (Zeng and Shields, 1999). Bahia and Anderson, 1993 reported that the glass transition

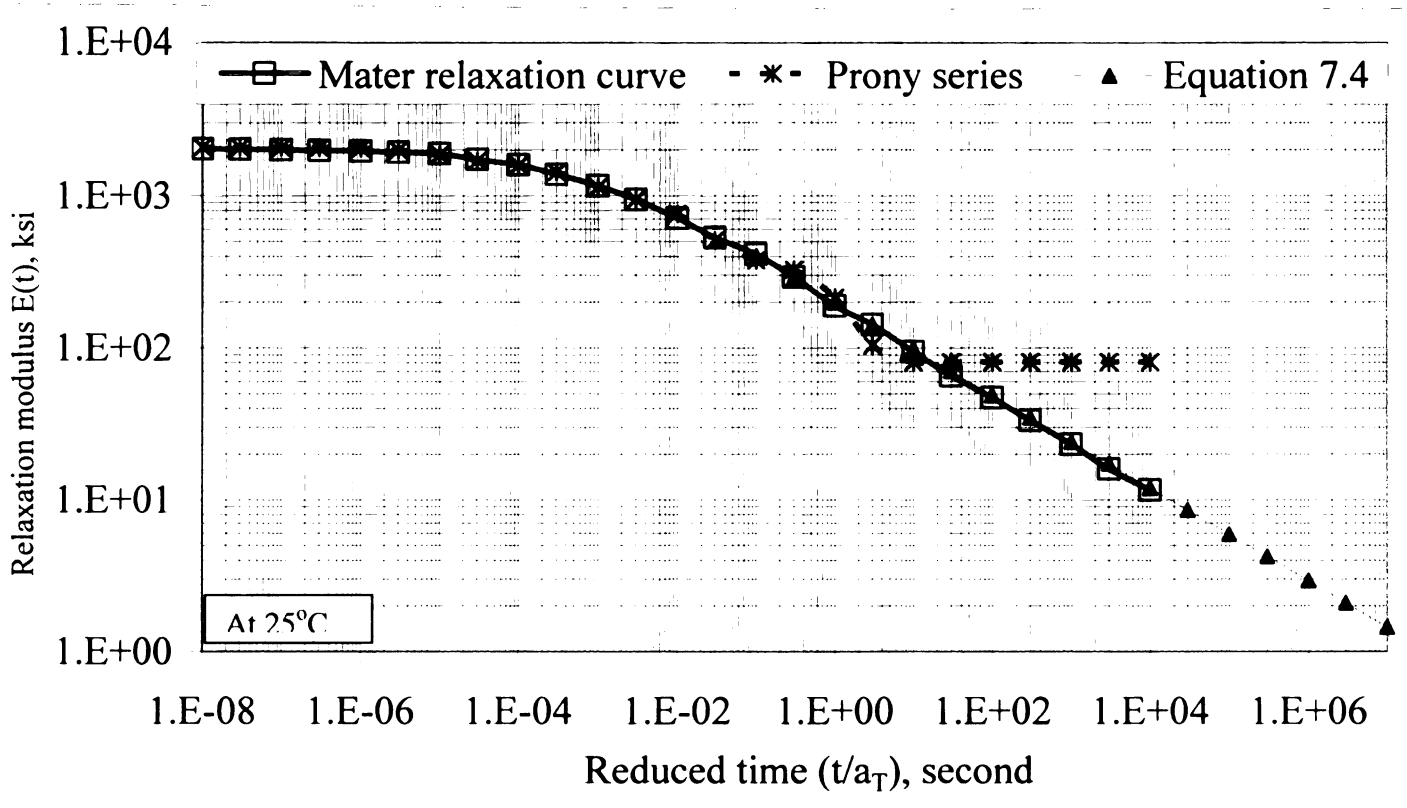


Figure 7.3 Comparison between the estimated relaxation moduli using the Prony series developed by Park (2000) and using equation 7.4 and the master relaxation modulus curve

temperature of asphalt binders ranges from 5°C to -35°C. In this study, the coldest measured temperature used in the analyses of thermal stresses is -18.1°C, which was assumed to be above the glass transition temperature. The measured pavement temperature data used in the analysis are described in the next section.

## 3.0 PAVEMENT TEMPERATURE DATA

Pavement temperature data collected by the Michigan Department of Transportation (MDOT) from 1994 to 1999 was utilized in the analysis of thermal stresses-induced at the top and bottom of the AC layer. MDOT installed thermo couples in flexible and composite pavements to measure air and pavement temperatures every 15 minutes for a continuous period of 5 years. For each pavement, a single thermo couple recorded the air temperature and a second recorded the pavement surface temperature. Two additional thermo couples were embedded at predetermined locations within the pavement as follows:

- For composite pavements, the thermo couples were embedded at the bottom of the AC layer and in the concrete slab.
- For flexible pavements, the thermocouples were embedded at about mid depth and at the bottom of the AC layer.

Table 7.1 provides a list of the pavement sections, depths of the embedded thermo couples and the recording period of the temperature data. For each pavement section, Table 7.2 shows the highest and lowest recorded surface temperatures. Figures 7.3 and 7.4 show the yearly and daily temperature variations at the pavement surface and at the

Table 7.1 List of the pavement sections, thermocouples locations and the time period during which for temperature data were recorded

| Nearby city | Route | Type | Thermocouples | | Depths from the surface of the additional thermocouples (in.) | | | Time period | |
|---|---|---|---|---|---|---|---|---|---|
| | | | Air | Surface | In the AC layer | At AC bottom | In the Concrete slab | Start | End |
| Brighton | US-23 | Composite | Yes | Yes | - | 7 | 10 | Jul-94 | Jul-99 |
| St. Johns | US-27 | Composite | Yes | Yes | - | 9.5 | 19 | Jul-94 | Sep-95 |
| Port Sanilac | M-25 | Composite | Yes | Yes | - | 6 | 10 | Sep-94 | Sep-99 |
| Farewell | M-115 | Composite | Yes | Yes | - | 3 | 10 | Jul-94 | Sep-99 |
| Alpena | US-23 | Composite | Yes | Yes | - | 6 | 10 | Jul-94 | Sep-99 |
| Brevot | US -2 | Flexible | Yes | Yes | 5 | 10 | - | Jul-94 | Apr-99 |
| Deerton | M-28 | Flexible | Yes | Yes | unknown | 12 | - | Jul-94 | Oct-99 |
| Carney | US-41 | Composite | Yes | Yes | - | 6 | 10 | Aug-94 | Sep-99 |
| Iron River | US-2 | Composite | Yes | Yes | - | 6 | 10 | Jul-94 | Sep-99 |

Note: There are some time intervals during the listed time periods that the thermocouples were malfunctioned.

Table 7.2 The lowest and the highest recorded pavement surface temperatures and the corresponding air temperatures and the temperatures at various depths in the pavements

| Nearby city | On the day with the lowest AC surface temperatures | | | | | | | On the day with the highest AC surface temperatures | | | | | | |
|---|---|---|---|---|---|---|---|---|---|---|---|---|---|---|
| | Date | Time | Temperature (°C) | | | | | Date | Time | Temperature (°C) | | | | |
| | | | Air | Surface | In the AC layer | Bottom of the AC layer | In the concrete slab | | | Air | Surface | In the AC layer | Bottom of the AC layer | In the concrete slab |
| Brighton | 2/3/96 | 7:39 | -23.4 | -19.8 | - | -15.1 | -11.4 | 7/14/95 | 14:24 | 37.3 | 50.9 | - | 39.2 | 33.2 |
| St. Johns | 2/12/95 | 4:36 | -18.9 | -15.1 | - | -7.9 | -2.0 | 6/19/95 | 15:04 | 37.7 | 50.6 | - | 35.2 | 27.8 |
| Port Sanilac | 2/3/96 | 4:00 | -23.5 | -15.8 | - | -10.9 | -7.1 | 7/14/95 | 14:48 | 42.8 | 53.4 | - | 40.3 | 32.5 |
| Farewell | 2/3/96 | 8:04 | -37.2 | -24.9 | - | -22.2 | -18.6 | 6/20/95 | 14:28 | 40.8 | 51.8 | - | 44.9 | 36.7 |
| Alpena | 2/3/96 | 8:41 | -27.1 | -21.3 | - | -17.1 | -14.4 | 6/19/95 | 14:24 | 43.1 | 52.6 | - | 40.2 | 33.8 |
| Brevot | 2/3/96 | 6:33 | -28.6 | -24.1 | -21.0 | -18.3 | - | 6/20/95 | 14:24 | 35.4 | 48.4 | 40.1 | 31.9 | - |
| Deerton | 2/4/96 | 8:24 | -32.9 | -23.8 | -19.7 | -16.9 | - | 6/18/95 | 14:42 | 34.1 | 50.7 | 39.6 | 32.2 | - |
| Carney | 2/2/96 | 7:45 | -33.6 | -24.7 | - | -18.3 | -15.2 | 6/19/95 | 13:48 | 35.6 | 54.2 | - | 38.6 | 33.8 |
| Iron River | 2/2/96 | 7:22 | -34.9 | -27.1 | - | -22.0 | -17.8 | 6/18/95 | 15:11 | 37.4 | 57.0 | - | 43.5 | 35.2 |

bottom of the AC layer on US-23 near Alpena. Examination of the data in Table 7.2 and Figures 7.4 and 7.5 indicate that:

- The range of the measured pavement surface temperatures is 57°C during the summer and -27°C during the winter (see Table 7.2).
- The pavement surface is subjected to greater temperature fluctuation than the bottom of the AC layer for both daily and yearly cycles (see Figures 7.4 and 7.5). Hence, it should be expected that the pavement surface is subjected to higher thermal stresses than the bottom of the AC layer.
- The temperature differences between the top and the bottom of the AC layer are more extreme in summer than in the winter.
- The pavement surface temperature reaches its minimum around 6:30 to 8:30 AM in winter and its maximum around 1:00 to 3:00 PM in summer.
- Finally, the thermocouples in US-27 by St. John, Carney and Iron River cities were malfunctioned on 2/02/1996 and the thermocouples in M-25 at Port Sanilac city were malfunctioned on 2/12/1995.

In the section below, the thermal stresses at the top and at the bottom of the AC layer are presented and discussed.

## 4.0 THERMAL STRESSES IN AC SURFACED PAVEMENTS

The analyses of thermal stresses in asphalt surface pavements were designed to accomplish the following objectives:

1. Assessment of the impact of the starting date of the calculation of thermal stress at a certain day on the magnitude of thermal stresses.

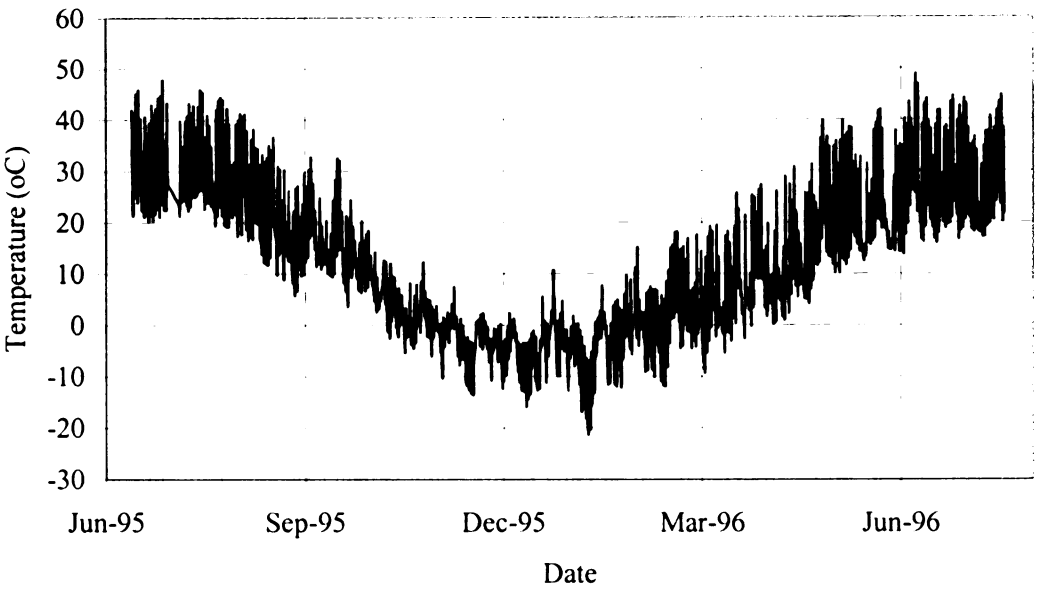


a) Variation in the pavement surface temperature during one year cycle

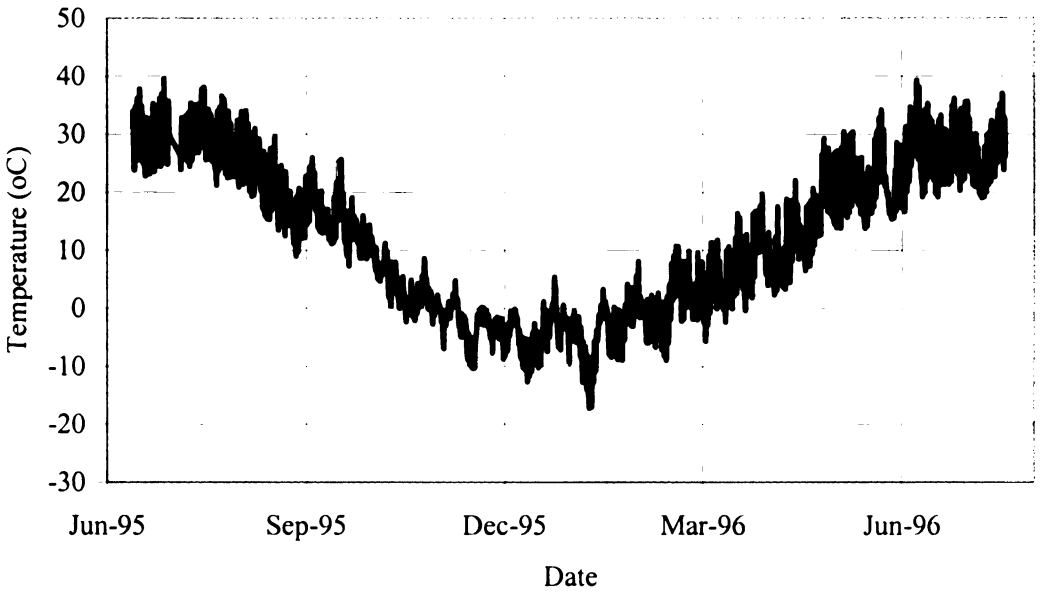


b) Variation of the temperature at the bottom of the AC layer during one year cycle

Figure 7.3 Yearly temperature variations at the surface and the bottom of the AC layer, US-23, Alpena, MI

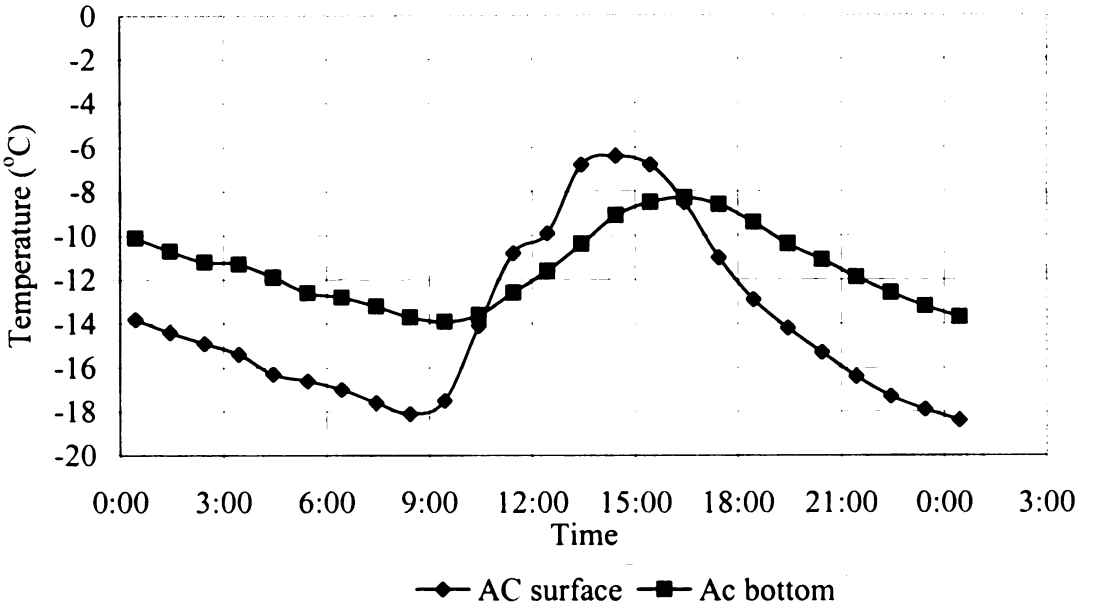


a) Low pavement surface temperatures (February 2, 1996)

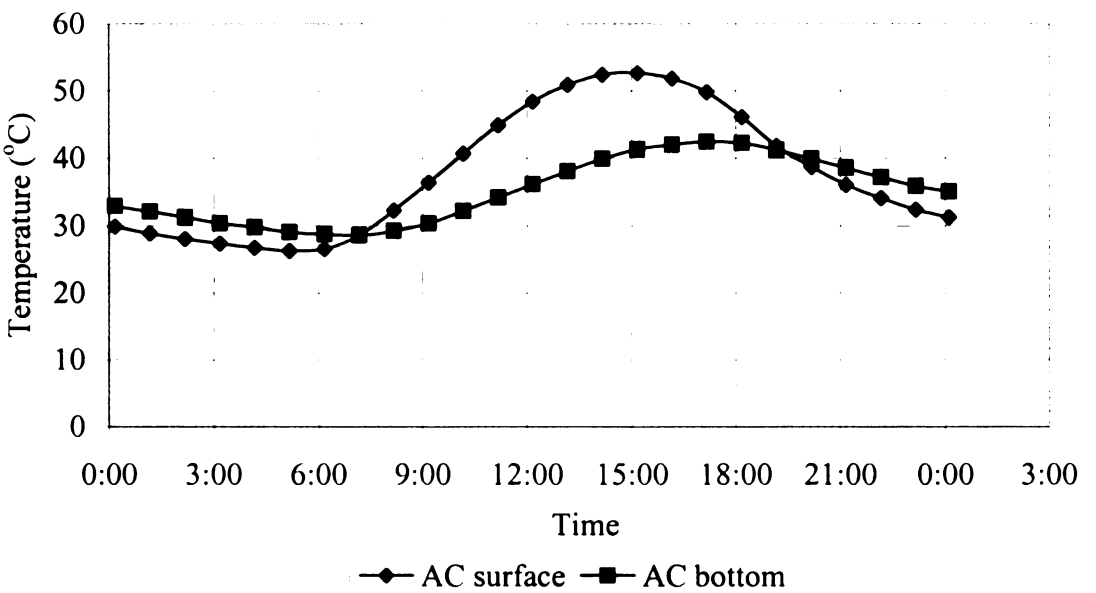


b) High pavement surface temperatures (June 19th, 1995)

Figure 7.4 Daily temperature variations at the surface and the bottom of the AC layer on the days at which the pavement surface experienced very low and very high temperatures (US-23, Alpena, MI)

2. Analyses of the variation in thermal stresses for one winter day (February 2, 1996) and for one summer day (June 19, 1996). The analyses were based on the pavement temperature data measured on US-23 near Alpena.

3. Assessment of the variation in thermal stresses for a single year. The analyses were based on the measured temperature data on US-23 near Alpena from August 1995 to August 1996.

4. Appraisal of the impact of the asphalt layer thickness on thermal stress induced on the coldest recorded day (February 2, 1996). The analysis was calculated for the following pavement sections:

   - US-23 by Brighton, AC thickness of 7-in.
   - M-115 by Farewell, AC thickness of 3-in.
   - US-23 by Alpena, AC thickness of 6-in.
   - US-2 by Brevot, AC thickness of 10-in.
   - M-28 by Deerton, AC thickness of 12-in.

The results of the analyses of thermal stresses at the top and bottom of the pavements are presented in the next section.

## 4.1. The Effect of the Duration Period on Thermal Stresses

The magnitude of the induced thermal stress is dependent on the temperature history of the pavement. Table 7.3 compares the calculated thermal stresses on February 2, 1996 and June 19, 1996 using duration periods of 3, 6.5 and 12 months. Results of the analyses indicated that:

1. The difference in the magnitudes of the calculated thermal stresses on a winter day due to different duration periods (different starting dates) is negligible relative to the magnitude of the induced thermal tensile stress. For a summer day, said difference, however small) could be equal in magnitude to the induced low magnitude thermal compressive stress (negative sign in the table).
2. The effect of the residual stress of a given day on the thermal stress in the pavement on another day decreases as the time period between the two days increases.
3. The magnitude of the cumulative residual stress of a given period on any given day is a function of the temperature fluctuation in that period.

Based on the above observations, one can conclude that the calculation of thermal stresses on any given day is relatively accurate if the analysis is based on a minimum period of three months. Said period is utilized in this study when historical temperature data were not available for longer periods. Nevertheless, it is recommended that, if temperature data are available, longer time periods be used.

## 4.2. Daily Thermal Stress Variation

For any given day, the induced-thermal stress varies with time. Such daily variations in thermal stresses on US-23 near Alpena, Michigan were analyzed for two days; February 2, 1996 and June 19, 1996. Figure 7.4 shows plots of the temperatures at the top and at the bottom of the AC layer on those days. Figure 7.5 shows the daily thermal stresses variation on those days. Examination of Figures 7.4 and 7.5 indicates that:

Table 7.3 Calculated thermals stresses at the surface and at the bottom of the AC layer for February 2 and June 19, 1996 using three time periods

| Start | End | Duration (month) | Thermal stress (psi) | | Start | End | Duration (month) | Thermal stress (psi) | |
|---|---|---|---|---|---|---|---|---|---|
| | | | AC surface | AC bottom | | | | AC surface | AC bottom |
| 11/2/95 | 2/2/96 | 3 | 112.9 | 56.2 | 3/19/95 | 6/19/95 | 3 | -2.4 | -2.9 |
| 7/11/95 | 2/2/96 | 6.5 | 114.5 | 57.9 | 12/19/94 | 6/19/95 | 6 | -3.9 | -4.4 |
| 2/2/95 | 2/2/96 | 12 | 114.5 | 54.7 | 7/28/94 | 6/19/95 | 10.5 | -1.3 | -2.1 |
| Average | | | 114.0 | 56.3 | Average | | | -2.5 | -3.1 |
| Maximum difference | | | 1.6 | 3.2 | Maximum difference | | | 2.6 | 2.3 |

- As expected, the pavement surface was subjected to higher variation of thermal stresses relative to the bottom of the AC layer.
- The variation in thermal stresses parallels the variation in the measured pavement temperatures at both the surface and the bottom of the AC layer. Further, the time lag between the peak thermal stresses at the surface and the bottom of the AC layer was similar to that between the peak temperatures at the same locations.
- The pavement surface experienced much higher variation in thermal stresses during winters than during summers. The variation in thermal stresses at the pavement surface on February 2, 1996 ranged from 40.8-psi compression to 109.0-psi tension. The peak surface tensile stress occurred at approximately 8:30 in the morning and the peak compressive surface stress at 2:20 in the afternoon. On June 19, 1996, the thermal stress varied from just above 4-psi compression to slightly less than 1-psi compression. No tensile stress was calculated at any time. These observations were expected because in the summer, the AC modulus is relatively low due to high temperature whereas it is relatively high in winter cold temperatures. Hence, in February, the thermal contraction and expansion of the AC layer result in high thermal tensile and compressive stresses while they produce low thermal stresses in summers.

## 4.3 Yearly Thermal Stress Variation

The yearly variation in thermal stresses at the top and at the bottom of the AC layer was analyzed for a single year on US-23 near Alpena by calculating the thermal stresses at 8:30 in the morning and at 2:20 in the afternoon for the second day of each month from

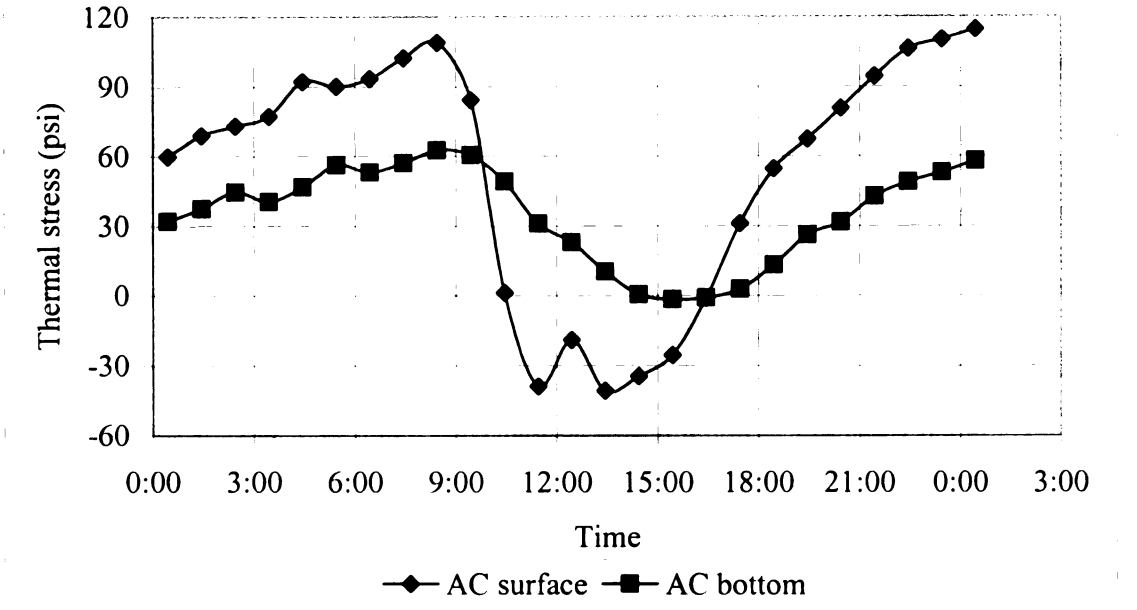


a) Thermal stresses on February 2nd, 1996

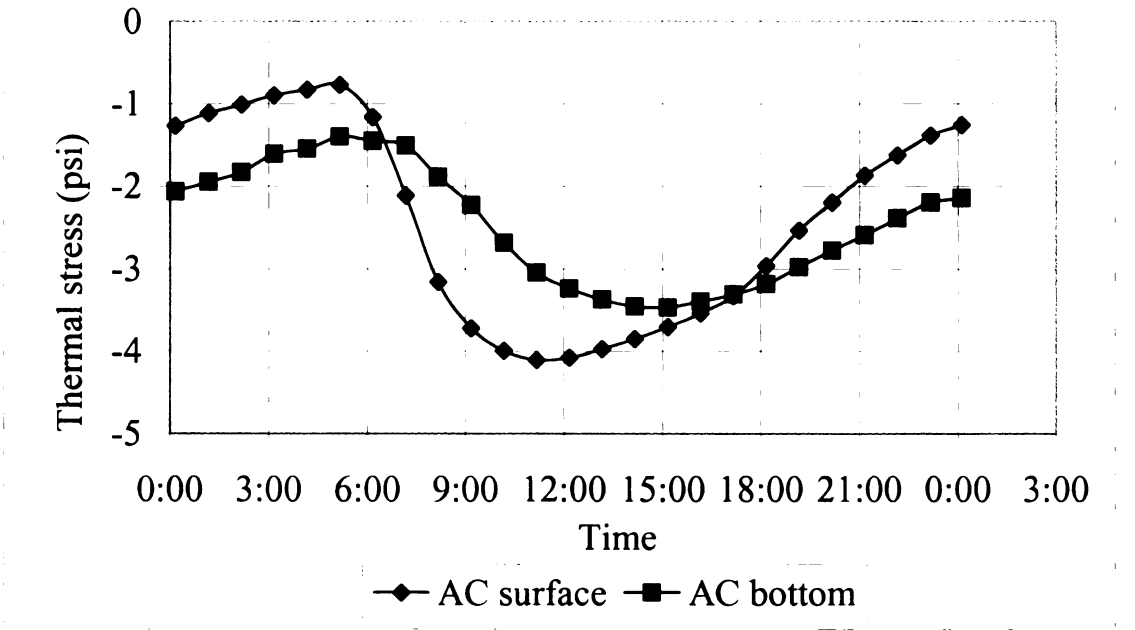


b) Thermal stresses on June 19th , 1996

Figure 7.5 Variations of thermal stresses throughout one day (February 2nd, 1996 and June 19th , 1996), (US-23, Alpena, MI)

August 1995 to August 1996. Results of the analyses are shown in Figure 7.6 and the temperatures for these days are shown in Figure 7.7. The two times on each second day of each month were selected to capture the possible high and low thermal stresses at the surface and at the bottom of the AC layer. Note that the daily times during which the thermal stress will reach its peak change over the course of the year. The intention herein is to calculate the critical stresses in winter which per section 4.2 occur on the pavement surface at 8:30 am and 2:20 pm. Nevertheless, examination of Figures 7.6 and 7.7 indicates that:

- Similar to the trend shown in Figure 7.5, the calculated thermal stress parallels the trend of pavement temperatures. That is, in general, the pavement temperature decreases continuously from August to February and then increases after February (see Figure 7.7). The pavement surface is subjected to the highest thermal tensile and compressive stresses in February.
- The AC layer was subjected to significant thermal stresses between November and May. The thermal stresses induced between June and October are relatively small.

## 4.4 Thermal Stress Variation between Test Sites

The effect of the AC layer thickness on the thermal stresses at the top and at the bottom of the AC layer was analyzed using five pavement sections with varying AC layer thickness. For each section, the thermal stress was calculated on February 2, 1996 at the time when the pavement surface temperature was the lowest for that day. Table 7.4 shows the calculated thermal stresses at the surface and at the bottom of the AC layers of the

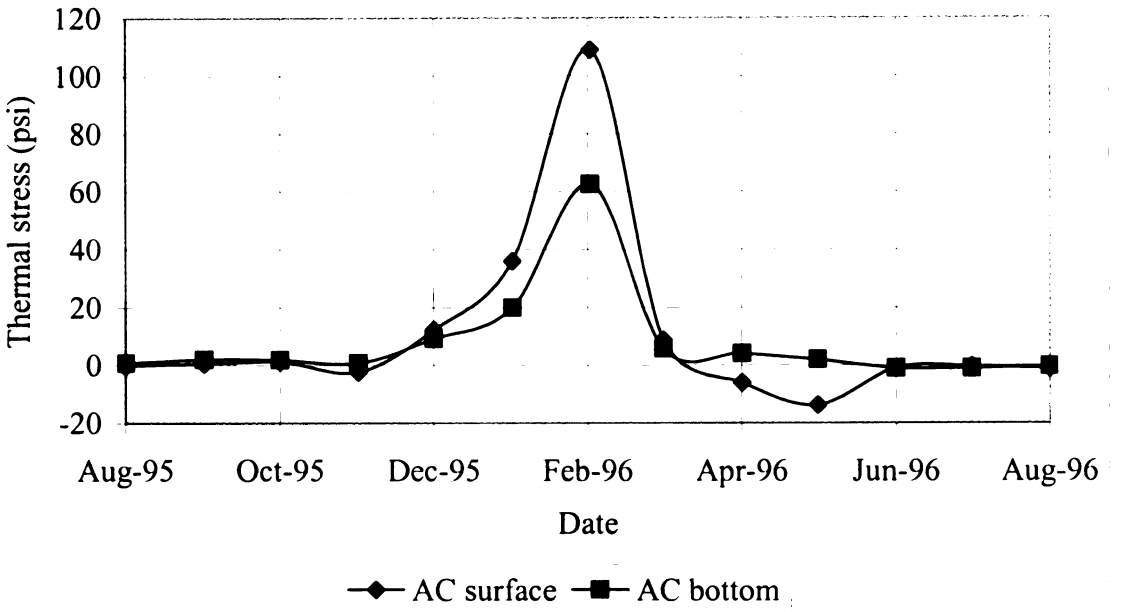


a) Thermal stresses around 8:30 AM

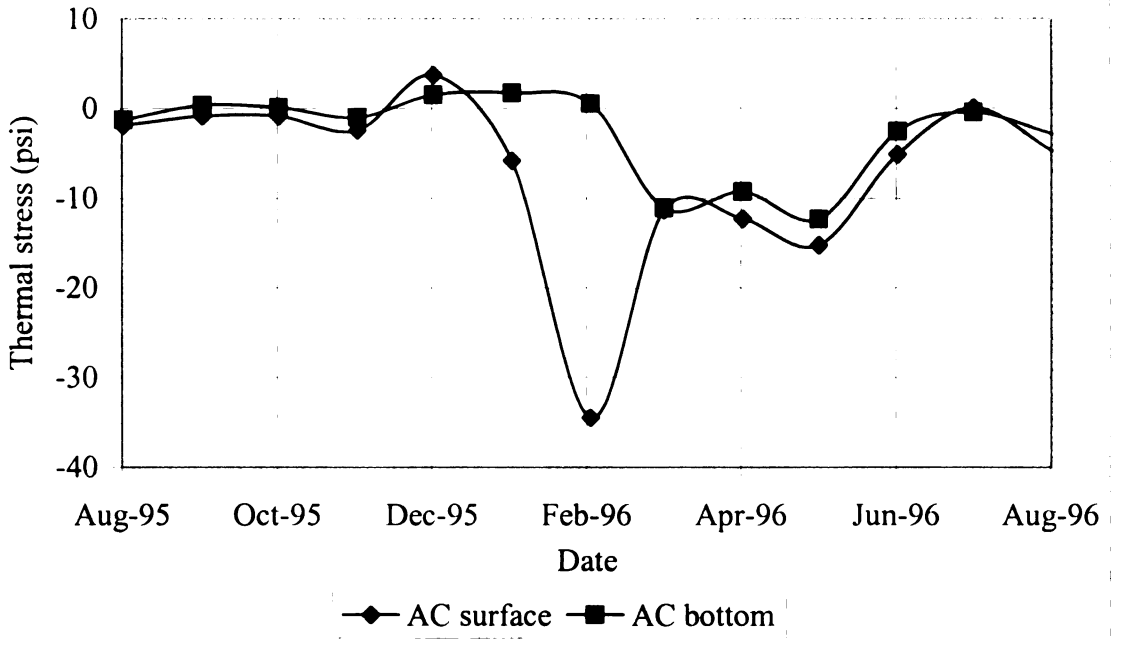


b) Thermal stresses around 2:20 PM

Figure 7.6 Variation in the thermal stresses throughout one year calculated around 8:30 AM and 2:20 PM (US-23, Alpena, MI)

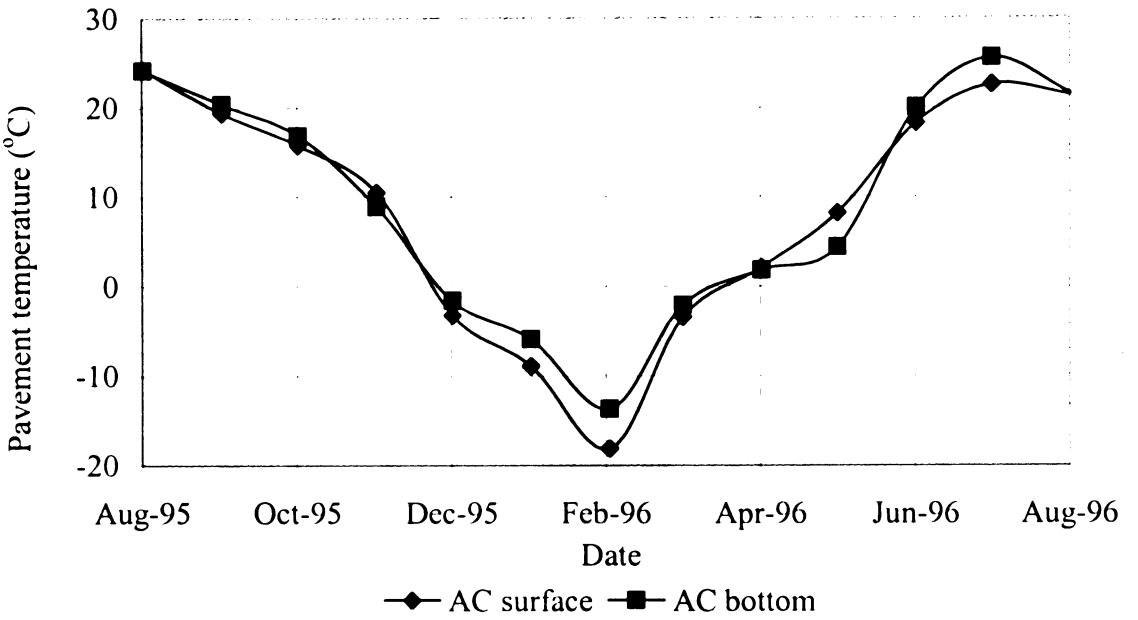


a) Pavement temperatures around 8:30 AM

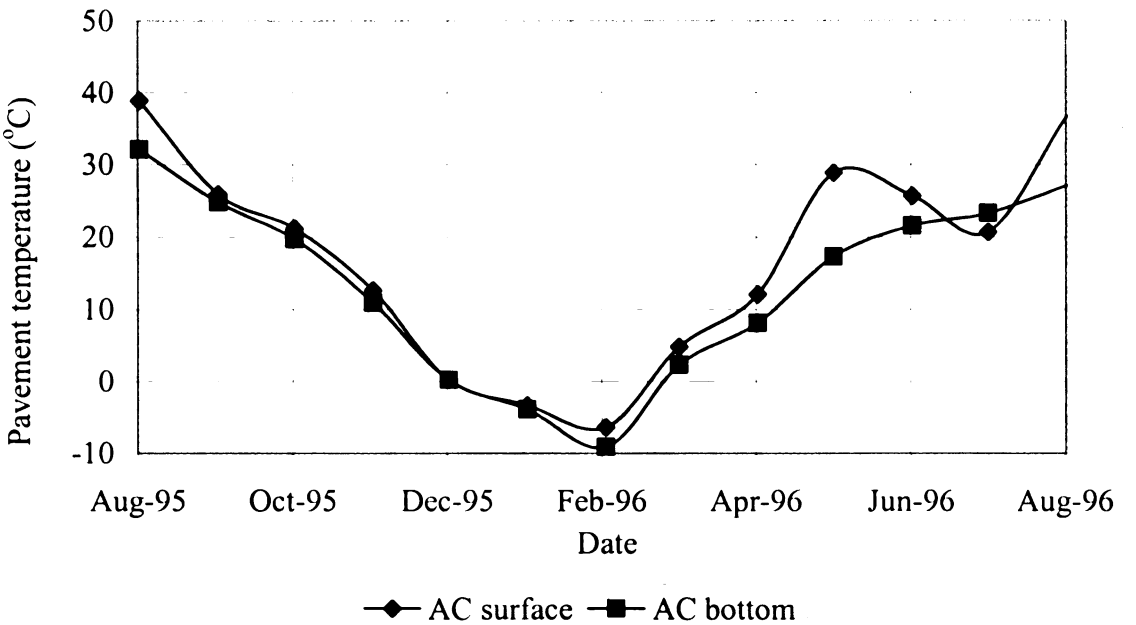


b) Pavement temperatures around 2:20 PM

Figure 7.7 Variation of the pavement temperatures around 8:30 AM and 2:20 PM throughout one year (US-23, Alpena, MI)

Table 7.4 The thermal stresses at the AC surface and at the AC bottom of five pavement sections in MI on February 2nd, 1996

| Pavement sections | Time (am) | Temperature (°C) | | Thermal stresses (psi) | | Thermal stress ratio | AC thickness (in.) | Difference between AC surface and AC bottom | | |
|---|---|---|---|---|---|---|---|---|---|---|
| | | | | | | | | | Thermal stress | |
| | | AC Surface | AC bottom | AC Surface | AC bottom | | | Temperature (°C) | Magnitude (psi) | As percent of the AC surface stress |
| Farewell | 8:19 | -20.5 | -18.3 | 130.7 | 99.4 | 1.31 | 3 | -2.2 | 31.3 | 24.0 |
| Alpena | 8:26 | -18.1 | -13.7 | 109 | 62.5 | 1.74 | 6 | -4.4 | 46.4 | 42.6 |
| Brighton | 8:39 | -17 | -12.3 | 97.2 | 54.9 | 1.77 | 7 | -4.7 | 42.2 | 43.5 |
| Brevot | 8:33 | -22.5 | -16.6 | 161.5 | 80.3 | 2.01 | 10 | -5.9 | 81.2 | 50.3 |
| Deerton | 9:54 | -21.1 | -14.6 | 121.5 | 53.6 | 2.27 | 12 | -6.5 | 67.9 | 55.9 |

five pavement sections, the thermal stress ratio between the top and the bottom of the AC layer, the temperature difference, the absolute difference in thermal stress at the top and bottom of the AC layer and the difference in stress as percent of the thermal stress at the pavement surface. Figure 7.8 depicts the stress ratio as a function of the AC layer thickness. Examination of the data in Table 7.4 and Figure 7.8 indicates that:

- For each pavement section, the lowest pavement surface temperature occurs during the morning of February 2, 1996.
- The ratio between the thermal stresses induced at the top and at the bottom of the AC layer increases as the AC thickness increases. This was expected because, at certain time of the day, higher AC thickness causes higher difference in temperatures between the top and the bottom of the AC layer.

One important point should be noted herein is that given the differential thermal stress between the top and the bottom of the AC layer and the high AC modulus at low temperatures, it is likely that the AC layers are subjected to curling during low temperatures. Finally, the findings of this chapter regarding the magnitudes and variations of thermal stresses induced at the AC surface and bottom are used in Chapter 8 for the calculation of the stress ratios.

## 5.0 SUMMARY

In this chapter, thermal stresses at the AC surface and the AC bottom were presented and discussed. Daily and yearly variations in the temperature data and the corresponding variations in thermal stresses were presented. It is shown that the thermal tensile stress at the AC surface is higher than that at the AC bottom.

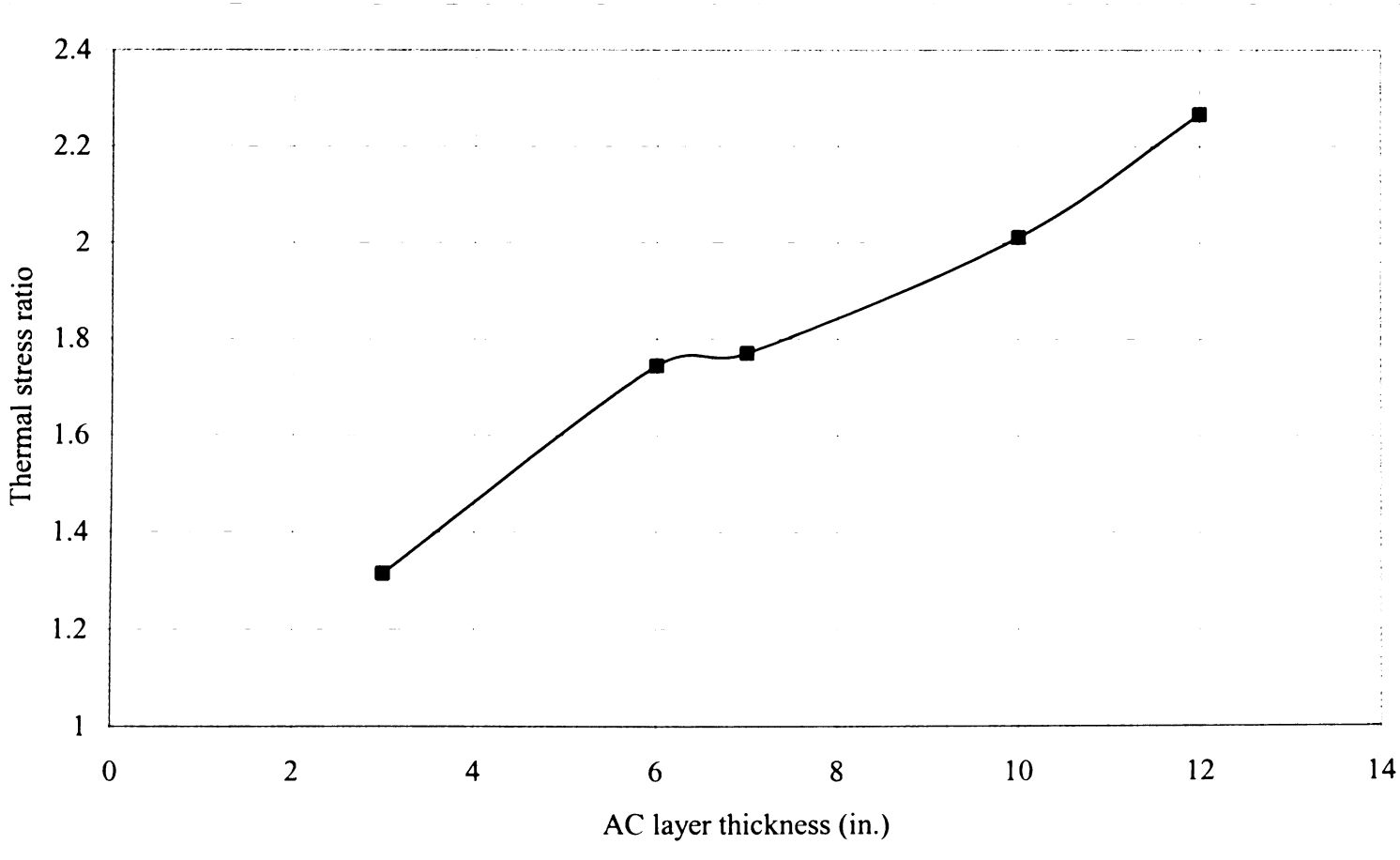


Figure 7.8 Thermal stress ratios between the top and the bottom of the AC layer versus the thickness of the AC layer

# CHAPTER 8

# MECHANISTIC ANALYSES OF LAOD-INDUCED STRESSES AT THE AC SURFACE AND AT THE AC BOTTOM

## 1.0 INTRODUCTION

In this study, all mechanistic analyses were conducted based on field and laboratory data, results of the backcalculation of layer moduli (see Chapter 6) and available information in the literature. The goal of the mechanistic analyses is to verify the hypotheses and to achieve the following objectives of this dissertation (Note that the full set of objectives is stated in Chapter 1):

1. Assess the sensitivity of top-down and bottom-up fatigue cracking potentials to the various causes of top-down cracks (TDC) and to their interactions.
2. For rubblized pavements only, assess the sensitivity of fatigue cracking potential to the outputs of the rubblization operation (the geometry of the interface between the rubblized material (RM) and the fractured concrete (FC) layers, and the thicknesses and moduli of the two layers).
3. Compare the potentials of crack initiation at the top and at the bottom of the AC layer using stress ratio.

The term "stress ratio" in the third objective refers to the ratio of the induced tensile stress to the tensile strength of the AC mix. Such ratio is thought to express the fatigue cracking potential better than the traditionally used tensile strain. Relative to the latter, many researchers have developed fatigue cracking models using the tensile strain (Huang, 1993, Yoder and Witczak, 1975). Such models indicate that higher tensile strain causes shorter fatigue life. The models however do not discriminate between high or low

viscosity AC binders or the high strain caused by high temperatures. Higher temperatures cause higher tensile strain but not necessarily shorter fatigue life. Indeed, in hot environment, rutting is the dominant distress in flexible pavements rather than fatigue cracking. Further, the AC mix properties and condition such as coarse, fine, dry and fat mixes, and segregation are not directly accounted for in the tensile strain models. Another advantage of evaluating the cracking potential using the stress ratio concept is that, some factors affect both the radial tensile stress and the tensile strength of the AC. Such factors include the AC mix design and temperature. Hence, the stress ratio can is a better indicator of fatigue cracking potential.

The induced tensile stresses in the AC layer, they can be divided into thermal tensile stresses and load-induced tensile stress. The former are calculated equation based on the viscoelastic properties of the AC mix (see Chapter 7). The latter are calculated using two-and three-dimensional (2-D and 3-D) analyses, which are presented and discussed in this chapter.

## 2.0 COMPUTER PROGRAMS USED IN THE MECHANISTIC ANALYSES

The load-induced horizontal tensile stresses at the top and at the bottom of the AC layer were analyzed using the following 2-D and 3-D computer programs:

- **CHEVRONX** – The CHEVRONX computer program provide a closed-form solution to linear elastic layer systems. The program is capable of calculating the stresses, strains and displacements of up to 5-layer pavement system subjected to a single wheel load.

- **MICHPAVE** - A 2-D finite element program capable of calculating the stresses, strains and displacements of up to 6-layer pavement system subjected to a single wheel load. In this study, the solution is based on linear elastic material properties although the program is capable of utilizing the non-linear material properties as well.
- **ABAQUS** - A multi-purpose finite element program capable of calculating the stresses, strains and displacements of multi-layer systems subjected to various load configurations and having a multitude of boundary conditions.

The assumptions, limitations and boundary conditions (degrees of freedom applied at the edges and at the bottom of the finite element model, the applied stresses and the tire-pavement contact area) used in the analyses of each of the three programs are listed in Table 8.1. As can be seen, the boundary conditions used in the three computer programs employed in this study are not the same.

The dimensions of the pavement models used in the programs are as follows:

- CHEVRONX – The pavement model is semi infinite with unlimited extents in the horizontal directions.
- MICHPAVE - The radius of the pavement model is 80.3 in., which is equal to 15 times the 5.35 in radius of the contact area. The total thickness of the pavement model including the roadbed soil (RB) is equal to 100 in.
- ABAQUS – The width and length of the full pavement model is 150 in. Like in MICHPAVE, the thickness of the model is 100 in.

To assess the impact of the boundary conditions and model dimensions and to compare the results of the three computer programs, several pavement cross-sections

Table 8.1 Assumptions used in the analyses and limitations of the CHEVRONX, MICHPAVE and ABAQUS programs

| Items | Assumptions | | |
|---|---|---|---|
| | CHEVRONX<br>A closed-form solution program | MICHPAVE<br>A 2-D finite element program | ABAQUS<br>A finite element program |
| Layer Interface | Full continuity (no slippage between the interfaces are allowed) | | |
| | Even interfaces | | Even and uneven interface |
| Symmetry | Axisymmetry around the z-axis (vertical axis) | | 2 planes of symmetry perpendicular to the x- and z-axes |
| Material properties | Linear elastic isotropic and homogeneous | | |
| Model dimensions | Infinite extent in horizontal direction | Finite width and thickness with special elements simulating infinitely deep roadbed soil | Finite width and thickness |
| | Infinite thickness for the bottom layer | | |
| Limitations | | | |
| Number of layers | 5 | 6 | Unlimited |
| Analyses types | Closed-form solution | 2-D analyses (Axisymmetry) | 3-D analysis |
| Boundary conditions | | | |
| At the walls of the model | No restraint | No displacement in the radial direction (perpendicular to the wall). | No displacement in the direction perpendicular to the planes of symmetry |
| | | | The other two walls have no restraint |
| At the bottom | No stress and displacement in all directions | No displacement in all directions | No displacement in all directions |
| At the surface | Free of shearing stress | No restraint | No restraint |
| Contact area | Circular, continuous and co-centered with the axis of symmetry | Circular, continuous and co-centered with the axis of symmetry | Circular and rectangular areas, w/ or w/o gaps, at various locations |
| Contact stress | Uniformly distributed vertical contact stress | Uniformly distributed vertical contact stress | Vertical, lateral and longitudinal contact stresses having uniform and/or non-uniform distributions |

consisting of 4 pavement layers and the RB were analyzed. In all analyses, 9,000-lb single wheel load and tire pressure of 100 psi were used. Various dimensions of the finite element models in MICHPAVE and ABAQUS were used in the analyses. Figure 8.1 depicts the results of the analyses for the smallest horizontal dimensions (80.3-in radius for MICHPAVE and 75-in width for ABAQUS) and for 100-in thick finite element models used in the analyses. The results indicate that despite the different boundary conditions at the edges and at the bottom of the models and the different model dimensions, the load-induced radial tensile stresses at the top and at the bottom of the AC layer calculated using the three programs are practically the same.

It should be noted that the assumptions of full continuity at the interfaces, and homogeneous and isotropic materials used in the analyses may not perfectly simulate field conditions. Therefore, the calculated stresses and strains in the AC layer could be different from those induced in the pavements. Since the results were used to compare the stresses at the top and bottom of the AC layer; the impact of said assumption is likely insignificant.

Finally, because of its robustness and its capability to analyze 6-layer systems, the MICHPAVE program was used in the 2-D analyses to assess the impacts of the pavement layers and roadbed soil properties on the stresses induced in the AC layer. The ABAQUS program was used in the 3-D analyses because of its capability to model the uneven interface between the RM and the FC layer, the tire-pavement interaction and dual wheels. Details of the 2- and 3-D analyses are presented in the sections below.

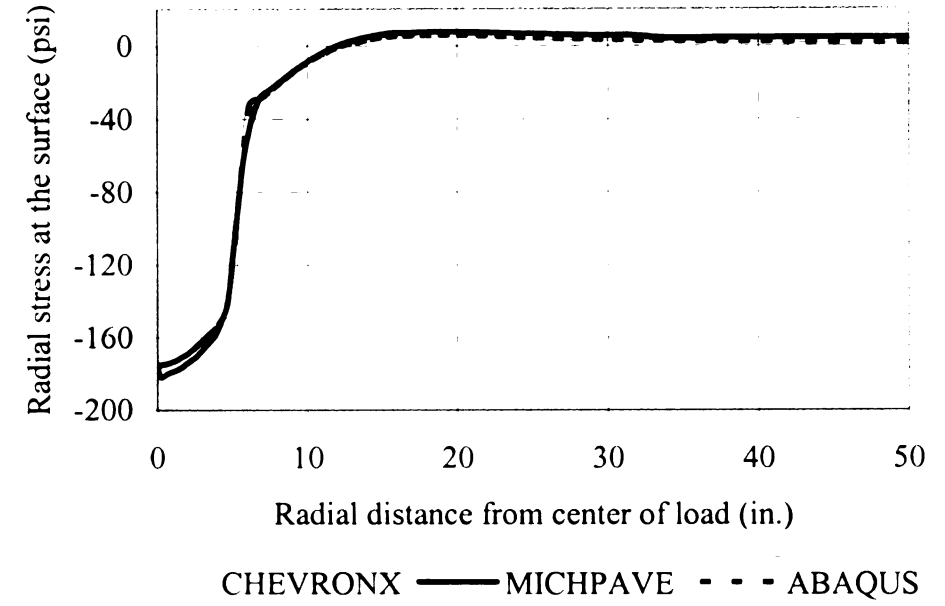


a) At the top of the AC layer

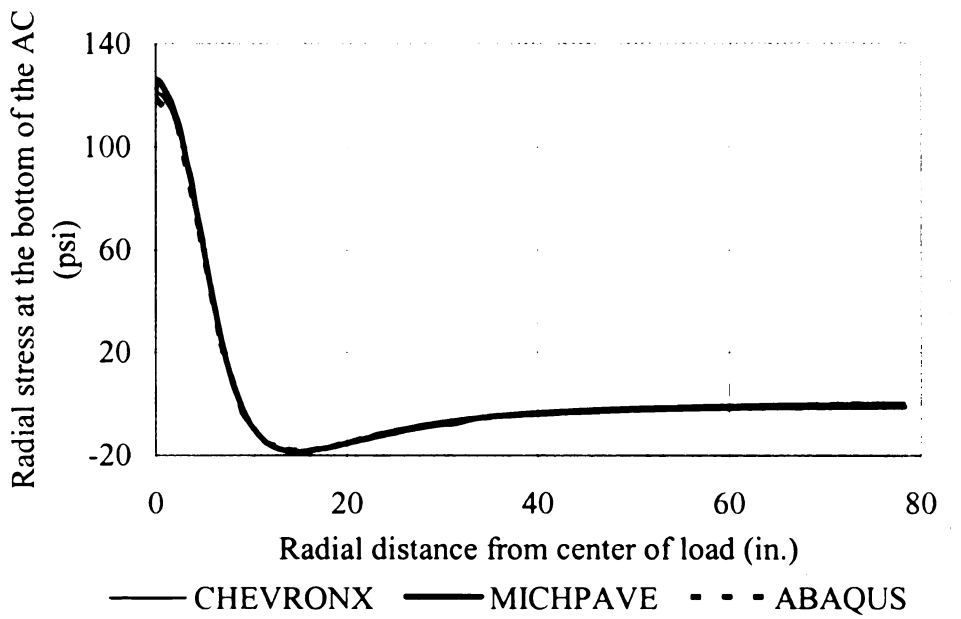


b) At the bottom of the AC layer

Figure 8.1 Comparison of the radial stresses at the top and at the bottom of the pavement obtained from the CHEVRONX, MICHPAVE and ABAQUS computer programs

## 3.0 MECHNAISTIC ANALYSES

Mechanistic analyses of the load-induced radial tensile stresses at the surface and at the bottom of the AC layer to various factors were conducted using 2-D and 3-D analyses. First, based on the literature review, three important points should be noted as follows:

1. The effects of the lateral contact stresses on the load-induced radial tensile stresses are independent of the pavement structure (Meyers et al, 1998).
2. The effects of the vertical load (or vertical contact stress) on the radial tensile stresses are dependent on the pavement structure (Molenaar, 1984, Gerritsen et al, 1987 and Myers et al, 1999).
3. The load-induced radial tensile stresses due to vertical, lateral and longitudinal contact stresses can be analyzed independently and the results could be combined using superposition (Soon, 2003) (see also section 5.0).

Based on these three points, the sensitivity of the load-induced radial tensile stresses due to the vertical contact stresses at the top and at the bottom of the AC layer to the pavement structure was analyzed using 2-D analyses. The results were used as a guideline to determine the critical pavement cross-sections that have potentials for high load-induced tensile stresses at the AC surface and at the AC bottom. These results were used to decrease the number of pavement sections to be included in the 3-D analyses. Finally, the 3-D analyses were conducted to assess the sensitivity of the load-induced radial tensile stresses in the AC layer to tire-pavement interaction and other parameters such as moduli and thicknesses of the pavement layers and the geometry of the interface between the RM and the FC layers in rubblized pavements.

## 4.0 TWO-DIMENSIONAL FINITE ELEMENT ANALYSES

The partial factorial matrix and the range of the values of the independent variables used in the analyses as well as the results of the analyses are presented and discussed in this section.

### 4.1 Partial Factorial

Because of the large number of variables involved in this study, partial factorial matrices were developed whereby the individual and the combined effects of these variables can be analyzed. The following variables were included in the 2-D analyses using the MICHPAVE computer program:

1. The AC surface course (ACS) modulus;
2. The AC base course (ACB) modulus and thickness;
3. The rubblized material (RM) thickness and modulus;
4. The fractured concrete (FC) modulus;
5. The combination of base and subbase (BS) modulus; and
6. The roadbed soil (RB) modulus.

In the analyses, the vertical load, the tire inflation pressure (vertical contact stress) and the thickness of the ACS were held at constant values of 9,000 pounds, 100 psi and 1.5 in., respectively. The general pavement model used in the 2-D sensitivity analyses is illustrated in Figure 8.2. The model consists of 6 layers; ACS, ACB, RM, FC, BS and RB. Table 8.2 provides the thicknesses and material properties of each layer used in the analyses. The range of the values of each variable listed in the tables represents the properties of rubblized, flexible and composite pavement sections.

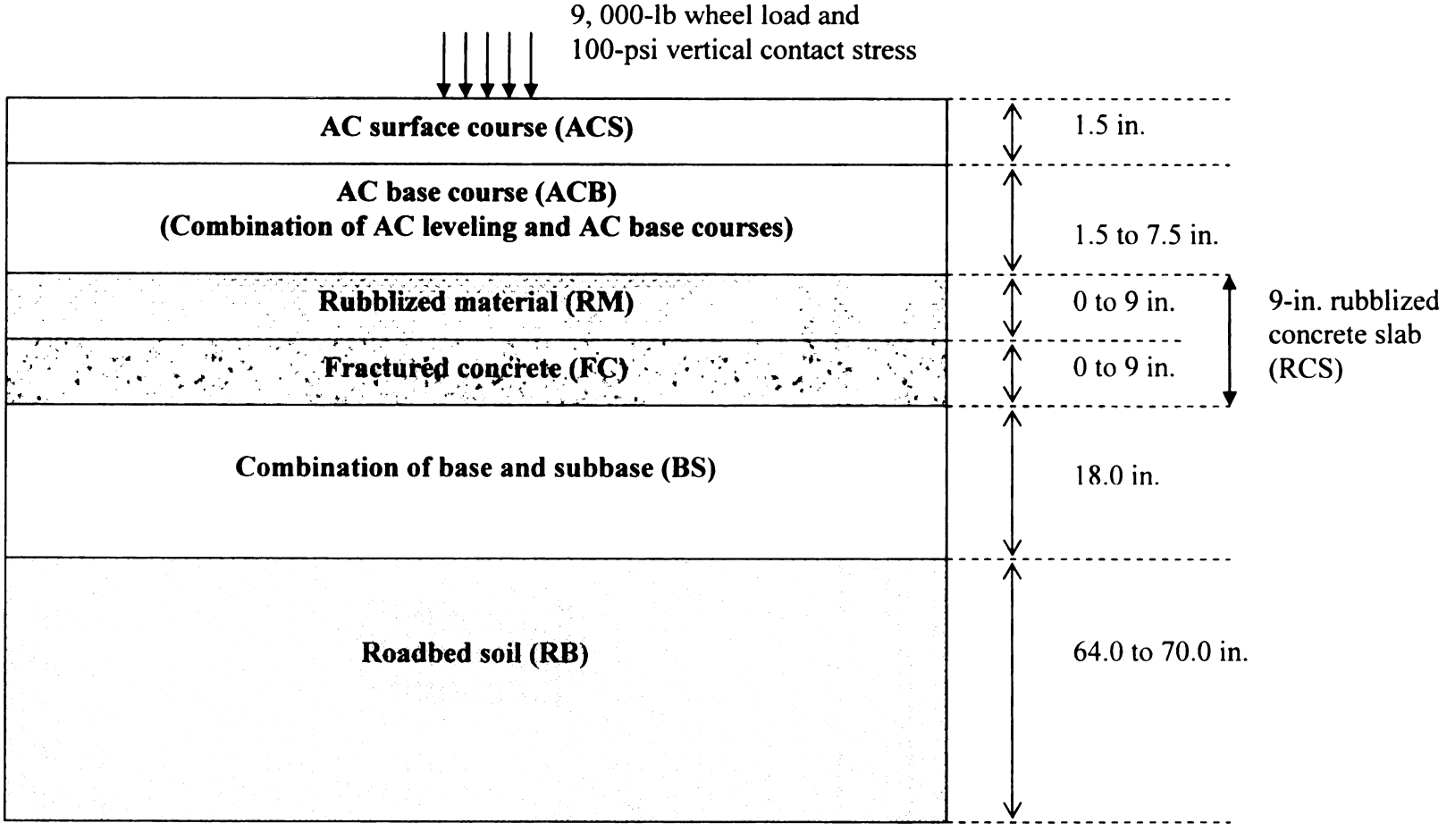


Figure 8.2 The pavement model used in the 2-D MICHPAVE analyses

Table 8.2 The range of pavement cross-sections and material properties used in the 2-D partial factorial sensitivity analyses

| AC courses/ Layers | Thickness (in.) | Modulus (ksi) | Poisson's ratio |
|---|---|---|---|
| AC surface course | **1.5** | 100, 300, **500**, 2000 | **0.3** |
| AC base course | 1.5, 2.5, **4.5**, 7.5 | 100, 300, **500**, 2000 | **0.3** |
| Total AC | 3, 4, **6**, 9 | | |
| Rubblized material | 0, 3, **5**, 7, 9 | 15, **30**, 50, 100 | 0.2, **0.4** |
| Fractured concrete | 9, 6, **4**, 2, 0 | 100, **500**, 1000, 2500 | **0.2** |
| Combination of base and subbase | **18** | 10, 20, **30**, 50 | **0.40** |
| Roadbed soil | 64, **67**, 69, 70 | 3, 5, **10**, 20 | **0.45** |

Note

1. The bolded and underlined figures represent the datum value of each variable.
2. The 0.2-Poisson's ratio was applied only to the rubblized material with the modulus of 100-ksi.
3. The thickness of the roadbed soil varies from one case to another to keep the total thickness of the finite element model at 100 in.

For example, when the RM thickness is set at 9 in. and its modulus at 30 ksi, the pavement section represents a conventional flexible pavement. On the other hand, when the FC thickness and modulus were set at 9 in. and 2,500 ksi, the pavement section represents a composite pavement. Further, the variations in the AC thicknesses represent pavements from low to heavy truck traffics and the variations in the moduli of the AC courses represent the effects of several factors including temperature, temperature gradient, aging, and the AC mix design. The ACS thickness was kept constant at 1.5 in. to model most state highway agency practices. Note that, the bolded and underlined figures in the table represent the datum values of each variable. In the analyses, when the effects of the variables on the induced radial stresses are analyzed, the values of the other variables were held at their datum values. Results of the analyses are presented in the next section.

## 4.2 Results of the 2-D Analyses

Table 8.3 provides the results of the partial factorial 2-D sensitivity analyses of 87 pavement sections including:

1. The varied pavement layers properties and/or RB moduli in each analysis.
2. The magnitudes of the radial stresses induced at the AC surface at the tire center and at the AC bottom under the tire center.
3. The magnitudes and locations of the maximum radial tensile stresses induced at the AC surface.
4. The magnitudes of the radial stresses induced at the AC surface at the tire edge (5.4-in. from the tire center).

Table 8.3 Results of the sensitivity analyses of the effects of the indicated properties on the radial stresses induced in the AC layer

| No. | AC surface course | | AC base course | | Radial stress at the tire center (psi) | | Maximum radial surface tensile stress | | Radial surface stress at the tire edge (psi) |
|---|---|---|---|---|---|---|---|---|---|
| | T (in.) | E (ksi) | T (in.) | E (ksi) | At the AC surface | At the AC bottom | Radial distance (in.) | Magnitude (psi) | |
| 1 | 1.5 | 100 | 4.5 | 100 | -106.3 | 36.8 | 6.7 | 7.8 | -19.8 |
| 2 | 1.5 | 100 | 4.5 | 300 | -89.7 | 98.6 | 14.7 | 3.9 | -24.0 |
| 3 | 1.5 | 100 | 4.5 | 500 | -81.2 | 136.8 | 15.6 | 3.2 | -23.7 |
| 4 | 1.5 | 100 | 4.5 | 2000 | -60.7 | 266.3 | 24.5 | 1.5 | -18.9 |
| 5 | 1.5 | 300 | 4.5 | 100 | -183.7 | 36.3 | 8.5 | 16.0 | -32.0 |
| 6 | 1.5 | 300 | 4.5 | 300 | -150.1 | 92.2 | 15.6 | 6.6 | -43.9 |
| 7 | 1.5 | 300 | 4.5 | 500 | -135.9 | 127.1 | 17.4 | 6.2 | -45.0 |
| 8 | 1.5 | 300 | 4.5 | 2000 | -94.5 | 253.6 | 25.4 | 3.8 | -36.4 |
| 9 | 1.5 | 500 | 4.5 | 100 | -245.3 | 35.8 | 8.5 | 26.1 | -40.2 |
| 10 | 1.5 | 500 | 4.5 | 300 | -192.7 | 89.5 | 16.5 | 7.8 | -57.1 |
| 11 | 1.5 | 500 | 4.5 | 500 | -174.7 | 122.1 | 18.3 | 7.7 | -60.0 |
| 12 | 1.5 | 500 | 4.5 | 2000 | -122.5 | 243.9 | 27.2 | 5.6 | -51.1 |
| 13 | 1.5 | 2000 | 4.5 | 100 | -577.8 | 30.8 | 9.4 | 76.1 | -95.2 |
| 14 | 1.5 | 2000 | 4.5 | 300 | -398.3 | 82.1 | 16.5 | 15.0 | -109.1 |
| 15 | 1.5 | 2000 | 4.5 | 500 | -345.2 | 110.4 | 22.7 | 13.0 | -116.3 |
| 16 | 1.5 | 2000 | 4.5 | 2000 | -249.5 | 209.3 | 31.7 | 13.8 | -117.2 |
| 17 | 1.5 | 100 | 1.5 | 500 | -123.5 | 197.0 | 9.4 | 15.2 | -18.5 |
| 18 | 1.5 | 300 | 1.5 | 500 | -216.8 | 200.1 | 10.3 | 27.4 | -38.2 |
| 19 | 1.5 | 500 | 1.5 | 500 | -280.3 | 202.3 | 10.3 | 34.2 | -53.8 |
| 20 | 1.5 | 2000 | 1.5 | 500 | -574.7 | 192.8 | 11.2 | 66.1 | -129.9 |
| 21 | 1.5 | 100 | 2.5 | 500 | -105.8 | 189.8 | 11.2 | 8.8 | -23.9 |
| 22 | 1.5 | 300 | 2.5 | 500 | -183.6 | 177.9 | 12.0 | 15.7 | -46.8 |
| 23 | 1.5 | 500 | 2.5 | 500 | -236.0 | 173.5 | 12.0 | 18.9 | -63.5 |
| 24 | 1.5 | 2000 | 2.5 | 500 | -469.2 | 161.6 | 13.8 | 33.8 | -133.9 |
| 25 | 1.5 | 100 | 7.5 | 500 | -65.4 | 81.6 | 27.2 | 1.3 | -18.9 |
| 26 | 1.5 | 300 | 7.5 | 500 | -102.4 | 76.7 | 31.7 | 3.3 | -34.0 |
| 27 | 1.5 | 500 | 7.5 | 500 | -130.5 | 73.8 | 31.7 | 4.7 | -45.0 |
| 28 | 1.5 | 2000 | 7.5 | 500 | -261.0 | 65.9 | 49.1 | 10.7 | -85.1 |
| 29 | 1.5 | 500 | 1.5 | 100 | -301.3 | 43.8 | 8.5 | 57.1 | -26.5 |
| 30 | 1.5 | 500 | 1.5 | 300 | -285.0 | 139.7 | 9.4 | 38.0 | -45.8 |
| 31 | 1.5 | 500 | 1.5 | 2000 | -255.9 | 483.6 | 12.0 | 27.8 | -67.3 |
| 32 | 1.5 | 500 | 2.5 | 100 | -279.6 | 44.3 | 8.5 | 42.1 | -35.6 |
| 33 | 1.5 | 500 | 2.5 | 300 | -247.3 | 123.2 | 11.2 | 21.1 | -56.7 |
| 34 | 1.5 | 500 | 2.5 | 2000 | -191.1 | 391.1 | 15.6 | 13.9 | -67.7 |
| 35 | 1.5 | 500 | 7.5 | 100 | -218.4 | 23.0 | 7.6 | 21.6 | -35.6 |
| 36 | 1.5 | 500 | 7.5 | 300 | -151.3 | 55.3 | 31.7 | 4.6 | -45.4 |
| 37 | 1.5 | 500 | 7.5 | 2000 | -84.2 | 132.4 | 47.3 | 3.4 | -32.3 |

The thicknesses (T) and moduli (E) of the other pavement layers and the roadbed soil moduli used in the 2-D analyses are as the datum values reported in Table 8.2

Table 8.3 Results of the sensitivity analyses of the effects of the indicated properties on the radial stresses induced in the AC layer (continued)

| No. | Rubblized material | | Fractured concrete | | Radial stress at the tire center (psi) | | Maximum radial surface tensile stress | | Radial surface stress at the tire edge (psi) |
|---|---|---|---|---|---|---|---|---|---|
| | T (in.) | E (ksi) | T (in.) | E (ksi) | At the AC surface | At the AC bottom | Radial distance (in.) | Magnitude (psi) | |
| 38 | 5 | 15 | 4 | 500 | -195.0 | 153.5 | 20.1 | 12.0 | -72.4 |
| 39 | 5 | 50 | 4 | 500 | -159.4 | 96.9 | 18.3 | 4.4 | -51.6 |
| 40 | 5 | 100 | 4 | 500 | -138.5 | 54.3 | 59.8 | 4.6 | -42.4 |
| 41 | 3 | 15 | 6 | 500 | -176.7 | 131.8 | 17.4 | 8.2 | -59.9 |
| 42 | 3 | 30 | 6 | 500 | -158.4 | 102.3 | 58.0 | 4.3 | -49.8 |
| 43 | 3 | 50 | 6 | 500 | -145.4 | 79.8 | 61.6 | 4.4 | -43.6 |
| 44 | 3 | 100 | 6 | 500 | -130.9 | 44.5 | 63.3 | 4.7 | -38.3 |
| 45 | 7 | 15 | 2 | 500 | -206.3 | 166.1 | 21.0 | 14.3 | -80.8 |
| 46 | 7 | 30 | 2 | 500 | -184.7 | 133.5 | 20.1 | 10.0 | -66.9 |
| 47 | 7 | 50 | 2 | 500 | -168.1 | 106.8 | 19.2 | 6.6 | -57.4 |
| 48 | 7 | 100 | 2 | 500 | -143.0 | 60.0 | 58.0 | 4.5 | -45.3 |
| 49 | 9 | 15 | 0 | - | -214.1 | 175.3 | 22.7 | 15.9 | -87.0 |
| 50 | 9 | 30 | 0 | - | -192.6 | 143.2 | 21.9 | 11.7 | -72.9 |
| 51 | 9 | 50 | 0 | - | -175.8 | 116.0 | 21.9 | 8.3 | -63.1 |
| 52 | 9 | 100 | 0 | - | -148.1 | 66.4 | 47.3 | 4.5 | -49.0 |
| 53 | 0 | - | 9 | 500 | -103.0 | -9.9 | 63.3 | 4.7 | -29.6 |
| 54 | 0 | - | 9 | 1000 | -90.0 | -26.3 | 66.9 | 4.6 | -23.9 |
| 55 | 0 | - | 9 | 2500 | -76.4 | -35.1 | 6.7 | 6.5 | -16.4 |
| 56 | 3 | 30 | 6 | 100 | -173.8 | 119.3 | 20.1 | 7.4 | -60.2 |
| 57 | 3 | 30 | 6 | 1000 | -151.9 | 97.1 | 61.6 | 4.3 | -45.1 |
| 58 | 3 | 30 | 6 | 2500 | -142.8 | 91.6 | 12.9 | 5.5 | -38.0 |
| 59 | 5 | 30 | 4 | 100 | -182.2 | 130.9 | 20.1 | 9.4 | -65.3 |
| 60 | 5 | 30 | 4 | 1000 | -171.5 | 119.2 | 17.4 | 7.1 | -57.6 |
| 61 | 5 | 30 | 4 | 2500 | -165.9 | 115.3 | 16.5 | 7.0 | -53.2 |
| 62 | 7 | 30 | 2 | 100 | -188.0 | 138.0 | 21.0 | 10.8 | -69.4 |
| 63 | 7 | 30 | 2 | 1000 | -183.7 | 132.0 | 20.1 | 9.8 | -66.2 |
| 64 | 7 | 30 | 2 | 2500 | -182.1 | 130.3 | 19.2 | 9.5 | -65.0 |
| 65 | 5 | 15 | 4 | 100 | -200.3 | 159.2 | 21.0 | 13.1 | -76.4 |
| 66 | 5 | 15 | 4 | 1000 | -192.2 | 151.1 | 19.2 | 11.6 | -70.2 |
| 67 | 5 | 15 | 4 | 2500 | -187.1 | 147.2 | 18.3 | 11.5 | -66.0 |
| 68 | 5 | 50 | 4 | 100 | -168.7 | 108.0 | 21.0 | 6.7 | -58.1 |
| 69 | 5 | 50 | 4 | 1000 | -155.9 | 93.7 | 59.8 | 4.3 | -49.1 |
| 70 | 5 | 50 | 4 | 2500 | -150.4 | 90.0 | 59.8 | 4.3 | -45.0 |
| 71 | 5 | 100 | 4 | 1000 | -135.6 | 51.0 | 65.1 | 4.6 | -40.4 |
| 72 | 5 | 100 | 4 | 2500 | -131.7 | 48.2 | 65.1 | 4.6 | -37.5 |

The thicknesses (T) and moduli (E) of the other pavement layers and the roadbed soil moduli used in the 2-D analyses are as the datum values reported in Table 8.2

Table 8.3 Results of the sensitivity analyses of the effects of the indicated properties on the radial stresses induced in the AC layer (continued)

| No. | Base and subbase | | Roadbed soil | | Radial stress at the tire center (psi) | | Maximum radial surface tensile stress | | Radial surface stress at the tire edge (psi) |
|---|---|---|---|---|---|---|---|---|---|
| | T (in.) | E (ksi) | T (in.) | E (ksi) | At the AC surface | At the AC bottom | Radial distance (in.) | Magnitude (psi) | |
| 73 | 18 | 50 | 67 | 20 | -165.9 | 117.8 | 16.5 | 10.8 | -52.2 |
| 74 | 18 | 30 | 67 | 20 | -171.8 | 121.3 | 18.3 | 9.5 | -57.2 |
| 75 | 18 | 20 | 67 | 20 | -176.2 | 123.9 | 19.2 | 8.7 | -61.0 |
| 76 | 18 | 10 | 67 | 20 | -183.3 | 127.7 | 23.6 | 7.8 | -67.2 |
| 77 | 18 | 50 | 67 | 10 | -168.3 | 118.4 | 16.5 | 9.1 | -54.5 |
| 78 | 18 | 20 | 67 | 10 | -179.4 | 124.8 | 21.0 | 6.9 | -64.1 |
| 79 | 18 | 10 | 67 | 10 | -186.3 | 128.5 | 31.7 | 6.9 | -70.1 |
| 80 | 18 | 50 | 67 | 5 | -170.1 | 118.8 | 17.4 | 7.9 | -56.1 |
| 81 | 18 | 30 | 67 | 5 | -177.0 | 122.7 | 19.2 | 6.2 | -62.2 |
| 82 | 18 | 20 | 67 | 5 | -182.1 | 125.5 | 58.0 | 5.8 | -66.6 |
| 83 | 18 | 10 | 67 | 5 | -189.3 | 129.4 | 56.2 | 6.9 | -72.9 |
| 84 | 18 | 50 | 67 | 3 | -170.9 | 119.0 | 17.4 | 7.4 | -56.9 |
| 85 | 18 | 30 | 67 | 3 | -178.2 | 123.0 | 59.8 | 5.5 | -63.3 |
| 86 | 18 | 20 | 67 | 3 | -183.6 | 125.9 | 59.8 | 6.3 | -68.0 |
| 87 | 18 | 10 | 67 | 3 | -191.0 | 129.9 | 59.8 | 7.5 | -74.6 |

The thicknesses (T) and moduli (E) of the other pavement layers used in the 2-D analyses are as the datum values reported in Table 8.2

Examination of the data in Table 8.3 indicates that:

1. For most cases, the maximum radial tensile stresses induced in the AC layer due to the vertical contact stresses are located at the AC bottom under the tire center.
2. There are three cases where the radial stresses induced at AC bottom under the tire center are compressive stresses (negative numbers in Table 8.3). For these cases, the maximum radial tensile stresses at the AC surface are less than 7 psi and located farther away from the tire center. Since the stress magnitudes are not significant and are not likely to cause crack initiation, they are not reported in Table 8.3.
3. There are seven cases where the maximum radial tensile stresses at the AC surface is greater than 30 percent of those induced at the AC bottom under the tire center. The ratios between ACS and ACB moduli for those cases are equal to or greater than three, which can not be supported by field and lab data. Further, if the high modulus ratios were due to the lower temperatures at AC surface relative to the AC bottom, the lower temperatures at AC surface also result in higher tensile strengths. Said high tensile strengths reduce stress ratios or the potentials of the crack initiation at the AC surface. Hence it is unlikely that the stresses induced in the AC layer due to the vertical contact stresses could result in top-down cracks prior to bottom-up cracks.
4. The radial stresses induced at the AC surface at the tire edge due to vertical contact stresses are compressive stresses varying from -16.4 psi to -133.9 psi depending on the pavement layer properties and RB modulus.

Table 8.4 summarizes the effects of pavement layer properties and RB moduli on the radial stresses induced at the AC bottom under the tire center and at the AC surface at the tire edge. Figures 8.3 through 8.16 provide plots of the effect of each variable on said stresses. Based on the results of the 2-D analyses, the critical pavement cross-sections for bottom-up (fatigue) cracks are those having:

- Low AC thickness, low ACS modulus and high ACB modulus.
- Low modulus of one or more layers beneath the AC layer. This includes the RM and FC layers in rubblized pavements, the base layer in conventional flexible pavements, and the roadbed soil.
- High RM layer thickness.

The critical cross sections for relatively high TDC potential are those having:

- High ACS modulus.
- High modulus of one or more layers beneath the AC layer. This includes the RM and FC layers in rubblized pavements, the base layer in conventional flexible pavements, and the roadbed soil. Note that, the deeper is the layer relative to the AC layer, the less significant is its impact on the radial stress at the tire edge.
- Low RM layer thickness.

Further, the effects of the AC thickness and the ACB modulus on the radial stresses induced at the tire edge vary from one pavement section to another depending on the entire pavement structure.

To this end, the five reasons listed in Table 8.4 for the effect of each variable on the radial stresses induced in the AC layer are detailed in the sections below.

Table 8.4 A summary of the sensitivity of the radial stress at the surface at the tire edge and at the AC bottom under the tire center due to various variables (as the value of the variable increases)

| Variables | | Radial stress | | Reasons | |
|---|---|---|---|---|---|
| | | At the AC bottom under the tire center | At the AC surface at tire edge | At the AC bottom under the tire center | At the AC surface at tire edge |
| Total AC thickness | | T decreases | C increases or decreases * | 1 and 2 | 1, 2 and 3 |
| AC surface course modulus | | T decreases | C increases | 1 and 2 | 2 |
| AC base course modulus | | T increases | C increases or decreases * | 2 | 1, 2 and 3 |
| Rubblized concrete | Thickness | T increases | C increases | 2, 4 and 5 | 2, 4 and 5 |
| | Modulus | T decreases | C decreases | 2, 4 and 5 | 2, 4 and 5 |
| Fractured concrete modulus | | T decreases | C decreases | 2, 4 and 5 | 2, 4 and 5 |
| Subbase modulus | | T decreases | C decreases | 2 and 4 | 2 and 4 |
| Roadbed soil modulus | | T decreases | C decreases | 2 and 4 | 2 and 4 |
| C = compression, T = tension | | | | | |
| Reasons<br>1. Flexural rigidity of the AC layer<br>2. Stress-strain relationship (Hooke's law)<br>3. Stress dissipation<br>4. Stiffness of the support of the AC layer<br>5. Location of the neutral axis | | | | | |

Note

"*": The impact of the independent variable on the radial stress at the tire edge depends on the overall pavement layer properties, especially the AC layer properties

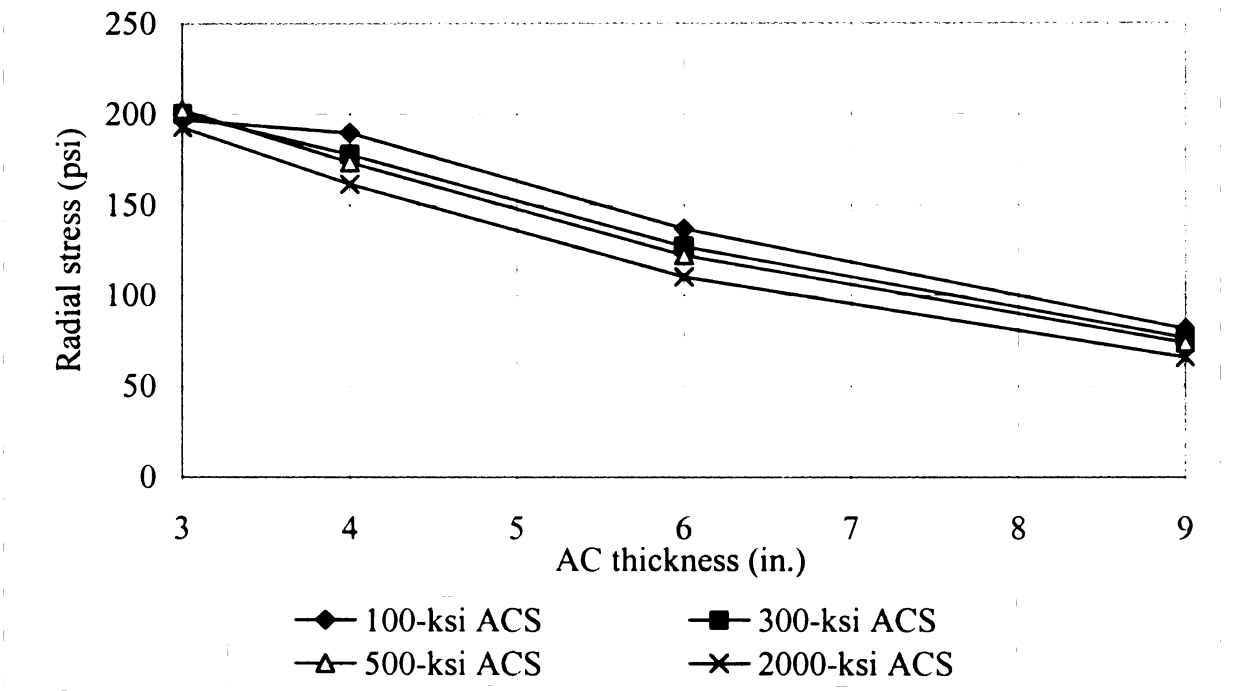


Figure 8.3 Radial tensile stresses at the AC bottom under the tire center versus the AC thicknesses for various AC surface course (ACS) moduli

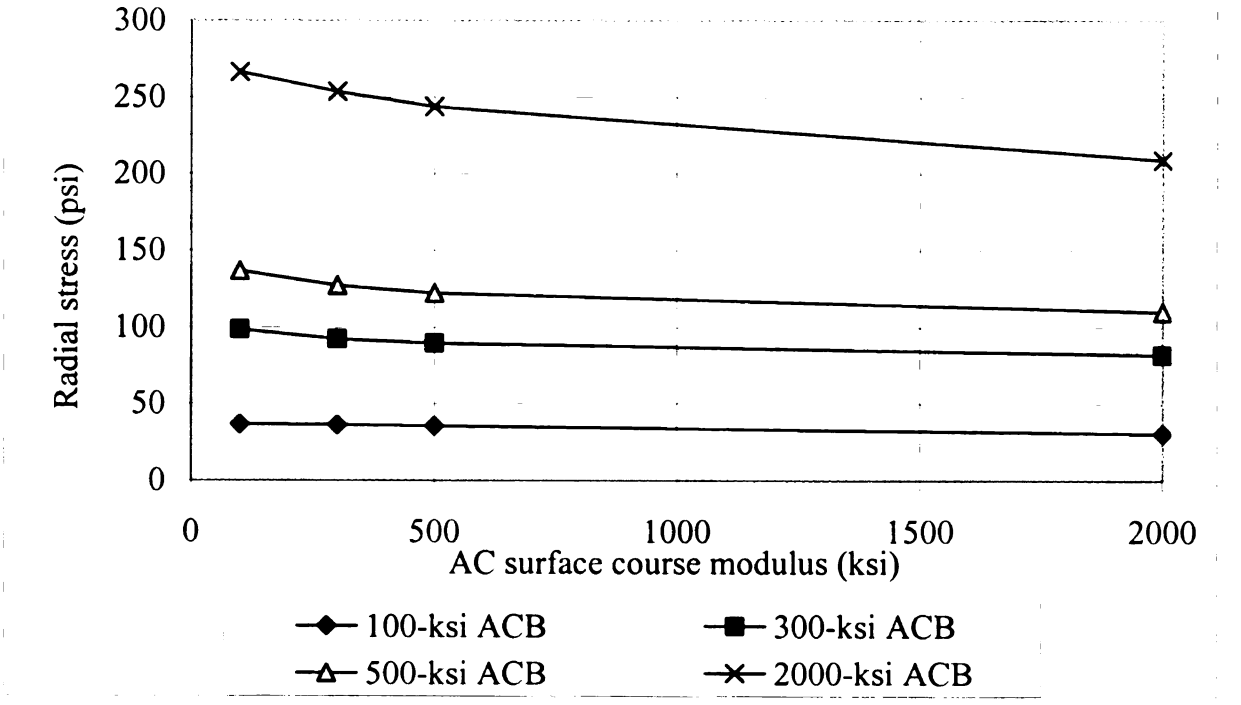


Figure 8.4 Radial tensile stresses at the AC bottom under the tire center versus the AC surface course moduli for various AC base course (ACB) moduli

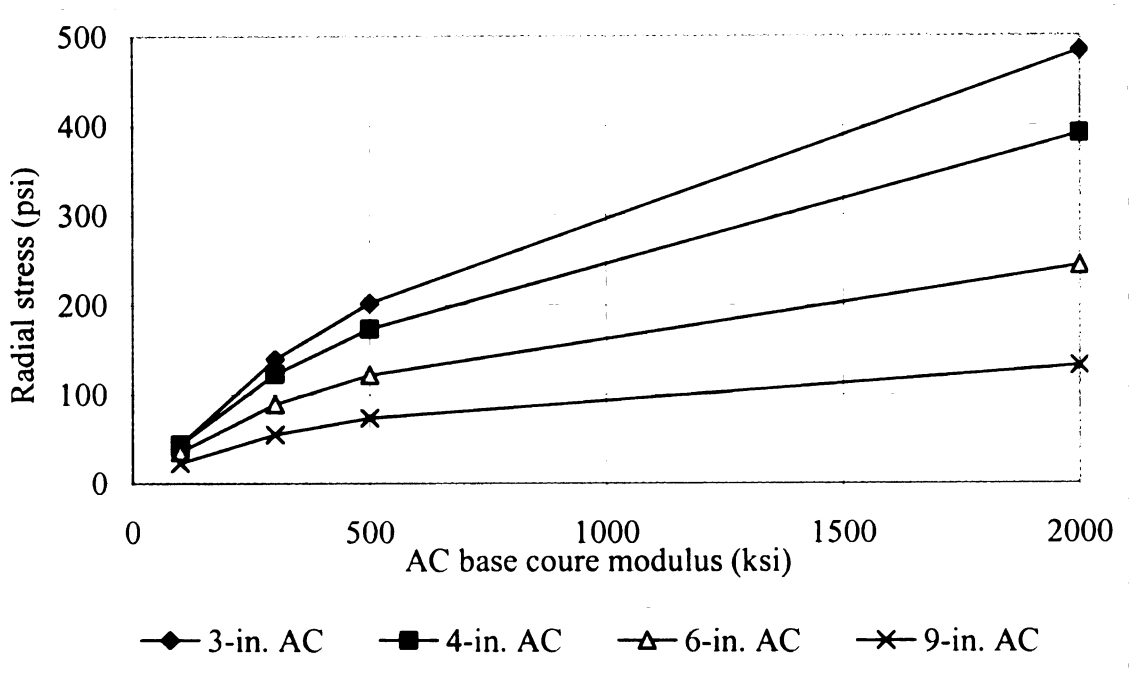


Figure 8.5 Radial tensile stresses at the AC bottom under the tire center versus the AC base course moduli for various AC thicknesses

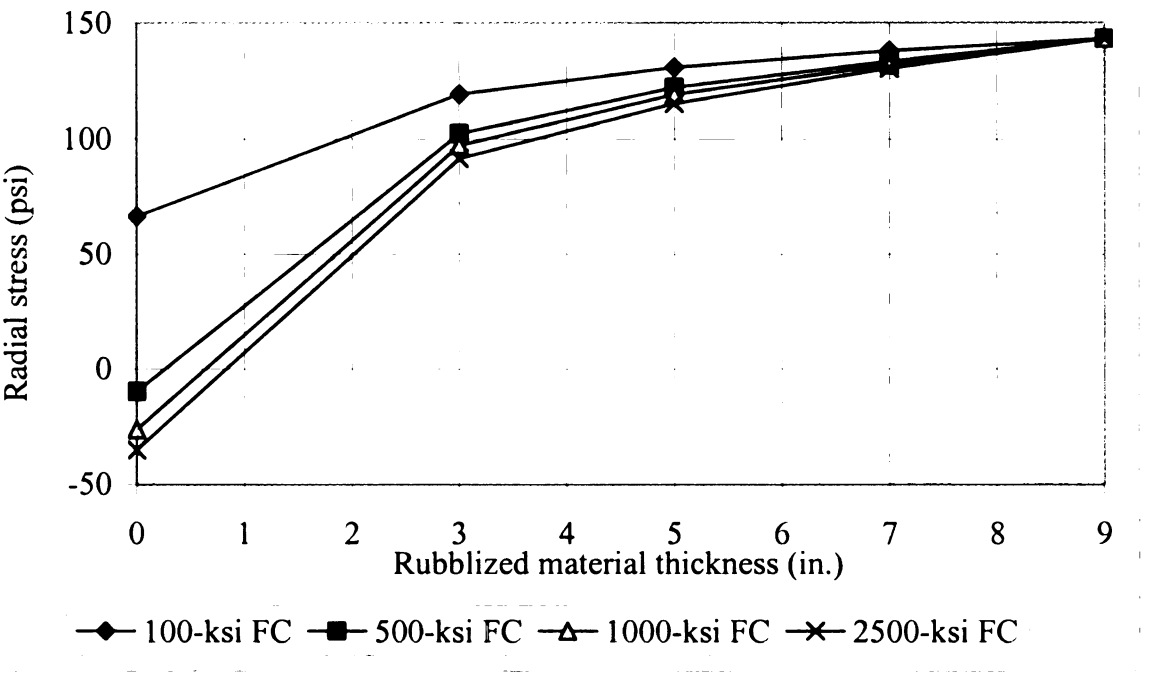


Figure 8.6 Radial tensile stresses at the AC bottom under the tire center versus the rubblized material thicknesses for various fractured concrete (FC) moduli

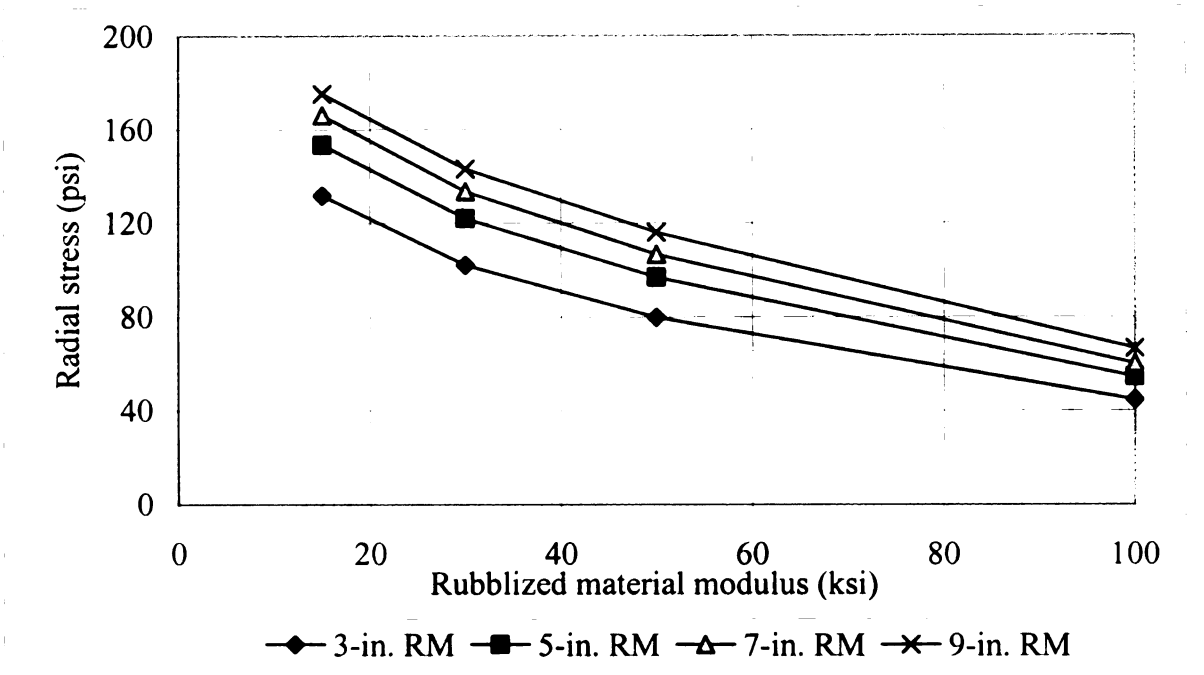


Figure 8.7 Radial tensile stresses at the AC bottom under the tire center versus the rubblized material (RM) moduli for various rubblized material thicknesses

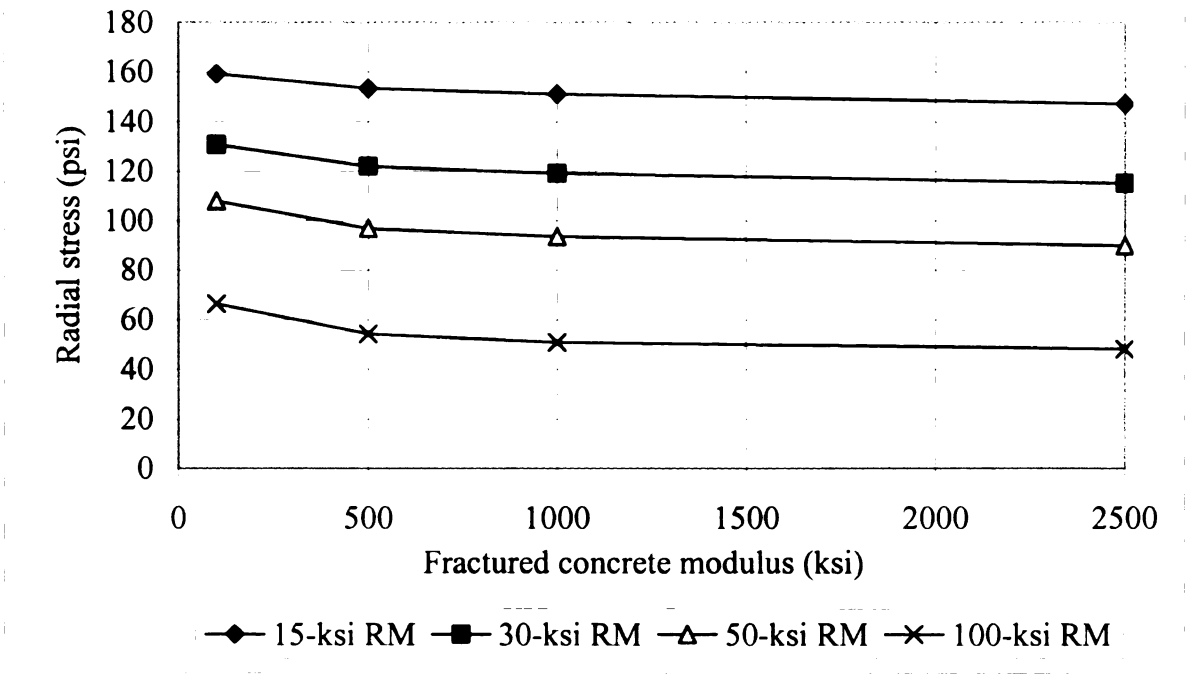


Figure 8.8 Radial tensile stresses at the AC bottom under the tire center versus the fractured concrete moduli for various rubblized material (RM) moduli

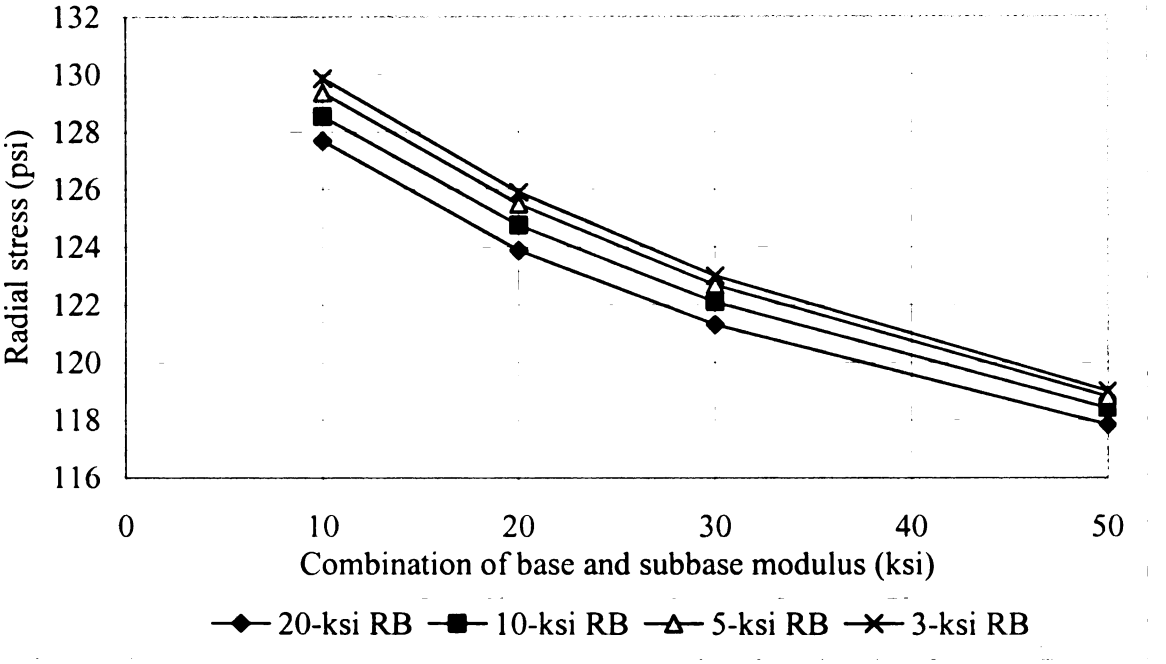


Figure 8.9 Radial tensile stresses at the AC bottom under the tire center versus the combination base and subbase moduli for various roadbed soil (RB) moduli

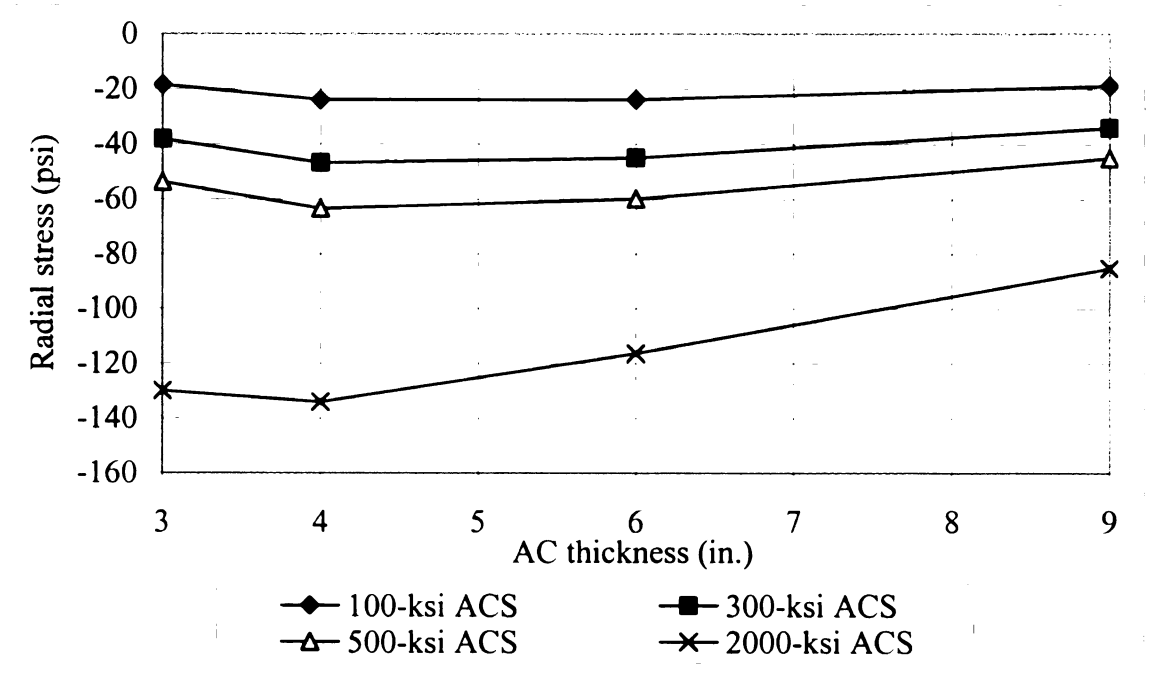


Figure 8.10 Radial tensile stresses at the AC surface at the tire edge versus the AC thicknesses for various AC surface course (ACS) moduli

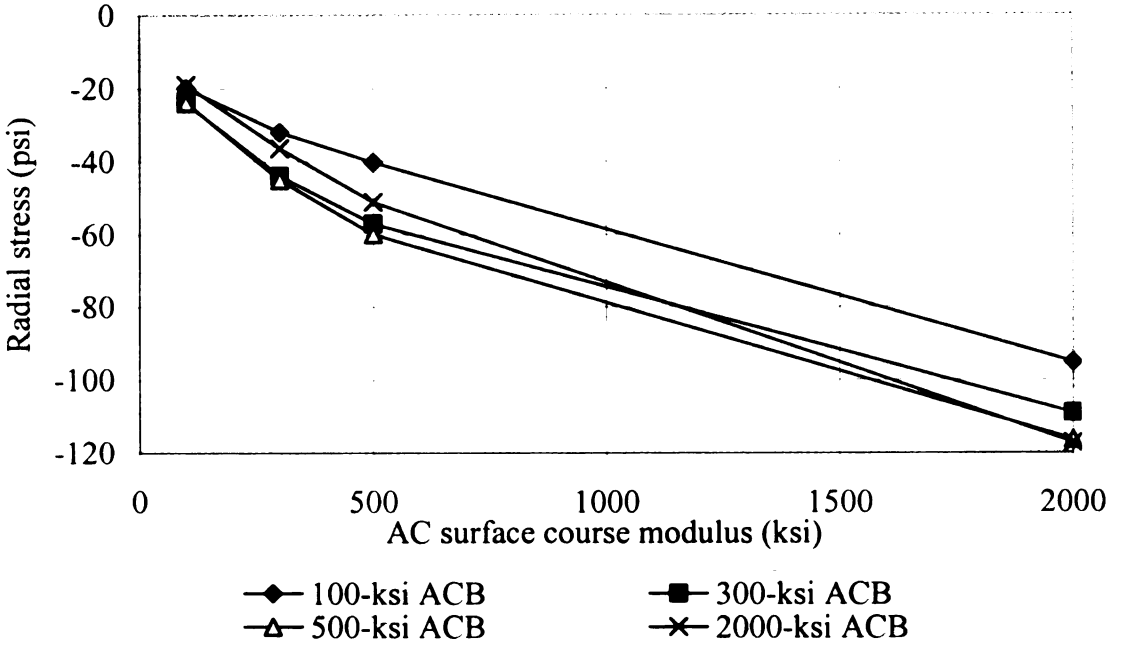


Figure 8.11 Radial tensile stresses at the AC surface at the tire edge versus the AC surface course moduli for various AC base course (ACB) moduli

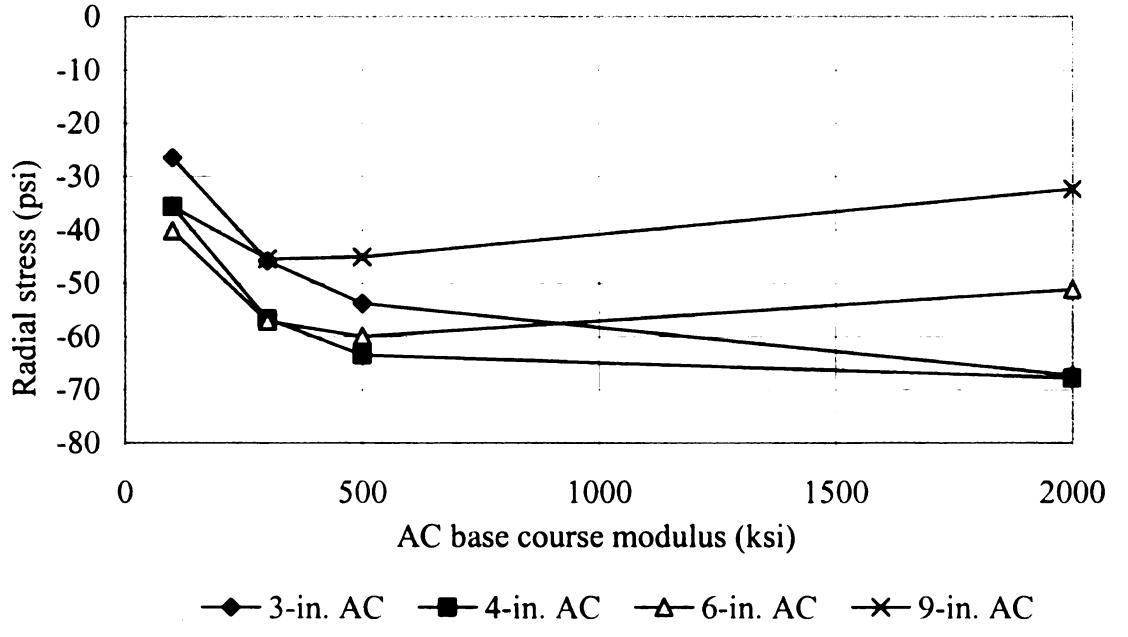


Figure 8.12 Radial tensile stresses at the AC surface at the tire edge versus the AC base course moduli for various AC thicknesses

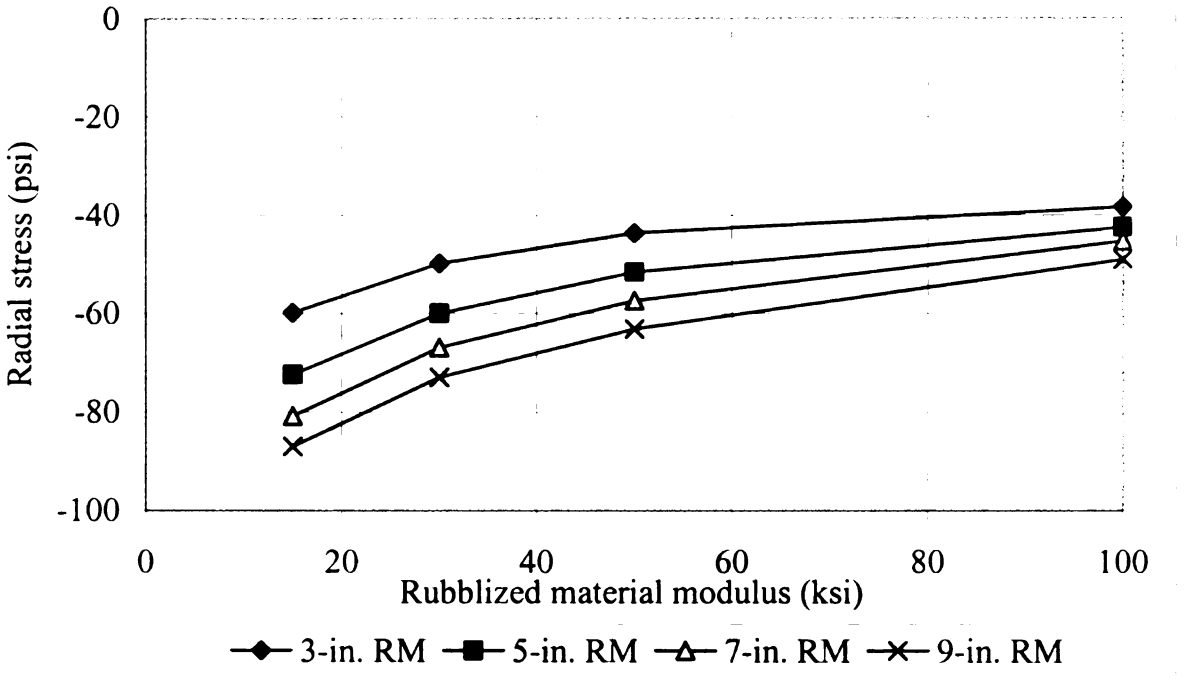


Figure 8.13 Radial tensile stresses at the AC surface at the tire edge versus the rubblized material (RM) moduli for various rubblized material thicknesses

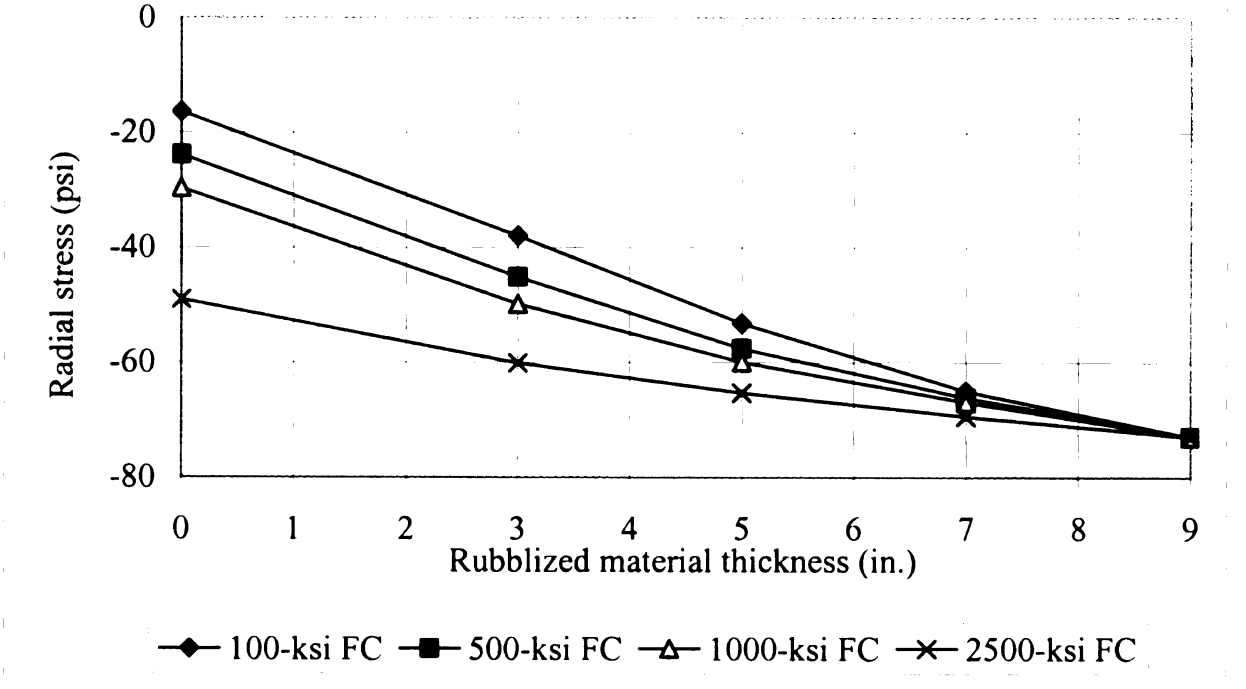


Figure 8.14 Radial tensile stresses at the AC surface at the tire edge versus the rubblized material thicknesses for various fractured concrete (FC) moduli

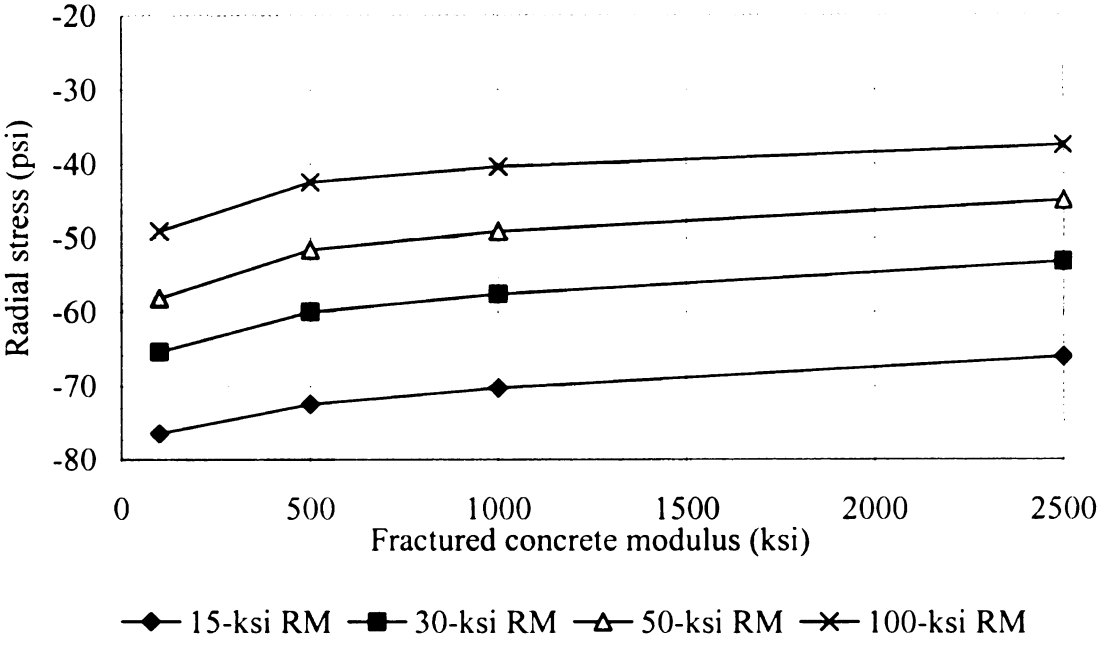


Figure 8.15 Radial tensile stresses at the AC surface at the tire edge versus the fractured concrete moduli for various rubblized material (RM) moduli

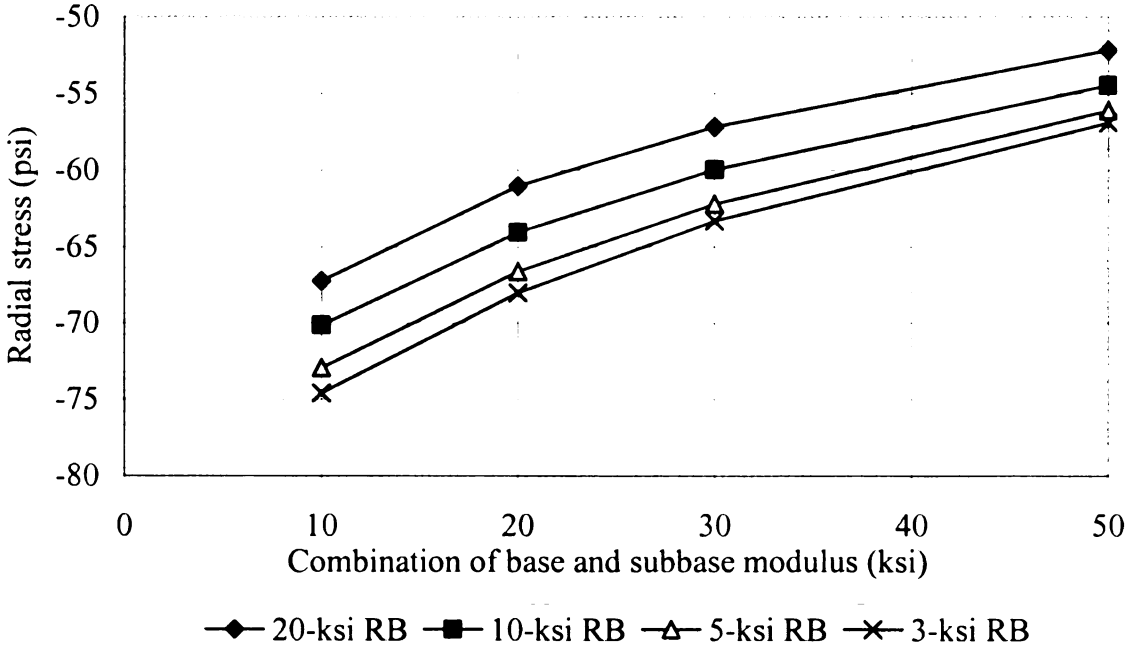


Figure 8.16 Radial tensile stresses at the AC surface at the tire edge versus the combination of base and subbase moduli for various roadbed soil (RB) moduli

### 4.2.1 Flexural Rigidity of the AC Layer

As an analogy to an elastic beam, the flexural rigidity of the AC layer is defined as the multiplication of the elastic modulus and the moment of inertia of the AC layer. Increases in the flexural rigidity of the AC layer result in lower flexural strains at the AC surface and the AC bottom under the tire center (compression at the top and tension at the bottom). Therefore increases in the AC thickness and/or or ACS and ACB moduli result in the decreases in the flexural or radial strain at the AC surface at the tire edge and at the AC bottom under the tire center. The effects of changes in the radial strains on the radial stresses are explained in the section below.

### 4.2.2 Stress-Strain Relationship (Hooke's Law)

The three-dimensional stress-strain relationship of any material in cylindrical coordinates can be expressed by Hook's law as follows (Yoder and Witczak, 1975):

$$\sigma_r = \varepsilon_r E + \nu(\sigma_t + \sigma_z) \tag{7.1}$$

Realizing that under the center of the load $\sigma_t = \sigma_r$, arranging terms and solving for $\sigma_r$ yield the following equation

$$\sigma_r = \frac{\varepsilon_r E + \nu\sigma_z}{(1-\nu)} \tag{7.2}$$

Where $\sigma_r$ = Radial stress;

$\varepsilon_r$ = Radial strain;

$\nu$ = Poisson ratio;

$\sigma_t$ = Tangential stress;

$\sigma_z$ = Vertical stress; and

E = Elastic modulus of the material.

As can be seen, equation 7.2 indicates that, increases in the radial strain and/or the elastic modulus result in the increases in the radial stress. Since increases in the radial strain is affected by the thickness and moduli of the AC layer; changes in these two variable causes changes in the induced radial stresses. The magnitude of the radial stresses at the tire edge is a function of the radial stresses induced at the tire center and the rate of stresses dissipation with the increasing radial distance from the tire center. The rate of stress dissipation is presented in section below.

### 4.2.3 Stress Decay

The stress decay rate is the rate at which the stress decreases with the increasing horizontal distance from the tire center. Graphically, it is the slope of the curves representing the relationship between the radial stresses and the radial distance from the tire center as shown in Figures 8.17 and 8.18. As can be seen from the figures, stiffer the AC layers (higher flexural rigidity) cause decreases in the stress decay rate. This is so because, in an analogy to an elastic beam, the stiffer AC layer would transfer the positive moment (compression at the top and tension at the bottom) to farther distance and hence the negative moment. The farther the distance between tire center and the negative moment is the lower

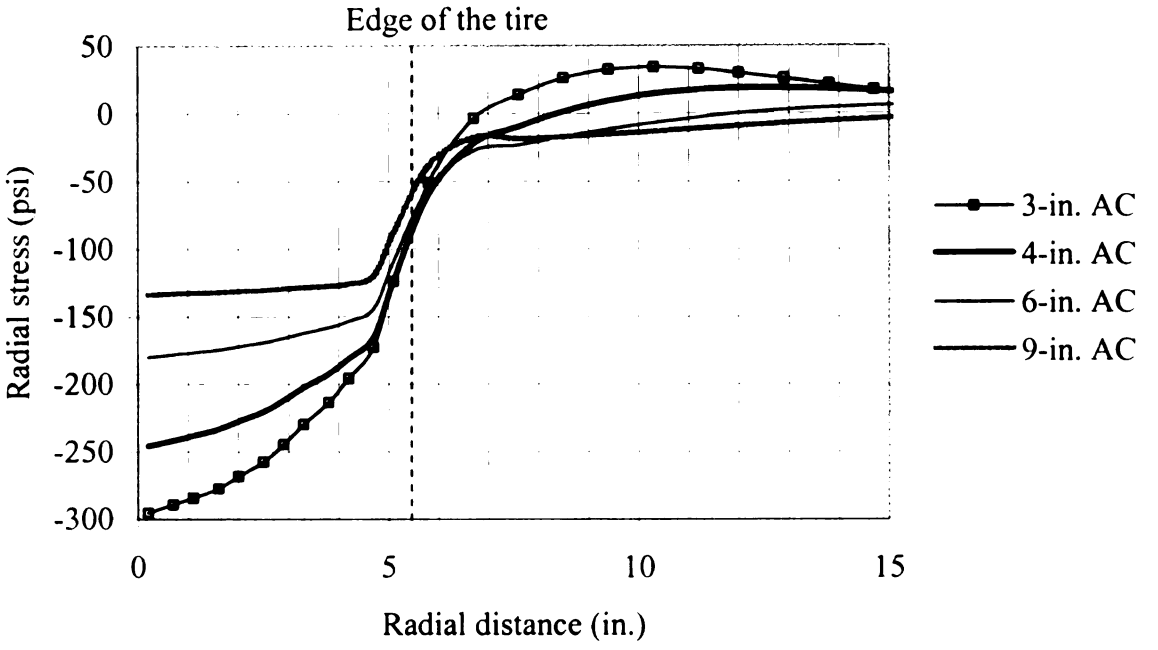


Figure 8.17 Lower stress decay rates due to higher AC thicknesses (500-ksi AC surface and AC base course moduli)

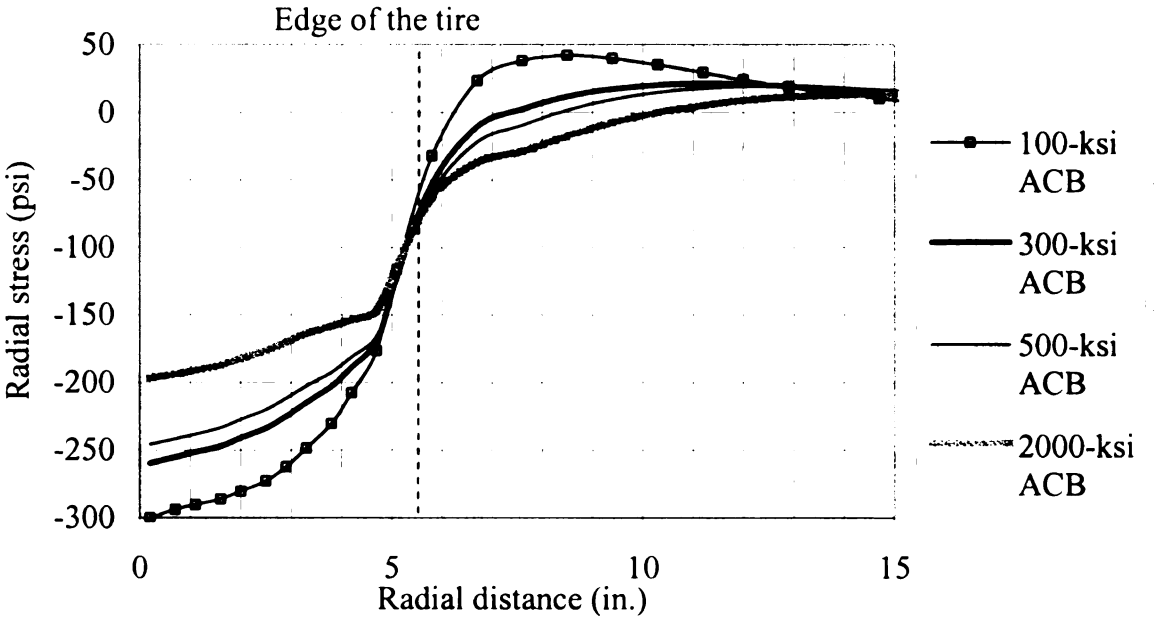


Figure 8.18 Lower stress decay rates due to higher AC base course (ACB) moduli (500-ksi AC surface course modulus and 4-in. total AC thickness)

the stress decay rate. Hence, increases in the AC thickness and/or in the ACS and ACB moduli result in lower stress decay rates. It should be noted that decreases in the radial stresses under the tire center may or may not causes decreases in the radial stresses at the tire edge. The latter stress is also a function of the rate of stress dissipation.

### 4.2.4 Stiffness of the Support of the AC Layer

Once again, in an analogy to a beam on elastic foundation, softer layer underneath the AC layer (softer support) results in higher deflection at the tire center as shown in Figure 8.19. The higher is the deflection, the sharper is the curvature and hence, the higher is the flexural strain at the AC surface and at the AC bottom under the tire center. Therefore, stiffening the support of the AC layer (increases in the moduli of the RM, the FC, BS and RB and decreases in the RM layer thickness) results in decreases in the radial stresses at the AC surface and AC bottom under the tire center and hence at the AC surface at the tire edge. Note that, later in this chapter, the results of 3-D analyses indicates that increases in the RM and FC moduli may result in either increases or decreases in the lateral tensile stresses at the tire edge (see more details in section 5.3). Nevertheless, in general, stiffening the support of the AC layer causes decreases in the radial compressive stresses at the AC surface at the tire edge.

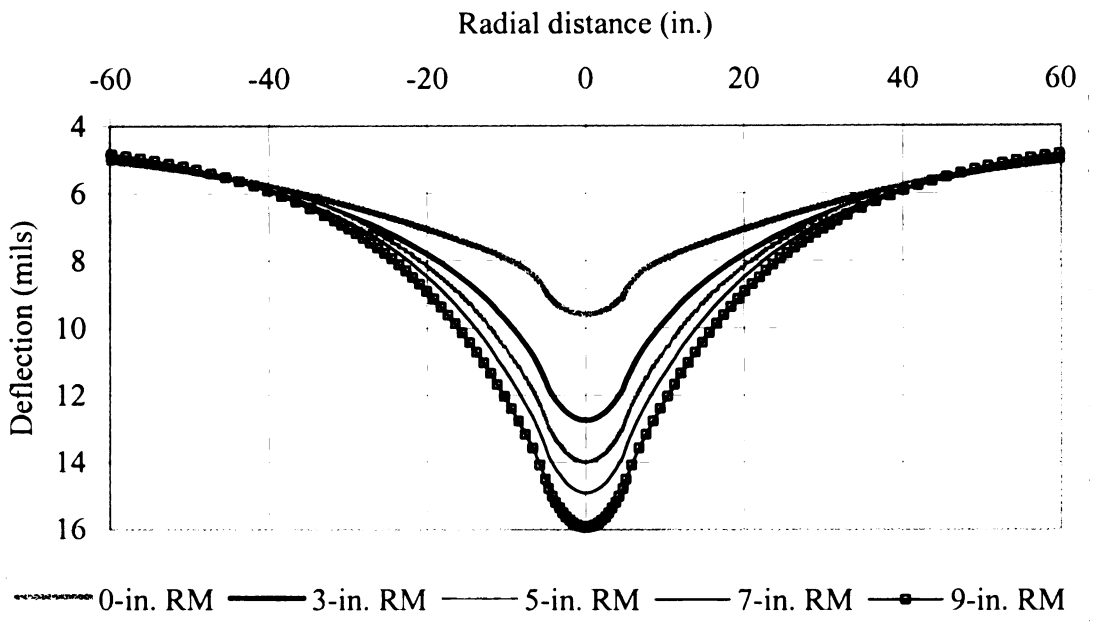


a) Different rubblized material thickness (30-ksi RM and 500-ksi FC)

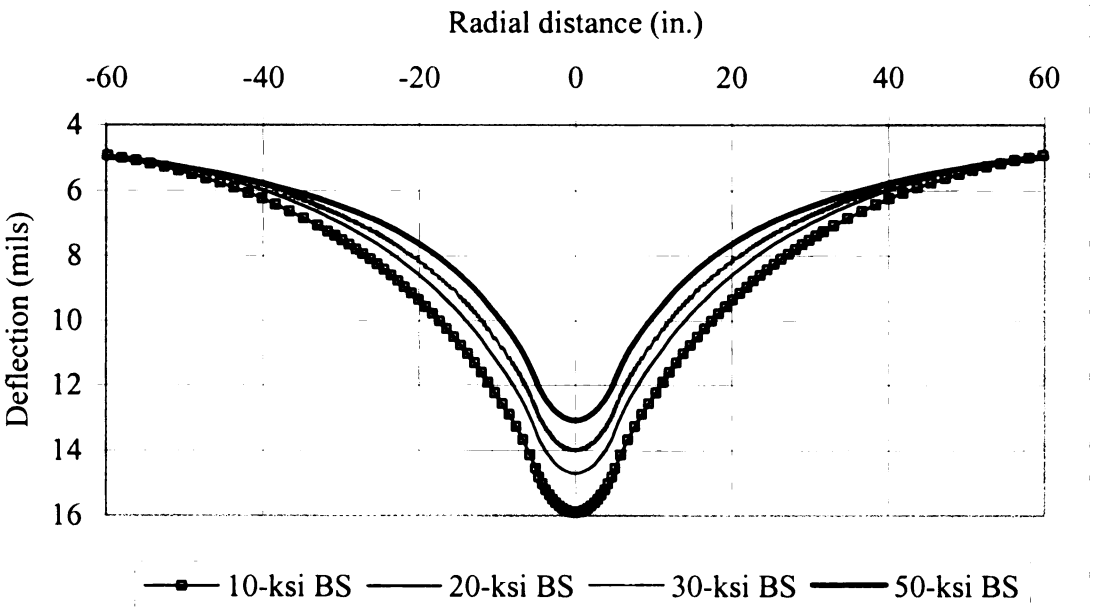


b) Different BS modulus

Figure 8.19 Variations in the peak deflections due to different rubblized material (RM) thicknesses and different base and subbase (BS) moduli

### 4.2.5 Location of the Neutral Axis

In beam theory, the neutral axis is the locus of points where the flexural stress is equal to zero. For a rubblized pavement, which could be modeled as a composite beam consisting of the AC and the RCS, the neutral axis is typically located in the AC layer. Increases in the RCS modulus (due to increases in the RM and FC moduli and/or decreases in the RM thickness) result in shifting the neutral axis toward the AC bottom. Said shifting of the neutral axis results in lower flexural stress at the AC bottom since the AC bottom is closer to the neutral. Further, when the modulus of the RCS is very high (full depth FC with the FC moduli are 500-ksi or greater), the flexural stresses at the bottom of the AC layer become compressive stresses as shown in Figure 8.6. This is because the neutral axis is located below the AC layer in the RCS, which is the scenario for all composite pavements.

## 5.0 THREE-DIMENSIONAL FINITE ELEMENT ANALYES

The wheel load and tire pressures of truck tires are much higher than those of passenger car tires. Therefore, higher magnitude stresses and strains are induced in the pavements due to the former. Further, two types of tires are used by the truck fleet in the USA (radial and bias ply). Since the radial tires are the predominant amongst the two types, the 3-D finite element analyses were conducted to determine the stresses induced in the pavement due to radial truck tire contact stresses.

The objective of the 3-D FEM analyses is to assess the effects of the following variables on the load-induced radial stresses at the top and bottom of the AC layer of

pavement structures:

1. The tire-pavement interaction, which includes vertical, lateral and longitudinal contact stresses and the contact areas.
2. The pavement layer moduli and thicknesses.
3. The geometry of the uneven interface between the RM and the FC layers in rubblized pavements.
4. The tire configurations (single vs. dual wheel).

The tire-pavement contact stresses, contact areas and the FEM model used in the analyses are described in the next two subsections.

## 5.1. Tire-Pavement Contact Area and Contact Stresses

As stated in Chapter 2, several researchers have measured the vertical, longitudinal and lateral shear stresses caused by straight rolling bias-ply and radial tires (Myers et al, 1999, Jacob, 1998, De Beer et al, 1997, and Pottinger and McIntyre 1999). Since no such measurements were conducted in this study, the contact stresses of a radial truck tire measured by Pottinger and McIntyre (1999) were used in the 3-D analyses. Figure 8.20 depicts the radial tire print used by Pottinger and McIntyre (1999) due to measured load and tire inflation pressure of 6,597 lb and 125 psi, respectively. This combination of wheel load and tire inflation pressure makes the tire an over-inflated one.

Nevertheless, Figures 8.21 and 8.22 illustrate 3-D plot of the variations in the measured vertical and lateral contact stresses for the radial tire tested by Pottinger and used in this study. Figures 2.23 and 2.24 illustrate the 2-D variations in the vertical and lateral contact stresses along and across the tire, respectively. As can be seen from the

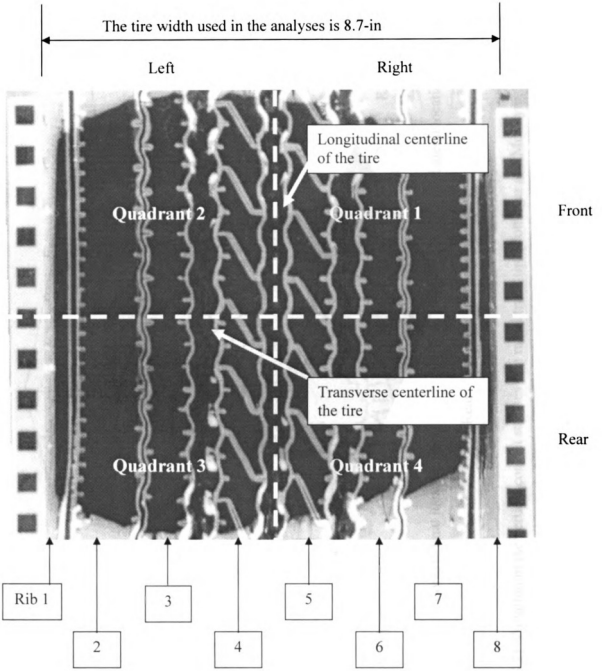


Figure 8.20 Lines of symmetry of the vertical and the lateral contact stresses of a radial truck tire having 8 ribs and 7 grooves (after Pottinger and McIntyre, 1999)

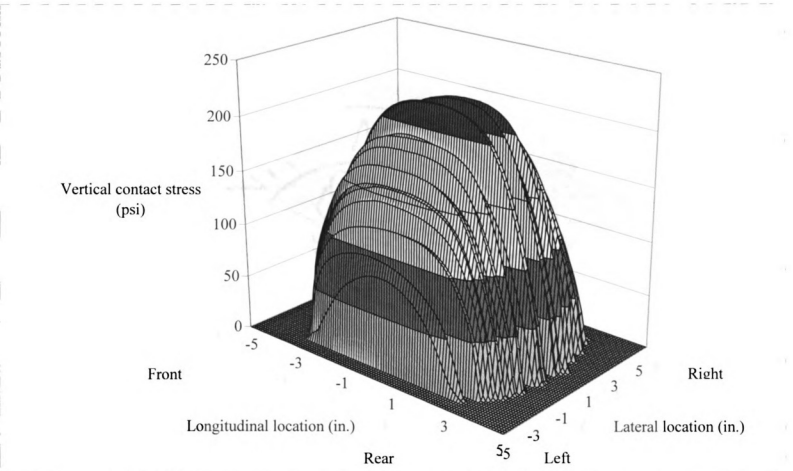


Figure 8.21 Variation in the vertical contact stresses of a radial truck tire (Pottinger and McIntyre, 1999)

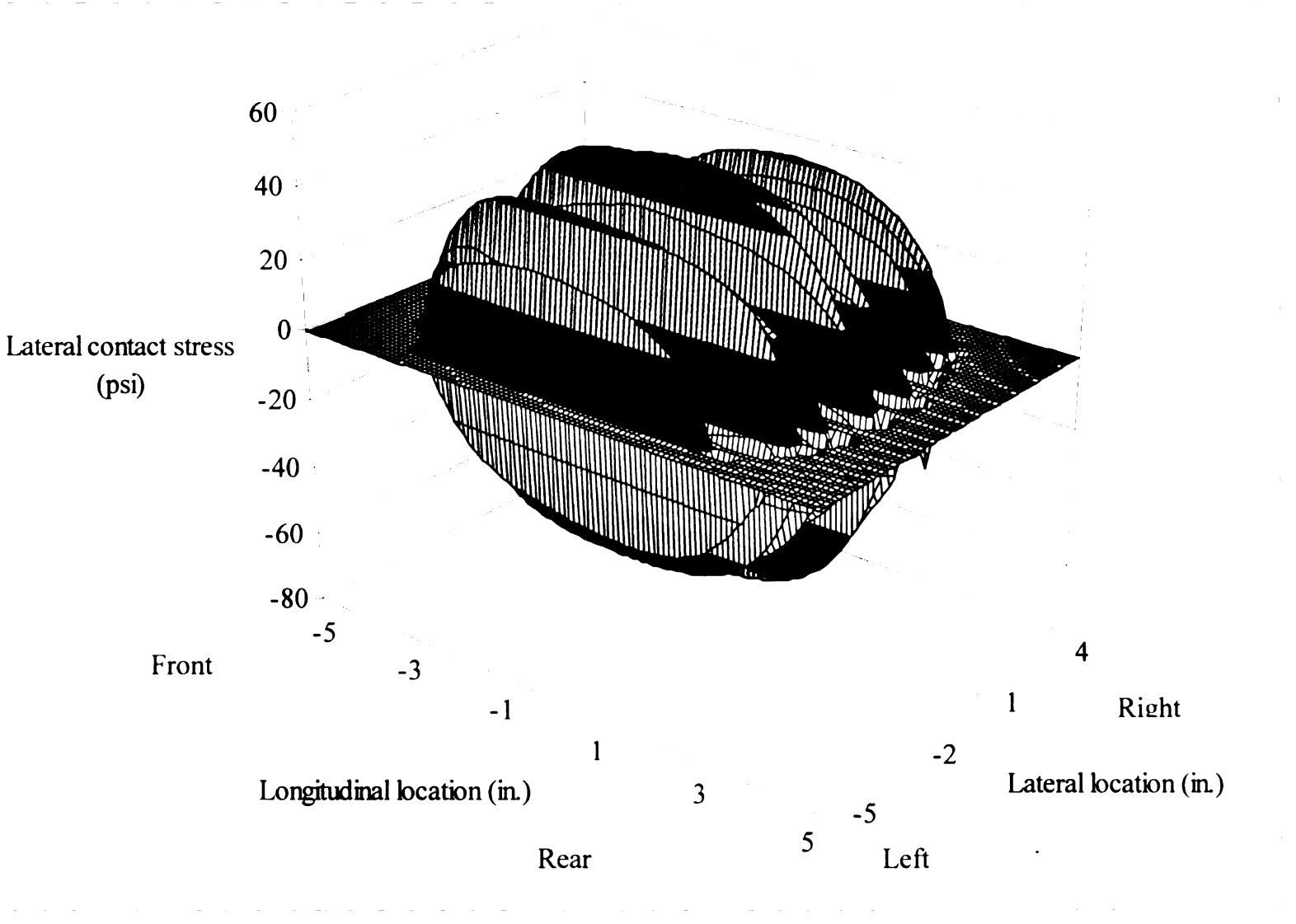


Figure 2.22 Variation in the lateral contact stresses of a radial truck tire (Pottinger and McIntyre, 1999)

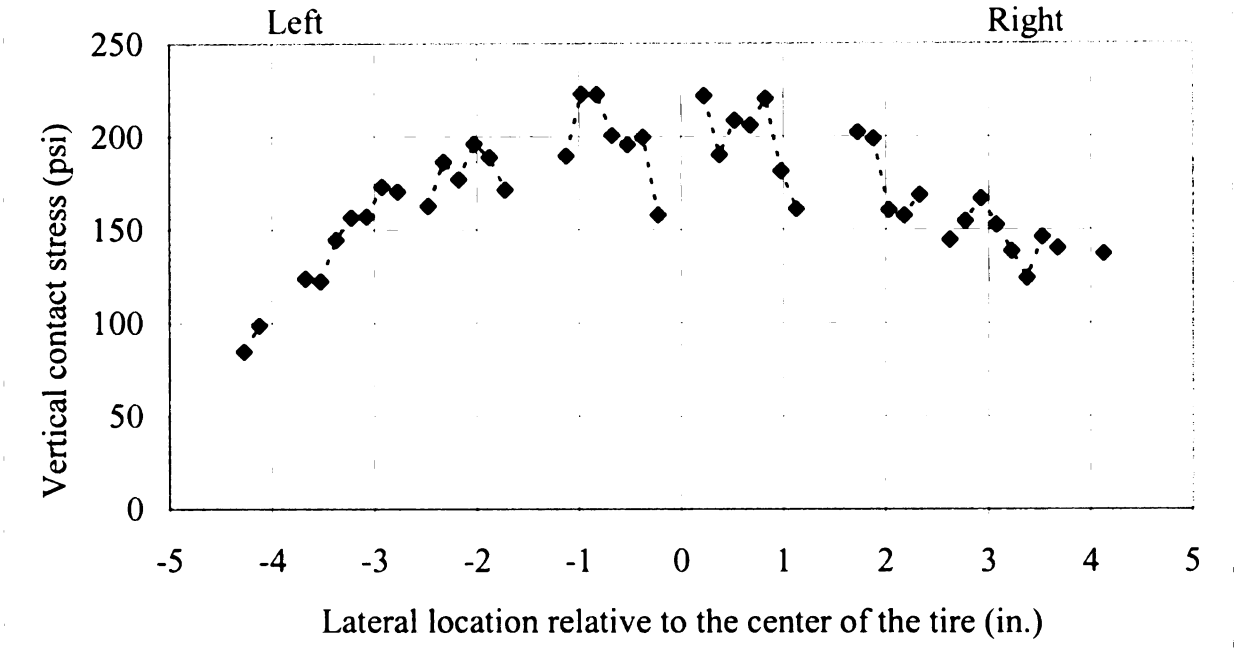


a) Vertical contact stresses

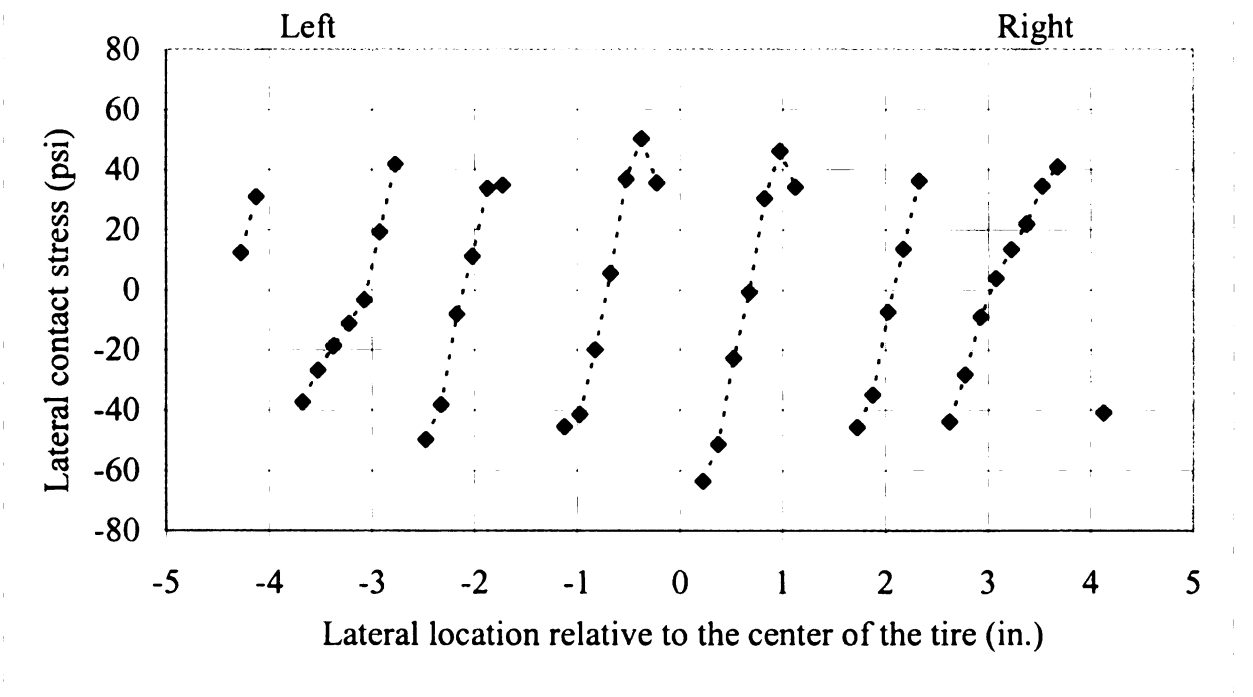


b) Lateral contact stresses

Figure 2.23 Variations in the measured vertical and lateral contact stresses across the tire along the lateral center line of a radial truck tire (after Pottinger and McIntyre, 1999)

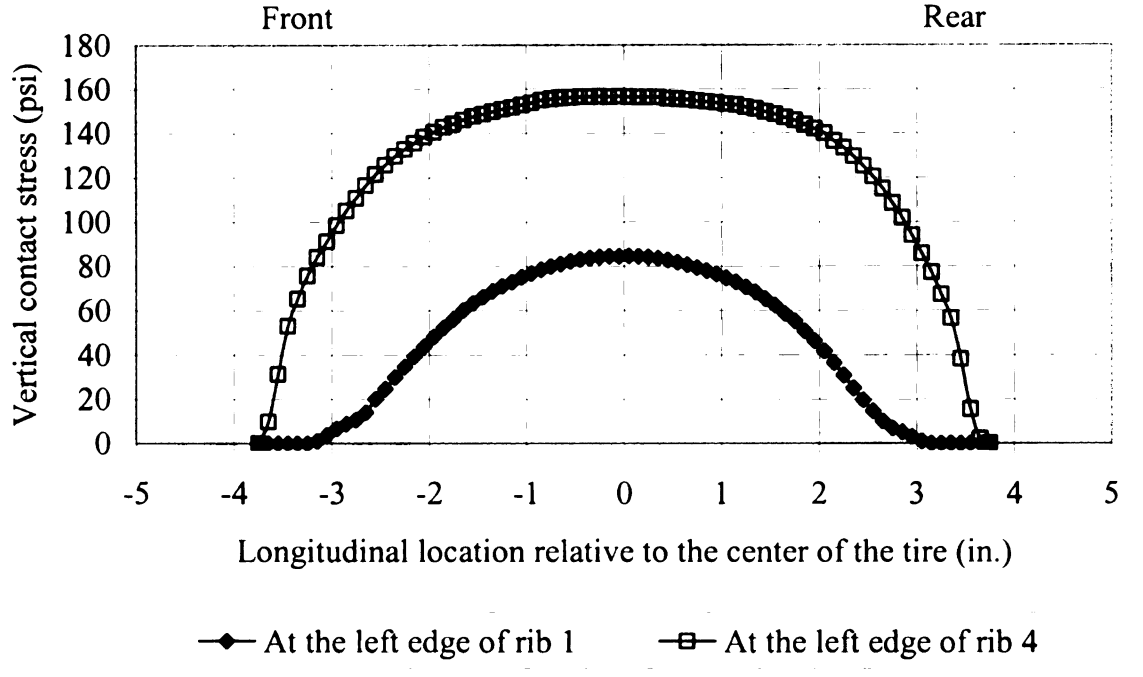


a) Vertical contact stress

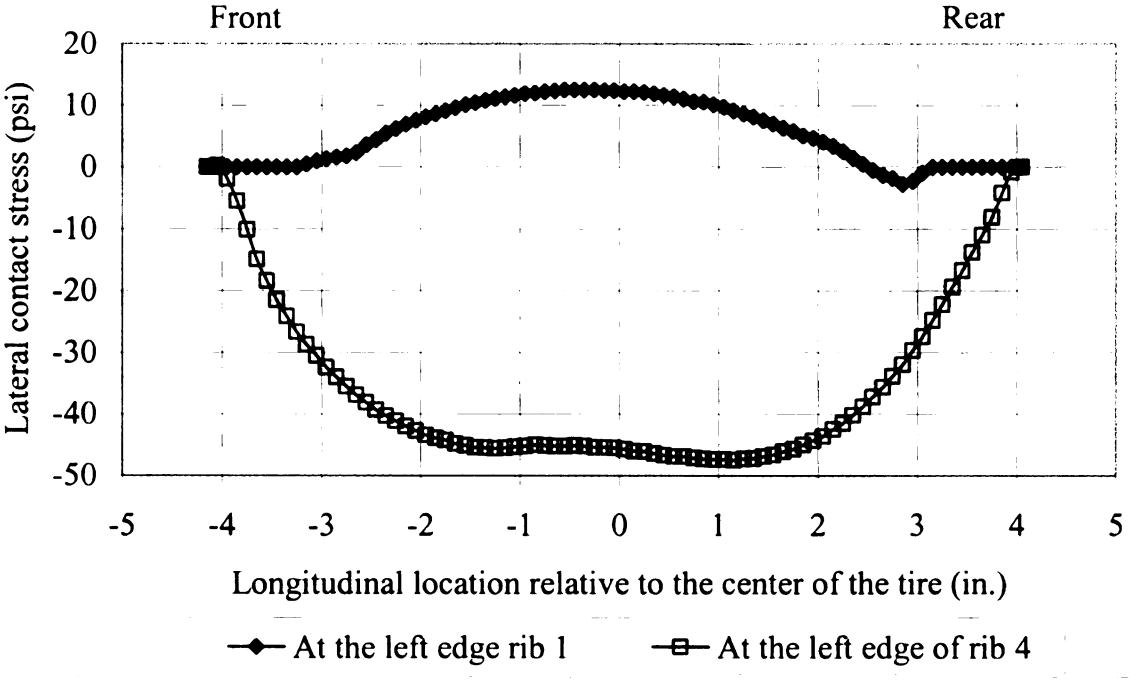


b) Lateral contact stress

Figure 2.24 Variations in the measured vertical and lateral contact stresses in the longitudinal direction along the edge of a radial truck tire (after Pottinger and McIntyre, 1999)

figures, the measured vertical and lateral contact stresses show symmetry about the transverse and the longitudinal centerlines of the tire. Figure 8.25 depicts the longitudinal contact stresses, which were measured at the left edge of rib 5 of the tire only. As can be seen from the figure, the measured longitudinal stresses showed no symmetry about the transverse centerline of the tire. In another study conducted by De Beer et al (1997), they measured the longitudinal contact stresses under all ribs of an over inflated tire as shown in Figure 8.26 The data in the figure indicate that the maximum longitudinal stresses are located under the longitudinal centerline of the tire (close to the edge of rib 5 in Pottinger's measurements). Unfortunately, the only contact stress data that were available in a digital form were those measured by Pottinger and McIntyre (1999). De Beer's and other data were available in the form of 3-D plots only, which cannot be digitized accurately. Therefore, in the analyses, Pottinger and McIntyre (1999) data were used. To overcome the shortcoming of the data relative to the longitudinal contact stresses, and to study the effects of the longitudinal contact stresses on the load-induced tensile stress at the edge of the tire, the stresses measured under the edge of rib 5 were assumed to act under the edge of the tire. Although this represents the worst case scenario, it was reasoned that if the impact of such high longitudinal contact stresses on the lateral stress in the pavement is negligible, then perhaps, the longitudinal contact stress can be neglected.

Due to symmetry, only the vertical and the lateral contact stress of quadrant 2 of the tire (see Figures 8.20) were used in the 3-D analyses. Hence, the total vertical wheel load is four times the 1743.75 lb vertical load on quadrant 2 or 6975 lb, which is slightly higher than the measured total vertical load of 6597 lb. Also, because of asymmetry of

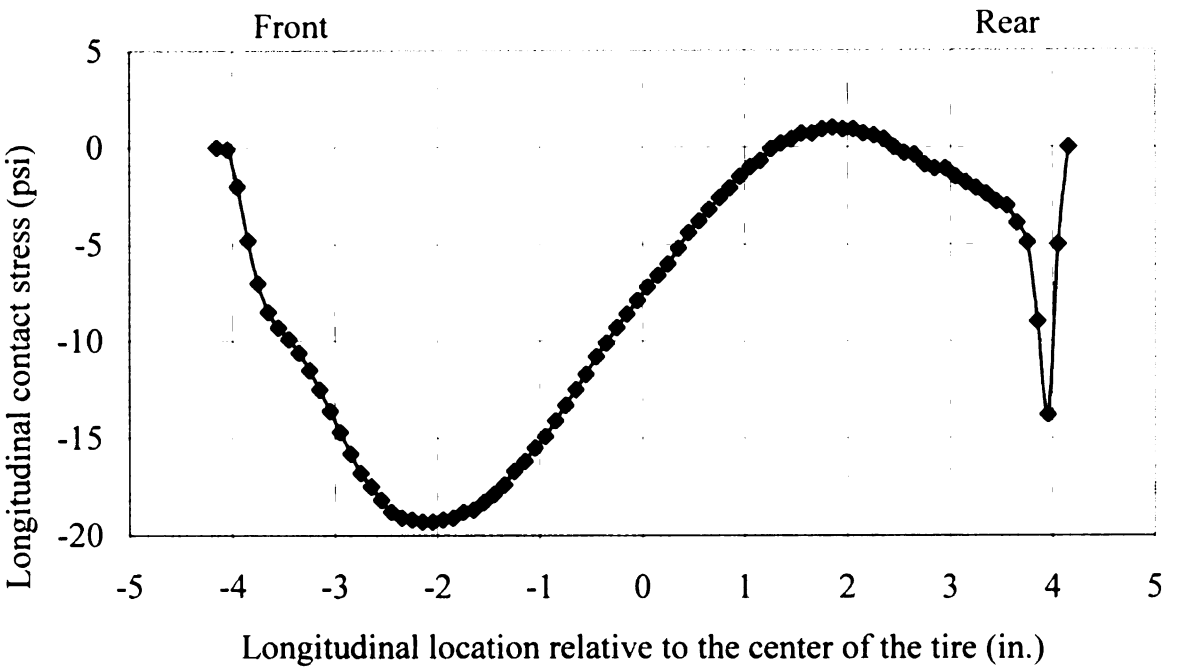


Figure 8.25 Variation in the longitudinal direction of the longitudinal contact stress along the left edge of rib 5 (after Pottinger and McIntyre, 1999)

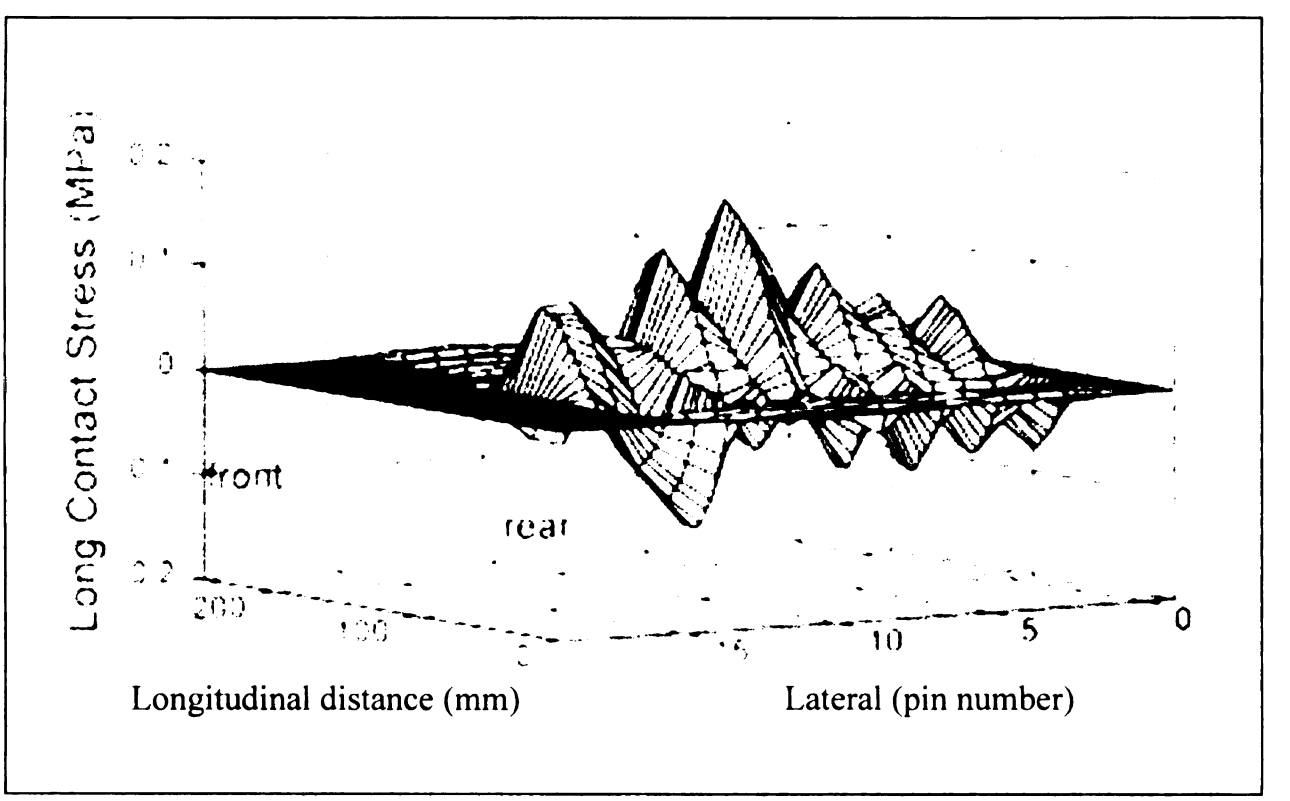


Figure 8.26 Variation in the longitudinal contact stresses of a radial truck tire subjected to the rated load (De Beer et al, 1997)

the longitudinal contact stresses, they were analyzed separately using the full contact length of ribs 1 and 2. The finite element models used in the 3-D analyses are presented in the next subsection.

## 5.2. Finite Element Models

The finite element models were generated using the IDEAS finite element (FEM) program and analyzed using the ABAQUS program. Figure 8.27 depicts a typical quarter model used in the 3-D analyses of the stresses induced at the top and bottom of the AC layer by the vertical and lateral contact stresses. The arrows on the two walls of the quarter model represent the boundary conditions simulating two planes of symmetry perpendicular to the x- and z-axes. Whereas the arrows at the bottom of the model represent the lower boundary condition, which was modeled as a hinge, allowing rotations but not translation in all directions. The dark area at the top of the model is the loaded area or the tire-pavement contact area. Once again, with the symmetrical properties, the quarter model simulates a pavement subjected to a single wheel load located at the center of the full model. The width, thickness and length (x, y and z dimensions) of the quarter model are 75, 100 and 75 in., respectively. Note that, said dimensions of the model result in negligible boundary or edge effects on the induced stresses in the AC layer as proven in section 3.0. Table 8.5 summarizes the physical dimensions of the layers and elements as well as the engineering characteristics of the materials simulated in the 3-D analysis.

Due to computing capacity problems, in all 3-d FEM analyses, the element sizes were designed as to minimize the total number of elements used in the quarter model.

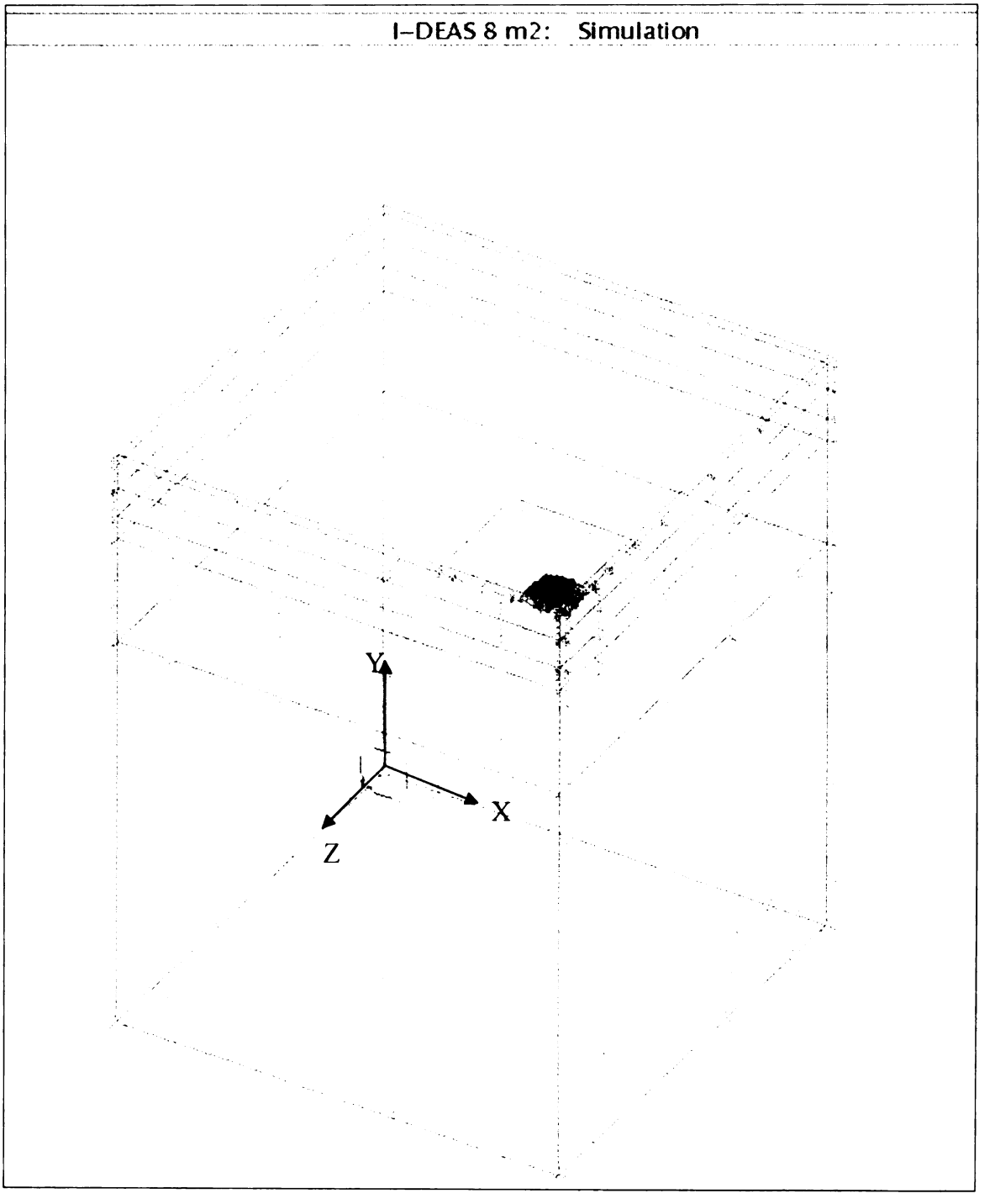


Figure 8.27 The quarter model used in the 3-D FEM analyses of the vertical and lateral contact stresses

Table 8.5 Thicknesses, element sizes, moduli and Poison ratios assigned to pavement layers and the roadbed soil in the 3-D analyses

| Layer | Modulus (ksi) | Poison ratio | Thickness (in.) | Element size (in.) | Element type |
|---|---|---|---|---|---|
| AC surface course | 100 - 2000 | 0.3 | 1.5 | 0.15, 1 and 2 | C3D20, C3D10 |
| AC base course | 100 - 2000 | 0.3 | 2.5, 4.5 and 7.5 | 2 | C3D10 |
| Rubblized material layer | 30, 100 | 0.4, 0.2 | 0 to 9 * | 2 | C3D10 |
| Fractured concrete layer | 500, 2500 | 0.2 | 0 to 9 * | 2 | C3D10 |
| Subbase | 30 | 0.4 | 18 | 6 | C3D10 |
| Roadbed soil | 10 | 0.45 | 64 ,67 and 69 | 9 | C3D10 |

Note: 1. C3D20 = 20-node quadratic brick element, C3D10 = 10-node quadratic tetrahedron element

2. The thicknesses of the rubblized material and fractured concrete layers varied from full depth rubblized material to full depth fractured concrete layers. There are also several models having uneven interface between the two layers.

Three element sizes were used in the AC surface course with the smallest element size of 0.15-in assigned to the vicinity of the contact area. The size of the elements increased as the distance from the loaded area increased. The largest size element in the AC layer used in the analysis was 2.0-in. Except for the 0.15-in. quadratic brick element whose meshes were assigned manually, all other elements were quadratic tetrahedron and they were automatically generated by the IDEAS program. Hence, the sizes of the tetrahedron elements reported in Table 8.5 are the target values specified in the IDEAS program. The actual exact element sizes vary within the layer because the IDEAS program uses the target element sizes as guideline and varies the actual element sizes to fit the elements in the layer and to match the element sizes between two adjacent layers.

Figure 8.28 depicts the model used for the longitudinal contact stresses. As can be seen the model (30-in. wide, 30-in. long and 100-in. thick) is smaller than the quarter model used for the vertical and lateral contact stresses. The dark area located at the center of the top of the model is the full-length contact area of ribs 1 and 2. Said contact area is longer than those used in the quarter model since no symmetrical plane was used in this model. As a result more elements were used in the contact area and its vicinity. Consequently, the model dimension was reduced to keep the total number of elements less than 150,000 as not to exceed the capacity of the computer system. Nevertheless, since the lateral and longitudinal stresses influence the induced lateral stresses over a relatively small zone (see sections 5.3.1 and 5.3.2), the dimensions of the model used in the analyses are sufficient to eliminate edge effects on the induced lateral stresses in the vicinity of the contact area.

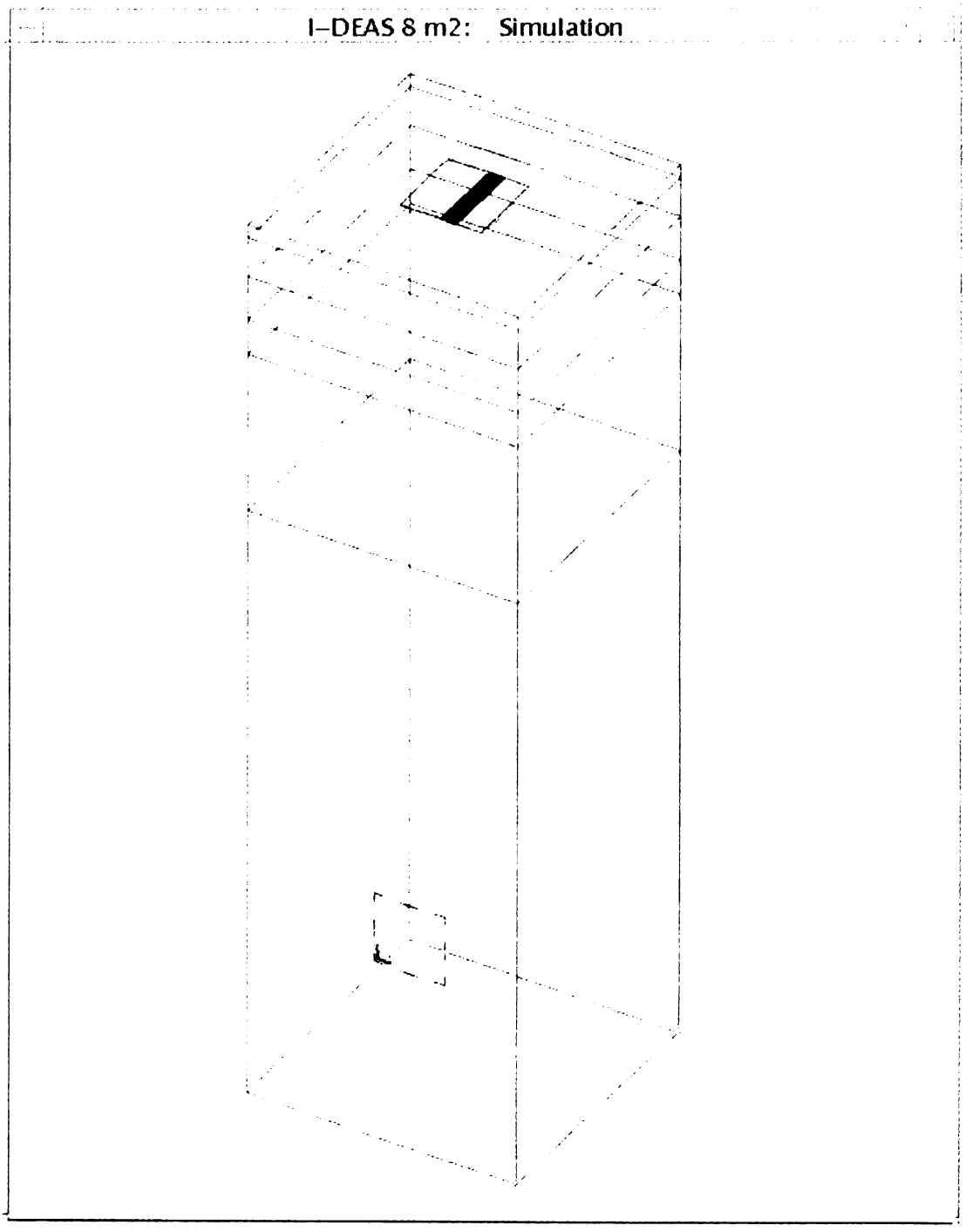


Figure 8.28 The model used in the 3-D FEM analysis of the lateral stresses induced in the AC layer due to the longitudinal contact stresses

## 5.3. Lateral Stresses Induced in the AC Layer by Tire-Pavement Contact Stresses

Recall that the objectives of the 3-D FEM analyses are to evaluate the lateral stresses induced in the AC layer by the tire-pavement contact stresses and to evaluate the effects of several factors on said stresses. These factors include the pavement layer properties (thickness and modulus), the geometry of the interface between the RM and the FC layers, and load configuration (single versus duel tires). Some of these factors influence only the effects of the vertical contact stress. Others influence the effects of the lateral contact stress; still others influence the effects of both contact stresses. The simultaneous analyses of the effects of both contact stresses on the lateral stresses induced at the top and bottom of the AC layer requires substantial number of FEM models each of which requires hundred of thousands of data entry; an overwhelming task. To simplify the problem, the effects of each contact stress were analyzed independently and the results were added based on the principles of superposition. Prior to the initiation of said analyses, a task was undertaken to proof that the superposition produces accurate results. This is presented in the next subsection.

### 5.3.1 Superposition

To confirm the accuracy of the results obtained by superposition, pavement section 1 of Table 8.6 was modeled and analyzed using the following configurations of contact stresses (all contact stresses were measured by Pottinger and McIntyre (1999):

- Case 1 - Vertical contact stresses only
- Case 2 - Lateral contact stresses only

Table 8.6 Pavement sections used in the 3-D analyses of the induced stresses in pavements due to the indicated contact stresses

| Contact stress | Section | Moduli (ksi) | | | | | | Thickness (in.) | | | | | |
|---|---|---|---|---|---|---|---|---|---|---|---|---|---|
| | | ACS | ACB | RM | FC | BS | RB | ACS | ACB | RM | FC | BS | RB |
| Lateral | 1 | 500 | 500 | 30 | 500 | 30 | 10 | 1.5 | 4.5 | 5 | 4 | 18 | 67 |
| Vertical | 1 | 500 | 500 | 30 | 500 | 30 | 10 | 1.5 | 4.5 | 5 | 4 | 18 | 67 |
| Longitudinal | 1 | 500 | 500 | 30 | 500 | 30 | 10 | 1.5 | 4.5 | 5 | 4 | 18 | 67 |
| Lateral and vertical | 1 | 500 | 500 | 30 | 500 | 30 | 10 | 1.5 | 4.5 | 5 | 4 | 18 | 67 |
| Lateral | 2 | 300 | 500 | 30 | 500 | 30 | 10 | 1.5 | 4.5 | 5 | 4 | 18 | 67 |
| Lateral | 3 | 1000 | 500 | 30 | 500 | 30 | 10 | 1.5 | 4.5 | 5 | 4 | 18 | 67 |
| Lateral | 4 | 500 | 300 | 30 | 500 | 30 | 10 | 1.5 | 4.5 | 5 | 4 | 18 | 67 |
| Lateral | 5 | 500 | 1000 | 30 | 500 | 30 | 10 | 1.5 | 4.5 | 5 | 4 | 18 | 67 |
| Lateral | 6 | 500 | 500 | - | 500 | 30 | 10 | 1.5 | 4.5 | - | 9 | 18 | 67 |
| Lateral | 7 | 500 | 500 | 30 | - | 30 | 10 | 1.5 | 4.5 | 9 | - | 18 | 67 |

ACS=AC surface course, ACB=AC base course, RM=rubblized material, FC=fractured concrete, BS=base and subbase, and RB=roadbed soil

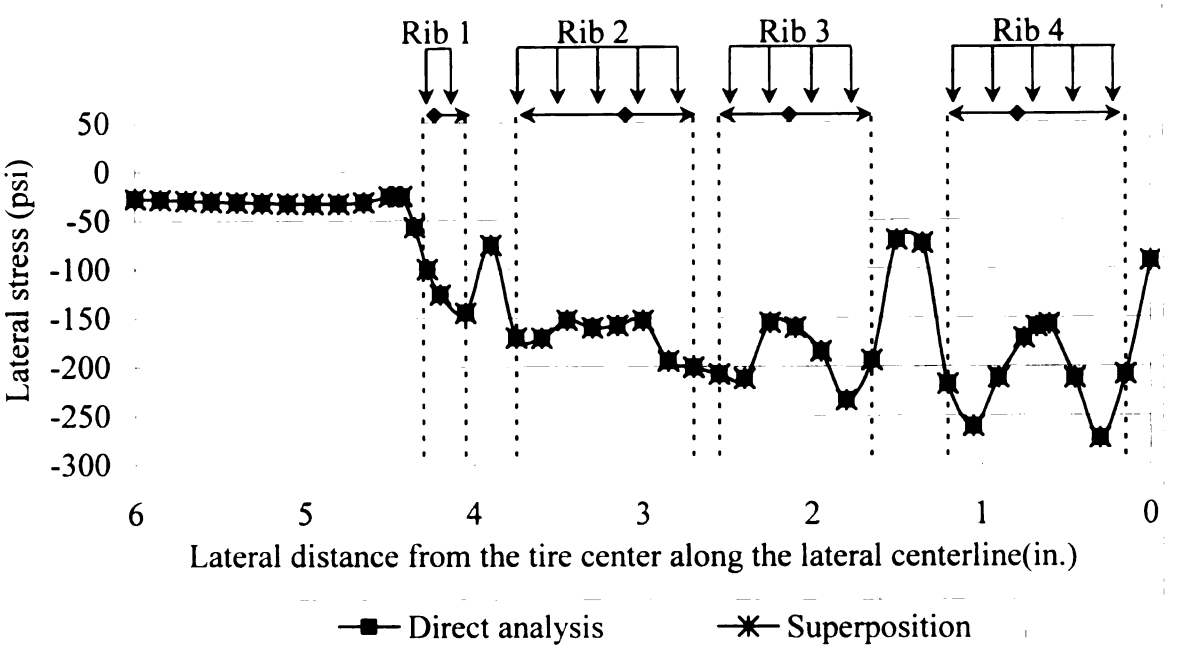


a) Comparison in the lateral direction

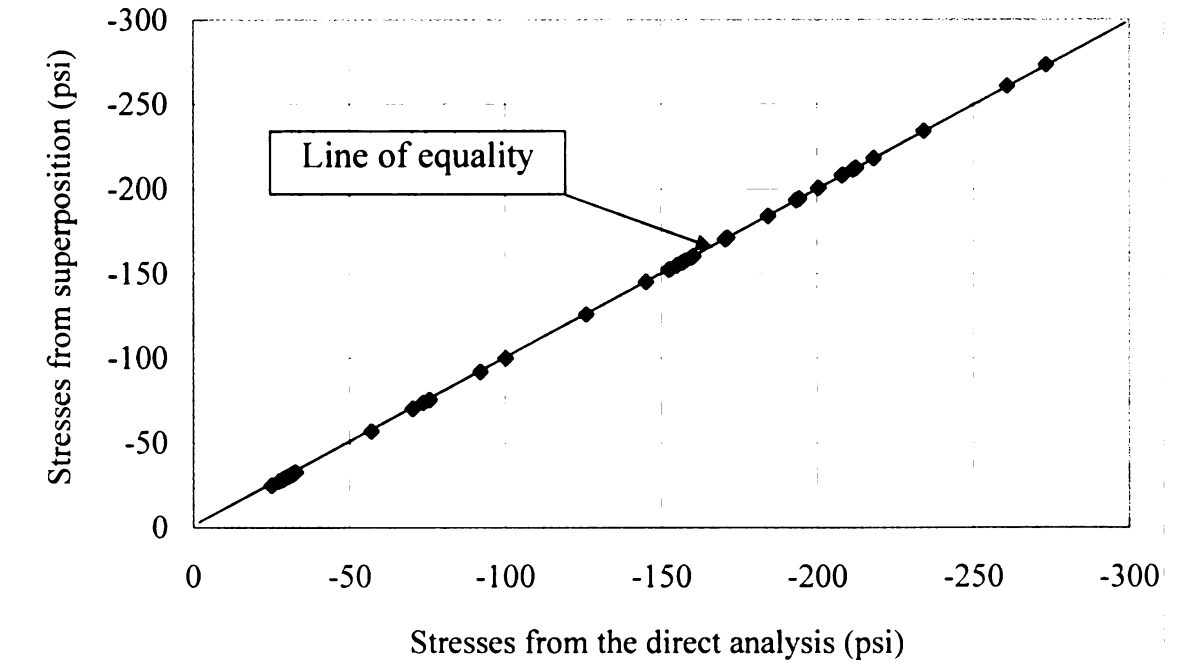


b) Comparison with the line of equality

Figure 8.29 Comparison of the lateral stresses induced at the AC surface by the vertical and lateral contact stresses obtained by superposition and by direct analyses of both contact stresses

➢ Case 3 - Combined vertical and lateral contact stresses

Figure 8.29 shows the lateral stresses induced at the AC surface obtained from the direct analysis of both the vertical and lateral contact stresses (case 3) and those obtained by superposition (case 1 + case 2). As can be seen from the figure, there are no significant differences between the lateral stresses obtained from the two analyses. Hence, superposition can be applied in the 3-D FEM analyses, which was expected because of the linear elastic material behavior used in the model. The implication of this finding is that, the stresses induced by individual contact stresses can be analyzed separately and the induced stresses can be combined later to obtain the total stresses induced by all components of the tire-pavement contact stresses. Results of the analyses of the lateral stresses induced at the top and bottom of the AC layer due to each contact stress component are presented in the next three subsections.

### 5.3.2 Lateral Contact Stresses

The lateral stressed induced at the AC surface of pavement sections 1 through 7 of Table 8.6 by the lateral contact stresses were analyzed. Figure 8.30a shows the variation in the induced lateral stress along the lateral centerline of the tire for all pavement sections. The induced lateral stresses were plotted again in Figure 8.30b depicts the lateral stresses induced at the AC surface of pavement section 1 versus that induced at the surface of pavement sections 2 through 7. As can be seen, all data falls along the line of equality (solid line in the figure). The results shown in Figure 8.30 indicate that:

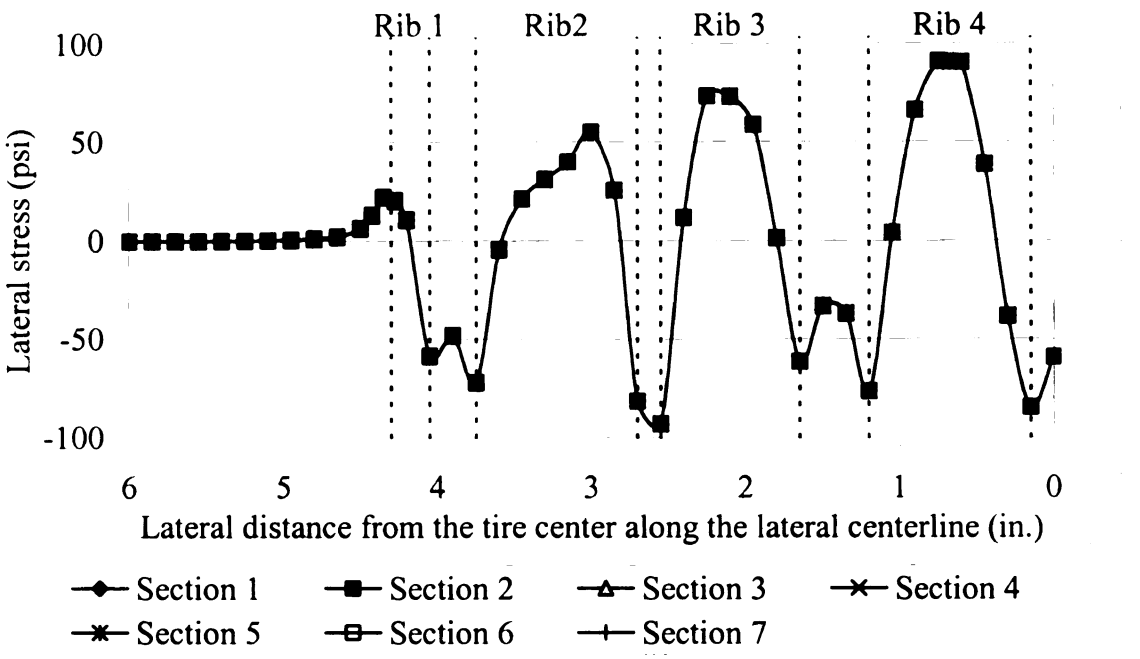


a) Comparison in the lateral direction

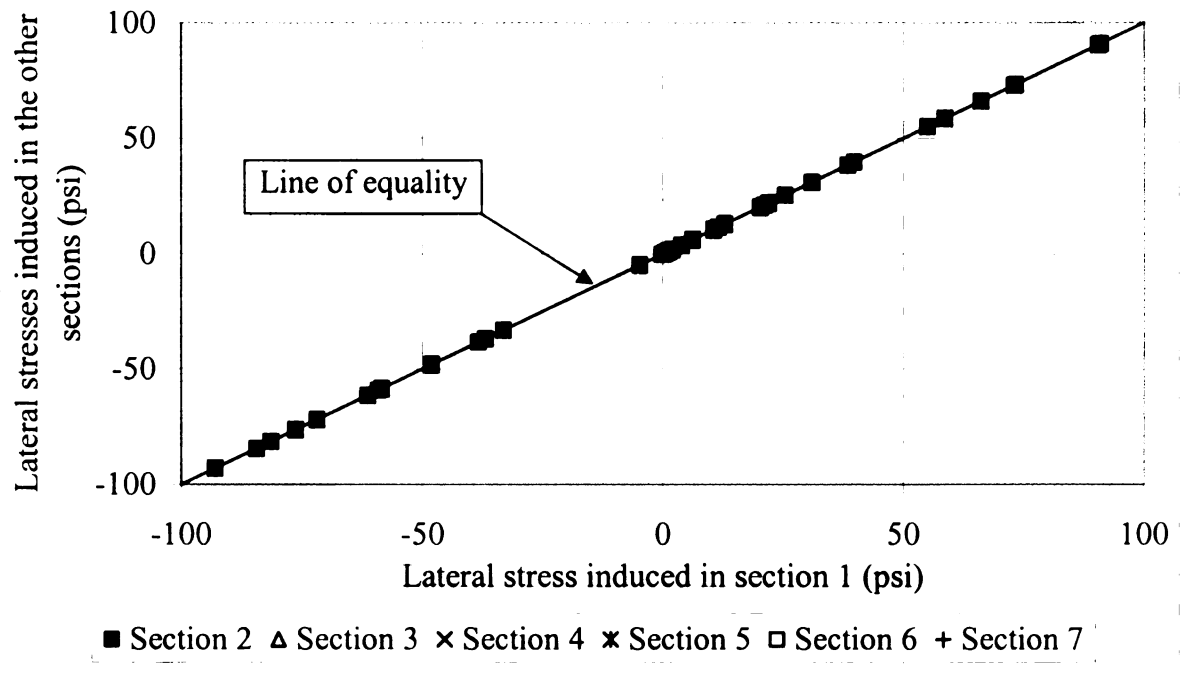


b) Comparison with the line of equality

Figure 8.30 Comparison of the lateral stresses obtained from pavement sections 1 through 7 of Table 8.6.

- The lateral stresses induced at the surface of the AC layer by the lateral contact stresses are independent of the pavement structure. This support the conclusions made by Meyers et al, (1998) and Molenaar, (1984) and stated in section 3 of this chapter.
- The outward (directed away from the center of the rib) lateral contact stresses under the inner ribs of the tire induce lateral tensile stresses under the ribs and lateral compressive stresses in the grooves at the AC surface.
- The inward (directed toward the tire center) lateral contact stresses under the outer rib (rib 1) induce lateral tensile stresses on the pavement surface at the tire edge. Said stresses decrease rapidly with increasing distance from the tire edge. The magnitude of the induced stresses decrease from a maximum of 22.04 psi at 0.075 in. from the tire edge to 0.04 psi at 0.9 in. from the tire edge. It should be noted that Meyers et al, (1998) analyzed another set of data (that were measured by Pottinger), which show outward lateral contact stresses under rib 1. They concluded that this contact stresses induced lateral tensile stress in the pavement surface under the center of rib 1.

The lateral stresses at the AC bottom induced by the lateral contact stresses were also analyzed. It was found that the magnitudes of the induced stresses are negligible (less than 0.2 psi). Hence, it can be concluded that the lateral stresses induced in the AC layer by the lateral contact stresses dissipate rapidly in both the vertical and the horizontal directions. Myers et al. (1998) arrived at similar conclusion regarding the shallow influence zone.

### 5.3.3 Longitudinal Contact Stresses

The 3-D analyses of the stresses induced by the longitudinal contact stress in the surface of the AC layer of pavement section 1 of Table 8.6 were conducted using the measured longitudinal contact stresses at the left edge of rib 5 of the tire tested by Pottinger and McIntyre (1999) (see Figure 8.20). Said stresses, which are the maximums, were the only longitudinal stresses measured and reported by Pottinger and McIntyre. In the analyses, they were assigned as the longitudinal contact stresses under ribs 1 and 2. Figure 8.31 depicts the lateral stresses induced at the AC surface due to the longitudinal contact stresses. As can be seen, the highest lateral tensile stresses of 2.2 psi is located at the front end of the tire while the highest lateral compressive stresses of-1.4 psi is located about the lateral centerline of the tire. In reality, the actual longitudinal contact stresses under ribs 1 and 2 are much lower than those used in the analyses, the actual lateral stresses induced at the tire edge are less than those obtained from the analyses. Hence, it can be concluded that the lateral stresses induced at the tire edge by the longitudinal contact stresses are insignificant.

Since the longitudinal and lateral contact stresses are both shear stresses applied to the AC surface, their influence on the lateral stresses induced at the pavement surface is independent of the pavement structure. Further, their influences on the lateral stresses induced at the bottom of the AC layer are negligible. Finally, based on the above results and discussions, the longitudinal contact stresses were neglected from any further analyses of the lateral stresses induced at the AC surface and at the AC bottom.

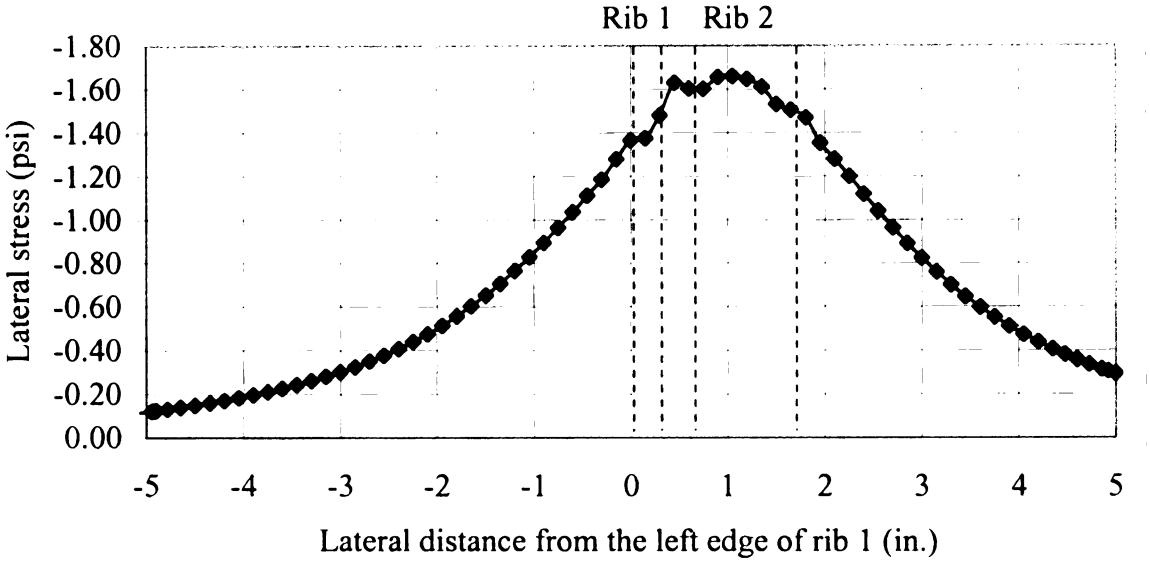


a) Variation in the induced lateral stresses along the lateral centerline of the tire

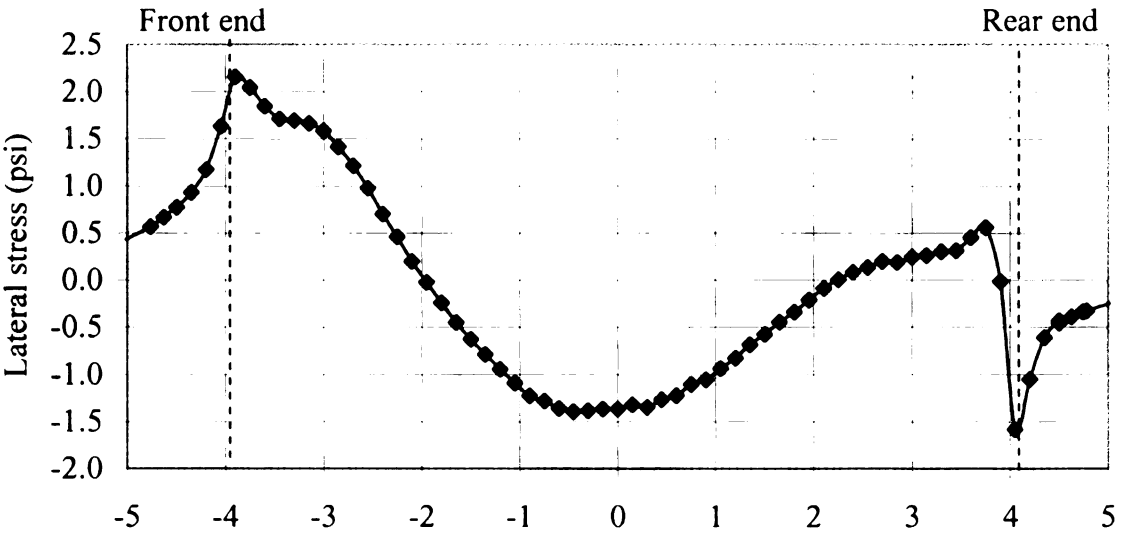


b) Variation in the induced lateral stresses along the edge of the outer rib (rib 1)

Figure 8.31 Lateral stresses induced at the pavement surface due to the longitudinal contact stresses

### 5.3.4 Vertical Contact Stresses and by Combination of Lateral and Vertical Contact Stresses

The lateral stresses induced in the AC layer due to the vertical contact stresses were analyzed using pavement sections with various properties of the AC, RM, FC, and BS layers and RB listed in Table 8.7. The data in the table indicate that the BS and RB properties used in the analyses are constants. The reasons are:

- It was shown in the 2-D analyses that the BS and the RB moduli have smaller impacts on the lateral stresses induced at the AC surface relative to the other layer moduli. This is because the effect of any layer on the stresses induced at the AC surface decreases with its depth.
- The effects of the BS and RB moduli on the lateral stresses induced at the AC bottom are the same as those reported in the 2-D analyses.

It should be noted that the moduli of the AC surface course (ACS) and the AC base course (ACB) of 100 and 300 ksi, respectively were used as a datum in the analyses of the effects of the moduli of the RM and FC layers. The two AC moduli are the consequence of negative temperature gradient (the ACS temperature is higher than that of the ACB) in the AC and they contribute to relatively high lateral tensile stresses at the tire edge.

Results of the analyses are listed in Table 8.8. Since the lateral stresses at the AC bottom induced by the by vertical contact stresses alone and by the vertical and lateral contact stresses are practically the same, only those due to the vertical contact stresses are reported in Table 8.8. Figures 8.32 through 8.36 illustrate the lateral stresses at the AC surface along the lateral centerline of the

Table 8.7 Thicknesses and moduli of pavement layers and roadbed soil used in the analyses of the tire-induced lateral stresses in the AC layer by vertical contact stresses and by the combination of vertical and lateral contact stresses

| Section | Modulus (ksi) | | | | | | Thickness (in.) | | | | | |
|---|---|---|---|---|---|---|---|---|---|---|---|---|
| | ACS | ACB | RM | FC | BS | RB | ACS | ACB | RM | FC | BS | RB |
| 1 | 100 | 500 | 30 | - | 30 | 10 | 1.5 | 4.5 | 9 | - | 18 | 67 |
| 2 | 500 | 500 | 30 | - | 30 | 10 | 1.5 | 4.5 | 9 | - | 18 | 67 |
| 3 | 2000 | 500 | 30 | - | 30 | 10 | 1.5 | 4.5 | 9 | - | 18 | 67 |
| 4 | 500 | 100 | 30 | - | 30 | 10 | 1.5 | 4.5 | 9 | - | 18 | 67 |
| 2 | 500 | 500 | 30 | - | 30 | 10 | 1.5 | 4.5 | 9 | - | 18 | 67 |
| 5 | 500 | 2000 | 30 | - | 30 | 10 | 1.5 | 4.5 | 9 | - | 18 | 67 |
| 6 | 100 | 300 | 30 | - | 30 | 10 | 1.5 | 2.5 | 9 | - | 18 | 69 |
| 7 | 100 | 300 | 30 | - | 30 | 10 | 1.5 | 4.5 | 9 | - | 18 | 67 |
| 8 | 100 | 300 | 30 | - | 30 | 10 | 1.5 | 7.5 | 9 | - | 18 | 64 |
| 7 | 100 | 300 | 30 | - | 30 | 10 | 1.5 | 4.5 | 9 | - | 18 | 67 |
| 9 | 100 | 300 | 30 | 500 | 30 | 10 | 1.5 | 4.5 | 5 | 4 | 18 | 67 |
| 10 | 100 | 300 | 100 | 500 | 30 | 10 | 1.5 | 4.5 | 5 | 4 | 18 | 67 |
| 11 | 100 | 300 | - | 500 | 30 | 10 | 1.5 | 4.5 | - | 9 | 18 | 67 |
| 12 | 100 | 300 | - | 2500 | 30 | 10 | 1.5 | 4.5 | - | 9 | 18 | 67 |

ACS = AC surface course, ACB = AC base course, RM = rubblized material, FC = fractured concrete, BS = base and subbase, and RB = roadbed soil

Table 8.8 Results of the 3-D analyses of the lateral stresses induced in the AC layer of the 12 pavement sections listed in Table 8.7

| Section number | Induced lateral stresses (psi) | | | Location and magnitude of the maximum lateral stresses induced at the AC surface due to vertical and lateral contact stresses | |
|---|---|---|---|---|---|
| | At the AC bottom under the tire center due to vertical and lateral contact stresses[1] | At the AC surface, 4.425-in. from the tire center (0.075-in from the edge of the tire) | | | |
| | | Due to vertical contact stress | Due to vertical and lateral contact stress | Distance from the center of the tire (in.) | Magnitude (psi) |
| 1 | 150.4 | -0.5 | 12.5 | 1.50 | 18.5 |
| 2 | 130.3 | -49.2 | -36.2 | 21.48 | 8.7 |
| 3 | 113.6 | -125.6 | -112.7 | 22.97 | 13.5 |
| 4 | 42.9 | -47.1 | -34.2 | 9.53 | 20.4 |
| 2 | 130.3 | -49.2 | -36.2 | 21.48 | 8.7 |
| 5 | 241.7 | -28.9 | -15.9 | 27.55 | 5.0 |
| 6 | 168.6 | -63.3 | 1.8 | 10.93 | 10.4 |
| 7 | 112.4 | -36.2 | 10.2 | 4.43 | 10.2 |
| 8 | 64.8 | -9.6 | 19.8 | 1.50 | 24.1 |
| 7 | 112.4 | -2.7 | 10.2 | 4.43 | 10.2 |
| 9 | 95.6 | 2.2 | 15.1 | 4.43 | 15.1 |
| 10 | 29.1 | 10.5 | 23.5 | 1.50 | 26.4 |
| 11 | -21.8 | 16.4 | 29.4 | 1.50 | 37.7 |
| 12 | -35.7 | 21.1 | 34.1 | 1.50 | 45.0 |

[1] The lateral stresses at the AC bottom induced by vertical contact stresses and by vertical and lateral contact stresses are practically the same.

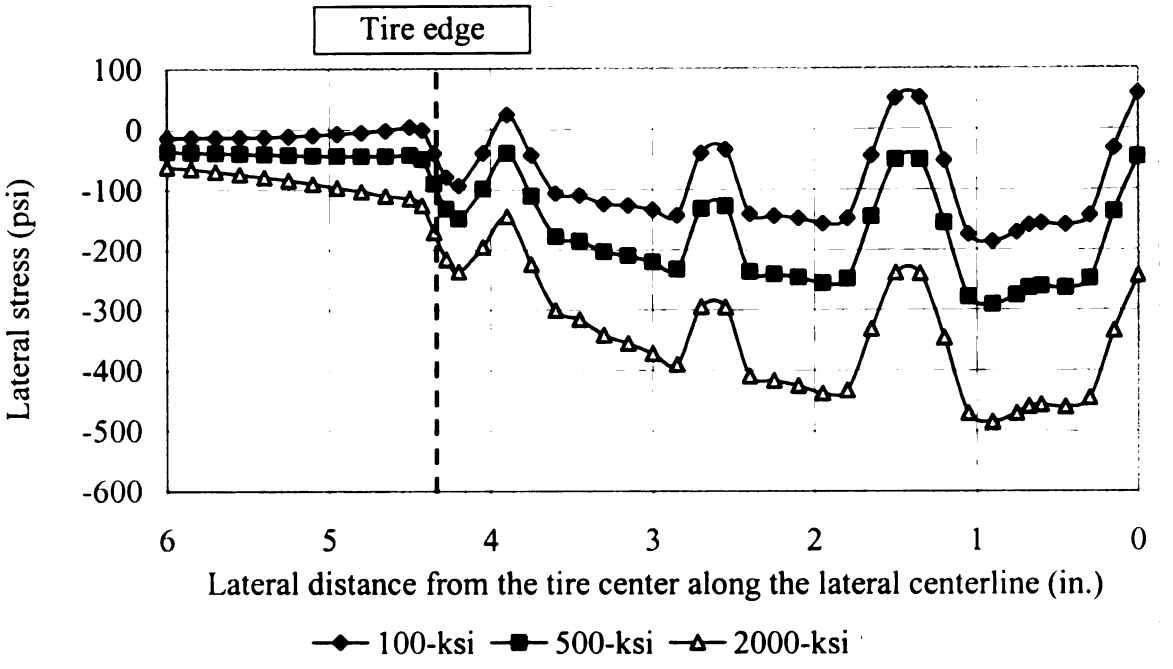


a) Lateral stresses induced by vertical contact stresses only

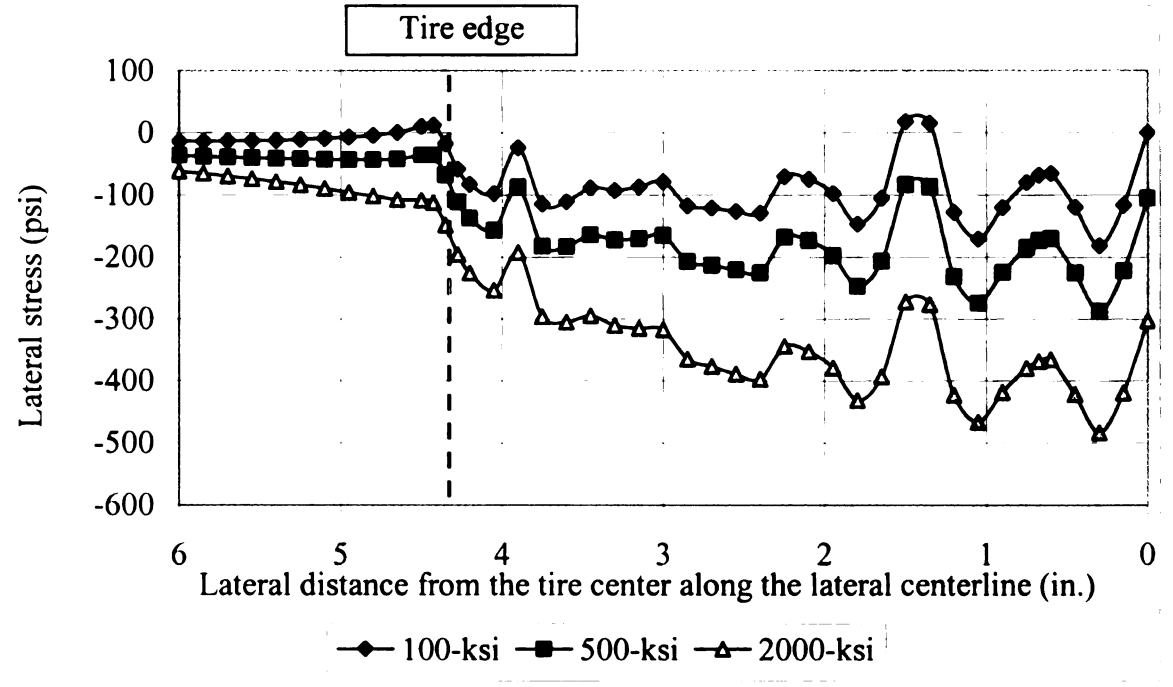


b) Lateral stresses induced by the combination of vertical and lateral contact stresses

Figure 8.32 The effects of the AC surface course modulus on the lateral stresses induced at the AC surface by vertical contact stresses and by the combination of vertical and lateral contact stresses

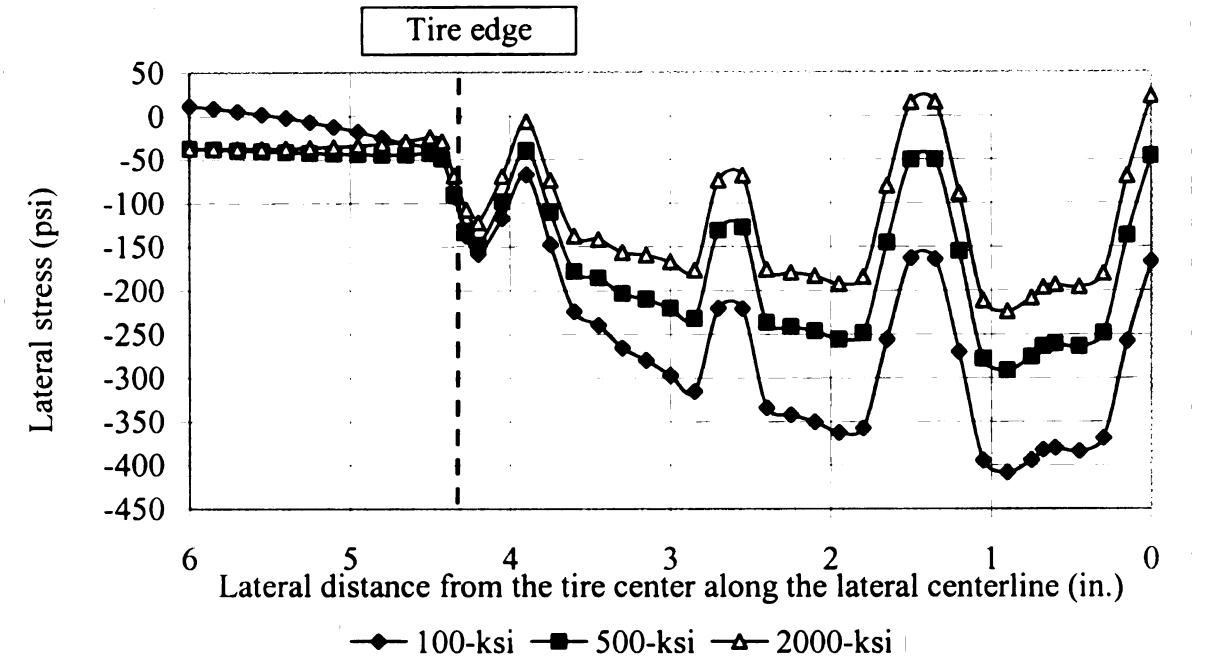


a) Lateral stresses induced by vertical contact stresses only

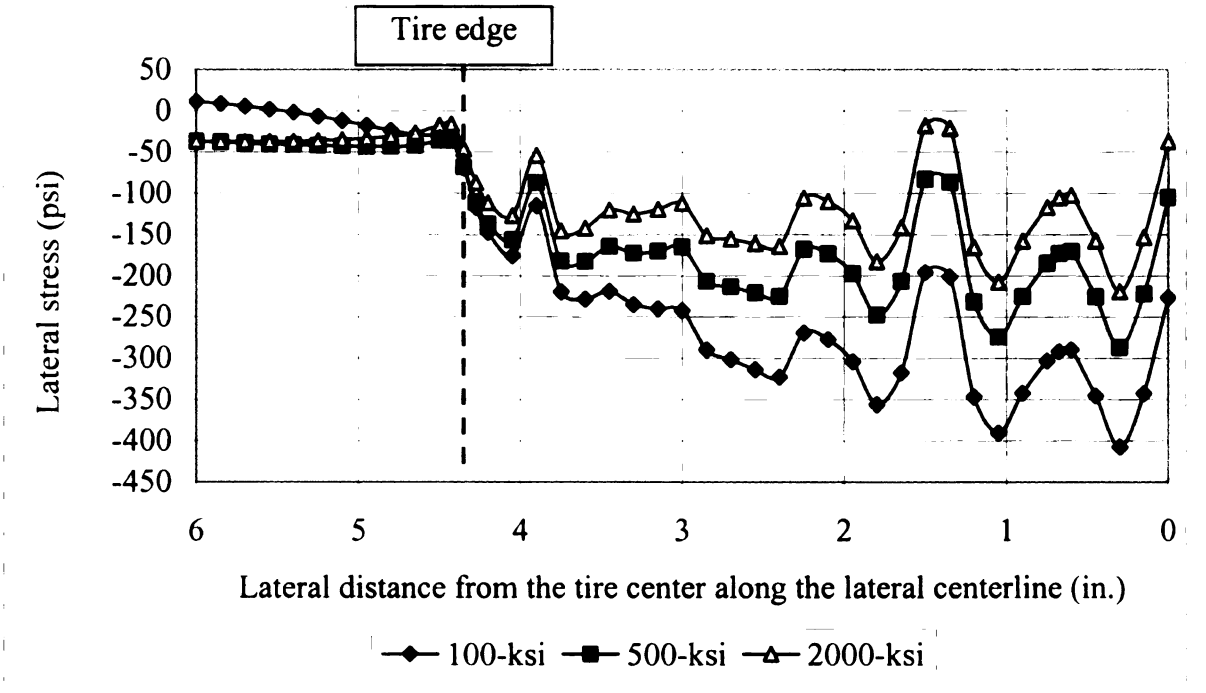


b) Lateral stresses induced by the combination of vertical and lateral contact stresses

Figure 8.33 The effects of the AC base course modulus on the lateral stresses induced at the AC surface by vertical contact stresses and by the combination of vertical and lateral contact stresses

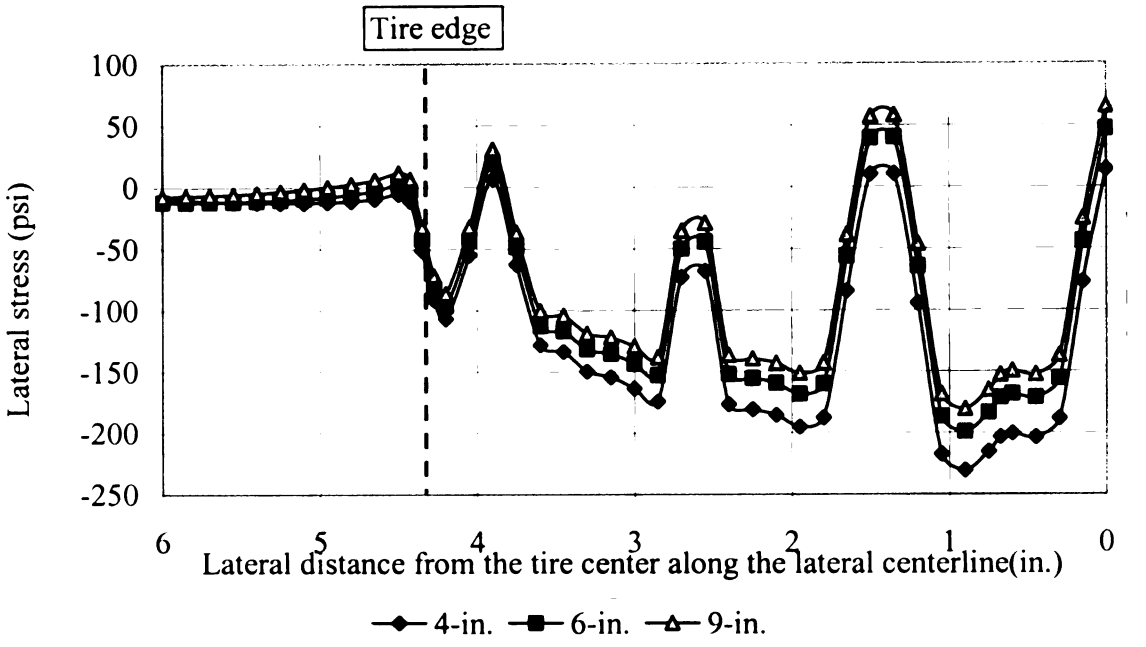


a) Lateral stresses induced by vertical contact stresses only

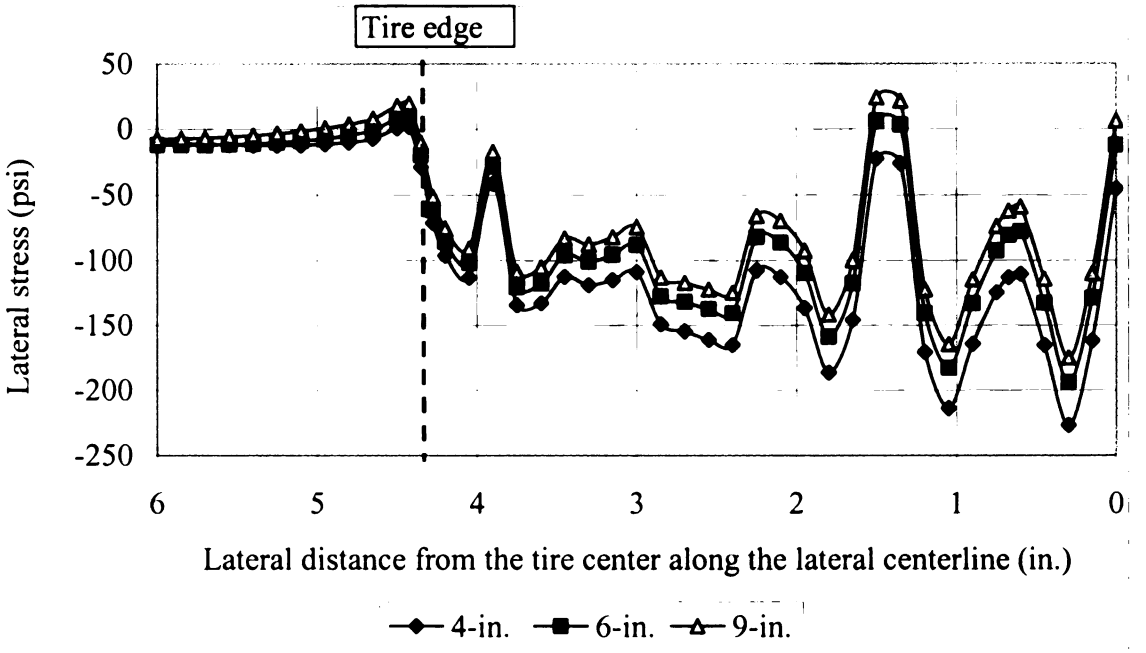


b) Lateral stresses induced by the combination of vertical and lateral contact stresses

Figure 8.34 The effects of the AC thickness on the lateral stresses induced at the AC surface by vertical contact stresses and by the combination of vertical and lateral contact stresses

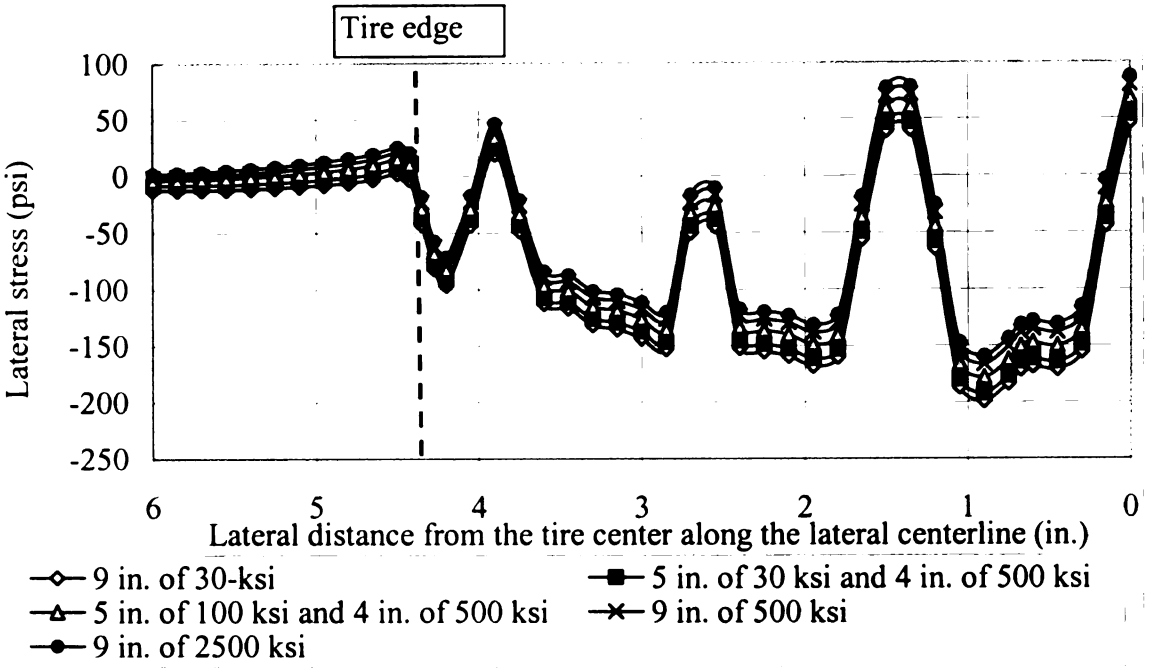


a) Lateral stresses induced by vertical contact stresses only

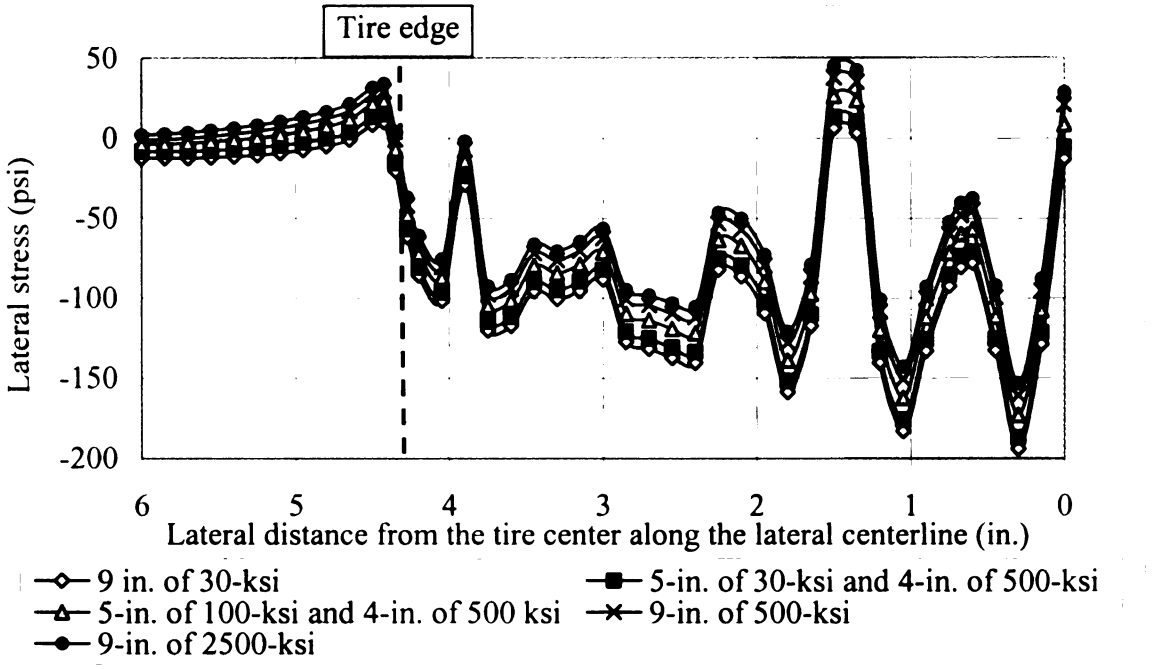


b) Lateral stresses induced by the combination of vertical and lateral contact stresses

Figure 8.35 The effects of properties of the rubblized concrete slab on the lateral stresses induced at the AC surface by vertical contact stresses and by the combination of vertical and lateral contact stresses

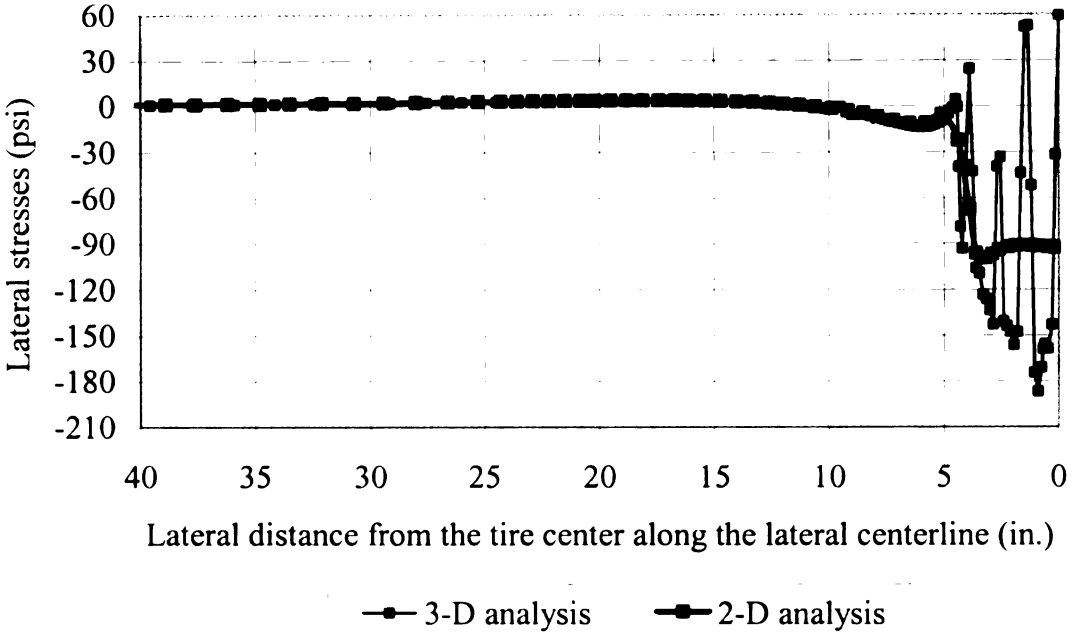


a) Induced lateral stresses at the AC surface

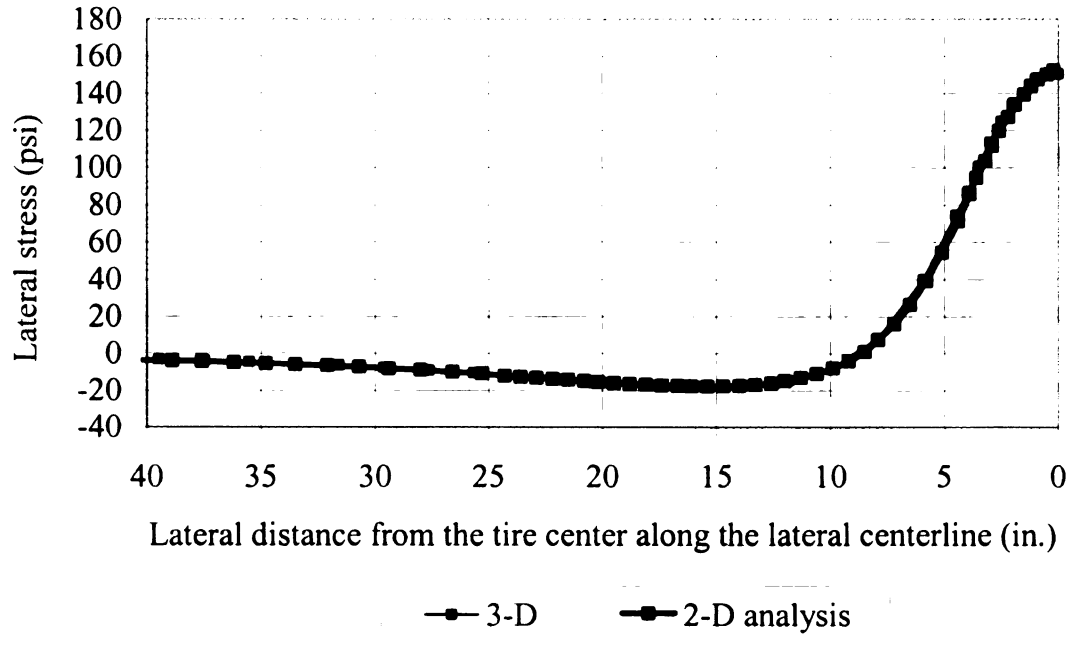


b) Induced lateral stresses at the AC bottom

Figure 8.36 The lateral stresses induced at the AC surface and the AC bottom by vertical contact stresses obtained from 2-D and 3-D analyses, pavement section 1 of Table 8.7

tire induced by the vertical and by combination of the vertical and lateral contact stresses. Examination of the figures and the data in Table 8.8 indicates that:

1. The vertical contact stresses alone induce at the AC surface high lateral compressive stresses under the tire ribs and lateral compressive or tensile stresses (depending on the groove location) under the tire grooves or at the tire edge. Although this observation was expected, it was not apparent from the results of the 2-D analyses because the ribs and grooves could not be modeled. Stated differently, in the 3-D analyses, the ribs and grooves of the tire were modeled by using several small contact areas (tire ribs) separated by no contact areas (grooves) whereas in the 2-D analyses, a single continuous circular contact area was used.
2. The combination of the vertical and lateral contact stresses causes:
   - Increase in the number of pavement sections having lateral tensile stresses at the tire edge because of the lateral tensile stresses induced at the tire edge by the lateral contact stresses.
   - Reversal in the lateral stresses from tension to compression in several pavement sections under some tire grooves.
3. The variations in the induced lateral stresses under the tire ribs and grooves at the AC surface in the vicinity of the tire dissipate with increasing distance from the tire (see Figure 8.36). This is so because according to St. Vernon principle, the effect of the shape of the contact area on the induced lateral stresses decreases with increasing distance from the contact area. The significance of this is that the load-induced

stresses at the AC bottom due to single wheel could be studied using 2-D analyses (no need to simulate tire ribs and grooves).

4. The lateral stresses induced at the AC surface at the tire edge increase as:
   - The ACS modulus decreases;
   - The AC thickness increases;
   - The RM and the FC moduli increase; and
   - The RM thickness decreases.

   Note that, increases in the ACB modulus may increase or decrease the lateral stresses induced at the tire edges as previously explained in section 4.2.3. The explanations for the effects of the ACS modulus, AC thickness, RM thickness and modulus and FC modulus on the lateral stresses at the AC surface at the tire edge are the same as those presented in section 4.0 for the 2-D analyses.

5. The lateral stresses induced at the AC bottom increases as:
   - The AC thickness and the ACS modulus decrease;
   - The ACB modulus increases;
   - The RM and the FC moduli decrease; and
   - The RM thickness decreases.

   The explanations for the effect of each of the above variables on the lateral stresses induced at the AC bottom are the same as those presented in section 4.0 for the 2-D analyses.

It should be noted that relative to the bottom of the AC layer, the maximum induced tensile stress could be located under the center of the tire or within a

fraction of an inch from the center depending on the geometry of the ribs and grooves of the tire. Hence, the term "tire center" used in this dissertation implies the vicinity of the tire center. Likewise, the term "edge of tire" implies 0 to 1-in from the edge of the tire.

## 5.4. The Effects of the Interface Geometry between the RM and the FC Layers

The effects of the interface geometry between the RM and the FC layers on the induced lateral stresses in the AC layer are analyzed and the results are summarized in Table 8.9. The various interface geometries used in the analyses are illustrated in Figures 8.37 through 8.39 and explained below.

- Geometry 1 is a uniform zigzag uneven interface with the thickness of the FC layer varying from 2 to 6 in.
- Geometries 2 and 3 are uneven interfaces having randomly generated boundaries.
- Geometries 4 through 6 are uneven interfaces with a RM channel under the tire (in the wheel path). Geometry 4 is repeated 4 times to accommodate the following widths of the RM channel: 4, 4.35, 5, and 9 in.
- Geometries 7 and 8 are uneven interfaces with a FC ridge under the tire (in the wheel path). Geometry 7 is repeated three times to accommodate the following widths of the FC ridge: 4, 4.35 and 5 in.
- Geometry 9 is an even interface with RM thicknesses of 5 and 0 in.

Relative to the interface geometries, two points should be noted as follows:

Table 8.9 Results of the 3-D analyses of the lateral stresses induced in the AC layer in rubblized pavement sections having the various interface geometries between the RM and the FC layers illustrated in Figures 8.37 to 8.39

| Geometry | Half channel/ half ridge width (in.) | Modulus (ksi) | | | | | | Thickness (in.) | | | | | | Lateral stress (psi) | | | | |
|---|---|---|---|---|---|---|---|---|---|---|---|---|---|---|---|---|---|---|
| | | | | | | | | | | | | | | At the AC surface | | | Maximum at the AC bottom | |
| | | | | | | | | | | | | | | At 0.075 in from the tire edge | Maximum | | | |
| | | ACS | ACB | RM | FC | BS | RB | ACS | ACB | RM | FC | BS | RB | | Distance from the tire center (in.) | Magnitude | Distance from the tire center (in.) | Magnitude |
| Uniform zigzag fractured concrete surface with thickness from 2 to 6 in. | | | | | | | | | | | | | | | | | | |
| 1 | - | 100 | 300 | 30 | 500 | 30 | 10 | 1.5 | 4.5 | N/A | N/A | 18 | 67 | 29.0 | 4.43 | 29.0 | 0.5 | 89.5 |
| Randomly generated interfaces | | | | | | | | | | | | | | | | | | |
| 2 | - | 100 | 300 | 30 | 500 | 30 | 10 | 1.5 | 4.5 | N/A | N/A | 18 | 67 | 19.2 | 4.43 | 19.2 | 0.0 | 81.6 |
| 3 | - | 100 | 300 | 30 | 500 | 30 | 10 | 1.5 | 4.5 | N/A | N/A | 18 | 67 | 11.8 | 4.43 | 11.8 | 0.0 | 105.1 |
| A RM channel under the tire | | | | | | | | | | | | | | | | | | |
| 4 | 4.00 | 100 | 300 | 30 | 500 | 30 | 10 | 1.5 | 4.5 | N/A | N/A | 18 | 67 | 30.6 | 4.43 | 30.6 | 0.5 | 63.7 |
| 4 | 4.35 | 100 | 300 | 30 | 500 | 30 | 10 | 1.5 | 4.5 | N/A | N/A | 18 | 67 | 29.9 | 4.43 | 29.9 | 0.5 | 65.4 |
| 4 | 5.00 | 100 | 300 | 30 | 500 | 30 | 10 | 1.5 | 4.5 | N/A | N/A | 18 | 67 | 28.3 | 4.43 | 28.3 | 0.5 | 73.2 |
| 4 | 9.00 | 100 | 300 | 30 | 500 | 30 | 10 | 1.5 | 4.5 | N/A | N/A | 18 | 67 | 15.1 | 4.43 | 15.1 | 0.5 | 98.2 |
| 5 | 4.35 | 100 | 300 | 30 | 500 | 30 | 10 | 1.5 | 4.5 | N/A | N/A | 18 | 67 | 30.3 | 4.43 | 30.3 | 0.5 | 58.7 |
| 6 | 4.35 | 100 | 300 | 30 | 500 | 30 | 10 | 1.5 | 4.5 | N/A | N/A | 18 | 67 | 17.0 | 4.43 | 17.0 | 0.0 | 92.3 |
| A FC ridge under the tire | | | | | | | | | | | | | | | | | | |
| 7 | 4.00 | 100 | 300 | 30 | 500 | 30 | 10 | 1.5 | 4.5 | N/A | N/A | 18 | 67 | 26.0 | 1.50 | 40.3 | 4.5 | 37.9 |
| 7 | 4.35 | 100 | 300 | 30 | 500 | 30 | 10 | 1.5 | 4.5 | N/A | N/A | 18 | 67 | 26.9 | 1.50 | 40.4 | 4.5 | 31.9 |
| 7 | 5.00 | 100 | 300 | 30 | 500 | 30 | 10 | 1.5 | 4.5 | N/A | N/A | 18 | 67 | 27.7 | 1.50 | 40.8 | 5.0 | 28.9 |
| 8 | 4.35 | 100 | 300 | 30 | 500 | 30 | 10 | 1.5 | 4.5 | N/A | N/A | 18 | 67 | 18.4 | 1.50 | 18.9 | 0.0 | 84.8 |
| Even interface | | | | | | | | | | | | | | | | | | |
| 9 | - | 100 | 300 | 30 | 500 | 30 | 10 | 1.5 | 4.5 | 5 | 4 | 18 | 67 | 15.1 | 4.43 | 15.1 | 0.0 | 95.6 |
| 9 | - | 100 | 300 | - | 500 | 30 | 10 | 1.5 | 4.5 | 0 | 9 | 18 | 67 | 29.4 | 1.50 | 37.7 | 49.3 | 0.30 |

ACS = AC surface course, ACB = AC base course, RM = rubblized material, FC = fractured concrete, BS = base and subbase, RB = roadbed soil, N/A = not available because the RM and FC thicknesses are not the same along the uneven interface.

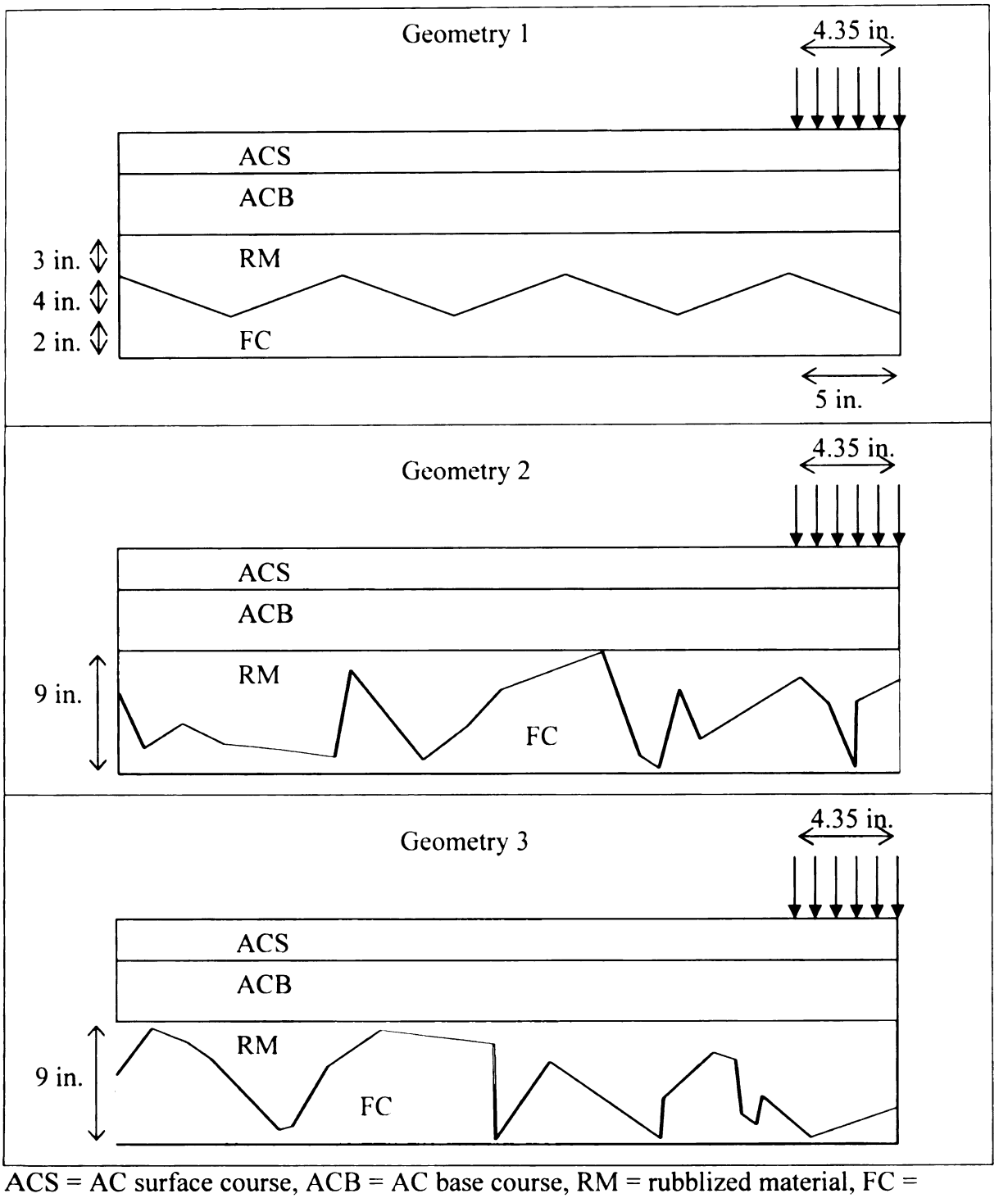


ACS = AC surface course, ACB = AC base course, RM = rubblized material, FC = fractured concrete

Figure 8.37 Geometries 1 through 3 of the interface between the RM and the FC layers used in the 3-D analyses of the effects of the uneven interface on the load-induced lateral stresses in the AC layer.

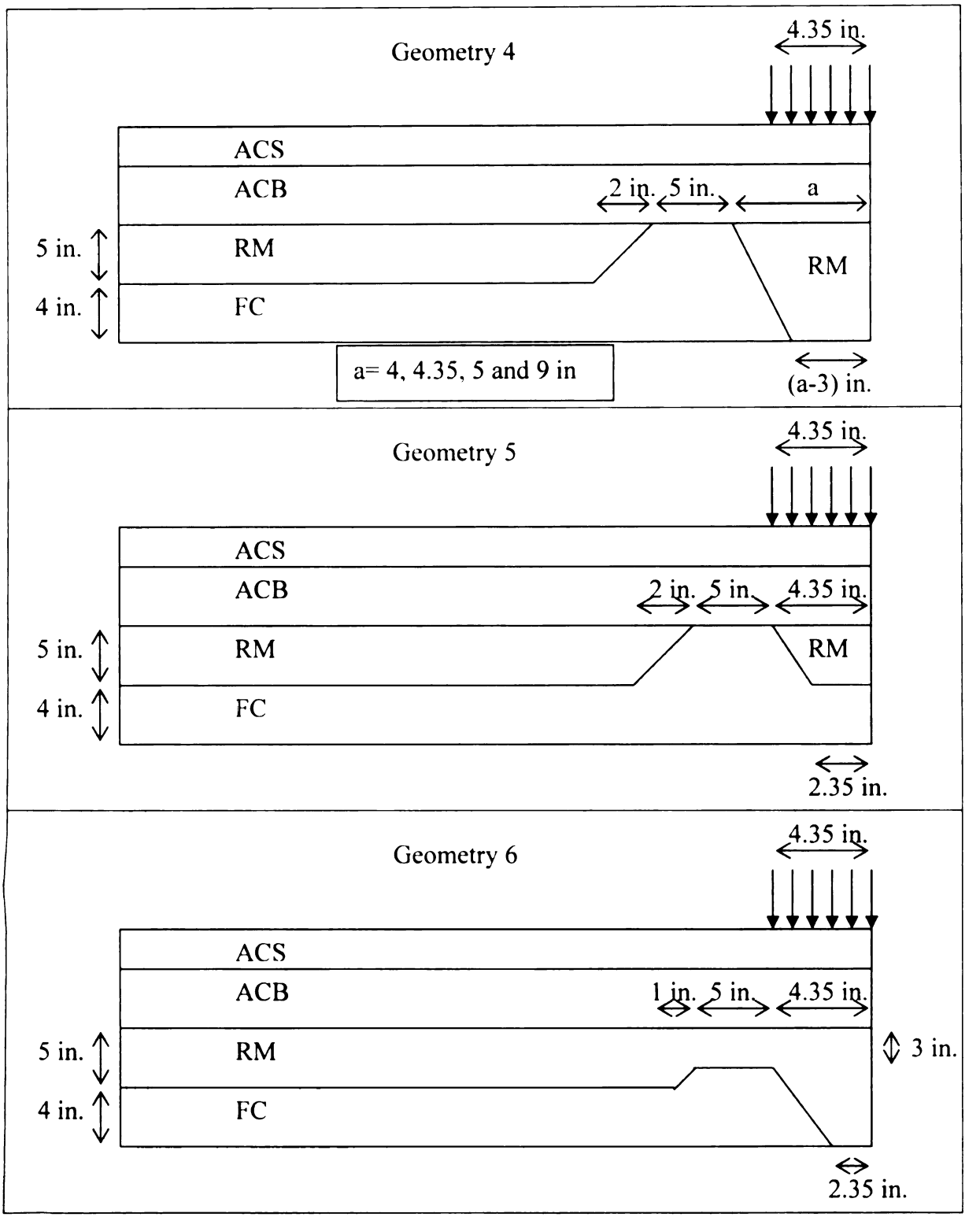


ACS = AC surface course, ACB = AC base course, RM = rubblized material, FC = fractured concrete

Figure 8.38 Geometries 4 through 6 of the interface between the RM and the FC layers used in the 3-D analyses of the effects of the uneven interface on the load-induced lateral stresses in the AC layer

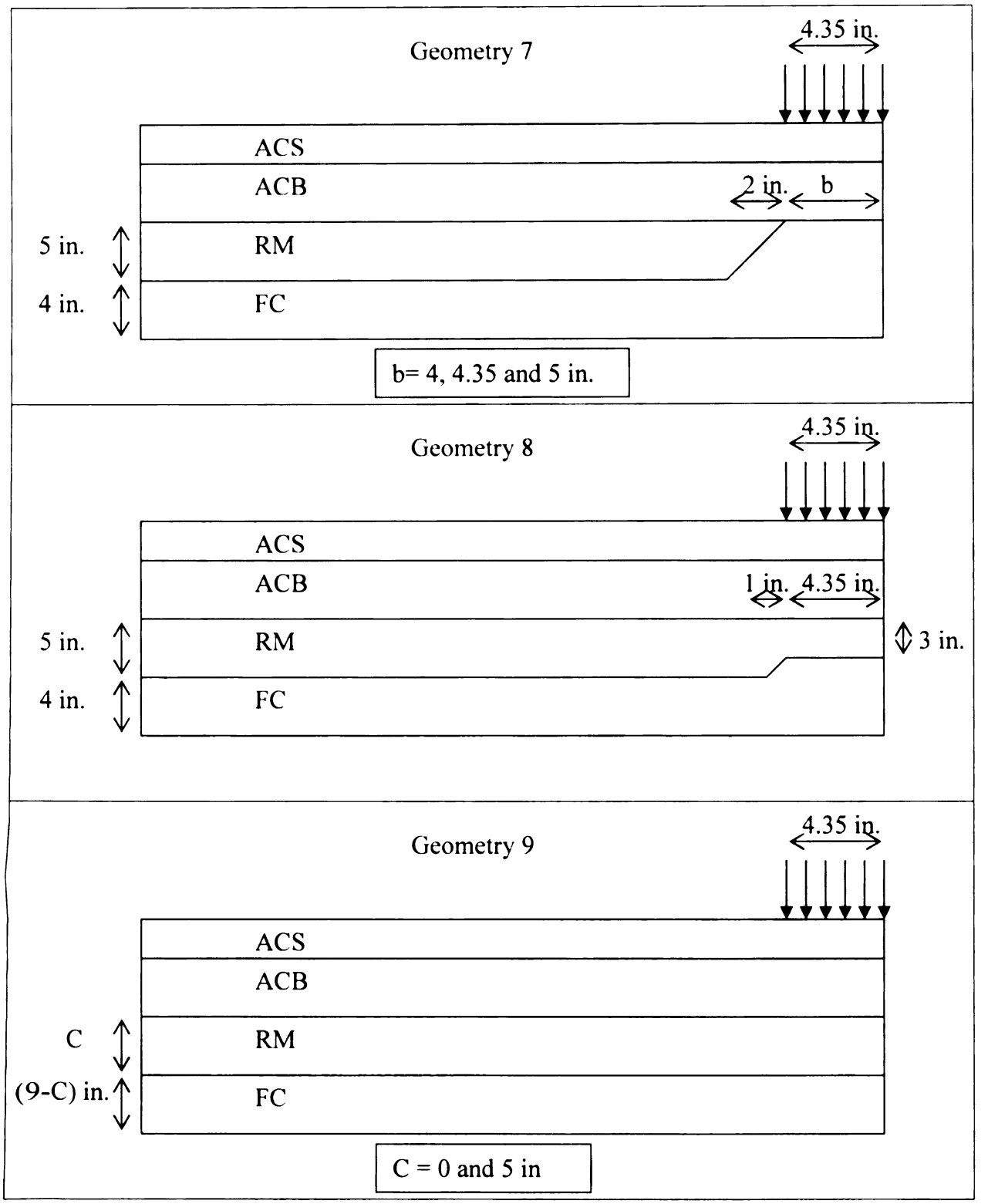


ACS = AC surface course, ACB = AC base course, RM = rubblized material, FC = fractured concrete

Figure 8.38 Geometries 7, 8 and 9 of the interface between the RM and the FC layers used in the 3-D analyses of the effects of the uneven interface on the load-induced lateral stresses in the AC layer

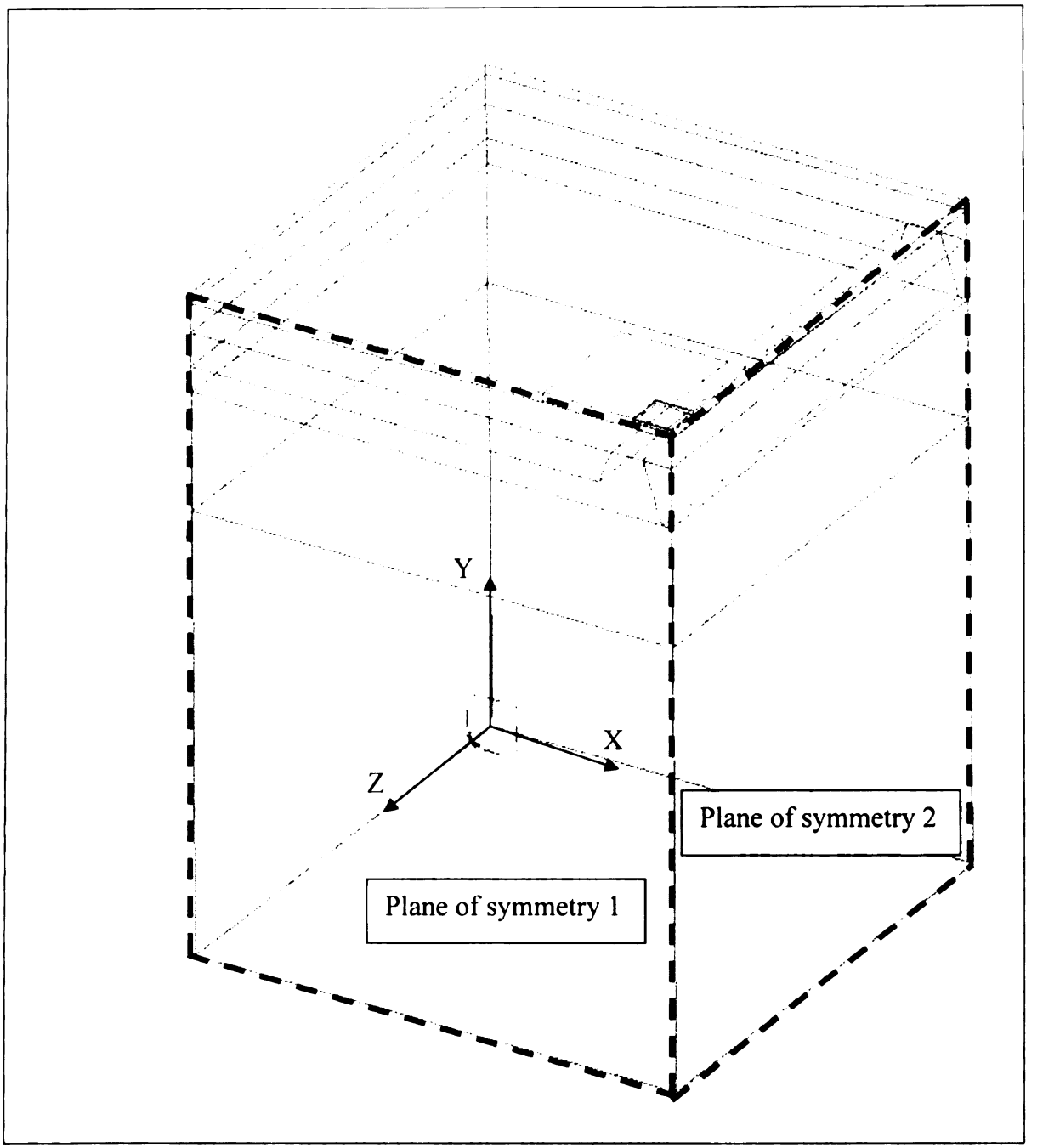


Figure 8.40 Three-dimensional view of the quarter model with the interface geometry 4 of Figure 8.38 (uneven interface with RM channel under the tire)

1. The widths of the loaded area, the RM channel and the FC ridge shown in Figures 8.37 through 8.39 are to be used in the 3-D FEM quarter model shown in Figure 8.40. Given the two planes of symmetry of the quarter model, the full widths of the contact area, the RM channel and the FC ridge in the full model are twice those stated in Figures 8.37 through 8.39.
2. All the interface geometries shown in 2-D in Figures 8.37 through 8.39 are the same throughout the length of the z-coordinate of the 3-D FEM quarter model shown in Figure 8.40.

Finally, Table 8.9 provides the thicknesses and moduli of all the layers used in 3-D analyses as well as the resulting lateral stresses induced at the AC surface and the AC bottom. Figure 8.41 depicts the lateral tensile stresses induced at the AC surface at the tire edge of pavements having various geometries of the interface between the RM and the FC layers (see Figure 8.37 through 8.39). Examination of the results listed in Table 8.9 and plotted in Figure 4.41 indicates that:

1. In most pavement sections, the maximum lateral tensile stresses at the AC surface are located at the tire edge. Whereas for those pavement sections with a FC ridge under the tire, the maximum stresses are located at 1.5 in. from the tire center between ribs 3 and 4. This is because the presence of the FC ridge under the tire decreases the lateral compressive stresses induced by the vertical contact stresses at the pavement surface under the tire.

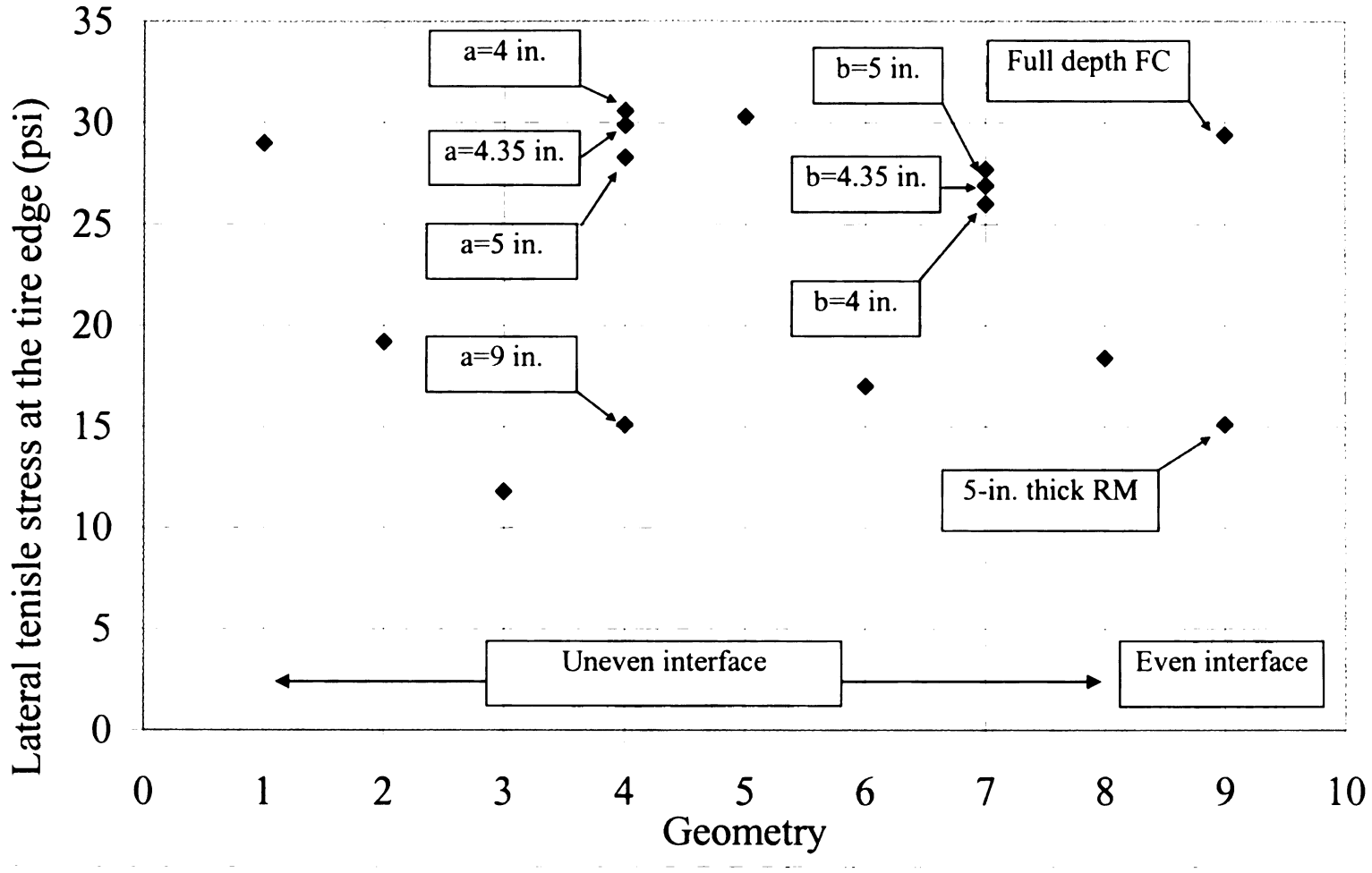


Figure 8.41 Lateral tensile stresses induced at the AC surface at the tire edge of pavement sections having the various geometries of the interface shown in Figure 8.37 through 8.40

2. In most pavement sections, the maximum lateral tensile stresses at the AC bottom are located under the tire center. Whereas pavement sections having 9-in thick FC ridge under the tire center, the lateral stresses under the tire are compressive (not listed in Table 8.9), which is similar to pavement sections with full depth FC or composite pavements.

3. As shown in Figure 8.41, the induced lateral stresses at the AC surface are function of the interface geometry between the RM and the FC layers. Uneven interfaces may results in lower or higher lateral tensile stresses at the AC surface relative to the even interfaces. For examples, geometry 9 (even interface) with RM thickness of 5 in. results in higher maximum lateral tensile stresses at the AC surface relative to geometry 3 but lower relative to geometries 1 and 2. Note that, the average thicknesses of the FC layer of section 9, geometries 1, 2 and 3 are 4, 4, 4.2 and 4.5 in., respectively.

4. The induced lateral stresses at the AC surface and at the AC bottom are function of the thickness and location of the FC ridge relative to the tire. When two full depth FC ridges are used (the FC is directly beneath the AC layer, one ridge is under the center of the tire and the other is under the edge of the tire, geometry 7), the induced lateral stresses at both locations are similar to those of the pavement section with full depth FC (geometry 9 with C = 0 in.). That is the lateral tensile stresses induced at the AC surface at the tire edge are relatively high and the lateral stresses induced at the AC bottom at the tire center are compressive stresses. When one full

depth FC ridge is located under the tire edge (geometry 4 with a = 4, 4.35 and geometry 5); the lateral stresses at the AC surface at the tire edge are similar to those of the pavement section with full depth FC and tensile lateral stresses are induced at the AC bottom. However, said tensile stresses at the Ac bottom are lower than those induced in the pavement section with even interface (geometry 9 with C = 5 in.). Finally, when a partial depth FC layer is used in the vicinity of the tire (geometry 4 with a = 9 in. and geometries 6 and 8), the induced lateral stresses at the AC surface and bottom are similar to those induced in pavement sections with even interface (geometry 9 with C = 5 in.) than to those with full depth FC (geometry 9 with c=0 in.).

5. Relative to geometries 4 and 5, as was expected, increasing width and depth of the RM channel under the tire cause decreases in the induced lateral tensile stresses at the AC surface at the tire edge and increases in the tensile stresses at the bottom of the AC layer.

6. Wider FC ridges under the tire cause higher lateral tensile stresses at the AC surface at the tire edge and lower lateral tensile stresses at the AC bottom under the tire center.

7. Interface geometry 4 with a = 4.35 in. has the most effect on the tensile stresses induced at the AC surface amongst all other geometries included in the analyses. This geometry was further analyzed using various properties of the AC, RM and FC layers.

Tables 8.10 through 8.12 provide the layer properties and the lateral stresses induced at the AC surface and the AC bottom of twelve pavement sections having uneven interface conforming to geometry 4. The reason that the RM and FC layer thicknesses are labeled "N/A" in the tables is that said thicknesses vary along the uneven interface. That is, each geometry of the uneven interface has its unique variations in the RM and FC layer thicknesses. In addition, the effects of the moduli of the BS layer and RB soil are not included in the 3-D analyses because they have relatively small impact on the stresses induced at the AC surface and the same effects on the lateral stresses at the AC bottom under the tire center as those reported in the 2-D analyses.

Examination of the data in the three tables indicates that:

1. The maximum induced lateral tensile stresses at the AC surface due to vertical and lateral contact stresses are located at the tire edge for the majority of the pavement sections with 4 and 6-in. AC layer (Tables 8.10 and 8.11). Whereas they are located at 1.5 in. from the tire center for the majority of the pavement sections with 9-in. AC layer (Table 8.12).
2. As can be seen in Table 8.11, decreases in the AC modulus (both ACS and ACB moduli) cause increases in the lateral tensile stresses at the tire edge. This is mainly because of the effects of the ACS modulus on the induced lateral stresses at the AC surface as explained in section 4.2.2. When the moduli of the AC courses are greater than 500 ksi, the magnitude of the maximum induced lateral tensile stresses at the AC surface is insignificant.
3. The lateral tensile stresses at the AC bottom under the tire center increases as:
   - The AC thickness and ACS modulus decrease;

Table 8.10 Results of 3-D analyses of the lateral stresses induced in the AC layer in pavement sections with 4-in. thick AC and a channel of rubblized material under the tire (Geometry 4 of Figure 8.32)

| Geometry | Half channel width (in.) | Modulus (ksi) | | | | | | Thickness (in.) | | | | | | Lateral stress (psi) | | | | |
|---|---|---|---|---|---|---|---|---|---|---|---|---|---|---|---|---|---|---|
| | | | | | | | | | | | | | | At the AC surface | | | Maximum at the AC bottom | |
| | | | | | | | | | | | | | | At 0.075-in from the tire edge | Maximum | | | |
| | | ACS | ACB | RM | FC | BS | RB | ACS | ACB | RM | FC | BS | RB | | Distance from the tire center (in.) | Magnitude | Distance from the tire center (in.) | Magnitude |
| 4 | 4.35 | 100 | 300 | 30 | 500 | 30 | 10 | 1.5 | 2.5 | N/A | N/A | 18 | 69 | 41.1 | 4.43 | 41.1 | 0.0 | 108.5 |
| 4 | 4.35 | 300 | 300 | 30 | 500 | 30 | 10 | 1.5 | 2.5 | N/A | N/A | 18 | 69 | 41.1 | 4.50 | 41.9 | 0.0 | 95.0 |
| 4 | 4.35 | 500 | 300 | 30 | 500 | 30 | 10 | 1.5 | 2.5 | N/A | N/A | 18 | 69 | 39.4 | 5.70 | 50.8 | 0.0 | 90.0 |
| 4 | 4.35 | 300 | 100 | 30 | 500 | 30 | 10 | 1.5 | 2.5 | N/A | N/A | 18 | 69 | 47.6 | 4.43 | 47.6 | 0.5 | 28.5 |
| 4 | 4.35 | 300 | 300 | 30 | 500 | 30 | 10 | 1.5 | 2.5 | N/A | N/A | 18 | 69 | 41.1 | 4.43 | 41.1 | 0.0 | 108.5 |
| 4 | 4.35 | 300 | 500 | 30 | 500 | 30 | 10 | 1.5 | 2.5 | N/A | N/A | 18 | 69 | 37.8 | 4.43 | 37.8 | 0.0 | 161.4 |
| 4 | 4.35 | 100 | 300 | 30 | 500 | 30 | 10 | 1.5 | 2.5 | N/A | N/A | 18 | 69 | 41.1 | 4.43 | 41.1 | 0.0 | 108.5 |
| 4 | 4.35 | 100 | 300 | 50 | 500 | 30 | 10 | 1.5 | 2.5 | N/A | N/A | 18 | 69 | 37.6 | 4.43 | 37.6 | 0.5 | 72.5 |
| 4 | 4.35 | 100 | 300 | 100 | 500 | 30 | 10 | 1.5 | 2.5 | N/A | N/A | 18 | 69 | 32.3 | 4.43 | 32.3 | 0.0 | 18.6 |
| 4 | 4.35 | 100 | 300 | 30 | 100 | 30 | 10 | 1.5 | 2.5 | N/A | N/A | 18 | 69 | 21.9 | 4.43 | 21.9 | 0.5 | 137.3 |
| 4 | 4.35 | 100 | 300 | 30 | 500 | 30 | 10 | 1.5 | 2.5 | N/A | N/A | 18 | 69 | 41.1 | 4.43 | 41.1 | 0.0 | 108.5 |
| 4 | 4.35 | 100 | 300 | 30 | 2500 | 30 | 10 | 1.5 | 2.5 | N/A | N/A | 18 | 69 | 48.7 | 4.43 | 48.7 | 0.0 | 92.9 |

ACS = AC surface course, ACB = AC base course, RM = rubblized material, FC = fractured concrete, BS = base and subbase, RB = roadbed soil, N/A = not available because the RM and FC thicknesses vary across the uneven interfaces

Table 8.11 Pavement layer thicknesses and moduli and the lateral stresses induced in the AC layer of the pavement sections with 6-in. AC and a channel of rubblized material under the tire (Geometry 4 of Figure 8.32)

| Geometry | Half channel width (in.) | Modulus (ksi) | | | | | | Thickness (in.) | | | | | | Lateral stress (psi) | | | | |
|---|---|---|---|---|---|---|---|---|---|---|---|---|---|---|---|---|---|---|
| | | | | | | | | | | | | | | At the AC surface | | | Maximum at the AC bottom | |
| | | | | | | | | | | | | | | At 0.075 in. from the tire edge | Maximum | | | |
| | | ACS | ACB | RM | FC | BS | RB | ACS | ACB | RM | FC | BS | RB | | Distance from the tire center (in.) | Magnitude | Distance from the tire center (in.) | Magnitude |
| 4 | 4.35 | 300 | 300 | 30 | 500 | 30 | 10 | 1.5 | 4.5 | N/A | N/A | 18 | 67 | 29.9 | 4.43 | 29.9 | 0.5 | 65.4 |
| 4 | 4.35 | 500 | 500 | 30 | 500 | 30 | 10 | 1.5 | 4.5 | N/A | N/A | 18 | 67 | 11.2 | 4.43 | 11.2 | 0.5 | 80.8 |
| 4 | 4.35 | 1000 | 1000 | 30 | 500 | 30 | 10 | 1.5 | 4.5 | N/A | N/A | 18 | 67 | -7.6 | 30.72 | 1.8 | 0.5 | 111.7 |
| 4 | 4.35 | 2000 | 2000 | 30 | 500 | 30 | 10 | 1.5 | 4.5 | N/A | N/A | 18 | 67 | -34.5 | 35.91 | 3.7 | 0.5 | 147.1 |
| 4 | 4.35 | 100 | 300 | 30 | 500 | 30 | 10 | 1.5 | 4.5 | N/A | N/A | 18 | 67 | 29.9 | 4.43 | 29.9 | 0.5 | 65.4 |
| 4 | 4.35 | 300 | 300 | 30 | 500 | 30 | 10 | 1.5 | 4.5 | N/A | N/A | 18 | 67 | 20.7 | 4.43 | 20.7 | 0.5 | 60.1 |
| 4 | 4.35 | 500 | 300 | 30 | 500 | 30 | 10 | 1.5 | 4.5 | N/A | N/A | 18 | 67 | 13.8 | 6.00 | 18.2 | 0.5 | 57.7 |
| 4 | 4.35 | 300 | 100 | 30 | 500 | 30 | 10 | 1.5 | 4.5 | N/A | N/A | 18 | 67 | 32.6 | 4.43 | 32.6 | 0.5 | 19.8 |
| 4 | 4.35 | 300 | 300 | 30 | 500 | 30 | 10 | 1.5 | 4.5 | N/A | N/A | 18 | 67 | 29.9 | 4.43 | 29.9 | 0.5 | 65.4 |
| 4 | 4.35 | 300 | 500 | 30 | 500 | 30 | 10 | 1.5 | 4.5 | N/A | N/A | 18 | 67 | 29.3 | 1.50 | 31.1 | 0.5 | 91.7 |
| 4 | 4.35 | 100 | 300 | 30 | 500 | 30 | 10 | 1.5 | 4.5 | N/A | N/A | 18 | 67 | 29.9 | 4.43 | 29.9 | 0.5 | 65.4 |
| 4 | 4.35 | 100 | 300 | 50 | 500 | 30 | 10 | 1.5 | 4.5 | N/A | N/A | 18 | 67 | 29.6 | 4.43 | 29.6 | 0.5 | 48.6 |
| 4 | 4.35 | 100 | 300 | 100 | 500 | 30 | 10 | 1.5 | 4.5 | N/A | N/A | 18 | 67 | 29.0 | 4.43 | 29.0 | 0.5 | 19.3 |
| 4 | 4.35 | 100 | 300 | 30 | 100 | 30 | 10 | 1.5 | 4.5 | N/A | N/A | 18 | 67 | 19.9 | 4.43 | 19.9 | 0.5 | 89.8 |
| 4 | 4.35 | 100 | 300 | 30 | 500 | 30 | 10 | 1.5 | 4.5 | N/A | N/A | 18 | 67 | 29.9 | 4.43 | 29.9 | 0.5 | 65.4 |
| 4 | 4.35 | 100 | 300 | 30 | 2500 | 30 | 10 | 1.5 | 4.5 | N/A | N/A | 18 | 67 | 34.5 | 4.43 | 34.5 | 0.5 | 50.3 |

ACS = AC surface course, ACB = AC base course, RM = rubblized material, FC = fractured concrete, BS = base and subbase, RB = roadbed soil, N/A = not available because the RM and FC thicknesses vary across the uneven interfaces

Table 8.12 Results of 3-D analyses of the lateral stresses induced in the AC layer in pavement sections with 9-in. thick AC and a channel of rubblized material under the tire (Geometry 4 of Figure 8.32)

| Geometry | Half channel width (in.) | Modulus (ksi) | | | | | | Thickness (in.) | | | | | | Lateral stress (psi) | | | | |
|---|---|---|---|---|---|---|---|---|---|---|---|---|---|---|---|---|---|---|
| | | | | | | | | | | | | | | At the AC surface | | | Maximum at the AC bottom | |
| | | | | | | | | | | | | | | At 0.075-in from the tire edge | Maximum | | | |
| | | ACS | ACB | RM | FC | BS | RB | ACS | ACB | RM | FC | BS | RB | | Distance from the tire center (in.) | Magnitude | Distance from the tire center (in.) | Magnitude |
| 4 | 4.35 | 100 | 300 | 30 | 500 | 30 | 10 | 1.5 | 7.5 | N/A | N/A | 18 | 64 | 28.8 | 1.50 | 32.8 | 0.5 | 38.2 |
| 4 | 4.35 | 300 | 300 | 30 | 500 | 30 | 10 | 1.5 | 7.5 | N/A | N/A | 18 | 64 | 18.8 | 4.43 | 18.8 | 0.5 | 36.3 |
| 4 | 4.35 | 500 | 300 | 30 | 500 | 30 | 10 | 1.5 | 7.5 | N/A | N/A | 18 | 64 | 11.3 | 4.50 | 11.6 | 0.5 | 35.4 |
| 4 | 4.35 | 300 | 100 | 30 | 500 | 30 | 10 | 1.5 | 7.5 | N/A | N/A | 18 | 64 | 28.4 | 4.43 | 28.4 | 0.5 | 11.8 |
| 4 | 4.35 | 300 | 300 | 30 | 500 | 30 | 10 | 1.5 | 7.5 | N/A | N/A | 18 | 64 | 28.8 | 1.50 | 32.8 | 0.5 | 38.2 |
| 4 | 4.35 | 300 | 500 | 30 | 500 | 30 | 10 | 1.5 | 7.5 | N/A | N/A | 18 | 64 | 29.4 | 1.50 | 41.2 | 0.5 | 52.6 |
| 4 | 4.35 | 100 | 300 | 30 | 500 | 30 | 10 | 1.5 | 7.5 | N/A | N/A | 18 | 64 | 28.8 | 1.50 | 32.8 | 0.5 | 38.2 |
| 4 | 4.35 | 100 | 300 | 50 | 500 | 30 | 10 | 1.5 | 7.5 | N/A | N/A | 18 | 64 | 28.9 | 1.50 | 33.6 | 0.5 | 29.7 |
| 4 | 4.35 | 100 | 300 | 100 | 500 | 30 | 10 | 1.5 | 7.5 | N/A | N/A | 18 | 64 | 29.3 | 1.50 | 35.0 | 0.5 | 14.6 |
| 4 | 4.35 | 100 | 300 | 30 | 100 | 30 | 10 | 1.5 | 7.5 | N/A | N/A | 18 | 64 | 23.9 | 1.50 | 28.1 | 0.5 | 51.8 |
| 4 | 4.35 | 100 | 300 | 30 | 500 | 30 | 10 | 1.5 | 7.5 | N/A | N/A | 18 | 64 | 28.8 | 1.50 | 32.8 | 0.5 | 38.2 |
| 4 | 4.35 | 100 | 300 | 30 | 2500 | 30 | 10 | 1.5 | 7.5 | N/A | N/A | 18 | 64 | 31.5 | 1.50 | 35.7 | 0.5 | 28.3 |

ACS = AC surface course, ACB = AC base course, RM = rubblized material, FC = fractured concrete, BS = base and subbase, RB = roadbed soil, N/A = not available because the RM and FC thicknesses vary across the uneven interfaces

- The ACS modulus increases; and
- The RM and FC layer moduli decrease.

These observations are the same as those of the 2-D analyses and those of the 3-D analyses of the pavement sections with even interface.

4. The lateral tensile stresses at the AC surface at the tire edge increases as:
   - The ACS modulus decrease;
   - The ACB modulus increases; and
   - The moduli of the FC increases.

   Increases in the AC thickness and the RM modulus may either increase or decrease the induced laterals stresses at the AC surface at the tire edge depending on the pavement structure. The AC thickness affects the flexural rigidity of the AC as explained in sections 4.2.1 and 4.2.3 and the RM modulus affects the stiffness of the AC support (see section 4.2.4).

Table 8.13 summarizes the effects of each pavement layer thicknesses and moduli on the lateral stresses in the AC layer obtained from the 2-D and 3-D analyses with even and uneven interfaces. Based on the data in Table 8.13, it was concluded that:

1. The effect of the pavement layer and roadbed soil properties on the lateral stresses induced at the AC bottom under the tire center are consistent in both 2-D and 3-D analyses that is said stresses increase as:
   - The AC thickness and the ACS modulus decrease;
   - The ACB modulus increases;

Table 8.13 A summary of the sensitivity of the lateral stress induced in the AC layer to various pavement layer and roadbed soil properties obtained from the 2-D and 3-D analyses

| Variables | | As the value of the variable increases the induced lateral stresses | | | | | |
|---|---|---|---|---|---|---|---|
| | | 2-D | | 3-D with even interface | | 3-D with uneven interface | |
| | | The AC bottom under the tire center | The AC surface at the tire edge | The AC bottom under the tire center | The AC surface at the tire edge | The AC bottom under the tire center | The AC surface at the tire edge |
| AC thickness | | T decreases | C increases or decreases [1] | T decreases | T increases | T decreases | T increases or decreases [2] |
| AC surface course modulus | | T decreases | C increases | T decreases | T decreases | T decreases | T decreases |
| AC base course modulus | | T increases | C increases or decreases [1] | T increases | T increases or decreases [1] | T increases | T increases |
| Rubblized concrete slab | Thickness | T increases | C increases | T increases | T decreases | - | - |
| | Modulus | T decreases | C decreases | T decreases | T increases | T decreases | T increases or decreases [2] |
| Fractured concrete modulus | | T decreases | C decreases | T decreases | T increases | T decreases | T increases |
| Subbase modulus | | T decreases | C decreases | - | - | - | - |
| Roadbed soil modulus | | T decreases | C decreases | - | - | - | - |
| C = compression, T = Tension | | | | | | | |

[1] The impact of the independent variable on the lateral stress at the tire edge depends on the pavement layer properties, especially the AC layer properties.

[2] The impact of the independent variable on the lateral stress at the tire edge depends on the geometry of the interface and the pavement layer properties.

- The RM thickness decreases; and
- The RM, FC, BS and RB moduli decrease.

The explanations for the above observations are listed in Table 8.4.

2. The ACS modulus has consistent and significant effect on the lateral tensile stresses at the AC surface at the tire edge in the 2-D and 3-D analyses. Increases in the ACS modulus cause decreases in the lateral tensile stresses at the tire edge because of its direct effect on the lateral compressive stresses at the AC surface at the tire center as explained in section 4.2.2. Whereas, the effects of the ACB modulus, AC thickness and RM and FC moduli on the lateral stresses induced at the tire edge vary from one pavement section to another depending on the pavement structural properties and the geometry of the interface between the RM and FC layers.

To this end, the lateral stresses induced in the AC layer were analyzed using a single wheel load. The effects of dual wheel load are analyzed and discussed in the next section.

## 5.5. The Lateral Stresses Induced in the AC Layer Due to Dual Wheel Load

The objectives of the analyses of the lateral stresses in this section are:

- Determine the lateral stresses induced in the AC layer by dual wheel load.
- Compare the lateral stresses induced in the AC layer by dual and single wheel loads.

To accomplish the above objectives, several 3-D analyses of the lateral stresses induced in the AC layers of rubblized pavements with even and uneven interfaces

between the RM and FC layers were conducted. The 3-D models, contact stresses and contact areas used in the analyses are presented below.

### 5.5.1 3-D Models, Contact Stresses and Contact Areas

By using 2 planes of symmetry, dual wheels were modeled as a half wheel and a single wheel was modeled as a quarter wheels in the 3-D quarter model used in the analyses. Figure 8.42 presents 2-D front views of the upper portions of the quarter models used in the finite element analyses. Note that, the vertical dashed lines in the figure represent the planes of symmetry perpendicular to the x-axis. Thus, only the left side of models 1 through 5 were modeled and analyzed. Finally, the group of arrows at the top of each model represents either a single or a duel wheel load. The wheel load and the contact stresses used in the analyses are presented below.

Recalling that, the single wheel load used in the previous sections is equal to 6,975 lb, which simulates half of the load on the steering axle of a truck. In this section, the analyses were conducted using a duel wheel load of 9,000 lb (Michigan center for truck safety, $6^{th}$ edition) and single wheel loads of 4,500 and 9,000 lb. The latter load was used for comparison purposes. Given the three wheel loads, the questions become:

- What is the size and shape of the contact area?
- What are the distributions of the vertical and lateral contact stresses over the contact area?

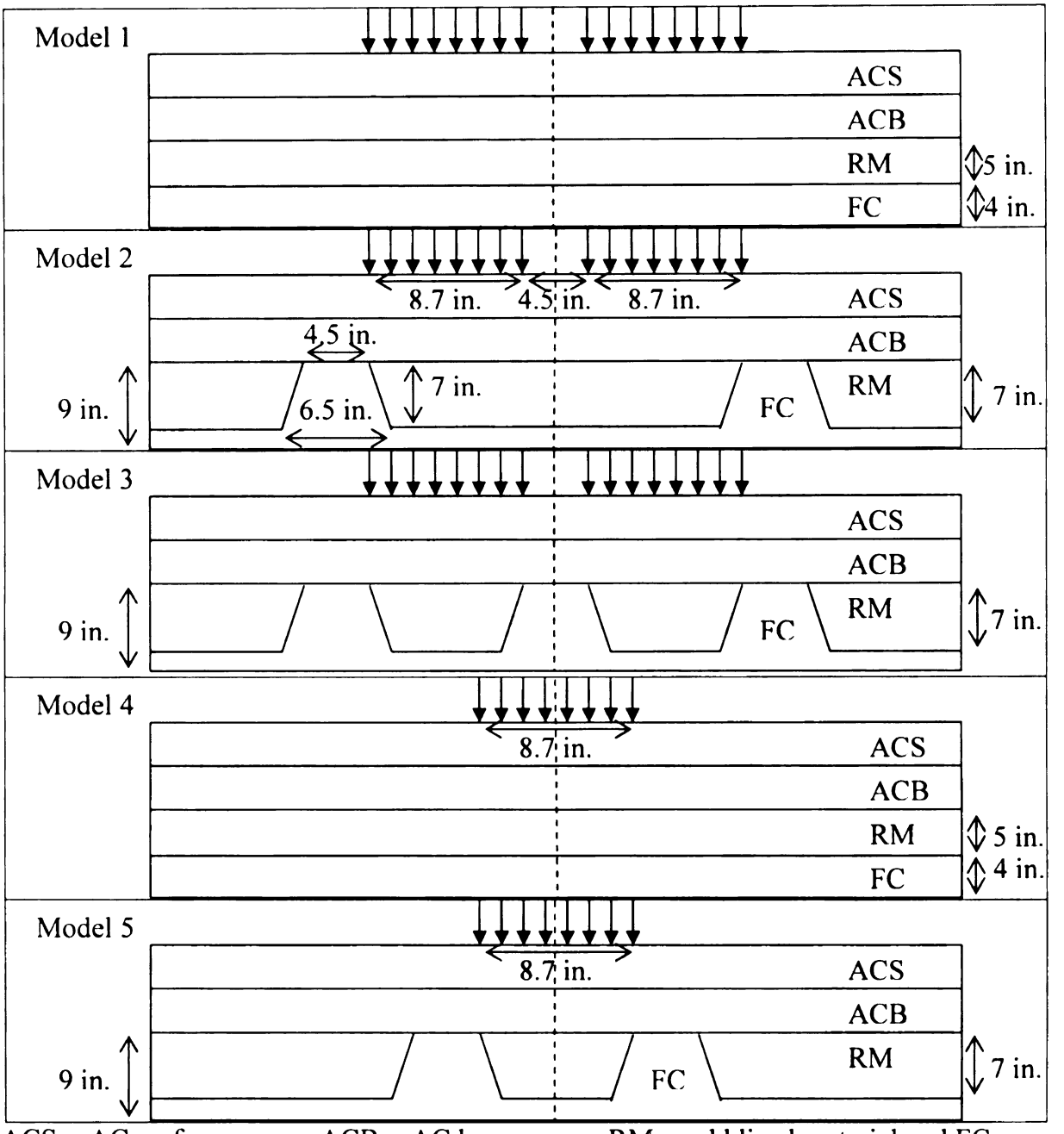


ACS = AC surface course, ACB = AC base course, RM = rubblized material and FC = fractured concrete

The vertical dashed lines at the centers of the models represent planes of symmetry.

A group of arrows represents a singe wheel.

All FC ridges and dual wheels have the same dimensions as those shown in model 2.

Figure 8.42 The upper portion of the models used in the analyses of lateral stresses induced by dual and single wheels

Accurate answers to the above questions cannot be obtained unless actual measurements of contact stresses and contact area were obtained. Such measurements were not available in a form that can be digitized. Since the objective is to compare the effects of a single wheel load to that of a duel, it was thought that any vertical and lateral contact stresses will suffice. Therefore, the following assumptions were made:

1. All tires for single and duel wheels are the same as that used in the earlier analyses; the radial truck tire that was tested by Pottinger and McIntyre (1999). This includes the ribs and grooves pattern and the width (not length) of the contact area of 8.7-in. This makes the effective contact width (which is equal to the difference between the total width of the contact area and the total groove width) of the tire equal to 6.6 in.
2. For simplicity, the contact width was assumed constant throughout the length of the contact area. Said length is 5.7 in. for the 4500 lb wheel load and 11.4 in. for the 9000-lb wheel load.

For ease of programming, uniform vertical contact stress of 120 psi was assumed. This corresponds to tire inflation pressure of 91 psi (see equation 2.1); which is lower than the inflation of 125 psi used by Pottinger and McIntyre (1999). Further, the assumed uniform vertical contact stress of 120-psi is lower than the one measured by Pottinger and McIntyre (1999) at the tire center and higher at the tire edge. According to De Beer et al (1997) and Figure 2.5, the lateral contact stresses should be lower than that measured by Pottinger and McIntyre (1999) at the tire center and higher at the tire edge. Based on this it was

decided to use the same lateral contact stresses as those measured by Pottinger and McIntyre (1999). Such lateral contact stresses should produce lower lateral stresses at the pavement surface at the tire edge than those corresponding to the 120 psi vertical stress.

It was further thought that, since the objective is to compare the impact of a single wheel load to a dual wheel load on the induced lateral stresses in the AC layer, the above assumptions would have minimum to no impact on the conclusions that can be drawn from the analyses.

### 5.5.2 Results of the 3-D analyses of Single and Dual Wheel Loads

Analyses of the effects of single and dual wheel loads on the induced lateral stresses in the AC layer were conducted using models 1 through 5 of Figure 8.42. Table 8.14 provides the wheel loads, pavement cross-sections and the modulus of each pavement layer and roadbed soil used in the analyses. For the 19 pavement sections listed in Table 8.14, Table 8.15 provides the lateral stresses induced at the AC surface at the tire edge and at the AC bottom under the tire center due to the uniform vertical contact stress of 120 psi and the lateral contact stress measured by Pottinger and McIntyre (1999). Examination of the data and the results listed in Tables 8.14 and 8.15 indicates that:

1. For rubblized pavements having even interface and subjected to the same load per tire (4,500 lb), dual wheels induce lower lateral tensile stresses at the AC bottom under the tire center relative to a single wheel. Whereas dual wheels may induce either higher or lower lateral stresses at the AC

Table 8.14 Pavement cross-sections, pavement layers and roadbed soil moduli used in the analyses of rubblized pavements subjected to the indicated wheel loads

| Section | Model | Interface | Wheel | Total load (lb) | Modulus (ksi) | | | | | | Thickness (in.) | | | | | |
|---|---|---|---|---|---|---|---|---|---|---|---|---|---|---|---|---|
| | | | | | ACS | ACB | RM | FC | BS | RB | ACS | ACB | RM | FC | BS | RB |
| 1 | 1 | Even | Dual | 9,000 | 100 | 300 | 30 | 2,500 | 30 | 10 | 1.5 | 4.5 | 5 | 4 | 18 | 67 |
| 2 | 1 | Even | Dual | 9,000 | 100 | 300 | 100 | 2,500 | 30 | 10 | 1.5 | 4.5 | 5 | 4 | 18 | 67 |
| 3 | 1 | Even | Dual | 9,000 | 100 | 300 | 30 | - | 30 | 10 | 1.5 | 4.5 | 9 | - | 18 | 67 |
| 4 | 1 | Even | Dual | 9,000 | 100 | 300 | - | 2,500 | 30 | 10 | 1.5 | 4.5 | - | 9 | 18 | 67 |
| 5 | 1 | Even | Dual | 9,000 | 500 | 300 | 30 | 2,500 | 30 | 10 | 1.5 | 4.5 | 5 | 4 | 18 | 67 |
| 6 | 2 | Uneven | Dual | 9,000 | 100 | 300 | 100 | 2,500 | 30 | 10 | 1.5 | 4.5 | N/A | N/A | 18 | 67 |
| 7 | 3 | Uneven | Dual | 9,000 | 100 | 300 | 100 | 2,500 | 30 | 10 | 1.5 | 4.5 | N/A | N/A | 18 | 67 |
| 8 | 4 | Even | Single | 4,500 | 100 | 300 | 30 | 2,500 | 30 | 10 | 1.5 | 4.5 | 5 | 4 | 18 | 67 |
| 9 | 4 | Even | Single | 4,500 | 100 | 300 | 100 | 2,500 | 30 | 10 | 1.5 | 4.5 | 5 | 4 | 18 | 67 |
| 10 | 4 | Even | Single | 4,500 | 100 | 300 | 30 | - | 30 | 10 | 1.5 | 4.5 | 9 | - | 18 | 67 |
| 11 | 4 | Even | Single | 4,500 | 100 | 300 | - | 2,500 | 30 | 10 | 1.5 | 4.5 | - | 9 | 18 | 67 |
| 12 | 4 | Even | Single | 4,500 | 500 | 300 | 30 | 2,500 | 30 | 10 | 1.5 | 4.5 | 5 | 4 | 18 | 67 |
| 13 | 4 | Even | Single | 9,000 | 100 | 300 | 30 | 2,500 | 30 | 10 | 1.5 | 4.5 | 5 | 4 | 18 | 67 |
| 14 | 4 | Even | Single | 9,000 | 100 | 300 | 100 | 2,500 | 30 | 10 | 1.5 | 4.5 | 5 | 4 | 18 | 67 |
| 15 | 4 | Even | Single | 9,000 | 100 | 300 | 30 | - | 30 | 10 | 1.5 | 4.5 | 9 | - | 18 | 67 |
| 16 | 4 | Even | Single | 9,000 | 100 | 300 | - | 2,500 | 30 | 10 | 1.5 | 4.5 | - | 9 | 18 | 67 |
| 17 | 4 | Even | Single | 9,000 | 500 | 300 | 30 | 2,500 | 30 | 10 | 1.5 | 4.5 | 5 | 4 | 18 | 67 |
| 18 | 5 | Uneven | Single | 4,500 | 100 | 300 | 100 | 2,500 | 30 | 10 | 1.5 | 4.5 | N/A | N/A | 18 | 67 |
| 19 | 5 | Uneven | Single | 9,000 | 100 | 300 | 100 | 2,500 | 30 | 10 | 1.5 | 4.5 | N/A | N/A | 18 | 67 |

ACS = AC surface course, ACB = AC base course, RM = rubblized material, FC = fractured concrete, BS = base and subbase, RB=roadbed soil, N/A = not available because the RM and FC thicknesses vary across the uneven interfaces

Table 8.15 Lateral stresses induced at the AC surface and AC bottom of the 19 rubblized pavement sections listed in Table 8.14

| Section | Model | Interface | Wheel | Total load (lb) | Lateral stress (psi) at 4.5-in. from the tire center (0.15 in. from the tire edge) induced by | | Lateral stresses at the AC bottom | |
|---|---|---|---|---|---|---|---|---|
| | | | | | Vertical contact stresses | Vertical and lateral contact stress[1] | Distance from the tire center (in.) | Lateral stress (psi) |
| 1 | 1 | Even | Dual | 9,000 | 15.7 | 22.0 | 0.0 | 44.7 |
| 2 | 1 | Even | Dual | 9,000 | 18.6 | 24.9 | 0.0 | 7.5 |
| 3 | 1 | Even | Dual | 9,000 | 12.6 | 18.9 | 0.0 | 60.9 |
| 4 | 1 | Even | Dual | 9,000 | 24.0 | 30.3 | 0.0 | -25.9 |
| 5 | 1 | Even | Dual | 9,000 | -13.4 | -7.1 | 0.0 | 41.1 |
| 6 | 2 | Uneven | Dual | 9,000 | 32.2 | 38.5 | 1.1[2] | 31.0 |
| 7 | 3 | Uneven | Dual | 9,000 | 25.6 | 31.9 | 0.0 | 20.4 |
| 8 | 4 | Even | Single | 4,500 | 17.2 | 23.5 | 0.0 | 55.8 |
| 9 | 4 | Even | Single | 4,500 | 21.8 | 28.1 | 0.0 | 15.0 |
| 10 | 4 | Even | Single | 4,500 | 12.3 | 18.6 | 0.0 | 69.8 |
| 11 | 4 | Even | Single | 4,500 | 27.8 | 34.1 | 0.0 | -23.0 |
| 12 | 4 | Even | Single | 4,500 | -27.5 | -21.2 | 0.0 | 49.6 |
| 13 | 4 | Even | Single | 9,000 | 8.0 | 14.3 | 0.0 | 87.2 |
| 14 | 4 | Even | Single | 9,000 | 15.8 | 22.1 | 0.0 | 20.4 |
| 15 | 4 | Even | Single | 9,000 | -1.2 | 5.1 | 0.0 | 113.8 |
| 16 | 4 | Even | Single | 9,000 | 26.0 | 32.3 | 0.0 | -33.9 |
| 17 | 4 | Even | Single | 9,000 | -56.2 | -49.9 | 0.0 | 79.7 |
| 18 | 5 | Uneven | Single | 4,500 | 25.6 | 31.9 | 0.5 | 33.0 |
| 19 | 5 | Uneven | Single | 9,000 | 24.5 | 30.8 | 0.5 | 46.5 |

[1] Assuming the same lateral contact stresses as those of the tire tested by Pottinger and McIntyre (1999)

[2] Toward the center of the dual wheel

surface at the tire edge relative to the single wheel depending on the pavement structural properties.

2. For rubblized pavements having even interface and subjected to the same total load of 9,000 lb, dual wheels induce lower lateral tensile stresses at the AC bottom under the tire center relative to a single wheel. Whereas in most cases, dual wheels induce higher lateral stresses at the AC surface at the tire edge relative to the single wheel.

3. As was expected, for rubblized pavements with full depth FC, both dual and single wheel loads induce:

   - Lateral compressive stress at the AC bottom under the tire center.
   - Higher lateral tensile stresses at the AC surface at the tire edge relative to the other rubblized pavements (with even interface).

4. For rubblized pavement sections having uneven interface with the dual and single wheels over a RM channel (sections 6, 18 and 19), relative to the 4500 and 9000-lb single wheel load, the 9,000-lb dual wheels induce:

   - Higher lateral tensile stresses at the AC surface at the tire edge.
   - Lower lateral tensile stress at the AC bottom under the tire center.

5. The uneven interface with a FC ridge between the two wheels of the dual wheels (section 7 of Table 8.14) produce lower lateral stresses at the tire edge relative to those without the FC ridge between the two wheels of the dual wheels (section 6 of Table 8.14). Further, the uneven interface results in only 6 psi lateral tensile stress at the AC surface at the middle between the dual wheels.

The differences between the lateral stresses at the AC surface and at the AC bottom induced by single and dual wheels can be explained using the concept of superposition of two 4,500-lb single wheel loads as follows:

1. Figure 8.43 illustrates the lateral stresses induced at the AC surface by the vertical contact stresses of each wheel of dual wheels. As can be seen in the figure, the lateral tensile stresses at the outer edge of the left wheel induced by the same (solid line) are enhanced by those induced by the right wheel (dashed line). Thus the induced lateral tensile stresses at the outer edge of the 9,000-lb dual wheel load are higher than those at the edge of a 4,500-lb single wheel. Further, the lateral stresses induced at the outer edge of the left wheel by the right wheel load can be either compressive or tensile depending on the pavement structural properties. Thus, as stated above, the lateral stresses at the edge of the 9,000-lb dual wheels can be either higher or lower than those at the edge of the 4,500-lb single wheel although the effects of the lateral contact stresses are the same for both single and duel wheels.
2. Figure 8.44 illustrates the lateral stresses induced at the AC bottom by the vertical contact stresses of each wheel of dual wheels. As can be seen in the figure, the lateral tensile stresses induced by the left wheel at the AC bottom under the left wheel are reduced by the lateral compressive stresses induced by the right wheel. Thus, as stated above, the lateral tensile stresses at the AC bottom under the tire center of the 9,000-lb dual wheels are lower than those under the tire center of the 4,500-lb single wheel.

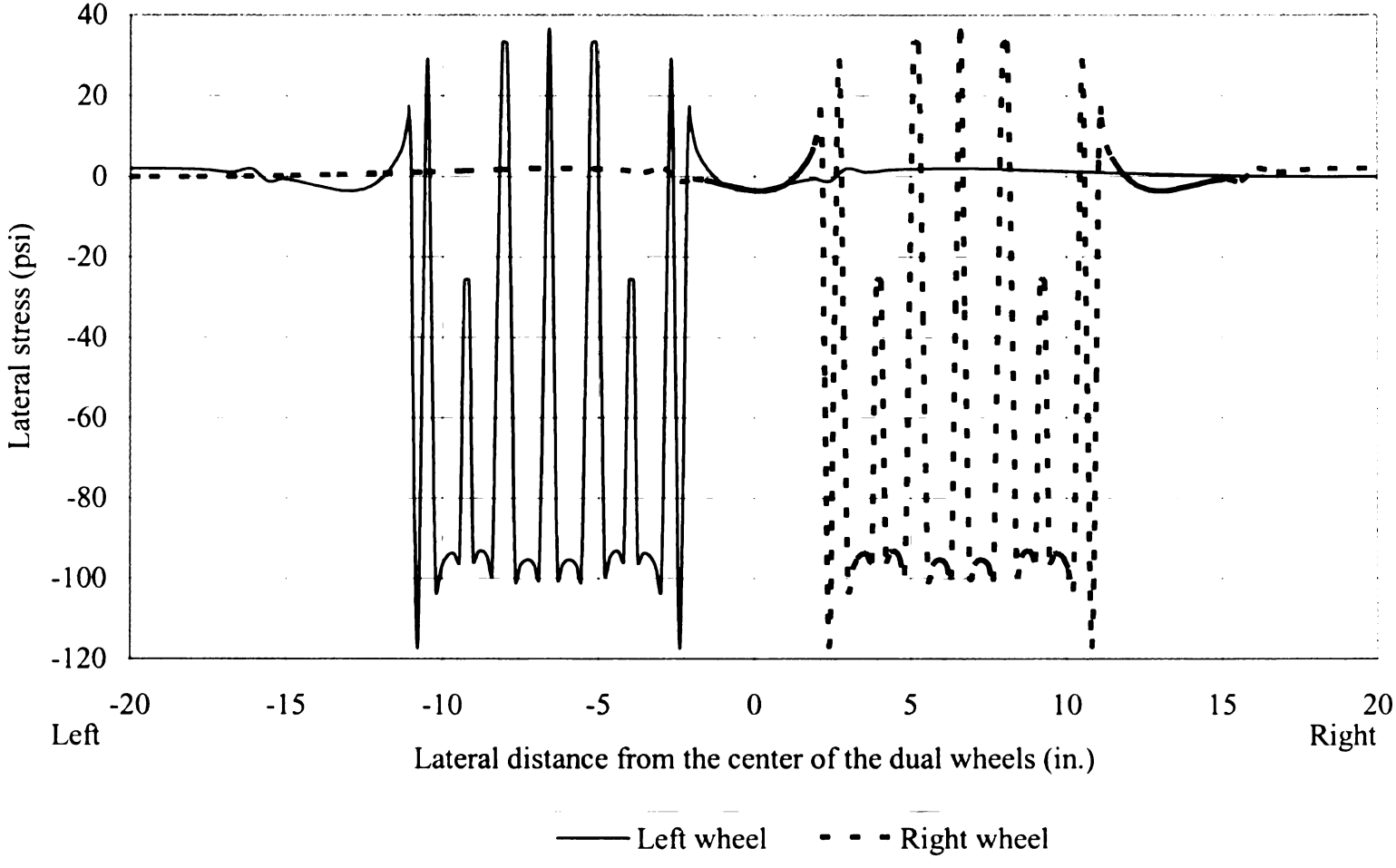


Figure 8.43 Lateral stresses at the AC surface induced by the vertical contact stresses of each wheel of the dual wheels

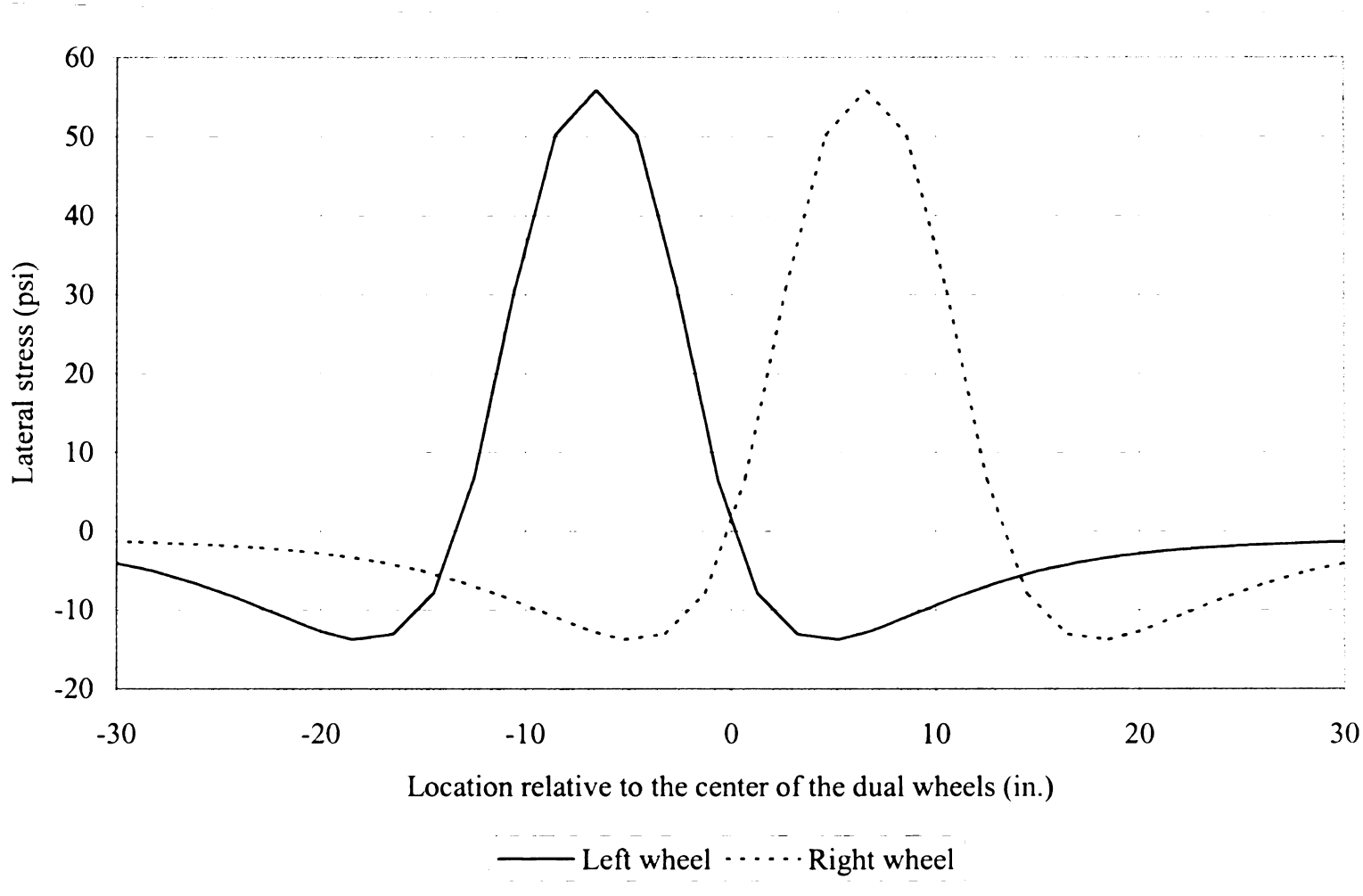


Figure 8.44 Lateral stresses at the AC bottom induced by the vertical contact stresses of each wheel of the dual wheels

Finally, based on the results of the 2- and 3-D analyses of various pavement sections using even and uneven interfaces and single and dual wheels, it can be concluded that:

1. Rubblized pavements are more likely to have higher load-induced tensile stresses at the pavement surface at the tire edge and lower load-induced tensile stresses at the AC bottom relative to flexible pavements. This is because of the higher modulus of the RCS relative to the modulus of the aggregate base and the geometry of the interface between the RM and FC layers.
2. For the same load per wheel and for the same vertical contacts stress, dual wheels induce lower lateral tensile stresses at the AC bottom whereas they may induce higher or lower lateral stresses at the AC surface at the tire edge relative to a single wheel.
3. Because the AC modulus is temperature dependent, the AC surface at the tire edge is subjected to load-induced lateral tensile stresses in high temperatures (e.g., summer) and lateral compressive stresses in colder temperatures (winter). Further, the high temperatures at the AC surface result in low tensile strength of the AC, which increases TDC potential.

## 6.0 STRESS RATIOS

In this section, the stresses ratios (the ratio of the induced tensile stresses to the tensile strength) at the AC surface and the AC bottom of representative rubblized and flexible pavements sections are analyzed and discussed. The AC moduli used in the analyses are based on the average backcalculated AC moduli of 24 rubblized and 12

flexible pavement sections at 68° F of 1,200 ksi and pavement temperature data collected by MDOT. The tensile strengths used in the analyses are based on the mid-range value of the results of the ITST tests at 68° F of 200 psi and the measured pavement temperatures (see Table 8.16). Table 8.16 provides the following information:

- The highest temperatures at the AC surface during 1994 through 1999 and the corresponding temperatures at the AC bottom of various asphalt pavements; all data were measured and provided by MDOT as discussed in Chapter 7.
- The approximate temperatures at mid depth of ACS and ACB and their corresponding moduli and indirect tensile strength (ITS). The mid depth temperatures of the ACS and ACB were calculated bases on an assumed AC surface course thickness of 1.5-in. and assumed linear variation of temperature with depth.
- The moduli and indirect tensile strength values which were adjusted to the mid-depth temperatures using equations 2.4 and 2.5.

Table 8.17 provides the properties of the rubblized and flexible pavements, the geometry of the interfaces between the RM and FC layers and the types of wheel loads used in the analyses. For a single wheel, the vertical and lateral contact stresses of the radial tire measured by Pottinger and McIntyre (1999) were used in the analyses whereas, for duel wheels, uniform vertical contact stresses of 120 psi and the above lateral contact stresses were used. The longitudinal contact stresses were not included in the analyses because they induce insignificant lateral stresses at the AC surface at the tire edge and at the AC bottom. Tables 8.18 and 8.19 provide the results of the 3-D analyses. The tables list the following information:

Table 8.16 The highest AC surface temperatures and the corresponding temperatures at the AC bottom measured by MDOT during 1994 through 1999, and the mid-depth temperatures of various asphalt pavements

| Nearby city | Route | Date | Time | Temperature (°F) | | AC thickness (in.) | Mid-depth Temperature (°F) | | Modulus (ksi) | | Indirect tensile strength (psi) | |
|---|---|---|---|---|---|---|---|---|---|---|---|---|
| | | | | AC Surface | AC bottom | | ACS | ACB | ACS | ACB | AC surface | AC bottom |
| Farewell | M-115 | 6/20/1995 | 14:28 | 123.6 | 102.6 | 3 | 121.4 | 110.8 | 166 | 208 | 29.2 | 44.3 |
| Alpena | US-23 | 6/19/1995 | 14:24 | 123.1 | 95.4 | 6 | 120.9 | 107.0 | 155 | 234 | 27.8 | 58.9 |
| Port Sanilac | M-25 | 7/14/1995 | 14:48 | 128.1 | 104.5 | 6 | 125.2 | 113.4 | 148 | 228 | 26.5 | 58.5 |
| Carney | US-41 | 6/19/1995 | 13:48 | 125.2 | 112.8 | 6 | 122.1 | 115.9 | 144 | 240 | 25.2 | 64.9 |
| Iron River | US-2 | 6/18/1995 | 15:11 | 126.7 | 104.4 | 6 | 123.9 | 112.7 | 117 | 183 | 21.3 | 48.2 |
| Brighton | US-23 | 7/14/1995 | 14:24 | 119.1 | 89.4 | 7 | 116.9 | 102.0 | 166 | 250 | 30.8 | 62.6 |
| St. Johns | US-27 | 6/19/1995 | 15:04 | 123.3 | 90.0 | 9.5 | 121.2 | 104.5 | 173 | 288 | 31.4 | 79.7 |
| Brevot | US -2 | 6/20/1995 | 14:24 | 129.6 | 101.5 | 10 | 126.1 | 112.0 | 201 | 345 | 35.8 | 97.3 |
| Deerton | M-28 | 6/18/1995 | 14:42 | 134.6 | 110.3 | 12 | 131.6 | 119.4 | 172 | 315 | 31.2 | 95.6 |
| Average temperatures of pavements of sections with 6-in. AC layer and the moduli and the indirect tensile strengths corresponding to the average temperatures | | | | 123.6 | 102.6 | 6 | 121.4 | 110.8 | 140 | 220 | 25.1 | 57.3 |

The moduli and ITS of the AC were calculated by assuming the AC surface course (ACS) and the AC base course (ACB) moduli of 1,200 ksi and their indirect tensile strength of 200 psi at 68 °F.

Table 8.17 Properties of the rubblized and flexible pavements, the interfaces between the RM and FC layers and the wheel loads used in the analyses of the load-induced stresses at the AC surface at the tire edge and at the AC bottom under the tire center.

| Pavement | Interface between RM and FC layers | Wheel | Modulus (ksi) | | | | | | Thickness (in.) | | | | | |
|---|---|---|---|---|---|---|---|---|---|---|---|---|---|---|
| | | | ACS | ACB | RM | FC | BS | RB | ACS | ACB | RM | FC | BS | RB |
| Rubblized pavement 1 | Even | Single and dual | 140 | 220 | 66 | 482 | 30 | 10 | 1.5 | 4.5 | 5 | 4 | 18 | 67 |
| Rubblized pavement 2 | Geometry 4 of Figure 8.33 | Single | 140 | 220 | 66 | 482 | 30 | 10 | 1.5 | 4.5 | N/A | N/A | 18 | 67 |
| Rubblized pavement 3 | Model 2 of Figure 8.36 | Dual | 140 | 220 | 66 | 482 | 30 | 10 | 1.5 | 4.5 | N/A | N/A | 18 | 67 |
| Flexible pavement | - | Single and dual | 140 | 220 | 30 | - | 30 | 10 | 1.5 | 4.5 | 9 | - | 18 | 67 |

ACS = AC surface course, ACB = AC base course, RM = rubblized material, FC = fractured concrete, BS = base and subbase, RB = roadbed soil, N/A = not available because the RM and FC thicknesses vary across the uneven interfaces

Table 8.18 Stress ratios at the AC surface and AC bottom of three pavement sections in Table 8.17 subjected to single wheel load

| | Rubblized pavement 1 | | | | Rubblized pavement 2 | | | | Flexible pavement | | | |
|---|---|---|---|---|---|---|---|---|---|---|---|---|
| | At AC surface at the tire edge | | | At the AC bottom under the tire center | At AC surface at the tire edge | | | At the AC bottom under the tire center | At AC surface at the tire edge | | | At the AC bottom under the tire center |
| Lateral stresses induced by vertical contact stress (psi) | 4.1 | | | 40.4 | 14.6 | | | 23.9 | -10.9 | | | 89.3 |
| Lateral stresses induced by lateral contact stress (psi) | 13 | | | 0.0 | 13 | | | 0.0 | 13 | | | 0.0 |
| Load-induced lateral stress (psi) | 17.1 | | | 40.4 | 27.6 | | | 23.9 | 2.1 | | | 89.3 |
| Thermal stress (psi) | -2.5 | | | -3.1 | -2.5 | | | -3.1 | -2.5 | | | -3.1 |
| Total lateral stress (psi) | 14.6 | | | 37.3 | 25.1 | | | 20.8 | -0.4 | | | 86.2 |
| | Regular strength | MD | S and MD | Regular strength | Regular strength | MD | S and MD | Regular strength | Regular strength | MD | S and MD | Regular strength |
| Indirect tensile strength (psi) | 25.1 | 21.8 | 16.6 | 57.3 | 25.1 | 21.8 | 16.6 | 57.3 | 25.1 | 21.8 | 16.6 | 57.3 |
| Stress ratio | 0.58 | 0.67 | 0.88 | 0.65 | 1 | 1.15 | 1.52 | 0.36 | -0.02 | -0.02 | -0.03 | 1.5 |

MD = Moisture damage, S = Segregation, Reductions in indirect tensile strength due to MD, and due to S and MD are 13 and 34 percent, respectively.

Table 8.19 Stress ratios at the AC surface and AC bottom of three pavement sections in Table 8.17 subjected to dual wheel load

| | Rubblized pavement 1 | | | | Rubblized pavement 3 | | | | Flexible pavement | | | |
|---|---|---|---|---|---|---|---|---|---|---|---|---|
| | At AC surface at the tire edge | | | At the AC bottom under the tire center | At AC surface at the tire edge | | | At the AC bottom under the tire center | At AC surface at the tire edge | | | At the AC bottom under the tire center |
| Lateral stresses induced by vertical contact stress (psi) | 12.5 | | | 17.5 | 12.5 | | | 13.3 | 6.6 | | | 47.6 |
| Lateral stresses induced by lateral contact stress (psi) | 6.3 | | | 0.0 | 6.3 | | | 0.0 | 6.3 | | | 0.0 |
| Load-induced lateral stress (psi) | 18.8 | | | 17.5 | 18.8 | | | 13.3 | 12.9 | | | 47.6 |
| Thermal stress (psi) | -2.5 | | | -3.1 | -2.5 | | | -3.1 | -2.5 | | | -3.1 |
| Total lateral stress (psi) | 16.3 | | | 14.4 | 16.3 | | | 10.2 | 10.4 | | | 44.5 |
| | Regular strength | MD | S and MD | Regular strength | Regular strength | MD | S and MD | Regular strength | Regular strength | MD | S and MD | Regular strength |
| Indirect tensile strength (psi) | 25.1 | 21.8 | 16.6 | 57.3 | 25.1 | 21.8 | 16.6 | 57.3 | 25.1 | 21.8 | 16.6 | 57.3 |
| Stress ratio | 0.65 | 0.75 | 0.99 | 0.25 | 1.04 | 1.2 | 1.58 | 0.18 | 0.42 | 0.48 | 0.63 | 0.78 |

MD = Moisture damage, S = Segregation, Reductions in indirect tensile strength due to MD, and due to S and MD are 13 and 34 percent, respectively.

- The lateral tensile stresses induced at the AC surface at the tire edge and at the AC bottom under the tire center of the rubblized and flexible pavement sections listed in Table 8.17.
- The thermal compressive stresses in the AC surface and AC bottom calculated for the afternoon of a summer day (see Table 7.3). The low thermal stresses in the table are due to the low relaxation modulus of the AC due to high temperatures. For more details, see Chapter 7.
- The indirect tensile strength at the AC surface and the AC bottom adjusted to their respective temperatures listed in Table 8.16.
- The reduced indirect tensile strengths due to moisture damage and due to segregation and moisture damage. Note that the reduced strength applies only to the pavement surface.
- The stress ratios at the AC surface at the tire edge and at the AC bottom.

Examination of the data in Tables 8.18 and 8.19 and comparing the stress ratios at the top and at the bottom of the AC layer for flexible and rubblized pavements indicates that:

1. As expected, the stress ratios at the AC surface at the tire edge of rubblized pavements with even and uneven interfaces between the RM and the FC layers are higher than those of flexible pavements. This implies that the TDC potential on rubblized pavements is higher than that on flexible pavements. This explains the field observations that the majority of rubblized pavements have TDC while few flexible pavement sections (higher surface age relative to the rubblized pavements) have shown TDC.

2. The stress ratio at the tire edge at the AC surface of rubblized pavements having uneven interface are higher than those of rubblized pavements having even interface. This verifies the hypothesis that the quality of the rubblization operation affects pavement performance.

3. For rubblized pavements, the stress ratios at the AC surface at the tire edge are very high (0.58 to 1.58) and, in general, are higher than those at the AC bottom. This observation also implies that the TDC potential is much higher than the bottom-up fatigue cracking potential. This finding is supported by field observations of 87 rubblized pavement projects. Only four projects have bottom-up fatigue cracks while 48 projects have longitudinal TDC at the edge of the wheel path with 33 of them showed some degrees of segregation. Finally, 19 projects were rehabilitated few years after construction due mainly to TDC. This observation verifies the hypothesis that TDC are fatigue cracks located at the edge of the wheel paths and caused by high stress ratios.

4. The stress ratios at the AC bottom under the tire of flexible pavements are higher than those at the AC surface at the tire edges of both single and dual wheels. This observation could be reversed if the confinement within the AC layer is accounted for in the analyses. The pavement surface has no confinement while the bottom of the AC layer is confined by two mechanisms; the equivalent to the earth pressure at rest within the AC layer due to its own weight and the frictional forces between the AC land the base layers as shown in Figure 8.45.

5. Although the stress ratios at the AC surface of rubblized pavements are generally higher than those at the bottom of the AC layer, their values increase if the AC

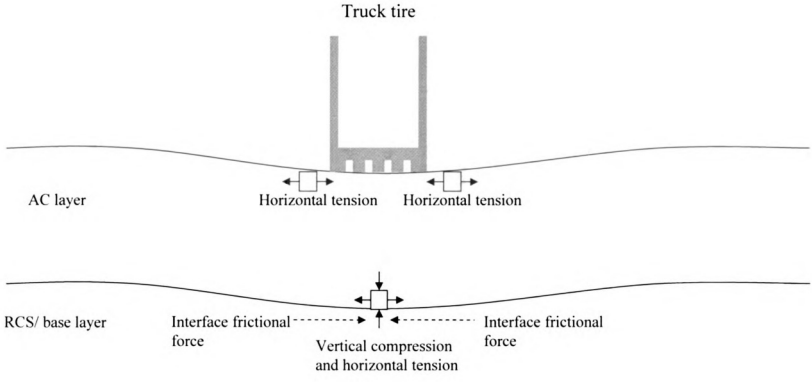


Figure 8.45 Confinement due to the interface frictional forces at the AC bottom

mix is susceptible to moisture damage and/or segregation as shown in the tables. Hence, segregation and moisture damage adversely affect the initiation and propagation of TDC. This finding supports the field observation that the majority of the longitudinal TDC were found at the edge of the wheel path and/or in the segregated areas.

6. Finally, for the same total load and for both rubblized and flexible pavements, the stress ratios at the edge of the dual wheels are higher than those at the edge of a single wheel whereas the stress ratios at the AC bottom under the dual wheels are lower than those under a single wheel. This implies that substituting dual wheels by a single one would under estimate the lateral stresses induced at the pavement surface and over predict the lateral tensile stresses at the bottom of the AC.

Finally, it should be noted that all the analyses of the load-induced stresses in the AC layer were conducted based on measured contact stresses under a radial tire rolling at a speed of about 0.2 mile per hour. Pottinger (1992) measured the contact stresses f rolling and stationary smooth radial tire. His results indicated that relative to a stationary tire, a rolling tire produces:

- Higher vertical contact stresses at the tire edges and lower at the tire center.
- Generally lower lateral contact stresses over the entire contact area.
- Higher longitudinal contact stresses whose resultant force acts against the traveling direction of the tire.

Based on the above observations, lateral stresses induced at the AC surface at the edges of a rolling tire may be either higher or lower than those induced at the edges of a

stationary tire. Whereas the strains and therefore, the stresses induced at the AC bottom decrease as the vehicle speed increases (Chatti et al, 1996 and 1997 and Dai et al, 1997).

## 7.0 SUMMARY

Two and three dimensional finite element analyses were conducted to evaluate the effects of the following variable on the lateral stresses induced at the top and bottom of the AC layer:

- Pavement layer thicknesses and moduli and the roadbed soil moduli.
- Geometry of the interface between the RM and FC layers in rubblized pavements.
- Load configurations.

Further, the interaction between thermal stresses, load-induced stresses and segregation and moisture damage in the AC layer were analyzed. It is shown that for rubblized pavements, the stress ratio at the top of the AC is much higher than that at the bottom.

# CHAPTER 9

# SUMMARY, CONCLUSIONS AND RECOMMENDATIONS

## 1.0 SUMMARY

Rubblization is one of the rehabilitation options for deteriorated concrete pavements. The main objectives of rubblization are to destroy the integrity of the concrete slabs and joints and to debond the temperature steel as to eliminate future reflective cracking potential. Pavement distress data indicate that the average service life of rubblized pavements is about 7 years, which is much shorter than the 20-year design life. The distress data indicate that the underperformance of rubblized pavements is manifested by various types of distress. Field investigation revealed that the two overwhelming types of distresses are top-down cracks (TDC) and reflective cracks.

TDC are longitudinal and/or transverse cracks that initiate at the pavement surface and propagate downward and outward. TDC have been found in asphalt, composite and concrete pavements. In asphalt surface pavements, TDC have been reported to cause reduction in their service lives in several countries including the USA. Currently, the only available procedure to identify TDC is to core the pavement section over existing cracks. Such procedure is expensive and laborious and therefore cannot be applied at the network level.

Recognizing the dimensions of the problems and the need of a full understanding of the causes of the underperformance of rubblized pavements, in general, and TDC, in particular, two research projects were initiated to address the problems. Both projects included extensive field and laboratory investigations of rubblized and flexible pavements and mechanistic analyses of stresses induced in the AC layers of the two

pavements. This study addresses field and laboratory investigations of rubblized pavements and mechanistic analyses of rubblized and flexible pavements. The other study (Schorsch, 2003) addresses field and laboratory investigation of flexible pavements.

Field investigation of the rubblization operation, the rubblizing equipment and their operating parameters and the conditions of the rubblized concrete slabs (RCS) revealed that the RCS typically consist of two distinctive layers; a rubblized material (RM) layer at the top and a fractured concrete (FC) layer at the bottom. After construction, three manual distress surveys of 84 rubblized pavement projects were conducted in 2001, 2002 and 2003. Nondestructive deflection tests (NDT) were also conducted on 27 rubblized and 14 flexible pavement test sites and cores were extracted from 25 rubblized and 13 flexible pavements test sites. The deflection data were used in the backcalculation of layer moduli while the cores were used to verify TDC and for laboratory investigation.

The laboratory investigation included core and cracks measurements, specific gravity tests, indirect tensile cyclic load tests and indirect tensile strength tests of the asphalt cores. The latter test was also used to assess the impact of temperature, segregation and moisture conditioning on the indirect tensile strength of some asphalt mixes. Results of the investigation indicated that high temperature and the combination of segregation and moisture damage results in substantial reduction of the indirect tensile strength of AC mixes.

Based on the results of field and laboratory investigations and on mechanistic analyses, it was shown that when the rubblization objectives are not fully satisfied,

premature distress would occur. Consequently, two procedures were developed; one procedure addresses the selection of candidate projects for rubblization and the other addresses the calibration of the rubblizing equipment as to improve the quality of the rubblization operation.

Based on their causes, TDC were classified into three categories; 1) longitudinal TDC (LTDC), 2) transverse TDC (TTDC) and 3) TDC in segregated areas. Further, a procedure to identify TDC and to differentiate them from regular longitudinal and/or transverse cracks was developed. The procedure was based on field observations and the understanding of TDC initiation and propagation mechanism.

Backcalculation of layer moduli were conducted using deflections from 24 rubblized and 12 flexible pavement test sites. To overcome the problems in the backcalculation of layer moduli, especially in rubblized pavements, a backcalculation procedure for rubblized and flexible pavements and a procedure to estimate the depth to stiff layer were developed and implemented in this study. The two procedures yielded reasonable and consistent results.

The backcalculated layer moduli were then used in 2- and 3-D mechanistic analyses of the stresses induced in the AC layer of rubblized and flexible pavements due to tire-pavement interaction. Measured tire-pavement contact stresses were obtained and used in the mechanistic analyses. In the analyses, factors affecting the magnitude and distribution of the induced stresses in the AC layers were analyzed. Such factors included the pavement cross-section, the pavement layer properties, the geometry of the interface between the RM and the FC layers and tire configuration. In the 2-D analyses, the wheel load was simulated using uniform vertical contact stresses. Whereas, measured contact

stresses of a radial truck tire and uniform vertical contact stresses were used in the 3-D analyses.

In addition, thermal stresses induced in the AC layer were calculated using the relaxation constitutive equations of the AC and pavement temperature data measured by the Michigan Department of Transportation (MDOT). The results indicated that high pavement temperatures cause insignificant thermal stresses while low temperature induces substantial tensile stresses in the AC layer. Further, the results indicated that the AC layer is subjected to daily cyclic thermal stresses.

Results of the two analyses of stresses induced in the AC layer were used to calculate the stress ratio (the ratio between the applied tensile stress and the tensile strength of the AC mix) at the top and bottom of the AC layer of rubblized and flexible pavements. It is shown that, during summer time, the stress ratio at the top of the AC layer of rubblized pavements is significantly higher than that at the bottom. Said high stress ratio causes the initiation of TDC while winter thermal stresses accelerate the propagation of TDC.

## 2.0 CONCLUSIONS

Based on the results of the filed and lab investigation conducted during the course of this study, the results of mechanistic analyses, and the results of the analyses of thermal stresses, various conclusions were drawn. The conclusions are divided into various categories and are presented below.

## 2.1 Hypotheses

The hypotheses stated in Chapter 1 of this thesis were verified.

1. LTDC at the edges of the wheel paths are fatigue cracks caused by high stress ratio and are likely to initiate in the summer.
2. TDC possess different characteristics than other cracks. These characteristics were used for TDC identification.
3. The underperformance of rubblized pavements is related to:

   a) the quality of the rubblization operation

   b) Construction

   c) AC mix design

## 2.2 Rubblized Pavements and Top-Down Cracks

1. The rubblized concrete slabs (RCS) consist of two layers; a rubblized material (RM) layer and a fractured concrete (FC) layer. The thickness of the RM and FC layers vary from 0.0-in to the original thickness of the concrete slab. The interface between the two layers is generally uneven.
2. Top-down cracks (TDC), reflective cracks and segregation are the dominant distresses on rubblized pavements.
3. Relative to their causes, TDC are classified into three categories; 1) longitudinal TDC (LTDC), 2) transverse TDC (TTDC) and 3) TDC in segregated areas. Most LTDC are observed at the edge of the wheel paths and/or in segregated areas.

4. Because of the uneven interface between the RM and the FC layers, and the poor quality of the rubblization operation, rubblized pavements are more vulnerable to TDC than both bottom-up cracking and flexible pavements.

## 2.3 NDT and Backcalculation of Layer Moduli

1. The variation in the structural capacity of rubblized pavements is much higher than conventional flexible pavements.
2. The pavement response to load is linear.
3. An algorithm to estimate the depth to stiff layer based on the backcalculation results of 3 and 4-layer systems was developed, implemented and verified.
4. The backcalculation of layer moduli of rubblized pavements is problematic due to the high variation in the RM layer thickness and the uneven interface between the RM and the FC layers. Consequently, a backcalculation procedure and algorithm were developed and implemented in rubblized and flexible pavements. The procedure produced reasonable and consistent results in both flexible and rubblized pavements.
5. A regression equation to estimate the thickness of the RM based on the backcalculated modulus of the RCS was developed.

## 2.4 Thermal Stresses

1. Low temperatures in winter result in high thermal tensile and compressive stresses whereas summer thermal stresses are relatively low.

2. High thermal tensile stresses in winter increase the potential for TTDC initiation and accelerate LTDC propagation.
3. Asphalt surfaced pavements are subjected to cyclic thermal stresses on a daily basis due to reversal in temperature gradient.

## 2.5 Mechanistic Analyses

1. Lateral stresses induced by the lateral contact stresses are independent of the pavement structures and are negligible at the AC bottom.
2. Lateral stresses induced by the longitudinal contact stresses are independent of the pavement structures and are negligible at the AC surface at the tire edge and at AC bottom.
3. The vertical and lateral contact stresses induce significant lateral stresses at the AC surface and at the AC bottom. Said stresses are affected by the properties of the pavement layers and roadbed soil, and the geometry of the interface between the RM and FC layers (the quality of the rubblization operation).
4. Analyses of the lateral stresses induced at the pavement surface require accurate 3-D modeling of the tire-pavement contact stresses and contact.
5. Dual wheels cannot be simulated using a single wheel in the analyses of the stresses induced the AC layer.
6. The tensile strength of asphalt mixes and the stress ratio are adversely affected by high temperatures, segregation and moisture damage.

## 3.0 RECOMMENDATIONS

Based on the results of field and lab investigations, the results of mechanistic analyses and the conclusions, the following recommendations were made.

1. Expand the mechanistic analyses to include various tire-pavement contact stresses, tire structures, loads and tire inflation pressures.
2. Evaluate the effects of slippage between the AC and the base layers on the load- and temperature-induced stresses.
3. Evaluate the effects of the confinement and interface frictional force on the tensile strength of the AC at the bottom of the AC layer.
4. Analyze curling of AC layer due to temperature gradients in the AC layer.
5. Evaluate and calibrate the new backcalculation procedure using larger database of measured deflection data. Likewise, evaluate and calibrate the new procedure for estimating the depth to stiff layer.

# APPENDIX A

## RUBBLIZED PAVEMENT PROJECTS IN MICHIGAN

This appendix provides information of all 87 rubblized pavement projects in Michigan (as of 2001) that were investigated in this study. The project information, obtained from the Michigan Department of Transportation (MDOT), include:

- MDOT control section and job number
- Beginning and ending mile posts (BMP and EMP) of the project (or segments of the project)
- Project location
- Construction completion date

Note that, one project may consist of one or more control sections and job numbers because the project is located in more than one political boundary (county, city, etc.). Further, one project may consist of one or more segments with different BMP and EMP because of the discontinuity in the rubblized areas due to bridges or political boundary. Further, some 4-lanes (2 lanes in each direction) projects were rubblized in both traffic directions whereas some others were only rubblized in one direction. When the direction is not specified in Table A1, it implies that the project was rubblized in both directions.

Table A1 List of 87 rubblized pavement projects in Michigan

| Project number | Control section | Job number | Route | Dir. | BMP | EMP | Project location | Completion date | Surveys | | |
|---|---|---|---|---|---|---|---|---|---|---|---|
| | | | | | | | | | 2001 | 2002 | 2003 |
| 1 | 16092 | 25559 | I-75 | | 13.19 | 15.22 | US-31 Interchange then Northerly to the South Approach of the Mackinaw Bridge | 12/6/1988 | Yes | Yes | Yes |
| 2 | 13081 | 24112 | I-94 | EB | 2.47 | 5.65 | West of Helmer Rd. Then Easterly to East of M-66 | 6/8/1988 | Yes | Yes | Yes |
| 2 | 13081 | 24112 | I-94 | WB | 2.47 | 5.65 | West of Helmer Rd. Then Easterly to East of M-66 | 6/8/1988 | Yes | Yes | Yes |
| 3 | 17062 | 26637 | M-28 | EB | 18.69 | 22.29 | West of Irish Line Road then Easterly to M-221 in Chippewa County | 9/12/1989 | Yes | No | No |
| 4 | 34031 | 28115 | M-66 | | 7.20 | 7.51 | From Portland Rd. Northerly to Grand River Ave.(M-66 Interchange with I-96) | 10/24/1989 | Yes | Yes | Yes |
| 4 | 34032 | 28115 | M-66 | | 0.00 | 0.45 | From Portland Rd. Northerly to Grand River Ave.(M-66 Interchange with I-96) | 10/24/1989 | Yes | Yes | Yes |
| 5 | 41131 | 21089 | US-131 | NB | 6.47 | 10.14 | South of Grand Rapids Starting South of 54th Street then Northerly to North of M-11 (28th Street). | 6/12/1990 | Yes | Yes | Yes |
| 5 | 41131 | 21089 | US-131 | SB | 6.47 | 10.32 | South of Grand Rapids Starting South of 54th Street then Northerly to North of M-11 (28th Street). | 6/12/1990 | Yes | Yes | Yes |
| 6 | 20014 | 26755 | I-75 | SB | 0.00 | 3.73 | The control section starts at JCT US-27 and ends at the south JCT I-75BL Grayling | 8/24/1990 | Yes | Yes | Yes |
| 7 | 47555 | 29902 | Old US-16 | | 0.00 | 1.41 | Old US-16/Grand River Ave. Brighton City Limits Westerly to Bendix Road | 10/29/1990 | Yes | Yes | Yes |
| 8 | 9042 | 28163 | M-25 | EB | 0.06 | 1.27 | From West of Flajole Rd. Then Easterly to East of the US-10/I-75 Interchange, Bay County | 8/24/1990 | Yes | Yes | Yes |
| 8 | 9101 | 28163 | US-10 | EB | 0.92 | 7.36 | From West of Flajole Rd. Then Easterly to East of the US-10/I-75 Interchange, Bay County | 11/1/1989 | Yes | Yes | Yes |
| 8 | 9101 | 28163 | US-10 | EB | 9.12 | 11.36 | From West of Flajole Rd. Then Easterly to East of the US-10/I-75 Interchange, Bay County | 9/8/1990 | Yes | Yes | Yes |
| 9 | 16032 | 26672 | M-27 | | 1.00 | 2.57 | From I-75 Northeasterly to the South City Limits of Cheboygan along Mullet Lake, Cheboygan County | 9/8/1990 | Yes | Yes | Yes |
| 9 | 16032 | 26672 | M-27 | | 9.31 | 9.58 | From I-75 Northeasterly to the South City Limits of Cheboygan along Mullet Lake, Cheboygan County | 9/8/1990 | Yes | Yes | Yes |
| 9 | 16032 | 26672 | M-27 | | 9.66 | 11.38 | From I-75 Northeasterly to the South City Limits of Cheboygan along Mullet Lake, Cheboygan County | 9/8/1990 | Yes | Yes | Yes |
| 10 | 16021 | 28111 | M-68 | | 0.00 | 7.71 | From Emment/Cheboygan County Line Easterly to South Intersection of M-68 and Old US-27 | 11/14/1990 | Yes | Yes | Yes |

Table A1 (cont'd)

| Project number | Control section | Job number | Route | Dir. | BMP | EMP | Project location | Completion date | Surveys | | |
|---|---|---|---|---|---|---|---|---|---|---|---|
| | | | | | | | | | 2001 | 2002 | 2003 |
| 11 | 34043 | 24662 | I-96 Ramps | | 11.63 | 12.03 | East Bound on and off Ramps in South West Quadrant of I-96 and M-66 Interchange | 5/20/1987 | Yes | Yes | Yes |
| 12 | 41033 | 26691 | M-37 | NB | 2.48 | 7.92 | From Alpine Church Street then northerly to north of Sparta Ave. | 8/14/1992 | Yes | Yes | Yes |
| 12 | 41033 | 26691 | M-37 | SB | 2.48 | 7.35 | From Alpine Church Street then northerly to north of Sparta Ave. | 8/14/1992 | Yes | Yes | Yes |
| 12 | 41033 | 26691 | M-37 | SB | 7.44 | 7.92 | From Alpine Church Street then northerly to north of Sparta Ave. | 8/14/1992 | Yes | Yes | Yes |
| 13 | 47013 | 29768 | US-23 | NB | 5.49 | 6.95 | South of I-96 in the City of Brighton then northerly to M-59 | 10/15/1992 | Yes | Yes | Yes |
| 13 | 47013 | 29768 | US-23 | SB | 5.49 | 6.95 | South of I-96 in the City of Brighton then northerly to M-59 | 10/15/1992 | Yes | Yes | Yes |
| 13 | 47014 | 29768 | US-23 | NB | 0.00 | 7.17 | South of I-96 in the City of Brighton then northerly to M-59 | 10/15/1992 | Yes | Yes | Yes |
| 13 | 47014 | 29768 | US-23 | SB | 0.00 | 7.17 | South of I-96 in the City of Brighton then northerly to M-59 | 10/15/1992 | Yes | Yes | Yes |
| 14 | 33084 | 28213 | I-96 | EB | 8.98 | 17.49 | West of Meridian Road then Easterly to M-52 | 10/27/1993 | Yes | Yes | Yes |
| 14 | 33084 | 28213 | I-96 | WB | 17.50 | 8.85 | West of Meridian Road then Easterly to M-52 | 10/27/1993 | Yes | Yes | Yes |
| 15 | 13033 | 29670 | I-194/M-66 | | 0.49 | 1.68 | North of I-94 then northerly to Jackson Street in the City of Battle Creek | 6/4/1993 | Yes | Yes | Yes |
| 16 | 41013 | 31067 | M-44 | EB | 0.70 | 2.67 | West River Drive Northeasterly to Belding Ave. In Kent County | 8/13/1993 | Yes | Yes | Yes |
| 16 | 41013 | 31067 | M-44 | WB | 0.70 | 2.67 | West River Drive Northeasterly to Belding Ave. In Kent County | 8/13/1993 | Yes | Yes | Yes |
| 17 | 33083 | 29581 | I-96 | EB | 2.11 | 3.69 | From 1.286 miles West of Cedar Street to 1.377 miles East of Cedar Street | 7/30/1994 | Yes | Yes | Yes |
| 18 | 33084 | 29581 | I-96 | EB | 0.00 | 1.07 | From 1.286 miles West of Cedar Street to 1.377 miles East of Cedar Street | 11/8/1995 | Yes | Yes | Yes |
| 19 | 3112 | 28143 | US-131 | NB | 3.07 | 8.56 | North of 124th Ave. northerly to south of 135th Avenue | 11/5/1993 | Yes | Yes | Yes |
| 19 | 3112 | 28143 | US-131 | SB | 3.07 | 3.52 | North of 124th Ave. northerly to south of 135th Avenue | 11/5/1993 | Yes | Yes | Yes |

Table A1 (cont'd)

| Project number | Control section | Job number | Route | Dir. | BMP | EMP | Project location | Completion date | Surveys | | |
|---|---|---|---|---|---|---|---|---|---|---|---|
| | | | | | | | | | 2001 | 2002 | 2003 |
| 19 | 3112 | 28143 | US-131 | SB | 3.76 | 8.56 | North of 124th Ave. northerly to south of 135th Avenue | 11/5/1993 | Yes | Yes | Yes |
| 20 | 83-81 | 33614 | Mackinaw Trail | | N/A | N/A | M-115 Northerly to US-131 in Wexford County | 9/30/1992 | Yes | Yes | No |
| 21 | 56-52 | 33121 | Saginaw Rd. | | 13.27 | 13.74 | Birchview St. Southeasterly to Meridian Rd in the Village of Sanford in Midland County | 9/26/1992 | No | Yes | Yes |
| 22 | 1052 | 31045 | US-23 | | 0.49 | 2.47 | South of M-72 to South of Lakeshore Dr. | 10/29/1996 | Yes | Yes | Yes |
| 23 | 25092 | 29727 | M-15 | | 8.61 | 8.90 | South of the South Village Limits of Otisville Northerly to North of Athletic Street in Otisville | 9/22/1994 | Yes | Yes | Yes |
| 24 | 37013 | 28116 | US-27 | NB | 8.95 | 11.72 | North of US-27 BR then Northerly to M-20 | 10/14/1993 | Yes | Yes | Yes |
| 24 | 37013 | 28116 | US-27 | SB | 8.95 | 11.36 | North of US-27 BR then Northerly to M-20 | 10/14/1993 | Yes | Yes | Yes |
| 24 | 37013 | 28116 | US-27 | SB | 11.45 | 11.72 | North of US-27 BR then Northerly to M-20 | 10/14/1993 | Yes | Yes | Yes |
| 25 | 56200 | 35269 | Saginaw Rd. | | 9.52 | 12.11 | Midland West County Line Easterly to Geneva Road and West of 9 Mile Road Easterly to Irish Road | 8/26/1994 | Yes | Yes | Yes |
| 25 | 56555 | 35266 | Saginaw Rd. | | 0.00 | 3.57 | Midland West County Line Easterly to Geneva Road and West of 9 Mile Road Easterly to Irish Road | 8/26/1994 | Yes | Yes | Yes |
| 26 | 56021 | 35139 | M-20 | WB | 6.05 | 10.59 | West of Castor Road easterly to Meridian Road | 10/22/1994 | Yes | Yes | Yes |
| 27 | 74012 | 29729 | M-53 | | 9.00 | 13.00 | Just South of Severance Road to North of M-81 | 8/25/1995 | Yes | Yes | No |
| 28 | 41033 | 31068 | M-37 | NB | 7.93 | 10.61 | From North of Sparta Avenue Northerly to North of 17 Mile Road | 9/13/1995 | Yes | Yes | Yes |
| 28 | 41033 | 31068 | M-37 | NB | 10.76 | 15.82 | From North of Sparta Avenue Northerly to North of 17 Mile Road | 9/13/1995 | Yes | Yes | Yes |
| 28 | 41033 | 31068 | M-37 | SB | 7.97 | 10.61 | From North of Sparta Avenue Northerly to North of 17 Mile Road | 9/13/1995 | Yes | Yes | Yes |
| 28 | 41033 | 31068 | M-37 | SB | 10.76 | 15.81 | From North of Sparta Avenue Northerly to North of 17 Mile Road | 9/13/1995 | Yes | Yes | Yes |
| 29 | 81063 | 26796 | US-12 | EB | 3.61 | 4.09 | West of Harris Road Easterly to West of Washtenaw/Wayne County Line | 11/9/1996 | Yes | Yes | Yes |
| 29 | 81063 | 26796 | US-12 | EB | 4.20 | 5.12 | West of Harris Road Easterly to West of Washtenaw/Wayne County Line | 11/9/1996 | Yes | Yes | Yes |
| 29 | 81063 | 26796 | US-12 | EB | 5.29 | 5.85 | West of Harris Road Easterly to West of Washtenaw/Wayne County Line | 11/9/1996 | Yes | Yes | Yes |

Table A1 (cont'd)

| Project number | Control section | Job number | Route | Dir. | BMP | EMP | Project location | Completion date | Surveys | | |
|---|---|---|---|---|---|---|---|---|---|---|---|
| | | | | | | | | | 2001 | 2002 | 2003 |
| 29 | 81063 | 26796 | US-12 | WB | 3.98 | 4.73 | West of Harris Road Easterly to West of Washtenaw/Wayne County Line | 11/9/1996 | Yes | Yes | Yes |
| 29 | 81063 | 26796 | US-12 | WB | 4.84 | 5.08 | West of Harris Road Easterly to West of Washtenaw/Wayne County Line | 11/9/1996 | Yes | Yes | Yes |
| 29 | 81063 | 26796 | US-12 | WB | 5.36 | 5.51 | West of Harris Road Easterly to West of Washtenaw/Wayne County Line | 11/9/1996 | Yes | Yes | Yes |
| 29 | 81063 | 26796 | US-12 | WB | 5.63 | 5.94 | West of Harris Road Easterly to West of Washtenaw/Wayne County Line | 11/9/1996 | Yes | Yes | Yes |
| 30 | 58111 | 34596 | M-50 | | 1.86 | 2.25 | From M-125 Easterly and Northerly to East of I-75 Interchange | 6/15/1996 | No | Yes | Yes |
| 31 | 70024 | 35987 | I-196 | EB | 12.59 | 15.59 | West of 32nd Avenue Interchange Northeasterly to East of the 44th Street Interchange | 9/30/1996 | Yes | Yes | Yes |
| 32 | 41401 | 37494 | Chicago Dr | | 0.01 | 0.37 | West City Limits of Grandville Easterly to Canal Avenue | 10/16/1995 | No | No | Yes |
| 33 | 61555 | 35396 | Airline Rd. | | 0.00 | 0.44 | From South of Pontaluna Road Northerly to North of Neal Street in the Village of Fruitport | 6/25/1996 | Yes | No | No |
| 34 | 39555 | 39212 | E. Michigan Ave | | 13.89 | 15.17 | Burgess Drive in the City of Galesburg (after M-96 intersection) to I-94 | 9/4/1996 | Yes | Yes | Yes |
| 35 | 65555 | 39235 | Old M-76/ County Rd. F-9 | | 5.24 | 6.60 | South of Rau Road to 60m (197 feet) South of Airport Road | 8/8/1996 | Yes | Yes | Yes |
| 36 | 3555 | 35605 | Blue Star Hwy | | 3.54 | 3.93 | South of Wiley Road Northerly to Washington Street in the Village of Douglas | 5/30/1997 | Yes | Yes | Yes |
| 36 | 3555 | 35605 | Blue Star Hwy | | 3.98 | 4.01 | South of Wiley Road Northerly to Washington Street in the Village of Douglas | 5/30/1997 | Yes | Yes | Yes |
| 37 | 3111 | 32373 | US-131 | NB | 6.73 | 7.96 | South of M-222 then Northerly to South of 124Th Avenue | 6/19/1997 | Yes | Yes | Yes |
| 37 | 3111 | 32373 | US-131 | SB | 6.73 | 7.96 | South of M-222 then Northerly to South of 124Th Avenue | 6/19/1997 | Yes | Yes | Yes |
| 37 | 3112 | 32373 | US-131 | NB | 0.02 | 1.94 | South of M-222 then Northerly to South of 124Th Avenue | 6/19/1997 | Yes | Yes | Yes |

Table A1 (cont'd)

| Project number | Control section | Job number | Route | Dir. | BMP | EMP | Project location | Completion date | Surveys | | |
|---|---|---|---|---|---|---|---|---|---|---|---|
| | | | | | | | | | 2001 | 2002 | 2003 |
| 37 | 3112 | 32373 | US-131 | NB | 2.08 | 3.10 | South of M-222 then Northerly to South of 124Th Avenue | 6/19/1997 | Yes | Yes | Yes |
| 37 | 3112 | 32373 | US-131 | SB | 0.02 | 0.89 | South of M-222 then Northerly to South of 124Th Avenue | 6/19/1997 | Yes | Yes | Yes |
| 37 | 3112 | 32373 | US-131 | SB | 1.18 | 1.94 | South of M-222 then Northerly to South of 124Th Avenue | 6/19/1997 | Yes | Yes | Yes |
| 37 | 3112 | 32373 | US-131 | SB | 2.08 | 3.10 | South of M-222 then Northerly to South of 124Th Avenue | 6/19/1997 | Yes | Yes | Yes |
| 38 | 61555 | 39233 | Third Ave | | 0.40 | 0.84 | Park Street Northerly to Pontaluna Road in the Village of Fruitport | 9/30/1996 | Yes | No | No |
| 39 | 70013 | 38179 | US-31 | NB | 1.23 | 8.28 | 8th Street Northerly to M-45 | 9/12/1997 | Yes | Yes | Yes |
| 39 | 70013 | 38179 | US-31 | NB | 8.93 | 13.01 | 8th Street Northerly to M-45 | 9/12/1997 | Yes | Yes | Yes |
| 40 | 28091 | 34060 | US-131 | | 0.00 | 0.13 | From Wexford/Grand Traverse County Line to Northerly to South of Elliott Rd. | 9/25/1997 | Yes | Yes | Yes |
| 40 | 83032 | 34060 | US-131 | | 12.97 | 18.66 | From North Village Limits of Manton Northerly to Wexford/Grand Traverse County Line | 9/25/1997 | Yes | Yes | Yes |
| 41 | 46082 | 32388 | M-50 | | 3.94 | 4.37 | East of Wyandotte St in Tecumseh to Rogers Highway | 9/29/1997 | Yes | Yes | Yes |
| 41 | 46082 | 32388 | M-50 | | 0.11 | 1.82 | East of M52 Easterly to West of West City Limits of Tecumseh | 9/29/1997 | Yes | Yes | Yes |
| 41 | 46082 | 32388 | M-50 | | 4.59 | 7.13 | East of Rogers Highway to West of Ford Highway | 9/29/1997 | Yes | Yes | Yes |
| 42 | 46082 | 32388 | M-50 | | 9.58 | 12.38 | East Village Limits of Britton to Lenawee/Monroe County Line | 7/15/1998 | Yes | Yes | Yes |
| 42 | 58041 | 32388 | M-50 | | 0.00 | 5.02 | Lenawee/Monroe County Line to West City Limits of Dundee | 7/15/1998 | Yes | Yes | Yes |
| 43 | 70024 | 35989 | I-196 | EB | 6.58 | 10.58 | From 64th Ave. Northeasterly to east of 32nd Ave. Interchange | 8/20/1997 | Yes | Yes | Yes |
| 44 | 12555 | 39160 | Broadway St. | | 0.01 | 0.04 | Coldwater Street to Charlotte Street in the Village of Union City | 10/25/1997 | Yes | Yes | Yes |
| 44 | 12555 | 39160 | Broadway St. | | 0.07 | 0.22 | Coldwater Street to Charlotte Street in the Village of Union City | 10/25/1997 | Yes | Yes | Yes |

Table A1 (cont'd)

| Project number | Control section | Job number | Route | Dir. | BMP | EMP | Project location | Completion date | Surveys | | |
|---|---|---|---|---|---|---|---|---|---|---|---|
| | | | | | | | | | 2001 | 2002 | 2003 |
| 45 | 13033 | 37138 | M-66/I-194 | NB | 0.06 | 0.49 | From 1/2 mile South of I-94 to Northerly to 1/2 mile North of I-94 in the City of Battle Creek | 8/22/1997 | Yes | Yes | Yes |
| 45 | 13033 | 37138 | M-66/I-194 | SB | 0.02 | 0.49 | From 1/2 mile South of I-94 to Northerly to 1/2 mile North of I-94 in the City of Battle Creek | 8/22/1997 | Yes | Yes | Yes |
| 46 | 37014 | 38206 | US-27 | NB | 7.15 | 14.43 | From Spring (Salt) Creek (B02) Northerly to the Chesapeake and Ohio Rail Road (R02) | 10/7/1997 | Yes | Yes | Yes |
| 46 | 37014 | 38206 | US-27 | SB | 7.21 | 14.51 | From Spring (Salt) Creek (B02) Northerly to the Chesapeake and Ohio Rail Road (R02) | 10/7/1997 | Yes | Yes | Yes |
| 47 | 37014 | 38206 | US-27 | NB | 1.54 | 7.71 | From North of River Road Northerly to South of Spring (Salt) Creek (B02) | 7/31/1998 | Yes | Yes | Yes |
| 47 | 37014 | 38206 | US-27 | SB | 1.57 | 7.14 | From North of River Road Northerly to South of Spring (Salt) Creek (B02) | 7/31/1998 | Yes | Yes | Yes |
| 48 | 58171 | 34113 | I-275 | NB | 0.47 | 1.96 | From I-75 Northerly to South of the US-24 Interchange | 1998 | Yes | Yes | Yes |
| 48 | 58171 | 34113 | I-275 | SB | 0.00 | 1.98 | From I-75 Northerly to South of the US-24 Interchange | 1998 | Yes | Yes | Yes |
| 49 | 82400 | 44388 | Lafayette St. | | 0.00 | 1.03 | Larned St. And Lafayette St. From I-375 to Mt. Elliot in the City of Detroit | 7/10/1998 | Yes | Yes | Yes |
| 49 | 82400 | 44388 | Larned St. | | 0.00 | 1.49 | Larned St. And Lafayette St. From I-375 to Mt. Elliot in the City of Detroit | 6/1/1998 | Yes | No | No |
| 50 | 74073 | 33937 | M-25 | | 0.48 | 4.94 | From the Northern Village Limits of Port Sanilac to the Northern Village Limits of Forester | 7/2/1998 | Yes | Yes | Yes |
| 51 | 44031 | 36021 | M-53 | | 0.00 | 1.59 | Macomb & Lapeer County Line Northerly to South Almont Village Limits | 9/30/1999 | Yes | Yes | Yes |
| 51 | 44031 | 36021 | M-53 | | 2.82 | 6.13 | North Village Limits of Almont Northerly to 298m (977ft) South of Ross Road | 9/30/1999 | Yes | Yes | Yes |
| 51 | 44031 | 36021 | M-53 | | 6.47 | 6.94 | 244m (800ft) North of Ross Road Northerly to 390m (1280ft) South of Hunter Creek Road | 9/30/1999 | Yes | Yes | Yes |
| 51 | 50012 | 36021 | M-53 | | 11.20 | 11.22 | From South of the Macomb & Lapeer County Line Northerly to North of Hunter Creek Road | 1999 | Yes | Yes | Yes |
| 52 | 21031 | 34050 | M-35 | | 1.42 | 3.09 | North of South Delta County Line Northerly to North of County Road A-35 | 7/23/1998 | Yes | No | No |

Table A1 (cont'd)

| Project number | Control section | Job number | Route | Dir. | BMP | EMP | Project location | Completion date | Surveys | | |
|---|---|---|---|---|---|---|---|---|---|---|---|
| | | | | | | | | | 2001 | 2002 | 2003 |
| 52 | 21031 | 34050 | M-35 | | 8.70 | 10.43 | South of County Road A-14 Northerly to South of Ford River | 7/23/1998 | Yes | No | No |
| 53 | 65555 | 44467 | Old M-76/ County Rd. F-9 | | 1.01 | 3.21 | South of Greenwood Road Northerly to South of Laporte Road | 8/20/1998 | Yes | Yes | Yes |
| 54 | 33555 | 35233 | Grand River Ave | | 0.10 | 1.06 | From East of M-52 to East of Elm Rd | 9/9/1998 | No | Yes | Yes |
| 54 | 41026 | 35988 | I-96 | EB | 5.87 | 6.10 | From West of Alpine Ave (M-37) Easterly to the Bridge over the Grand River | 10/30/1998 | Yes | Yes | Yes |
| 54 | 41026 | 35988 | I-96 | EB | 4.73 | 5.64 | From West of Alpine Ave (M-37) Easterly to the Bridge over the Grand River | 10/30/1998 | Yes | Yes | Yes |
| 54 | 41026 | 35988 | I-96 | WB | 5.51 | 6.07 | From West of Alpine Ave (M-37) Easterly to the Bridge over the Grand River | 10/30/1998 | Yes | Yes | Yes |
| 54 | 41026 | 35988 | I-96 | WB | 4.76 | 5.20 | From West of Alpine Ave (M-37) Easterly to the Bridge over the Grand River | 10/30/1998 | Yes | Yes | Yes |
| 54 | 41131 | 35988 | I-296 | SB | 17.36 | 17.88 | From East of Alpine Ave (M-37) Easterly to the Bridge over West River Dr. | 10/30/1998 | Yes | Yes | Yes |
| 55 | 41029 | 45068 | I-196 | EB | 4.08 | 6.61 | West(South) of 36th Street Northeasterly to East(North) of Market Street (Indian Mounds Dr.) | 7/31/1998 | Yes | Yes | Yes |
| 55 | 41029 | 35990 | I-196 | EB | 1.15 | 4.08 | West(South) of 36th Street Northeasterly to East(North) of Market Street (Indian Mounds Dr.) | 7/31/1998 | Yes | Yes | Yes |
| 55 | 41131 | 35988 | I-296 | NB | 17.59 | 17.76 | From East of Alpine Ave (M-37) Easterly to the Bridge over West River Dr. | 10/30/1998 | Yes | Yes | Yes |
| 56 | 41029 | 45068 | I-196 | WB | 4.11 | 6.66 | West(South) of 36th Street Northeasterly to East(North) of Market Street (Indian Mounds Dr.) | 7/31/1998 | Yes | Yes | Yes |
| 56 | 41029 | 35990 | I-196 | WB | 1.12 | 4.11 | West(South) of 36th Street Northeasterly to East(North) of Market Street (Indian Mounds Dr.) | 7/31/1998 | Yes | Yes | Yes |
| 57 | 39405 | 46994 | Portage Rd. | | 0.00 | 2.14 | From Centre Avenue Northerly to East Milham Avenue in the City of Portage | 11/29/1998 | Yes | Yes | Yes |
| 58 | 64555 | 39385 | Third Street | | 0.13 | 0.44 | Garfield Road Northerly to Oceana Drive (US-31BR) in the Village of New Era | 8/30/1998 | Yes | No | No |

Table A1 (cont'd)

| Project number | Control section | Job number | Route | Dir. | BMP | EMP | Project location | Completion date | Surveys | | |
|---|---|---|---|---|---|---|---|---|---|---|---|
| | | | | | | | | | 2001 | 2002 | 2003 |
| 59 | 81076 | 32390 | US-23 | NB | 0.54 | 6.62 | North of Milan then Northerly to North of Bemis Road | 11/11/1997 | Yes | Yes | Yes |
| 59 | 81076 | 32390 | US-23 | SB | 0.54 | 6.43 | North of Milan then Northerly to North of Bemis Road | 11/11/1997 | Yes | Yes | Yes |
| 60 | 26011 | 45410 | M-18 | | 4.86 | 12.00 | From the Tobacco River Northerly to M-61 | 7/31/1999 | Yes | Yes | Yes |
| 61 | 67021 | 45053 | US-10 | | 1.94 | 2.63 | From Patterson Road (220th Avenue) Easterly to 200th Avenue, in the City of Reed City | 10/30/1998 | Yes | Yes | Yes |
| 61 | 67022 | 45053 | US-10 | | 0.00 | 1.52 | From Patterson Road (220th Avenue) Easterly to 200th Avenue, in the City of Reed City | 10/30/1998 | Yes | Yes | Yes |
| 62 | 25092 | 45534 | M-15 | | 9.50 | 10.41 | South of North Street in the Village of Otisville Northerly to North of M-57 | 10/1/1998 | Yes | No | Yes |
| 63 | 39060 | 39503 | E. Michigan Ave | | 0.99 | 3.61 | 358 m (1175 ft) East of 40th Street Easterly of 960 m (3150 ft) East of 42nd Street in Kalamazoo County | 10/1/1998 | Yes | Yes | Yes |
| 64 | 25042 | 36020 | I-69 | | 0.04 | 5.93 | West of M-13 Easterly to West of Elms Road | 9/1/1998 | Yes | Yes | Yes |
| 65 | 23012 | 32386 | Lansing Rd. | NB | 10.69 | 13.01 | Northeast of Guinea Road Northeasterly to Southwest of Creyts Road | 10/28/1998 | Yes | Yes | Yes |
| 65 | 23012 | 32386 | Lansing Rd. | SB | 10.66 | 13.01 | Northeast of Guinea Road Northeasterly to Southwest of Creyts Road | 10/28/1998 | Yes | Yes | Yes |
| 66 | 38061 | 34106 | M-60 | EB | 12.65 | 16.41 | From South of Spring Arbor Road Northerly to I-94 in Spring Arbor | 10/30/1998 | Yes | Yes | Yes |
| 66 | 38061 | 34106 | M-60 | WB | 12.65 | 16.42 | From South of Spring Arbor Road Northerly to I-94 in Spring Arbor | 10/30/1998 | Yes | Yes | Yes |
| 67 | 1052 | 32335 | US-23 | | 16.37 | 16.39 | From South of the Alcona/Alpena County Line Northerly to the Alcona/Alpena County Line | 11/1/1999 | Yes | Yes | Yes |
| 67 | 4031 | 32335 | US-23 | | 0.00 | 0.24 | From Alcona/Alpena County Line Northerly to South of Ossineke Road | 11/1/1999 | Yes | Yes | Yes |
| 67 | 4031 | 32335 | US-23 | | 0.45 | 0.91 | From Alcona/Alpena County Line Northerly to South of Ossineke Road | 11/1/1999 | Yes | Yes | Yes |
| 67 | 4031 | 32335 | US-23 | | 1.40 | 2.25 | From Alcona/Alpena County Line Northerly to South of Ossineke Road | 11/1/1999 | Yes | Yes | Yes |

Table A1 (cont'd)

| Project number | Control section | Job number | Route | Dir. | BMP | EMP | Project location | Completion date | Surveys | | |
|---|---|---|---|---|---|---|---|---|---|---|---|
| | | | | | | | | | 2001 | 2002 | 2003 |
| 67 | 4031 | 44350 | US-23 | | 4.22 | 7.89 | From South of Ossineke Road Northerly to North of Cranberry Creek | 11/1/1999 | Yes | Yes | Yes |
| 68 | 67022 | 44986 | US-10 | | 9.66 | 12.09 | 1.08 Miles East of 110th Avenue Easterly to 0.25 Miles East of 100th Avenue | 9/30/1999 | Yes | Yes | Yes |
| 69 | 5011 | 44109 | US-31 | | 0.92 | 3.02 | 0.923 Miles North of South Antrim County Line Northerly to just South of River Street in Elk Rapids | 8/25/1999 | Yes | Yes | Yes |
| 70 | 10032 | 44113 | US-31 | | 11.43 | 13.87 | 209 m (686 ft) East of Carman Rd Easterly to 20 m (66 ft) West of Reynolds Road | 9/30/1999 | Yes | Yes | Yes |
| 70 | 10032 | 44113 | US-31 | | 13.91 | 14.34 | 209 m (686 ft) East of Carman Rd Easterly to 20 m (66 ft) West of Reynolds Road | 9/30/1999 | Yes | Yes | Yes |
| 71 | 58042 | 43523 | M-50 | | 0.14 | 4.52 | From West of Lewis Avenue Easterly to West of Rainsville Road | 6/15/1999 | Yes | Yes | Yes |
| 72 | 39052 | 48864 | E. Michigan Ave | | 0.00 | 2.41 | From 980 m (3215 ft) East of 42nd Street to Mercury Dr. In Kalamazoo County | 6/11/1999 | Yes | Yes | Yes |
| 73 | 25081 | 38028 | M-21 | | 4.98 | 7.29 | From Morrish Road Easterly to East of Lincor Parkway | 10/30/1999 | No | Yes | Yes |
| 74 | 41133 | 33914 | US-131 | NB | 3.20 | 8.69 | From M-46 (West Segment) Northerly to Kent/Montcalm County Line | 9/10/1999 | Yes | Yes | Yes |
| 74 | 41133 | 33914 | US-131 | SB | 3.21 | 8.69 | From M-46 (West Segment) Northerly to Kent/Montcalm County Line | 9/10/1999 | Yes | Yes | Yes |
| 74 | 59012 | 33914 | US-131 | NB | 0.00 | 4.21 | From Kent/Montcalm County Line Northerly to North of Cannonsville Road | 9/10/1999 | Yes | Yes | Yes |
| 74 | 59012 | 33914 | US-131 | SB | 0.00 | 4.23 | From Kent/Montcalm County Line Northerly to North of Cannonsville Road | 9/10/1999 | Yes | Yes | Yes |
| 75 | 39405 | 49551 | Portage Rd. | | 0.00 | 1.13 | From Lakeview Drive Northerly to Centre Avenue | 9/15/1999 | Yes | Yes | Yes |
| 76 | 41013 | 45797 | M-44 | | 2.67 | 2.82 | From 230m (755 ft) South of Belding Road Northerly to Belding Road | 8/22/1999 | Yes | Yes | Yes |
| 76 | 41401 | 49321 | Wolverine Blvd | | 0.00 | 1.39 | From Belding Road Northerly to 10 Mile Road | 8/22/1999 | Yes | Yes | Yes |

Table A1 (cont'd)

| Project number | Control section | Job number | Route | Dir. | BMP | EMP | Project location | Completion date | Surveys | | |
|---|---|---|---|---|---|---|---|---|---|---|---|
| | | | | | | | | | 2001 | 2002 | 2003 |
| 77 | 56555 | 48370 | Saginaw Rd. | | 7.11 | 9.51 | From East of Castor Rd. Easterly to 280m (919 ft) East of Trillium Lane | 9/30/1999 | Yes | Yes | Yes |
| 78 | 39405 | 50708 | Shaver Rd. | | 1.28 | 1.93 | From 70.89 m North of the North Oakland Drive Northerly to South of Vanderbilt Avenue | 10/30/1999 | Yes | Yes | Yes |
| 79 | 35032 | 35985 | US-23 | | 19.12 | 22.01 | Gaston Way Road Northerly to the Iosco/Alcona County line | 2000 | Yes | Yes | Yes |
| 80 | 53022 | 37974 | US-10 | | 3.50 | 6.55 | Custer East Village Limits Easterly to 134.7m (442 ft) East of Budzynski Rd (Control) | 2000 | Yes | Yes | Yes |
| 80 | 53022 | 37974 | US-10 | | 6.55 | 9.40 | 134.7m (442 ft) East of Budzynski Rd Easterly to 429.4 m (1409ft) East of Campbell Rd | 2000 | Yes | Yes | Yes |
| 81 | 37011 | 38205 | US-27 BR | | 0.00 | 0.46 | Gore of US-27 BR Exit Ramp from US-27 Northerly to South of end of duel roadway | 2000 | Yes | Yes | Yes |
| 81 | 41033 | 38190 | M-37/M-46 | | 15.74 | 17.12 | South of Fruitridge Road Northerly to Kent/Muskegon County Line | 5/12/2000 | Yes | Yes | Yes |
| 81 | 61171 | 38190 | M-37/M-46 | | 0.00 | 0.57 | Kent /Muskegon County Line Northerly to West Village Limits of Casnovia | 5/12/2000 | Yes | Yes | Yes |
| 82 | 37013 | 38205 | US-27 | | 8.06 | 9.01 | North of Shepherd Road Northerly to North of US-27 BR (North of Summerton Rd. To north of US-27 BR) | 2000 | Yes | Yes | Yes |
| 82 | 37014 | 38205 | US-27 | | 0.00 | 1.53 | M-20 Northerly to South of River Road | 2000 | Yes | Yes | Yes |
| 83 | 25402 | 50078 | Beecher Rd. | | 0.00 | 0.99 | River Road to Linden Road | 2000 | No | Yes | Yes |
| 83 | 65041 | 45865 | I-75 | SB | 6.62 | 9.34 | Cook Road Northerly to North of Gray Road | 5/17/2001 | Yes | Yes | Yes |
| 83 | 65041 | 45865 | I-75 | NB | 6.54 | 9.54 | Cook Road Northerly to North of Gray Road | 5/17/2001 | Yes | Yes | Yes |
| 84 | 65041 | 50649 | I-75 | SB | 9.34 | 11.27 | North of Gray Road Northerly to South of Ski Park Road | 5/17/2001 | Yes | Yes | Yes |
| 84 | 65041 | 50649 | I-75 | NB | 9.54 | 11.37 | North of Gray Road Northerly to South of Ski Park Road | 5/17/2001 | Yes | Yes | Yes |
| 85 | 58042 | 50711 | M-50 | | 4.53 | 6.87 | West of Rainsville Road Easterly to Westwood Boulevard | 7/6/2001 | No | Yes | Yes |
| 86 | 18555 | 55091 | Clare Ave | | N/A | N/A | North of Arnold Lake Road Northerly to North of Long Lake Road | 5/15/2001 | No | Yes | Yes |

Table A1 (cont'd)

| Project number | Control section | Job number | Route | Dir. | BMP | EMP | Project location | Completion date | Surveys | | |
|---|---|---|---|---|---|---|---|---|---|---|---|
| | | | | | | | | | 2001 | 2002 | 2003 |
| 87 | 41401 | 50230 | Chicago Dr. | | 0.00 | 1.17 | Wilson Ave to Ivanrest Ave | 2001 | No | Yes | Yes |
| 87 | 41402 | 50251 | Chicago Dr. | | 1.17 | 1.77 | Ivanrest Ave to East City Limits of the City of Grandville | 2001 | No | Yes | Yes |

## REFERENCES


1. Annual Book of ASTM Standards - Section 4 - Construction, 1994, Vol. 04.03 Road and Paving Materials; Paving Management Technologies, The American Society for Testing and Materials, Philadelphia, Pennsylvania.

2. American Association of State Highway and Transportation Officials, "AASHTO Guide for Design of Pavement Structures", pp. 106-112, Washington D.C., 1993

3. Bahia U.H. and D.A. Anderson, "Glass Transition Behavior and Physical Hardening of Asphalt Binders," *Proceedings of the Association of Asphalt Paving Technologists*, Volume 62, 1993, pp 93-129.

4. Baladi, G.Y., "Integrated Material and Structural Design Method for Flexible Pavements," Volumes I and II, final report, FHWA/RD-88-109 and 110, Washington, D.C. December 1988

5. Baladi, G. Y. and T. Svasdisant, "Identify Causes for Underperforming Rubblized Concrete Pavement Projects," Final Report, RC-1416, Michigan State University, East Lansing, MI, 2002

6. Bensalem, A., A. J., Broen, M. E. Nunn, D. B. Merrill, and W. G. Lloyd, "Finite Element Modeling of fully Flexible Pavements: Surface Cracking and Wheel Interaction," *Proceedings of the Second International Symposium on 3D Finite Element For Pavement Analysis, Design, and Research,* West Virginia, 2000, pp. 103-121

7. Brown, E.R. and C.E. Bassett, "Effects of Maximum Aggregate Size on Rutting Potential and Other Properties of Asphalt-Aggregate Mixtures," In *Transportation Research Record 1259*, TRB, National Research Council, Washington, D.C., 1990, pp. 107-119

8. Brown, E. R., R. Collins, and J.R. Brownfield, "Investigation of Segregation of Asphalt Mixtures in the State of Georgia," In *Transportation Research Record 1217*, TRB, National Research Council, Washington, D.C, 1989, pp. 1-8

9. Button, J.W., D. Perdomo, and R.L. Lytton, "Influence of Aggregate on Rutting in Asphalt concrete Pavements," In *Transportation Research Record 1259*, TRB, National Research Council, Washington, D.C., 1990, pp. 141-152

10. Chang, C.M., "Detecting Segregation in Bituminous Pavements and Relating its Effects to Performance," A Ph.D. Thesis, Department of Civil and Environmental Engineering, Michigan State University, 2000.

11. Chang, C.M., G.Y. Baladi, and T.F. Wolff, "Using Pavement Distress Data to Assess the Impact of Construction on Pavement Performance," In *Transportation Research Record 1761*, TRB, National Research Council, Washington, D.C., 2001, pp 15-25

12. Chang, C.M., G.Y. Baladi, and T.F. Wolff, "Detecting Segregation in Bituminous Pavements," In T*ransportation Research Record* 1813, TRB, National Research Council, Washington, D.C., 2002, pp 77-86

13. Chapuis, R.P. and A. Gatien, "Temperature Dependent Tensile strength of Asphalt Mixtures in Relation to field Cracking Data," ASTM STP 1265, 1995, pp. 180-193

14. Chatti, K., H.B. Kim, K.K. Yun, J.P. Mahoney, and C.L. Monismith, "Field Investigation into Effects of Vehicle Speed and Tire Pressure on Asphalt Concrete Pavement Strains," In *Transportation Research Record 1539*, TRB, National Research Council, Washington, D.C., 1996, pp 66-71

15. Clark, S. M., Mechanics of Pneumatic Tires, U.S. Department of Transportation, National Highway Traffic Safety Administration, Washington, D. C., 1981

16. Dai, S.T., D. Van Deusen, M. De Beer, D. Rettner and G. Cochran, "Investigation of Flexible Pavement Response to Truck Speed and FWD Load through Instrumented Pavements," *Proceedings of the 8th International Conference on Asphalt Pavements*, Seattle, 1997, pp. 141-160

17. Dauzats, M., and A. Rampal, "Mechanism of Surface Cracking in Wearing Courses," *Proceedings of the 6th International Conference on Asphalt Pavements*, Ann Arbor, 1987, pp. 232-247

18. De Beer, M. and C. Fisher, "Contact Stresses of Pneumatic Tires Measured with the Vehicle-Road Surface Pressure Transducer Array (VRSPTA) System for the University of California at Berkley (UCB) and the Nevada Automotive Test Center (NATC)", Volume 1 and 2, 1997

19. De Beer, M., C. Fisher, and F.J. Jooste, "Determination of Pneumatic Tyre/Pavement Interface Contact Stresses Under Moving Loads and Some Effects on Pavement with Thin Asphalt Surfacing Layers," *Proceedings of the 8th International Conference on Asphalt Pavements*, Seattle, 1997, pp. 179-227

20. Gerritsen, A.H., C.A.P.M. van Gurp, J.P.J. van der Heide, A.A A. Molenaar, and A.C. Pronk, "Prediction and Prevention of Surface Cracking in Asphaltic Pavements," *Proceedings of the 6th International Conference on Asphalt Pavements*, Ann Arbor, 1987, pp. 378-391

21. Gillespie, T. D., "Fundamentals of Vehicle Dynamics", Society of Automotive Engineers, Pennsylvania, 1992

22. Groenendijk, J., "Accelerated testing and Surface Cracking of Asphaltic Concrete Pavements," A PhD dissertation. Department of Civil Engineering, Delft University of Technology, the Netherlands, 1998

23. Haddad, Y. M., "Viscoelasticity of engineering Materials," Chapman & Hall, London, 1995.

24. Harvey, John T. and Bor-Wen Tsai, "Effects of Asphalt Content and Air Void Content on Mix Fatigue and Stiffness," in ***Transportation Research Record*** *1543*, National Research Council, Washington, D.C.,1996, pp. 38-45

25. Heukelom, W., "Observations on the Rheology and Fracture of Bitumens and Asphalt Mixes," *Proceedings of the Association of Asphalt Paving Technologists,* Volume 35, 1966, pp. 358-399

26. Hiltunen D. R. and R. Rogue, "A Mechanics-Based Prediction Model for Thermal Cracking of Asphalt Concrete Pavements," Proceedings *Association of Asphalt paving Technologists*, Volume 63,1994, pp.81-117

27. Himeno, K., T. Ikeda, T. Kamijima, and T. Abe, "Distribution of Tire Contact Pressure of Vehicles and its Influence on Pavement Distress," *Proceedings of the* $8^{th}$ *International Conference on Asphalt Pavements*, Seattle, 1997, pp. 129-139

28. Huang, Yang H., "Pavement Analysis and Design," Prentice-Hall Inc., New Jersey, 1993

29. Hugo, F., and T.W. Kennedy, "Surface Cracking of Asphalt Mixtures in Southern Africa," *Proceedings of the Association of Asphalt Paving Technologists*, Volume 54, 1985, pp 454-501

30. Irwin, L.H., S.W. Yang, and R.N. Stubstad, "Deflection Reading Accuracy and Layer Thickness Accuracy in Backcalculation of Pavement Layer Moduli." The American Society for Testing and Material, STP 1026, 1989, Bush and Baladi, editors, pp. 229-244.

31. Jacobs, M.M.J., P. C. Hopman, and A.A.A. Molenaar, "Application of Fracture mechanics and Principles to Analyze Cracking in Asphalt Concrete (With Discussion)," *Proceedings of the Association of Asphalt Paving Technologists*, Volume 65, 1996, pp 1-39

32. Jung, D. and T. S. Vinson, "Thermal stress Restrained Specimen Test to Evaluate Low Temperature Cracking of Asphalt-Aggregate Mixtures," In *Transportation*

*Research Record 1417*, National Research Council, Washington, D.C., 1993, pp. 12-20

33. Khattak, Jamal, "Engineering Characteristics of Polymer Modified Asphalt Mixtures," A PhD Dissertation, Department of Civil and Environmental Engineering, Michigan State University, Michigan, 1999

34. Khedaywi, T.S. and T.D. White, "Development and Analysis of Laboratory Techniques for Simulating Segregation," In *Transportation Research Record 1492*, TRB, National Research Council, Washington, D.C., 1995, pp 36-45

35. Kim, K.W. and H.M. El Hussein, "Effect of Differential Thermal Contraction on Fracture Toughness of Asphalt Materials at Low Temperatures," *Proceedings of the Association of Asphalt Paving Technologists*, Volume 64, 1996, pp. 474-499.

36. Kim, Y.R. and Y.C. Lee, "Interrelationships Among Stiffnesses of Asphalt Aggregate Mixtures," *Proceedings of the Association of Asphalt Paving Technologists*, Volume 64, 1996, pp. 575-610.

37. Marker, V., "Symposium-Compaction of Asphalt Concrete," *Proceedings of the Association of Asphalt Paving Technologists*, Volume 36, 1967, pp. 288-294

38. Matsuno, S., and T. Nishizawa, "Mechanism of Longitudinal Surface Cracking in Asphalt Pavement," Proceedings of the 7th International Conference on Asphalt Pavements, Nottingham, 1992, pp. 277-291

39. Malan, G.W., P.J. Straus, and F. Hugo, "A Field Study of Premature Surface Cracking in Asphalt (With Discussion)," *Proceedings of the Association of Asphalt Paving Technologists*, Volume 58, 1988, pp 142-162

40. Markwick, A.H.D., and J.H. Starks, "Stresses Between Tire and Road." Journal of the Institution of Civil Engineers, Vol. 16,1940-1941, pp 309-325

41. Michigan Center for Truck safety, "Truck Driver's Guidebook," 6th Edition.

42. Mohammad, L.N. and H.R. Paul, "Evaluation of Indirect Tensile Test for Determining Structural Properties of Asphalt Mix," In *Transportation Research Record 1417*, TRB, National Research Council, Washington, D.C., 1993, pp. 58-63

43. Molenaar, A.A.A., "Fatigue and Reflective Cracking due to Traffic (With Discussion)," *Proceedings of the Association of Asphalt Paving Technologists*, Volume 53, 1984, pp 440-474

44. Myers, L.A., R. Roque, and B.E. Ruth, "Mechanisms of Surface-Initiated Longitudinal Wheel Path Cracks in High-Type Bituminous Pavements," *Proceedings of the Association of Asphalt Paving Technologists*, Volume 67, 1998, pp 401-432

45. Myers, L.A., R. Roque, B.E. Ruth, and C. Drakos, "Measurement of Contact Stresses for Different Truck Tire Types to Evaluate Their Influence on Near-Surface Cracking and Rutting," In *Transportation Research Record 1655*, TRB, National Research Council, Washington, D.C., 1999, pp. 175-184

46. Myers, L.A., R. Roque and B. Birgisson, "Propagation Mechanisms for Surface-Initiated Longitudinal Wheel Path Cracks," In *Transportation Research Record 1778*, TRB, National Research Council, Washington, D.C., 2001, pp. 113-121

47. Myers, L. and R. Roque, "Top-Down Crack Propagation in Bituminous Pavements and Implications for Pavement management," *Proceedings of the Association of Asphalt Paving Technologists*, Volume 71, 2002, p 651-670

48. Niederquell, M.G., G.Y. Baladi, and K. Chatti, "Rubblization of Concrete Pavements: Field Investigation," In *Transportation Research Record 1730*, TRB, National Research Council, Washington, D.C., 2001, pp. 150-160

49. Park, D.Y., "Effect of Temperature and Loading Time on the Stiffness Properties of HMAC in Flexible Pavements," A Ph.D. dissertation, Department of Civil and Environmental Engineering, Michigan State University, Michigan, 2000

50. Per Ullidtz , "Pavement Analysis", Elsevier Science Publishing Company, New York, New York, 1987.

51. Pottinger M., "The Three-Dimensional Contact Patch Stress Field of Solid and Pneumatic Tires," Tire Science and Technology, TSTCA, volume 20 number 1, 1992, pp. 3-32.

52. Pottinger, M.G., and J.E. McIntrye, "Effects if suspension Alignment and Modest Cornering on the footprint Behavior of Performance Tires and Heavy Duty Radial Tires," Tire Science and Technology, TSTCA, volume 27 number 3, 1999, pp.128-160.

53. Rickards, I., S. Goodman, J. Pagani, A.O.A.E. Halim, and R. Haas, "Practical Realization of a New concept for Asphalt Compaction," In *Transportation Research Record 1730*, TRB, National Research Council, Washington, D.C., 1999, pp. 27-35

54. Roque, R., and B.E. Ruth., "Mechanisms of Modeling of Surface Cracking in Asphalt Pavements," Proceedings of the Association of Asphalt Paving Technologists, Volume 59, 1990, pp. 396-421

55. Roque, R., L.A. Myers, and B. Birgisson, "Evaluating Measured Tire Contact Stresses to Predict Pavement Response and Performance." In *Transportation Research Record 1716*, TRB, National Research Council, Washington, D.C., 2000, pp 73-81

56. Schorsch, M., "Determining the Causes of Top-Down Cracks in Bituminous Pavements", A Master dissertation, Department of Civil and Environmental Engineering, Michigan State University, Michigan, 2003

57. Shahin, Y., "Design System for Minimizing Asphalt Concrete Thermal Cracking," The 4th International Conference Structure Design of Asphalt Pavement, Ann Arbor, Volume 1, 1977, pp. 920-932.

58. Siddharthan, R.V. and P.E. Sebaaly, "Investigation of Asphalt Concrete Layer Strains from Wide-Base Tires," In *Transportation Research Record 1655*, TRB, National Research Council, Washington, D.C., 1999, pp 168-174

59. Soon, See Chaw, "Tire-Induced Surface Stresses in Flexible Pavements", Accepted for Publication in Transportation Research Record and Presented at TRB Annual meeting, Washington, D.C., 2003.

60. Svasdisant T., M. Schorsch, G.Y. Baladi, and S. Pinyosunun, "Mechanistic Analysis of Top-down Cracks in Asphalt Pavement," In *Transportation Research Record 1809*, TRB, National Research Council, Washington, D.C., 2002, pp 126-136

61. Tielking, J.T., and M.A. Abraham, "Measurement of Truck Tire Footprint Pressure." In *Transportation Research Record 1435*, TRB, National Research Council, Washington, D.C., 1994, pp 92-99

62. Uhlmeyer, J. S., K. Willoughby, L.M. Pierce, and J. P. Mahoney, "Top-Down Cracking in Washington State Asphalt Concrete Wearing Courses," In *Transportation Research Record 1730*, TRB, National Research Council, Washington, D.C., 2000, pp. 110-116

63. Wambura, J.H.G., J. Maina, and H. R. Smith., "Kenya Bituminous Materials Study," In *Transportation Research Record 1681*, TRB, National Research Council, Washington, D.C., 1999, pp. 129-137

64. Yoder, E. J. and M. W. Witczak, "Principles of Pavement Design," 2nd Edition, John Wiley & Son, 1975

65. Zeng, M. and D. H. Shields, "Nonlinear Thermal Expansion and Contraction of Asphalt Concrete," Canadian Journal of Civil Engineering, Volume 26, 1999, pp. 26-34.

66. Zubeck, H.K. and T.S. Vinson, "Prediction of Low-Temperature Cracking of Asphalt Concrete Mixtures with Thermal Stress Restrained Specimen Test Results," In *Transportation Research Record 1545*, TRB, National Research Council, Washington, D.C., 1996, pp. 50-58

MICHIGAN STATE UNIVERSITY LIBRARIES
3 1293 02461 8781